

EDITOR'S PICK 2021: HIGHLIGHTS IN MOLECULAR AND CELLULAR PATHOLOGY

EDITED BY: Ramani Ramchandran

PUBLISHED IN: Frontiers in Cell and Developmental Biology



frontiers

Frontiers eBook Copyright Statement

The copyright in the text of individual articles in this eBook is the property of their respective authors or their respective institutions or funders. The copyright in graphics and images within each article may be subject to copyright of other parties. In both cases this is subject to a license granted to Frontiers.

The compilation of articles constituting this eBook is the property of Frontiers.

Each article within this eBook, and the eBook itself, are published under the most recent version of the Creative Commons CC-BY licence.

The version current at the date of publication of this eBook is CC-BY 4.0. If the CC-BY licence is updated, the licence granted by Frontiers is automatically updated to the new version.

When exercising any right under the CC-BY licence, Frontiers must be attributed as the original publisher of the article or eBook, as applicable.

Authors have the responsibility of ensuring that any graphics or other materials which are the property of others may be included in the CC-BY licence, but this should be checked before relying on the CC-BY licence to reproduce those materials. Any copyright notices relating to those materials must be complied with.

Copyright and source acknowledgement notices may not be removed and must be displayed in any copy, derivative work or partial copy which includes the elements in question.

All copyright, and all rights therein, are protected by national and international copyright laws. The above represents a summary only. For further information please read Frontiers' Conditions for Website Use and Copyright Statement, and the applicable CC-BY licence.

ISSN 1664-8714

ISBN 978-2-88974-412-1

DOI 10.3389/978-2-88974-412-1

About Frontiers

Frontiers is more than just an open-access publisher of scholarly articles: it is a pioneering approach to the world of academia, radically improving the way scholarly research is managed. The grand vision of Frontiers is a world where all people have an equal opportunity to seek, share and generate knowledge. Frontiers provides immediate and permanent online open access to all its publications, but this alone is not enough to realize our grand goals.

Frontiers Journal Series

The Frontiers Journal Series is a multi-tier and interdisciplinary set of open-access, online journals, promising a paradigm shift from the current review, selection and dissemination processes in academic publishing. All Frontiers journals are driven by researchers for researchers; therefore, they constitute a service to the scholarly community. At the same time, the Frontiers Journal Series operates on a revolutionary invention, the tiered publishing system, initially addressing specific communities of scholars, and gradually climbing up to broader public understanding, thus serving the interests of the lay society, too.

Dedication to Quality

Each Frontiers article is a landmark of the highest quality, thanks to genuinely collaborative interactions between authors and review editors, who include some of the world's best academicians. Research must be certified by peers before entering a stream of knowledge that may eventually reach the public - and shape society; therefore, Frontiers only applies the most rigorous and unbiased reviews.

Frontiers revolutionizes research publishing by freely delivering the most outstanding research, evaluated with no bias from both the academic and social point of view. By applying the most advanced information technologies, Frontiers is catapulting scholarly publishing into a new generation.

What are Frontiers Research Topics?

Frontiers Research Topics are very popular trademarks of the Frontiers Journals Series: they are collections of at least ten articles, all centered on a particular subject. With their unique mix of varied contributions from Original Research to Review Articles, Frontiers Research Topics unify the most influential researchers, the latest key findings and historical advances in a hot research area! Find out more on how to host your own Frontiers Research Topic or contribute to one as an author by contacting the Frontiers Editorial Office: frontiersin.org/about/contact

EDITOR'S PICK 2021: HIGHLIGHTS IN MOLECULAR AND CELLULAR PATHOLOGY

Topic Editor:

Ramani Ramchandran, Medical College of Wisconsin, United States

Citation: Ramchandran, R., ed. (2022). Editor's Pick 2021: Highlights in Molecular and Cellular Pathology. Lausanne: Frontiers Media SA.
doi: 10.3389/978-2-88974-412-1

Table of Contents

- 04** *Novel Aspects of Extracellular Vesicles in the Regulation of Renal Physiological and Pathophysiological Processes*
Juan Pablo Rigalli, Eric Raul Barros, Vera Sommers, René J. M. Bindels and Joost G. J. Hoenderop
- 11** *Nicotinamide Mononucleotide: A Promising Molecule for Therapy of Diverse Diseases by Targeting NAD⁺ Metabolism*
Weiqi Hong, Fei Mo, Ziqi Zhang, Mengyuan Huang and Xiawei Wei
- 38** *Bergerin as a Novel Urate-Lowering Therapeutic Strategy for Hyperuricemia*
Mo Chen, Chenyi Ye, Jianing Zhu, Peiyu Zhang, Yujie Jiang, Xiaoyong Lu and Huaxiang Wu
- 51** *Circular RNAs: Functions and Clinical Significance in Cardiovascular Disease*
Lei Zhang, Yuan Zhang, Yin Wang, Yanfang Zhao, Han Ding and Peifeng Li
- 64** *The Role of the Microbiome in Driving RA-Related Autoimmunity*
Cristopher M. Rooney, Kulveer Mankia and Paul Emery
- 79** *Recent Advances in Pathophysiology, Drug Development and Future Perspectives of SARS-CoV-2*
Desh Deepak Singh, Ihn Han, Eun-Ha Choi and Dharmendra K. Yadav
- 95** *Exploring Additional Valuable Information From Single-Cell RNA-Seq Data*
Yunjin Li, Qiyue Xu, Duoqiao Wu and Geng Chen
- 113** *b3galt6 Knock-Out Zebrafish Recapitulate β 3GalT6-Deficiency Disorders in Human and Reveal a Trisaccharide Proteoglycan Linkage Region*
Sarah Delbaere, Adelbert De Clercq, Shuji Mizumoto, Fredrik Noborn, Jan Willem Bek, Lien Alluyn, Charlotte Gistelinck, Delfien Syx, Phil L. Salmon, Paul J. Coucke, Göran Larson, Shuhei Yamada, Andy Willaert and Fransiska Malfait
- 130** *N6-Methyladenosine Induced miR-34a-5p Promotes TNF- α -Induced Nucleus Pulposus Cell Senescence by Targeting SIRT1*
Hao Zhu, Bao Sun, Liang Zhu, Guoyou Zou and Qiang Shen
- 143** *Umbilical Cord Blood-Derived Exosomes From Very Preterm Infants With Bronchopulmonary Dysplasia Impaired Endothelial Angiogenesis: Roles of Exosomal MicroRNAs*
Xin-qi Zhong, Qin Yan, Zhuang-gui Chen, Chun-hong Jia, Xiu-hong Li, Zi-yan Liang, Jian Gu, Hui-ling Wei, Chang-yu Lian, Jing Zheng and Qi-liang Cui



Novel Aspects of Extracellular Vesicles in the Regulation of Renal Physiological and Pathophysiological Processes

Juan Pablo Rigalli¹, Eric Raul Barros^{1,2}, Vera Sommers¹, René J. M. Bindels¹ and Joost G. J. Hoenderop^{1*}

¹ Department of Physiology, Radboud Institute for Molecular Life Sciences, Radboud University Medical Center, Nijmegen, Netherlands, ² Department of Endocrinology, School of Medicine, Pontificia Universidad Católica de Chile, Santiago, Chile

OPEN ACCESS

Edited by:

Adelaide Fernandes,
University of Lisbon, Portugal

Reviewed by:

Mariateresa Giullano,
University of Campania Luigi Vanvitelli,
Italy

David Otaegui,
Biodonostia Health Research Institute
(IIS Biodonostia), Spain

*Correspondence:

Joost G. J. Hoenderop
joost.hoenderop@radboudumc.nl

Specialty section:

This article was submitted to
Molecular Medicine,
a section of the journal
Frontiers in Cell and Developmental
Biology

Received: 13 January 2020

Accepted: 23 March 2020

Published: 15 April 2020

Citation:

Rigalli JP, Barros ER, Sommers V,
Bindels RJM and Hoenderop JGJ
(2020) Novel Aspects of Extracellular
Vesicles in the Regulation of Renal
Physiological and Pathophysiological
Processes.
Front. Cell Dev. Biol. 8:244.
doi: 10.3389/fcell.2020.00244

Extracellular vesicles (EV) are nanosized particles released by a large variety of cells. They carry molecules such as proteins, RNA and lipids. While urinary EVs have been longer studied as a source of biomarkers for renal and non-renal disorders, research on EVs as regulatory players of renal physiological and pathological processes has experienced an outbreak recently in the past decade. In general, the microenvironment and (patho)physiological state of the donor cells affect the cargo of the EVs released, which then determines the effect of these EVs once they reach a target cell. For instance, EVs released by renal epithelial cells modulate the expression and function of water and solute transporting proteins in other cells. Also, EVs have been demonstrated to regulate renal organogenesis and blood flow. Furthermore, a dual role of EVs promoting, but also counteracting, disease has also been reported. EVs released by renal tubular cells can reach fibroblasts, monocytes, macrophages, T cells and natural killer cells, thus influencing the pathogenesis and progression of renal disorders like acute kidney injury and fibrosis, nephrolithiasis, renal transplant rejection and renal cancer, among others. On the contrary, EVs may also exert a cytoprotective role upon renal damage and promote recovery of renal function. In the current review, a systematic summary of the key studies from the past 5 years addressing the role of EVs in the modulation of renal physiological and pathophysiological processes is provided, highlighting open questions and discussing the potential of future research.

Keywords: extracellular vesicles, exosomes, renal physiology, renal disorders, renal injury

INTRODUCTION

Extracellular vesicles (EVs) are a group of membrane-enclosed nanosized particles released from a large variety of cell types (Théry et al., 2019). EVs are classified according to their origin as exosomes for those of endosomal origin and microvesicles for plasma membrane-derived vesicles. All vesicles incorporate molecules from their cell of origin, including proteins (Pisitkun et al., 2004), nucleic acids (Miranda et al., 2010) and lipids (Del Boccio et al., 2012). In the kidney, research has focused mainly on urinary EVs (uEVs), released by the tubular and urinary tract cells, and their potential as biomarkers of kidney-related diseases (Street et al., 2017). However, in the last 5 years more interest

has been placed in the role of EVs as essential regulators in renal physiology and pathophysiology (Wang et al., 2017). In this review, the latest discoveries on the regulatory role of EVs in health and disease are discussed.

For the sake of clarity, and in agreement with the International Society for EVs (Théry et al., 2019), the term EV for the different populations of vesicles will be used, since isolation methods and markers do not allow to fully distinguish exosomes from other vesicles.

EVS IN THE REGULATION OF PHYSIOLOGICAL PROCESSES IN THE KIDNEY

EV-Mediated Intrarenal Communication

EVs released by different segments of the nephron carry RNAs and proteins capable of communicating signals in an upstream to downstream fashion within the nephron (Alvarez et al., 2012). For instance, Gildea et al. (2014) described the uptake of proximal tubule EVs by distal convoluted tubule and collecting duct cells as well as by the same proximal cells. Furthermore, it was reported that decrease in reactive oxygen species (ROS) production in proximal tubule cells by dopaminergic stimulation was transferred to distal tubule- and collecting duct cells by EVs secreted by the proximal cells. Conversely, the increase in ROS in proximal tubule cells exposed to angiotensin II was not transferred via EVs to cells downstream (Gildea et al., 2014). This observation indicates certain specificity of EV-mediated communication toward particular treatments and phenotypes. From the cellular point of view, the cargo of the EVs might be specifically influenced by particular stimuli applied to the donor cell and therefore determine EV activity upon reaching the target cell.

A more recent study demonstrated that treatment of cortical collecting duct cells with desmopressin (i.e., synthetic vasopressin analog) stimulated uptake of EVs released by proximal tubule and collecting duct cells (Oosthuyzen et al., 2016). An overview on renal physiological processes mediated by EVs and the bioactive components within the EV cargo is graphically depicted in **Figure 1**.

Regulation of Tubular Transport Processes

Within the cargo of renal EVs, different ion-, organic compound- and water transporters, their codifying RNAs, as well as microRNAs (miRNAs) targeting their expression can be found. In this regard, EVs from cortical collecting duct cells carry higher protein levels of aquaporin 2 (AQP2) after exposure of the donor cells to desmopressin (Street et al., 2011). Moreover, these EVs had the ability to transfer functional AQP2 to other collecting duct cells. Since AQP2 plays a key role in water reabsorption in this segment and, thus, in the concentration of urine (van Lieburg et al., 1995), increased water permeability due to exposure to EVs could be expected. These observations suggest a potential role of

EVs in the mediation of physiological responses after changes in the hydration status (Street et al., 2011).

Additionally, a comprehensive study using next-generation sequencing evaluated the diversity of miRNAs present in uEVs and their impact on the expression of renal transporters and channels (Gracia et al., 2017). Based on the 10 most abundant miRNAs found (miR-10b-5p, miR-10a-5p, miR-30a-5p, miR-26a-5p, miR-22-3p, miR-204-5p, miR-181a-5p, miR-27b-3p, miR-30d-5p, miR-192-5p), the renal outer medullary potassium channel (ROMK, Kir1.1), the plasma membrane calcium-transporting ATPase (PMCA1) and the amino acid transporter SNAT2 (*SLC38A2*) appeared as candidates to be regulated by these EVs. In fact, addition of the vesicles to the human proximal cells HKC-8 resulted in a decrease in the mRNA and protein levels of SNAT2. The decrease in *SLC38A2* mRNA levels suggests lower mRNA stability due to the presence of targeting miRNAs in the vesicles. Similarly, PMCA1 and ROMK protein expression were down-regulated by uEVs in human collecting duct (HCD) cells (Gracia et al., 2017). This report indicates a potential regulatory role of EVs also in calcium and potassium reabsorption. Additionally, the transport of amino acids may be regulated by EVs.

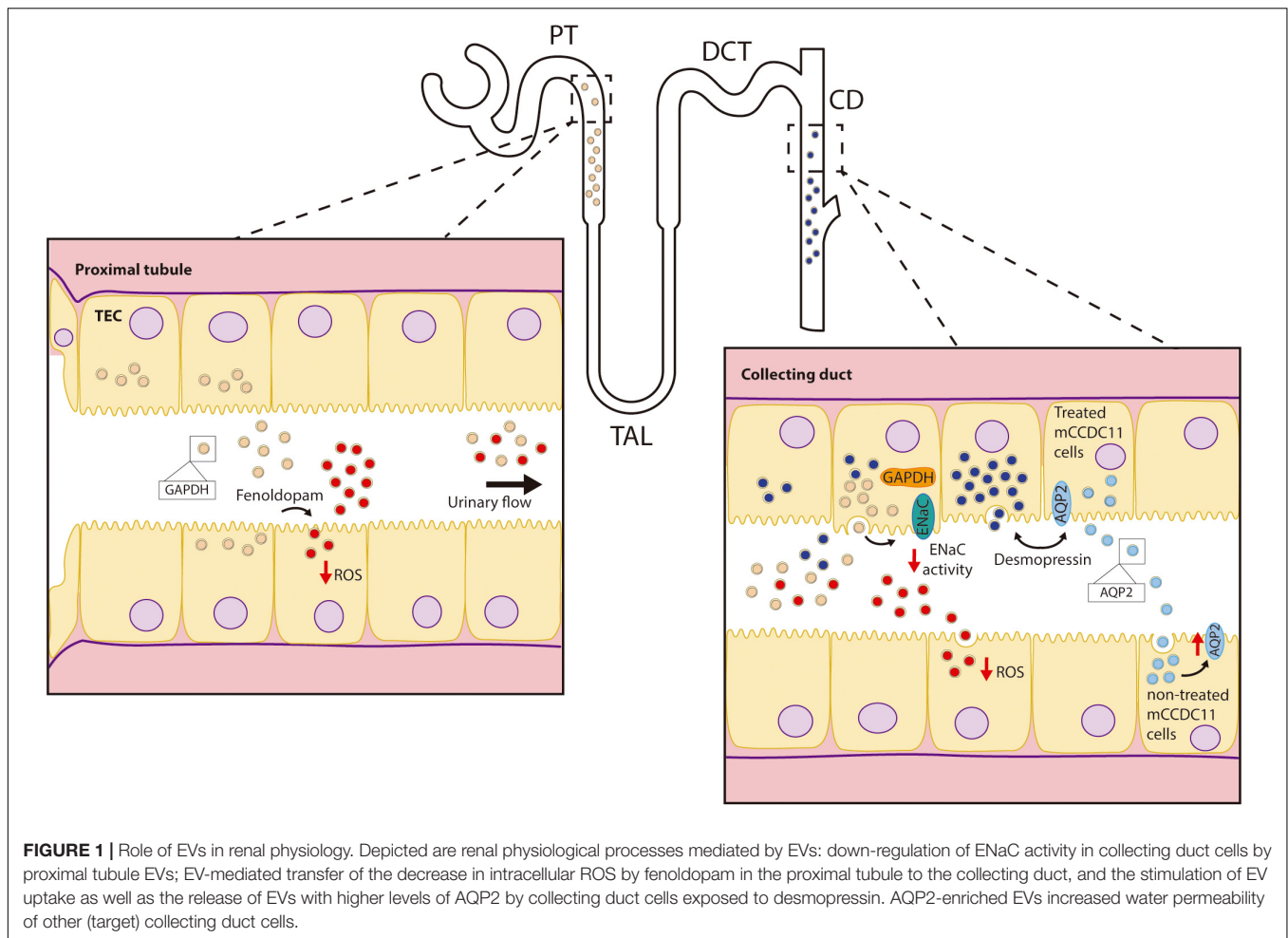
The epithelial sodium channel (ENaC) is expressed in the distal part of the nephron and plays a significant role in sodium homeostasis. Jella et al. (2016) described an acute inhibition of ENaC activity in collecting duct cells after exposure to EVs released from proximal cells. The effect was observed majorly for apical vesicles, thus indicating a potential proximal to distal communication mechanism along the nephron via pro-urine flow. The authors attributed the inhibitory action to EV-carried glyceraldehyde-3-phosphate-dehydrogenase (GAPDH), as immunoprecipitation studies demonstrated the physical interaction between GAPDH and ENaC.

Regulation of Renal Blood Flow

A recent study showed in a mouse model that application of acupuncture with low frequency electrical stimulation (Acu/LFES) to the hindlimb muscles increases renal blood flow, compared to mice treated with acupuncture without electrical stimulation (Su et al., 2018). Administration of the inhibitor of exosome release GW4869 (Menck et al., 2017) prevented the increase in the blood flow by Acu/LFES. Further mechanistic information was obtained using miRNA deep sequencing analysis, which displayed increased levels of miR-181d in serum EVs from Acu/LFES mice. Subsequently, binding of miR-181d to the 3'UTR of angiotensinogen mRNA and lower angiotensinogen levels were observed for Acu/LFES, probably accounting for the hemodynamic effects described above (Su et al., 2018). These findings point EVs as an additional factor regulating renal blood flow. Moreover, the described study provides a proof-of-concept for EV-mediated communication at a systemic level with the kidney as a target.

Organogenesis

Nephrogenesis requires a complex exchange from inductive signals between the ureteric bud (UB) and the metanephric



mesenchyme (MM) in which the activation of the Wnt pathway in the latter plays a vital role (Wang et al., 2018). Hereby, a stimulatory effect of UB-derived EVs on the formation of pre-tubular aggregates in MM organoids has been described. Mechanistically, MM cells take up UB-derived EVs carrying miR-27a/b, miR-135a/b, miR-155, and miR-499. These miRNAs target the complex of APC (adenomatous polyposis coli), axin, GSK3 β (glycogen synthase kinase 3), and CK1 α (casein kinase 1 α) and, thus, stimulate the nuclear accumulation of β -catenin (Krause et al., 2018).

EVS IN THE REGULATION OF RENAL PATHOPHYSIOLOGICAL PROCESSES

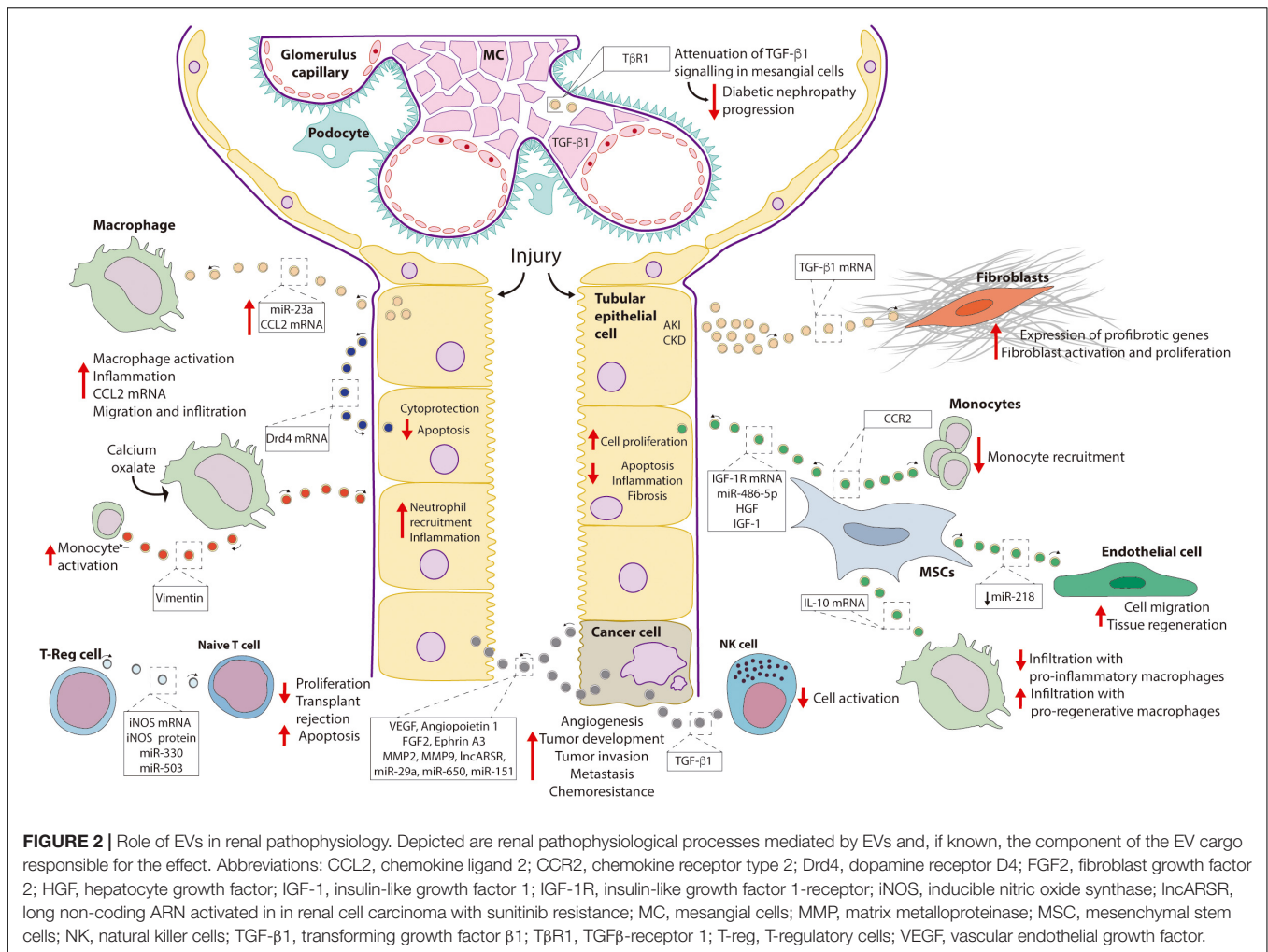
Kidney Injury and Regeneration

Acute kidney injury (AKI) is characterized by the coexistence of damage and counteracting regenerative processes. So far, there is abundant evidence supporting the participation of EVs, both stimulating the progression of the injury as well as playing a cytoprotective role and promoting tissue regeneration. In this regard, the different cargo content of the vesicles could be the key to explain these opposing effects.

The latest findings on the participation of EVs in renal injury are discussed here. The reviewed data are depicted in Figure 2.

Role of EVs Promoting Renal Injury

Tubulointerstitial inflammation is a complication of AKI. Mice models of ischemia-reperfusion injury and unilateral ureteral obstruction exhibited a higher content of miR-23a in EVs released by tubular cells compared to sham-operated animals. In particular, miR-23a downregulated the protein A20, a negative regulator of NF κ B signaling, finally leading to macrophage activation (Li et al., 2019). In addition, an increase in chemokine ligand 2 (CCL2) mRNA content was observed in EVs from kidneys of mice exposed to lipopolysaccharide and in uEVs of rats with 5/6 nephrectomy, experimental models of AKI and chronic kidney disease (CKD), respectively (Lv et al., 2018). Hereby, filtered albumin is likely to be a factor directing changes in the EV cargo, as exposure of tubular epithelial cells (TECs) to albumin *in vitro* reproduced the increase in CCL2 mRNA content observed in the vesicles *in vivo*. Furthermore, macrophage migration was more stimulated by EVs from albumin-treated TECs than by control EVs.



Fibroblast proliferation and activation are associated with renal fibrosis. A study with a mice model of AKI (unilateral ureteral obstruction) described higher levels of TGF-β1 (transforming growth factor β1) mRNA in renal EVs respect to control animals. Addition of these EVs to fibroblasts led to higher proliferation and up-regulation of α-smooth muscle actin (α-SMA) (Borges et al., 2013). In addition, EVs from mouse and human TECs exposed to hypoxic conditions also exhibited a higher potential to induce fibroblast proliferation and activation. These effects were prevented by transfection of donor cells with a siRNA against TGF-β1 (Borges et al., 2013).

EVs may also inhibit renal regeneration. The epidermal growth factor (EGF), which signals through the epidermal growth factor receptor (EGFR) is an essential molecule for epithelial regeneration. A study using a mouse proximal tubule cell line described stimulation of EV release by scratch wounding. Treatment with agonists and inhibitors of the EGF signaling pathway supported an inverse association between EV release and EGFR-mediated wound healing. In line with this, inhibition of exosome release with GW4869 and manumycin A increased EGFR activation and wound healing. These findings provided

novel evidence that EVs may not only instigate the injury process but may also inhibit physiological regeneration mechanisms (Zhou et al., 2017).

Cytoprotective Effect of EVs

TGF-β1 signaling is necessary for extracellular matrix secretion by mesangial cells, and thus, for glomerulosclerosis and diabetic nephropathy progression. In this regard, clearance of the TβR1 receptor (i.e., TGF-β1 receptor) by loading into EVs has been demonstrated as a mechanism mediating down-regulation of TGF-β1 signaling in mesangial cells (Van Krieken et al., 2017).

EVs released by mesenchymal stem cells (MSCs) can contribute to tissue regeneration. For instance, EVs from human bone marrow MSCs increased proliferation of proximal tubule cells exposed to the nephrotoxic agent cisplatin. Beneficial effects of the EVs were prevented by silencing IGF-1R (insulin-like growth factor 1-receptor) in the donor cells (Tomasoni et al., 2013). A further study suggested a beneficial role of EVs from bone marrow MSCs by buffering extracellular levels of free chemokine ligand 2 (CCL2), thus preventing monocyte activation. The effect was attributed to the chemokine receptor type 2 (CCR2) present in the EVs (Shen et al., 2016).

Likewise, improved renal function and reduced macrophage infiltration was observed in a mice model of diabetic nephropathy administered intravenously with EVs from bone marrow MSC. Beneficial effects may be explained by the down-regulation of adhesion molecules for macrophages (e.g., ICAM1) in the endothelial cells of the glomeruli and the peritubular capillaries by the EVs (Nagaishi et al., 2016).

Similarly, in a study using a model renal artery stenosis in pigs with metabolic syndrome, treatment with adipose tissue MSC EVs improved renal function. Reduced renal infiltration by pro-inflammatory macrophages and increased infiltration by pro-regenerative macrophages was observed. Effects were dependent on the presence of the anti-inflammatory cytokine interleukin-10 (IL-10) mRNA in the EVs (Eirin et al., 2017).

The endothelium of blood vessels constitutes a third source of MSC EVs. An analysis of miRNAs enriched in renal artery-derived vascular progenitor cells (RAPCs) highlighted the miR-218, which targets Robo1, a protein linked to endothelial cell migration. Interestingly, while under control conditions, RAPC release EVs enriched in miR-218, suppressing Robo1 expression and cell migration, exposure of RAPC to pro-oxidant conditions (i.e., tissue damage) results in a decrease in the content of miR-218 in the vesicles and, therefore, Robo1 up-regulation and increase of endothelial cell migration (i.e., regeneration of blood vessels) (Pang et al., 2017). In line with these observations, another related study reported the potential of EVs from human cord endothelial colony forming cells (ECFCs) to attenuate renal damage in a mouse model of ischemia-reperfusion (Viñas et al., 2016). Here, miR-486-5p was demonstrated as the critical component of the EVs improving renal function and reducing inflammation (Viñas et al., 2016).

Nephrolithiasis

Recently, some lines of evidence pointed to the role of EVs in the pathogenesis of nephrolithiasis. For instance, a study evaluating the effect of different concentrations of calcium oxalate, one of the main components of kidney stones, on proximal cells, reported an increase in the release of EVs by elevated levels of oxalate (He et al., 2017).

Interstitial deposition of calcium oxalate constitutes one of the complications of nephrolithiasis. Hereby, macrophages seem to play a dual role in removing deposited crystals but also promoting inflammation. EVs isolated from macrophages previously exposed to calcium oxalate exhibited a different cargo of proteins with respect to EVs from control macrophages (Singhto and Thongboonkerd, 2018). When TECs were exposed to EVs from calcium oxalate-treated macrophages, increased inflammation and neutrophil recruitment were observed (Singhto and Thongboonkerd, 2018). Furthermore, EVs from calcium oxalate treated cells exhibited a higher capacity to bind crystals promoting their dissemination into the extracellular matrix, ultimately contributing to interstitial deposits (Singhto and Thongboonkerd, 2018). Interestingly, most of the proinflammatory effects were abolished by knock-down of vimentin in the donor macrophages, clearly indicating a role of this protein in the observed effects (Singhto et al., 2018).

Renal Transplant Rejection and Tolerance

Organ rejection represents a common complication of transplanted patients. Participation of EVs stimulating allograft tolerance has been proposed. Specifically, EVs released by T regulatory (T-reg) cells have been reported to inhibit proliferation and stimulate apoptosis of naïve T cells *in vitro*. Inducible nitric oxide synthase (iNOS) mRNA and protein, which were enriched in the EVs, as well as miR-330 and miR-503 were necessary mediators of these effects. Noteworthy, a similar effect was also observed in a rat model of kidney transplantation, where intravenous and intrasplenic administration of EVs from T-regs improved renal function and prolonged allograft survival (Aiello et al., 2017).

Conversely, a role of EVs promoting host immune response and rejection has also been described. Patients diagnosed with transplant glomerulopathy after receiving a kidney transplant had circulating EVs with increased expression of fibronectin and collagen-IV (Sharma et al., 2018) and higher concentrations of antibodies against collagen IV and fibronectin (Angaswamy et al., 2014) compared with patients receiving a kidney transplant without this diagnosis. In this regard, a previous study with a rat model of renal transplantation showed that the immune response to collagen IV plays a role in allograft rejection (Joosten et al., 2002). Other studies pointed out a role of EVs released by endothelial cells in promoting inflammation and stimulating the immune response of the host (Cardinal et al., 2018). These findings not only suggest a potential role of circulating EVs in the prediction of transplant rejection but also raise possible therapeutic targets in order to counteract the rejection process.

Renal Cancer

EVs can mediate intercellular communication also between tumor cells. In this regard, a pro-angiogenic and pro-metastatic role of EVs from CD105-positive cancer stem cells *in vitro* and *in vivo* has been described. Indeed, EVs derived from CD105-positive cells carried multiple proangiogenic mRNAs including VEGF, angiopoietin 1, fibroblast growth factor 2, ephrin A3, matrix metalloprotease 2, and matrix metalloproteinase 9. These factors were absent in EVs from CD105-negative cells. The same study also reported the presence of miRNAs with participation in tumor invasion and metastasis such as miR-29a, miR-650, and miR-151 in CD105⁺ derived EVs (Grange et al., 2011).

EVs released by renal cancer cells may also facilitate the evasion of the tumor cells from the immune system of the patient. In this regard, an inhibitory action of EVs released by cells from clear cell renal cell carcinoma on natural killer cells was described. The effect was attributed to TGFβ1 carried by the EVs (Xia et al., 2017).

Furthermore, EVs play a key role in drug resistance in renal cancer. In this case, a long non-coding RNA, named lncARSR (i.e., lncRNA activated in renal cell carcinoma with sunitinib resistance) was described as the bioactive component of EVs mediating chemoresistance. Once in the target (sunitinib sensitive) cell, lncARSR competes with the action of miR-34a and

miR-449 preventing down-regulation of the membrane proteins AXL and c-Met which, ultimately, mediate resistance to sunitinib (Qu et al., 2016).

DISCUSSION

Besides their well-acknowledged role as a source of biomarkers, the past decade has witnessed EVs emerge as key players in cell-cell communication at autocrine, paracrine, and systemic level. Although a vast volume of information is already available for non-renal tissues, their participation in renal pathophysiology is a relatively novel field. Also, the heterogeneous nature of the nephron epithelium has reduced the study of EV-mediated processes to the utilization of *in vitro* models or pooled samples (e.g., uEVs) where relevant regulatory phenomena may remain undiscovered. Hereby, the use of microperfusion techniques to isolate EVs from specific segments of the nephron may constitute a promising tool (Cheng et al., 2013). Furthermore, a vast amount of the experimental evidence available results from *in vitro* studies and, therefore, need validation *in vivo* or in more complex models in order to be translated into a clinical setting. In this regard, *organ-on-a-chip* platforms may allow to culture, and thus scrutinize the effects of EVs, released by a donor cell on a target cell also mimicking physiological flow conditions and combining different segments from the nephron in one platform.

Tackling EV participation orchestrating pathophysiological responses, for instance, in acute kidney damage, can constitute a therapeutic alternative to mitigate inflammatory damage and fibrosis. Moreover, enrichment of EVs in particular components may allow to target physiological processes with therapeutic purposes, stimulate EV-mediated regenerative mechanisms and counteract those situations where EV contribute to disease development. For instance, several studies highlighted a clear regenerative role of EVs obtained from MSC. In this regard, EVs isolated from bone marrow MSCs could be used as preventive and regenerative therapy in cases where acute kidney damage is expected (e.g., treatments with highly nephrotoxic drugs).

Research on the role of EVs in kidney function may lead to the identification of novel biomarkers. Although, uEVs

constitute a well-acknowledged source of information with diagnostic potential, several studies also described a role of plasma EVs conveying information about renal physiological and pathophysiological status (reviewed in Erdbrügger and Le, 2016). Importantly, different isolation and analysis methods, as well as the different nature of biological samples constitute a limitation toward obtaining a reliable picture of EV-mediated processes. The implementation of normalization procedures, for instance, by using EV pools from the general population (Witwer et al., 2013) or EV-mimetic particles (Lozano-Andrés et al., 2019) may provide more comparable results for different isolation techniques.

In conclusion, a significant volume of high-level studies has appeared during the past years, describing the participation of EVs regulating the normal function of the kidney as well as promoting and counteracting pathophysiological responses. While this may already bear therapeutic potential, considering the high diversity of the EV cargo, future studies will probably find EVs involved in increasing processes within the kidney and mediating communication between the kidney and other organs. This would likely result in more mechanisms that could be targeted in the aim of developing novel therapeutic strategies.

AUTHOR CONTRIBUTIONS

JR, EB, and JH conceived the manuscript. JR, EB, and VS drafted the manuscript. JR, EB, VS, RB and JH edited the manuscript. All authors approved the final version.

ACKNOWLEDGMENTS

JR is supported by a fellowship from the Radboud Excellence Initiative (Radboud University, Nijmegen, Netherlands). EB holds CONICYT-PhD (Chile) and Faculty of Medicine, Pontificia Universidad Católica de Chile (PUC) Ph.D. fellowships. JH is supported by Netherlands Organization for Scientific Research (NWO, VICI 016.130.668).

REFERENCES

- Aiello, S., Rocchetta, F., Longaretti, L., Faravelli, S., Todeschini, M., Cassis, L., et al. (2017). Extracellular vesicles derived from T regulatory cells suppress T cell proliferation and prolong allograft survival. *Sci. Rep.* 7:11518. doi: 10.1038/s41598-017-08617-3
- Alvarez, M. L., Khosroheidari, M., Kanchi Ravi, R., and DiStefano, J. K. (2012). Comparison of protein, microRNA, and mRNA yields using different methods of urinary exosome isolation for the discovery of kidney disease biomarkers. *Kidney Int.* 82, 1024–1032. doi: 10.1038/ki.2012.256
- Angaswamy, N., Klein, C., Tiriveedhi, V., Gaut, J., Anwar, S., Rossi, A., et al. (2014). Immune responses to collagen-IV and fibronectin in renal transplant recipients with transplant glomerulopathy. *Am. J. Transplant.* 14, 685–693. doi: 10.1111/ajt.12592
- Borges, F. T., Melo, S. A., Özdemir, B. C., Kato, N., Revuelta, I., Miller, C. A., et al. (2013). TGF- β 1-containing exosomes from injured epithelial cells activate fibroblasts to initiate tissue regenerative responses and fibrosis. *J. Am. Soc. Nephrol.* 24, 385–392. doi: 10.1681/ASN.2012101031
- Cardinal, H., Dieudé, M., and Hébert, M. J. (2018). Endothelial dysfunction in kidney transplantation. *Front. Immunol.* 9:1130. doi: 10.3389/fimmu.2018.01130
- Cheng, C. J., Baum, M., and Huang, C. L. (2013). Kidney-specific WNK1 regulates sodium reabsorption and potassium secretion in mouse cortical collecting duct. *Am. J. Physiol. Ren. Physiol.* 304, F397–F402. doi: 10.1152/ajprenal.00589.2012
- Del Boccio, P., Raimondo, F., Pieragostino, D., Morosi, L., Cozzi, G., Sacchetta, P., et al. (2012). A hyphenated microLC-Q-TOF-MS platform for exosomal lipidomics investigations: application to RCC urinary exosomes. *Electrophoresis* 33, 689–696. doi: 10.1002/elps.201100375
- Eirin, A., Zhu, X. Y., Puranik, A. S., Tang, H., McGurren, K. A., van Wijnen, A. J., et al. (2017). Mesenchymal stem cell-derived extracellular vesicles attenuate kidney inflammation. *Kidney Int.* 92, 114–124. doi: 10.1016/j.kint.2016.12.023
- Erdbrügger, U., and Le, T. H. (2016). Extracellular vesicles in renal diseases: more than novel biomarkers? *J. Am. Soc. Nephrol.* 27, 12–26. doi: 10.1681/ASN.2015010074
- Gildea, J. J., Seaton, J. E., Victor, K. G., Reyes, C. M., Bigler Wang, D., Pettigrew, A. C., et al. (2014). Exosomal transfer from human renal proximal tubule

- cells to distal tubule and collecting duct cells. *Clin. Biochem.* 47, 89–94. doi: 10.1016/j.clinbiochem.2014.06.018
- Gracia, T., Wang, X., Su, Y., Norgett, E. E., Williams, T. L., and Moreno, P. (2017). Urinary exosomes contain microRNAs capable of paracrine modulation of tubular transporters in kidney. *Sci. Rep.* 7:40601. doi: 10.1038/srep40601
- Grange, C., Tapparo, M., Collino, F., Vitillo, L., Damasco, C., Deregis, M. C., et al. (2011). Microvesicles released from human renal cancer stem cells stimulate angiogenesis and formation of lung premetastatic niche. *Cancer Res.* 71, 5346–5356. doi: 10.1158/0008-5472.CAN-11-0241
- He, Z., Guan, X., Liu, Y., Tao, Z., Liu, Q., Wu, J., et al. (2017). Alteration of exosomes secreted from renal tubular epithelial cells exposed to high-concentration oxalate. *Oncotarget* 8, 92635–92642. doi: 10.18632/oncotarget.21517
- Jella, K. K., Yu, L., Yue, Q., Friedman, D., Duke, B. J., and Alli, A. A. (2016). Exosomal GAPDH from proximal tubule cells regulate ENaC activity. *PLoS One* 11:e0165763. doi: 10.1371/journal.pone.0165763
- Joosten, S. A., van Dixhoorn, M. G. A., Borrias, M. C., Benediktsson, H., van Veelen, P. A., van Kooten, C., et al. (2002). Antibody response against perlecan and collagen types IV and VI in chronic renal allograft rejection in the rat. *Am. J. Pathol.* 160, 1301–1310. doi: 10.1016/S0002-9440(10)62557-6
- Krause, M., Rak Raszeska, A., Naillat, F., Saarela, U., Schmidt, C., Ronkainen, V. P., et al. (2018). Exosomes as secondary inductive signals involved in kidney organogenesis. *J. Extracell. Vesicles* 7:1422675. doi: 10.1080/20013078.2017.1422675
- Li, Z. L., Lv, L. L., Tang, T. T., Wang, B., Feng, Y., Zhou, L. T., et al. (2019). HIF-1 α inducing exosomal microRNA-23a expression mediates the cross-talk between tubular epithelial cells and macrophages in tubulointerstitial inflammation. *Kidney Int.* 95, 388–404. doi: 10.1016/j.kint.2018.09.013
- Lozano-Andrés, E., Libregts, S. F., Toribio, V., Royo, F., Morales, S., López-Martín, S., et al. (2019). Tetraspanin-decorated extracellular vesicle-mimetics as a novel adaptable reference material. *J. Extracell. Vesicles* 8, 1573052. doi: 10.1080/20013078.2019.1573052
- Lv, L. L., Feng, Y., Wen, Y., Wu, W. J., Ni, H. F., Li, Z. L., et al. (2018). Exosomal CCL2 from tubular epithelial cells is critical for albumin-induced tubulointerstitial inflammation. *J. Am. Soc. Nephrol.* 29, 919–935. doi: 10.1681/ASN.2017050523
- Menck, K., Sönmez, C., Worst, T. S., Schulz, M., Dihazi, G. H., Streit, F., et al. (2017). Neutral sphingomyelinases control extracellular vesicles budding from the plasma membrane. *J. Extracell. Vesicles* 6:1378056. doi: 10.1080/20013078.2017.1378056
- Miranda, K. C., Bond, D. T., McKee, M., Skog, J., Păunescu, T. G., Da Silva, N., et al. (2010). Nucleic acids within urinary exosomes/microvesicles are potential biomarkers for renal disease. *Kidney Int.* 78, 191–199. doi: 10.1038/ki.2010.106
- Nagaishi, K., Mizue, Y., Chikenji, T., Otani, M., Nakano, M., Konari, N., et al. (2016). Mesenchymal stem cell therapy ameliorates diabetic nephropathy via the paracrine effect of renal trophic factors including exosomes. *Sci. Rep.* 6:34842. doi: 10.1038/srep34842
- Oosthuizen, W., Scullion, K. M., Ivy, J. R., Morrison, E. E., Hunter, R. W., Starkey Lewis, P. J., et al. (2016). Vasopressin regulates extracellular vesicle uptake by kidney collecting duct cells. *J. Am. Soc. Nephrol.* 27, 3345–3355. doi: 10.1681/ASN.2015050568
- Pang, P., Abbott, M., Chang, S. L., Abdi, M., Chauhan, N., Mistri, M., et al. (2017). Human vascular progenitor cells derived from renal arteries are endothelial-like and assist in the repair of injured renal capillary networks. *Kidney Int.* 91, 129–143. doi: 10.1016/j.kint.2016.07.037
- Pisitkun, T., Shen, R. F., and Knepper, M. A. (2004). Identification and proteomic profiling of exosomes in human urine. *Proc. Natl. Acad. Sci. U.S.A.* 101, 13368–13373. doi: 10.1073/pnas.0403453101
- Qu, L., Ding, J., Chen, C., Wu, Z. J., Liu, B., Gao, Y., et al. (2016). Exosome-transmitted lncARSR promotes sunitinib resistance in renal cancer by acting as a competing endogenous RNA. *Cancer Cell* 29, 653–668. doi: 10.1016/j.ccell.2016.03.004
- Sharma, M., Ravichandran, R., Bansal, S., Bremner, R. M., Smith, M. A., and Mohanakumar, T. (2018). Tissue-associated self-antigens containing exosomes: role in allograft rejection. *Hum. Immunol.* 79, 653–658. doi: 10.1016/j.humimm.2018.06.005
- Shen, B., Liu, J., Zhang, F., Wang, Y., Qin, Y., Zhou, Z., et al. (2016). CCR2 positive exosome released by mesenchymal stem cells suppresses macrophage functions and alleviates ischemia/reperfusion-induced renal injury. *Stem Cells Int.* 2016:1240301. doi: 10.1155/2016/1240301
- Singhto, N., Kanlaya, R., Nilnumkhum, A., and Thongboonkerd, V. (2018). Roles of macrophage exosomes in immune response to calcium oxalate monohydrate crystals. *Front. Immunol.* 9:316. doi: 10.3389/fimmu.2018.00316
- Singhto, N., and Thongboonkerd, V. (2018). Exosomes derived from calcium oxalate-exposed macrophages enhance IL-8 production from renal cells, neutrophil migration and crystal invasion through extracellular matrix. *J. Proteomics* 185, 64–76. doi: 10.1016/j.jpro.2018.06.015
- Street, J. M., Birkhoff, W., Menzies, R. I., Webb, D. J., Bailey, M. A., and Dear, J. W. (2011). Exosomal transmission of functional aquaporin 2 in kidney cortical collecting duct cells. *J. Physiol.* 589, 6119–6127. doi: 10.1111/jphysiol.2011.220277
- Street, J. M., Koritzinsky, E. H., Glispie, D. M., Star, R. A., and Yuen, P. S. T. (2017). Urine exosomes: an emerging trove of biomarkers. *Adv. Clin. Chem.* 78, 103–122. doi: 10.1016/bs.acc.2016.07.003
- Su, Z., Yuan, Y., Yu, M., Liu, Y., Klein, J. D., and Wang, X. H. (2018). Electrically stimulated acupuncture increases renal blood flow through exosome-carried miR-181. *Am. J. Physiol. Ren. Physiol.* 315, F1542–F1549. doi: 10.1152/ajprenal.00259.2018
- Théry, C., Witwer, K. W., Aikawa, E., Alcaraz, M. J., Anderson, J. D., Andriantsitohaina, R., et al. (2019). Minimal information for studies of extracellular vesicles 2018 (MISEV2018): a position statement of the International Society for Extracellular Vesicles and update of the MISEV2014 guidelines. *J. Extracell. Vesicles* 8:1535750. doi: 10.1080/20013078.2018.1535750
- Tomasoni, S., Longaretti, L., Rota, C., Morigi, M., Conti, S., Gotti, E., et al. (2013). Transfer of growth factor receptor mRNA via exosomes unravels the regenerative effect of mesenchymal stem cells. *Stem Cells Dev.* 22, 772–780. doi: 10.1089/scd.2012.0266
- Van Krieken, R., Chen, G., Gao, B., Read, J., Al Saleh, H. A., Li, R., et al. (2017). Sterol Regulatory Element Binding Protein (SREBP)-1 is a novel regulator of the Transforming Growth Factor (TGF)- β receptor I (T β RI) through exosomal secretion. *Cell. Signal.* 29, 158–167. doi: 10.1016/j.cellsig.2016.11.004
- van Lieburg, A. F., Knoers, N. V. A. M., and Deen, P. (1995). Discovery of aquaporins: a breakthrough in research on renal water transport. *Pediatr. Nephrol.* 9, 228–234. doi: 10.1007/BF00860757
- Viñas, J. L., Burger, D., Zimpelmann, J., Haneef, R., Knoll, W., Campbell, P., et al. (2016). Transfer of microRNA-486-5p from human endothelial colony forming cell-derived exosomes reduces ischemic kidney injury. *Kidney Int.* 90, 1238–1250. doi: 10.1016/j.kint.2016.07.015
- Wang, X., Wilkinson, R., Kildey, K., Potriquet, J., Mulvenna, J., Lobb, R. J., et al. (2017). Unique molecular profile of exosomes derived from primary human proximal tubular epithelial cells under diseased conditions. *J. Extracell. Vesicles* 6:1314073. doi: 10.1080/20013078.2017.1314073
- Wang, Y., Zhou, C. J., and Liu, Y. (2018). Wnt signaling in kidney development and disease. *Prog. Mol. Biol. Transl. Sci.* 153, 181–207. doi: 10.1016/bs.pmbts.2017.11.019
- Witwer, K. W., Buzás, E. I., Bemis, L. T., Bora, A., Lässer, C., Lötvall, J., et al. (2013). Standardization of sample collection, isolation and analysis methods in extracellular vesicle research. *J. Extracell. Vesicles* 2:20360. doi: 10.3402/jev.v2i0.20360
- Xia, Y., Zhang, Q., Zhen, Q., Zhao, Y., Liu, N., Li, T., et al. (2017). Negative regulation of tumor-infiltrating NK cell in clear cell renal cell carcinoma patients through the exosomal pathway. *Oncotarget* 8, 37783–37795. doi: 10.18632/oncotarget.16354
- Zhou, X., Zhang, W., Yao, Q., Zhang, H., Dong, G., Zhang, M., et al. (2017). Exosome production and its regulation of EGFR during wound healing in renal tubular cells. *Am. J. Physiol. Ren. Physiol.* 312, F963–F970. doi: 10.1152/ajprenal.00078.2017

Conflict of Interest: The authors declare that the research was conducted in the absence of any commercial or financial relationships that could be construed as a potential conflict of interest.

Copyright © 2020 Rigalli, Barros, Sommers, Bindels and Hoenderop. This is an open-access article distributed under the terms of the Creative Commons Attribution License (CC BY). The use, distribution or reproduction in other forums is permitted, provided the original author(s) and the copyright owner(s) are credited and that the original publication in this journal is cited, in accordance with accepted academic practice. No use, distribution or reproduction is permitted which does not comply with these terms.



Nicotinamide Mononucleotide: A Promising Molecule for Therapy of Diverse Diseases by Targeting NAD⁺ Metabolism

WeiQi Hong^{1†}, Fei Mo^{2†}, Ziqi Zhang², Mengyuan Huang¹ and Xiawei Wei^{1*}

¹ Laboratory of Aging Research and Cancer Drug Target, State Key Laboratory of Biotherapy, National Clinical Research Center for Geriatrics, West China Hospital, Sichuan University, Chengdu, China, ² West China Hospital and State Key Laboratory of Biotherapy, Sichuan University, Department of Biotherapy, Chengdu, China

OPEN ACCESS

Edited by:

Mario Antonio Blanchet,
School of Medicine, Johns Hopkins
University, United States

Reviewed by:

Tibor Kristian,
University of Maryland, Baltimore,
United States

Pei Wang,
Second Military Medical University,
China

Takashi Nakagawa,
University of Toyama, Japan

*Correspondence:

Xiawei Wei
weixiaweiscu@126.com;
xiaweivei@scu.edu.cn

[†] These authors have contributed
equally to this work

Specialty section:

This article was submitted to
Molecular Medicine,
a section of the journal
*Frontiers in Cell and Developmental
Biology*

Received: 21 December 2019

Accepted: 24 March 2020

Published: 28 April 2020

Citation:

Hong W, Mo F, Zhang Z, Huang M
and Wei X (2020) Nicotinamide
Mononucleotide: A Promising
Molecule for Therapy of Diverse
Diseases by Targeting NAD⁺
Metabolism.
Front. Cell Dev. Biol. 8:246.
doi: 10.3389/fcell.2020.00246

NAD⁺, a co-enzyme involved in a great deal of biochemical reactions, has been found to be a network node of diverse biological processes. In mammalian cells, NAD⁺ is synthesized, predominantly through NMN, to replenish the consumption by NADase participating in physiologic processes including DNA repair, metabolism, and cell death. Correspondingly, aberrant NAD⁺ metabolism is observed in many diseases. In this review, we discuss how the homeostasis of NAD⁺ is maintained in healthy condition and provide several age-related pathological examples related with NAD⁺ unbalance. The sirtuins family, whose functions are NAD-dependent, is also reviewed. Administration of NMN surprisingly demonstrated amelioration of the pathological conditions in some age-related disease mouse models. Further clinical trials have been launched to investigate the safety and benefits of NMN. The NAD⁺ production and consumption pathways including NMN are essential for more precise understanding and therapy of age-related pathological processes such as diabetes, ischemia-reperfusion injury, heart failure, Alzheimer's disease, and retinal degeneration.

Keywords: nicotinamide adenine dinucleotide (NAD), nicotinamide mononucleotide (NMN), aging, diabetes, obesity, Alzheimer's disease

INTRODUCTION

Nicotinamide adenine dinucleotide (NAD) is a vital metabolic redox co-enzyme found in eukaryotic cells and is necessary for over 500 enzymatic reactions. It plays a crucial role in various biological processes, including metabolism, aging, cell death, DNA repair, and gene expression (Rajman et al., 2018; Okabe et al., 2019). Thus, NAD⁺ is critical for human health and longevity.

The co-enzyme was first discovered by Harden and Young in 1906 as a component that enhanced the rate of alcohol fermentation in yeast extracts (Harden and Young, 1906). Over subsequent years, the chemical composition of the co-enzyme was established as an adenine, a reducing sugar group and a phosphate by Hans von Euler-Chelpin (von Euler and Myrback, 1930). Then, in 1936, Warburg suggested that NAD⁺ could play a role in redox reactions (Warburg and Christian, 1936). By 1960, it was assumed that all biochemical investigations on NAD⁺ had been exhausted. In 1963, Chambon and Mandel reported that NAD⁺ is a co-substrate for the addition

of poly-ADP-ribose to proteins, and this prompted a series of studies on poly-ADP-ribose and poly-ADP-ribose polymerases (PARPs) (Chambon et al., 1963; Yoshino et al., 2018). In the last decade, new interests in NAD⁺ emerged because of its association with sirtuins, a family of NAD-dependent protein deacetylases (SIRT1–7) (Rajman et al., 2018). Roy Frye showed that mammalian sirtuins could metabolize NAD⁺ and that NAD⁺ had a protein ADP-ribosyltransferase activity (Frye, 1999). Guarente and Imai made a phenomenal discovery that yeast SIR2 (silent information regulator 2) and the mouse ortholog SIRT1 have NAD⁺-dependent protein deacetylase activity (Imai et al., 2000). Previously, several studies had shown that sirtuins play a critical role in regulating multiple cellular functions, such as cell growth, energy metabolism, stress resistance, inflammation, and circadian rhythm neuronal function, among others (Imai and Yoshino, 2013; Rajman et al., 2018). The deficiency of NAD⁺ is closely associated with diverse pathophysiological conditions, including type 2 diabetes (T2D), obesity, heart failure, Alzheimer's disease (AD), and cerebral ischemia. The NAD⁺ levels decline in multiple organs with age, and this contributes to the development of various age-related diseases (Yoshino et al., 2011; Gomes et al., 2013; Mouchiroud et al., 2013; Mills et al., 2016). Therefore, NAD⁺ supplementation could be an effective therapy for the treatment of the conditions mentioned above.

Nicotinamide mononucleotide (NMN) is one of the intermediates in NAD⁺ biosynthesis and is a bioactive nucleotide formed by the reaction between a phosphate group and a nucleoside containing ribose and nicotinamide (NAM) (Poddar et al., 2019). NAM is directly converted to NMN by nicotinamide phosphoribosyltransferase (NAMPT). The molecular weight of NMN is 334.221 g/mol (Poddar et al., 2019). There are two anomeric forms of NMN named alpha and beta, and the latter is the active form (Poddar et al., 2019). NMN is found in various types of natural foods, such as vegetables, fruits, and meat. Edamame and broccoli contain 0.47–1.88 and 0.25–1.12 mg NMN/100 g, respectively, whereas avocado and tomato contain 0.36–1.60 and 0.26–0.30 mg NMN/100 g, respectively. However, raw beef only contains 0.06–0.42 mg NMN/100 g (Mills et al., 2016). Recent preclinical studies have demonstrated that the administration of NMN could compensate for the deficiency of NAD⁺, and NMN supplementation was able to effect diverse pharmacological activities in various diseases.

In this review, NAD⁺ biosynthesis pathways and the possible reason for its age-related decline are described. Also, a summary of studies on the role of NAD⁺ deprivation in causing human diseases and how the application of NMN could have positive effects on those diseases is provided.

NAD⁺ BIOSYNTHESIS PATHWAYS

Three different NAD⁺ biosynthesis pathways have been described in mammalian cells (**Figure 1**): (1) Preiss–Handler, in which NAD is synthesized from nicotinic acid (NA); (2) *de novo* synthesis, which starts from tryptophan; and (3) salvage pathway, which is most predominant in mammalian cells.

The Preiss–Handler Pathway

This pathway starts with conversion of NA to the nicotinic acid mononucleotide (NAMN) by the enzyme nicotinic acid phosphoribosyltransferase (NAPRT) (Preiss and Handler, 1958). Afterward, NAMN is used for nicotinic acid adenine dinucleotide (NAAD⁺) biosynthesis by nicotinamide/nicotinic acid mononucleotide adenyltransferase (NMNAT1/2/3). Finally, NAD⁺ synthetase (NADS) transforms NAAD⁺ to NAD⁺ with ammonia and ATP action as extra ingredients (Yang and Sauve, 2016).

De novo Synthesis From Tryptophan

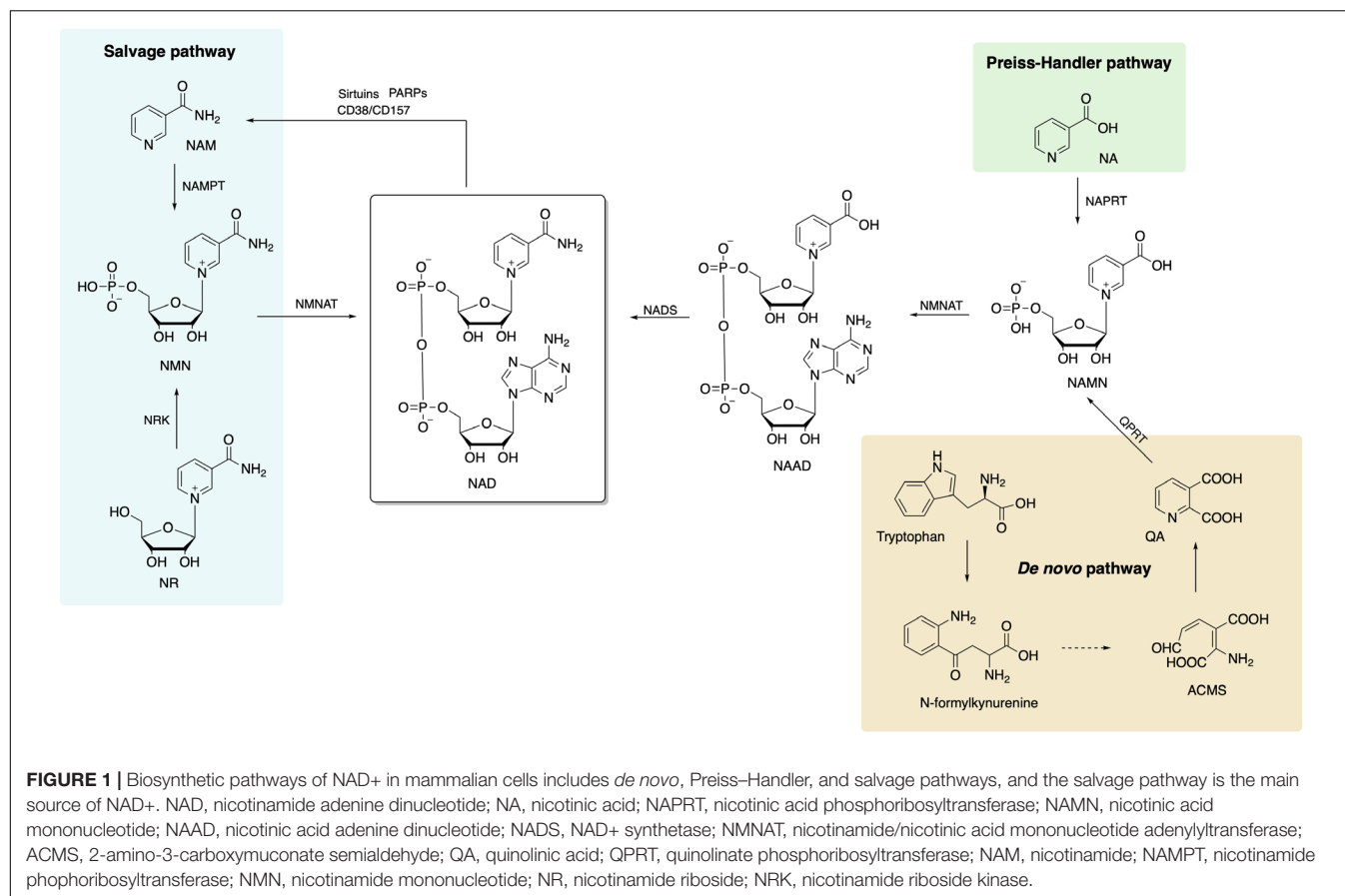
The eight-step *de novo* synthesis pathway is initiated by indoleamine 2,3-dioxygenase (IDO) or tryptophan 2,3-dioxygenase (TDO) that convert tryptophan to *N*-formylkynurenine (Salter et al., 1991). Through formamidase (KFase), *N*-formylkynurenine is then transformed to be kynurenine, to which hydroxyl is added via kynurenine 3-hydroxylase (K3H). The product, 3-hydroxy-kynurenine, is converted to 3-hydroxyanthranilate followed by 2-amino-3-carboxymuconate semialdehyde (ACMS) via kynureninase (Kyase) and 3-hydroxyanthranilate-3,4-dioxygenase. ACMS then cyclizes to form quinolinic acid (QA) that participates in NAMN biosynthesis with quinolinic acid phosphoribosyltransferase (QPRT) (Yang and Sauve, 2016). The last two steps are the same as the Preiss–Handler pathway that NAD⁺ is synthesized sequentially from NAMN and NAAD by NMNAT 1/2/3 and NADS.

The Salvage Pathway

The salvage pathway is the primary source of NAD⁺ in mammalian cells. The degradation of NAD⁺ and subsequent generation of NAM (as a by-product) are achieved by NAD-consuming enzymes, such as sirtuins, PARPs, CD38, CD157, and sterile alpha and TIR motif-containing protein 1 (SARM1) (Okabe et al., 2019). There are only two steps in the salvage pathway. The rate of NAD⁺ synthesis in this pathway is mostly determined by NAMPT that converts NAM and 5-phosphoribosyl-1-pyrophosphate (PRPP) to NMN in the first step. Then, NMN, the substrate for NAMPT, is conjugated to ATP and converted to NAD in the second step.

The NAMPT exists in two forms in mammals, that is, intracellular NAMPT (iNAMPT) in the cytoplasm and nucleus and extracellular NAMPT (eNAMPT) in the plasma or extracellular space (Revollo et al., 2007). The SIRT1-dependent deacetylation of iNAMPT predisposes the protein to secretion in adipocytes (Yoon et al., 2015). Various types of cells, including mature adipocytes, pancreatic β -cells, myocytes, epithelial cells, and hepatocytes (Revollo et al., 2007; Garten et al., 2010; Zhao et al., 2014) secrete and release eNAMPT to the plasma or extracellular space.

Also, another NAD precursor, nicotinamide riboside (NR), is incorporated into cells using equilibrative nucleoside transporters (ENTs) (Nikiforov et al., 2011) and phosphorylated to NMN by nicotinamide riboside kinase (NRK1/2) intracellularly (Ratajczak et al., 2016). Conversion of extracellular NMN to NR mediated by enzyme CD73 is required for cell



uptake and intracellular synthesis of NAD⁺ (Grozio et al., 2013; Ratajczak et al., 2016). NAD⁺ biosynthesis in kidney and brown adipose tissue has been shown to decrease after administration of NMN in NRK1 knockout mice (Ratajczak et al., 2016). However, a recent study identified Slc12a8 as a specific transporter of NMN, which is highly expressed in the small intestine (Grozio et al., 2019). In the study, Slc12a8 expression was upregulated in the small intestines of aged mouse in response to a decrease of NAD⁺. These findings suggested that the uptake pathway of NMN could be via a cell- or tissue-specific manner.

Given that the salvage pathway is the main and the most efficient route for NAD⁺ biosynthesis, NMN or NR supplementation is becoming the preferred option of improving NAD⁺ levels that is devoid of side effects. Currently, increasing numbers of clinical trials using NMN and NR have been approved and are geared toward the treatment of various diseases, which further demonstrate that NMN is a suitable and safe drug for use in humans.

EFFECT OF AGING ON NAD⁺ LEVELS

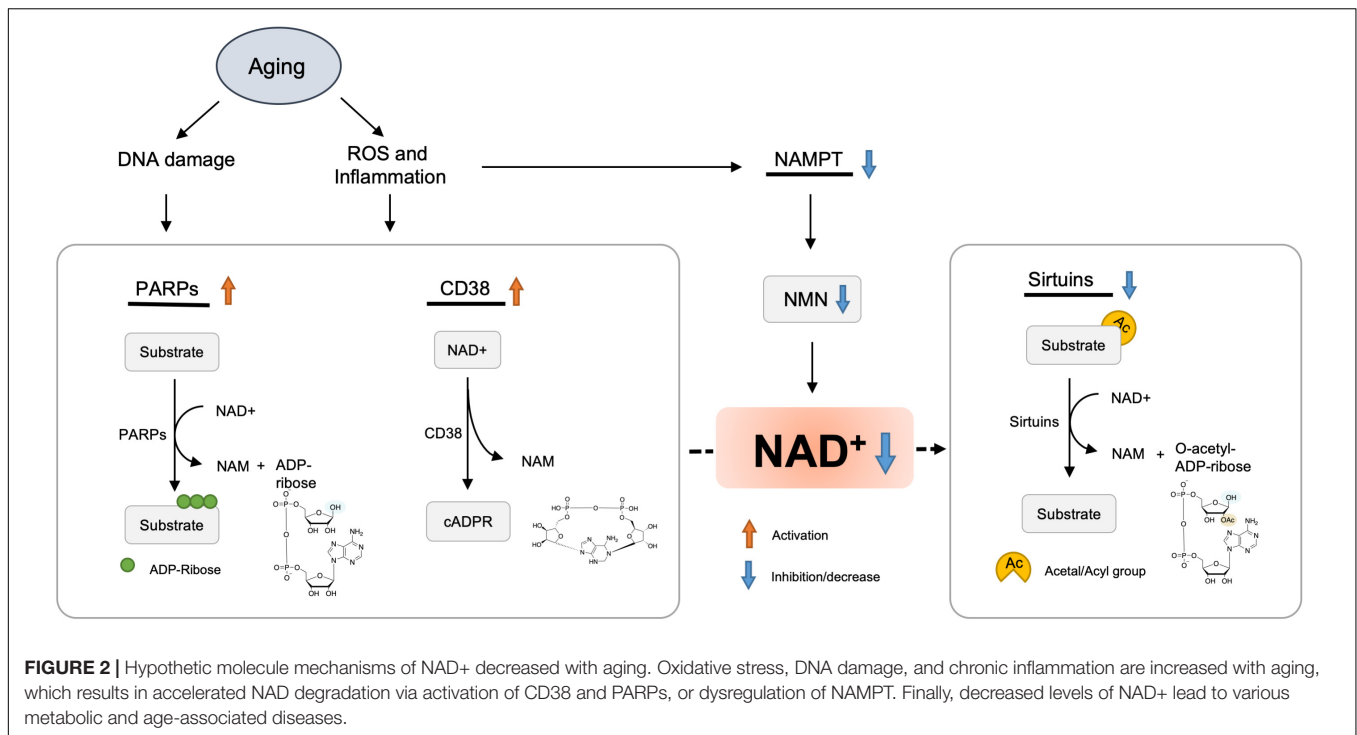
NAD⁺ Biosynthetic Pathways Decline With Age

The decline in NAD⁺ biosynthetic pathways in the course of aging could be a possible explanation for the reduction

of NAD⁺ levels. NAMPT controls NAD⁺ levels, thereby influencing the activity of NAD-dependent enzymes, including sirtuins and PARPs.

A study demonstrated that the NAD⁺ levels and NAMPT protein levels declined significantly in multiple organs, including the pancreas, white adipose tissue (WAT), and skeletal muscle of old mice (Yoshino et al., 2011). However, exercise training increased NAMPT expression in the skeletal muscles (Costford et al., 2010). NAD⁺ levels and exercise capacity were preserved in aged transgenic mice with muscle-specific NAMPT transgene expression (Frederick et al., 2016). These results suggested that the deficiency of NAMPT result in a reduction of NAD⁺ levels in the aged mice, and exercise may elevate NAMPT expression, thus restoring the NAD⁺ levels (Figure 2).

Inflammation and oxidative stress caused by aging have been shown to reduce the NAMPT-mediated NAD⁺ biosynthesis (Yoshino et al., 2011; Figure 2). Besides, *Nampt* gene encoding is controlled by BMAL1/CLOCK complex, a heterodimeric complex of core circadian transcription factors, which is suppressed by inflammatory cytokines (Cavadini et al., 2007). Therefore, the development of chronic inflammation in the course of aging may contribute to the inhibition of NAMPT-mediated NAD⁺ biosynthesis and CLOCK/BMAL-mediated circadian machinery (Imai and Guarente, 2014).



NAD⁺-Consuming Enzymes Are Activated With Age

PARP1

PARPs were initially considered to be DNA damage repair agents in the 1960s (Chini et al., 2017). The accumulation of DNA damage during aging could activate PARP, among which PARP-1 acts as a major cellular NAD⁺-consuming enzyme (Imai and Guarente, 2014). Cockayne syndrome (CS) is an aging-related progressive neurodegeneration that occurs as a result of mutations in either Cockayne syndrome group A (CSA) or B (CSB) proteins (Gitiaux et al., 2015; Scheibye-Knudsen et al., 2014). In CS mice, PARP inhibitor or NAD⁺ supplementation reversed decline in SIRT1 activation and mitochondrial function caused by aberrant PARP activation (Scheibye-Knudsen et al., 2014). Consistently, another inhibitor of PARP, PJ34, or knockout boosted the levels of NAD⁺, SIRT1 activity, and oxidative metabolism (Bai et al., 2011).

CD38

The CD38 enzyme and its homolog CD157 were initially described as plasma membrane antigens on thymocytes and T lymphocytes. Their role in NAD⁺ consumption have been revealed; that is, CD157/BST-1 could hydrolyze NR (Preugschat et al., 2014) and CD38 hydrolyzes NAD⁺ to generate NAM, adenosine diphosphoribose (ADPR), and cyclic ADPR (cADPR). In addition, CD38 also hydrolyzes cADPR (De Flora et al., 2004) and NMN (Grozio et al., 2013).

In mammals, the level of NAD⁺ and mitochondrial function decreased partially through regulation of SIRT3 as the expression and activity of CD38 protein increased in various tissues during aging (Camacho-Pereira et al., 2016). Administration of CD38

inhibitors elevated intracellular NAD⁺ level (Escande et al., 2013; Boslett et al., 2017). Consistently, CD38 knockout mice displayed significantly higher NAD⁺ level in multiple organs (Young et al., 2006).

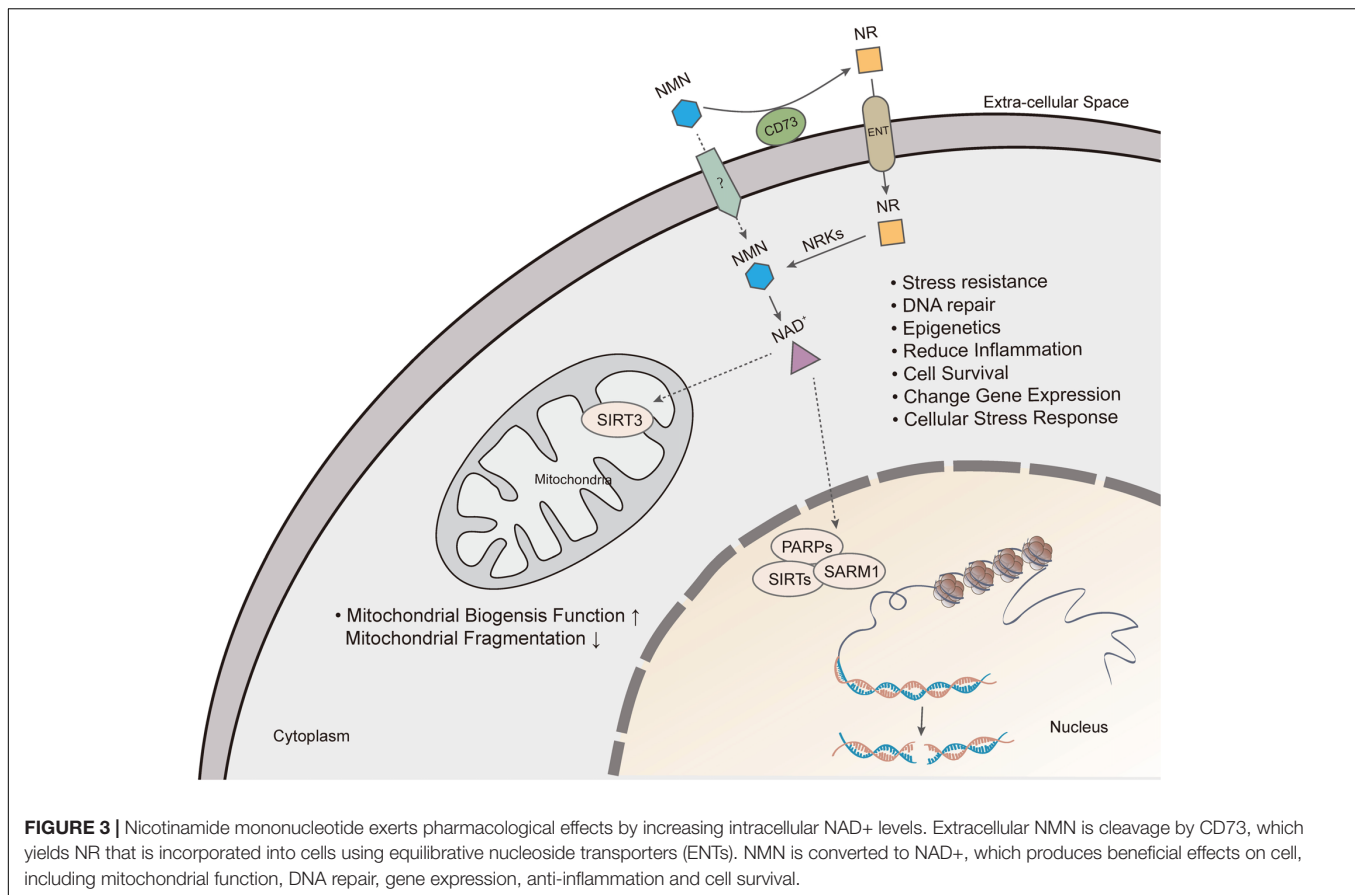
Sterile Alpha and TIR Motif-Containing 1 (SARM1) Protein

The toll/interleukin-1 receptor (TIR) domain of sterile alpha and TIR motif-containing 1 (SARM1) protein presents NADase activity (Rajman et al., 2018) that is involved in axonal degeneration after axon injury. In response to neuronal injury, the TIR domain of SARM1 cleaves NAD⁺ to generate ADP ribose (ADPR) and cyclic ADPR, which may contribute to axonal degeneration (Essuman et al., 2017). Paradoxically, overexpression of enzymes in NAD⁺ biosynthesis pathway or supplying NR could inhibit SARM1-induced axon destruction (Gerdtts et al., 2015).

In summary, there are many ways of restoring NAD⁺ level depletion caused by aging or other diseases, including improving NAMPT expression, providing NAD⁺ precursors, or inhibiting NAD⁺-consuming enzymatic activities of PARP, CD38, and SARM1. Currently, supplementation with NMN or NR is considered a viable and highly efficient strategy of increasing NAD⁺ levels (Figure 3).

DIABETES

The global prevalence of diabetes has increased dramatically over the past four decades. According to the WHO report, the number of people with diabetes rose from 108 million in 1980 to 422 million in 2014. T2D is characterized by insulin resistance



and subsequent impairment of insulin secretion (Okabe et al., 2019). The metabolism of NAD⁺ plays a crucial role in insulin sensitivity and secretion and is sometimes disrupted by obesity and aging.

Revollo et al. showed that eNAMPT was necessary for NAD⁺ biosynthesis (Revollo et al., 2007). Declined NAD⁺ levels and glucose-stimulated insulin secretion (GSIS) in pancreatic β cells and impaired glucose tolerance were observed in $\text{Nampt}^{+/-}$ mice. Similar blood glucose and plasma insulin levels were observed in $\text{Nampt}^{+/-}$ and control mice after NMN (i.p. 500 mg/kg) treatment. Also, FK866, an inhibitor of NAMPT, reduced NAD⁺ levels, and glucose-stimulated insulin secretion in primary islets, whereas NMN treatment reversed the defects (Revollo et al., 2007). These results demonstrated that Nampt-mediated NAD⁺ biosynthesis is critical for β cell function, and that NMN treatment can ameliorate the deficiency in NAD biosynthesis and glucose-stimulated insulin secretion.

Obesity and diabetes are inextricably linked. MicroRNAs (miRNAs) are key regulators of metabolism, by which SIRT1 expression is regulated in healthy conditions and metabolic diseases (Lee and Kemper, 2010). In the dietary obese mice, the elevation of hepatic microRNA-34a (miR-34a) inhibited the expression of NAMPT and SIRT1, which was responsible for the decrease in NAD⁺ levels and SIRT1 activity (Choi et al., 2013). The reduction of SIRT1 activity resulted in transcriptional responses of decreased fatty acid β -oxidation

and increased lipogenesis and inflammation (Choi et al., 2013). Mice overexpressing miR-34a were intraperitoneally injected with NMN (500 mg/kg) for 10 days consecutively, the effects caused by hepatic overexpression of miR-34a were reversed, and glucose tolerance was enhanced (Choi et al., 2013). These results suggested that NMN could be a potential agent for the treatment of obesity-associated T2D involving SIRT1 dysfunction.

Because of the high intake of dietary sugar, the risk of metabolic syndrome and T2D has been on the increase in humans (Malik et al., 2010). Fructose consumption contributes to the development of pro-inflammatory effect in rodent models, which is involved in the process of insulin resistance and the onset of T2D (Roncal-Jimenez et al., 2011). Fructose-rich diet (FRD) results in T2D-like symptoms, including hyperglycemia, dyslipidemia, and inflammation (Roncal-Jimenez et al., 2011). FRD-fed mice showed an increased expression of IL-1 β and TNF- α , which are pro-inflammatory phenotypes. The GSIS and leucine-stimulated insulin secretion (LSIS) were significantly reduced in FRD-fed mice, which was associated with islet dysfunction caused by a decrease of eNAMPT in plasma, whereas the administration of NMN at the dose of 500 mg/kg eliminated the adverse effects of FRD on GSIS and LSIS in mice (Caton et al., 2011).

FRD increased the expression of Inos (induces cellular stress and cell death) and Bax (pro-apoptotic gene) genes and reduced the expression of Pdx1, Glut2, and Gk genes, which are all

essential for glucose detection and beta-cell differentiation. These changes in gene expression were restored by NMN treatment. Moreover, the decrease in expression of Sirt1 and Sirt3 genes in FDR mice were reversed by NMN treatment. These results suggested that NMN could improve islet function by influencing the expression of genes related to anti-inflammatory, islet beta-cell differentiation, and SIRT1 activation.

Yoshino et al. revealed that the administration of NMN was highly effective in combating diet- and age-induced T2D (Yoshino et al., 2011). In their study, mice fed with high-fat diet (HFD) displayed significantly reduced NAMPT protein and NAD⁺ levels in the liver and WAT and not in skeletal muscle as was expected. The HFD-induced male and female diabetic mice after receiving intraperitoneal administration of NMN (500 mg/kg/day) for 10 and 7 consecutive days, respectively, exhibited restored NAD⁺ levels in the liver and WAT. Impaired glucose and insulin tolerance were significantly improved in diabetic female mice. The effect of NMN in reversing impaired glucose tolerance was milder in males compared to females, and insulin tolerance remained unchanged in male mice.

Yoshino et al. also confirmed that NMN improves hepatic insulin sensitivity by reversing the expression of genes related to oxidative stress, inflammatory response, immune response, and lipid metabolism (Yoshino et al., 2011). For example, the expression of the glutathione S-transferase alpha two gene (*Gsta2*), which is crucial for the maintenance of hepatic insulin by protecting lipid peroxidation products, was suppressed by HFD but activated by NMN. Other genes that are related to insulin resistance were significantly influenced by NMN in HFD-induced mice, such as interleukin 1 β , *lipin1*, and pyruvate dehydrogenase kinase 4 (*Pdk4*). Also, Yoshino et al. revealed that SIRT1 was responsible for gene expression dynamics, and its suppression by HFD was restored by NMN.

Aging is one of the highest risk factors for developing T2D (Moller et al., 2003). Previous studies have shown that progressive decline in β cell function in the course of aging contributes to the pathophysiology of T2D (Basu et al., 2003). As mentioned above, NAD⁺ and NAMPT levels declined during aging (Yoshino et al., 2011). Administration of NMN (500 mg/kg/day) for 11 consecutive days resulted in significant improvement in glucose tolerance and utilization in aged mice. Also, hyperlipidemia induced by HFD was also reversed by this treatment. Meanwhile, NMN did not have other effects on glucose homeostasis in non-diabetic old mice (Yoshino et al., 2011). Mills et al. (2016) also demonstrated that long-term (12 months) administration of NMN ameliorated age-associated decreased insulin sensitivity. Triglyceride levels in the liver were lower after 12-month NMN administration, which indicated a decline in insulin resistance. Mice that were put on long-term NMN intervention showed a tendency of plasma fatty acids (FFA), which is consistent with improved insulin sensitivity (Mills et al., 2016).

Moynihan et al. (2005) reported that an increase in Sirt1 dosage in pancreatic β cells improved GSIS and glucose tolerance in beta cell-specific Sirt1-overexpression (BESTO) transgenic mice at 3 and 8 months of age. However, the same cohort of BESTO mice did not show these beneficial effects at 18–24 months of age (Ramsey et al., 2008). It has been reported that

Sirt1 improves glucose-stimulated insulin secretion through the repression of *Ucp2* and improvement of ATP levels in pancreatic β cells (Bordone et al., 2006; Ramsey et al., 2008), which was abolished in aged mice, resulting in maintenance of a high level of Sirt1 protein. Also, NMN plasma levels declined significantly in aged BESTO mice, which suggested that a decrease in Sirt1 activity and loss of the glucose-responsiveness in BESTO mice resulted from the decline in systemic NAD biosynthesis. Thus, intraperitoneal injection of NMN (500 mg/kg) into 20-month-old BESTO mice led to an enhancement in GSIS and improvement in glucose tolerance in the aged BESTO females instead of males.

Generally, these discoveries demonstrated that NMN could be a promising drug for obese-associated and age-induced T2D through the role it plays in the enhancement of NAD⁺ biosynthesis and Sirt1 activity.

OBESITY

Obesity is associated with insulin resistance in multiple organs. It is a systemic metabolic derangement, which is involved in the pathogenesis of many diseases such as T2D, non-alcoholic fatty liver disease (NAFLD), atherogenic dyslipidemia, and cardiovascular disease (Reaven, 1988). It has been reported that the dysfunction of adipose tissue could result in obesity-associated metabolic disorders in multiple organs because adipose tissue has effects on maintaining the functional integrity of whole-body metabolic health (Stromsdorfer et al., 2016). Significantly reduced iNAMPT has been manifested in adipocyte as a result of HFD (Yoshino et al., 2011; Chalkiadaki and Guarente, 2012), however, elevated eNAMPT was detected in obesity (Catalán et al., 2011). Compared with clear function of iNAMPT in NMN synthesis, the significance of eNAMPT is controversial. In response to cellular stress, nutritional cues, or inflammatory cytokines, adipocytes secreted eNAMPT through PI3K-AKT pathway (Haider et al., 2006), SIRT1-mediated pathway (Yoon et al., 2015), or other unknown pathway (Tanaka et al., 2007). The role of eNAMPT has been indicated to be inflammatory promotion, inflammatory suppression (Revollo et al., 2007; Li et al., 2008; Pillai et al., 2013; Zhao et al., 2013; Jing et al., 2014), enhancement of food intake (Brunetti et al., 2012), and regulation of insulin resistance as well as plasma free fatty acid concentration (Stromsdorfer et al., 2016; Nielsen et al., 2018). The function of eNAMPT remains elusive in recent research, demonstrating that low concentration of dimeric eNAMPT benefited for beta cell function through NAD⁺, however, a higher monomeric eNAMPT level presented hostile effect on beta cell function (Sayers et al., 2020). Obesity has also been associated with the dampened NAD⁺/SIRT pathway in adipose tissue (Jukarainen et al., 2016). These findings suggested that NAMPT-mediated NAD⁺ biosynthesis in adipose tissue could be involved in the regulation of whole-body glucose metabolism.

Adipocyte-specific Nampt knockout (ANKO) mice showed a severe multi-organ insulin resistance, including adipose tissue, liver, and skeletal muscle, independently with an increase in whole-body adiposity and weight. The plasma FFA availability

and local adipose tissue inflammation were also increased in the ANKO mice (Stromsdorfer et al., 2016). The plasma concentration of two key adipokines, namely, adiponectin and adipisin, were significantly reduced in ANKO mice. It has been reported that adiponectin and adipisin regulate insulin sensitivity and glucose homeostasis (Kadowaki et al., 2006). Phosphorylation of cyclin-dependent kinase 5 (CDK5) and peroxisome proliferator-activated receptor γ (PPAR γ) was increased in adipose tissue of the ANKO mice, which led to a significant decline in gene expression of obesity-linked specific targets of phosphorylated PPAR γ , including adiponectin and adipisin. As was expected, NAD⁺ levels in adipose tissue from the ANKO mice were significantly increased after oral administration of NMN (500 mg/kg) for 4–6 weeks. The NMN treatment also improved multi-organ insulin sensitivity and normalized plasma insulin and FFA concentrations in the ANKO mice. Moreover, the phosphorylation of PPAR γ (Ser273) and CDK5 in visceral adipose tissue (VAT) was reduced by the NMN treatment. Accordingly, the plasma concentrations and gene expression of adiponectin and adipisin in adipose tissue were enhanced (Stromsdorfer et al., 2016). Therefore, these results provided evidence that NMN could be a therapeutic molecule for obesity-associated systemic metabolic derangements, particularly multi-organ insulin resistance. ANKO and brown adipocyte-specific Nampt knockout (BANKO) mice both showed impaired gene programs involved in thermogenesis, mitochondrial biogenesis, and FFA metabolism in BAT (Yamaguchi et al., 2019). However, only ANKO mice have a blunted thermogenic response (lower temperature in rectal and BAT, and whole-body oxygen consumption) to acute cold exposure, fasting, and administration of β -adrenergic agonists. Altered function in WAT may contribute to this difference. Lack of NAMPT in WAT decreased adrenergic-mediated lipolysis through inactivation of the NAD⁺–SIRT1–caveolin-1 axis, which reduced the release of FFAs as fuel source for BAT thermogenesis. NMN administration normalized these metabolic abnormalities, including increasing BAT NAD⁺ levels, decreasing BAT weight and BAT whitening as well as restoring gene expression of caveolin-1 in WAT and those involved in thermogenesis, mitochondrial function, and FFA metabolism in BAT. Moreover, ANKO mice treated with NMN showed greater cold tolerance compared with ANKO mice (Yamaguchi et al., 2019).

Several studies have confirmed that physical exercises have various health benefits, especially in obesity-related cases (Vieira et al., 2009; Ross et al., 2015), which, in part, results from the upregulation of mitochondrial activity because of increased NAD levels. Mouse models showed that NAD⁺ levels in metabolic organs and mitochondrial biogenesis could be improved by physical exercises (Ross et al., 2015). Thus, taking physical exercises is thought to be an effective way of increasing NAD⁺ levels. To compare the efficiency of increasing NAD⁺ levels between NMN supplementation and exercise, HFD-induced obese mice were given NMN (500 mg/kg) for 17 days or treadmill running (45 min/day) was implemented for 6 days per week for 6 weeks. According to the results, NMN treatment increased NAD⁺ levels in muscles and the liver, but exercise increased NAD⁺ levels in muscles only. The liver mass and triglyceride

content were significantly reduced, and citrate synthase activity was increased after NMN treatment in HFD-fed mice, which suggested that NMN could increase catabolism of fats. Exercises and NMN have a similar effect on glucose intolerance induced by obesity, however, these two interventions are tissue-specific with a different impact on mitochondrial function in muscles and the liver (Uddin et al., 2016). Uddin et al. (2017) also showed that NMN could reduce the effects of maternal obesity as compared to exercise. Maternal overnutrition is often associated with increased infant birth weight, adiposity, and high risk of long-term obesity in later life of the offspring (Castillo-Laura et al., 2015). Thus, it is important to investigate new strategies for reducing the risk in future generations. A study found that treadmill exercise (for 9 weeks) and NMN injection (for 15 days) both reduced adiposity and improved glucose tolerance and mitochondrial function. Moreover, NMN showed stronger effects on liver fat catabolism and synthesis than exercise. This study suggested that NMN treatment might be an effective option for reversing negative effects caused by maternal obesity (Uddin et al., 2017).

Long-term administration of NMN can significantly reduce age-associated body weight gain in a dose-dependent manner. A study conducted a 12-month-long administration of NMN (from 5 to 17 months) in mice. The results indicated that the 100- and 300-mg/kg dose of NMN was able to reduce the mice's weight by 4 and 9%, respectively, compared to the control mice. No difference was observed in body length between NMN-treated and control mice. NMN-treated mice also maintained higher levels of food and water consumption compared to control mice, which suggested that NMN did not cause severe side effects, such as growth defect and loss of appetite (Mills et al., 2016). In conclusion, the administration of NMN could be an effective option for maintaining body weight and reversing metabolic dysfunctions caused by obesity.

ISCHEMIA–REPERFUSION INJURY

Ischemia is known to decrease oxygen and ATP levels in tissues, leading to cell necrosis. Reperfusion is a reoxygenation process whereby blood re-enters a previously ischemic tissue, and this often causes calcium overload and production of ROS (Sanada et al., 2011). Ischemia followed by reperfusion has been reported to trigger severe tissue damage, for which ischemic preconditioning (IPC) is a confirmed preventative strategy (Sanada et al., 2011).

It has been reported that activation of SIRT1 can protect the heart from ischemia and reperfusion (I/R)-induced injury (Hsu et al., 2010). SIRT1 upregulates cardioprotective molecules, such as MnSOD (antioxidants), Trx1 (antioxidants), and Bcl-xL (anti-apoptotic), while it decreases pro-apoptotic molecules, including Bax and cleaved caspase-3. FoxO1, a transcription factor deacetylated by Sirt1, partially mediates the SIRT1-induced upregulation of MnSOD (Hsu et al., 2010), which protects the heart from oxidative stress. Moreover, maintaining NAMPT expression is critical for prevention of myocardial injury caused by I/R (Hsu et al., 2009). The deacetylase activity of SIRT1 is

dependent on NAD⁺. Thus, enhancing NAD⁺ may promote SIRT1-mediated IPC.

NMN has been shown to confer protection on the heart in ischemic and reperfusion conditions (Yamamoto et al., 2014). Yamamoto et al. found that IPC upregulates NAMPT and the protective effect of IPC on heart during I/R injury is attenuated in Nampt^{+/-} mice, suggesting that NAMPT mediates the protective effect of IPC. The NAD⁺ levels in heart were decreased after 30 min of ischemia and transiently normalized by NMN administration. Implementation of two patterns of NMN administration, once 30 min before ischemia or 4 times repetitive administration just before and during reperfusion, reduced the infarct size by 44 and 29%, respectively. However, a single administration of NMN 12 h before ischemia and once immediately before reperfusion did not significantly reduce the infarct size. These findings suggest that NMN reduces infarct size after by I/R, and this effect is timing-dependent. Notably, NMN attenuated the increase in acetylation of FoxO1 during myocardial ischemia, but NMN failed to reduce the infarct size in Sirt1-KO mice, indicating that the protective effect of NMN on the heart following I/R injury is partly mediated by Sirt1.

NMN suppressed cardiomyocyte apoptosis in the peri-infarct area after I/R and significantly improves left ventricle (LV) systolic function caused by I/R. In addition, NMN activates autophagy during myocardial ischemia, which is consistent with the finding that NAMPT and SIRT1 promote autophagy in cardiomyocytes (Hsu et al., 2009). An *ex vivo* experiment showed that NMN attenuated myocardial I/R injury in aged rats (Hosseini et al., 2019b). Rats treated with NMN showed improved myocardial function and reduced infarct size. Besides, NMN exerted positive effects on mitochondrial function by improving the antioxidant system, restoring oxidative stress, and reducing mitochondrial ROS production and membrane depolarization. Importantly, the combination of NMN and melatonin could produce stronger cardioprotection.

Glycolytic stimulation during ischemia and enhanced acidosis during reperfusion are additional mechanisms for NMN-induced cardioprotection (Nadtochiy et al., 2018). Under normal conditions, cardiac ATP production is executed by β -oxidation of fatty acids (Stanley et al., 2005). Generating ATP via glycolysis is usually considered a manifestation of cardiac pathology and heart failure (Stanley et al., 2005). However, recent studies show that glycolysis has cardioprotective effects (Gohil et al., 2010). Nadtochiy et al. reported that NMN stimulates glycolysis and increases ATP production during ischemia, which partially contributes to NMN-induced cardioprotection (Nadtochiy et al., 2018). IR injury triggers the opening of the mitochondrial permeability transition pore (mPTP). Acid pH maintains the closed state of PT pores during ischemia, however, changes in pH during reperfusion promote mitochondrial pore opening (Griffiths and Halestrap, 1995). Addition of acidic media offers cardioprotection by maintaining the closed state of PT pore in early reperfusion (Cohen et al., 2007). It is worth noting that acidosis may promote mPTP in energetic mitochondria by stimulating Pi uptake (Kristian et al., 2001). NMN elevates cardiac lactate and pyruvate to induce acidosis, which protects against IR-induced injury (Nadtochiy et al., 2018).

Park et al. (2016) showed that NMN antagonizes global cerebral ischemia injury. Ischemic insults increase the production of free radicals, which causes DNA oxidative damage and PARP1 activation, and uncontrolled PARP1 activation decreases NAD⁺, which further decreases ATP synthesis, leading to cell death (Strosznajder et al., 2003). Conversely, NMN maintains normal cellular NAD⁺ levels by inhibiting the NAD⁺ catabolism of PARP1 to improve bioenergetics metabolism of post-ischemic tissue and ameliorate brain damage. NMN treatment at 30 min after initiation of reperfusion reduces hippocampal CA1 neuron cell death and improves ischemia-induced hippocampal dysfunction involved in spatial working memory (Park et al., 2016). The NAD⁺ levels in hippocampal tissue are significantly reduced after forebrain ischemia, and NMN inhibits this decrease in NAD⁺. Meanwhile, studies show that hippocampal PARP protein levels are significantly increased in mice with cerebral ischemia, accompanied by elevated ROS production. Interestingly, this effect is blocked by administration of NMN at the start of reperfusion. Notably, when administered at a dose of 62.5 mg/kg, NMN produced optimal treatment effects compared to other doses (500, 250, 125, and 31.25 mg/kg), suggesting that high dosage of NMN may introduce adverse effects on post-ischemic neurons. In fact, accumulation of NMN in nerve injury promotes axonal degeneration (Di Stefano et al., 2015) and NMN deamidase delays Wallerian degeneration and rescues axonal outgrowth defects (Di Stefano et al., 2017). Recently, Klimova et al. (2020) revealed a novel link between mitochondrial NAD⁺ metabolism, mitochondrial dynamics, and ROS production in cerebral ischemia. They showed that NMN treatment prevents post-ischemic depletion of mitochondrial NAD⁺, suppresses mitochondrial fragmentation, and reduces ROS generation via SIRT3-dependent mechanisms (Klimova et al., 2020). The activity of superoxide dismutase 2 (SOD2), a key mitochondrial antioxidant enzyme, was inhibited by an increase in its acetylation after ischemia, which can be reversed by NMN treatment. Moreover, NMN also prevents ischemia-induced phosphorylation of mitochondrial fission Dynamin-related protein (Drp1) (Klimova et al., 2020).

Wang P. et al. (2011) have already demonstrated that NAMPT protected against ischemic stroke through promoting neuronal survival via the SIRT1-dependent AMPK pathway. As the NAMPT enzymatic product, NMN alleviates cerebral infarction size, neurological deficit, and neuronal cell death (Wang P. et al., 2011). Furthermore, the important role of NAMPT-NAD cascade in regenerative neurogenesis after ischemic stroke has been underscored by Zhao et al. (2015), and delayed NMN supplementation for 7 days with the first administration at 12 h after cerebral ischemia improved post-ischemic regenerative neurogenesis.

HEART FAILURE AND CARDIOMYOPATHIES

Heart failure is the end stage of heart disease development and refers to the inability of the heart to pump sufficient blood to match the metabolic requirements of tissues due

to impaired systole and/or diastole. Generally, heart failure is always associated with enlarged heart and dilated ventricles (Pillai et al., 2005).

Heart failure is one of diseases that are associated with mitochondrial respiratory dysfunction (Karamanlidis et al., 2013). It was found that deletion of *Ndufs4*, a protein critical for assembly and/or stability of complex I, resulted in a significant loss of complex I function in the heart. The cardiac-specific *Ndufs4* KO (cKO) mice not only showed normal longevity and cardiac function in unstressed condition, but also exhibited normal myocardial energetics and contractile function during baseline workload or acute increases of workload. However, after chronic increases of workload including pressure overload and repeated pregnancy, the cKO mice with complex I deficiency developed heart failure and high cell death, and could not be explained by oxidative stress mechanism. Complex I deficiency significantly decreased NAD⁺/NADH ratio, which inhibited sirt3 activity, increased mitochondrial protein acetylation, and sensitized mPTP. Additionally, it has been shown that NMN treatment rescues NAD⁺/NADH ratio and mitochondria protein acetylation in cKO hearts, and normalizes the sensitivity of the mPTP (Karamanlidis et al., 2013).

Lee et al. reported that mitochondrial protein hyperacetylation, which is caused by elevated NADH/NAD⁺, increases the risk of development of heart failure by two distinct mechanisms (Lee et al., 2016). Malate aspartate shuttle (MAS) modulates communication between cytosolic and mitochondrial NAD⁺ redox states, transferring electrons from cytosolic NADH generated from glycolysis into mitochondria for oxidative phosphorylation (LaNoue and Williamson, 1971; Lee et al., 2016). During mitochondrial dysfunction, hyperacetylation of MAS decreases cytosolic NAD⁺/NADH ratio, thereby inducing mPTP-related cell death and the development of heart failure (Elrod et al., 2010). Lee et al. (2016) also identified that the acetylation of lysine-70 on oligomycin-sensitive conferring protein (OSCP) sensitized mPTP opening by promoting its interaction with cyclophilin D (CypD), a regulator of mPTP. Thus, administration of NMN reverses hyperacetylation of these proteins by normalizing the NAD⁺ redox balance, thereby protecting mice from heart failure.

Kruppel-like factor 4 (KLF4) is critical for cardiac mitochondrial homeostasis. Accordingly, mice with cardiac-specific deficiency of KLF4 (CM-K4KO) are more sensitive to pressure overload-induced heart failure (Liao et al., 2015). Zhang et al. found that cardiac KLF4 deficiency led to hyperacetylation of mitochondrial proteins, including SOD2, CypD, and long-chain Acyl-CoA dehydrogenase (LCAD), which impaired mitochondrial metabolic function and predisposed the CM-K4KO hearts to stress-induced dysfunction (Zhang et al., 2017). Meanwhile, the expression of Sirt3, NAD⁺, and NAMPT were reduced in the KLF4-deficient heart, all of which decreased deacetylase activity in the mitochondria. Moreover, NMN increased NAD⁺ levels and normalized the mitochondrial protein acetylation levels in cardiac tissue. Remarkably, NMN preserved the cardiac contractile function and protected CM-K4KO mice from heart failure during

pressure overload. LCAD is a fatty acid oxidation (FAO) enzyme, which oxidizes long-chain fatty acid, the main fuel of heart. The activity of this enzyme is dependent on Sirt3-NAD⁺ deacetylation (Hirschey et al., 2010), and acute NMN treatment increased mitochondrial FAO, indicating that NMN improves cardiac energetics and heart function. CM-K4KO hearts showed high rates of cell death in myocardium when subjected to stress, and NMN administration prevented cell death in pressure-overloaded hearts. Finally, NMN was found to preserve the mitochondrial ultrastructure and reduce ROS and inflammation in CM-K4KO myocardium partially through Sirt3-dependent deacetylation and activation of SOD2 in response to oxidative stress (Zhang et al., 2017). In summary, short-term administration of NMN may confer protection against cardiac mitochondrial homeostasis and prevent heart failure.

Martin et al. (2017) reported that NMN improves cardiac function and bioenergetics in a SIRT3-dependent manner in a Friedreich's ataxia (FRDA) cardiomyopathy model, a mouse genetic cardiomyopathy model with frataxin-KO (*Fxn*^{-/-}, FXN-KO). NMN (500 mg/kg) administered two times per week for 4–5 weeks improves diastolic function and normalizes the defective cardiac contractility in FXN-KO. A shortened ejection time (ET) represents impaired contractility or severe LV dysfunction in patients with heart failure or idiopathic-dilated cardiomyopathy (Dujardin et al., 1998). FXN-KO mice show a shortened ET, whereas NMN treatment significantly increases ET (Martin et al., 2017).

NMN supplementation also improves cardiac energy utilization and decreases energy wastage in the FXN-KO heart. Cardiac efficiency (CE), a ratio of energy used for mechanical work to overall energy available, is decreased in FXN-KO. Also, FXN-KO mice also shows an increased ventriculoarterial coupling (VC) ratio, another parameter representing the efficiency of converting ventricular mechanical energy (ME) into hydraulic energy in the aorta during systole (Suga, 1990; Walley, 2016). NMN treatment normalizes both CE and VC in the FXN-KO heart failure model. Pressure-volume area (PVA) is the sum of ME and potential energy (PE) (Suga, 1990). In FXN-KO hearts, a large proportion of PVA is consumed as PE, rather than ME, which indicates greater energy wastage in heart failure. However, NMN treatment improves myocardial energy utilization by normalizing the proportion of PE in PVA.

Additionally, the study reported that NMN-induced reduction in energy wastage paralleled the remarkable decrease in whole-body energy expenditure (EE) due to decreased FA metabolism and a SIRT3-dependent carbohydrate metabolism (Martin et al., 2017). FXN-KO mouse show elevated whole-body daily FA oxidation and serum triacylglycerides, while NMN supplementation blocks this elevation. Moreover, NMN reduces tissue lactate production and inhibits glycolysis by decreasing systemic and cardiac glucose utilization in the FXN-KO heart, thereby improving CE and function (Martin et al., 2017). Importantly, the therapeutic effects of NMN are mediated by deacetylation of SIRT3 in FXN-KO hearts (Martin et al., 2017). In summary, these findings provide preclinical evidence

that NMN could be a promising drug for heart failure and cardiomyopathies.

VASCULAR DYSFUNCTION

Cardiovascular disease (CVD) is the leading cause of mortality worldwide. Aging is a developmental risk factor for the disease. Vascular endothelial dysfunction and large elastic artery stiffness are two antecedents and predictors of clinical CVD (Mitchell, 2014). Vascular oxidative stress contributes to vascular endothelial dysfunction and large elastic artery stiffness (Bachschmid et al., 2013). Excessive superoxide reduces the bioavailability of nitric oxide (NO), a vasoprotective, and vasodilatory molecule, and thus causes alterations of structural proteins such as collagen and elastin, in large elastic arteries (Seals et al., 2014). Vascular endothelial dysfunction and large elastic artery stiffness are assessed by endothelium-dependent dilation (EDD) and aortic pulse wave velocity (aPWV), respectively (de Picciotto et al., 2016). Old mice showed impaired carotid artery EDD, and oral supplement of NMN (300 mg/kg) for 8 weeks restored EDD in the old mice by assisting in regaining NO-mediated dilation and reducing arterial oxidative stress (de Picciotto et al., 2016). Also, NMN restored the expression and activity of the SIRT1 in the arteries of old mice in accordance with previous studies, which revealed that the reduced expression and activity of SIRT1 contributes to impaired EDD in aging arteries (Donato et al., 2011; Gano et al., 2014) and by applying SIRT1 activator, the EDD was improved by partly reducing the oxidative stress (Gano et al., 2014).

An increase in stiffness of large elastic artery with age reduces the artery's ability to buffer increase in pressure churned out by systolic ejection (de Picciotto et al., 2016). The type I collagen, a load-bearing protein in the arterial wall, is augmented during aging, while the main structural protein, elastin, diminishes in old arteries (Diez, 2007). Treatment using NMN also reduced the large elastic stiffness in aged mice by reversing the accumulation of whole-vessel type I collagen and enhancing arterial elastin (de Picciotto et al., 2016). A recent study showed that the protective effects of NMN supplement on vascular function are associated with increased anti-aging miRNA expression profile in the aorta of aged mice (Kiss et al., 2019b).

The brain, which is, a metabolically active organ, relies on the blood circulation to deliver nutrients and eliminate metabolic waste products (Tarantini et al., 2017). Cerebromicrovascular health is critical for brain perfusion, which helps in the maintenance of healthy cerebral function. Adjustment in cerebral blood flow maintains cellular homeostasis and function through neurovascular coupling (NVC), in response to the increased neuronal activity (Tarantini et al., 2017). Microvascular endothelium releases the vasodilator (NO) in response to increased neuronal and astrocytic activation (Toth et al., 2014). Several lines of evidence suggest that NVC responses are impaired in the course of aging, hence contributing to age-related cognitive impairment (Toth et al., 2014; Balbi et al., 2015). Emerging studies have revealed that an increase in mitochondrial oxidative

stress and mitochondrial dysfunction results in impairment of neurovascular during the aging process (Springo et al., 2015).

A report by a recent study on aged mice showed that NMN could restore the function of cerebromicrovascular endothelium and NVC responses (Tarantini et al., 2019). NMN (i.p. 500 mg/kg) was injected in male aged mice (24 months old) for 14 consecutive days. The treatment restored the NO mediation of NVC in aged mice by reestablishing NO release, which resulted in endothelial NO-mediated vasodilation in the aortas of aged mice. The NO mediation of NVC responses is weakened by age-related mitochondrial oxidative stress. NMN increased the activation of SIRT1, which reversed mtDNA-encoded subunits, attenuated mtROS production, and improved mitochondrial bioenergetics. Thus, NMN can restore the protective effects of cerebromicrovascular by improving endothelial function, attenuating endothelial oxidative stress, and improving NVC responses in aged mice (Tarantini et al., 2019).

Age-related NAD⁺ depletion and consequential SIRT1 dysregulation are associated with impaired angiogenic processes in cerebromicrovascular. However, a study indicated that NMN could rescue angiogenic capacity in aged cerebromicrovascular endothelial cells (ECs) (Kiss et al., 2019a). Recently, the same team identified 590 genes differentially expressed in the aged neurovascular unit, 204 of which were shifted back toward youthful expression levels by NMN (Kiss et al., 2020). NMN supplementation reverses age-related changes in neurovascular gene expression, including SIRT1 activation, mitochondrial protection, anti-inflammatory, and anti-apoptotic (Kiss et al., 2020).

A steady decline in tissue perfusion has been observed in humans from the age of 40, which often results in organ dysfunction and general body weakness in the last decades of life (Le Couteur and Lakatta, 2010). The number and function of ECs decline with age, resulting in increased apoptosis of ECs in the muscle, diminished neovascularization, and loss of blood vessels (Wang et al., 2014). These changes reduce muscle mass and endurance during aging (Prior et al., 2016). Abhirup et al. reported that SIRT1 in ECs is necessary for the response to pro-angiogenic signals secreted from myocytes and treatment with NMN improved blood flow and endurance in elderly mice by increasing capillary density (Das et al., 2018). In the same study, the number and density of ECs and capillaries in skeletal muscle for endurance were significantly decreased in the old mice, which could have been associated with impaired angiogenesis. Endothelial-specific SIRT1 knockout mice (ESKO) exhibited the same phenotype of aging, including reduced density of capillaries and decreased exercise endurance. Overexpression of endothelial SIRT1 sensitizes ECs to vascular endothelial growth factor, which improves the muscle neovascularization and hence increases capillary density and endurance. Moreover, NAD⁺/SIRT1 negatively regulates Notch signaling (Guarani et al., 2011), an indispensable signaling pathway for blood vessel formation (Blanco and Gerhardt, 2013).

Thus, NMN could restore angiogenesis in old mice through SIRT1-mediated inhibition of Notch signaling. NMN (400 mg/kg/day) was administered to old mice through drinking

water for 2 months. The drug restored the number and density of capillaries, increased soluble oxygen (sO_2) levels, and improved endurance in the old mice. However, these effects were abolished in SIRT1 knockout mice. Also, exogenous hydrogen sulfide (H_2S) augmented the effect of NMN.

All these studies suggest that NMN could be a favorable agent for therapy against various diseases related to a decrease in blood flow brought about by cardiovascular dysfunction.

INTRACEREBRAL HEMORRHAGE

Intracerebral hemorrhage (ICH) is a primary brain injury resulting from mechanical damage that causes a hematoma. It can sometimes progress to a secondary injury, which is mainly subsequent pathophysiologic changes, including blood–brain barrier (BBB) destruction, hemoglobin-induced iron overload, neural cell death, neuroinflammation, and oxidative stress (Zhou et al., 2014; Wei et al., 2017b). A study suggested that NMN could be a promising agent for the treatment of ICH (Wei et al., 2017b). A single dose of NMN (300 mg/kg) was injected into CD1 mice 30 min after treatment with collagen-induced intracerebral hemorrhage (cICH). The NMN treatment relieved the edema that had been induced by cICH and improved neurological function. Treatment using NMN reduced cell death and oxidative stress in hemorrhage area. Moreover, it suppressed the cICH-induced microglia activation and neutrophil infiltration and inhibited inflammatory-associated factors, including $TNF-\alpha$ and IL-6. The intercellular adhesion molecule-1 (ICAM-1) protein, an adhesion molecule, is essential for the process of neuroinflammation activation after ICH. The NMN treatment also inhibited an increase in ICAM-1 after cICH (Sozzani et al., 2015; Wei et al., 2017b).

The secondary stage of ICH mainly results from toxicity caused by hemin, which is a breakdown product of hemoglobin. It causes cell death and induces extensive local inflammation/oxidative stress. Hemin can induce HO-1, a ubiquitous enzyme, which oxidatively cleaves pro-oxidant heme to produce biliverdin and carbon monoxide. NMN also elevates the nuclear Nrf2 protein expression to upregulate HO-1 protein expression in brain tissues, thereby inhibiting neuroinflammation and oxidative stress and contributing to the neuroprotection in ICH (Mylroie et al., 2015; Wei et al., 2017b). Finally, a prolonged NMN treatment for 7 days significantly arrested body weight decline and neurological deficit caused by ICH.

Carrie et al. also reported that NMN supplement preserved mitochondrial function, mitigated inflammation, and increased survival rate in hemorrhagic shock (Sims et al., 2018). Lactic acidosis, which is a by-product of anaerobic metabolism, is used to estimate the success of resuscitation in injured patients (Broder and Weil, 1964). High lactate levels reflect tissue hypoperfusion, which is, in turn, related to the severity and survivability of the shock (Rixen and Siegel, 2005). Pretreatment (400 mg/kg/day for 5 days, oral) and resuscitation (400 mg/kg, intravenous) with NMN significantly reduced serum lactate levels during a fixed pressure hemorrhagic shock.

The NAD^+ concentration in various tissue decreases rapidly with the severity of the injury during hemorrhagic shock (Wurth et al., 1973), which can result in dysfunction of vital organs. Under hypoxic conditions, the mitochondrial electron transport chain becomes inefficient in reoxidizing NADH to the NAD (Wheaton and Chandel, 2011). The NMN treatment can compensate for the decrease in NAD^+ levels and preserved the NAD/NADH ratio in both kidneys and livers. Adenosine triphosphate reserves are also depleted following hemorrhagic shock and resuscitation, and NMN treatment also restores the reserves in the kidney, but, not the liver. This could be caused by elevated ATP consumption in the liver. Treatment with NMN preserves the impaired complex I-dependent (CI-dependent) respiration following hemorrhagic shock and resuscitation.

Hemorrhagic shock and resuscitation are usually accompanied by increased cytokine levels, oxidative stress, and insulin-resistant hyperglycemia, which indicates the existence of inflammation (Sims et al., 2018). Circulating levels of the cytokine IL-6 are as predictors of mortality in human patients (Stensballe et al., 2009). Treatment with NMN significantly reduces serum IL-6 cytokine levels and ameliorated shock-induced hyperglycemia. The most important is that NMN can enhance physiologic reserve and improve survival after hemorrhagic shock. Pretreatment with NMN increases the ability of animals to tolerate longer periods of hypoperfusion. Resuscitation with NMN significantly improves the survival.

Tissue plasminogen activator (tPA) is used for therapy in case of acute brain ischemia. The window of tPA therapy is within 0–4.5 h. A delayed tPA therapy dose not decrease infarction but worsens hemorrhagic transformation (Wei et al., 2017a; Zhang et al., 2009). Wei et al. (2017a) suggested that NMN could attenuate delayed tPA-induced hemorrhagic transformation after cerebral ischemia without changing tPA thrombolytic activity. In the study, delayed tPA therapy resulted in a high mortality rate in middle cerebral artery occlusion (MCAO) mice. However, a single dose of NMN (300 mg/kg) injection (i.p.) reduced the mortality rate. NMN also attenuated the delayed tPA-induced severe infarction volume and brain edema. The cerebral hemorrhage caused by delayed tPA was fatal, but NMN significantly decreased the cerebral hemorrhage and higher hemoglobin level in the ipsilateral hemisphere of delayed tPA mice. The administration of NMN also inhibited neural apoptosis and ameliorated microglial activation and reduced neuroinflammation in delayed tPA-treatment mice.

It has been reported that disruption of BBB could be a reason for tPA-induced hemorrhagic transformation (Kastrup et al., 2008). The tPA activates matrix metalloproteinases (MMPs), which destroys tight junction proteins (TJPs) (Rempe et al., 2016). Consistent with previous findings, the protein levels of TJPs (claudins, occludin, and zonular occludens-1) were downregulated, and the activities of MMP9 and MMP2 were enhanced in delayed tPA treatment, which implied that the BBB integrity had been compromised. The NMN treatment significantly reversed these changes and protected BBB integrity. Thus, NMN could be a potential agent for the therapy of tPA-induced hemorrhagic transformation.

It was also reported that NMN is able to protect brain in both the early and the chronic phase of cryoinjury (Zhang et al., 2015). These studies demonstrated that NMN could be a remedy for ICH of various causes.

NEUROPROTECTIVE AND COGNITIVE FUNCTION

Cognitive decline is one of the many symptoms of aging, and regulation of adult neurogenesis could be a therapeutic strategy in overcoming the condition. There are two distinct populations of neural stem cells (NSCs) in the brain, which are found in the subgranular zone (SGZ) and subventricular zone (SVZ). They can self-renew and differentiate into transient amplifying progenitors, that is, neural stem/progenitor cells (NSPCs). The NSPCs undergo finite, lineage-restricted cell divisions to differentiate into the major cell types of the brain, such as neurons, oligodendrocytes, and astrocytes (Artegiani and Calegari, 2012; Jadasz et al., 2012). Studies have revealed that aging is a negative regulator of NSPC proliferation, whereas NSPCs could be reactivated in the aged brain (Artegiani and Calegari, 2012). Thus, restoring the function of NSPCs could effectively prevent age-associated cognitive decline.

Liana and Shin-ichiro established that, in response to insult-induced demyelination, NAMPT-mediated NAD⁺ biosynthesis was critical for NSPC self-renewal, proliferation, and differentiation into oligodendrocytes (Stein and Imai, 2014). The study found that levels of NAD⁺ and expression of NAMPT in hippocampus were declining with age. However, the long-term NMN administration was able to maintain the NSPC pool. Moreover, they found that NMN administration reduced defects in oligodendrogenesis caused by decrease in NAD⁺ levels. Thus, NMN could be a promising agent for maintaining the NSPC pool and reactivating NSPCs, which can improve remyelination caused by aging and neurodegenerative diseases (Stein and Imai, 2014). Also, Zhao et al. (2015) reported that NMN was able to induce NSC proliferation (via SIRT1 and SIRT2) and promote NSC differentiation (via SIRT1, SIRT2, and SIRT6).

Mental disorders such as anxiety are prevalent among older people and account for 10–20% of the total mental diseases in the population, most of which is dementia or major depressive disorder (Regier et al., 1988). Late-life anxiety disorder results in substantial financial burden on individuals and society. Sean et al. discovered that old mice developed cognitive hypersensitivity in response to aversive stimulation during contextual fear condition tests, which was associated with the age-related changes in emotionality and sensory processing (Johnson et al., 2018). Moreover, specific knockdown of NAMPT in the hippocampal CA1 region recapitulated the same age-associated cognitive hypersensitivity, whereas dentate gyrus specific NAMPT knockdown mice did not show cognitive hypersensitivity.

Sean et al. found that calcium/calmodulin-dependent serine protein kinase (Cask), a crucial multidomain scaffold protein at the synapse and in cell junctions (Hsueh, 2006), is the downstream effector in response to the reduction in NAD⁺

and is also downregulated in the hippocampus during aging (Johnson et al., 2018). Therefore, Sean et al. proposed a model to demonstrate that the levels of NAMPT and NAD⁺ in hippocampal neurons, particularly in CA1 neurons, decline during aging, leading to a decrease in SIRT1 activity and subsequent downregulation of Cask expression in the aged hippocampus. Cask interacts with the GluN2B subunit of N-methyl-D-aspartate receptor (NMDAR) for the transport of GluN2B-containing vesicles (Jeyifous et al., 2009), and the reduction in Cask could cause dysfunction of GluN2B-containing NMDARs at the synapse, which could contribute to a wide range of cognitive and behavioral impairments during aging (Johnson et al., 2018). The NMN supplementation, even in a short time, could reduce cognitive hypersensitivity and improve the sensory processing aspect of some aversive stimuli and possibly other related behaviors (Johnson et al., 2018). Therefore, the NMN administration could prevent and treat such cognitive impairments and enhance the quality of life in old age.

NMN also prevented aging-induced cognitive impairment by improving cerebrovascular (Kiss et al., 2019a; Tarantini et al., 2019) and mitochondrial function, and reducing apoptosis in the prefrontal cortex and hippocampus of aged animals (Hosseini et al., 2019a). Lu et al. (2014) reported that NMN improved energy activity and survival rate in an *in vitro* model of Parkinson's disease. Fang et al. (2016) also demonstrated that NR and NMN were able to normalize neuromuscular function and memory by regulation of mitophagy and enhancement of DNA repair in mice and worm models of ataxia-telangiectasia (AT), an autosomal recessive disease with progressive neurodegeneration.

A study indicated that NAMPT enzymatic activity enhancer P7C3 could have a neuroprotective effect in a mouse model of amyotrophic lateral sclerosis (ALS) (Tesla et al., 2012), and the levels of iNAMPT in ALS patients were lower than those of age-matched controls (Wang et al., 2017). Wang et al. (2017) silenced NAMPT in the projection neurons of adult mice and created Thy1-YFP-Nampt^{-/-} cKO mice that notably exhibited general motor abnormalities, muscle atrophy, progressive motor function deficits, and a shorter lifespan, some of which are the key features of ALS. Loss of NAMPT in projection neurons led to mitochondrial metabolic dysfunction and destroyed the mitochondrial homeostasis. Wang et al. reported that NAMPT knockdown disrupts the balance between mitochondrial fission/fusion and causes more fragmentation, which could lead to subsequent neuronal degeneration. The thy1-YFP-Nampt^{-/-} cKO mice exhibited neurodegeneration in the brain, especially in the motor cortex and increased acetylation proteins, which implied that NAD⁺-related perturbations induced a reduction in Sirt3 activity. Also, many lines of evidence have shown that increasing Sirt1 and Sirt3 deacetylation activities have a neuroprotective role in motor neuron degeneration diseases, such as ALS (Fu et al., 2012; Watanabe et al., 2014).

The thy1-YFP-Nampt^{-/-} cKO mice also showed widespread abnormalities of the neuromuscular junctions (NMJs), which is known to disrupt synaptic connectivity and cause defective synaptic transmission. Remarkably, NMN (400 mg/kg) treatment lessened disease severity, restored motor function, and extended

the life span of Thy1-YFP-Nampt^{-/-} cKO mice. Recently, this same team reported that loss of NAMPT in projection neurons cause detrimental effects on the function and structure of NJM, including impaired synaptic vesicle cycling, morphological changes to the motor endplate, alterations of skeletal muscle contractile responses, and noticeable sarcomere misalignment (Lundt et al., 2020). These detrimental effects were reverse by administration of NMN (400 mg/kg/day) for 14 days. However, NMN treatment did not restore skeletal muscle mitochondria morphology change caused by deletion of Nampt (Lundt et al., 2020). Thus, NMN is a potential therapeutic drug for motor neuron (MN) degenerative diseases, including ALS. Increasing the NAD⁺ salvage pathway could reduce the symptoms of neurodegenerative diseases.

ALZHEIMER'S DISEASE

AD is progressive dementia characterized by memory loss at an early stage of the disease progression. Currently, there is no effective therapy for AD treatment. Also, its molecular basis has not been elucidated (Gong et al., 2003). Thus, there is a need to focus on finding effective therapeutic drugs for the disease.

Mitochondrial dysfunction is a feature of many neurodegenerative diseases, including Alzheimer's disease (AD), Parkinson's disease (PD), and Huntington's disease (HD) (Hroudova et al., 2014). Morphological and functional abnormalities of mitochondria may lead defects in the electron transport chain and ATP production, which are associated with AD (Hroudova et al., 2014; Long et al., 2015). The NAD⁺ as a cofactor is crucial for the tricarboxylic acid cycle, mitochondrial oxidative phosphorylation, and glycolysis-related enzymatic reactions, and the levels of NAD⁺ in the cell are critical for neuronal survival (Liu et al., 2008). Thus, preventing NAD⁺ depletion and boosting cellular energy could be a therapy for neurodegenerative disease (Long et al., 2015).

A study reported that NMN improved NAD⁺ catabolism and changed mitochondrial morphological dynamics in mice with AD (Long et al., 2015). In the study, AD chimeric amyloid precursor protein APP_(swe)/PS1_(ΔE9) double transgenic (AD-Tg) mice showed deficits in mitochondrial oxygen consumption rates (OCRs) in the brain and muscle at 3 months of age. The NMN (100 mg/kg) was subcutaneously injected to AD-Tg female and male mice consecutively for 28 days, which reversed mitochondrial OCR deficiencies in the AD model. Still, in the same study, full-length mutant human APP levels were significantly increased in the brain of AD-Tg mice compared to non-transgenic (NTG) mice. The administration of NMN decreased full-length mutant APP expression in AD-Tg mice. Immunoreactivity of SIRT1 and CD38 was also significantly increased in AD-Tg compared to NTG mice, which could be attributed to NAD⁺ catabolism. The AD mice pre-treated with NMN showed a lower SIRT1 immunoreactivity compared to Ag-TD mice, but still had a higher SIRT1 compared to NTG mice.

The mitochondrial morphology is vital for its functions, such as mitochondrial respiration and calcium homeostasis, among others. Fusion and fission are two fundamental processes in

mitochondria, which are essential for cellular survival and disease vulnerability. The protection of the nervous system is associated with the fusion, and fission processes, both of which contribute to the damaged organelles' elimination (Escobar-Henriques and Anton, 2013). NMN administration increased the length of mitochondria and decreased fragmentation in the hippocampal sub-region (Long et al., 2015). A study reported that NMN alters mitochondrial dynamics by SIRT3-dependent mechanism (Klimova et al., 2019). Nina et al. also showed that the levels of the active form of fission protein, phosphorylated Drp1 (S616) (pDrp1), were significantly decreased in hippocampal mitochondria after a single-dose NMN treatment, and the same result was observed in AD-Tg mice (Long et al., 2015). NMN also decreased the acetylation of mitochondrial proteins, such as mitochondrial SOD2, which is an important antioxidant enzyme and one of the targets of SIRT3. The SOD2 catalyzes superoxide into hydrogen peroxide and oxygen, which is then converted to water by glutathione peroxidase (Chen et al., 2011). Studies have shown that mitochondrial morphologies are associated with the generation of ROS, and the accumulation of ROS could induce more mitochondrial fragmentation (Willems et al., 2015). Thus, NMN treatment reduced hippocampal ROS through SIRT3-dependent deacetylation of SOD2, which resulted in lowering mitochondrial fragmentation via pDrp1 (S616).

The Aβ oligomers have been widely reported to be responsible for AD pathology. They usually accumulate in AD frontal cortex levels of up to 70-fold compared to normal brains (Gong et al., 2003). Wistar rats with an intracerebroventricular infusion of Aβ₁₋₄₂ oligomer were used as AD mouse models. Intraperitoneal NMN (500 mg/kg) treatment improved their cognitive and memory functions, which might have been as a result of NMN reducing oxidative stress actions (Wang et al., 2016). Long-term potentiation (LPT), a mechanism for memory and learning functions, is significantly inhibited by Aβ oligomers, but NMN treatment was able to prevent this inhibition in organotypic hippocampal slice cultures (OHCs). Oxidative stress and a high concentration of ROS have toxic effects on synaptic transmission, which is essential in neurodegeneration (Guidi et al., 2006). Administration of NMN prevented the accumulation of ROS induced by Aβ₁₋₄₂ oligomer in OHCs, which could have been the reason for memory and learning improvement. The NMN treatment also attenuated the neuronal cell death and reduction of NAD⁺ and ATP in Aβ₁₋₄₂ oligomer-treated hippocampal slices (Wang et al., 2016).

The c-Jun N-terminal kinases (JNKs) are a family of multifunction-signaling protein kinases that respond to various cellular stresses and inflammatory mediators (Mehan et al., 2011). However, aberrant activation of JNK is associated with pathogenesis of Alzheimer's disease. A study demonstrated that NMN could reverse AD by inhibiting JNK activation in the hippocampus and cerebral cortex of AD-Tg mice (Yao et al., 2017). Administration of NMN ameliorated amyloid-induced synaptic loss and dysfunction, and reversed cognitive impairments in AD-Tg mice, including severe impairment of spatial learning, spatial memory and contextual memory.

Also, NMN decreased β-amyloid production and amyloid plaque burden (Yao et al., 2017). The NMN regulated the

expression of APP cleavage secretase in AD-Tg mice, including elevation of sAPP α and reduction of sAPP β . A previous study indicated that phosphorylation of APP on threonine 668 could promote β -secretase cleavage of APP, resulting in more A β generation (Colombo et al., 2009). SIRT1 activation promoted non-amyloidogenic α -secretase processing of the amyloid precursor protein by inhibiting rho-associated kinase (ROCK1) expression (Qin et al., 2006). These results showed that NMN might enhance non-amyloidogenic APP processing and hence decrease A β pathology in AD-Tg mice. Neuroinflammation, a crucial response for the development of AD (Morales et al., 2014), was shown to be inhibited by NMN treatment in AD-Tg mice (Yao et al., 2017), including decrease in IL-6, IL-1 β , and TNF α . These proinflammatory cytokines stimulate β -secretase and γ -secretase to generate more A β in the brain through a JNK-dependent MAPK pathway (Liao et al., 2004). In conclusion, NMN improved cognitive abilities and decreased amyloid plaque, loss of synapse, β -secretase, and neuroinflammation, at least partially by inhibition of JNK activation.

These studies demonstrate that NMN could be a viable intervention for managing AD.

RETINAL DEGENERATION AND CORNEAL INJURY

The photoreceptor is crucial for light transduction, which is necessary for vision, and there are two classes of photoreceptors: rods and cones. Rod and cone photoreceptors mediate dim and precise central vision in ambient light, respectively (Lin et al., 2016). Death of photoreceptors results in vision loss, and this occurs in many diseases, including age-related macular degeneration (AMD), retinitis pigmentosa (RP), and Leber congenital amaurosis (LCA) (Wright et al., 2010). It has been reported that mutations in NMNAT1 cause LCA, as a result of reduced NAD $^{+}$ biosynthesis and impaired protein folding (Koeneke et al., 2012). Thus, NAD $^{+}$ biosynthesis has a role in photoreceptor function and survival.

Knockout mice lacking Nampt in rod photoreceptors (Nampt $^{-rod/-rod}$) and cone photoreceptors (Nampt $^{-cone/-cone}$) showed a decreased retinal NAD $^{+}$ level and a degenerative phenotype, including vascular attenuation, optic nerve atrophy, outer nuclear layer thickness reduction, and retinal function impairment (Lin et al., 2016). Retinal NAD $^{+}$ deficiency was observed in multiple mouse models with retinal dysfunction, including light-induced degeneration, streptozotocin (STZ)-induced diabetic retinopathy, and aging-associated retinal dysfunction. NAD $^{+}$ deficiency in photoreceptors causes significant glycolytic and mitochondrial dysfunction under basal conditions and impairs the normal response to moderate metabolic stresses, which results in photoreceptor cell death and retinal degeneration (Lin et al., 2016). Besides, photoreceptors are susceptible to defects in energy homeostasis because of their limited mitochondrial reserve (Kooragayala et al., 2015). Lin et al. (2016) demonstrated that SIRT3 and SIRT5 are both critical for photoreceptor survival and retinal homeostasis.

It is through SIRT3 that NAD $^{+}$ deficiency causes aberrant hyperacetylation of mitochondrial proteins, hence contributing to mitochondrial dysfunction.

Nampt is critical for energy metabolism in retinal cells and its deficiency results in impairment of retinal homeostasis. Downstream production of Nampt is a potential approach to relieve the impairment. Intraperitoneal injections of NMN (150 mg/kg) for 4 weeks improved scotopic and photopic retinal function and reduced photoreceptor death in Nampt $^{-rod/-rod}$ and Nampt $^{-cone/-cone}$ mice. Also, intraperitoneal injections of NMN (300 mg/kg) for 10 days were able to protect the retina from light-induced injury (Lin et al., 2016).

Mills et al. reported that long-term NMN administration ameliorated age-associated pathological changes in the eyes (Mills et al., 2016). The mutation in rd8 of C57BL/6N mice induced accumulation of subretinal microglia and macrophages with age, which was consistent with an increase in light-colored spots in the fundus of the eyes (Aredo et al., 2015; Mills et al., 2016). The C57BL/6N mice at 17 months of age showed several light-colored spots in the fundus. However, the spots were significantly reduced in the fundus of the aged mice, which were on a long-term NMN supplementation. The long-term supplementation prevented rod cell dysfunction and improved scotopic b and photopic b waves in aged C57BL/6N, which suggested that the function of Muller/bipolar cell and cone cell was enhanced by NMN supplementation (Mills et al., 2016). The functioning of the lacrimal gland in humans and rodents gradually decreases with age (Zoukhri, 2006). Notably, long-term NMN administration significantly increased tear production in aged mice (Mills et al., 2016).

The cornea is one of the most densely innervated tissues in the human body and corneal innervations play a critical role in the regulation of epithelial homeostasis (Bonini et al., 2003). Neurotrophic keratopathy, a degenerative corneal disease with an impairment of trigeminal nerve, shows corneal epithelial defects, ulcer, and even perforation (Bonini et al., 2003). Li et al. demonstrated that corneal denervation impaired the epithelial NAD $^{+}$ levels by reducing the expression of NAMPT. This process led to deactivation of SIRT1, pAKR, and pCREB, and caused the apoptosis of corneal epithelial cells (Li et al., 2019). NMN treatment significantly reduced the wound area and slowed down the corneal nerve fiber degeneration in the denervated mice. The supplement of NMN restored the activation levels of SIRT1, AKT, and CREB, and reversed the cell apoptosis and epithelial defects (Li et al., 2019). A recent study also reported that subconjunctival injection of NMN or other NAD $^{+}$ precursors effectively prevented ultraviolet B light (UVB)-induced tissue damage and EC apoptosis in the mouse cornea through reactivating AKT signaling (Zhao et al., 2020). These findings demonstrate that NMN could be a therapeutic agent for treating diverse diseases that are associated with blindness.

ACUTE KIDNEY INJURY (AKI)

Approximately 1.33 million people worldwide suffer from AKI every year, resulting in a substantial economic and social burden

on patients and society. The condition is associated with a high mortality rate exceeding 50% of those affected and the development of chronic kidney disease and other types of organ dysfunctions (Lewington et al., 2013). Aging is an independent risk factor for AKI (Kane-Gill et al., 2015), and various age-related factors contribute to the increased susceptibility to AKI (Fan et al., 2013), including diabetes, hypertension, vascular diseases, and some iatrogenic factors (Kane-Gill et al., 2015).

Studies have revealed that SIRT1 and SIRT3 are critical in protecting the kidney from injury (Fan et al., 2013; Morigi et al., 2015). Guan et al. reported that the administration of NMN could prevent age-associated susceptibility to AKI by restoring renal SIRT1 activity (Guan et al., 2017). The study found that kidneys of aged mice were more susceptible to cisplatin-induced AKI, and the NAD⁺ levels and SIRT1 expression were low in aged kidney. NAMPT and NMNAT were significantly lower in the kidney cortex of the old mice compared with those of the young mice. Four days of NMN treatment restored NAD⁺ levels in the kidneys and protected them from age-associated AKI. However, this protective effect of NMN was inhibited by SIRT1 deficiency, indicating that the renal protective effect of NMN was dependent on SIRT1. NMN treatment also protects the kidney from ischemia–reperfusion injury. Mice with NMN administration showed less ischemia–reperfusion injury and better kidney function compared with mice treated with PBS, which includes decreased blood urea nitrogen (BUN) and lower serum creatinine levels, and ameliorated tubular damage (Guan et al., 2017). Moreover, it has been shown that NMN could alleviate diabetic nephropathy nephritic fibrosis by inhibiting endogenous Nampt (Chen et al., 2017).

In conclusion, the findings of these studies show that NMN could be a potential therapeutic agent for AKI because of its ability to restore NAD⁺ and SIRT levels in the kidney.

ALCOHOLIC LIVER DISEASE

As the most common chronic liver disease, alcoholic liver disease (ALD) is caused by chronic alcohol consumption and can develop from alcoholic fatty liver (AFL) to alcoholic steatohepatitis (ASH) (Seitz et al., 2018). Ethanol-induced NAD⁺ depletion is involved in the development of ethanol-induced steatosis, oxidative stress, steatohepatitis, and insulin resistance (Luo et al., 2017). However, NMN treatment maintained the NAD⁺ levels and restored the alterations of TCA cycle metabolites that is induced by ethanol (Assiri et al., 2019). NMN also successfully prevented an ethanol-induced increase in plasma levels of alanine aminotransferase (ALT) and aspartate aminotransferase (AST), two damage biomarkers of liver. RNA-seq analysis revealed that ethanol changed the expression of 1778 genes, 25% of which were altered by NMN treatment (Assiri et al., 2019). The mitogen-activated protein kinases (MAPK) pathway was one of the signaling pathways that were significantly affected by NMN. Previous studies have demonstrated that activating transcription factor 3 (Atf3) is associated with NAD⁺/NADH ratios and can be induced by ethanol (Mohammadnia et al., 2015). Elevated Atf3 also correlated with increased ALT and

AST (Allen-Jennings et al., 2002). Moreover, Atf3 overexpression has been found in patients with alcoholic steatohepatitis (Mohammadnia et al., 2015). Interestingly, NMN normalized extracellular signal-regulated kinase1/2 (Erk1/2) signaling and reduced the expression of Atf3 (Assiri et al., 2019).

OTHER DISEASES AND IMPROVEMENT OF PHYSICAL FUNCTION

Associated with the loss of oocyte quality, reproductive aging in female mammals is an irreversible process that accompanies decreased levels of NAD⁺ (Bertoldo et al., 2020). However, administration of NMN can hopefully restore oocyte quality and fertility in aged mice and reverse the adverse effect of maternal age on developing embryo, suggesting that NMN can rescue female reproductive function in mammals (Bertoldo et al., 2020). Multigenerational obesity-induced perturbations in oocyte-secreted factor signal can also be normalized by NMN supplementation (Bertoldo et al., 2018). However, NMN does not protect the ovarian reserve from radiotherapy and chemotherapy, such as γ -irradiation or cyclophosphamide (Stringer et al., 2019).

Depression is a major mental health problem and has especially large effects on individual health and social burden. Previous studies have suggested that mitochondrial dysfunction and decreased ATP production contribute to depression (Allen et al., 2018). Recently, Xie et al. reported that in a corticosterone (CORT)-induced depressed mouse model, NMN could alleviate depression-like behaviors by improving mitochondrial energy metabolism via enhancing the activity of SIRT3 (Xie et al., 2020). Transcriptome and metabolome analysis demonstrated that NMN inhibited CORT-induced lipid synthesis, stimulated β -oxidation and glycolysis, and improved the TCA cycle to enhance ATP production in mitochondria.

Besides, NMN has also been reported to enhance skeletal muscle mitochondrial oxidative metabolism in aged mice (Gomes et al., 2013), improve hepatic mitochondrial function in circadian mutant mice (Peek et al., 2013), reduce DNA damage, and protect against irradiation-induced alterations in white blood cell counts, lymphocytes, and hemoglobin (Li et al., 2017). Recently, a study reported that NMN treatment improved mesenchymal stromal cells self-renewal with promoted osteogenesis and reduced adipogenesis via the SIRT1 pathway in aged and irradiated adult mice (Song et al., 2019). Moreover, NMN supplement can alleviate aluminum-induced bone injuries via suppression of the thioredoxin-interacting protein (TXNIP)–NLRP3 inflammasome pathway (Liang et al., 2019). These findings further demonstrate that NMN can be used to treat a variety of diseases involving NAD⁺ decline (Figure 4 and Table 1).

POSSIBLE DETRIMENTAL EFFECTS OF NMN SUPPLEMENTARY

Although the benefits of NMN are obvious, some studies suggest that people need to use it with caution. Keeping NMN at

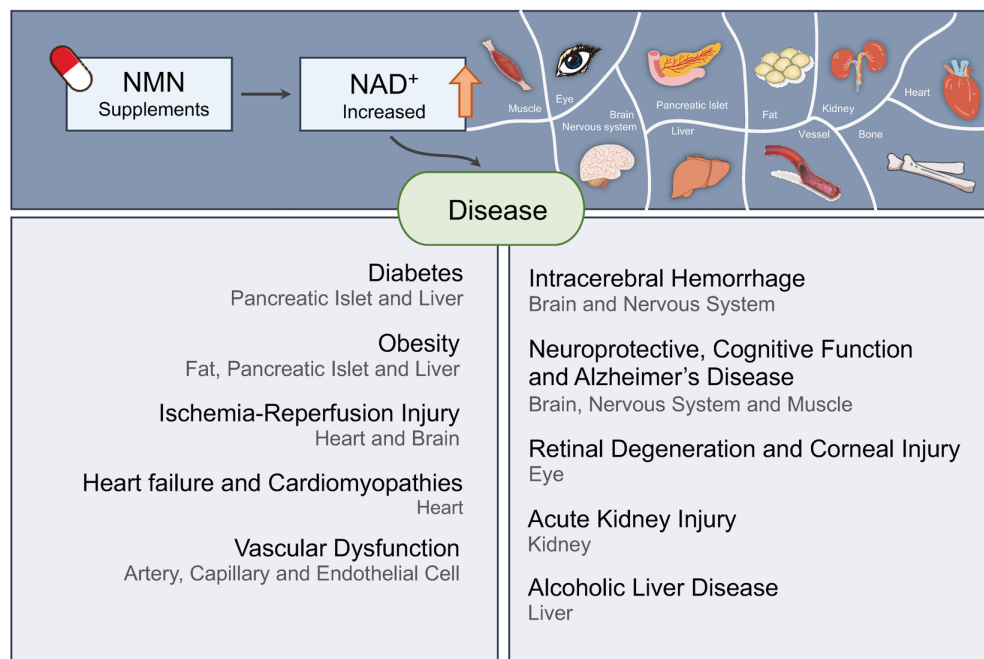


FIGURE 4 | Nicotinamide mononucleotide ameliorates various diseases by increasing NAD⁺ levels in human. NMN is a promising molecule for therapy of diverse diseases, including diabetes, obesity, ischemia–reperfusion injury, heart failure, Alzheimer's disease, retinal degeneration, acute kidney injury, and so on.

a low level was beneficial to the axon survival (Di Stefano et al., 2017). NMN accumulation could promote Wallerian or Wallerian-like degeneration, which was involved with the physical neurite injury. Inhibiting NAMPT or maintaining NMNAT activity could preserve the structure and function of the transected axons and the distal axon stump by preventing the increase of NMN. It is worth noting that since a long-term NAD⁺ depletion would become harmful for protection of axons, a time window of inhibiting the NMN accumulation was shown after the acute injury (Di Stefano et al., 2015). To decrease the level of NMN and maintain the production of NAD⁺, nicotinic acid riboside (NAR) was introduced in treating chemotherapy-induced axon degeneration by generating NAD⁺ through an alternative pathway that bypassed NMN formation (Liu et al., 2018).

It was reported that a lower dosage of NMN could be more effective and safer, for example, the brain may be more sensitive to the concentration of NMN (Park et al., 2016). A lower-dose administration of NMN resulted in improved female infertility with enhanced oocyte quality. Overdose of NMN may have some adverse effects on other aspects of fertility (Bertoldo et al., 2020). NMN administered by intraperitoneal injection increased oxidative stress of sperm and reduced sperm quality in male offspring of obese mothers with HFD, whereas oral administration of NMN did not have these effects (Youngson et al., 2019). These data indicated that the effects of NMN were complex and the therapeutic dose or mode of administration needs more investigation in the future.

Carefully, NAD turnover in tumor cells is higher than nontumor cells. The expression levels of NAMPT were found

to be elevated and have a positive relationship with the stage of tumor progression in many types of tumor, indicating that downregulation of NAMPT/NAD⁺ may become a strategy for anti-cancer therapy (Wang B. et al., 2011; Gujar et al., 2016). It is noteworthy that SIRT1, as downstream targets, has both tumor-suppressor and oncogenic roles under different circumstances (Chalkiadaki and Guarente, 2015). Thus, efficiency and long-term safety of NMN should be precisely assessed in further preclinical and clinical studies.

HUMAN CLINICAL STUDY

Given that NMN has shown high efficacy and benefits in various mouse models of human disease, several clinical trials of NMN have been conducted to investigate its clinical applicability (Table 2). This has led to some capsule formulations of NMN being approved and put on the market as health supplements (Poddar et al., 2019).

The first phase I human clinical study (UMIN000021309) for NMN has been initiated by an international collaborative team between Keio University School of Medicine in Tokyo and Washington University School of Medicine in St. Louis. The aim of this study is to examine the safety and bioavailability of NMN in human bodies. This research is led by Hiroshi Itoh, a professor of Endocrinology, Metabolism and Nephrology, Tokyo and Shin-ichiro Imai, a professor of Developmental Biology, at Washington University (Tsubota, 2016). Recently, they reported that a single oral administration of NMN up to 500 mg was safe and effectively metabolized in healthy subjects without causing severe adverse

TABLE 1 | Therapeutic effects of NMN administration *in vivo*.

Disease	Model	Intervention	Effects	References
Diabetes	Nampt-deficient heterozygous (Nampt +/−) mice	NMN (i.p. 500 mg/kg) Single	Improved the defects in NAD biosynthesis and glucose-stimulated insulin secretion	Revollo et al., 2007
	Adenoviral-mediated hepatic overexpression of miR-34a in mice	NMN (i.p. 500 mg/kg) 10 days	Improved glucose tolerance and increased expression of fatty acid β-oxidation genes	Choi et al., 2013
	Fructose-rich diet (FRD) mice	NMN (i.p. 500 mg/kg) Single	Improved insulin secretion and protected against inflammation	Caton et al., 2011
	High-fat diet (HFD)-induced and age-induced diabetic mice	NMN (i.p. 500 mg/kg) HFD-induced diabetes (7–10 days) aged-induced diabetes 11 days	Improved glucose tolerance and enhanced hepatic insulin sensitivity in HFD-induced diabetic mice. Improved glucose tolerance and lipid profiles in aged-induced diabetic mice	Yoshino et al., 2011
	C57BL/6N mice	NMN (drinking water. 100, 300 mg/kg) 12 months	Improved age-associated decreased insulin sensitivity and plasma metabolism	Mills et al., 2016
	Aged beta cell-specific Sirt1 overexpression (BESTO) mice	NMN (i.p. 500 mg/kg) Single	Improved glucose tolerance and insulin secretion in the aged BESTO females	Ramsey et al., 2008
Obesity	Adipocyte-specific Nampt knockout (ANKO) mice	NMN (drinking water. 500 mg/kg) 4–6 weeks	Improved multi-organ insulin sensitivity, increased adiponectin production and normalized plasma FFA concentrations	Stromsdorfer et al., 2016
	Adipocyte-specific Nampt knockout (ANKO) mice	NMN (drinking water. 500–1000 mg/kg) 8 weeks	Restored thermogenesis in ANKO mice, and normalized the expression of genes involved in thermogenesis, mitochondrial biogenesis, and FFA metabolism	Yamaguchi et al., 2019
	High-fat diet (HFD)-induced obese mice	NMN (i.p. 500 mg/kg) 17 days	Improved glucose tolerance, liver citrate synthase activity, and reduced liver triglyceride content	Uddin et al., 2016
	HFD-consuming offspring of obese mothers	NMN (i.p. 500 mg/kg) 18 days	Reduced adiposity and improved glucose tolerance and mitochondrial function	Uddin et al., 2017
Ischemia–reperfusion injury	C57BL/6N mice	NMN (drinking water. 100, 300 mg/kg) 12 months	Reduced age-associated body weight gain	Mills et al., 2016
	Ischemia/reperfusion heart injury in C57BL/6J mice	NMN (i.p. 500 mg/kg) Once or 4 times	Reduced the infarct area and improved left ventricle (LV) systolic function after I/R	Yamamoto et al., 2014
	Global cerebral ischemia in C57BL/6 mice	NMN (i.p. 31.25, 62.5, 125, 250, and 500 mg/kg) Single	Reduced hippocampal CA1 neurons cell death and improved ischemia-induced hippocampal dysfunction involved in spatial working memory (62.5 mg/kg produced optimal treatment effects)	Park et al., 2016
	Global cerebral ischemia in C57BL/6 mice	NMN (i.p. 62.5 mg/kg) Single	Prevented post-ischemic depletion of mitochondrial NAD ⁺ , suppressed mitochondrial fragmentation, and reduced ROS generation	Klimova et al., 2020
	Middle cerebral artery occlusion (MCAO) in Sprague-Dawley rats	NMN (i.c.v. 10 mg/ml with 2 μl) Single	Alleviated cerebral infarction size, neurological deficit, and neuronal cell death	Wang P. et al., 2011
	Middle cerebral artery occlusion (MCAO) in C57BL/6J mice	NMN (i.p. 500 mg/kg) 7 days with the first dose at 3 h (early) or 12 h (delayed) post MCAO	Alleviated brain infarction and neurological deficit, increased animal survival, and accelerated body weight recovery (early NMN administration). Improved post-ischemic regenerative neurogenesis (delayed NMN administration)	Zhao et al., 2015
Heart failure and cardiomyopathies	Cardiac-specific deletion of Ndufs4 (cKO) in mice	NMN (i.p. 500 mg/kg) twice in 3 days	Decreased the NADH/NAD ⁺ ratio and mitochondria protein acetylation in cKO hearts, and normalized the sensitivity of the mitochondria permeability transition pore (mPTP)	Karamanlidis et al., 2013
	Transverse aortic constriction (TAC)-stressed mice, cKO mice	NMN (i.p. 500 mg/kg) 33 days (every 3 days)	Suppressed mitochondrial protein hyperacetylation, improved cardiac function, and reduced pathologic hypertrophy induced by pressure overload	Lee et al., 2016
	TCA in cardiac-specific deficiency of Klf4 (CM-K4KO) mice	NMN (i.p. 500 mg/kg) 5 days	Protected mice from pressure overload-induced heart failure, prevented cell death, preserved mitochondrial ultrastructure and reduced ROS in heart	Zhang et al., 2017
	Cardiac-specific Fxn KO mice (FXN-KO) (Friedreich's ataxia cardiomyopathy model)	NMN (i.p. 500 mg/kg) 4–5 weeks (twice weekly)	Improved diastolic function, normalized the defective cardiac contractility, improved cardiac energy utilization and decreased energy wastage and whole-body energy expenditure in FXN-KO mice	Martin et al., 2017

(Continued)

TABLE 1 | Continued

Disease	Model	Intervention	Effects	References
Vascular dysfunction	Aged (26–28 months) C57Bl/6 mice	NMN (drinking water: 300 mg/kg) 8 weeks	Improved artery endothelium-dependent dilation (EDD) and NO-mediated EDD, reduced arterial oxidative stress and large elastic artery stiffness	de Picciotto et al., 2016
	Aged (24-month-old) C57BL/6 mice	NMN (i.p. 500 mg/kg) 14 days	Rescued neurovascular coupling (NVC) responses, and increased endothelial NO-mediated vasodilation	Tarantini et al., 2019
	Aged (24-month-old) C57BL/6 mice	NMN (i.p. 500 mg/kg) 14 days	Reversed age-related changes in miRNA expression profile in the aged mouse aorta	Kiss et al., 2019b
	Aged (24-month-old) C57BL/6 mice	NMN (i.p. 500 mg/kg) 14 days	Reversed age-related changes in neurovascular gene expression, including SIRT1 activation, mitochondrial protection, anti-inflammatory, and anti-apoptotic	Kiss et al., 2020
	Aged (18-month-old) C57BL/6J mice	NMN (drinking water: 400 mg/kg) 2 months	Improved blood flow and endurance in elderly mice by increasing capillary density	Das et al., 2018
Intracerebral hemorrhage	Collagenase-induced intracerebral hemorrhage (cICH) in CD1 mice	NMN (i.v. 300 mg/kg) Single (acute) NMN (i.v. and i.p. 300 mg/kg) 7 days (prolonged)	Relieved the edema, improved neurological function, reduced cell death and oxidative stress, and inhibited neuroinflammation in cICH. Promoted the recovery of body weight and neurological function (prolonged administration)	Wei et al., 2017b
	Hemorrhagic shock in Long-Evans rats	NMN (400 mg/kg) Pretreatment (drinking water) for 5 days and during resuscitation with once (i.v.)	Inhibited inflammation, improved cellular metabolism, and promoted survival following hemorrhagic shock.	Sims et al., 2018
	Tissue plasminogen activator (tPA)-treated CD1 mice with MCAO	NMN (i.p. 300 mg/kg) Single	Prevented delayed tPA-induced brain damage, cerebral hemorrhage, neural apoptosis, and neuroinflammation, and protected blood-brain barrier integrity	Wei et al., 2017a
Neuroprotective and cognitive function	C57BL/6N mice	NMN (drinking water, 100, 300 mg/kg) 12 months	Maintained the neural stem/progenitor cells (NSPCs) pool	Stein and Imai, 2014
	Aged (20-month-old) C57BL/6 mice	NMN (p.o. 300 mg/kg) 3 weeks	Improved cognitive hypersensitivity (age-related changes in sensory processing and emotionality) in old mice	Johnson et al., 2018
	Aged (24-month-old) C57BL/6 mice	NMN (i.p. 500 mg/kg) 14 days	Improved cognitive function in aged mice	Tarantini et al., 2019
	Aged (24-month-old) Wistar rats	NMN (i.p. 100 mg/kg) every other day for 28 days	Alleviated aging-induced cognitive impairment, improved learning and memory in aged animals	Hosseini et al., 2019a
	Projection-neuron-specific and inducible Nampt conditional knockout (Thy1-YFP-Nampt ^{-/-} cKO) mice	NMN (i.p. 400 mg/kg) Started on day 11 post- tamoxifen administration	Alleviated disease severity, restored motor function, and prolonged the lifespan	Wang et al., 2017
Alzheimer's disease	Thy1-YFP-Nampt ^{-/-} cKO mice	NMN (i.p. 400 mg/kg) 14 days	Reversed the detrimental effects on vesicle cycling, endplate morphology and muscle contractility	Lundt et al., 2020
	Ataxia-telangiectasia mutated (ATM)-deficient mice (Atm ^{-/-} mice) (Ataxia telangiectasia mouse model)	NMN (drinking water, 12 mM) 2 weeks	Restored deficit in motor function and improved memory in Atm ^{-/-} mice	Fang et al., 2016
	APP _(SWE) /PS1 _(ΔE9) double transgenic (AD-Tg) mice	NMN (s.c. 100 mg/kg) every other day for 28 days	Increased mitochondrial function and decreased amyloid precursor protein (APP) expression	Long et al., 2015
	C57BL/6 mice and neuron-specific expression of mitochondria-targeted enhanced yellow fluorescent protein (mito-eYFP) transgenic mice	NMN (i.p. 62.5 mg/kg) Single	Inhibited mitochondrial fission, decreased mitochondrial protein acetylation, and reduced ROS in the hippocampus	Klimova et al., 2019
	Intracerebroventricular infusion of Aβ _{1–42} oligomer in Wistar rats	NMN (i.p. 500 mg/kg) 10 days	Improved cognitive function	Wang et al., 2016

(Continued)

TABLE 1 | Continued

Disease	Model	Intervention	Effects	References
Retinal degeneration and corneal injury	APP _(SWE) /PS1 _(ΔE9) double transgenic (AD-Tg) mice	NMN (s.c. 100 mg/kg) every other day for 28 days	Improved cognitive abilities and decreased amyloid plaque, loss of synapse, β-secretase, and neuroinflammation	Yao et al., 2017
	Rod-specific Namp1 KO mice (Namp1 ^{rod/rod}) Cone-specific Namp1 KO mice (Namp1 ^{cone/cone}) Light-induced retinal dysfunction (129S1/SvImJ mice)	NMN (i.p. 150 mg/kg) 4 weeks for Namp1 ^{rod/rod} and Namp1 ^{cone/cone} mice NMN (i.p. 300 mg/kg) 10 days for 129S1/SvImJ mice	Prevented photoreceptor degeneration and improved vision in Namp1 ^{rod/rod} and Namp1 ^{cone/cone} mice. Protected the retina from light-induced injury in 129S1/SvImJ mice	Lin et al., 2016
	C57BL/6N mice	NMN (drinking water, 100, 300 mg/kg) 12 months	Ameliorated age-associated pathological changes in the eyes, and increased tear production in aged mice	Mills et al., 2016
	Corneal denervation in C57BL/6 mice	NMN (251 ng/eye) subconjunctival injection 2 days	Reduced wound area and slowed down the corneal nerve fibers degeneration in the denervated mice	Li et al., 2019
Acute kidney injury (AKI)	Ultraviolet B light (UVB)-induced injury in C57BL/6 mice	NMN (500 mM, 5 μl/eye) subconjunctival injection 2 days	Prevented ultraviolet B light (UVB)-induced tissue damage and endothelial cell apoptosis in the mouse cornea	Zhao et al., 2020
	Cisplatin-induced AKI or ischemia reperfusion injury in 129S2/Sv mice, and C57BL/6 mice	NMN (i.p. 500 mg/kg) 4 days	Protected renal function from cisplatin-induced AKI and ischemia reperfusion injury	Guan et al., 2017
Alcoholic liver disease (ALD)	Lieber–DeCarli chronic ethanol model in C57BL/6 J mice	NMN (i.p. 500 mg/kg) every other day for 6 weeks	Prevented an ethanol-induced increase in plasma alanine aminotransferase (ALT) and aspartate aminotransferase (AST), and changed the gene expression that were modulated by ethanol	Assiri et al., 2019
Other diseases	C57BL6/JAusb mice	NMN (drinking water, 0.5 and 2 g/L) for 4 weeks	Restored oocyte quality and enhanced ovulation rate and fertility in aged mice	Bertoldo et al., 2020
	HFD-consuming offspring of obese mothers	NMN (i.p. 500 mg/kg) 18 days	Ameliorated multigenerational obesity-induced perturbations in oocyte-secreted factor signal	Bertoldo et al., 2018
	Corticosterone (CORT)-induced depression in C57BL/6 mice	NMN (p.o. 300 mg/kg) 2 weeks	Alleviated depression-like behaviors	Xie et al., 2020
	C57BL/6J	NMN (i.p. 500 mg/kg) 7 days	Enhanced skeletal muscle mitochondrial oxidative metabolism in aged mice	Gomes et al., 2013
	Bmal1 KO mice	NMN (i.p. 250 mg/kg). Single NMN (i.p. 500 mg/kg) 10 days	Increased hepatic mitochondrial respiration	Peek et al., 2013
	Old C57BL/6J mice and young irradiated C57BL/6J mice	NMN (i.p. 500 mg/kg) 7 days. NMN (p.o. 2000 mg/kg) 8 days	Reduced DNA damage and protected against irradiation-induced changes in white blood cell counts, lymphocytes, and hemoglobin	Li et al., 2017
	Aged C57BL/6J (12-month-old) mice, and sublethal irradiation in adult (2-month-old) C57BL/6J mice	NMN (drinking water. 300 mg/kg) 3 months	Stimulated osteogenesis of endogenous mesenchymal stromal cells (MSCs), and protected bone from aging and irradiation induced damage in mice	Song et al., 2019
	AlCl ₃ -treated Sprague–Dawley rats	NMN (i.p. 20 mg/kg) 4 weeks	Alleviated aluminum-induced bone loss	Liang et al., 2019
	Brain cryoinjury in Balb/c mice	NMN (i.c.v. 5 mM with 7 μl) Single	Protected brain in both the early and the chronic phase of cryoinjury	Zhang et al., 2015
	Adipocyte-specific Namp1 knockout (ANKO) mice	NMN (i.p. 500 mg/kg) Single	Restored physical activity in ANKO mice	Yoon et al., 2015

IP, intraperitoneal; IV, intravenous; PO, per oral; SC, subcutaneous; ICV, intracerebroventricular.

TABLE 2 | Human clinical trials of NMN.

Molecule	Objectives	Subjects and sample size	Intervention	Study design	Region and Institute	Phase	Trial number
NMN	Evaluate the safety and kinetics of NMN in healthy volunteers	Healthy men 40–60 years (<i>n</i> = 10)	NMN P.O. single time	Non-randomized non-label uncontrolled	Keio University School of Medicine in Japan	I	UMIN000021309
NMN	Evaluate the safety and kinetics of long-term NMN and its effect on glucose metabolism in healthy volunteers.	Healthy men 40–60 years (<i>n</i> = 30)	NMN P.O. 8 weeks	Non-randomized non-label uncontrolled	Keio University School of Medicine in Japan.	II	UMIN000030609
NMN	Evaluate the effect of the dietary (NMN) on key cardiovascular and metabolic functions in healthy women.	Postmenopausal women pre-diabetic BMI 25.0–44.9 55–75 years (<i>n</i> = 25)	Placebo or 250 mg/day NMN P.O. 8 weeks	Randomized double-blinded placebo-controlled	Washington University School of Medicine in United States of America	Active, not recruiting	NCT03151239
NMN	Evaluate the safety and effect of long-term NMN on various hormonal levels in healthy human.	Healthy men and women 50–70 years (<i>n</i> = 20)	100 or 200 mg/day NMN P.O. 24 weeks	Randomized double-blinded dose comparison	Hiroshima University in Japan	Not applicable	UMIN000025739
NMN	Evaluate the effect of NMN on the body composition in the elder	Healthy men no smoking BMI 22–28 ~65 years (<i>n</i> = 42)	Placebo or 250 mg/day NMN P.O. 12 weeks	Randomized double-blind placebo-controlled	The University of Tokyo Hospital in Japan	Not applicable	UMIN000036321

events. The major final metabolites of NMN were significantly increased in a dose-dependent manner by NMN administration. However, the team failed to detect NMN in plasma samples in this study. In a further study, they will detect the levels of NMN in plasma and NAD⁺ in peripheral blood mononuclear cells (Irie et al., 2019).

Itoh is also conducting a phase II study (UMIN000030609) to assess the safety of long-term NMN in healthy subjects, the kinetics of NMN and metabolites of NAM, and the effect of daily administration of NMN on glucose metabolism. Other clinical trials of NMN are ongoing at Washington University to examine the effect of NMN on insulin sensitivity, endothelial function, blood lipids, body fat and liver fat, and fat tissue and muscle tissue markers of cardiovascular and metabolic health. Additionally, a study (UMIN000025739) has been initiated at Hiroshima University, Institute of Biomedical and Health Sciences to evaluate the effect of long-term oral administration of NMN on various hormones in healthy volunteers. Recently, a new clinical study (UMIN000036321) was initiated at the University of Tokyo Hospital to evaluate the effect of NMN oral administration on the body composition in elderly persons.

In summary, despite the tremendous research efforts aimed at exploiting the therapeutic potential of NMN to treat metabolic and aging-related diseases, the clinical and toxicological evidence to support its utility is currently insufficient (Poddar et al., 2019). Thus, further research is needed to increase the prospects of developing drugs based on NMN.

PERSPECTIVE

Among various NAD⁺ precursors, NMN and NR seem to increase NAD levels more effectively than NAM in rodents

(Rajman et al., 2018). Since NAM acts as a feedback inhibitor to suppress sirtuins and PARPs, the benefits of increase in NAD⁺ levels may be compromised (Bitterman et al., 2002). Additionally, because of the shorter resident time, high-dose administration, and some side effects of NAM, it was not the preferred choice compared with NMN and NR (Kawamura et al., 2016).

It is difficult to compare NMN with NR, both of which are subjected to first-pass metabolism and the quick conversion to other NAD⁺ intermediates before uptake *in vivo* (Frederick et al., 2016; Ratajczak et al., 2016). NR, instead of NMN, is unstable and quickly converted into NAM in murine plasma (Ratajczak et al., 2016). Some differences regarding the pharmacological effects of NMN and NR should be noted. As mentioned above, NMN improves cardiac function in a SIRT3-dependent manner in an FRDA cardiomyopathy model (Martin et al., 2017), whereas NR does not (Stram et al., 2017). Exploring the pharmacokinetics of NMN and NR *in vivo* could help determine the optimal concentration of them in different regions and facilitate understanding the mechanisms of their pharmacological actions. Head-to-head study should be performed to compare NMN and NR in the future.

Besides making a choice between NMN and NR, more precise data about the dosage and more detailed mechanism are needed. Some researches attempted to utilize novel methods to achieve integral understanding (Assiri et al., 2019; Kiss et al., 2020; Xie et al., 2020). In order to understand the complex NMN-related network changes, high-throughput methods are indispensable, such as methylation profiling, transcriptome, proteome, and metabolomics. In addition, the multifunctional role of NAD⁺ indicates that NAD⁺ might function in various organelles. It would be intriguing to decipher NAD⁺-related mechanism in subcellular compartment.

Further researches are compelling to reveal links between NAD⁺-related pathway and other disease-related pathway. More importantly, efficiency and safety should be precisely assessed in NMN clinical application.

CONCLUSION

NAD⁺ metabolism has been proven to be an essential part of biochemical reaction that acts as a link between various physiologic processes. During aging, weakened NAD⁺ biosynthesis and accelerated NAD⁺ consumption lead to dysfunction in multiple tissues. Depressed NAD⁺ levels disturb many biochemical processes, for instance, abnormal deacetylation activity of sirtuins. Downstream alterations of abnormal sirtuin activity include transcription pattern, mitochondrial permeability, mtROS production, and oxidative stress response. As an intermediate in NAD⁺ biosynthesis, NMN is a promising agent to reinforce NAD⁺ metabolism and alleviate age-related pathologic processes *in vivo*, which has promoted NMN to stage of clinical trial. More details of NAD⁺ metabolism

pathway and applications of NMN are fascinating for further researches.

AUTHOR CONTRIBUTIONS

WH wrote the initial manuscript. MH and ZZ created the figures. FM contributed writing material and new ideas. XW revised the manuscript and approved the final version. All authors read and approved the final manuscript.

FUNDING

This work was supported by the National Natural Science Foundation of China (No. 81602492), the National Key Research and Development Program of China (No. 2016YFA0201402), the National Major Scientific and Technological Special Project for “Significant New Drugs Development” (No. 2018ZX09733001), and the Excellent Youth Foundation of Sichuan Scientific Committee Grant in China (No. 2019JDJQ0008).

REFERENCES

- Allen, J., Romay-Tallon, R., Brymer, K. J., Caruncho, H. J., and Kalynchuk, L. E. (2018). Mitochondria and mood: mitochondrial dysfunction as a key player in the manifestation of depression. *Front. Neurosci.* 12:386. doi: 10.3389/fnins.2018.00386
- Allen-Jennings, A. E., Hartman, M. G., Kociba, G. J., and Hai, T. (2002). The roles of ATF3 in liver dysfunction and the regulation of phosphoenolpyruvate carboxykinase gene expression. *J. Biol. Chem.* 277, 20020–20025. doi: 10.1074/jbc.M200727200
- Aredo, B., Zhang, K., Chen, X., Wang, C. X., Li, T., and Ufret-Vincenty, R. L. (2015). Differences in the distribution, phenotype and gene expression of subretinal microglia/macrophages in C57BL/6N (Crb1 rd8/rd8) versus C57BL/6J (Crb1 wt/wt) mice. *J. Neuroinflammation* 12:6. doi: 10.1186/s12974-014-0221-4
- Artegiani, B., and Calegari, F. (2012). Age-related cognitive decline: can neural stem cells help us? *Aging* 4, 176–186. doi: 10.18632/aging.100446
- Assiri, M. A., Ali, H. R., Marentette, J. O., Yun, Y., Liu, J., Hirschey, M. D., et al. (2019). Investigating RNA expression profiles altered by nicotinamide mononucleotide therapy in a chronic model of alcoholic liver disease. *Hum. Genomics* 13:65. doi: 10.1186/s40246-019-0251-1
- Bachschmid, M. M., Schildknecht, S., Matsui, R., Zee, R., Haeussler, D., Cohen, R. A., et al. (2013). Vascular aging: chronic oxidative stress and impairment of redox signaling-consequences for vascular homeostasis and disease. *Ann. Med.* 45, 17–36. doi: 10.3109/07853890.2011.645498
- Bai, P., Canto, C., Oudart, H., Brunyanszki, A., Cen, Y., Thomas, C., et al. (2011). PARP-1 inhibition increases mitochondrial metabolism through SIRT1 activation. *Cell Metab.* 13, 461–468. doi: 10.1016/j.cmet.2011.03.004
- Balbi, M., Ghosh, M., Longden, T. A., Jatava Vega, M., Gesierich, B., Hellal, F., et al. (2015). Dysfunction of mouse cerebral arteries during early aging. *J. Cereb. Blood Flow Metab.* 35, 1445–1453. doi: 10.1038/jcbfm.2015.107
- Basu, R., Breda, E., Oberg, A. L., Powell, C. C., Dalla Man, C., Basu, A., et al. (2003). Mechanisms of the age-associated deterioration in glucose tolerance: contribution of alterations in insulin secretion, action, and clearance. *Diabetes Metab. Res. Rev.* 52, 1738–1748. doi: 10.2337/diabetes.52.7.1738
- Bertoldo, M. J., Listijono, D. R., Ho, W. J., Riepsamen, A. H., Goss, D. M., Richani, D., et al. (2020). NAD(+) repletion rescues female fertility during reproductive aging. *Cell Rep.* 30, 1670–1681.e7. doi: 10.1016/j.celrep.2020.01.058
- Bertoldo, M. J., Uddin, G. M., Youngson, N. A., Agapiou, D., Walters, K. A., Sinclair, D. A., et al. (2018). Multigenerational obesity-induced perturbations in oocyte-secreted factor signalling can be ameliorated by exercise and nicotinamide mononucleotide. *Hum. Reprod. Open* 2018:hoy010. doi: 10.1093/hropen/hoy010
- Bitterman, K. J., Anderson, R. M., Cohen, H. Y., Latorre-Esteves, M., and Sinclair, D. A. (2002). Inhibition of silencing and accelerated aging by nicotinamide, a putative negative regulator of yeast sir2 and human SIRT1. *J. Biol. Chem.* 277, 45099–45107. doi: 10.1074/jbc.M205670200
- Blanco, R., and Gerhardt, H. (2013). VEGF and Notch in tip and stalk cell selection. *Cold Spring Harb. Perspect. Med.* 3:a006569. doi: 10.1101/cshperspect.a006569
- Bonini, S., Rama, P., Olzi, D., and Lambiase, A. (2003). Neurotrophic keratitis. *Eye* 17, 989–995. doi: 10.1038/sj.eye.6700616
- Bordone, L., Motta, M. C., Picard, F., Robinson, A., Jhala, U. S., Apfeld, J., et al. (2006). Sirt1 regulates insulin secretion by repressing UCP2 in pancreatic beta cells. *PLoS Biol.* 4:e31. doi: 10.1371/journal.pbio.0040031
- Boslett, J., Hemann, C., Zhao, Y. J., Lee, H. C., and Zweier, J. L. (2017). Luteolinidin protects the postischemic heart through CD38 inhibition with preservation of NAD(P)(H). *J. Pharmacol. Exp. Ther.* 361, 99–108. doi: 10.1124/jpet.116.239459
- Broder, G., and Weil, M. H. (1964). Excess lactate: an index of reversibility of shock in human patients. *Science* 143, 1457–1459. doi: 10.1126/science.143.3613.1457
- Brunetti, L., Recinella, L., Di Nisio, C., Chiavaroli, A., Leone, S., Ferrante, C., et al. (2012). Effects of visfatin/PBEF/NAMPT on feeding behaviour and hypothalamic neuromodulators in the rat. *J. Biol. Regul. Homeost. Agents* 26, 295–302.
- Camacho-Pereira, J., Tarrago, M. G., Chini, C. C. S., Nin, V., Escande, C., Warner, G. M., et al. (2016). CD38 dictates age-related NAD decline and mitochondrial dysfunction through an SIRT3-dependent mechanism. *Cell Metab.* 23, 1127–1139. doi: 10.1016/j.cmet.2016.05.006
- Castillo-Laura, H., Santos, I. S., Quadros, L. C., and Matijasevich, A. (2015). Maternal obesity and offspring body composition by indirect methods: a systematic review and meta-analysis. *Cad. Saude. Publica* 31, 2073–2092. doi: 10.1590/0102-311x00159914
- Catalán, V., Gómez-Ambrosi, J., Rodríguez, A., Ramírez, B., Silva, C., Rotellar, F., et al. (2011). Association of increased visfatin/PBEF/NAMPT circulating concentrations and gene expression levels in peripheral blood cells with lipid metabolism and fatty liver in human morbid obesity. *Nutr. Metab. Cardiovasc. Dis.* 21, 245–253. doi: 10.1016/j.numecd.2009.09.008
- Caton, P. W., Kieswich, J., Yaqoob, M. M., Holness, M. J., and Sugden, M. C. (2011). Nicotinamide mononucleotide protects against pro-inflammatory cytokine-mediated impairment of mouse islet function. *Diabetologia* 54, 3083–3092. doi: 10.1007/s00125-011-2288-0

- Cavadini, G., Petrzilka, S., Kohler, P., Jud, C., Tobler, I., Birchler, T., et al. (2007). TNF- α suppresses the expression of clock genes by interfering with E-box-mediated transcription. *Proc. Natl. Acad. Sci. U.S.A.* 104, 12843–12848. doi: 10.1073/pnas.0701466104
- Chalkiadaki, A., and Guarente, L. (2012). High-fat diet triggers inflammation-induced cleavage of SIRT1 in adipose tissue to promote metabolic dysfunction. *Cell Metab.* 16, 180–188. doi: 10.1016/j.cmet.2012.07.003
- Chalkiadaki, A., and Guarente, L. (2015). The multifaceted functions of sirtuins in cancer. *Nat. Rev. Cancer* 15, 608–624. doi: 10.1038/nrc3985
- Chambon, P., Weill, J. D., and Mandel, P. (1963). Nicotinamide mononucleotide activation of new DNA-dependent polyadenylic acid synthesizing nuclear enzyme. *Biochem. Biophys. Res. Commun.* 11, 39–43. doi: 10.1016/0006-291x(63)90024-x
- Chen, Y., Liang, Y., Hu, T., Wei, R., Cai, C., Wang, P., et al. (2017). Endogenous Namp1 upregulation is associated with diabetic nephropathy inflammatory-fibrosis through the NF- κ B p65 and Sirt1 pathway; NMN alleviates diabetic nephropathy inflammatory-fibrosis by inhibiting endogenous Namp1. *Exp. Ther. Med.* 14, 4181–4193. doi: 10.3892/etm.2017.5098
- Chen, Y., Zhang, J., Lin, Y., Lei, Q., Guan, K. L., Zhao, S., et al. (2011). Tumour suppressor SIRT3 deacetylates and activates manganese superoxide dismutase to scavenge ROS. *EMBO Rep.* 12, 534–541. doi: 10.1038/embor.2011.65
- Chini, C. C. S., Tarrago, M. G., and Chini, E. N. (2017). NAD and the aging process: role in life, death and everything in between. *Mol. Cell. Endocrinol.* 455, 62–74. doi: 10.1016/j.mce.2016.11.003
- Choi, S. E., Fu, T., Seok, S., Kim, D. H., Yu, E., Lee, K. W., et al. (2013). Elevated microRNA-34a in obesity reduces NAD $^{+}$ levels and SIRT1 activity by directly targeting NAMPT. *Aging Cell* 12, 1062–1072. doi: 10.1111/ace.12135
- Cohen, M. V., Yang, X. M., and Downey, J. M. (2007). The pH hypothesis of postconditioning: staccato reperfusion reintroduces oxygen and perpetuates myocardial acidosis. *Circulation* 115, 1895–1903. doi: 10.1161/circulationaha.106.675710
- Colombo, A., Bastone, A., Ploia, C., Scip, A., Salmona, M., Forloni, G., et al. (2009). JNK regulates APP cleavage and degradation in a model of Alzheimer's disease. *Neurobiol. Dis.* 33, 518–525. doi: 10.1016/j.nbd.2008.12.014
- Costford, S. R., Bajpeyi, S., Pasarica, M., Albarado, D. C., Thomas, S. C., Xie, H., et al. (2010). Skeletal muscle NAMPT is induced by exercise in humans. *Am. J. Physiol. Endocrinol. Metab.* 298, E117–E126. doi: 10.1152/ajpendo.00318.2009
- Das, A., Huang, G. X., Bonkowski, M. S., Longchamp, A., Li, C., Schultz, M. B., et al. (2018). Impairment of an endothelial NAD $^{+}$ -H2S signaling network is a reversible cause of vascular aging. *Cell* 173, 74–89.e20. doi: 10.1016/j.cell.2018.02.008
- De Flora, A., Zocchi, E., Guida, L., Franco, L., and Bruzzzone, S. (2004). Autocrine and paracrine calcium signaling by the CD38/NAD $^{+}$ /cyclic ADP-ribose system. *Ann. N. Y. Acad. Sci.* 1028, 176–191. doi: 10.1196/annals.1322.021
- de Picciotto, N. E., Gano, L. B., Johnson, L. C., Martens, C. R., Sindler, A. L., Mills, K. F., et al. (2016). Nicotinamide mononucleotide supplementation reverses vascular dysfunction and oxidative stress with aging in mice. *Aging Cell* 15, 522–530. doi: 10.1111/ace.12461
- Di Stefano, M., Loreto, A., Orsomando, G., Mori, V., Zamporlini, F., Hulse, R. P., et al. (2017). NMN deamidase delays wallerian degeneration and rescues axonal defects caused by NMNAT2 deficiency in vivo. *Curr. Biol.* 27, 784–794. doi: 10.1016/j.cub.2017.01.070
- Di Stefano, M., Nascimento-Ferreira, I., Orsomando, G., Mori, V., Gilley, J., Brown, R., et al. (2015). A rise in NAD precursor nicotinamide mononucleotide (NMN) after injury promotes axon degeneration. *Cell Death. Differ.* 22, 731–742. doi: 10.1038/cdd.2014.164
- Diez, J. (2007). Arterial stiffness and extracellular matrix. *Adv. Cardiol.* 44, 76–95. doi: 10.1159/000096722
- Donato, A. J., Magerko, K. A., Lawson, B. R., Durrant, J. R., Lesniewski, L. A., and Seals, D. R. (2011). SIRT-1 and vascular endothelial dysfunction with ageing in mice and humans. *J. Physiol.* 589(Pt 18), 4545–4554. doi: 10.1113/jphysiol.2011.211219
- Dujardin, K. S., Tei, C., Yeo, T. C., Hodge, D. O., Rossi, A., and Seward, J. B. (1998). Prognostic value of a Doppler index combining systolic and diastolic performance in idiopathic-dilated cardiomyopathy. *Am. J. Cardiol.* 82, 1071–1076. doi: 10.1016/s0002-9149(98)00559-1
- Elrod, J. W., Wong, R., Mishra, S., Vagnozzi, R. J., Sakthivel, B., Goonasekera, S. A., et al. (2010). Cyclophilin D controls mitochondrial pore-dependent Ca $^{2+}$ exchange, metabolic flexibility, and propensity for heart failure in mice. *J. Clin. Invest.* 120, 3680–3687. doi: 10.1172/jci43171
- Escande, C., Nin, V., Price, N. L., Capellini, V., Gomes, A. P., Barbosa, M. T., et al. (2013). Flavonoid apigenin is an inhibitor of the NAD $^{+}$ ase CD38: implications for cellular NAD $^{+}$ metabolism, protein acetylation, and treatment of metabolic syndrome. *Diabetes Metab. Res. Rev.* 62, 1084–1093. doi: 10.2337/db12-1139
- Escobar-Henriques, M., and Anton, F. (2013). Mechanistic perspective of mitochondrial fusion: tubulation vs. fragmentation. *Biochim. Biophys. Acta* 1833, 162–175. doi: 10.1016/j.bbamcr.2012.07.016
- Essuman, K., Summers, D. W., Sasaki, Y., Mao, X., DiAntonio, A., and Milbrandt, J. (2017). The SARM1 Toll/Interleukin-1 receptor domain possesses intrinsic NAD $^{+}$ cleavage activity that promotes pathological axonal degeneration. *Neuron* 93, 1334–1343.e5. doi: 10.1016/j.neuron.2017.02.022
- Fan, H., Yang, H. C., You, L., Wang, Y. Y., He, W. J., and Hao, C. M. (2013). The histone deacetylase, SIRT1, contributes to the resistance of young mice to ischemia/reperfusion-induced acute kidney injury. *Kidney Int.* 83, 404–413. doi: 10.1038/ki.2012.394
- Fang, E. F., Kassahun, H., Croteau, D. L., Scheibye-Knudsen, M., Marosi, K., Lu, H., et al. (2016). NAD $^{+}$ replenishment improves lifespan and healthspan in ataxia telangiectasia models via mitophagy and DNA repair. *Cell Metab.* 24, 566–581. doi: 10.1016/j.cmet.2016.09.004
- Frederick, D. W., Loro, E., Liu, L., Davila, A. Jr., Chellappa, K., Silverman, I. M., et al. (2016). Loss of NAD homeostasis leads to progressive and reversible degeneration of skeletal muscle. *Cell Metab.* 24, 269–282. doi: 10.1016/j.cmet.2016.07.005
- Frye, R. A. (1999). Characterization of five human cDNAs with homology to the yeast SIR2 gene: Sir2-like proteins (sirtuins) metabolize NAD and may have protein ADP-ribosyltransferase activity. *Biochem. Biophys. Res. Commun.* 260, 273–279. doi: 10.1006/bbrc.1999.0897
- Fu, J., Jin, J., Cichewicz, R. H., Hageman, S. A., Ellis, T. K., Xiang, L., et al. (2012). trans-(-)-epsilon-Viniferin increases mitochondrial sirtuin 3 (SIRT3), activates AMP-activated protein kinase (AMPK), and protects cells in models of Huntington Disease. *J. Biol. Chem.* 287, 24460–24472. doi: 10.1074/jbc.M112.382226
- Gano, L. B., Donato, A. J., Pasha, H. M., Hearon, C. M. Jr., Sindler, A. L., and Seals, D. R. (2014). The SIRT1 activator SRT1720 reverses vascular endothelial dysfunction, excessive superoxide production, and inflammation with aging in mice. *Am. J. Physiol. Heart Circ. Physiol.* 307, H1754–H1763. doi: 10.1152/ajpheart.00377.2014
- Garten, A., Petzold, S., Barnikol-Oettler, A., Korner, A., Thasler, W. E., Kratzsch, J., et al. (2010). Nicotinamide phosphoribosyltransferase (NAMPT/PBEF/visfatin) is constitutively released from human hepatocytes. *Biochem. Biophys. Res. Commun.* 391, 376–381. doi: 10.1016/j.bbrc.2009.11.066
- Gerds, J., Brace, E. J., Sasaki, Y., DiAntonio, A., and Milbrandt, J. (2015). SARM1 activation triggers axon degeneration locally via NAD $^{+}$ destruction. *Science* 348, 453–457. doi: 10.1126/science.1258366
- Gitiaux, C., Blin-Rochemaure, N., Hully, M., Echaniz-Laguna, A., Calmels, N., Bahi-Buisson, N., et al. (2015). Progressive demyelinating neuropathy correlates with clinical severity in Cockayne syndrome. *Clin. Neurophysiol.* 126, 1435–1439. doi: 10.1016/j.clinph.2014.10.014
- Gohil, V. M., Sheth, S. A., Nilsson, R., Wojtovich, A. P., Lee, J. H., Perocchi, F., et al. (2010). Nutrient-sensitized screening for drugs that shift energy metabolism from mitochondrial respiration to glycolysis. *Nat. Biotechnol.* 28, 249–255. doi: 10.1038/nbt.1606
- Gomes, A. P., Price, N. L., Ling, A. J., Moslehi, J. J., Montgomery, M. K., Rajman, L., et al. (2013). Declining NAD $^{+}$ induces a pseudohypoxic state disrupting nuclear-mitochondrial communication during aging. *Cell* 155, 1624–1638. doi: 10.1016/j.cell.2013.11.037
- Gong, Y., Chang, L., Viola, K. L., Lacor, P. N., Lambert, M. P., Finch, C. E., et al. (2003). Alzheimer's disease-affected brain: presence of oligomeric A β ligands (ADDLs) suggests a molecular basis for reversible memory loss. *Proc. Natl. Acad. Sci. U.S.A.* 100, 10417–10422. doi: 10.1073/pnas.1834302100
- Griffiths, E. J., and Halestrap, A. P. (1995). Mitochondrial non-specific pores remain closed during cardiac ischaemia, but open upon reperfusion. *Biochem. J.* 307(Pt 1), 93–98. doi: 10.1042/bj3070093
- Grozio, A., Mills, K. F., Yoshino, J., Bruzzzone, S., Sociali, G., Tokizane, K., et al. (2019). Slc12a8 is a nicotinamide mononucleotide transporter. *Nat. Metab.* 1, 47–57. doi: 10.1038/s42255-018-0009-4

- Grozio, A., Sociali, G., Sturla, L., Caffa, I., Soncini, D., Salis, A., et al. (2013). CD73 protein as a source of extracellular precursors for sustained NAD⁺ biosynthesis in FK866-treated tumor cells. *J. Biol. Chem.* 288, 25938–25949. doi: 10.1074/jbc.M113.470435
- Guan, Y., Wang, S. R., Huang, X. Z., Xie, Q. H., Xu, Y. Y., Shang, D., et al. (2017). Nicotinamide mononucleotide, an NAD(+) precursor, rescues age-associated susceptibility to AKI in a sirtuin 1-Dependent manner. *J. Am. Soc. Nephrol.* 28, 2337–2352. doi: 10.1681/ASN.2016040385
- Guarani, V., DeFlorian, G., Franco, C. A., Kruger, M., Phng, L. K., Bentley, K., et al. (2011). Acetylation-dependent regulation of endothelial Notch signalling by the SIRT1 deacetylase. *Nature* 473, 234–238. doi: 10.1038/nature09917
- Guidi, I., Galimberti, D., Lonati, S., Novembrino, C., Bamonti, F., Tiriticco, M., et al. (2006). Oxidative imbalance in patients with mild cognitive impairment and Alzheimer's disease. *Neurobiol. Aging* 27, 262–269. doi: 10.1016/j.neurobiolaging.2005.01.001
- Gujar, A. D., Le, S., Mao, D. D., Dadey, D. Y. A., Turski, A., Sasaki, Y., et al. (2016). An NAD⁺-dependent transcriptional program governs self-renewal and radiation resistance in glioblastoma. *Proc. Natl. Acad. Sci. U.S.A.* 113, E8247–E8256. doi: 10.1073/pnas.1610921114
- Haider, D. G., Schaller, G., Kapiotis, S., Maier, C., Luger, A., and Wolzt, M. (2006). The release of the adipocytokine visfatin is regulated by glucose and insulin. *Diabetologia* 49, 1909–1914. doi: 10.1007/s00125-006-0303-7
- Harden, A., and Young, W. (1906). The alcoholic ferment of yeast-juice. Part II. The conferment of yeast-juice. *Proc. R. Soc. Lond. Ser. B* 78, 369–375. doi: 10.1098/rspb.1906.0070
- Hirschey, M. D., Shimazu, T., Goetzman, E., Jing, E., Schwer, B., Lombard, D. B., et al. (2010). SIRT3 regulates mitochondrial fatty-acid oxidation by reversible enzyme deacetylation. *Nature* 464, 121–125. doi: 10.1038/nature08778
- Hosseini, L., Farokhi-Sisakht, F., Badalzadeh, R., Khabbaz, A., Mahmoudi, J., and Sadigh-Eteghad, S. (2019a). Nicotinamide mononucleotide and melatonin alleviate aging-induced cognitive impairment via modulation of mitochondrial function and apoptosis in the prefrontal cortex and hippocampus. *Neuroscience* 423, 29–37. doi: 10.1016/j.neuroscience.2019.09.037
- Hosseini, L., Vafaee, M. S., and Badalzadeh, R. (2019b). Melatonin and nicotinamide mononucleotide attenuate myocardial ischemia/reperfusion injury via modulation of mitochondrial function and hemodynamic parameters in aged rats. *J. Cardiovasc. Pharmacol. Ther.* 25, 240–250. doi: 10.1177/1074248419882002
- Hroudova, J., Singh, N., and Fisar, Z. (2014). Mitochondrial dysfunctions in neurodegenerative diseases: relevance to Alzheimer's disease. *Biomed. Res. Int.* 2014:175062. doi: 10.1155/2014/175062
- Hsu, C. P., Oka, S., Shao, D., Hariharan, N., and Sadoshima, J. (2009). Nicotinamide phosphoribosyltransferase regulates cell survival through NAD⁺ synthesis in cardiac myocytes. *Circ. Res.* 105, 481–491. doi: 10.1161/CIRCRESAHA.109.203703
- Hsu, C. P., Zhai, P., Yamamoto, T., Maejima, Y., Matsushima, S., Hariharan, N., et al. (2010). Silent information regulator 1 protects the heart from ischemia/reperfusion. *Circulation* 122, 2170–2182. doi: 10.1161/CIRCULATIONAHA.110.958033
- Hsueh, Y. P. (2006). The role of the MAGUK protein CASK in neural development and synaptic function. *Curr. Med. Chem.* 13, 1915–1927. doi: 10.2174/092986706777585040
- Imai, S., Armstrong, C. M., Kaeblerlein, M., and Guarente, L. (2000). Transcriptional silencing and longevity protein Sir2 is an NAD-dependent histone deacetylase. *Nature* 403, 795–800. doi: 10.1038/35001622
- Imai, S., and Guarente, L. (2014). NAD⁺ and sirtuins in aging and disease. *Trends Cell Biol.* 24, 464–471. doi: 10.1016/j.tcb.2014.04.002
- Imai, S., and Yoshino, J. (2013). The importance of NAMPT/NAD/SIRT1 in the systemic regulation of metabolism and ageing. *Diabetes Obes. Metab.* 15(Suppl. 3), 26–33. doi: 10.1111/dom.12171
- Irie, J., Inagaki, E., Fujita, M., Nakaya, H., Mitsuishi, M., Yamaguchi, S., et al. (2019). Effect of oral administration of nicotinamide mononucleotide on clinical parameters and nicotinamide metabolite levels in healthy Japanese men. *Endocr. J.* 67, 153–160. doi: 10.1507/endocrj.EJ19-0313
- Jadasz, J., Aigner, L., Rivera, F. J., and Kury, P. (2012). The remyelination Philosopher's Stone: stem and progenitor cell therapies for multiple sclerosis. *Cell Tissue Res.* 349, 331–347. doi: 10.1007/s00441-012-1331-x
- Jeyifous, O., Waites, C. L., Specht, C. G., Fujisawa, S., Schubert, M., Lin, E. I., et al. (2009). SAP97 and CASK mediate sorting of NMDA receptors through a previously unknown secretory pathway. *Nat. Neurosci.* 12, 1011–1019. doi: 10.1038/nn.2362
- Jing, Z., Xing, J., Chen, X., Stetler, R. A., Weng, Z., Gan, Y., et al. (2014). Neuronal NAMPT is released after cerebral ischemia and protects against white matter injury. *J. Cereb. Blood Flow Metab.* 34, 1613–1621. doi: 10.1038/jcbfm.2014.119
- Johnson, S., Wozniak, D. F., and Imai, S. (2018). CA1 Nampt knockdown recapitulates hippocampal cognitive phenotypes in old mice which nicotinamide mononucleotide improves. *NPJ Aging Mech. Dis.* 4:10. doi: 10.1038/s41514-018-0029-z
- Jukarainen, S., Heinonen, S., Ramo, J. T., Rinnankoski-Tuikka, R., Rappou, E., Tummers, M., et al. (2016). Obesity is associated with low NAD(+)/SIRT pathway expression in adipose tissue of BMI-discordant monozygotic twins. *J. Clin. Endocrinol. Metab.* 101, 275–283. doi: 10.1210/jc.2015-3095
- Kadowaki, T., Yamauchi, T., Kubota, N., Hara, K., Ueki, K., and Tobe, K. (2006). Adiponectin and adiponectin receptors in insulin resistance, diabetes, and the metabolic syndrome. *J. Clin. Invest.* 116, 1784–1792. doi: 10.1172/jci29126
- Kane-Gill, S. L., Sileanu, F. E., Murugan, R., Trietley, G. S., Handler, S. M., and Kellum, J. A. (2015). Risk factors for acute kidney injury in older adults with critical illness: a retrospective cohort study. *Am. J. Kidney Dis.* 65, 860–869. doi: 10.1053/j.ajkd.2014.10.018
- Karamanlidis, G., Lee, C. F., Garcia-Menendez, L., Kolwicz, S. C. Jr., Suthammarak, W., Gong, G., et al. (2013). Mitochondrial complex I deficiency increases protein acetylation and accelerates heart failure. *Cell Metab.* 18, 239–250. doi: 10.1016/j.cmet.2013.07.002
- Kastrup, A., Groschel, K., Ringer, T. M., Redecker, C., Cordesmeier, R., Witte, O. W., et al. (2008). Early disruption of the blood-brain barrier after thrombolytic therapy predicts hemorrhage in patients with acute stroke. *Stroke* 39, 2385–2387. doi: 10.1161/strokeaha.107.505420
- Kawamura, T., Mori, N., and Shibata, K. (2016). β -Nicotinamide mononucleotide, an anti-aging candidate compound, is retained in the body for longer than nicotinamide in rats. *J. Nutr. Sci. Vitaminol.* 62, 272–276. doi: 10.3177/jnsv.6.2.272
- Kiss, T., Balasubramanian, P., Valcarcel-Ares, M. N., Tarantini, S., Yabluchanskiy, A., Csipo, T., et al. (2019a). Nicotinamide mononucleotide (NMN) treatment attenuates oxidative stress and rescues angiogenic capacity in aged cerebrovascular endothelial cells: a potential mechanism for the prevention of vascular cognitive impairment. *Geroscience* 41, 619–630. doi: 10.1007/s11357-019-00074-2
- Kiss, T., Giles, C. B., Tarantini, S., Yabluchanskiy, A., Balasubramanian, P., Gautam, T., et al. (2019b). Nicotinamide mononucleotide (NMN) supplementation promotes anti-aging miRNA expression profile in the aorta of aged mice, predicting epigenetic rejuvenation and anti-atherogenic effects. *Geroscience* 41, 419–439. doi: 10.1007/s11357-019-00095-x
- Kiss, T., Nyul-Toth, A., Balasubramanian, P., Tarantini, S., Ahire, C., Yabluchanskiy, A., et al. (2020). Nicotinamide mononucleotide (NMN) supplementation promotes neurovascular rejuvenation in aged mice: transcriptional footprint of SIRT1 activation, mitochondrial protection, anti-inflammatory, and anti-apoptotic effects. *Geroscience* doi: 10.1007/s11357-020-00165-5 [Epub ahead of print].
- Klimova, N., Fearnow, A., Long, A., and Kristian, T. (2020). NAD(+) precursor modulates post-ischemic mitochondrial fragmentation and reactive oxygen species generation via SIRT3 dependent mechanisms. *Exp. Neurol.* 325:113144. doi: 10.1016/j.expneurol.2019.113144
- Klimova, N., Long, A., and Kristian, T. (2019). Nicotinamide mononucleotide alters mitochondrial dynamics by SIRT3-dependent mechanism in male mice. *J. Neurosci. Res.* 97, 975–990. doi: 10.1002/jnr.24397
- Koenekoop, R. K., Wang, H., Majewski, J., Wang, X., Lopez, I., Ren, H., et al. (2012). Mutations in NMNAT1 cause leber congenital amaurosis and identify a new disease pathway for retinal degeneration. *Nat. Genet.* 44, 1035–1039. doi: 10.1038/ng.2356
- Kooragayala, K., Gotoh, N., Cogliati, T., Nellissery, J., Kaden, T. R., French, S., et al. (2015). Quantification of oxygen consumption in retina ex vivo demonstrates limited reserve capacity of photoreceptor mitochondria. *Invest. Ophthalmol. Vis. Sci.* 56, 8428–8436. doi: 10.1167/iov.15-17901
- Kristian, T., Bernardi, P., and Siesjö, B. K. (2001). Acidosis promotes the permeability transition in energized mitochondria: implications for

- reperfusion injury. *J. Neurotrauma* 18, 1059–1074. doi: 10.1089/08977150152693755
- LaNoue, K. F., and Williamson, J. R. (1971). Interrelationships between malate-aspartate shuttle and citric acid cycle in rat heart mitochondria. *Metabolism* 20, 119–140. doi: 10.1016/0026-0495(71)90087-4
- Le Couteur, D. G., and Lakatta, E. G. (2010). A vascular theory of aging. *J. Gerontol. A Biol. Sci. Med. Sci.* 65, 1025–1027. doi: 10.1093/gerona/gql135
- Lee, C. F., Chavez, J. D., Garcia-Menendez, L., Choi, Y., Roe, N. D., Chiao, Y. A., et al. (2016). Normalization of NAD⁺ redox balance as a therapy for heart failure. *Circulation* 134, 883–894. doi: 10.1161/CIRCULATIONAHA.116.022495
- Lee, J., and Kemper, J. K. (2010). Controlling SIRT1 expression by microRNAs in health and metabolic disease. *Aging* 2, 527–534. doi: 10.18632/aging.100184
- Lewington, A. J., Cerda, J., and Mehta, R. L. (2013). Raising awareness of acute kidney injury: a global perspective of a silent killer. *Kidney Int.* 84, 457–467. doi: 10.1038/ki.2013.153
- Li, J., Bonkowski, M. S., Moniot, S., Zhang, D., Hubbard, B. P., Ling, A. J., et al. (2017). A conserved NAD(+) binding pocket that regulates protein-protein interactions during aging. *Science* 355, 1312–1317. doi: 10.1126/science.aad8242
- Li, Y., Ma, X., Li, J., Yang, L., Zhao, X., Qi, X., et al. (2019). Corneal denervation causes epithelial apoptosis through inhibiting NAD⁺ biosynthesis. *Invest. Ophthalmol. Vis. Sci.* 60, 3538–3546. doi: 10.1167/iovs.19-26909
- Li, Y., Zhang, Y., Dorweiler, B., Cui, D., Wang, T., Woo, C. W., et al. (2008). Extracellular Nampt promotes macrophage survival via a nonenzymatic interleukin-6/STAT3 signaling mechanism. *J. Biol. Chem.* 283, 34833–34843. doi: 10.1074/jbc.M805866200
- Liang, H., Gao, J., Zhang, C., Li, C., Wang, Q., Fan, J., et al. (2019). Nicotinamide mononucleotide alleviates Aluminum induced bone loss by inhibiting the TXNIP-NLRP3 inflammasome. *Toxicol. Appl. Pharmacol.* 362, 20–27. doi: 10.1016/j.taap.2018.10.006
- Liao, X., Zhang, R., Lu, Y., Prosdocimo, D. A., Sangwung, P., Zhang, L., et al. (2015). Kruppel-like factor 4 is critical for transcriptional control of cardiac mitochondrial homeostasis. *J. Clin. Invest.* 125, 3461–3476. doi: 10.1172/jci79964
- Liao, Y. F., Wang, B. J., Cheng, H. T., Kuo, L. H., and Wolfe, M. S. (2004). Tumor necrosis factor- α , interleukin-1 β , and interferon- γ stimulate gamma-secretase-mediated cleavage of amyloid precursor protein through a JNK-dependent MAPK pathway. *J. Biol. Chem.* 279, 49523–49532. doi: 10.1074/jbc.M402034200
- Lin, J. B., Kubota, S., Ban, N., Yoshida, M., Santeford, A., Sene, A., et al. (2016). NAMPT-Mediated NAD(+) biosynthesis is essential for vision in mice. *Cell Rep.* 17, 69–85. doi: 10.1016/j.celrep.2016.08.073
- Liu, D., Pitta, M., and Mattson, M. P. (2008). Preventing NAD(+) depletion protects neurons against excitotoxicity: bioenergetic effects of mild mitochondrial uncoupling and caloric restriction. *Ann. N. Y. Acad. Sci.* 1147, 275–282. doi: 10.1196/annals.1427.028
- Liu, H.-W., Smith, C. B., Schmidt, M. S., Cambronne, X. A., Cohen, M. S., Migaud, M. E., et al. (2018). Pharmacological bypass of NAD(+) salvage pathway protects neurons from chemotherapy-induced degeneration. *Proc. Natl. Acad. Sci. U.S.A.* 115, 10654–10659. doi: 10.1073/pnas.1809392115
- Long, A. N., Owens, K., Schlappal, A. E., Kristian, T., Fishman, P. S., and Schuh, R. A. (2015). Effect of nicotinamide mononucleotide on brain mitochondrial respiratory deficits in an Alzheimer's disease-relevant murine model. *BMC Neurol.* 15:19. doi: 10.1186/s12883-015-0272-x
- Lu, L., Tang, L., Wei, W., Hong, Y., Chen, H., Ying, W., et al. (2014). Nicotinamide mononucleotide improves energy activity and survival rate in an in vitro model of Parkinson's disease. *Exp. Ther. Med.* 8, 943–950. doi: 10.3892/etm.2014.1842
- Lundt, S., Zhang, N., Wang, X., Polo-Parada, L., and Ding, S. (2020). The effect of NAMPT deletion in projection neurons on the function and structure of neuromuscular junction (NMJ) in mice. *Sci. Rep.* 10:99. doi: 10.1038/s41598-019-57085-4
- Luo, G., Huang, B., Qiu, X., Xiao, L., Wang, N., Gao, Q., et al. (2017). Resveratrol attenuates excessive ethanol exposure induced insulin resistance in rats via improving NAD(+)/NADH ratio. *Mol. Nutr. Food Res.* 61:1700087. doi: 10.1002/mnfr.201700087
- Malik, V. S., Popkin, B. M., Bray, G. A., Despres, J. P., Willett, W. C., and Hu, F. B. (2010). Sugar-sweetened beverages and risk of metabolic syndrome and type 2 diabetes: a meta-analysis. *Diabetes Care* 33, 2477–2483. doi: 10.2337/dc10-1079
- Martin, A. S., Abraham, D. M., Hershberger, K. A., Bhatt, D. P., Mao, L., Cui, H., et al. (2017). Nicotinamide mononucleotide requires SIRT3 to improve cardiac function and bioenergetics in a Friedreich's ataxia cardiomyopathy model. *JCI Insight* 2:93885. doi: 10.1172/jci.insight.93885
- Mehan, S., Meena, H., Sharma, D., and Sankhla, R. (2011). JNK: a stress-activated protein kinase therapeutic strategies and involvement in Alzheimer's and various neurodegenerative abnormalities. *J. Mol. Neurosci.* 43, 376–390. doi: 10.1007/s12031-010-9454-6
- Mills, K. F., Yoshida, S., Stein, L. R., Grozio, A., Kubota, S., Sasaki, Y., et al. (2016). Long-term administration of nicotinamide mononucleotide mitigates age-associated physiological decline in mice. *Cell Metab.* 24, 795–806. doi: 10.1016/j.cmet.2016.09.013
- Mitchell, G. F. (2014). Arterial stiffness and hypertension. *Hypertension* 64, 13–18. doi: 10.1161/hypertensionaha.114.00921
- Mohammadnia, A., Yaqubi, M., and Fallahi, H. (2015). Predicting transcription factors in human alcoholic hepatitis from gene regulatory network. *Eur. Rev. Med. Pharmacol. Sci.* 19, 2246–2253.
- Moller, N., Gormsen, L., Fuglsang, J., and Gjedsted, J. (2003). Effects of ageing on insulin secretion and action. *Horm. Res.* 60(Suppl. 1), 102–104. doi: 10.1159/000071233
- Morales, I., Guzman-Martinez, L., Cerda-Troncoso, C., Farias, G. A., and Maccioni, R. B. (2014). Neuroinflammation in the pathogenesis of Alzheimer's disease. A rational framework for the search of novel therapeutic approaches. *Front. Cell. Neurosci.* 8:112. doi: 10.3389/fncel.2014.00112
- Morigi, M., Perico, L., Rota, C., Longaretti, L., Conti, S., Rottoli, D., et al. (2015). Sirtuin 3-dependent mitochondrial dynamic improvements protect against acute kidney injury. *J. Clin. Invest.* 125, 715–726. doi: 10.1172/JCI77632
- Mouchiroud, L., Houtkooper, R. H., Moulhan, N., Katsyuba, E., Ryu, D., Canto, C., et al. (2013). The NAD(+) /Sirtuin pathway modulates longevity through activation of mitochondrial UPR and FOXO signaling. *Cell* 154, 430–441. doi: 10.1016/j.cell.2013.06.016
- Moynihan, K. A., Grimm, A. A., Plueger, M. M., Bernal-Mizrachi, E., Ford, E., Cras-Meneur, C., et al. (2005). Increased dosage of mammalian Sir2 in pancreatic beta cells enhances glucose-stimulated insulin secretion in mice. *Cell Metab.* 2, 105–117. doi: 10.1016/j.cmet.2005.07.001
- Myroie, H., Dumont, O., Bauer, A., Thornton, C. C., Mackey, J., Calay, D., et al. (2015). PKCepsilon-CREB-Nrf2 signalling induces HO-1 in the vascular endothelium and enhances resistance to inflammation and apoptosis. *Cardiovasc. Res.* 106, 509–519. doi: 10.1093/cvr/cvv131
- Nadtochiy, S. M., Wang, Y. T., Nehrke, K., Munger, J., and Brookes, P. S. (2018). Cardioprotection by nicotinamide mononucleotide (NMN): involvement of glycolysis and acidic pH. *J. Mol. Cell Cardiol.* 121, 155–162. doi: 10.1016/j.jymcc.2018.06.007
- Nielsen, K. N., Peics, J., Ma, T., Karavaeva, I., Dall, M., Chubanava, S., et al. (2018). NAMPT-mediated NAD(+) biosynthesis is indispensable for adipose tissue plasticity and development of obesity. *Mol. Metab.* 11, 178–188. doi: 10.1016/j.molmet.2018.02.014
- Nikiforov, A., Dolle, C., Niere, M., and Ziegler, M. (2011). Pathways and subcellular compartmentation of NAD biosynthesis in human cells: from entry of extracellular precursors to mitochondrial NAD generation. *J. Biol. Chem.* 286, 21767–21778. doi: 10.1074/jbc.M110.213298
- Okabe, K., Yaku, K., Tobe, K., and Nakagawa, T. (2019). Implications of altered NAD metabolism in metabolic disorders. *J. Biomed. Sci.* 26:34. doi: 10.1186/s12929-019-0527-8
- Park, J. H., Long, A., Owens, K., and Kristian, T. (2016). Nicotinamide mononucleotide inhibits post-ischemic NAD(+) degradation and dramatically ameliorates brain damage following global cerebral ischemia. *Neurobiol. Dis.* 95, 102–110. doi: 10.1016/j.nbd.2016.07.018
- Peek, C. B., Affinati, A. H., Ramsey, K. M., Kuo, H. Y., Yu, W., Sena, L. A., et al. (2013). Circadian clock NAD⁺ cycle drives mitochondrial oxidative metabolism in mice. *Science* 342:1243417. doi: 10.1126/science.1243417
- Pillai, J. B., Isbatan, A., Imai, S., and Gupta, M. P. (2005). Poly(ADP-ribose) polymerase-1-dependent cardiac myocyte cell death during heart failure is mediated by NAD⁺ depletion and reduced Sir2alpha deacetylase activity. *J. Biol. Chem.* 280, 43121–43130. doi: 10.1074/jbc.M506162200

- Pillai, V. B., Sundaresan, N. R., Kim, G., Samant, S., Moreno-Vinasco, L., Garcia, J. G. N., et al. (2013). Nampt secreted from cardiomyocytes promotes development of cardiac hypertrophy and adverse ventricular remodeling. *Am. J. Physiol. Heart Circ. Physiol.* 304, H415–H426. doi: 10.1152/ajpheart.00468.2012
- Poddar, S. K., Sifat, A. E., Haque, S., Nahid, N. A., Chowdhury, S., and Mehedi, I. (2019). Nicotinamide mononucleotide: exploration of diverse therapeutic applications of a potential molecule. *Biomolecules* 9:34. doi: 10.3390/biom9010034
- Preiss, J., and Handler, P. (1958). Biosynthesis of diphosphopyridine nucleotide. I. Identification of intermediates. *J. Biol. Chem.* 233, 488–492.
- Preugschat, F., Carter, L. H., Boros, E. E., Porter, D. J., Stewart, E. L., and Shewchuk, L. M. (2014). A pre-steady state and steady state kinetic analysis of the N-ribosyl hydrolase activity of hCD157. *Arch. Biochem. Biophys.* 564, 156–163. doi: 10.1016/j.abb.2014.09.008
- Prior, S. J., Ryan, A. S., Blumenthal, J. B., Watson, J. M., Katzel, L. I., and Goldberg, A. P. (2016). Sarcopenia is associated with lower skeletal muscle capillarization and exercise capacity in older adults. *J. Gerontol. A Biol. Sci. Med. Sci.* 71, 1096–1101. doi: 10.1093/gerona/glw017
- Qin, W., Yang, T., Ho, L., Zhao, Z., Wang, J., Chen, L., et al. (2006). Neuronal SIRT1 activation as a novel mechanism underlying the prevention of Alzheimer disease amyloid neuropathology by calorie restriction. *J. Biol. Chem.* 281, 21745–21754. doi: 10.1074/jbc.M602909200
- Rajman, L., Chwalek, K., and Sinclair, D. A. (2018). Therapeutic potential of NAD-Boosting molecules: the in vivo evidence. *Cell Metab.* 27, 529–547. doi: 10.1016/j.cmet.2018.02.011
- Ramsey, K. M., Mills, K. F., Satoh, A., and Imai, S. (2008). Age-associated loss of Sirt1-mediated enhancement of glucose-stimulated insulin secretion in beta cell-specific Sirt1-overexpressing (BESTO) mice. *Aging Cell* 7, 78–88. doi: 10.1111/j.1474-9726.2007.00355.x
- Ratajczak, J., Joffraud, M., Trammell, S. A., Ras, R., Canela, N., Boutant, M., et al. (2016). NRK1 controls nicotinamide mononucleotide and nicotinamide riboside metabolism in mammalian cells. *Nat. Commun.* 7:13103. doi: 10.1038/ncomms13103
- Reaven, G. M. (1988). Banting lecture 1988. Role of insulin resistance in human disease. *Diabetes* 37, 1595–1607. doi: 10.2337/diab.37.12.1595
- Regier, D. A., Boyd, J. H., Burke, J. D. Jr., Rae, D. S., Myers, J. K., Kramer, M., et al. (1988). One-month prevalence of mental disorders in the United States. Based on five epidemiologic catchment area sites. *Arch. Gen. Psychiatry* 45, 977–986. doi: 10.1001/archpsyc.1988.01800350011002
- Rempe, R. G., Hartz, A. M. S., and Bauer, B. (2016). Matrix metalloproteinases in the brain and blood-brain barrier: versatile breakers and makers. *J. Cereb. Blood Flow Metab.* 36, 1481–1507. doi: 10.1177/0271678x16655551
- Revollo, J. R., Korner, A., Mills, K. F., Satoh, A., Wang, T., Garten, A., et al. (2007). Nampt/PBEF/Visfatin regulates insulin secretion in beta cells as a systemic NAD biosynthetic enzyme. *Cell Metab.* 6, 363–375. doi: 10.1016/j.cmet.2007.09.003
- Rixen, D., and Siegel, J. H. (2005). Bench-to-bedside review: oxygen debt and its metabolic correlates as quantifiers of the severity of hemorrhagic and post-traumatic shock. *Crit. Care* 9, 441–453. doi: 10.1186/cc3526
- Roncal-Jimenez, C. A., Lanaspas, M. A., Rivard, C. J., Nakagawa, T., Sanchez-Lozada, L. G., Jalal, D., et al. (2011). Sucrose induces fatty liver and pancreatic inflammation in male breeder rats independent of excess energy intake. *Metabolism* 60, 1259–1270. doi: 10.1016/j.metabol.2011.01.008
- Ross, R., Hudson, R., Stotz, P. J., and Lam, M. (2015). Effects of exercise amount and intensity on abdominal obesity and glucose tolerance in obese adults: a randomized trial. *Ann. Intern. Med.* 162, 325–334. doi: 10.7326/m14-1189
- Salter, M., Beams, R. M., Critchley, M. A., Hodson, H. F., Iyer, R., Knowles, R. G., et al. (1991). Effects of tryptophan 2,3-dioxygenase inhibitors in the rat. *Adv. Exp. Med. Biol.* 294, 281–288. doi: 10.1007/978-1-4684-5952-4_25
- Sanada, S., Komuro, I., and Kitakaze, M. (2011). Pathophysiology of myocardial reperfusion injury: preconditioning, postconditioning, and translational aspects of protective measures. *Am. J. Physiol. Heart Circ. Physiol.* 301, H1723–H1741. doi: 10.1152/ajpheart.00553.2011
- Sayers, S. R., Beavil, R. L., Fine, N. H. F., Huang, G. C., Choudhary, P., Pacholarz, K. J., et al. (2020). Structure-functional changes in eNAMPT at high concentrations mediate mouse and human beta cell dysfunction in type 2 diabetes. *Diabetologia* 63, 313–323. doi: 10.1007/s00125-019-05029-y
- Scheibye-Knudsen, M., Mitchell, S. J., Fang, E. F., Iyama, T., Ward, T., Wang, J., et al. (2014). A high-fat diet and NAD(+) activate Sirt1 to rescue premature aging in cockayne syndrome. *Cell Metab.* 20, 840–855. doi: 10.1016/j.cmet.2014.10.005
- Seals, D. R., Kaplon, R. E., Gioscia-Ryan, R. A., and LaRocca, T. J. (2014). You're only as old as your arteries: translational strategies for preserving vascular endothelial function with aging. *Physiology* 29, 250–264. doi: 10.1152/physiol.00059.2013
- Seitz, H. K., Bataller, R., Cortez-Pinto, H., Gao, B., Gual, A., Lackner, C., et al. (2018). Alcoholic liver disease. *Nat. Rev. Dis. Primers* 4:16. doi: 10.1038/s41572-018-0014-7
- Sims, C. A., Guan, Y., Mukherjee, S., Singh, K., Botolin, P., Davila, A., et al. (2018). Nicotinamide mononucleotide preserves mitochondrial function and increases survival in hemorrhagic shock. *JCI Insight* 3:e120182. doi: 10.1172/jci.insight.120182
- Song, J., Li, J., Yang, F., Ning, G., Zhen, L., Wu, L., et al. (2019). Nicotinamide mononucleotide promotes osteogenesis and reduces adipogenesis by regulating mesenchymal stromal cells via the SIRT1 pathway in aged bone marrow. *Cell Death Dis.* 10:336. doi: 10.1038/s41419-019-1569-2
- Sozzani, S., Del Prete, A., Bonocchi, R., and Locati, M. (2015). Chemokines as effector and target molecules in vascular biology. *Cardiovasc. Res.* 107, 364–372. doi: 10.1093/cvr/cvv150
- Springo, Z., Tarantini, S., Toth, P., Tucsek, Z., Koller, A., Sonntag, W. E., et al. (2015). Aging exacerbates pressure-induced mitochondrial oxidative stress in mouse cerebral arteries. *J. Gerontol. A Biol. Sci. Med. Sci.* 70, 1355–1359. doi: 10.1093/gerona/glu244
- Stanley, W. C., Recchia, F. A., and Lopaschuk, G. D. (2005). Myocardial substrate metabolism in the normal and failing heart. *Physiol. Rev.* 85, 1093–1129. doi: 10.1152/physrev.00006.2004
- Stein, L. R., and Imai, S. (2014). Specific ablation of Nampt in adult neural stem cells recapitulates their functional defects during aging. *EMBO J.* 33, 1321–1340. doi: 10.1002/emboj.201386917
- Stensballe, J., Christiansen, M., Tonnesen, E., Espersen, K., Lippert, F. K., and Rasmussen, L. S. (2009). The early IL-6 and IL-10 response in trauma is correlated with injury severity and mortality. *Acta Anaesthesiol. Scand.* 53, 515–521. doi: 10.1111/j.1399-6576.2008.01801.x
- Stram, A. R., Pride, P. M., and Payne, R. M. (2017). NAD+ replacement therapy with nicotinamide riboside does not improve cardiac function in a model of mitochondrial heart disease. *FASEB J* 31, 602–602.615. doi: 10.1096/fasebj.31.1_supplement.602.15
- Stringer, J., Groenewegen, E., Liew, S. H., and Hutt, K. J. (2019). Nicotinamide mononucleotide does not protect the ovarian reserve from cancer treatments. *Reproduction* doi: 10.1530/rep-19-0337 [Epub ahead of print].
- Stromsdorfer, K. L., Yamaguchi, S., Yoon, M. J., Moseley, A. C., Franczyk, M. P., Kelly, S. C., et al. (2016). NAMPT-Mediated NAD(+) biosynthesis in adipocytes regulates adipose tissue function and multi-organ insulin sensitivity in mice. *Cell Rep.* 16, 1851–1860. doi: 10.1016/j.celrep.2016.07.027
- Strosznajder, R. P., Gadamski, R., Czapski, G. A., Jesko, H., and Strosznajder, J. B. (2003). Poly(ADP-ribose) polymerase during reperfusion after transient forebrain ischemia: its role in brain edema and cell death. *J. Mol. Neurosci.* 20, 61–72. doi: 10.1385/jmn:20:1:61
- Suga, H. (1990). Ventricular energetics. *Physiol. Rev.* 70, 247–277. doi: 10.1152/physrev.1990.70.2.247
- Tanaka, M., Nozaki, M., Fukuhara, A., Segawa, K., Aoki, N., Matsuda, M., et al. (2007). Visfatin is released from 3T3-L1 adipocytes via a non-classical pathway. *Biochem. Biophys. Res. Commun.* 359, 194–201. doi: 10.1016/j.bbrc.2007.05.096
- Tarantini, S., Tran, C. H. T., Gordon, G. R., Ungvari, Z., and Csiszar, A. (2017). Impaired neurovascular coupling in aging and Alzheimer's disease: contribution of astrocyte dysfunction and endothelial impairment to cognitive decline. *Exp. Gerontol.* 94, 52–58. doi: 10.1016/j.exger.2016.11.004
- Tarantini, S., Valcarcel-Ares, M. N., Toth, P., Yabluchanskiy, A., Tucsek, Z., Kiss, T., et al. (2019). Nicotinamide mononucleotide (NMN) supplementation rescues cerebrovascular endothelial function and neurovascular coupling responses and improves cognitive function in aged mice. *Redox Biol.* 24:101192. doi: 10.1016/j.redox.2019.101192

- Tesla, R., Wolf, H. P., Xu, P., Drawbridge, J., Estill, S. J., Huntington, P., et al. (2012). Neuroprotective efficacy of aminopropyl carbazoles in a mouse model of amyotrophic lateral sclerosis. *Proc. Natl. Acad. Sci. U.S.A.* 109, 17016–17021. doi: 10.1073/pnas.1213960109
- Toth, P., Tarantini, S., Tucek, Z., Ashpole, N. M., Sosnowska, D., Gautam, T., et al. (2014). Resveratrol treatment rescues neurovascular coupling in aged mice: role of improved cerebrovascular endothelial function and downregulation of NADPH oxidase. *Am. J. Physiol. Heart Circ. Physiol.* 306, H299–H308. doi: 10.1152/ajpheart.00744.2013
- Tsubota, K. (2016). The first human clinical study for NMN has started in Japan. *NPJ Aging Mech. Dis.* 2:16021. doi: 10.1038/npjamd.2016.21
- Uddin, G. M., Youngson, N. A., Doyle, B. M., Sinclair, D. A., and Morris, M. J. (2017). Nicotinamide mononucleotide (NMN) supplementation ameliorates the impact of maternal obesity in mice: comparison with exercise. *Sci. Rep.* 7:15063. doi: 10.1038/s41598-017-14866-z
- Uddin, G. M., Youngson, N. A., Sinclair, D. A., and Morris, M. J. (2016). Head to head comparison of short-term treatment with the NAD(+) precursor nicotinamide mononucleotide (NMN) and 6 weeks of exercise in obese female mice. *Front. Pharmacol.* 7:258. doi: 10.3389/fphar.2016.00258
- Vieira, V. J., Valentine, R. J., Wilund, K. R., Antao, N., Baynard, T., and Woods, J. A. (2009). Effects of exercise and low-fat diet on adipose tissue inflammation and metabolic complications in obese mice. *Am. J. Physiol. Endocrinol. Metab.* 296, E1164–E1171. doi: 10.1152/ajpendo.00054.2009
- von Euler, H., and Myrback, K. (1930). Co-zynase, XVII. *Hoppe Seylers Zeitschrift Fur Physiologische Chemie* 190, 93–100. doi: 10.1515/bchm2.1930.190.3-6.93
- Walley, K. R. (2016). Left ventricular function: time-varying elastance and left ventricular aortic coupling. *Crit. Care* 20:270. doi: 10.1186/s13054-016-1439-6
- Wang, B., Hasan, M. K., Alvarado, E., Yuan, H., Wu, H., and Chen, W. Y. (2011). NAMPT overexpression in prostate cancer and its contribution to tumor cell survival and stress response. *Oncogene* 30, 907–921. doi: 10.1038/ncr.2010.468
- Wang, P., Xu, T.-Y., Guan, Y.-F., Tian, W.-W., Viollet, B., Rui, Y.-C., et al. (2011). Nicotinamide phosphoribosyltransferase protects against ischemic stroke through SIRT1-dependent adenosine monophosphate-activated kinase pathway. *Ann. Neurol.* 69, 360–374. doi: 10.1002/ana.22236
- Wang, H., Listrat, A., Meunier, B., Gueugneau, M., Coudy-Gandilhon, C., Combaret, L., et al. (2014). Apoptosis in capillary endothelial cells in ageing skeletal muscle. *Aging Cell* 13, 254–262. doi: 10.1111/accel.12169
- Wang, X., Hu, X., Yang, Y., Takata, T., and Sakurai, T. (2016). Nicotinamide mononucleotide protects against beta-amyloid oligomer-induced cognitive impairment and neuronal death. *Brain Res.* 1643, 1–9. doi: 10.1016/j.brainres.2016.04.060
- Wang, X., Zhang, Q., Bao, R., Zhang, N., Wang, Y., Polo-Parada, L., et al. (2017). Deletion of nampt in projection neurons of adult mice leads to motor dysfunction, neurodegeneration, and death. *Cell Rep.* 20, 2184–2200. doi: 10.1016/j.celrep.2017.08.022
- Warburg, O., and Christian, W. (1936). Pyridine, the hydrogen transferring element of fermentation enzymes. (*Pyridine-nucleotide.*) *Biochemische Zeitschrift* 287, 291–328.
- Watanabe, S., Ageta-Ishihara, N., Nagatsu, S., Takao, K., Komine, O., Endo, F., et al. (2014). SIRT1 overexpression ameliorates a mouse model of SOD1-linked amyotrophic lateral sclerosis via HSF1/HSP70i chaperone system. *Mol. Brain* 7:62. doi: 10.1186/s13041-014-0062-1
- Wei, C. C., Kong, Y. Y., Hua, X., Li, G. Q., Zheng, S. L., Cheng, M. H., et al. (2017a). NAD replenishment with nicotinamide mononucleotide protects blood-brain barrier integrity and attenuates delayed tissue plasminogen activator-induced haemorrhagic transformation after cerebral ischaemia. *Br. J. Pharmacol.* 174, 3823–3836. doi: 10.1111/bph.13979
- Wei, C. C., Kong, Y. Y., Li, G. Q., Guan, Y. F., Wang, P., and Miao, C. Y. (2017b). Nicotinamide mononucleotide attenuates brain injury after intracerebral hemorrhage by activating Nrf2/HO-1 signaling pathway. *Sci. Rep.* 7:717. doi: 10.1038/s41598-017-00851-z
- Wheaton, W. W., and Chandel, N. S. (2011). Hypoxia. 2. Hypoxia regulates cellular metabolism. *Am. J. Physiol. Cell Physiol.* 300, C385–C393. doi: 10.1152/ajpcell.00485.2010
- Willems, P. H., Rossignol, R., Dieteren, C. E., Murphy, M. P., and Koopman, W. J. (2015). Redox homeostasis and mitochondrial dynamics. *Cell Metab.* 22, 207–218. doi: 10.1016/j.cmet.2015.06.006
- Wright, A. F., Chakarova, C. F., Abd El-Aziz, M. M., and Bhattacharya, S. S. (2010). Photoreceptor degeneration: genetic and mechanistic dissection of a complex trait. *Nat. Rev. Genet.* 11, 273–284. doi: 10.1038/nrg2717
- Wurth, M. A., Sayeed, M. M., and Baue, A. E. (1973). Nicotinamide adenine dinucleotide (n.d.) content of liver with hemorrhagic shock. *Proc. Soc. Exp. Biol. Med.* 144, 654–658. doi: 10.3181/00379727-144-37656
- Xie, X., Yu, C., Zhou, J., Xiao, Q., Shen, Q., Xiong, Z., et al. (2020). Nicotinamide mononucleotide ameliorates the depression-like behaviors and is associated with attenuating the disruption of mitochondrial bioenergetics in depressed mice. *J. Affect. Disord.* 263, 166–174. doi: 10.1016/j.jad.2019.11.147
- Yamaguchi, S., Franczyk, M. P., Chondronikola, M., Qi, N., Gunawardana, S. C., Stromsdorfer, K. L., et al. (2019). Adipose tissue NAD(+) biosynthesis is required for regulating adaptive thermogenesis and whole-body energy homeostasis in mice. *Proc. Natl. Acad. Sci. U.S.A.* 116, 23822–23828. doi: 10.1073/pnas.1909917116
- Yamamoto, T., Byun, J., Zhai, P., Ikeda, Y., Oka, S., and Sadoshima, J. (2014). Nicotinamide mononucleotide, an intermediate of NAD+ synthesis, protects the heart from ischemia and reperfusion. *PLoS One* 9:e98972. doi: 10.1371/journal.pone.0098972
- Yang, Y., and Sauve, A. A. (2016). NAD(+) metabolism: bioenergetics, signaling and manipulation for therapy. *Biochim. Biophys. Acta* 1864, 1787–1800. doi: 10.1016/j.bbapap.2016.06.014
- Yao, Z., Yang, W., Gao, Z., and Jia, P. (2017). Nicotinamide mononucleotide inhibits JNK activation to reverse Alzheimer disease. *Neurosci. Lett.* 647, 133–140. doi: 10.1016/j.neulet.2017.03.027
- Yoon, M. J., Yoshida, M., Johnson, S., Takikawa, A., Usui, I., Tobe, K., et al. (2015). SIRT1-Mediated eNAMPT secretion from adipose tissue regulates hypothalamic NAD+ and function in mice. *Cell Metab.* 21, 706–717. doi: 10.1016/j.cmet.2015.04.002
- Yoshino, J., Baur, J. A., and Imai, S. I. (2018). NAD(+) intermediates: the biology and therapeutic potential of NMN and NR. *Cell Metab.* 27, 513–528. doi: 10.1016/j.cmet.2017.11.002
- Yoshino, J., Mills, K. F., Yoon, M. J., and Imai, S. (2011). Nicotinamide mononucleotide, a key NAD(+) intermediate, treats the pathophysiology of diet- and age-induced diabetes in mice. *Cell Metab.* 14, 528–536. doi: 10.1016/j.cmet.2011.08.014
- Young, G. S., Choleris, E., Lund, F. E., and Kirkland, J. B. (2006). Decreased cADPR and increased NAD+ in the Cd38-/- mouse. *Biochem. Biophys. Res. Commun.* 346, 188–192. doi: 10.1016/j.bbrc.2006.05.100
- Youngson, N. A., Uddin, G. M., Das, A., Martinez, C., Connaughton, H. S., Whiting, S., et al. (2019). Impacts of obesity, maternal obesity and nicotinamide mononucleotide supplementation on sperm quality in mice. *Reproduction* 158, 169–179. doi: 10.1530/REP-18-0574
- Zhang, L., Chopp, M., Jia, L., Cui, Y., Lu, M., and Zhang, Z. G. (2009). Atorvastatin extends the therapeutic window for tPA to 6 h after the onset of embolic stroke in rats. *J. Cereb. Blood Flow Metab.* 29, 1816–1824. doi: 10.1038/jcbfm.2009.105
- Zhang, R., Shen, Y., Zhou, L., Sangwung, P., Fujioka, H., Zhang, L., et al. (2017). Short-term administration of nicotinamide mononucleotide preserves cardiac mitochondrial homeostasis and prevents heart failure. *J. Mol. Cell Cardiol.* 112, 64–73. doi: 10.1016/j.yjmcc.2017.09.001
- Zhang, X. Q., Lu, J. T., Jiang, W. X., Lu, Y. B., Wu, M., Wei, E. Q., et al. (2015). NAMPT inhibitor and metabolite protect mouse brain from cryoinjury through distinct mechanisms. *Neuroscience* 291, 230–240. doi: 10.1016/j.neuroscience.2015.02.007
- Zhao, B., Zhang, M., Han, X., Zhang, X.-Y., Xing, Q., Dong, X., et al. (2013). Cerebral ischemia is exacerbated by extracellular nicotinamide phosphoribosyltransferase via a non-enzymatic mechanism. *PLoS One* 8:e85403. doi: 10.1371/journal.pone.0085403
- Zhao, C., Li, W., Duan, H., Li, Z., Jia, Y., Zhang, S., et al. (2020). NAD(+) precursors protect corneal endothelial cells from UVB-induced apoptosis. *Am. J. Physiol. Cell Physiol.* 318, C796–C805. doi: 10.1152/ajpcell.00445.2019
- Zhao, Y., Guan, Y. F., Zhou, X. M., Li, G. Q., Li, Z. Y., Zhou, C. C., et al. (2015). Regenerative neurogenesis after ischemic stroke promoted by nicotinamide phosphoribosyltransferase-nicotinamide adenine dinucleotide cascade. *Stroke* 46, 1966–1974. doi: 10.1161/STROKEAHA.115.009216

- Zhao, Y., Liu, X. Z., Tian, W. W., Guan, Y. F., Wang, P., and Miao, C. Y. (2014). Extracellular visfatin has nicotinamide phosphoribosyltransferase enzymatic activity and is neuroprotective against ischemic injury. *CNS Neurosci. Ther.* 20, 539–547. doi: 10.1111/cns.12273
- Zhou, Y., Wang, Y., Wang, J., Anne Stetler, R., and Yang, Q. W. (2014). Inflammation in intracerebral hemorrhage: from mechanisms to clinical translation. *Prog. Neurobiol.* 115, 25–44. doi: 10.1016/j.pneurobio.2013.11.003
- Zoukhri, D. (2006). Effect of inflammation on lacrimal gland function. *Exp. Eye Res.* 82, 885–898. doi: 10.1016/j.exer.2005.10.018

Conflict of Interest: The authors declare that the research was conducted in the absence of any commercial or financial relationships that could be construed as a potential conflict of interest.

Copyright © 2020 Hong, Mo, Zhang, Huang and Wei. This is an open-access article distributed under the terms of the Creative Commons Attribution License (CC BY). The use, distribution or reproduction in other forums is permitted, provided the original author(s) and the copyright owner(s) are credited and that the original publication in this journal is cited, in accordance with accepted academic practice. No use, distribution or reproduction is permitted which does not comply with these terms.



Bergenin as a Novel Urate-Lowering Therapeutic Strategy for Hyperuricemia

Mo Chen^{1†}, Chenyi Ye^{2†}, Jianing Zhu¹, Peiyu Zhang¹, Yujie Jiang¹, Xiaoyong Lu^{1*} and Huaxiang Wu^{1*}

¹ Department of Rheumatology, The Second Affiliated Hospital, School of Medicine, Zhejiang University, Hangzhou, China,

² Department of Orthopedic, The Second Affiliated Hospital, School of Medicine, Zhejiang University, Hangzhou, China

OPEN ACCESS

Edited by:

Claudia Fiorillo,
University of Florence, Italy

Reviewed by:

Blanka Stiburkova,
Institute of Rheumatology, Prague,
Czechia
Venkata Saroja Voruganti,
The University of North Carolina
at Chapel Hill, United States
Gregory Tsay,
Chung Shan Medical University,
Taiwan

*Correspondence:

Xiaoyong Lu
luxyzju18@zju.edu.cn
Huaxiang Wu
wuhx8855@zju.edu.cn;
wuhx8855@163.com

[†] These authors have contributed
equally to this work and share first
authorship

Specialty section:

This article was submitted to
Molecular Medicine,
a section of the journal
Frontiers in Cell and Developmental
Biology

Received: 04 May 2020

Accepted: 10 July 2020

Published: 29 July 2020

Citation:

Chen M, Ye C, Zhu J, Zhang P,
Jiang Y, Lu X and Wu H (2020)
Bergenin as a Novel Urate-Lowering
Therapeutic Strategy
for Hyperuricemia.
Front. Cell Dev. Biol. 8:703.
doi: 10.3389/fcell.2020.00703

Bergenin is a C-glucoside of 4-O-methyl gallic acid isolated from several medicinal plants and has multiple biological activities. The aim of this study was to assess the potential usefulness of bergenin in hyperuricemia. We found that bergenin reduced serum urate levels in hyperuricemia mice by promoting renal and gut uric acid excretion. Bergenin treatment increased *Abcg2* expression both in the kidneys and intestine, while the expression of *Slc2a9* was suppressed in the kidney and increased in the intestine. Moreover, bergenin induced *ABCG2* expression in HK-2 and Caco-2 cells, as well as *SLC2A9* in Caco-2 cells, via the activation of *PPAR* γ . Nevertheless, bergenin suppressed *SLC2A9* expression in HK-2 cells by inhibiting the nuclear translocation of p53. Furthermore, bergenin decreased the serum levels of IL-6, IL-1 β , and TNF- α in hyperuricemia mice, and promoted a polarization shift from the M1 to M2 phenotype in RAW264.7 cells. In conclusion, these findings provide evidence supporting the further development of bergenin as a novel therapeutic strategy for hyperuricemia.

Keywords: hyperuricemia, bergenin, *ABCG2*, *SLC2A9*, urate-lowering therapeutic

INTRODUCTION

The global burden of gout remains substantial, and in many parts of the world, its incidence has increased over the past years (Kuo et al., 2015). In 2015–2016, the prevalence of hyperuricemia in the United States was 20.2% (22.8 million) in males and 20.0% (24.4 million) in females (Chen-Xu et al., 2019). Moreover, individuals with asymptomatic hyperuricemia are at high risk of developing a variety of diseases, including gouty arthritis, renal damage, hypertension, diabetes mellitus, and metabolic syndrome (Dalbeth et al., 2019). Recent evidence has shown a link between high urate exposure and an increased inflammatory capacity across several tissues and immune cell types (Joosten et al., 2020). Urate-lowering therapies (ULT), including xanthine oxidase inhibitors and uricosuric drugs, often cause severe side effects. Therefore, according to evidence-based international guidelines, such therapies are only recommended in people with established conditions, such as gout and kidney stones (Dalbeth et al., 2019; Joosten et al., 2020). Hence, the development of safe and effective hyperuricemia therapies remains an unmet clinical need.

Nowadays it has become clearly that altered urate transport, both in the gut and the kidneys, has a central role in the pathogenesis of hyperuricaemia and gout (Dalbeth et al., 2019). Furthermore, genome-wide association studies (GWAS) have identified numerous loci that are associated with hyperuricemia and gout (Kawamura et al., 2019; Nakatochi et al., 2019).

Serum urate levels are primarily regulated by the activity of the four transporters solute carrier family 2, facilitated glucose transporter member (SLC2A9), solute carrier family 22 member 12 (SLC22A12), solute carrier family 17 member 1 (SLC17A1), and ATP-binding cassette transporter, subfamily G, member 2 (ABCG2), in the kidneys, and of ABCG2 in the intestine (Nakayama et al., 2017).

Bergenin is the C-glucoside of 4-O-methyl gallic acid and can be found in several medicinal plants, including *Bergenia crassifolia* and *Corylopsis spicata* (Liang et al., 2017). Bergenin has been reported to have multiple biological activities, including antiarthritic (Jain et al., 2014; Singh et al., 2017), immunomodulatory (Wang et al., 2017; Kumar et al., 2019), antidiabetic (Veerapur et al., 2012), osteogenic (Hou et al., 2019), neuroprotective (Barai et al., 2019; Ji et al., 2019), and wound-healing effects (Mukherjee et al., 2013). Wang et al. (2017) showed that bergenin attenuated colitis by activating the peroxisome proliferator-activated receptor (PPAR) γ . Moreover, Veerapur et al. (2012) found that bergenin exerted the antidiabetic effect and could bind the PPAR ligand-binding domain. PPAR γ regulates the expression of various genes by directly binding to peroxisome proliferator response elements (Mandard and Patsouris, 2013).

Although PPAR γ has been reported to regulate the expression of ABCG2 (Szatmari et al., 2006; To and Tomlinson, 2013; Wang et al., 2016), the relevance of bergenin as a therapeutic agent for hyperuricemia remains unclear. The aim of this study was to explore the potential clinical usefulness of bergenin in hyperuricemia. To this end, we investigated the effects of bergenin on hyperuricemia *in vitro* and *in vivo*, as well as the potential biological mechanisms underlying these effects.

MATERIALS AND METHODS

Reagents and Antibodies

Bergenin (purity >99%) was purchased from JingZhu Biological Technology (Nanjing, China). Uric acid, allopurinol, yeast polysaccharide, and HEPES were purchased from Sigma-Aldrich (United States). Potassium oxonate (PO), rosiglitazone, GW9662, WR-1065, and Pifithrin- β were purchased from MedChemExpress (United States). Antibodies against acetylated-p53, p53 and PPAR γ were obtained from Cell Signaling Technology (United States). Antibodies against Lamin A/C, Glyceraldehyde-3-phosphate dehydrogenase (GAPDH), and β -actin were obtained from Santa Cruz Biotechnology (United States). Antibodies against SLC2A9 and ABCG2 were obtained from Novus (United States) and Abcam (United States), respectively. Penicillin/streptomycin and TRIzol reagent were purchased from Invitrogen Life Technologies (United States).

Animals

Male C57BL/6 mice (6–8 weeks old) were provided by the Academy of Medical Sciences of Zhejiang Province. Mice were given *ad libitum* access to food and water. All experiments were conducted in accordance with the Animal Care and Use Committee guidelines of Zhejiang province. All experimental

procedures were approved by the Institutional Animal Care and Use Committee of Zhejiang University.

Control mice were fed a standard diet. To induce hyperuricemia, mice were given 25% yeast polysaccharide (YP) mixed in daily diet and intraperitoneal injected of PO (250 mg/kg) at 8:00 a.m. every day. Mice of the treatment group were subjected to intragastric administration of either of two concentrations (40 or 80 mg/kg) of bergenin, while the same volume of normal saline (NS) was used as a control. Intragastric administration of 25 mg/kg allopurinol was performed as a positive control (Figure 1).

Measurement of Uric Acid and Creatinine in Serum and Urine

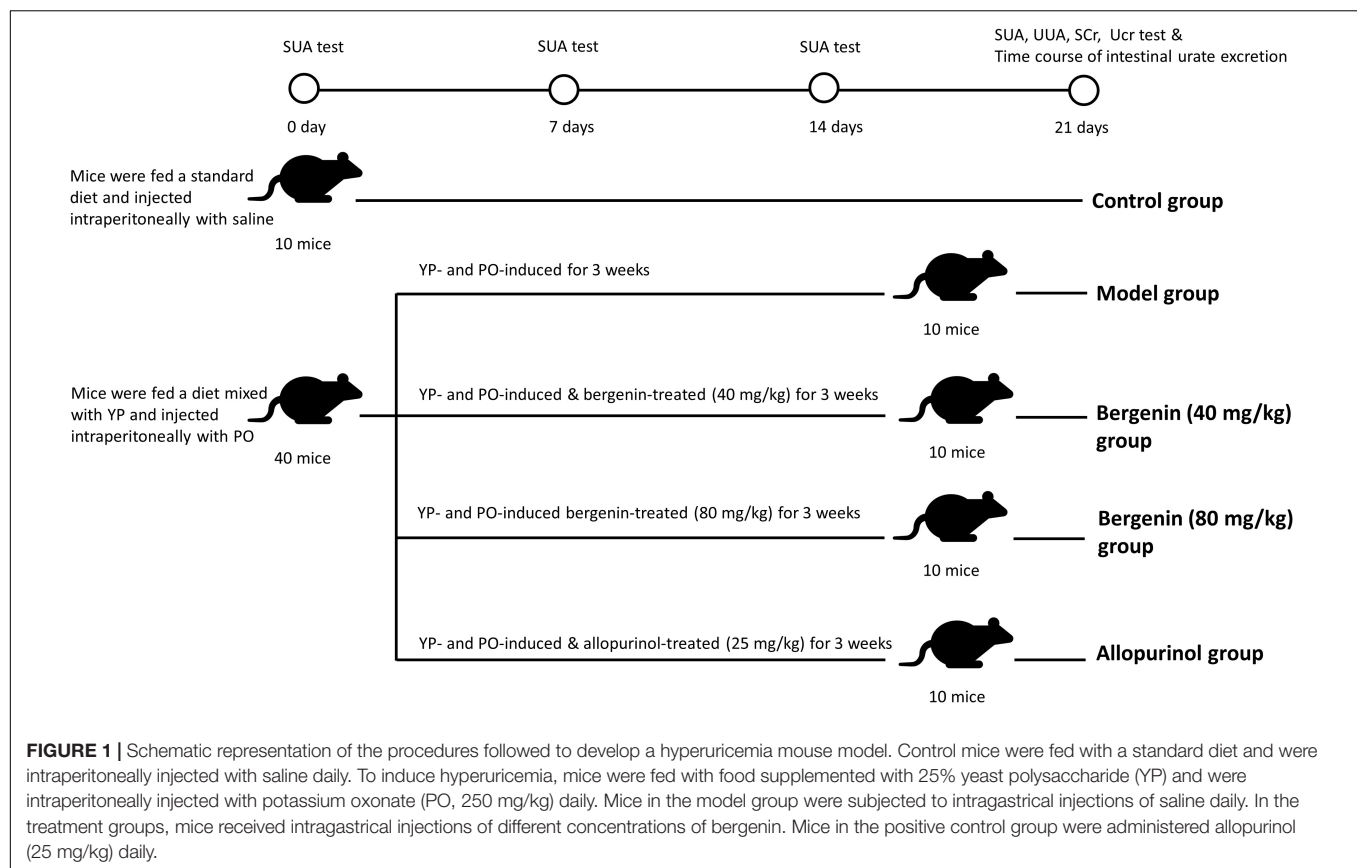
To measure the serum uric acid levels (SUA), we collected blood samples 2 h after treatment on days 0, 7, 14, and 21. The day before sacrificing, urine samples were collected from mice with metabolic changes within 24 h. Mice were sacrificed 2 h after the last treatment, and blood samples were collected. Uric acid and creatinine levels in serum and urine were determined using the phosphotungstic acid method and a Jaffe reaction kit, respectively (Nanjing Jiancheng Biological Technology Co., Ltd., China). Fractional excretion of urate (FEur) was calculated as per a previously reported method (Perez-Ruiz et al., 2002): $FEur = (U_{ur} \text{ Scr}) / (S_{ur} U_{cr}) \times 100\%$. Sur, serum urate level; Scr, serum creatinine level; U_{ur}, Urinary urate level; U_{cr}, Urinary creatinine level.

Transintestinal Urate Transport Analysis

Intestinal urate excretion was determined according to a previously described method (Ichida et al., 2012). Briefly, after overnight fasting, mice were anesthetized with 2% isoflurane inhalation using an isoflurane delivery system 2 h after the last treatment. Subsequently, mice were cannulated with polyethylene tubing at the upper duodenum and middle jejunum, making an intestinal loop at the upper half of the intestine. The intestinal contents were slowly removed by saline and air. Efflux buffer (saline containing 0.3 mM PO) was added into the intestinal loop; the bugger was collected at the indicated time points, and urate concentrations were quantified. Intestinal urate excretion was calculated using the following equation: intestinal urate excretion = (urate concentration in the intestinal loop) \times (volume of efflux buffer in the intestinal loop) (length of the whole small intestine/length of the intestinal loop). Urate concentration was determined using the QuantiChrom Uric Acid Assay Kit (Bioassay Systems, United States).

Histological Examination

After mice were sacrificed, kidney tissues were collected and cleaned, followed by fixation in 4% paraformaldehyde for at least 48 h at room temperature. Specimens were embedded in paraffin wax, and 3-mm thick sections were prepared. After mounting the sections onto polylysine-coated slides, hematoxylin and eosin, as well as Masson's stainings were performed on consecutive tissue sections. Images were obtained using a microscope.



Xanthine Oxidase Activity Measurement

Xanthine oxidase (XO) activity in liver tissues was measured using a Xanthine Oxidase Activity Assay Kit (Sigma, United States) according to the manufacturer's instructions. XO activity was determined by a coupled enzyme assay, which results in a colorimetric (570 nm) fluorometric product, which is proportional to the hydrogen peroxide generated. XO activity was expressed as nanomoles of uric acid per min per mg of total protein (mU/mg).

Cytokine Measurement

Blood samples were collected 2 h after the last treatment. The concentrations of IL-1 β , TNF α , IL-6, IL-10, and IL-1Ra were determined using the respective ELISA kits (BOSTER, China for IL-1Ra and NEOBIOSCIENCE, China for the rest) according to the manufacturer's instructions.

Cell Culture

HK-2, Caco-2, and RAW264.7 cells were kindly provided by Stem Cell Bank, Chinese Academy of Sciences (Shanghai, China). HK-2 cells were maintained in Dulbecco's modified Eagle medium (DMEM)/F12 medium (Gibco, United States) containing 10% fetal bovine serum (FBS; Gibco, Australia). Caco-2 and RAW264.7 cells were cultured in high-glucose DMEM (Gibco, United States) supplemented with 10% FBS (Gibco,

Australia). Cells were maintained in a humidified incubator containing 5% CO₂ at 37°C.

Inhibitors were dissolved in DMSO or double-distilled water (ddH₂O). Prior to treatments, we cultured cells overnight in serum-free medium to induce growth arrest. Cells were treated with bergenin and indicated inhibitors in a humidified incubator containing 5% CO₂ at 37°C, with or without stimulation with soluble uric acid for an additional 12 h. The final concentrations and incubation times were as follow: rosiglitazone (30 μ M, 2 h), GW9662 (10 μ M, 2 h), WR-1065 (1 mM, 2 h), and Pifithrin- β (10 μ M, 2 h). Following the addition of HEPES at a final concentration of 25 mM, cells were treated with uric acid or the solvent (10 mM NaOH). The solution was filtered through a 0.22- μ m pore size filter (Millipore, Shanghai, China) before use.

CCK-8

The effect of bergenin on the viability of HK-2 and Caco-2 cells was evaluated using the CCK8 assay. Cells were treated with different concentrations of bergenin, followed by incubation with 10% CCK-8 (Dojindo, Kumamoto, Japan) in 100 μ L of high-glucose serum-free DMEM for 4 h at 37°C. Absorbance at 450 nm was measured on a microplate reader (ELX808; BioTek, Winooski, VT, United States).

Extraction of Subcellular Fractions

For total protein extraction, cells were washed with ice-cold phosphate-buffered saline (PBS) and lysed in

radioimmunoprecipitation assay (RIPA) lysis buffer supplemented with proteasome inhibitors (Beyotime, Shanghai, China).

Nuclear and cytoplasmic extracts were prepared using the NE-PER Nuclear Cytoplasmic Extraction Reagent Kit (Pierce, Rockford, IL, United States) according to the manufacturer's instructions. Briefly, cells were washed in PBS. Ice-cold CER I buffer was added to the cell pellet and vortexed vigorously for 15 s. After a 10-min incubation on ice, ice-cold CER II buffer was added to the cells. Samples were incubated on ice for 1 min, followed by centrifugation for 5 min at $16,000 \times g$. Subsequently, the supernatant containing the cytoplasmic extract was immediately transferred to a pre-chilled tube.

Western Blot Analysis

Equal amounts of protein were separated by 8–12% sodium dodecyl sulfate-polyacrylamide gel electrophoresis and transferred onto polyvinylidene fluoride membranes (Millipore). Membranes were blocked in 5% non-fat dry milk for 2 h at room temperature, followed by overnight incubation at 4°C with the appropriate primary antibody: GAPDH (1:2000), ABCG2 (1:1000), SLC2A9 (1:1000), PPAR γ (1:1000), p53 (1:1000), acetylated-p53, β -actin (1:1000), or Lamin A/C (1:1000). Horseradish peroxidase (HRP)-conjugated goat anti-rabbit or goat anti-mouse IgG (1:5000; Cell Signaling Technology) secondary antibody was applied for 1 h at room temperature. Membranes were covered with enhanced chemiluminescence solution (Millipore) and exposed to film. Signal intensity was measured using the Bio-Rad XRS chemiluminescence detection system (Bio-Rad, Hercules, CA, United States).

Immunofluorescence

HK-2 and Caco-2 cells were seeded onto 24-well plates. After treatment, cells were fixed in 4% paraformaldehyde for 15 min, washed with PBS, and permeabilized with or without 0.1% Triton X-100 (Beyotime) for 30 min. After blocking in 10% goat serum for 60 min, slides were incubated with a rabbit p53 antibody (1:200) overnight at 4°C. Samples were then incubated with Alexa Fluor 488-conjugated goat anti-rabbit IgG antibody (Invitrogen) for 2 h, and nuclei were stained with 4',6-diamidino-2-phenylindole (DAPI, Sigma, United States). Samples were observed under a fluorescence microscope (Leica, Solms, Germany).

Real-Time Quantitative Polymerase Chain Reaction (RT-qPCR)

Total RNA was isolated using TRIzol reagent (Invitrogen) and quantified by measuring the absorbance at 260 nm (NanoDrop 2000; Thermo Fisher Scientific, Waltham, MA, United States). Complementary single-stranded DNA was synthesized from total RNA by reverse transcription (PrimerScript RT Master Mix, TaKaRa, Kyoto, Japan). RT-qPCR reactions were prepared using the SYBR Premix Ex Taq Kit (TaKaRa) in a total volume of 20 μ L. All reactions were prepared in duplicates and were run on an ABI StepOnePlus System (Applied Biosystems, Warrington, United Kingdom). The PCR temperature cycling conditions were

as follows: 95°C for 30 s followed by 40 cycles at 95°C for 5 s and 60°C for 30 s. Relative gene expression was analyzed using the $2^{-\Delta\Delta C_t}$ method. The primer sequences used are provided in **Supplementary Table S1**.

Transfection of Cells With Small Interfering RNA (siRNA)

Cells were seeded onto 6-well plates and cultured overnight in DMEM/F12 or DMEM without FBS and antibiotics. siRNA transfections were carried out using Lipofectamine 2000 (Invitrogen) according to the manufacturer's instructions. Briefly, 10 μ L of siRNA and 5 μ L of Lipofectamine 2000 reagent were combined in a total of 300 μ L of Opti-MEM I (Gibco, Invitrogen). Thereafter, 700 μ L of Opti-MEM I was added to the mixture, and the mixture was added to each well. After incubation for 6 h, fresh DMEM or DMEM/F12 containing 10% FBS was added to each well. Cells were incubated for an additional 48–72 h. PPAR- γ siRNAs and the negative control siRNAs were purchased from GenePharma (Shanghai, China).

Luciferase Reporter Assay

Cells were transfected with luciferase reporter constructs PPAR γ -Luc (Promega, United States) or p53-Luc (Promega, United States) as previously described (Ye et al., 2019). Cells were then treated with uric acid (UA, 8 mg/dL) and/or bergenin for 12 h. Subsequently, luciferase activity was measured using a luciferase assay system (Promega, United States).

Statistical Analysis

Statistical analysis was performed using the SPSS statistical software for Windows, version 19.0 (IBM, Armonk, NY, United States). All experiments were performed at least in triplicate, and the data were expressed as mean \pm standard error of the mean (SEM). Statistical significance was determined using one-way analysis of variance (ANOVA) followed by Fisher's Least Significant Difference (LSD) test when comparing more than two groups. P values ≤ 0.05 were considered statistically significant. The correlation between variables was evaluated by the Pearson correlation test. Two-sided P values < 0.05 were considered statistically significant.

RESULTS

Bergenin Ameliorates Hyperuricemia in Mice Treated With Potassium Oxonate (PO) and Yeast Polysaccharide (YP)

The procedure followed to develop a hyperuricemia mouse model is illustrated in **Figure 1**. Compared with control mice, SUA levels were significantly higher in hyperuricemia mice after day 7, and remained elevated between day 14 ($407.41 \pm 79.09 \mu\text{mol/L}$ vs. $194.07 \pm 25.85 \mu\text{mol/L}$; $P < 0.01$) and day 21 ($439.39 \pm 48.11 \mu\text{mol/L}$ vs. $220.60 \pm 35.28 \mu\text{mol/L}$; $P < 0.01$). SUA elevation was suppressed by bergenin (80 mg/kg) and allopurinol administration. While bergenin at 80 mg/kg profoundly decreased SUA levels ($253.18 \pm 31.74 \mu\text{mol/L}$)

compared to hyperuricemia mice, no significant difference was observed at day 21 after administration of 40 mg/kg bergenin ($397.39 \pm 52.69 \mu\text{mol/L}$; **Figure 2A**). This finding suggests that the effects of bergenin are dose-dependent to some degree. It is worth noting that SUA level of the Bergenin (80 mg/kg) group stabilized at baseline levels from day 1 to day 21. As expected, SUA levels were significantly lower in allopurinol-treated mice (positive control) compared with control mice. No significant differences in SUA levels were observed between the mice in the bergenin (80 mg/kg) group and the allopurinol group.

Scr, FEur, intestinal urate excretion rate, and hepatic XO activity were assessed at day 21. Scr levels were higher in hyperuricemia mice compared with control mice; however, the difference did not reach statistical significance ($P > 0.05$) (**Figure 2B**). In hyperuricemic mice, FEur was decreased; bergenin (40 mg/kg, 80 mg/kg) treatment rescued FEur. Furthermore, urate excretion from the intestine was significantly increased in mice treated with bergenin (80 mg/kg) compared with hyperuricemic mice ($P < 0.01$; **Figure 2D**). While allopurinol reduced hepatic XO activity ($P < 0.01$), it did not affect uric acid excretion in the kidneys and intestine ($P > 0.05$) compared with hyperuricemia mice (**Figures 2C–E**). Additionally, bergenin had no effect on XO activity in liver and jejunum (**Figure 2E**, **Supplementary Figure S1**).

Histological analysis revealed that the ultrastructure of the kidneys was intact in mice treated with PO and YP. Compared with control mice, degeneration and necrosis were observed in tubular epithelial cells of hyperuricemic mice (**Figure 2F**). Bergenin (80 mg/kg) and allopurinol treatment ameliorated PO- and YP-induced pathological lesions. No histological changes were observed in the intestine of hyperuricemic or bergenin-treated mice (**Supplementary Figure S2**).

Bergenin Regulates the Expression of Urate Transporters in the Kidney

To determine the effects of bergenin on uric acid excretion in the kidneys, we analyzed the expression of urate transporters involved in urate export and reuptake in the kidney. We found no significant differences in the mRNA levels of the genes encoding urate transporter 1 (*Urat1*) and PDZ domain-containing 1 (*Pdzk1*) among the different groups ($P > 0.05$; **Figure 3A**). *Abcg2* expression was lower in hyperuricemic mice compared with control mice; nevertheless, its expression in hyperuricemic mice was rescued by bergenin (40 mg/kg, 80 mg/kg) treatment, both at the mRNA and protein levels ($P < 0.01$) (**Figures 3A,E**). Bergenin at 80 mg/kg and 40 mg/kg resulted in 2-fold and 1.5-fold increases in *Abcg2* mRNA levels, respectively.

In contrast, *Slc2a9* expression was higher in hyperuricemic mice compared with control mice, and bergenin (80 mg/kg) suppressed *Slc2a9* expression, which was evident both at the mRNA and protein levels ($P < 0.01$). Although bergenin treatment (40 mg/kg) decreased SLC2A9 protein levels ($P < 0.05$, compared to the model group), no difference was observed at the mRNA level (**Figures 3A,E**). Hyperuricemic mice exhibited a reduction in PPAR γ expression ($P < 0.01$, compared to control

mice), PPAR γ expression was restored by bergenin (40 mg/kg, 80 mg/kg; **Figure 3E**).

Bergenin Regulates the Expression of Urate Transporters in the Intestine

RT-qPCR analyses revealed no significant differences in the expression of *Pdzk1* and solute carrier family 17 member 3 (*Slc17a3*) in the intestine among the groups ($P > 0.05$; **Figures 3B–D**). In the colon, bergenin (40 mg/kg, 80 mg/kg) significantly increased *Abcg2* mRNA and protein levels (**Figures 3B,F**). Hyperuricemic mice had lower *Abcg2* mRNA and protein levels compared with the control group, which were restored by bergenin (40 mg/kg, 80 mg/kg) treatment (**Figures 3C,G**). In the jejunum, the expression of *Abcg2* was increased in hyperuricemic mice, and its expression was elevated by bergenin in a dose-dependent manner, both at the mRNA and protein levels (**Figures 3D,H**). These RT-qPCR and western blot findings were also confirmed by immunofluorescence (**Supplementary Figure S3**).

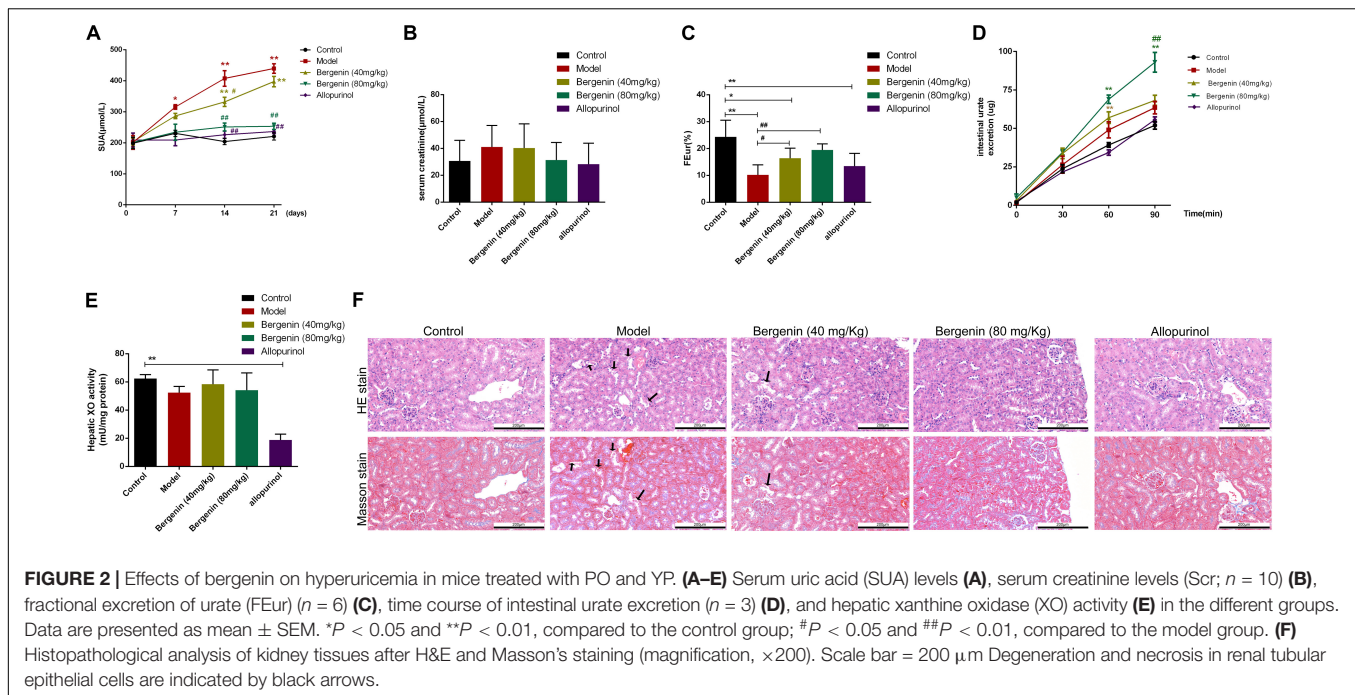
Compared to control mice, hyperuricemic mice exhibited decreased expression of *Slc2a9* in the ileum and jejunum, both at the mRNA and protein levels ($P < 0.01$). Administration of bergenin significantly restored *Slc2a9* expression in the ileum and jejunum (**Figures 3C,D,G,H**). The mRNA levels of *Slc2a9* were increased by approximately 2-fold and 4-fold after administration of bergenin at 40 and 80 mg/kg, respectively, suggesting a dose-dependent effect. On the other hand, RT-qPCR and western blot analyses showed no changes in *Slc2a9* expression in the colon (**Figures 3B,F**). SLC2A9 expression in intestine was further confirmed by immunofluorescence (**Supplementary Figure S3**).

PPAR γ was expressed at lower levels in the ileum and jejunum of hyperuricemic mice ($P < 0.01$, compared with control mice), but not in the colon. Bergenin treatment enhanced PPAR γ expression in a dose-dependent manner (**Figures 3F–H**).

Bergenin Reduces Pro-inflammatory Cytokine Serum Levels

Several studies suggested that hyperuricemia and soluble uric acid levels are associated with systemic inflammation (Joosten et al., 2020). Therefore, we investigated the effects of bergenin on the serum levels of several inflammatory cytokines. IL-1 β , TNF- α , and IL-6 serum levels were significantly increased in hyperuricemic mice; bergenin treatment reduced the serum levels of these cytokines. Notably, bergenin at 80 mg/kg reduced the serum levels of IL-1 β , TNF- α , and IL-6 by 16%, 25%, and 57%, respectively (**Figures 4A,C,E**). In contrast, no significant difference was observed in the serum levels of IL-1Ra or IL-18 (**Figures 4G,I**). Additionally, SUA levels were positively correlated with IL-1 β , TNF- α and IL-6 serum levels and were negatively correlated with those of IL-1Ra (**Figures 4B,D,F,H**). No correlation between SUA and IL-18 (**Figure 4J**).

To gain further insight into the effects of bergenin on inflammatory responses, we treated RAW267.4 cells with UA (8 mg/dL) or bergenin (50 μM). Exposure to UA polarized RAW267.4 cells toward an inflammatory (M1) phenotype with upregulation of inducible nitric oxide synthase (iNos)



and downregulation of *IL-10*. In contrast, bergenin treatment polarized RAW267.4 cells toward an anti-inflammatory (M2) phenotype, with high expression of Arginase-1 (*Arg-1*), *IL-10*, and *CD206* and low expression of *Tnf- α* and *iNos*. RAW267.4 cells pretreated with bergenin prior to UA exposure acquired an M2 phenotype, with increased *Arg-1*, *IL-10*, and *CD206* expression and low *Tnf- α* and *iNos* expression (Figure 4K).

Bergenin *in vitro* Treatment Regulates the Expression of ABCG2 and SLC2A9 in HK-2 Human Renal Proximal Tubular Epithelial Cells

We found that bergenin at 10–100 μ M did not affect the viability of HK-2 cells (Figure 5A). Hence, we pretreated HK-2 cells with 10, 30, 50, or 100 μ M bergenin for 2 h, followed by treatment with 8 mg/dL UA for 10 h. UA decreased *ABCG2* expression at the mRNA and protein level ($P < 0.05$, compared to the control group). UA-mediated *ABCG2* downregulation was rescued by bergenin treatment (50 and 100 μ M). In contrast, *SLC2A9* mRNA and protein levels were increased after UA treatment ($P < 0.05$, compared to the control group). Pretreatment with bergenin (50 and 100 μ M) suppressed UA-induced *SLC2A9* upregulation (Figures 5B,C); however, lower concentrations of bergenin did not affect *SLC2A9* expression. No significant increase was observed in *ABCG2* and *SLC2A9* expression in cells treated with 30 μ M bergenin alone (Figures 5B,C).

Bergenin Promotes ABCG2 Expression by Activating PPAR γ in HK-2 Cells

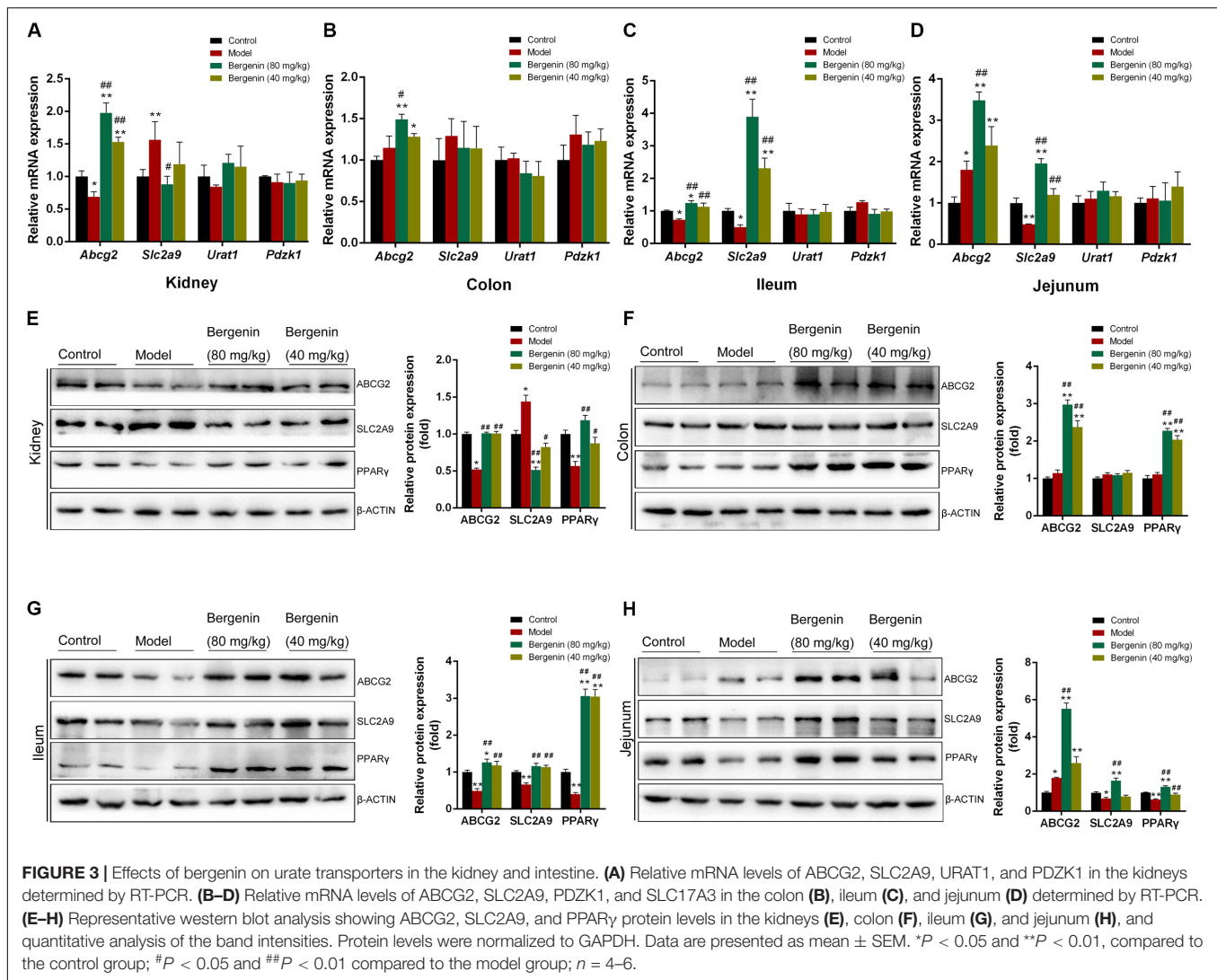
Luciferase reporter assays revealed that UA significantly reduced the expression and transcriptional activity of PPAR γ , both

of which were restored by bergenin (Figures 5C,D). siRNA-mediated PPAR γ silencing decreased the mRNA and protein levels of ABCG2. Moreover, bergenin treatment failed to enhance ABCG2 expression after PPAR γ knockdown. PPAR γ silencing did not affect the expression of SLC2A9, regardless of the presence of bergenin (Figures 5E,F).

Similarly to bergenin, pretreatment of HK-2 cells with the PPAR γ agonist rosiglitazone before stimulation with UA increased the expression of PPAR γ and ABCG2. In contrast, pretreatment with the PPAR γ antagonist GW9662 enhanced the UA-mediated downregulation of PPAR γ and ABCG2 (Figure 5G). Additionally, bergenin failed to restore ABCG2 expression in cells treated with GW9662 and UA (Figure 5G). These results suggest that bergenin regulates the expression of ABCG2 by activating PPAR γ .

Bergenin Reduces SLC2A9 Expression by Diminishing Nuclear Translocation of p53 in HK-2 Cells

As the previous research indicated SLC2A9 was a direct target gene of p53 (Itahana et al., 2015), we next investigated the effects of bergenin and UA on p53 signaling. Although bergenin and UA had no effects in the total p53 and acetylated p53 levels (Figure 5H), UA significantly decreased p53 levels in the cytoplasm and increased its levels in the nucleus. These results suggest that UA promotes p53 protein translocation from the cytoplasm to the nucleus. Interestingly, bergenin suppressed nuclear translocation of p53 (Figure 5H). Immunofluorescence and luciferase reporter analyses confirmed these results (Figures 5I,J).



Pifithrin- β (PFT- β), a potent *p53* inhibitor, significantly suppressed the UA-induced SLC2A9 upregulation. On the other hand, the *p53* agonist WR-1065 reinforced SLC2A9 upregulation. Bergenin treatment failed to suppress SLC2A9 expression in HK-2 cells treated with WR-1065 and UA (Figure 5K).

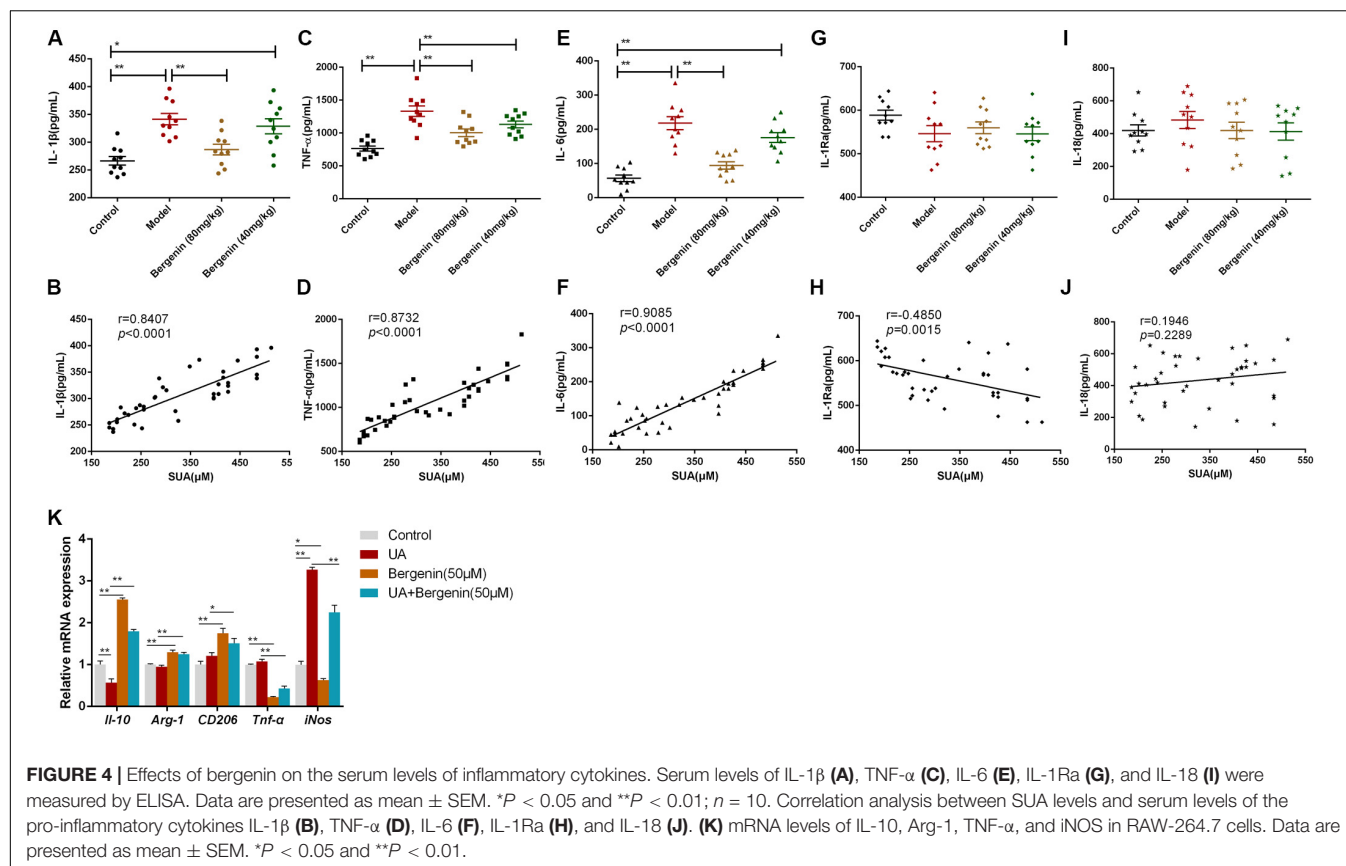
Bergenin *in vitro* Treatment Promotes the Expression of ABCG2 and SLC2A9 in Intestinal Epithelial Cells

We next used Caco-2 cells as an *in vitro* model of human intestinal epithelial cells to examine the effects of bergenin on intestinal urate transporters. We found that treatment with bergenin at 10–100 μ M for 12 h had no effects on the viability of Caco-2 cells (Figure 6A). We then pretreated Caco-2 cells with bergenin for 2 h, followed by treatment with UA at 8 mg/dL for 10 h. UA increased ABCG2 mRNA and protein levels and downregulated SLC2A9 levels. Treatment with bergenin alone increased the protein levels of ABCG2 and SLC2A9. Compared to cells treated with UA alone,

ABCG2 and SLC2A9 were significantly upregulated when cells were treated with UA and 100 μ M bergenin (P < 0.01) (Figures 6B,C).

Bergenin Promotes ABCG2 and SLC2A9 Expression by Activating PPAR γ in Caco-2 Cells

Similar to HK-2 cells, UA significantly inhibited PPAR γ activity in Caco-2 cells, which was restored by bergenin (Figures 6C,D). Interestingly, siRNA-mediated PPAR γ silencing reduced the expression of both ABCG2 and SLC2A9. In addition, bergenin treatment failed to enhance ABCG2 and SLC2A9 expression after PPAR γ silencing (Figures 6E,F). PPAR γ activation by rosiglitazone significantly enhanced the UA-mediated ABCG2 and SLC2A9 upregulation (P < 0.01). In contrast, pretreatment with GW9662 enhanced the UA-mediated downregulation of PPAR γ , ABCG2, and SLC2A9. Furthermore, bergenin failed to restore ABCG2 and SLC2A9 expression in cells treated with GW9662 and UA (Figure 6G).



Bergenin Does Not Affect the p53 Signaling Pathway in Caco-2 Cells

Bergenin treatment did not alter the total p53 and acetylated p53 levels in Caco-2 cells (Figure 6H). Additionally, immunofluorescence analyses indicated that bergenin did not promote nuclear translocation of p53 (Figure 6I).

DISCUSSION

As serum urate levels are associated with the development of gout, interventions that reduce serum urate concentrations have been investigated for their potential to prevent gout (Dalbeth et al., 2019). In this study, we assessed the effect of bergenin on hyperuricemia using a mouse model. We showed for the first time that bergenin has uricosuric properties, reducing serum urate levels in hyperuricemic mice. We also provided evidence that its urate-lowering effects are mediated by increasing *Abcg2* expression in the kidneys and intestine, as well as *Slc2a9* downregulation in the kidneys. Furthermore, we demonstrated that bergenin downregulates IL-6, IL-1 β , and TNF- α serum levels in hyperuricemic mice and polarizes RAW264.7 cells toward an M2 phenotype.

ABCG2 is a high-capacity urate exporter expressed in the intestine and kidneys, and ABCG2 dysfunction strongly increases serum urate levels and the risk of gout development (Ichida et al., 2012; Dalbeth et al., 2019). In this study, we

found that although *Abcg2* expression was increased in the jejunum, its levels were decreased in the kidneys and ileum of hyperuricemic mice. After treatment with bergenin, *Abcg2* was significantly upregulated in the kidneys, jejunum, ileum, and colon, enhancing renal and intestine urate excretion. These findings may partly explain the anti-hyperuricemic effects of bergenin. *PPAR γ* is a ligand-regulated transcription factor involved in various pathophysiological processes, including metabolism, inflammatory responses, and tumorigenesis (Berger and Moller, 2002; Mandard and Patsouris, 2013). Herein, we showed that *PPAR γ* expression was decreased under high-UA conditions both *in vitro* and *in vivo*. Importantly, bergenin restored *ABCG2* expression by activating *PPAR γ* . These findings suggest that *PPAR γ* enhances *ABCG2* expression, which is consistent with previous studies (Szatmari et al., 2006; Wang et al., 2016). It is noteworthy that in Caco-2 cells, although *PPAR γ* was decreased after treatment with UA, *ABCG2* expression was upregulated. This could be explained by the fact that UA is not a specific *PPAR γ* antagonist. In a previous study, we showed that soluble UA induced *ABCG2* expression in Caco-2 cells via the TLR4-NLRP3 inflammasome and PI3K/Akt signaling pathways (Chen et al., 2018). Additionally, the *ABCG2* is the only associated locus with the early onset and/or a family history (Stiburkova et al., 2019). And it has been reported (Roberts et al., 2017) *ABCG2* rs2231142 predicts a poor response to first-line ULT, allopurinol. We will verify the impact of bergenin in the case of *ABCG2* variants with reduced function in the future.

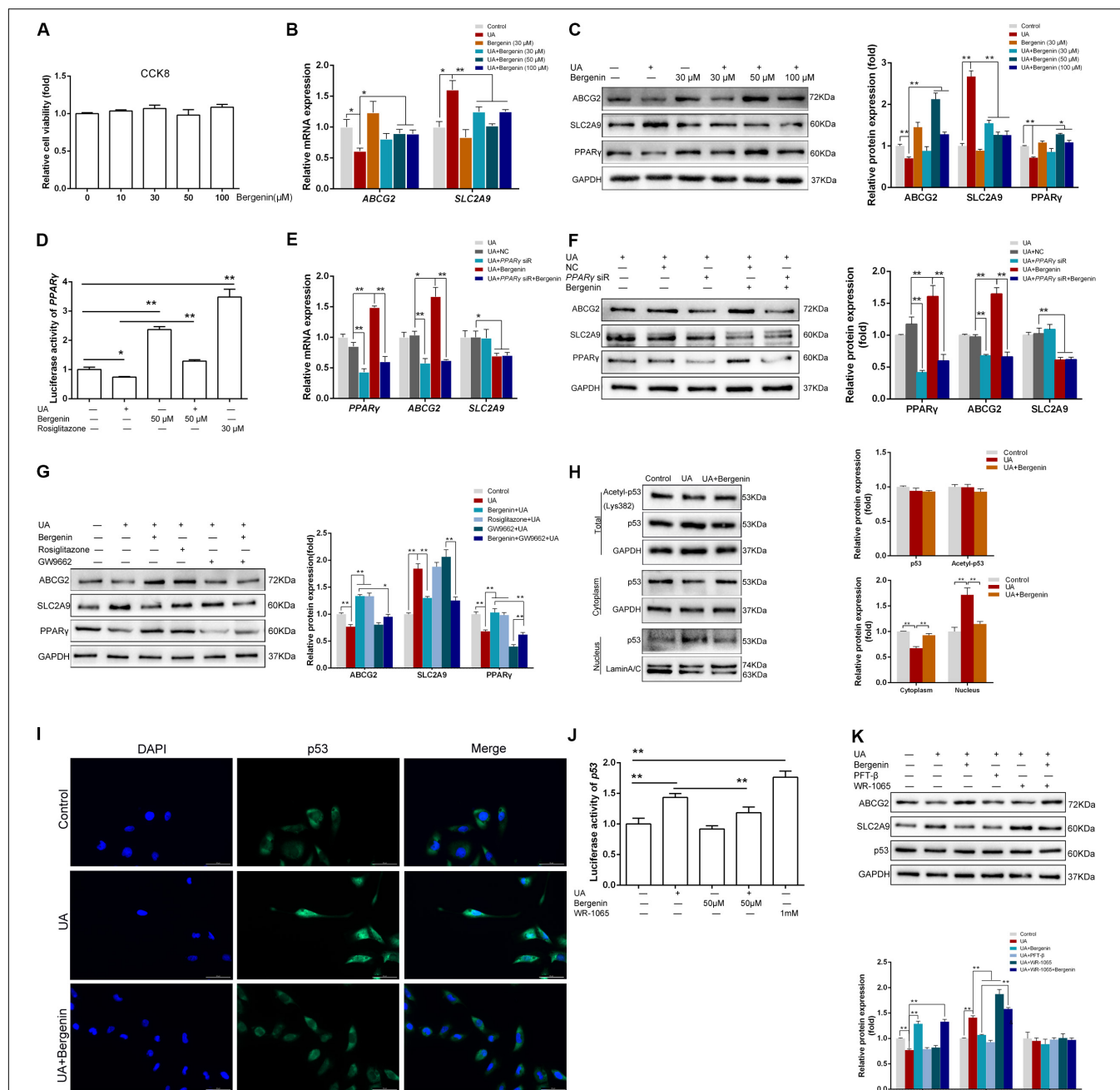


FIGURE 5 | Bergenin regulates the expression of ABCG2 and SLC2A9 in HK-2 cell lines. **(A)** HK-2 cell lines were treated with bergenin (10, 30, 50, or 100 μ M) for 12 h, and cell viability was determined by the CCK8 assay. **(B)** HK-2 cell lines were pretreated with bergenin (0, 30, 50, or 100 μ M) for 2 h, followed by treatment with 8 mg/dL uric acid (UA) for 10 h. Relative mRNA levels of ABCG2 and SLC2A9 were determined by RT-qPCR. **(C)** Representative western blot showing ABCG2, SLC2A9, and PPAR γ protein levels. Protein levels were normalized to GAPDH. **(D)** Transcriptional activity of PPAR γ , as determined by luciferase assay. **(E)** Cells were transfected with PPAR γ siRNA or scrambled siRNA for 48 h. Cells were then pretreated with or without 50 μ M bergenin for 2 h, followed by exposure to 8 mg/dL UA for another 10 h. Relative mRNA levels of ABCG2, SLC2A9, and PPAR γ were determined by RT-qPCR. **(F)** Representative western blot showing ABCG2, SLC2A9, and PPAR γ protein levels. Protein levels were normalized to GAPDH. **(G)** Cells were pretreated with bergenin (50 μ M) or rosiglitazone (PPAR γ agonist) for 2 h, followed treatment with 8 mg/dL UA for another 10 h, with or without GW9662 (PPAR γ inhibitor). ABCG2, SLC2A9, and PPAR γ protein levels were determined by western blotting. Protein levels were normalized to GAPDH. **(H)** Total p53 and acetylated p53 levels were measured by western blot analysis. Protein levels were normalized to GAPDH. Cytoplasmic and nuclear extracts were prepared for western blot analyses. Cytoplasmic protein levels were normalized to GAPDH, whereas nuclear protein levels were normalized to Lamin A/C. **(I)** Representative immunofluorescence images (magnification, $\times 400$) showing p53 expression (green). Nuclei were stained with DAPI (blue). Scale bar = 50 μ m. **(J)** Transcriptional activity of p53, as determined by luciferase assay. **(K)** Cells were pretreated with bergenin (50 μ M) or the p53 inhibitor Pifithrin- β (PFT- β) for 2 h, followed by treatment with 8 mg/dL UA for another 10 h, with or without WR-1065 (p53 agonist). ABCG2, SLC2A9, and p53 protein levels were determined by western blot analysis. Protein levels were normalized to GAPDH. Data are presented as mean \pm SEM. * P < 0.05 and ** P < 0.01, n = 3.

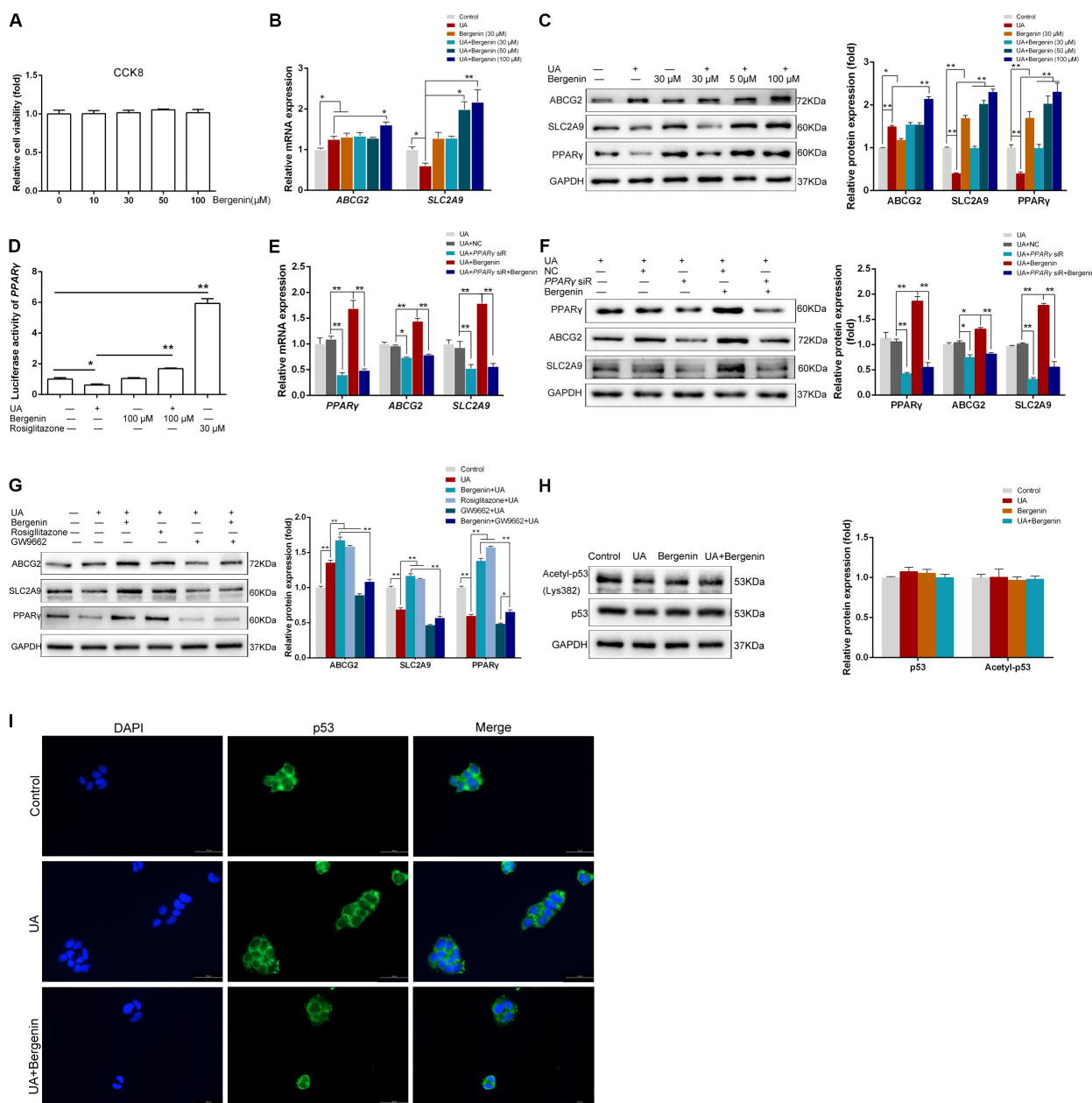
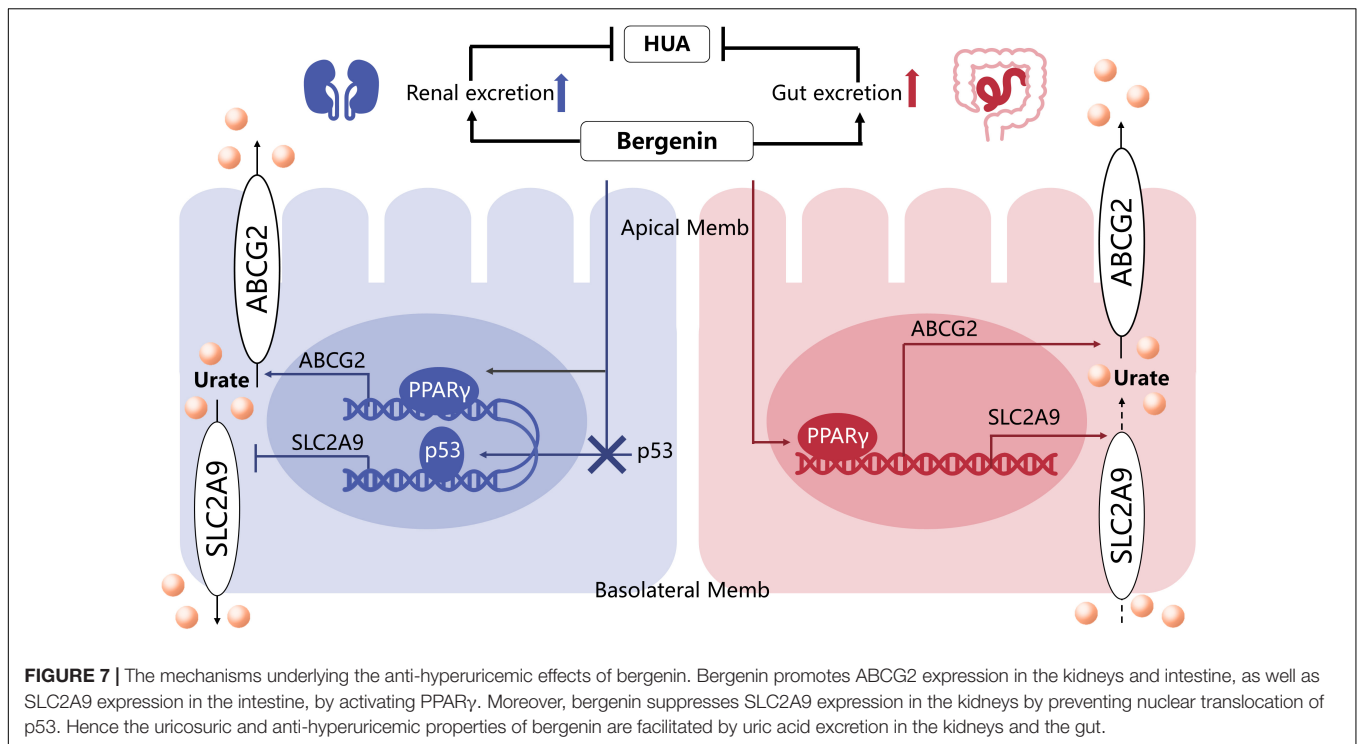


FIGURE 6 | Bergenin regulates the expression of ABCG2 and SLC2A9 in Caco-2 cell lines. **(A)** Cells were treated with bergenin (10, 30, 50, and 100 μ M) for 12 h, and cell viability was determined by the CCK8 assay. **(B)** Caco-2 cells were pretreated with 0, 30, 50, or 100 μ M bergenin for 2 h, followed by treatment with 8 mg/dL UA for 10 h. Relative mRNA levels of ABCG2, and SLC2A9, as determined by RT-qPCR. **(C)** Representative western blots showing ABCG2, SLC2A9, and PPAR γ protein levels. Protein levels were normalized to GAPDH. **(D)** Transcriptional activity of PPAR γ , as determined by luciferase assays. **(E)** Cells were transfected with PPAR γ siRNA or scrambled siRNA for 48 h. Cells were then pretreated with or without 100 μ M bergenin for 2 h, followed by incubation with 8 mg/dL UA for another 10 h. Relative mRNA levels of ABCG2, SLC2A9, and PPAR γ , as determined by RT-qPCR. **(F)** Representative western blots showing ABCG2, SLC2A9, and PPAR γ protein levels. Protein levels were normalized to GAPDH. **(G)** Cells were pretreated with bergenin (100 μ M) or rosiglitazone (PPAR γ agonist) for 2 h followed by incubation with 8 mg/dL UA for another 10 h, with or without GW9662 (PPAR γ inhibitor). ABCG2, SLC2A9, and PPAR γ protein levels were determined by western blotting. Protein levels were normalized to GAPDH. **(H)** Total p53 and acetylated p53 levels were determined by western blot analysis. Protein levels were normalized to GAPDH. **(I)** Representative immunofluorescence images (magnification, $\times 400$) showing p53 expression (green). Nuclei were stained with DAPI (blue). Scale bar = 50 μ m.

SLC2A9 is widely expressed, including in the liver, kidneys, intestine, brain, placenta, lungs, and peripheral leucocytes (Phay et al., 2000; DeBosch et al., 2014). In kidneys, *SLC2A9* is

responsible for reabsorption of urate at the basolateral membrane in the proximal renal tubule (Dinour et al., 2010). Herein, we demonstrated that bergenin decreased *SLC2A9* expression by



inhibiting the nuclear translocation of p53, which indicated that bergenin might not only have effect on urate excretion, but also urate reabsorption in the kidneys. Consistently, Itahana et al. (2015) showed that *SLC2A9* was a direct target gene of the tumor suppressor *p53*. Interestingly, we found no association between *SLC2A9* and *p53* levels in Caco-2 cells. Caco-2 is a well-characterized human colon adenocarcinoma cell line widely used to investigate mechanisms of drug absorption or characterize intestinal transporters. Caco-2 cells harbor *p53* mutations (Lee et al., 2008; Sun et al., 2008), which is a limitation of using this cell line model to assess the relevance of *p53* pathway in the anti-hyperuricemic effects of bergenin. In addition to the liver and kidneys, *SLC2A9* is also expressed on the apical and basolateral gut enterocyte membranes in mice (Lu et al., 2019). Gut enterocyte-specific *Slc2a9*-knockout mice exhibited increased serum urate levels with impaired enterocyte urate transport kinetics. Moreover, these mice developed early onset metabolic syndromes, including hypertension, dyslipidemia, and hyperinsulinemia, suggesting a role of *Slc2a9* in regulating enterocyte urate clearance (DeBosch et al., 2014). The upregulation of *Slc2a9* in the jejunum and ileum reported herein could have contributed to increased urate excretion from the intestine observed after bergenin treatment.

We also detected the xanthine oxidase activity in ileum and jejunum besides livers. The xanthine oxidase activity was almost undetectable in the ileum. No significant difference were found in the jejunum among the groups (Supplementary Figure S1B). However, Yoon et al. (2016) have shown *in vivo* XO inhibitory and antihyperuricemic effects of *Corylopsis coreana* Uyeki, containing and identified bergenin as one of constituents. As a herbal medicine, *Corylopsis coreana* Uyeki might also include

some other constituents responsible for the XO inhibitory activity. Synergizing action of a combination of several active components may be another possibility.

The crosstalk between PPAR γ and *SIRT1* plays an important role in the regulation of metabolism and inflammation (Han et al., 2010; Chou et al., 2017). Furthermore, p53 acetylation at Lys382, the primary target site of *SIRT1*, increases the ability of p53 to activate transcription (Feng et al., 2015; Nakamura et al., 2017). Therefore, we used siRNAs targeting *SIRT1* to explore the interaction. *SIRT1* silencing did not affect the expression of PPAR γ , ABCG2, or *SLC2A9* in HK-2 and Caco-2 cells, regardless of exposure to bergenin (Supplementary Figure S4).

Increasing evidence suggests that not only crystalline urate, but soluble urate could promote metabolic inflammation, activate innate immunity, and trigger epigenetic alterations that amplify pro-inflammatory responses (Crişan et al., 2017; Joosten et al., 2020). Studies in patients with asymptomatic hyperuricemia have shown that increased serum urate concentrations are associated with inflammatory responses, including increased IL-6, IL-1 β , TNF- α , and IL-18 levels and decreased IL-1Ra and IL-10 levels (Crişan et al., 2016; Crişan et al., 2017). Kim et al. (2015) reported that hyperuricemia induced NLRP3 activation in macrophages, accelerated macrophage recruitment, and promoted M1 phenotype polarization, contributing to diabetic nephropathy progression. These findings suggest that in addition to urate-lowering therapies, immunomodulatory therapies may also be helpful in hyperuricemia treatment. Bergenin is a plant-derived compound with well-documented anti-inflammatory properties (Veerapur et al., 2012). Notably, bergenin inhibited collagen-induced arthritis and ameliorated experimental colitis in mice by reducing the serum levels of

IL-2, IL-6, and TNF- α (Jain et al., 2014; Wang et al., 2017; Lopes de Oliveira et al., 2019). In this study, we found that the serum levels of IL-1 β , TNF- α , and IL-6 were increased in hyperuricemic mice and positively correlated with SUA. Bergenin treatment reduced the serum levels of IL-1 β , TNF- α , and IL-6 in hyperuricemic mice.

M1 macrophages are characterized by TNF- α and iNOS expression and mediate tissue damage and initiate inflammatory responses by secreting high levels of various pro-inflammatory cytokines, including IL-1 α , TNF- α , and IL-1 β (Shapouri-Moghaddam et al., 2018). To protect against excessive tissue damage and inflammation, macrophages can acquire an M2 phenotype, expressing several anti-inflammatory molecules, such as IL-10 and IL-1Ra (Shapouri-Moghaddam et al., 2018). In this study, we showed that bergenin treatment *in vitro* induced *Il-10*, *CD206* and *Arg-1* expression in macrophages while decreasing *Tnf- α* and *iNos* expression at the same time, suggesting a shift from the M1 to M2 phenotype. M2 polarization in macrophages after bergenin treatment can, therefore, be one of the mechanisms responsible for the anti-inflammatory effects of bergenin reported in previous studies. Nevertheless, the in-depth mechanisms involved in the inflammatory effects of bergenin in hyperuricemia need further investigation.

CONCLUSION

In summary (Figure 7), these findings indicated that bergenin not only can promote renal and gut uric acid excretion via regulating the expression of *ABCG2* and *SLC2A9* but also attenuate inflammation and induce a macrophage polarization shift from the M1 phenotype to M2. Thus, bergenin is a promising candidate as a novel therapeutic strategy for hyperuricemia, either for supplement of the existing ULT or potential intervention in metabolic inflammation.

REFERENCES

- Barai, P., Raval, N., Acharya, S., Borisa, A., Bhatt, H., and Acharya, N. (2019). Neuroprotective effects of bergenin in Alzheimer's disease: investigation through molecular docking, *in vitro* and *in vivo* studies. *Behav. Brain Res.* 356, 18–40. doi: 10.1016/j.bbr.2018.08.010
- Berger, J., and Moller, D. E. (2002). The mechanisms of action of PPARs. *Annu. Rev. Med.* 53, 409–435. doi: 10.1146/annurev.med.53.082901.104018
- Chen, M., Lu, X., Lu, C., Shen, N., Jiang, Y., Chen, M., et al. (2018). Soluble uric acid increases PDZK1 and ABCG2 expression in human intestinal cell lines via the TLR4-NLRP3 inflammasome and PI3K/Akt signaling pathway. *Arthritis Res. Ther.* 20:20. doi: 10.1186/s13075-018-1512-4
- Chen-Xu, M., Yokose, C., Rai, S. K., Pillinger, M. H., and Choi, H. K. (2019). Contemporary prevalence of gout and hyperuricemia in the United States and decadal trends: the National health and nutrition Examination Survey, 2007–2016. *Arthritis Rheumatol.* 71, 991–999. doi: 10.1002/art.40807
- Chou, H. C., Wen, L. L., Chang, C. C., Lin, C. Y., Jin, L., and Juan, S. H. (2017). From the Cover: L-Carnitine via PPARgamma- and Sirt1-dependent mechanisms attenuates epithelial-mesenchymal transition and renal fibrosis caused by perfluorooctanesulfonate. *Toxicol. Sci.* 160, 217–229. doi: 10.1093/toxsci/kfx183

DATA AVAILABILITY STATEMENT

The raw data supporting the conclusions of this article will be made available by the authors, without undue reservation, to any qualified researcher.

ETHICS STATEMENT

The animal study was reviewed and approved by Institutional Animal Care and Use Committee of Zhejiang University.

AUTHOR CONTRIBUTIONS

HW and XL contributed to design and funding sources to this study. MC and CY drafted the manuscript. MC, JZ, PZ, and YJ did all the *in vitro* parts of the study. All authors have contributed significantly and read and approved the final manuscript.

FUNDING

This work was supported by the National Natural Science Foundation of China (No. 81571577), Key Research and Development Program of Zhejiang Province (No. 2020C3044), Scientific Research Fund of Zhejiang Provincial Education Department, Medicine and Health Science and Technology Project of Zhejiang Province (No. 2017192934), and Science and Technology Plan Project of Zhejiang Province (No. 2017C37128).

SUPPLEMENTARY MATERIAL

The Supplementary Material for this article can be found online at: <https://www.frontiersin.org/articles/10.3389/fcell.2020.00703/full#supplementary-material>

- Crisan, T. O., Cleophas, M. C., Oosting, M., Lemmers, H., Toenhake-Dijkstra, H., Netea, M. G., et al. (2016). Soluble uric acid primes TLR-induced proinflammatory cytokine production by human primary cells via inhibition of IL-1Ra. *Ann. Rheum. Dis.* 75, 755–762. doi: 10.1136/annrheumdis-2014-206564
- Crisan, T. O., Cleophas, M. C. P., Novakovic, B., Erler, K., Van De Veerdonk, F. L., Stunnenberg, H. G., et al. (2017). Uric acid priming in human monocytes is driven by the AKT-PRAS40 autophagy pathway. *Proc. Natl. Acad. Sci. U.S.A.* 114, 5485–5490. doi: 10.1073/pnas.1620910114
- Dalbeth, N., Choi, H. K., Joosten, L. A. B., Khanna, P. P., Matsuo, H., Perez-Ruiz, F., et al. (2019). Gout. *Nat. Rev. Dis. Primers* 5:69. doi: 10.1038/s41572-019-0115-y
- DeBosch, B. J., Kluth, O., Fujiwara, H., Schurmann, A., and Moley, K. (2014). Early-onset metabolic syndrome in mice lacking the intestinal uric acid transporter SLC2A9. *Nat. Commun.* 5:4642. doi: 10.1038/ncomms5642
- Dinour, D., Gray, N. K., Campbell, S., Shu, X., Sawyer, L., Richardson, W., et al. (2010). Homozygous SLC2A9 mutations cause severe renal hypouricemia. *J. Am. Soc. Nephrol.* 21, 64–72. doi: 10.1681/ASN.2009040406
- Feng, Y., Liu, T., Dong, S. Y., Guo, Y. J., Jankovic, J., Xu, H., et al. (2015). Rotenone affects p53 transcriptional activity and apoptosis via targeting SIRT1 and H3K9 acetylation in SH-SY5Y cells. *J. Neurochem.* 134, 668–676. doi: 10.1111/jnc.13172

- Han, L., Zhou, R., Niu, J., McNutt, M. A., Wang, P., and Tong, T. (2010). SIRT1 is regulated by a PPAR[gamma]-SIRT1 negative feedback loop associated with senescence. *Nucleic Acids Res.* 38, 7458–7471. doi: 10.1093/nar/gkq609
- Hou, W., Ye, C., Chen, M., Li, W., Gao, X., He, R., et al. (2019). Bergenin activates SIRT1 as a novel therapeutic agent for osteogenesis of bone mesenchymal stem cells. *Front. Pharmacol.* 10:618. doi: 10.3389/fphar.2019.00618
- Ichida, K., Matsuo, H., Takada, T., Nakayama, A., Murakami, K., Shimizu, T., et al. (2012). Decreased extra-renal urate excretion is a common cause of hyperuricemia. *Nat. Commun.* 3:764. doi: 10.1038/ncomms1756
- Itahana, Y., Han, R., Barbier, S., Lei, Z., Rozen, S., and Itahana, K. (2015). The uric acid transporter SLC2A9 is a direct target gene of the tumor suppressor p53 contributing to antioxidant defense. *Oncogene* 34, 1799–1810. doi: 10.1038/nc.2014.119
- Jain, S. K., Singh, S., Khajuria, A., Guru, S. K., Joshi, P., Meena, S., et al. (2014). Pyrano-isochromanones as IL-6 inhibitors: synthesis, in vitro and in vivo antiarthritic activity. *J. Med. Chem.* 57, 7085–7097. doi: 10.1021/jm500901e
- Ji, Y., Wang, D., Zhang, B., and Lu, H. (2019). Bergenin ameliorates MPTP-induced Parkinson's disease by activating PI3K/Akt signaling pathway. *J. Alzheimers Dis.* 72, 823–833. doi: 10.3233/JAD-190870
- Joosten, L. A. B., Crisan, T. O., Bjornstad, P., and Johnson, R. J. (2020). Asymptomatic hyperuricaemia: a silent activator of the innate immune system. *Nat. Rev. Rheumatol.* 16, 75–86. doi: 10.1038/s41584-019-0334-3
- Kawamura, Y., Nakaoka, H., Nakayama, A., Okada, Y., Yamamoto, K., Higashino, T., et al. (2019). Genome-wide association study revealed novel loci which aggravate asymptomatic hyperuricaemia into gout. *Ann. Rheum. Dis.* 78, 1430–1437. doi: 10.1136/annrheumdis-2019-215521
- Kim, S. M., Lee, S. H., Kim, Y. G., Kim, S. Y., Seo, J. W., Choi, Y. W., et al. (2015). Hyperuricemia-induced NLRP3 activation of macrophages contributes to the progression of diabetic nephropathy. *Am. J. Physiol. Renal. Physiol.* 308, F993–F1003. doi: 10.1152/ajprenal.00637.2014
- Kumar, S., Sharma, C., Kaushik, S. R., Kulshreshtha, A., Chaturvedi, S., Nanda, R. K., et al. (2019). The phytochemical bergenin as an adjunct immunotherapy for tuberculosis in mice. *J. Biol. Chem.* 294, 8555–8563. doi: 10.1074/jbc.RA119.008005
- Kuo, C. F., Grainge, M. J., Zhang, W., and Doherty, M. (2015). Global epidemiology of gout: prevalence, incidence and risk factors. *Nat. Rev. Rheumatol.* 11, 649–662. doi: 10.1038/nrrheum.2015.91
- Lee, W., Belkhir, A., Lockhart, A. C., Merchant, N., Glaeser, H., Harris, E. I., et al. (2008). Overexpression of OATP1B3 confers apoptotic resistance in colon cancer. *Cancer Res.* 68, 10315–10323. doi: 10.1158/0008-5472.CAN-08-1984
- Liang, C., Pei, S., Ju, W., Jia, M., Tian, D., Tang, Y., et al. (2017). Synthesis and in vitro and in vivo antitumor activity study of 11-hydroxyl esterified bergenin/cinnamic acid hybrids. *Eur. J. Med. Chem.* 133, 319–328. doi: 10.1016/j.ejmech.2017.03.053
- Lopes de Oliveira, G. A., Alarcón De La Lastra, C., Rosillo, M., Castejon Martinez, M. L., Sánchez-Hidalgo, M., Rolim Medeiros, J. V., et al. (2019). Preventive effect of bergenin against the development of TNBS-induced acute colitis in rats is associated with inflammatory mediators inhibition and NLRP3/ASC inflammasome signaling pathways. *Chemico Biol. Interact.* 297, 25–33. doi: 10.1016/j.cbi.2018.10.020
- Lu, J., Dalbeth, N., Yin, H., Li, C., Merriman, T. R., and Wei, W. H. (2019). Mouse models for human hyperuricaemia: a critical review. *Nat. Rev. Rheumatol.* 15, 413–426. doi: 10.1038/s41584-019-0222-x
- Mandard, S., and Patsouris, D. (2013). Nuclear control of the inflammatory response in mammals by peroxisome proliferator-activated receptors. *PPAR Res.* 2013:613864. doi: 10.1155/2013/613864
- Mukherjee, H., Ojha, D., Bharitkar, Y. P., Ghosh, S., Mondal, S., Kaity, S., et al. (2013). Evaluation of the wound healing activity of *Shorea robusta*, an Indian ethnomedicine, and its isolated constituent(s) in topical formulation. *J. Ethnopharmacol.* 149, 335–343. doi: 10.1016/j.jep.2013.06.045
- Nakamura, K., Zhang, M., Kageyama, S., Ke, B., Fujii, T., Sosa, R. A., et al. (2017). Macrophage heme oxygenase-1-SIRT1-p53 axis regulates sterile inflammation in liver ischemia-reperfusion injury. *J. Hepatol.* 67, 1232–1242. doi: 10.1016/j.jhep.2017.08.010
- Nakatochi, M., Kanai, M., Nakayama, A., Hishida, A., Kawamura, Y., Ichihara, S., et al. (2019). Genome-wide meta-analysis identifies multiple novel loci associated with serum uric acid levels in Japanese individuals. *Commun. Biol.* 2:115. doi: 10.1038/s42003-019-0339-0
- Nakayama, A., Nakaoka, H., Yamamoto, K., Sakiyama, M., Shaukat, A., Toyoda, Y., et al. (2017). GWAS of clinically defined gout and subtypes identifies multiple susceptibility loci that include urate transporter genes. *Ann. Rheum. Dis.* 76, 869–877. doi: 10.1136/annrheumdis-2016-209632
- Perez-Ruiz, F., Calabozo, M., Erauskin, G. G., Ruibal, A., and Herrero-Beites, A. M. (2002). Renal underexcretion of uric acid is present in patients with apparent high urinary uric acid output. *Arthritis Rheum.* 47, 610–613. doi: 10.1002/art.10792
- Phay, J. E., Hussain, H. B., and Moley, J. F. (2000). Cloning and expression analysis of a novel member of the facilitative glucose transporter family, SLC2A9 (GLUT9). *Genomics* 66, 217–220. doi: 10.1006/geno.2000.6195
- Roberts, R. L., Wallace, M. C., Phipps-Green, A. J., Topless, R., Drake, J. M., Tan, P., et al. (2017). ABCG2 loss-of-function polymorphism predicts poor response to allopurinol in patients with gout. *Pharmacogenomics J.* 17, 201–203. doi: 10.1038/tpj.2015.101
- Shapouri-Moghaddam, A., Mohammadian, S., Vazini, H., Taghadosi, M., Esmaili, S. A., Mardani, F., et al. (2018). Macrophage plasticity, polarization, and function in health and disease. *J. Cell. Physiol.* 233, 6425–6440. doi: 10.1002/jcp.26429
- Singh, R., Kumar, V., Bharate, S. S., and Vishwakarma, R. A. (2017). Synthesis, pH dependent, plasma and enzymatic stability of bergenin prodrugs for potential use against rheumatoid arthritis. *Bioorg. Med. Chem.* 25, 5513–5521. doi: 10.1016/j.bmc.2017.08.011
- Stiburkova, B., Pavelcova, K., Pavlikova, M., Jesina, P., and Pavelka, K. (2019). The impact of dysfunctional variants of ABCG2 on hyperuricemia and gout in pediatric-onset patients. *Arthritis Res. Ther.* 21:77. doi: 10.1186/s13075-019-1860-8
- Sun, H., Chow, E. C., Liu, S., Du, Y., and Pang, K. S. (2008). The Caco-2 cell monolayer: usefulness and limitations. *Expert Opin. Drug Metab. Toxicol.* 4, 395–411. doi: 10.1517/17425255.4.4.395
- Szatmari, I., Vamosi, G., Brazda, P., Balint, B. L., Benko, S., Szeles, L., et al. (2006). Peroxisome proliferator-activated receptor gamma-regulated ABCG2 expression confers cytoprotection to human dendritic cells. *J. Biol. Chem.* 281, 23812–23823. doi: 10.1074/jbc.M604890200
- To, K. K., and Tomlinson, B. (2013). Targeting the ABCG2-overexpressing multidrug resistant (MDR) cancer cells by PPARgamma agonists. *Br. J. Pharmacol.* 170, 1137–1151. doi: 10.1111/bph.12367
- Veerapur, V. P., Prabhakar, K. R., Thippeswamy, B. S., Bansal, P., Srinivasan, K. K., and Unnikrishnan, M. K. (2012). Antidiabetic effect of *Ficus racemosa* Linn. stem bark in high-fat diet and low-dose streptozotocin-induced type 2 diabetic rats: a mechanistic study. *Food Chem.* 132, 186–193. doi: 10.1016/j.foodchem.2011.10.052
- Wang, J., Zhu, X. X., Liu, L., Xue, Y., Yang, X., and Zou, H. J. (2016). SIRT1 prevents hyperuricemia via the PGC-1alpha/PPARgamma-ABCG2 pathway. *Endocrine* 53, 443–452. doi: 10.1007/s12020-016-0896-7
- Wang, K., Li, Y. F., Lv, Q., Li, X. M., Dai, Y., and Wei, Z. F. (2017). Bergenin, acting as an agonist of PPARgamma, ameliorates experimental colitis in mice through improving expression of SIRT1, and therefore inhibiting NF-kappaB-mediated macrophage activation. *Front. Pharmacol.* 8:981. doi: 10.3389/fphar.2017.00981
- Ye, C., Hou, W., Chen, M., Lu, J., Chen, E., Tang, L., et al. (2019). IGF1BP2 acts as a negative regulator of RANKL-induced osteoclastogenesis and oestrogen deficiency-induced bone loss. *Cell Prolif.* 53:e12752. doi: 10.1111/cpr.12752
- Yoon, I.-S., Park, D.-H., Ki, S.-H., and Cho, S.-S. (2016). Effects of extracts from *Corylopsis coreana* Uyeki (Hamamelidaceae) flos on xanthine oxidase activity and hyperuricemia. *J. Pharm. Pharmacol.* 12, 1597–1603. doi: 10.1111/jph.12626

Conflict of Interest: The authors declare that the research was conducted in the absence of any commercial or financial relationships that could be construed as a potential conflict of interest.

Copyright © 2020 Chen, Ye, Zhu, Zhang, Jiang, Lu and Wu. This is an open-access article distributed under the terms of the Creative Commons Attribution License (CC BY). The use, distribution or reproduction in other forums is permitted, provided the original author(s) and the copyright owner(s) are credited and that the original publication in this journal is cited, in accordance with accepted academic practice. No use, distribution or reproduction is permitted which does not comply with these terms.



Circular RNAs: Functions and Clinical Significance in Cardiovascular Disease

Lei Zhang^{1*}, Yuan Zhang¹, Yin Wang¹, Yanfang Zhao², Han Ding¹ and Peifeng Li^{1*}

¹ Institute for Translational Medicine, The Affiliated Hospital of Qingdao University, Qingdao University, Qingdao, China,

² Institute of Biomedical Research, School for Life Science, Shandong University of Technology, Zibo, China

OPEN ACCESS

Edited by:

Rebecca Ann Wingert,
University of Notre Dame,
United States

Reviewed by:

Myriam Gorospe,
National Institutes of Health (NIH),
United States

Bin Liu,
Mississippi State University,
United States

Dachun Xu,
Tongji University, China

*Correspondence:

Lei Zhang
leizhang@qdu.edu.cn

Peifeng Li
peifli@qdu.edu.cn

Specialty section:

This article was submitted to
Molecular Medicine,
a section of the journal
Frontiers in Cell and Developmental
Biology

Received: 16 July 2020

Accepted: 09 September 2020

Published: 29 September 2020

Citation:

Zhang L, Zhang Y, Wang Y,
Zhao Y, Ding H and Li P (2020)
Circular RNAs: Functions and Clinical
Significance in Cardiovascular
Disease.
Front. Cell Dev. Biol. 8:584051.
doi: 10.3389/fcell.2020.584051

Cardiovascular disease (CVD) causes high morbidity and mortality worldwide. Accumulating research has indicated the possible roles played by circular RNAs (circRNAs) in the pathogenesis of CVD. CircRNAs are non-coding RNAs with covalently closed loop structures. CircRNAs can function by acting as miRNA sponges, RNA binding protein sponges, mRNA transcriptional regulators and templates for protein translation. The specific characteristics of circRNAs such as high stability, abundant distribution, and tissue- and developmental stage-specific expression make them potential biomarkers for the diagnosis and prognosis of CVD. In this paper, we systematically summarized the current knowledge regarding the biogenesis, biological properties and the action mechanisms of circRNAs, elucidated the roles played by circRNAs in the pathogenesis of CVD, and explored the diagnostic potential of circRNAs in CVD. With in-depth studies, an increasing number of molecular mechanisms underlying the participation of circRNAs in CVD may be elucidated, and the application of circRNAs in the clinical diagnosis and prevention of CVD may eventually be realized.

Keywords: cardiovascular disease, circular RNAs, pathogenesis, diagnosis, clinical application

INTRODUCTION

Cardiovascular disease (CVD) is one of the leading causes of morbidity and mortality worldwide. In recent decades, scientists have made considerable progress in the diagnosis and treatment of CVD. However, the increasing tendency of the mortality rate of CVD has not been stopped to date. Therefore, novel and effective strategies for the diagnostic and therapeutic interventions of CVD are strongly warranted. A growing number of studies have determined that non-coding RNAs, such as microRNAs (miRNAs) and long non-coding RNAs (lncRNAs), participate in the pathological processes of CVD and can serve as biological markers in diagnosis, prognosis and clinical treatment (Yang et al., 2016; Zhang L. et al., 2018, 2020). In the last several years, circular RNAs (circRNAs) have also been reported to be associated with CVD.

CircRNAs are covalently closed loop structures with no 5' cap and 3' polyadenylated tail. CircRNAs were first identified in plant viruses (Kolakofsky, 1976) and were thought to have no function or very limited function (Nigro et al., 1991; Cocquerelle et al., 1992; Capel et al., 1993). Subsequently, the existence of circRNAs has also been reported in many organisms, such as yeast (Schroeder et al., 1983) and humans (Cocquerelle et al., 1993). The rapid development of prediction, detection and screening technologies for circRNAs facilitates the discovery of different types of circRNAs. Studies have reported that circRNAs might participate in the regulation of physiological and pathological processes of different kinds of CVD (Fan et al., 2017; Lim et al., 2020), such as myocardial infarction (MI) (Geng et al., 2016; Cai et al., 2019), cardiac senescence

(Du et al., 2016; Chen et al., 2018) and coronary artery disease (CAD) (Holdt et al., 2016; Dang et al., 2017; Shan et al., 2017). CircRNAs have a variety of characteristics, including high stability, tissue- and developmental-specific expression, and the altered expression in the pathological and normal conditions of various diseases (Werfel et al., 2016; Siede et al., 2017; Gupta et al., 2018). Due to these characteristics, circRNAs exhibit considerable potential as biomarkers for the detection of CVD from human blood samples (Vausort et al., 2016; Zhao et al., 2017). In this paper, we will summarize the available knowledge on the biogenesis of circRNAs, the functions of circRNAs, the roles of circRNAs in CVD and the diagnostic potential of circRNAs in CVD.

BIOGENESIS OF CircRNAs

CircRNAs are divided into three categories: exonic circRNAs (ecircRNAs or ecRNAs) (Zhang et al., 2014), circular intronic RNAs (ciRNAs) (Zhang et al., 2013) and exon-intron circRNAs (EIciRNAs) (Li et al., 2015). CircRNAs are generated from pre-mRNAs through backsplicing. Four mechanisms of circRNA formation have been revealed. The 5' end of the intron (splice donor site, GU) and the 3' end of the intron (splice acceptor site, AG) can be covalently bound to generate an exon-containing lariat, which will be internally spliced thereafter to form an exonic circle (Jeck et al., 2013; Jeck and Sharpless, 2014) (**Figure 1A**). The RNA base motifs (e.g., Alu repeats) in the introns of pre-mRNA can pair with the complementary sequences (Jeck et al., 2013; Zhang et al., 2014), and direct cyclization subsequently occurs to generate ecRNAs (introns removed) or EIciRNAs (introns retained) (Jeck et al., 2013) (**Figure 1B**). In the introns, the C-rich element close to the branch and the GU-rich element close to the 5' splice site can bind together, and then the other exons and introns are removed by the spliceosome to form ciRNAs (Zhang et al., 2013) (**Figure 1C**). The bridging of RNA binding proteins (RBPs) with pre-mRNAs has also been elaborated to facilitate the production of circRNAs (ecRNAs or EIciRNAs) (Ashwal-Fluss et al., 2014; Conn et al., 2015) (**Figure 1D**).

Multiple factors participate in the biogenesis of circRNAs. Quaking (QKI) and Muscleblind (MBL) proteins function as regulatory activators of the biogenesis of circRNAs (Ashwal-Fluss et al., 2014; Conn et al., 2015). In contrast, an adenosine deaminase acting on RNA-1 inhibits the circRNA formation by destroying the stem structures (Rybak-Wolf et al., 2015). Serine-arginine and heterogeneous nuclear ribonucleoprotein can regulate the generation of circRNAs in *Drosophila* (Kramer et al., 2015).

BIOLOGICAL PROPERTIES OF CircRNAs

CircRNAs have some common characteristics and the most important ones are elaborated as follows.

- (1) Wide distribution and diversity. CircRNAs are found in many eukaryotic organisms ranging from plants to animals and in all tissues (Jeck et al., 2013). In humans, over 30,000

circRNAs have been found and the number will increase in the future (Xu et al., 2017; Zeng X. X. et al., 2017).

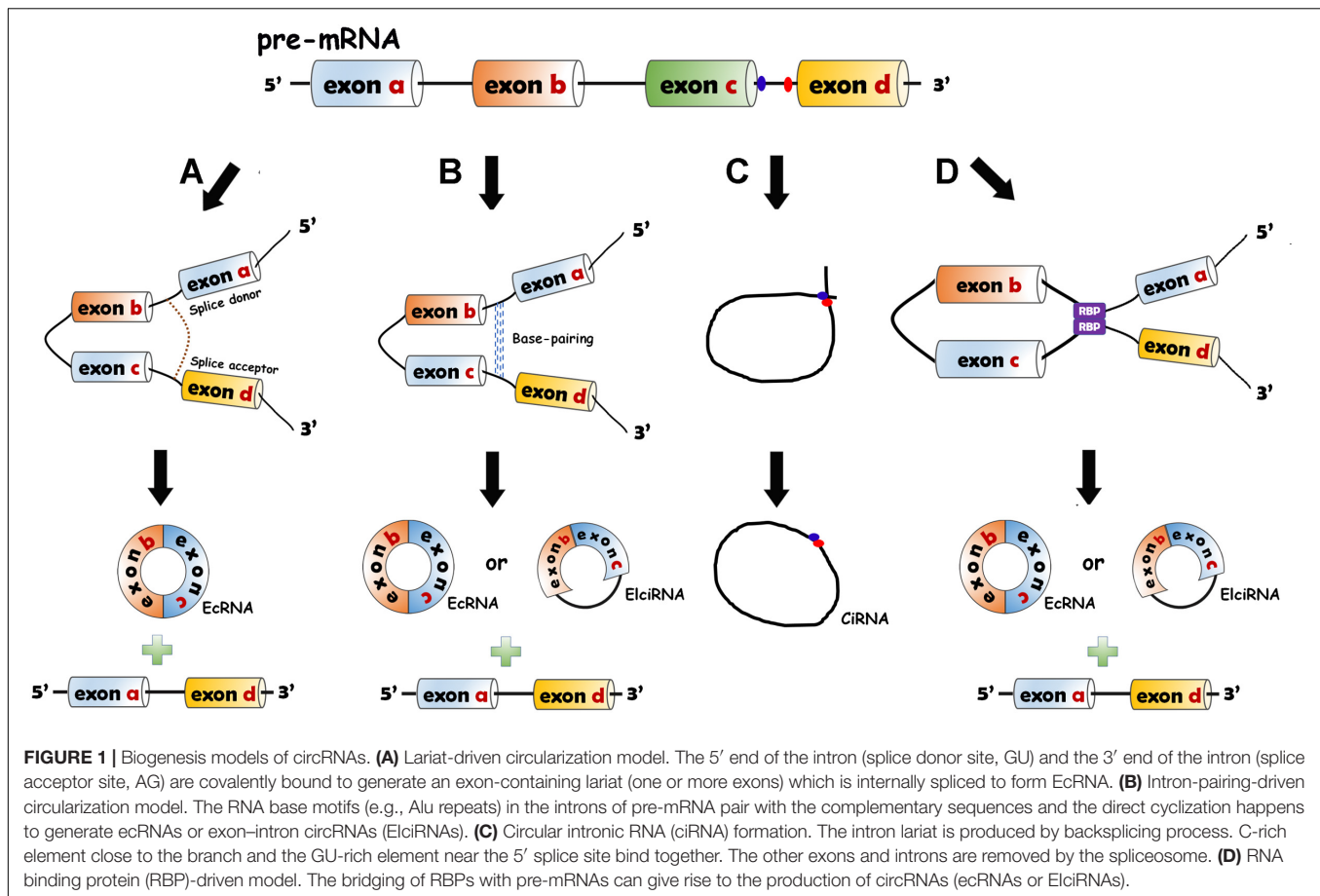
- (2) High stability. Because of the covalently closed structures, circRNAs are resistant to the degradation by ribonuclease (RNase) and are more stable than linear RNAs (Suzuki et al., 2006).
- (3) Specific expression. CircRNAs are specifically expressed in different tissues, cells and developmental stages (Jakobi et al., 2016; Li Y. S. et al., 2017; Xu et al., 2017). circRNAs have different profiles at four stages of heart differentiation (Li Y. S. et al., 2017). Significant alterations have been detected at different developmental stages in cardiomyocytes derived from induced pluripotent stem cells (Siede et al., 2017).
- (4) Evolutionary conservation. Many circRNAs seem to be evolutionarily conserved among species (Jeck et al., 2013; AbouHaidar et al., 2014). Jeck et al. (2013) found the homology of 2121 circRNAs between human fibroblasts and mouse genome. Werfel et al. (2016) reported high homology of 1288 circRNAs across human, mouse and rat. However, Werfel et al. (2016) also revealed that only a small number of circRNAs were conserved. Other studies have also illustrated that many circRNAs are specific to species (Aufiero et al., 2019; Lim et al., 2020).
- (5) Dynamic expression profiles between normal and pathological conditions. A lot of circRNAs have altered expression related to diseases. Zheng et al. (2016) revealed altered expression of many circRNAs between normal tissues and cancerous tissues. In many other diseases, the expression differences of circRNAs have also been verified (Werfel et al., 2016; Siede et al., 2017; Gupta et al., 2018). Some studies reported lack of dynamic expression of circRNAs in specific diseases (Werfel et al., 2016; Tan et al., 2017).

THE UNDERLYING MECHANISMS OF CircRNA FUNCTIONS

The characteristics of circRNAs, such as wide distribution, high stability, expression specificity and localization, indicate that circRNAs have various biological functions. Recent studies have illustrated that circRNAs can function through different mechanisms (**Figure 2**).

Some CircRNAs Act as miRNA Sponges

CircRNAs contain miRNA response elements (MREs) that facilitate the binding of circRNAs and miRNAs. This binding decreases the level of functional miRNAs and thus increases the expression of miRNA targets (Hansen et al., 2013a; Tay et al., 2014). This process is known as the "sponge effect," as circRNAs can absorb miRNAs similar to sponges (**Figure 2A**). Many circRNAs can function as miRNA sponges. CiRS-7/CDR1_{as} contains more than 70 binding sites for miR-7 that are involved in the pathogenesis of various diseases (Hansen et al., 2013b; Pan et al., 2018; Liu et al., 2019). The binding of ciRS-7/CDR1_{as} to miR-7 causes downregulation of miR-7 and elevated levels



of miR-7 target genes. Sry, a testis-specific circRNA, has 16 conserved MREs for miR-138 (Hansen et al., 2013a). The activity of miR-138 is inhibited due to the sponge effect and the miR-138 target genes are upregulated (Hansen et al., 2013a). CircHIPK3 have different MREs (total number: 18) which allow it to bind to nine different miRNAs (Zheng et al., 2016). HRCR can bind to miR-223 which promotes the pathogenesis of cardiac hypertrophy and heart failure (HF) (Wang et al., 2016). CircNFIB can competitively absorb miR-433 to enhance cardiac fibroblast proliferation induced by the stimulation of TGF- β (Zhu et al., 2019). CircRNA_000203 can directly sponge miR-26b-5p and miR-140-3p to regulate the occurrence of cardiac hypertrophy (Li et al., 2019).

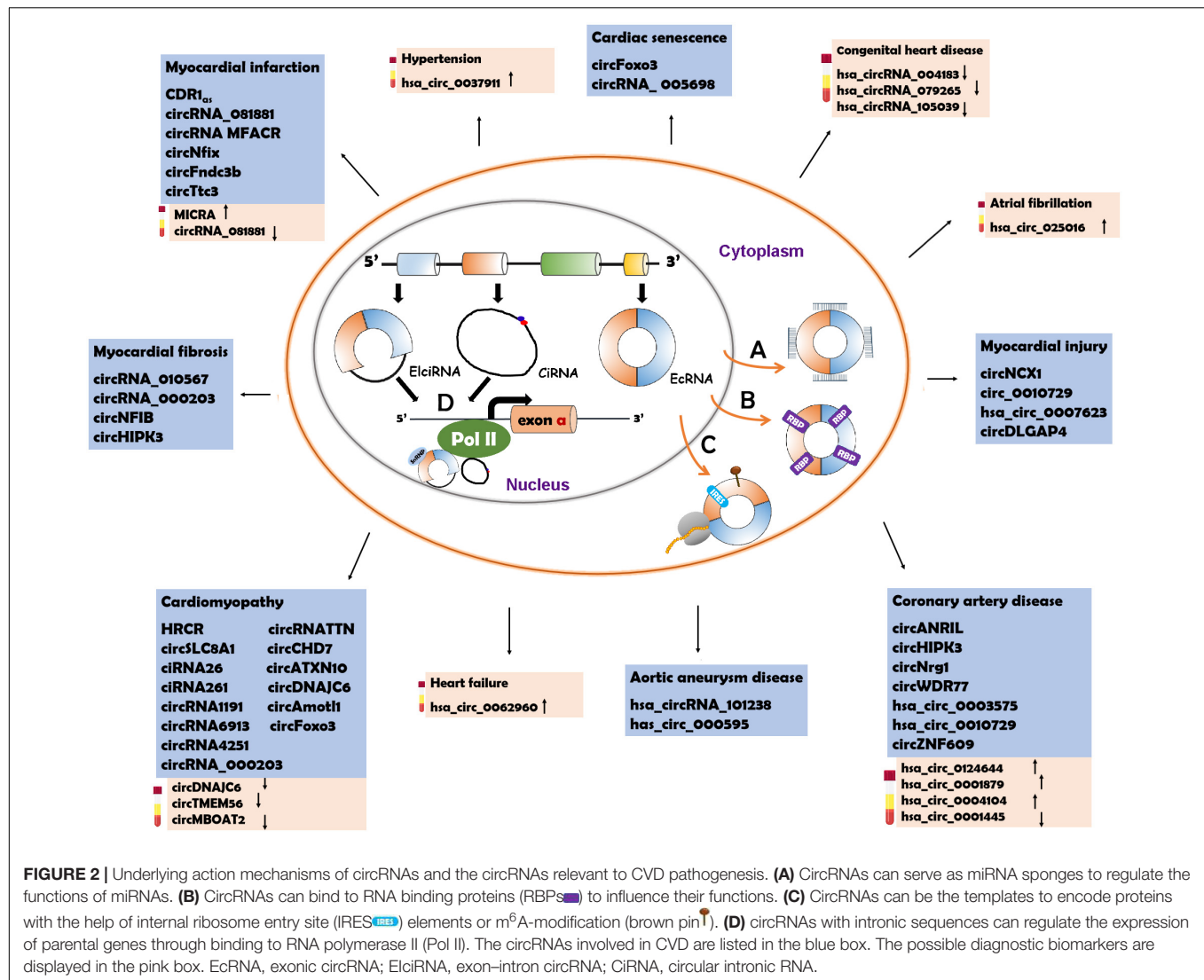
Some CircRNAs Serve as RBP Sponges

CircRNAs can interact with RBPs and inhibit RBP activity (Figure 2B). CircMbl is produced from the same pre-mRNA as the MBL protein and can absorb MBL proteins to regulate the subsequent physiological processes (Ashwal-Fluss et al., 2014). CircPABPN1 can bind to HuR, which is a well-known RBP, to prevent the interaction between HuR and PABPN1 mRNA, suppressing the translation of PABPN1 mRNA (Abdelmohsen et al., 2017). CircANRIL competitively recruits PES1 (an essential 60S-preribosomal assembly factor), leading to inhibition of

ribosome biogenesis (Holdt et al., 2016). CircFoxo3 participates in the processes of cardiomyocyte senescence and cell cycle progression through interacting with different RBPs, such as anti-senescent protein ID-1, transcription factor E2F1, anti-stress proteins FAK, p21 (cyclin-dependent kinase inhibitor 1) and CDK2 (cyclin-dependent kinase 2) (Du et al., 2017). CircAmotl1 can protect cardiomyocytes and promote cell proliferation and wound repair by binding to the cardioprotective molecules (PDK1 and AKT1) and to STAT3 (signal transducer and activator of transcription 3) (Yang Z. G. et al., 2017; Zeng Y. et al., 2017).

Some CircRNAs Encode Peptides

Studies conducted in recent years have demonstrated that circRNAs can serve as templates for protein translation (Chen and Sarnow, 1995; Wesselhoeft et al., 2018) (Figure 2C). It was first observed in prokaryotes that circRNAs were able to encode proteins. In 1986, studies in hepatitis D virus showed that circRNAs could be translated into functional proteins (Kos et al., 1986). In *Escherichia coli*, a circRNA was also reported to act as a translation template (Perriman and Ares, 1998). CircRNAs lack a 5' cap and a 3' polyadenylated tail which are typical translation initiation structures of linear RNAs. Nevertheless, instead of recruiting ribosomes, circRNA translation is initiated with the help of specific elements, such as IRES (internal ribosome entry



site) and *N*-methyladenosine (m⁶A) (Chen and Sarnow, 1995; Wesselhoeft et al., 2018). When IRESs are introduced into a circRNA, the synthetic circRNA initiates translation (Chen and Sarnow, 1995). CircZNF609 has an IRES element and can be translated into a protein that functions in myoblast proliferation (Legnini et al., 2017). CircFBXW7 can be translated into a functional protein that plays a role in the inhibition of glioma tumorigenesis with the assistance of the IRES element (Yang et al., 2018). m⁶A modification has been illustrated to facilitate the translation of linear mRNAs in a cap-independent manner (Meyer et al., 2015). Some circRNAs also employ m⁶A to initiate translation (Yang Y. et al., 2017). The m⁶A reader YTHDF3 can interact with circRNAs and subsequently recruit translation initiation factors to drive the initiation of circRNA translation (Yang Y. et al., 2017). In a study based on ribosome profiling of *Drosophila* heads, circMbl3 was demonstrated to be the template for splicing-dependent translation (Pamudurti et al., 2017). Another recent study found that circβ-catenin could be translated into the β-CATENIN isoform, a functional protein

that activates the Wnt/β-catenin pathway and promotes tumor development in liver cancer (Liang et al., 2019).

Some CircRNAs Regulate the Transcription of Parental Genes

Of the three types of circRNAs, ecRNAs account for the majority and are predominantly located in the cytosol (Hansen et al., 2013a; Memczak et al., 2013). The cytoplasmic localization of ecRNAs facilitates their functions as miRNA sponges, RBP sponges and translational templates. CiRNAs and EicRNAs are confined to the nucleus due to their intronic sequences (Zhang et al., 2013). Recent studies have verified the roles of nucleus-localized ciRNA and EicRNA in the transcriptional regulation of their parental genes (Zhang et al., 2013; Li et al., 2015) (Figure 2D). CiRNAs can directly interact with RNA polymerase II (Pol II) and enhance parental gene transcription (Zhang et al., 2013), whereas EicRNAs bind to the U1 small nuclear ribonucleoproteins (snRNPs) at first, and the complex promotes

the interaction with Pol II (Li et al., 2015). CiRNA-ankrd52 can bind to Pol II of the pre-mRNA of the *ANKRD52* gene to promote transcription, while the knockdown of *ciankrd52* may cause a significant transcriptional decrease in the parental gene (Zhang et al., 2013). CircEIF3J and circPAIP2 are EICiRNAs that can form a complex with U1 snRNP and Pol II (Li et al., 2015). In general, ciRNAs and EICiRNAs can serve as transcription regulators of their parental genes.

CircRNA IDENTIFICATION AND RESEARCH DATABASES

Various methods have been developed to identify and study the functions of circRNAs. RNA-seq, microarray, Northern Blot and RT-PCR analyses are the most widely used. RNA-seq can identify new circRNA species and quantify circRNA expression. Next-generation sequencing and depletion of ribosomal RNA methods may be cooperatively utilized for circRNA-seq. The microarray method can only detect and quantify known circRNAs approximately and the results require further confirmation. For high-throughput sequencing, reliable and precise algorithms are of vital importance. Many algorithms have been developed, such as circRNA-finder, MapSplice, CIRCexplorer, and CIRI (Hansen et al., 2016). The combined use of these algorithms may improve the accuracy and sensitivity of circRNA identification. Northern Blot and RT-PCR methods only validate known circRNAs dependent on an exonuclease-RNase R, which cleaves linear RNAs from the 3' end (Asha et al., 1983). With circular structures, circRNAs can avoid the cleavage of RNase R. Thus, in the extraction process, total RNA is digested by RNase R to discard the linear RNAs (Szabo and Salzman, 2016). The collected RNAs are then combined with specific probes (Northern Blot method) or reverse-transcribed to obtain cDNAs of circRNAs (RT-PCR method). Aside from these methods for circRNA identification, some other methods are employed to analyze the subcellular localization (fluorescence *in situ* hybridization) or the interaction between circRNAs and miRNAs/RBPs (e.g., RNA immunoprecipitation and dual luciferase reporter assay) (Li Y. et al., 2018; Zirkel and Papantonis, 2018). In addition to these known methods, simpler and more efficient methods are still urgently needed for the identification and characterization of circRNAs.

To elucidate the roles of circRNAs, many online databases have been developed (Table 1). Different databases emphasize on different aspects of circRNA research including prediction, identification, protein-coding annotation, circRNA-miRNA interactions and circRNA-RBP interactions. The combined use of these databases may help to establish a foundation for the further studies of circRNAs.

CircRNAs AND CARDIOVASCULAR DISEASES

With the use of advanced technologies in sequencing and data analysis, a lot of circRNAs have been detected in human hearts

and been reported to be associated with CVD (Jakobi et al., 2016; Werfel et al., 2016; Fan et al., 2017; Tan et al., 2017) (Table 2 and Figure 2). Moreover, circRNAs have been observed to have great potential as biomarkers for the diagnosis and prognosis of CVD (Vausort et al., 2016; Sonnenschein et al., 2019; Wu et al., 2019; Vilades et al., 2020) (Table 3 and Figure 2).

Myocardial Infarction

Myocardial infarction provokes cardiac remodeling and is often complicated by arrhythmia, shock or HF. CDR1_{as} has been determined to sponge miR-7 and to have elevated levels in mice with MI (Geng et al., 2016). The increased levels of CDR1_{as} can upregulate PARP and SP1, the targets of miR-7, which may subsequently enlarge the size of MI (Geng et al., 2016). CircRNA_081881 has been found to be associated with acute MI. CircRNA_081881 has seven binding sites for miR-548, and the competitive binding upregulates the expression of PPAR γ which can protect the heart from acute MI (Deng et al., 2016). MTP18 participates in the development of MI. CircRNA MFACR could absorb miR-652-3p to increase the expression of MTP18 and subsequently promote the progression of MI (Wang et al., 2017). CircNfix has been revealed to promote the degradation of Ybx1 and sponge miR-214. The downregulation of circNfix inhibited cardiomyocyte apoptosis after MI and promoted cardiac regeneration and repair (Huang et al., 2019). CircFndc3b exhibited significantly decreased expression levels in post-MI mouse hearts. CircFndc3b could function through interacting with RBP-FUS which regulates the expression and the signaling pathway of vascular endothelial growth factor-A (VEGF-A). The overexpression of circFndc3b in post-MI mouse hearts could decrease cardiomyocyte apoptosis and fibrosis, enhance neovascularization, reduce infarct size and attenuate left ventricular dysfunction after MI (Garikipati et al., 2019). CircTtc3 was reported to be significantly upregulated in rats with MI (Cai et al., 2019). CircTtc3 could recruit miR-15b-5p to repress its inhibitory effect on Arl2, an ADP-ribosylation factor relevant to cardiomyocyte viability (Cai et al., 2019). The knockdown of circTtc3 exacerbated the symptoms of cardiac dysfunction post-MI, suggesting that circTtc3 plays a role in the cardiac protection in MI (Cai et al., 2019).

Myocardial Fibrosis

Myocardial fibrosis is a disease condition in which normal myocardium is replaced by non-beating cardiac fibroblasts, resulting in diastole difficulty. CircRNA_010567 exhibited significantly increased levels in both diabetic mouse myocardium and Angiotensin-II (Ang-II)-induced cardiac fibroblasts (CFs) (Zhou and Yu, 2017). CircRNA_010567 was found to recruit miR-141. The competitive binding of circRNA_010567 and miR-141 released the inhibitory effect of TGF- β 1, a pro-fibrotic factor, thereby promoting myocardial fibrosis (Zhou and Yu, 2017). CircRNA_000203 was also revealed to be elevated in diabetic mouse myocardium and Ang-II-induced CFs (Tang et al., 2017). CircRNA_000203 could sponge miR-26b-5p to attenuate the inhibition of its targets, Col1a2 and CTGF, which are fibrosis-associated proteins. Thus, the

TABLE 1 | Database for circRNA research.

Name	URL	Function
circBase	http://www.circbase.org/	Collects the circular RNA information of many species, such as human, mouse, <i>C. elegans</i> , etc.
CircInteractome	https://circinteractome.nia.nih.gov/	Maps RBP- and miRNA-binding sites on human circRNAs; Designs primers and siRNA sequence of circRNAs.
CircNet	http://circnet.mbc.nctu.edu.tw/	Integrates the following information: identification of new circRNAs; genome annotation of circRNAs; the expression profile of circRNAs; the network of circRNA-miRNA -mRNA.
circRNABase	http://starbase.sysu.edu.cn/mirCircRNA.php	Integrates the published data to construct the interaction network of miRNA and circRNA, or circRNA and RBP.
circRNADb	http://reprod.njmu.edu.cn/circrnadb	Summarizes circRNAs that encode proteins; contains 32,914 human circRNAs.
Circ2Traits	http://gyanxet-beta.com/circdb/	Collects circRNAs potentially associated with human diseases or traits.
CIRCpedia	http://www.picb.ac.cn/rnomics/circpedia/	Provides annotations on circRNAs and variable shear events of different cell lines/tissues
Deepbase	http://deepbase.sysu.edu.cn/	Emphasizes the interaction of ceRNA molecular network; integrates the information related to circRNAs.
TSCD	http://gb.whu.edu.cn/TSCD/	Provides information of tissue-specific circRNAs in main tissues of human and mouse.
circRNA disease	http://cgga.org.cn:9091/circRNADisease/	Includes the data of the association between circRNAs and disease, the expression of circRNAs in the patients, the detection methods of circRNA
CSCD	http://gb.whu.edu.cn/CSCD	Collects cancer-specific circRNAs; elaborates the interaction between miRNA and circRNA, or circRNA and RBP; predicts variable splicing of related genes.

TSCD, tissue specific circRNA database; *CSCD*, cancer-specific circRNA database; *RBP*, RNA binding protein.

upregulation of circRNA_000203 may promote the proliferation of CFs (Tang et al., 2017). CircNFIB was downregulated in primary adult CFs treated with TGF- β (Zhu et al., 2019). Overexpression of circNFIB attenuates CF proliferation while inhibition of circNFIB promotes CF proliferation, indicating the cardioprotective role of circNFIB (Zhu et al., 2019). CircHIPK3 was upregulated in CFs treated with Ang-II (Ni et al., 2019). CircHIPK3 was revealed to sponge miR-29b-3p which can target fibrosis-associated proteins such as Col1a2, Col3a1 and α -SMA. The elevated level of circHIPK3 ultimately enhanced the function of Col1a2, Col3a1 and α -SMA, thereby promoting myocardial fibrosis (Ni et al., 2019). In general, circRNA_010567, circRNA_000203 and circHIPK3 are profibrotic while circNFIB is antifibrotic.

Myocardial Injury

Myocardial injury as well as apoptosis is usually correlated to HF, MI, and ischemia-reperfusion (I/R) injury. CircNCX1 was found to have elevated levels during oxidative stress (Li M. et al., 2018). CircNCX1 could bind to miR-133a-3p and subsequently increase the activity of cell death-inducing protein 1 (CDIP1), inducing apoptosis and I/R injury (Li M. et al., 2018). Circ_0010729 was elucidated to play a role in the injury of human cardiomyocytes induced by oxygen-glucose-deprivation (OGD) (Jin and Chen, 2019). The downregulation of circ_0010729 attenuated the OGD-induced cell injury by activating the mTOR and MEK/ERK pathways (Jin and Chen, 2019). Hsa_circ_0007623 was confirmed to have cardioprotective effects in isoproterenol-induced acute ischemia mice. Hsa_circ_0007623 was able to bind to miR-297 and repress the inhibitory effect of miR-297 on VEGF-A, thereby promoting cell proliferation, migration and angiogenesis (Zhang Q. et al., 2020). Wang S. et al. (2019) speculated that circDLGAP4 may regulate cardiomyocyte apoptosis in myocardial I/R injury through targeting miR-143. However, no additional experimental evidence has been reported to date.

Cardiomyopathy

Cardiomyopathy is a disease with abnormal heart muscles. The muscles are stretched, weakened, or have other structural changes, causing pump difficulties of heart. Most patients with cardiomyopathy will have HF (Molkentin et al., 1998; Aaronson and Sackner-Bernstein, 2006; Rajabi et al., 2007; van Rooij et al., 2008; Authors/Task Force et al., 2014; Wang et al., 2016; Lim et al., 2019). Hypertrophic cardiomyopathy (HCM, cardiac hypertrophy) and dilated cardiomyopathy (DCM, cardiac dilatation) are two common subtypes of cardiomyopathy. When HCM happens, the heart muscles are stretched and become thick, thereby decreasing or blocking the blood flow. In DCM, the heart muscles are weakened, leading to the loss of pumping power of the heart. HRCR could bind to miR-223-5p to decrease its activity and could subsequently upregulate its target, ARC (apoptosis inhibitor with CARD domain), resulting in the inhibition of HCM and HF (Wang et al., 2016). CircSLC8A1 has recently been demonstrated to be the sponge of miR-133a (Lim et al., 2019). The knockdown of circSLC8A1 in cardiomyocytes lessened the hypertrophy induced by pressure overload, whereas the overexpression of circSLC8A1 caused HF (Lim et al., 2019). CircRNA_000203 can bind to miR-26b-5p and miR-140-3p to increase the expression level of their target gene-GATA4 (Li et al., 2019). The elevated level of GATA4 promotes the occurrence of cardiac hypertrophy (Li et al., 2019). Several circRNAs (ciRNA26, ciRNA261, circRNA1191, circRNA4251, and circRNA6913) were reported to exhibit altered expression in cardiac cells with HCM when they were cultured in high levels and normal levels of D-glucose, respectively (Meng et al., 2019). These circRNAs might be sponges of more than 60 miRNAs, suggesting that they have vital functions in HCM.

RBM20 plays a critical role in the splicing of many cardiac genes, whose mutation will cause aggressive DCM (Brauch et al., 2009). RBM20 can regulate the generation of TTN

TABLE 2 | CircRNAs with CVD.

CVD type	CircRNAs	Source	Action mechanism	Regulation	References
Myocardial infarction	CDR1 _{as}	Mouse myocardial tissue	Sponge miR-7	Up	Geng et al. (2016)
	CircRNA_081881	Blood	Sponge miR-548	Down	Deng et al. (2016)
	CircRNA MFACR	A/R and I/R mouse models	Sponge miR-652-3p	Up	Wang et al. (2017)
	CircNfix	Mouse heart section	Dual function as miR-214 sponge and inducing YBX1 degradation	Down	Huang et al. (2019)
	CircFndc3b	Mouse hearts	Interact with RBP-FUS	Down	Garikipati et al. (2019)
	CircTtc3	Rat myocardium	Sponge miR-15b-5p	Up	Cai et al. (2019)
Myocardial fibrosis	CircRNA_010567	Mouse myocardium, cardiac fibroblasts	Sponge miR-141	Up	Zhou and Yu (2017)
	CircRNA_000203	Mouse myocardium, cardiac fibroblasts	Sponge miR-26b-5p	Up	Tang et al. (2017)
	CircNFIB	Mouse heart tissue	Sponge miR-433	Down	Zhu et al. (2019)
	CircHIPK3	Mouse cardiac fibroblasts	Sponge miR-29b-3p	UP	Ni et al. (2019)
	CircNCX1	Mouse cardiomyocytes	Sponge miR-133a-3p	Up	Li M. et al. (2018)
Myocardial injury	Circ_0010729	Human cardiomyocytes	Sponge miR-145-5p	Down	Jin and Chen (2019)
	Hsa_circ_0007623	Acute ischemia mice	Sponge miR-297	Up	Zhang Q. et al. (2020)
	CircDLGAP4	Myocardial ischemia-reperfusion injury	Sponge miR-143	Up	Wang S. et al. (2019)
	HRCR	Mouse cardiomyocytes	Sponge miR-223-5p	Down	Wang et al. (2016)
Cardiomyopathy	CircSLC8A1	Mouse cardiomyocytes	Sponge miR-133a	—	Lim et al. (2019)
	CircRNA_000203	NMVCs	Sponge miR-26b-5p and miR-140-3p	Up	Li et al. (2019)
	CiRNA26	Mouse cardiomyocytes	Sponge several miRNAs	Down	Meng et al. (2019)
	CiRNA261	Mouse cardiomyocytes	Sponge several miRNAs	Up	Meng et al. (2019)
	CircRNA1191	Mouse cardiomyocytes	Sponge several miRNAs	Down	Meng et al. (2019)
	CircRNA6913	Mouse cardiomyocytes	Sponge several miRNAs	Up	Meng et al. (2019)
	CircRNA4251	Mouse cardiomyocytes	Sponge several miRNAs	Down	Meng et al. (2019)
	CircRNATTN 1/2/4/5	DCM patient with a heterozygous mutation in <i>RBM20</i> (E913K).	Unknown	Down	Khan et al. (2016)
	CircSLC8A1	Human dilated cardiomyopathy	Unknown	Up	Siede et al. (2017)
	CircCHD7	Human dilated cardiomyopathy	Unknown	Up	Siede et al. (2017)
	CircATXN10	Human dilated cardiomyopathy	Unknown	Up	Siede et al. (2017)
	CircDNAJC6	Human dilated cardiomyopathy	Unknown	Down	Siede et al. (2017)
	CircSLC8A1	Heart tissues from DCM patient	Unknown	Up	Lei et al. (2018)
	CircAmotl1	Human neonatal cardiac tissue	Interact with AKT and PDK1	Up	Zeng Y. et al. (2017)
	CircFoxo3	Mouse heart tissue	Interact with ID-1, E2F1, FAK, and HIF1a	Up	Du et al. (2017)
	Hsa_circ_000595	Aortic smooth muscle cells	Sponge miR-19a	Up	Zheng et al. (2015)
	Hsa_circRNA_101238	Human aortic segments	Sponge miR-320a	Up	Zou et al. (2017)

(Continued)

TABLE 2 | Continued

CVD type	CircRNAs	Source	Action mechanism	Regulation	References
Cardiac senescence	CircRNA005698	Sow cardiac muscle	Sponge seven miRNAs	Up	Chen et al. (2018)
	CircFoxo3	Mouse heart tissue	Interact with ID-1, E2F1, FAK, and HIF1a	Up	Du et al. (2017)
Coronary artery disease	CircANRIL	Mouse cardiac fibroblast	p21 and CDK2	Up	Du et al. (2016)
		Human peripheral blood	Interact with PES1	Down	Holdt et al. (2016)
	CircHIPK3	Different cell lines	Interact with INK4/ARF	Down	Burd et al. (2010)
		Diabetic retinopathy	Sponge miR-30a-3p	Up	Shan et al. (2017)
	CircNrg1	MASMCs	Sponge miR-193b-5p	Down	Sun et al. (2019)
	CircWDR77	VSMCs	Sponge miR-124	Up	Chen et al. (2017)
	Nine circRNAs	VSMCs	Sponge miR-130a-3p	–	Pan et al. (2017)
	Hsa_circ_0003575	HUVECs	Sponge miR-9-5p and miR-199-3p	Up	Li C. Y. et al. (2017)
	Hsa_circ_0010729	HUVECs	Sponge miR-186	Up	Dang et al. (2017)
	CircZNF609	HUVECs	Sponge miR-615-5p	Up	Liu et al. (2017)

VSMC, vascular smooth mother cell; SMC, smooth mother cell; PBMC, peripheral blood mononuclear cell; HUVEC, human umbilical vein endothelial cells.

circRNA which might be involved in DCM (Khan et al., 2016). CircSLC8A1, circCHD7, and circATXN10 were found to have elevated expression levels in DCM patients compared with control patients, while circDNAJC6 expression levels were reduced (Siede et al., 2017). The increased expression level of circSLC8A1 was also observed in another study in dilated heart tissue compared with control tissues (Lei et al., 2018). CircAmotl1 has been reported to bind to PDK1 and AKT1, two cardioprotective molecules (Zeng Y. et al., 2017). This interaction activated AKT1 through phosphorylation and facilitated the nuclear translocation of AKT1 to protect cardiomyocytes in doxorubicin-induced cardiomyopathy (Zeng Y. et al., 2017). CircFoxo3 has been determined to promote doxorubicin-induced ventricular dilatation (Du et al., 2017).

Aortic Aneurysm Disease

Aortic dissection is the most serious aneurysm disease. Through screening of aortic tissues from patients with aortic dissection aneurysms, Zheng et al. (2015) found an obviously upregulated circRNA, hsa_circ_000595. Hsa_circ_000595 was found to promote apoptosis in vascular smooth mother cells (VSMCs) under hypoxic conditions through upregulating miR-19a expression. Zou et al. (2017) found 162 circRNAs with abnormal expression by microarray analysis of three thoracic aortic dissection (TAD) patients and three control subjects, in which hsa_circRNA_101238 was notably increased. Hsa_circRNA_101238 could sponge miR-320a to inhibit its activity, thereby increasing the levels of its target, MMP9 protein (a TAD related protein) (Zou et al., 2017).

Cardiac Senescence

Cardiac senescence greatly depresses heart function. Through high throughput RNA-seq, Chen et al. (2018) identified 22 circRNAs with dynamic expression in cardiac muscle during aging. Some of them might regulate the pro-coagulation process. CircRNA005698 was found to be a sponge for seven miRNAs and might be a biomarker for cardiac senescence (Chen et al., 2018). CircFoxo3 was reported to bind to several RBPs (ID-1, E2F1, FAK and HIF1a) and inhibit their activities, thereby promoting cardiomyocyte senescence (Du et al., 2017). CircFoxo3 could also absorb two G1 to S phase transition-related proteins (p21 and CDK2) and suppress their functions in the cell cycle, leading to cell cycle repression (Du et al., 2016).

Hypertension

Hypertension is a common chronic disease and a major risk factor for CVD. Through profiling of plasma, Wu et al. (2017) identified 59 circRNAs that exhibited altered expression between hypertensive patients and healthy controls. Additionally, a profiling with blood found 351 circRNAs that had different levels from patients with chronic thromboembolic pulmonary hypertension and healthy people (Miao et al., 2017). However, due to the small cohort (five patients and five controls for both studies), all the results in these studies require further validation. Overall, the number of studies on circRNAs in

TABLE 3 | Circulating circRNAs as diagnostic biomarkers of CVD.

CVD type	CircRNAs	Source	Regulation	References
Myocardial infarction	MICRA	Peripheral blood	Up	Vausort et al. (2016)
	CircRNA_081881	Plasma	Down	Deng et al. (2016)
Congenital heart diseases	Hsa_circRNA_004183	Plasma	Down	Wu et al. (2019)
	Hsa_circRNA_079265	Plasma	Down	Wu et al. (2019)
	Hsa_circRNA_105039	Plasma	Down	Wu et al. (2019)
Hypertension	Hsa_circ_0037911	Whole blood	Up	Bao et al. (2018)
Cardiomyopathy	CircDNAJC6	Serum	Down	Sonnenschein et al. (2019)
	CircTMEM56	Serum	Down	Sonnenschein et al. (2019)
	CircMBOAT2	Serum	Down	Sonnenschein et al. (2019)
Heart failure	Hsa_circ_0062960	Plasma	Up	Sun et al. (2020)
Coronary artery disease	Hsa_circ_0124644	Peripheral blood	Up	Zhao et al. (2017)
	Hsa_circ_0001879	PBMCs	Up	Wang L. et al. (2019)
	Hsa_circ_0004104	PBMCs	Up	Wang S. et al. (2019)
	Hsa_circ_0001445	Plasma	Down	Vilades et al. (2020)
Atrial fibrillation	Hsa_circ_025016	Plasma	Up	Zhang J. et al. (2018)

PBMCs, peripheral blood mononuclear cells.

hypertension remains small. More studies should be conducted to elucidate the mechanisms.

Coronary Artery Disease

Coronary artery disease is a chronic disease mainly caused by atherosclerosis. miRNAs have been shown to function in all pathogenesis processes of CAD (Zhang L. et al., 2018, 2020), such as endothelial dysfunction, lipid metabolism disorder, proliferation and differentiation of smooth muscle cells (SMCs). Recently, circRNAs have also been found to participate in the development of CAD. CircANRIL was testified to interact with PES1 to suppress pre-rRNA maturation and subsequently restrain the biogenesis of ribosomes, which consequently enhances the stability of anti-atherogenic cells (Holdt et al., 2016). The high level of circANRIL might reduce the severity of CAD (Holdt et al., 2016). Thus, circANRIL plays an atheroprotective role. In addition, circANRIL was also illustrated to play a role in the formation of atherosclerosis by regulating the expression of INK4/ARF (Burd et al., 2010). CircHIPK3 was found to have elevated level in diabetic retinopathy. CircHIPK3 could promote endothelial proliferation and vascular dysfunction through binding to miR-30a-3p which can target VEGFC and WNT2 (Shan et al., 2017). Neuregulin-1 (NRG1) participates in vascular physiopathology (Odiote et al., 2012). CircNrg1 was revealed to sponge miR-193b-5p which could target its host mRNA, *Nrg1*. The overexpression of circNrg1 led to an elevated level of NRG1, whereas the silencing of circNrg1 decreased the level of NRG1 (Sun et al., 2019). CircWDR77 was determined to be increased in VSMCs treated with high glucose (Chen et al., 2017). CircWDR77 could sponge miR-124 to increase the activity of its target, FGF-2 (fibroblast growth factor 2), thereby promoting VSMC proliferation and migration (Chen et al., 2017). Pan et al. (2017) identified 24 circRNAs which were differentially expressed by circRNA microarray. Among these circRNAs, nine circRNAs were found

to sponge hsa-miR-130a-3p and then increase the level of TRPM3 which regulates the proliferation and contractility of VSMCs in cooperation with cholesterol (Pan et al., 2017). OxLDL treatment can be employed to induce endothelial cells injury to simulate the pathogenesis of atherosclerosis or CAD. Hsa_circ_0003575 was found to have elevated expression in oxLDL-induced HUVECs (human umbilical vein endothelial cells) (Li C. Y. et al., 2017). The study elaborated that hsa_circ_0003575 could regulate endothelial cells proliferation and angiogenesis probably through interacting with miR-9-5p and miR-199-3p (Li C. Y. et al., 2017). Dang et al. (2017) performed a circRNA microarray in hypoxia-induced HUVECs to identify 36 circRNAs with abnormal expression, and they reported that hsa_circ_0010729 was upregulated. Hsa_circ_0010729 could sponge miR-186 to regulate vascular endothelial cell proliferation and apoptosis via targeting HIF-1 α . Circular RNA-ZNF609 was reported to have increased expression in HUVECs under high glucose and hypoxia stress, both *in vivo* and *in vitro*. CircZNF609 could regulate endothelial cell function by binding to miR-615-5p which targets the transcription factor MEF2A. The knockdown of circZNF609 promoted endothelial cell migration and inhibited endothelial cell apoptosis (Liu et al., 2017).

CircRNAs AS BIOMARKERS FOR CVD

Currently, a variety of circulating molecules, such as proteins and miRNAs, have been illustrated to have diagnostic potential for CVD. Such proteins as troponins, creatine kinase-MB and myoglobin have been widely used in the clinic. However, these proteins are not specific and are not applicable for the early diagnosis. Additionally, these proteins are easily influenced by such factors as the heart-associated diseases, medication, patient genetic background, and age (Chen et al., 2008; Lawrie et al., 2008). Therefore, protein biomarkers have limited diagnostic value. Circulating miRNAs have been elaborated to have high

specificity and strong potential for early diagnosis. However, circulating miRNAs have not been applied in the clinic due to their low content and time-consuming detection (Zhang L. et al., 2018). Circulating circRNAs have many features resembling circulating miRNAs including high stability, sensitivity and specificity, which are essential for biomarkers. Meanwhile, the circulating levels of circRNAs are not low, and some circRNAs even have high content, making detection easier. Many studies have revealed the considerable potential of circulating circRNAs as novel and promising biomarkers for the early diagnosis of CVD (**Table 3** and **Figure 2**).

CircZNF609 (MICRA) had lower levels in the peripheral blood of MI patients than in healthy controls (Vausort et al., 2016). Circulating MICRA was demonstrated to have a high value of predicting left ventricular dysfunction (Vausort et al., 2016). CircRNA_081881 was downregulated in the plasma of AMI patients and might be a promising target for AMI diagnosis and therapy (Deng et al., 2016). The level of hsa_circ_0124644 was increased in the peripheral blood of CAD patients and was found to have a significant association with CAD. Receiver operating characteristic (ROC) analysis revealed that circulating hsa_circ_0124644 might be a potential diagnostic biomarker for CAD (Zhao et al., 2017). Hsa_circ_0001879 and hsa_circ_0004104 were found to have increased levels in the peripheral blood mononuclear cells (PBMCs) of CAD patients (Wang L. et al., 2019). ROC analysis revealed their high accuracy in the diagnosis of CAD. Furthermore, the combination of hsa_circ_0001879, hsa_circ_0004104 and CAD risk factors had the highest value to discriminate CAD patients from healthy controls (Wang L. et al., 2019). Atrial fibrillation (AF) is a common complication after coronary artery bypass grafting (CABG) (Maesen et al., 2012). Hsa_circ_025016 was upregulated in the plasma of patients with new-onset AF after isolated off-pump CABG. ROC analysis revealed a high diagnostic value (Zhang J. et al., 2018). The analysis with a large validation cohort confirmed the diagnostic power of hsa_circ_025016 (Zhang J. et al., 2018). All results indicated that hsa_circRNA_025016 might be a promising biomarker for the prediction of new-onset AF after isolated off-pump CABG (Zhang J. et al., 2018). Sun et al. (2020) performed circRNA microarrays and found significantly upregulated plasma levels of hsa_circ_0112085, hsa_circ_0062960, hsa_circ_0053919 and hsa_circ_0014010 in HF patients. ROC analysis revealed that hsa_circ_0062960 had great potential to be a diagnostic biomarker of HF (Sun et al., 2020). A study using whole blood revealed that the hsa_circ_0037911 level was significantly increased in hypertensive patients in contrast to the control group (Bao et al., 2018). Another study revealed reduced expression levels of circRNAs (DNAJC6, TMEM56 and MBOAT2) in the serum of patients with HCM (Sonnenschein et al., 2019). All three circRNAs had high discrimination power between HCM patients and the control cohort. Moreover, circTMEM56 and circDNAJC6 could be indicators of disease severity in patients with HCM (Sonnenschein et al., 2019). Wu et al. (2019) reported three notably downregulated circRNAs (hsa_circRNA_004183, hsa_circRNA_079265 and hsa_circRNA_105039) in the plasma of children with congenital heart diseases (CHD) and employed

ROC analyses to determine their potential to be biomarkers. They found the great potential of three circRNAs as novel non-invasive diagnostic biomarkers for CHD (Wu et al., 2019). Hsa_circ_0001445 was shown to have lower plasma levels in CAD patients than in the control group (Vilades et al., 2020). Hsa_circ_0001445 is secreted into circulation through being packaged in extracellular vesicles of coronary SMCs (Vilades et al., 2020). The coronary atherosclerotic condition abolished the association of hsa_circ_0001445 and vesicles, leading to the downregulation of plasma hsa_circ_0001445 (Vilades et al., 2020). Therefore, hsa_circ_0001445 might be considered an effective and novel predictor of CAD (Vilades et al., 2020). In general, these studies have illuminated the potential role of circulating circRNAs as biomarkers for the diagnosis and prognosis of CVD.

CONCLUSION AND FUTURE PERSPECTIVES

Base on our exploration, the results from a variety of studies have confirmed that circRNAs can participate in the pathogenesis of CVD mainly through acting as miRNA sponges and interacting with RBPs. CircRNAs are widely distributed in different tissues and have tissue- and developmental stage-specific expression. In addition, circRNAs are stable and abundantly present in the circulatory system. Therefore, circRNAs might be promising biomarkers for the diagnosis of CVD, and accumulating research has confirmed this possibility. The clinical use of circRNAs as diagnostic biomarkers will greatly facilitate the prevention and treatment of CVD. However, there are some problems that should be solved before clinical application of circRNAs.

First, there is no generally accepted methodology on the measurement procedures of circulating circRNAs, which might result in the lack of consistency in various studies. Hence, a standardized methodology should be formulated before clinical use. Second, the sample sizes are small in most studies. The insufficient samples might lead to deviation in the test results. A larger cohort is necessary for correct conclusions. Finally, despite these findings, the underlying mechanisms of the functions of many circulating circRNAs have not been elucidated, and our knowledge is still insufficient, which represents a considerable obstacle to clinical application. More and deeper studies should be performed to explore the potential molecular mechanisms.

In summary, studies have confirmed that circRNAs are closely involved in the progression of CVD and might be promising biomarkers for CVD. These findings may provide a new avenue for the prevention, diagnosis and therapeutic intervention of CVD in the future.

AUTHOR CONTRIBUTIONS

LZ and YZhang drafted the manuscript. YZhao and HD edited the manuscript. YW revised the manuscript. PL and LZ conceived the idea and framework of the review and made

the final proofreading. All authors read and approved the final manuscript.

FUNDING

This work was supported by the National Natural Science Foundation of China (Grant Numbers: 91849209 and 31430041)

REFERENCES

- Aaronson, K. D., and Sackner-Bernstein, J. (2006). Risk of death associated with nesiritide in patients with acutely decompensated heart failure. *JAMA* 296, 1465–1466. doi: 10.1001/jama.296.12.1465
- Abdelmohsen, K., Panda, A. C., Munk, R., Grammatikakis, I., Dudekula, D. B., De, S., et al. (2017). Identification of HuR target circular RNAs uncovers suppression of PABPN1 translation by CircPABPN1. *RNA Biol.* 14, 361–369. doi: 10.1080/15476286.2017.1279788
- AbouHaidar, M. G., Venkataraman, S., Golshani, A., Liu, B. L., and Ahmad, T. (2014). Novel coding, translation, and gene expression of a replicating covalently closed circular RNA of 220 nt. *Proc. Natl. Acad. Sci. U.S.A.* 111, 14542–14547. doi: 10.1073/pnas.1402814111
- Asha, P. K., Blouin, R. T., Zaniewski, R., and Deutscher, M. P. (1983). Ribonuclease BN: identification and partial characterization of a new tRNA processing enzyme. *Proc. Natl. Acad. Sci. U.S.A.* 80, 3301–3304. doi: 10.1073/pnas.80.11.3301
- Ashwal-Fluss, R., Meyer, M., Pamudurti, N. R., Ivanov, A., Bartok, O., Hanan, M., et al. (2014). circRNA biogenesis competes with pre-mRNA splicing. *Mol. Cell* 56, 55–66. doi: 10.1016/j.molcel.2014.08.019
- Aufiero, S., Reckman, Y. J., Pinto, Y. M., and Creemers, E. E. (2019). Circular RNAs open a new chapter in cardiovascular biology. *Nat. Rev. Cardiol.* 16, 503–514.
- Authors/Task Force, M., Elliott, P. M., Anastasakis, A., Borger, M. A., Borggrefe, M., Cecchi, F., et al. (2014). 2014 ESC Guidelines on diagnosis and management of hypertrophic cardiomyopathy: the Task Force for the Diagnosis and Management of Hypertrophic Cardiomyopathy of the European Society of Cardiology (ESC). *Eur. Heart J.* 35, 2733–2779. doi: 10.1093/eurheartj/ehu284
- Bao, X., Zheng, S., Mao, S., Gu, T., Liu, S., Sun, J., et al. (2018). A potential risk factor of essential hypertension in case-control study: Circular RNA hsa_circ_0037911. *Biochem. Biophys. Res. Commun.* 498, 789–794. doi: 10.1016/j.bbrc.2018.03.059
- Brauch, K. M., Karst, M. L., Herron, K. J., de Andrade, M., Pellikka, P. A., Rodeheffer, R. J., et al. (2009). Mutations in ribonucleic acid binding protein gene cause familial dilated cardiomyopathy. *J. Am. Coll. Cardiol.* 54, 930–941. doi: 10.1016/j.jacc.2009.05.038
- Burd, C. E., Jeck, W. R., Liu, Y., Sanoff, H. K., Wang, Z., and Sharpless, N. E. (2010). Expression of linear and novel circular forms of an INK4/ARF-associated non-coding RNA correlates with Atherosclerosis risk. *PLoS Genet.* 6:e1001233. doi: 10.1371/journal.pgen.1001233
- Cai, L., Qi, B., Wu, X., Peng, S., Zhou, G., Wei, Y., et al. (2019). Circular RNA Ttc3 regulates cardiac function after myocardial infarction by sponging miR-15b. *J. Mol. Cell Cardiol.* 130, 10–22. doi: 10.1016/j.yjmcc.2019.03.007
- Capel, B., Swain, A., Nicolis, S., Hacker, A., Walter, M., Koopman, P., et al. (1993). Circular transcripts of the testis-determining gene Sry in adult mouse testis. *Cell* 73, 1019–1030. doi: 10.1016/0092-8674(93)90279-y
- Chen, C. Y., and Sarnow, P. (1995). Initiation of protein synthesis by the eukaryotic translational apparatus on circular RNAs. *Science* 268, 415–417. doi: 10.1126/science.7536344
- Chen, J., Zou, Q., Lv, D., Wei, Y., Raza, M. A., Chen, Y., et al. (2018). Comprehensive transcriptional landscape of porcine cardiac and skeletal muscles reveals differences of aging. *Oncotarget* 9, 1524–1541. doi: 10.18632/oncotarget.23290
- Chen, J. J., Cui, L. Q., Yuan, J. L., Zhang, Y. Q., and Sang, H. J. (2017). Circular RNA WDR77 target FGF-2 to regulate vascular smooth muscle cells proliferation and migration by sponging miR-124. *Biochem. Biophys. Res. Commun.* 494, 126–132. doi: 10.1016/j.bbrc.2017.10.068

and Innovative Talent Program of Qingdao City, China (18-1-2-6-zhc).

ACKNOWLEDGMENTS

The authors would like to thank Liang Xu for the help in the manuscript revision.

- Chen, X., Ba, Y., Ma, L., Cai, X., Yin, Y., Wang, K., et al. (2008). Characterization of microRNAs in serum: a novel class of biomarkers for diagnosis of cancer and other diseases. *Cell Res.* 18, 997–1006. doi: 10.1038/cr.2008.282
- Cocquerelle, C., Daubersies, P., Majerus, M. A., Kerckaert, J. P., and Bailleul, B. (1992). Splicing with inverted order of exons occurs proximal to large introns. *EMBO J.* 11, 1095–1098.
- Cocquerelle, C., Mascrez, B., Hetuin, D., and Bailleul, B. (1993). Mis-splicing yields circular RNA molecules. *FASEB J.* 7, 155–160. doi: 10.1096/fasebj.7.1.7678559
- Conn, S. J., Pillman, K. A., Toubia, J., Conn, V. M., Salamanidis, M., Phillips, C. A., et al. (2015). The RNA binding protein quaking regulates formation of circRNAs. *Cell* 160, 1125–1134. doi: 10.1016/j.cell.2015.02.014
- Dang, R. Y., Liu, F. L., and Li, Y. (2017). Circular RNA hsa_circ_0010729 regulates vascular endothelial cell proliferation and apoptosis by targeting the miR-186/HIF-1 α axis. *Biochem. Biophys. Res. Commun.* 490, 104–110. doi: 10.1016/j.bbrc.2017.05.164
- Deng, Y. Y., Zhang, W. P., She, J. Q., Zhang, L. S., Chen, T., Zhou, J., et al. (2016). Circular RNA related to PPAR gamma function as ceRNA of microRNA in human acute myocardial infarction. *J. Am. Coll. Cardiol.* 68, C51–C52. doi: 10.1016/j.jacc.2016.07.189
- Du, W. W., Yang, W., Chen, Y., Wu, Z. K., Foster, F. S., Yang, Z., et al. (2017). Foxo3 circular RNA promotes cardiac senescence by modulating multiple factors associated with stress and senescence responses. *Eur. Heart J.* 38, 1402–1412. doi: 10.1093/eurheartj/ehw001
- Du, W. W., Yang, W., Liu, E., Yang, Z., Dhaliwal, P., and Yang, B. B. (2016). Foxo3 circular RNA retards cell cycle progression via forming ternary complexes with p21 and CDK2. *Nucl. Acids Res.* 44, 2846–2858. doi: 10.1093/nar/gkw027
- Fan, X., Weng, X., Zhao, Y., Chen, W., Gan, T., and Xu, D. (2017). Circular RNAs in Cardiovascular Disease: An Overview. *Biomed. Res. Int.* 2017:5135781. doi: 10.1155/2017/5135781
- Garikipati, V. N. S., Verma, S. K., Cheng, Z. J., Liang, D. M., Truongcao, M. M., Cimini, M., et al. (2019). Circular RNA CircFndc3b modulates cardiac repair after myocardial infarction via FUS/VEGF-A axis. *Nat. Commun.* 10:4317.
- Geng, H. H., Li, R., Su, Y. M., Xiao, J., Pan, M., Cai, X. X., et al. (2016). The circular RNA Cdr1as promotes myocardial infarction by mediating the regulation of miR-7a on its target genes expression. *PLoS One* 11:e0151753. doi: 10.1371/journal.pone.0151753
- Gupta, S. K., Garg, A., Bar, C., Chatterjee, S., Foinquinos, A., Milting, H., et al. (2018). Quaking inhibits doxorubicin-mediated cardiotoxicity through regulation of cardiac circular RNA expression. *Circ. Res.* 122, 246–254. doi: 10.1161/Circresaha.117.311335
- Hansen, T. B., Jensen, T. I., Clausen, B. H., Bramsen, J. B., Finsen, B., Damgaard, C. K., et al. (2013a). Natural RNA circles function as efficient microRNA sponges. *Nature* 495, 384–388. doi: 10.1038/nature11993
- Hansen, T. B., Kjems, J., and Damgaard, C. K. (2013b). Circular RNA and miR-7 in cancer. *Cancer Res.* 73, 5609–5612.
- Hansen, T. B., Venø, M. T., Damgaard, C. K., and Kjems, J. (2016). Comparison of circular RNA prediction tools. *Nucl. Acids Res.* 44:e58. doi: 10.1093/nar/gkv1458
- Holdt, L. M., Stahringer, A., Sass, K., Pichler, G., Kulak, N. A., Wilfert, W., et al. (2016). Circular non-coding RNA ANRIL modulates ribosomal RNA maturation and atherosclerosis in humans. *Nat. Commun.* 7:12429. doi: 10.1038/ncomms12429
- Huang, S. L., Li, X. Z., Zheng, H., Si, X. Y., Li, B., Wei, G. Q., et al. (2019). Loss of super-enhancer-regulated circRNA Nfix induces cardiac regeneration after myocardial infarction in adult mice. *Circulation* 139, 2857–2876. doi: 10.1161/Circulationaha.118.038361

- Jakobi, T., Czaja-Hasse, L. F., Reinhardt, R., and Dieterich, C. (2016). Profiling and validation of the circular RNA repertoire in adult murine hearts. *Genom. Proteom. Bioinf.* 14, 216–223. doi: 10.1016/j.gpb.2016.02.003
- Jeck, W. R., and Sharpless, N. E. (2014). Detecting and characterizing circular RNAs. *Nat. Biotechnol.* 32, 453–461. doi: 10.1038/nbt.2890
- Jeck, W. R., Sorrentino, J. A., Wang, K., Slevin, M. K., Burd, C. E., Liu, J. Z., et al. (2013). Circular RNAs are abundant, conserved, and associated with ALU repeats. *RNA* 19, 141–157. doi: 10.1261/rna.035667.112
- Jin, Q. F., and Chen, Y. Y. (2019). Silencing circular RNA circ_0010729 protects human cardiomyocytes from oxygen-glucose deprivation-induced injury by up-regulating microRNA-145-5p. *Mol. Cell Biochem.* 462, 185–194.
- Khan, M. A., Reckman, Y. J., Aufiero, S., van den Hoogenhof, M. M., van der Made, I., Beqqali, A., et al. (2016). RBM20 regulates circular RNA production from the titin gene. *Circ. Res.* 119, 996–1003. doi: 10.1161/CIRCRESAHA.116.309568
- Kolakofsky, D. (1976). Isolation and characterization of Sendai virus DI-RNAs. *Cell* 8, 547–555.
- Kos, A., Dijkema, R., Arnberg, A. C., van der Meide, P. H., and Schellekens, H. (1986). The hepatitis delta (delta) virus possesses a circular RNA. *Nature* 323, 558–560. doi: 10.1038/32358a0
- Kramer, M. C., Liang, D., Tatomer, D. C., Gold, B., March, Z. M., Cherry, S., et al. (2015). Combinatorial control of Drosophila circular RNA expression by intronic repeats, hnRNPs, and SR proteins. *Genes Dev.* 29, 2168–2182. doi: 10.1101/gad.270421.115
- Lawrie, C. H., Gal, S., Dunlop, H. M., Pushkaran, B., Liggins, A. P., Pulford, K., et al. (2008). Detection of elevated levels of tumour-associated microRNAs in serum of patients with diffuse large B-cell lymphoma. *Br. J. Haematol.* 141, 672–675. doi: 10.1111/j.1365-2141.2008.07077.x
- Legnini, I., Di Timoteo, G., Rossi, F., Morlando, M., Briganti, F., Sthandier, O., et al. (2017). Circ-ZNF609 is a circular RNA that can be translated and functions in myogenesis. *Mol. Cell* 66, 22–37. doi: 10.1016/j.molcel.2017.02.017
- Lei, W., Feng, T., Fang, X., Yu, Y., Yang, J., Zhao, Z. A., et al. (2018). Signature of circular RNAs in human induced pluripotent stem cells and derived cardiomyocytes. *Stem. Cell Res. Rev.* 9:56.
- Li, C. Y., Ma, L., and Yu, B. (2017). Circular RNA hsa_circ_0003575 regulates oxLDL induced vascular endothelial cells proliferation and angiogenesis. *Biomed. Pharmacother.* 95, 1514–1519. doi: 10.1016/j.biopha.2017.09.064
- Li, H., Xu, J. D., Fang, X. H., Zhu, J. N., Yang, J., Pan, R., et al. (2019). Circular RNA circRNA_000203 aggravates cardiac hypertrophy via suppressing miR26b-5p and miR-140-3p binding to Gata4. *Cardiovasc. Res.* 116, 1323–1334. doi: 10.1093/cvr/cvz215
- Li, M., Ding, W., Tariq, M. A., Chang, W., Zhang, X., Xu, W., et al. (2018). A circular transcript of nrx1 gene mediates ischemic myocardial injury by targeting miR-133a-3p. *Thrombosis* 8, 5855–5869. doi: 10.7150/thno.27285
- Li, Y., Chen, B., and Huang, S. (2018). Identification of circRNAs for miRNA Targets by Argonaute2 RNA immunoprecipitation and luciferase screening assays. *Methods Mol. Biol.* 1724, 209–218. doi: 10.1007/978-1-4939-7562-4_17
- Li, Y. S., Zhang, J. W., Huo, C. Q., Ding, N., Li, J. Y., Xiao, J., et al. (2017). Dynamic organization of lncrna and circular rna regulators collectively controlled cardiac differentiation in humans. *Ebiomedicine* 24, 137–146. doi: 10.1016/j.ebiom.2017.09.015
- Li, Z. Y., Huang, C., Bao, C., Chen, L., Lin, M., Wang, X. L., et al. (2015). Exon-intron circular RNAs regulate transcription in the nucleus. *Nat. Struct. Mol. Biol.* 22, 256–264. doi: 10.1038/nsmb.2959
- Liang, W. C., Wong, C. W., Liang, P. P., Shi, M., Cao, Y., Rao, S. T., et al. (2019). Translation of the circular RNA circ-catenin promotes liver cancer cell growth through activation of the Wnt pathway. *Genome Biol* 20:84.
- Lim, T. B., Aliwarga, E., Luu, T. D. A., Li, Y. P., Ng, S. L., Annadurai, L., et al. (2019). Targeting the highly abundant circular RNA circSlc8a1 in cardiomyocytes attenuates pressure overload induced hypertrophy. *Cardiovasc Res* 115, 1998–2007. doi: 10.1093/cvr/cvz130
- Lim, T. B., Lavenia, A., and Foo, R. S. (2020). Circles in the heart and cardiovascular system. *Cardiovasc. Res.* 116, 269–278. doi: 10.1093/cvr/cvz227
- Liu, C., Yao, M. D., Li, C. P., Shan, K., Yang, H., Wang, J. J., et al. (2017). Silencing of circular RNA-ZNF609 ameliorates vascular endothelial dysfunction. *Theranostics* 7, 2863–2877. doi: 10.7150/thno.19353
- Liu, L., Liu, F. B., Huang, M., Xie, K., Xie, Q. S., Liu, C. H., et al. (2019). Circular RNA circS-7 promotes the proliferation and metastasis of pancreatic cancer by regulating miR-7-mediated EGFR/STAT3 signaling pathway. *Hepatob. Pancreat. Dis. Int.* 18, 580–586. doi: 10.1016/j.hbpd.2019.03.003
- Maesen, B., Nijs, J., Maessen, J., Allesie, M., and Schotten, U. (2012). Post-operative atrial fibrillation: a maze of mechanisms. *Europace* 14, 159–174. doi: 10.1093/europace/eur208
- Memczak, S., Jens, M., Elefsinioti, A., Torti, F., Krueger, J., Rybak, A., et al. (2013). Circular RNAs are a large class of animal RNAs with regulatory potency. *Nature* 495, 333–338. doi: 10.1038/nature11928
- Meng, Z. Y., Chen, C., Cao, H. L., Wang, J. Y., and Shen, E. (2019). Whole transcriptome sequencing reveals biologically significant RNA markers and related regulating biological pathways in cardiomyocyte hypertrophy induced by high glucose. *J. Cell Biochem.* 120, 1018–1027. doi: 10.1002/jcb.27546
- Meyer, K. D., Patil, D. P., Zhou, J., Zinoviev, A., Skabkin, M. A., Elemento, O., et al. (2015). 5' UTR m(6)A promotes cap-independent translation. *Cell* 163, 999–1010. doi: 10.1016/j.cell.2015.10.012
- Miao, R., Wang, Y., Wan, J., Leng, D., Gong, J., Li, J., et al. (2017). Microarray expression profile of circular RNAs in chronic thromboembolic pulmonary hypertension. *Medicine* 96:e7354. doi: 10.1097/MD.00000000000007354
- Molkentin, J. D., Lu, J. R., Antos, C. L., Markham, B., Richardson, J., Robbins, J., et al. (1998). A calcineurin-dependent transcriptional pathway for cardiac hypertrophy. *Cell* 93, 215–228.
- Ni, H., Li, W., Zhuge, Y., Xu, S., Wang, Y., Chen, Y., et al. (2019). Inhibition of circHIPK3 prevents angiotensin II-induced cardiac fibrosis by sponging miR-29b-3p. *Int. J. Cardiol.* 292, 188–196. doi: 10.1016/j.ijcard.2019.04.006
- Nigro, J. M., Cho, K. R., Fearon, E. R., Kern, S. E., Ruppert, J. M., Oliner, J. D., et al. (1991). Scrambled exons. *Cell* 64, 607–613. doi: 10.1016/0092-8674(91)90244-s
- Odiote, O., Hill, M. F., and Sawyer, D. B. (2012). Neuregulin in cardiovascular development and disease. *Circ. Res.* 111, 1376–1385. doi: 10.1161/CIRCRESAHA.112.267286
- Pamudurti, N. R., Bartok, O., Jens, M., Ashwal-Fluss, R., Stottmeister, C., Ruhe, L., et al. (2017). Translation of CircRNAs. *Mol. Cell* 66, 9–21e27. doi: 10.1016/j.molcel.2017.02.021
- Pan, H., Li, T., Jiang, Y., Pan, C., Ding, Y., Huang, Z., et al. (2018). Overexpression of circular RNA ciRS-7 Abrogates the tumor suppressive effect of miR-7 on gastric cancer via PTEN/PI3K/AKT signaling pathway. *J. Cell Biochem.* 119, 440–446. doi: 10.1002/jcb.26201
- Pan, R. Y., Liu, P., Zhou, H. T., Sun, W. X., Song, J., Shu, J., et al. (2017). Circular RNAs promote TRPM3 expression by inhibiting hsa-miR-130a-3p in coronary artery disease patients. *Oncotarget* 8, 60280–60290. doi: 10.18632/oncotarget.19941
- Perriman, R., and Ares, M. (1998). Circular mRNA can direct translation of extremely long repeating-sequence proteins in vivo. *RNA* 4, 1047–1054. doi: 10.1017/S135583829898061x
- Rajabi, M., Kassiotis, C., Razeghi, P., and Taegtmeyer, H. (2007). Return to the fetal gene program protects the stressed heart: a strong hypothesis. *Heart Fail Rev.* 12, 331–343.
- Rybak-Wolf, A., Stottmeister, C., Glazar, P., Jens, M., Pino, N., Giusti, S., et al. (2015). Circular RNAs in the mammalian brain are highly abundant, conserved, and dynamically expressed. *Mol. Cell* 58, 870–885. doi: 10.1016/j.molcel.2015.03.027
- Schroeder, R., Breitenbach, M., and Schweyen, R. J. (1983). Mitochondrial circular RNAs are absent in sporulating cells of *Saccharomyces cerevisiae*. *Nucl. Acids Res* 11, 1735–1746. doi: 10.1093/nar/11.6.1735
- Shan, K., Liu, C., Liu, B. H., Chen, X., Dong, R., Liu, X., et al. (2017). Circular noncoding RNA HIPK3 mediates retinal vascular dysfunction in diabetes mellitus. *Circulation* 136, 1629–1642. doi: 10.1161/CIRCULATIONAHA.117.029004
- Siede, D., Rapti, K., Gorska, A. A., Katus, H. A., Altmüller, J., Boeckel, J. N., et al. (2017). Identification of circular RNAs with host gene-independent expression in human model systems for cardiac differentiation and disease. *J. Mol. Cell Cardiol.* 109, 48–56. doi: 10.1016/j.yjmcc.2017.06.015
- Sonnenschein, K., Wilczek, A. L., de Gonzalo-Calvo, D., Pfanne, A., Derda, A. A., Zwadlo, C., et al. (2019). Serum circular RNAs act as blood-based biomarkers for hypertrophic obstructive cardiomyopathy. *Sci. Rep.* 9:20350.
- Sun, Y., Jiang, X., Lv, Y., Liang, X., Zhao, B., Bian, W., et al. (2020). Circular rna expression profiles in plasma from patients with heart failure related to platelet activity. *Biomolecules* 10:187. doi: 10.3390/biom10020187

- Sun, Y., Zhang, S. L., Yue, M. M., Li, Y., Bi, J., and Liu, H. R. (2019). Angiotensin II inhibits apoptosis of mouse aortic smooth muscle cells through regulating the circNRG-1/miR-193b-5p/NRG-1 axis. *Cell. Death Dis.* 10:362.
- Suzuki, H., Zuo, Y. H., Wang, J. H., Zhang, M. Q., Malhotra, A., and Mayeda, A. (2006). Characterization of RNase R-digested cellular RNA source that consists of lariat and circular RNAs from pre-mRNA splicing. *Nucl. Acids Res.* 34:e63. doi: 10.1093/nar/gkl151
- Szabo, L., and Salzman, J. (2016). Detecting circular RNAs: bioinformatic and experimental challenges. *Nat. Rev. Genet.* 17, 679–692. doi: 10.1038/nrg.2016.114
- Tan, W. L., Lim, B. T., Anene-Nzelu, C. G., Ackers-Johnson, M., Dashi, A., See, K., et al. (2017). A landscape of circular RNA expression in the human heart. *Cardiovas. Res.* 113, 298–309. doi: 10.1093/cvr/cvw250
- Tang, C. M., Zhang, M., Huang, L., Hu, Z. Q., Zhu, J. N., Xiao, Z., et al. (2017). CircRNA_000203 enhances the expression of fibrosis-associated genes by derepressing targets of miR-26b-5p, Col1a2 and CTGF in cardiac fibroblasts. *Sci. Rep.* 7:40342. doi: 10.1038/srep40342
- Tay, Y., Rinn, J., and Pandolfi, P. P. (2014). The multilayered complexity of ceRNA crosstalk and competition. *Nature* 505, 344–352. doi: 10.1038/nature12986
- van Rooij, E., Marshall, W. S., and Olson, E. N. (2008). Toward microRNA-based therapeutics for heart disease: the sense in antisense. *Circ. Res.* 103, 919–928. doi: 10.1161/CIRCRESAHA.108.183426
- Vausort, M., Salgado-Somoza, A., Zhang, L., Leszek, P., Scholz, M., Teren, A., et al. (2016). Myocardial infarction-associated circular RNA predicting left ventricular dysfunction. *J. Am. Coll. Cardiol.* 68, 1247–1248. doi: 10.1016/j.jacc.2016.06.040
- Vilades, D., Martinez-Camblor, P., Ferrero-Gregori, A., Bar, C., Lu, D. C., Xiao, K., et al. (2020). Plasma circular RNA hsa_circ_0001445 and coronary artery disease: performance as a biomarker. *Faseb J.* 34, 4403–4414. doi: 10.1096/fj.201902507R
- Wang, K., Gan, T. Y., Li, N., Liu, C. Y., Zhou, L. Y., Gao, J. N., et al. (2017). Circular RNA mediates cardiomyocyte death via miRNA-dependent upregulation of MTP18 expression. *Cell Death Differ.* 24, 1111–1120. doi: 10.1038/cdd.2017.61
- Wang, K., Long, B., Liu, F., Wang, J. X., Liu, C. Y., Zhao, B., et al. (2016). A circular RNA protects the heart from pathological hypertrophy and heart failure by targeting miR-223. *Eur. Heart J* 37, 2602–2611. doi: 10.1093/eurheartj/ehv713
- Wang, L., Shen, C., Wang, Y., Zou, T., Zhu, H., Lu, X., et al. (2019). Identification of circular RNA Hsa_circ_0001879 and Hsa_circ_0004104 as novel biomarkers for coronary artery disease. *Atherosclerosis* 286, 88–96. doi: 10.1016/j.atherosclerosis.2019.05.006
- Wang, S., Chen, J. Y., Yu, W. Q., and Deng, F. (2019). Circular RNA DLGAP4 ameliorates cardiomyocyte apoptosis through regulating BCL2 via targeting miR-143 in myocardial ischemia-reperfusion injury. *Int. J. Cardiol.* 279, 147–147. doi: 10.1016/j.ijcard.2018.09.023
- Werfel, S., Nothjunge, S., Schwarzmayr, T., Strom, T. M., Meitinger, T., and Engelhardt, S. (2016). Characterization of circular RNAs in human, mouse and rat hearts. *J. Mol. Cell Cardiol.* 98, 103–107. doi: 10.1016/j.yjmcc.2016.07.007
- Wesselhoeft, R. A., Kowalski, P. S., and Anderson, D. G. (2018). Engineering circular RNA for potent and stable translation in eukaryotic cells. *Nat. Commun.* 9:2629.
- Wu, J. H., Li, J. Q., Liu, H., Yin, J. W., Zhang, M. J., Yu, Z. B., et al. (2019). Circulating plasma circular RNAs as novel diagnostic biomarkers for congenital heart disease in children. *J. Clin. Lab. Anal.* 33:e22998. doi: 10.1002/jcla.22998
- Wu, N., Jin, L., and Cai, J. (2017). Profiling and bioinformatics analyses reveal differential circular RNA expression in hypertensive patients. *Clin. Exp. Hypertens* 39, 454–459. doi: 10.1080/10641963.2016.1273944
- Xu, T. Y., Wu, J., Han, P., Zhao, Z. M., and Song, X. F. (2017). Circular RNA expression profiles and features in human tissues: a study using RNA-seq data. *Bmc Genom.* 18:680. doi: 10.1186/s12864-017-4029-23
- Yang, Y., Fan, X., Mao, M., Song, X., Wu, P., Zhang, Y., et al. (2017). Extensive translation of circular RNAs driven by N(6)-methyladenosine. *Cell Res.* 27, 626–641. doi: 10.1038/cr.2017.31
- Yang, Y., Gao, X., Zhang, M., Yan, S., Sun, C., Xiao, F., et al. (2018). Novel role of FBXW7 circular RNA in repressing glioma tumorigenesis. *J. Natl. Cancer Inst.* 110:435. doi: 10.1093/jnci/djx166
- Yang, Z. G., Awan, F. M., Du, W. W., Zeng, Y., Lyu, J., Wu, et al. (2017). The circular RNA interacts with STAT3, increasing its nuclear translocation and wound repair by modulating Dnmt3a and miR-17 function. *Mol. Ther.* 25, 2062–2074. doi: 10.1016/j.ymthe.2017.05.022
- Yang, Z. G., Guo, X. B., Li, G. M., Shi, Y. L., and Li, L. P. (2016). Long noncoding RNAs as potential biomarkers in gastric cancer: opportunities and challenges. *Cancer Lett.* 371, 62–70. doi: 10.1016/j.canlet.2015.11.011
- Zeng, X. X., Lin, W., Guo, M. Z., and Zou, Q. (2017). A comprehensive overview and evaluation of circular RNA detection tools. *PLoS Comp. Biol.* 13:e1005420. doi: 10.1371/journal.pcbi.1005420
- Zeng, Y., Du, W. W., Wu, Y., Yang, Z., Awan, F. M., Li, X., et al. (2017). A circular RNA binds to and activates AKT phosphorylation and nuclear localization reducing apoptosis and enhancing cardiac repair. *Theranostics* 7, 3842–3855. doi: 10.7150/thno.19764
- Zhang, J., Xu, Y. L., Xu, S., Liu, Y., Yu, L. M., Li, Z., et al. (2018). Plasma circular RNAs, Hsa_circRNA_025016, predict postoperative atrial fibrillation after isolated off-pump coronary artery bypass grafting. *J. Am. Heart Assoc.* 7:e006642. doi: 10.1161/JAHA.117.006642
- Zhang, L., Zhang, Y., Xue, S., Ding, H., Wang, Y., Qi, H. Z., et al. (2020). Clinical significance of circulating microRNAs as diagnostic biomarkers for coronary artery disease. *J. Cell Mol. Med.* 24, 1146–1150. doi: 10.1111/jcmm.14802
- Zhang, L., Zhang, Y., Zhao, Y. F., Wang, Y., Ding, H., Xue, S., et al. (2018). Circulating miRNAs as biomarkers for early diagnosis of coronary artery disease. *Expert Opin Ther Pat* 28, 591–601. doi: 10.1080/13543776.2018.1503650
- Zhang, Q., Sun, W. X., Han, J., Cheng, S. Y., Yu, P., Shen, L., et al. (2020). The circular RNA hsa_circ_0007623 acts as a sponge of microRNA-297 and promotes cardiac repair. *Biochem. Biophys. Res. Co.* 523, 993–1000. doi: 10.1016/j.bbrc.2019.12.116
- Zhang, X. O., Wang, H. B., Zhang, Y., Lu, X. H., Chen, L. L., and Yang, L. (2014). Complementary sequence-mediated exon circularization. *Cell* 159, 134–147. doi: 10.1016/j.cell.2014.09.001
- Zhang, Y., Zhang, X. O., Chen, T., Xiang, J. F., Yin, Q. F., Xing, Y. H., et al. (2013). Circular intronic long noncoding RNAs. *Mol. Cell* 51, 792–806. doi: 10.1016/j.molcel.2013.08.017
- Zhao, Z. Z., Li, X. J., Gao, C. Y., Jian, D. D., Hao, P. Y., Rao, L. X., et al. (2017). Peripheral blood circular RNA hsa_circ_0124644 can be used as a diagnostic biomarker of coronary artery disease. *Sci. Rep.* 7:39918. doi: 10.1038/srep39918
- Zheng, C., Niu, H., Li, M., Zhang, H., Yang, Z., Tian, L., et al. (2015). Cyclic RNA hsa_circ000595 regulates apoptosis of aortic smooth muscle cells. *Mol. Med. Rep.* 12, 6656–6662. doi: 10.3892/mmr.2015.4264
- Zheng, Q. P., Bao, C. Y., Guo, W. J., Li, S. Y., Chen, J., Chen, B., et al. (2016). Circular RNA profiling reveals an abundant circHIPK3 that regulates cell growth by sponging multiple miRNAs. *Nat. Commun.* 7:11215. doi: 10.1038/ncomms11215
- Zhou, B., and Yu, J. W. (2017). A novel identified circular RNA, circRNA_010567, promotes myocardial fibrosis via suppressing miR-141 by targeting TGF-beta 1. *Biochem. Biophys. Res. Commun.* 487, 769–775. doi: 10.1016/j.bbrc.2017.04.044
- Zhu, Y., Pan, W., Yang, T., Meng, X., Jiang, Z., Tao, L., et al. (2019). Upregulation of circular RNA CircNFIB attenuates cardiac fibrosis by sponging miR-433. *Front. Genet.* 10:564. doi: 10.3389/fgene.2019.00564
- Zirkel, A., and Papantonis, A. (2018). Detecting circular RNAs by RNA fluorescence in situ hybridization. *Methods Mol. Biol.* 1724, 69–75. doi: 10.1007/978-1-4939-7562-4_6
- Zou, M., Huang, C., Li, X., He, X., Chen, Y., Liao, W., et al. (2017). Circular RNA expression profile and potential function of hsa_circRNA_101238 in human thoracic aortic dissection. *Oncotarget* 8, 81825–81837. doi: 10.18632/oncotarget.18998

Conflict of Interest: The authors declare that the research was conducted in the absence of any commercial or financial relationships that could be construed as a potential conflict of interest.

Copyright © 2020 Zhang, Zhang, Wang, Zhao, Ding and Li. This is an open-access article distributed under the terms of the Creative Commons Attribution License (CC BY). The use, distribution or reproduction in other forums is permitted, provided the original author(s) and the copyright owner(s) are credited and that the original publication in this journal is cited, in accordance with accepted academic practice. No use, distribution or reproduction is permitted which does not comply with these terms.



The Role of the Microbiome in Driving RA-Related Autoimmunity

Cristopher M. Rooney¹, Kulveer Mankia^{1,2} and Paul Emery^{1,2*}

¹ Leeds Institute of Rheumatic and Musculoskeletal Medicine, University of Leeds, Chapel Allerton Hospital, Leeds, United Kingdom, ² Musculoskeletal Biomedical Research Unit, Chapel Allerton Hospital, Leeds, United Kingdom

OPEN ACCESS

Edited by:

Francesco Ria,
Catholic University of the Sacred
Heart, Italy

Reviewed by:

Sayed-Amir Marashi,
University of Tehran, Iran
Marco Giammanco,
University of Palermo, Italy

*Correspondence:

Paul Emery
p.emery@leeds.ac.uk

Specialty section:

This article was submitted to
Molecular Medicine,
a section of the journal
Frontiers in Cell and Developmental
Biology

Received: 26 February 2020

Accepted: 07 September 2020

Published: 29 September 2020

Citation:

Rooney CM, Mankia K and
Emery P (2020) The Role of the
Microbiome in Driving RA-Related
Autoimmunity.
Front. Cell Dev. Biol. 8:538130.
doi: 10.3389/fcell.2020.538130

Once referred to as “normal commensal flora” the human microbiome plays an integral role between health and disease. The host mucosal surface replete with a multitude of immune cells is a vast arena constantly sensing and responding to antigen presentation and microbial by-products. It is this key role that may allow the microbiome to prime or protect the host from autoimmune disease. Rheumatoid arthritis (RA) is a chronic, disabling inflammatory condition characterized by a complex multifactorial etiology. The presence of certain genetic markers has been proven to increase susceptibility to RA however it does not guarantee disease development. Given low concordance rates demonstrated in monozygotic twin studies there is a clear implication for the involvement of external players in RA pathogenesis. Since the historical description of rheumatoid factor, numerous additional autoantibodies have been described in the sera of RA patients. The presence of anti-cyclic citrullinated protein antibody is now a standard test, and is associated with a more severe disease course. Interestingly these antibodies are detectable in patient's sera long before the clinical signs of RA occur. The production of autoantibodies is driven by the lack of tolerance of the immune system, and how tolerance is broken is a crucial question for understanding RA development. Here we review current literature on the role of the microbiome in RA development including periodontal, gut and lung mucosa, with particular focus on proposed mechanisms of host microbiome interactions. We discuss the use of Mendelian randomization to assign causality to the microbiome and present considerations for future studies.

Keywords: Initiation of autoimmunity, host-microbiome interaction, gut microbiome, oral microbiome, lung microbiome, rheumatoid arthritis

INTRODUCTION

Complex interactions govern the symbiosis that exists between the human body as the host and our microbiome. It is conceivable to imagine that defense mechanisms capable of continual surveillance for infection but tolerant of our own “healthy microbiome” have evolved (Kamada et al., 2013; Mezouar et al., 2018), allowing the microbiome to prime or protect us from disease. Initial microbiome research focused on descriptions of variant microbiome populations within specific disease states, e.g., diabetes, obesity, inflammatory bowel disease

(Tilg and Moschen, 2014; Tralongo et al., 2014; Tomasello et al., 2015; Castaner et al., 2018; Sharma and Tripathi, 2019) or temporal shifts observed over the course of a disease (Kong et al., 2012; Kelly et al., 2016). Autoimmune disorders are a primary group of disorders hypothesized to be triggered by interactions of the microbiome and the host (Chervonsky, 2013). Intriguingly the target tissue which characterizes the clinical syndrome is often distant from the assumed instigating microbial impetus, this scenario is exemplified by rheumatoid arthritis (RA).

As the number of microbiome studies increase and greater details unfold regarding the microbiomes' physiological role we believe it is important to emphasize two elements of microbiome research. Firstly, strictly speaking the term microbiome refers to all microorganisms and the collection of all their genes and genomes within a microbial community associated with a distinct anatomical region (Lederberg and McCray, 2001). Therefore this definition would encompass all living organisms at that site, including bacterial, viral, fungal and archaeal populations. This is an important concept as tools for analysis of these complex communities can be divided broadly into functional or taxonomic characterization. Primarily, the former relies on metagenomic shotgun sequencing and the latter on 16S rRNA sequencing but overlap exists, where hypothesized function can be inferred from 16S rRNA sequencing (Ortiz-Estrada et al., 2019) and of course, metagenomics shotgun sequencing is also capable of taxonomic resolution. Taxonomic variation using 16S rRNA often only reports the bacterial portion of the microbiome, albeit the largest and potentially most active microbial component. It is worth noting the fungal, viral and much of the archaeal populations are not reported in 16S rRNA analysis performed. Secondly, it is often cited that the gut microbiome houses up to 10^{14} bacterial cells. While there is agreement that the gut microbiome is indeed the largest human microbiome in terms of cell biomass and genetic potential, the original estimates of bacterial cells outnumbering human cells by 10:1 is likely an over estimation (Sender et al., 2016). Sender et al. (2016) investigated these numbers and found the original estimates stemmed from a single paper published in 1972 (Luckey, 1972) which assumed a homogenous bacterial population density along the alimentary canal, and overestimated the capacity of the human colon thereby amplifying bacterial numbers. Newer estimates suggest a more modest ratio of 1:1 of bacterial to human cell biomass (Sender et al., 2016), however this of course this does not take into account genetic potential and subsequent metabolic pathways which still favor the microbiome as having numerical dominance in terms of transcriptional and subsequent functional activity.

This review article focuses on the mechanistic relationships between the microbiome and the human host and how bacterial perturbations could trigger or potentiate the autoimmune response in RA. Building upon previous review articles (Rosenbaum and Asquith, 2016; Wells et al., 2019; König, 2020) we have included a synopsis of the unique immune adaptations at potential offending mucosal sites, focusing on the molecular interactions and a summary of the animal model supporting the mucosal origins hypothesis of RA. We highlight potential new efforts to assign causality to the microbiome using Mendelian

randomization on available curated datasets and finally propose some future consideration for further research.

THE MICROBIOME AND RA AUTOIMMUNITY

Numerous factors impact the microbiome such as vaginal delivery versus cesarean section in newborns, diet, and antibiotic administration (Hasan and Yang, 2019) with the overriding determinant being anatomical site (Cho and Blaser, 2012). The diversity of a microbiome can be categorized based on which organisms are present, their relative abundance, their temporality and their metabolic activity. Great variation of the microbiota between individuals, and even temporally within the same individual has been demonstrated at the lower taxonomic units (Costello et al., 2009). Each of these streams holds the potential for disease progression or enhancement. For example, the priming of the immune system with a specific antigen exposure or infection with a predominant bacterium and subsequent induction of a pro-inflammatory status could impact disease states.

Rheumatoid arthritis is a chronic, disabling autoimmune disease characterized by a complex multifactorial etiology. The presence of certain genetic markers has been proven to increase susceptibility to RA, however these do not guarantee RA development (Stahl et al., 2010). A 15% concordance has been demonstrated in monozygotic twin studies which clearly indicates a role for environmental factors in disease development (Aho et al., 1986). Furthermore the use of antimicrobials in RA treatment has been established for some time, (Brown et al., 1971) however, the exact mechanism by which they exert their effect is unknown, as is the target group of organisms (Nagra et al., 2019). The production of autoantibodies is driven by the lack of tolerance of the immune system, and how tolerance is broken is a crucial question for understanding RA development. Since the historical description of rheumatoid factor (RF), an IgM antibody directed against IgG, numerous additional autoantibodies have been described in the sera of RA patients. These autoantibodies are directed against various joint components (cartilage, collagen) and non-joint components (enzymes, nuclear proteins, stress proteins) and although are not diagnostically important may contribute to disease by immune complex formation and deposition. The presence of anti-cyclic citrullinated protein antibody (ACPA) is now a standard test for RA, and is associated with a more severe disease course. Interestingly these antibodies are detectable in patient's sera long before the clinical signs of RA (i.e., clinical arthritis) occur (Nielen et al., 2004). Within this phase of antibody positivity but without arthritis, the joint synovium shows no inflammatory changes (Berglin et al., 2006; Van De Sande et al., 2011). ACPA represent a collection of autoantibodies of various isotypes (IgG, IgM, and IgA) directed against the neutrally charged non-essential amino acid citrulline. The creation of ACPAs is brought about by a process called citrullination, which is the post-translational modification of arginine, catalyzed by peptidylarginine deiminase (PAD) enzymes resulting in the

substitution of arginine to citrulline. This process decreases the proteins ability to form hydrogen bonds due to a lack of positively charged amino acids introducing a structural change within the peptide sequence and subsequent immunogenicity (Kurowska et al., 2017). PAD enzymes are highly conserved throughout evolution, in humans there are five main types of PAD genes (Chavanas et al., 2004) which display both tissue and substrate specificity and are involved in a plethora of physiological functions including tissue structure, apoptosis and immune regulation (Wegner et al., 2010), of note PAD2 and PAD4 are likely more important in RA development given their isolation in the synovium of RA patients (Foulquier et al., 2007). As mentioned ACPAs may be heterogeneous in terms of their fine specificity to antigens but are highly specific for RA when compared to RF (Kurowska et al., 2017).

The presence of circulating serum ACPA represent a state of systemic autoimmunity, combination of ACPA titers with symptomatology, imaging and major histocompatibility complex (HLA)-DRB1, prediction models can be developed to identify those at the highest risk of progression to RA (Van De Stadt et al., 2013; Rakieh et al., 2015). As previously mentioned, the multifactorial etiology of RA encompasses genetic risk, with the “shared epitope” (SE) accounting for the strongest genetic risk factor (Gregersen et al., 1987; Raychaudhuri et al., 2012; Deane et al., 2017). The SE is located within the third hypervariable region of HLA DRB1 molecule and encodes a five amino acid sequence (Huizinga et al., 2005) with some alleles possessing a higher binding affinity for citrullinated peptides spurring the investigation for a “RA antigen.” The identification of such an antigen is an exciting concept which may provide a malleable risk factor in which RA disease may be moderated or ameliorated. Environmental risk factors are a perpetual interest in RA, as mentioned the use of drugs with antimicrobial properties for the treatment of RA (Ogrendik, 2013) provide a rationale for a possible role of bacteria in RA pathogenesis. Furthermore, infections with specific organisms have been associated with an increased risk of RA development; these include *Porphyromonas gingivalis* (discussed within “Periodontal Microbiome and ACPA” section), *Proteus mirabilis*, *Mycobacterium tuberculosis*, and *Mycoplasma* spp. (Li et al., 2013) the hypothesized mechanism of action includes molecular mimicry and activation of the immune system via a “super-antigen.” Recently gastrointestinal and urogenital infections were shown to be associated with a lower risk developing RA (Sandberg et al., 2015). The authors’ hypothesize that these infections and/or their subsequent treatment with antibiotics may induce a deviation in microbiome composition that has an overall protective effect i.e., disrupting an already high risk microbiome. Smoking status has a long established link with RA as demonstrated by numerous epidemiological studies (Karlson et al., 1999; Criswell et al., 2002; Padyukov et al., 2004; Sugiyama et al., 2010), this combined with the strong link to periodontal disease (PD) (Kasser et al., 1997; Mercado et al., 2001; Pischon et al., 2008; Scher et al., 2012; Äyräväinen et al., 2017) provides clear evidence for the role of the oral microbiome in the development of RA. Continuing along the lines of a microbial impetus for RA, Scher et al. (2013) demonstrated individuals diagnosed with

new onset RA had a different microbiome when compared to healthy controls, while Zhang et al. (2015) demonstrated perturbations in both the oral and gut microbiomes could be used to identify those with RA from healthy controls. They also demonstrated that treatment of RA with disease modifying drugs resulted in reversion of the microbiome composition comparable to that of the healthy controls, which undoubtedly is a secondary phenomenon but serves to highlight the interaction between the gut microbiome and joint inflammation. Therefore, understanding the microbiomes role will be paramount in completing this etiological puzzle of RA. In this review we will focus on the mechanisms by which the microbiome may initiate autoimmunity.

THE NICHE ENVIRONMENT OF THE MICROBIOME

The oral microbiome acts a portal of entry to the human body and therefore has adapted to endure a multitude of physical insults including rapid fluctuations in temperature, pH and external pollutants (air and climate) (Idris et al., 2017). The oral cavity forming the initial segment of the alimentary canal shares many physiological features with the gastrointestinal tract, and indeed the function of gastrointestinal immune cells is far better understood. Distinct to the oral cavity, salivary secretions are a primary component of the oral immune system, and have evolved with the ability to rapidly neutralize microbial threats via the production of large quantities of secretory IgA, mainly in a dimeric form (Brandtzaeg, 2013). The unique properties of the secretory IgA allows it to resist proteolytic cleavage while preventing bacterial aggregation and biofilm formation, a precursor to PD. Stimulus for the production of the IgA comes from inductor sites such as mucosa-associated lymphoid tissue (MALT) (Wu et al., 2014) in particular nasopharynx-associated lymphoid tissue (Brandtzaeg et al., 1999).

The gastrointestinal (GI) tract is a unique organ providing a pivotal dual role of digestion and maintenance of immune homeostasis. The enormous numbers of antigens presented to the GI tract in the form of food, environmental and microbial antigens are processed at the highly efficient mucosal barrier, which can be divided into three physically distinct elements; the epithelial barrier, the lamina propria and the gut-associated lymphoid tissue (GALT). GALT is further divided into Peyer’s patches (PP), isolated lymphoid follicles and mesenteric lymph nodes (MLN) which together constitute the largest lymphatic network in the body (Mowat, 2003; Ahluwalia et al., 2017). There are a variety of mechanisms by which the gut is capable of antigen uptake. Briefly antigens can enter via microfold (M) cells and are presented by dendritic cells (DC) to underlying T cells within the PP. Alternatively the DC may enter the lymphatic drainage network and present to next MLN. Direct intraluminal antigen sampling may also occur as DC are capable of extending the dendrite through the epithelial barrier directly into the colonic lumen. Furthermore, follicular associated enterocytes may pass antigens to DC cells or via MHC class II presentation to CD4+ cells (Ahluwalia et al., 2017) see **Figure 1**. The first line of

immune defense relies on a family of receptors known as pattern recognition receptors (PRRs), these receptors are expressed on innate immune cells and include Toll-Like receptors (TLR) which allow identification of pathogen-associated molecular patterns (PAMPs). Upon sensing a PAMP, TLR enables activation of the immune system and induces subsequent inflammation to eradicate the invading organism (Kumar et al., 2011; Ahluwalia et al., 2017), is it through PAMPs that the mucosal immune system maintains constant surveillance.

Akin to the gastrointestinal system, the mucosal surface of the lung is also exposed to a vast array of antigens, hence the resident immune cells of the bronchial tree must also delineate between potential harmful and innocuous stimuli (Joshua et al., 2017). The lung mucosal barrier in addition to recognition of PAMP's during pathogen invasion, can also identify damage-associated molecular patterns (DAMP's) commonly induced by smoking, which may further perpetuate PAMP recognition and subsequent TLR activation (Joshua et al., 2017). Within the lungs, local inflammation fosters the development of inducible bronchus associated lymphoid tissue (iBALT) which is architecturally similar to other non-encapsulated secondary lymphoid structures (PP), having distinct B and T cell elements with supporting APC's (Carragher et al., 2008). The presence of iBALT therefore confers the mucosal lining of the lungs the ability to generate and potentiate autoantibody production.

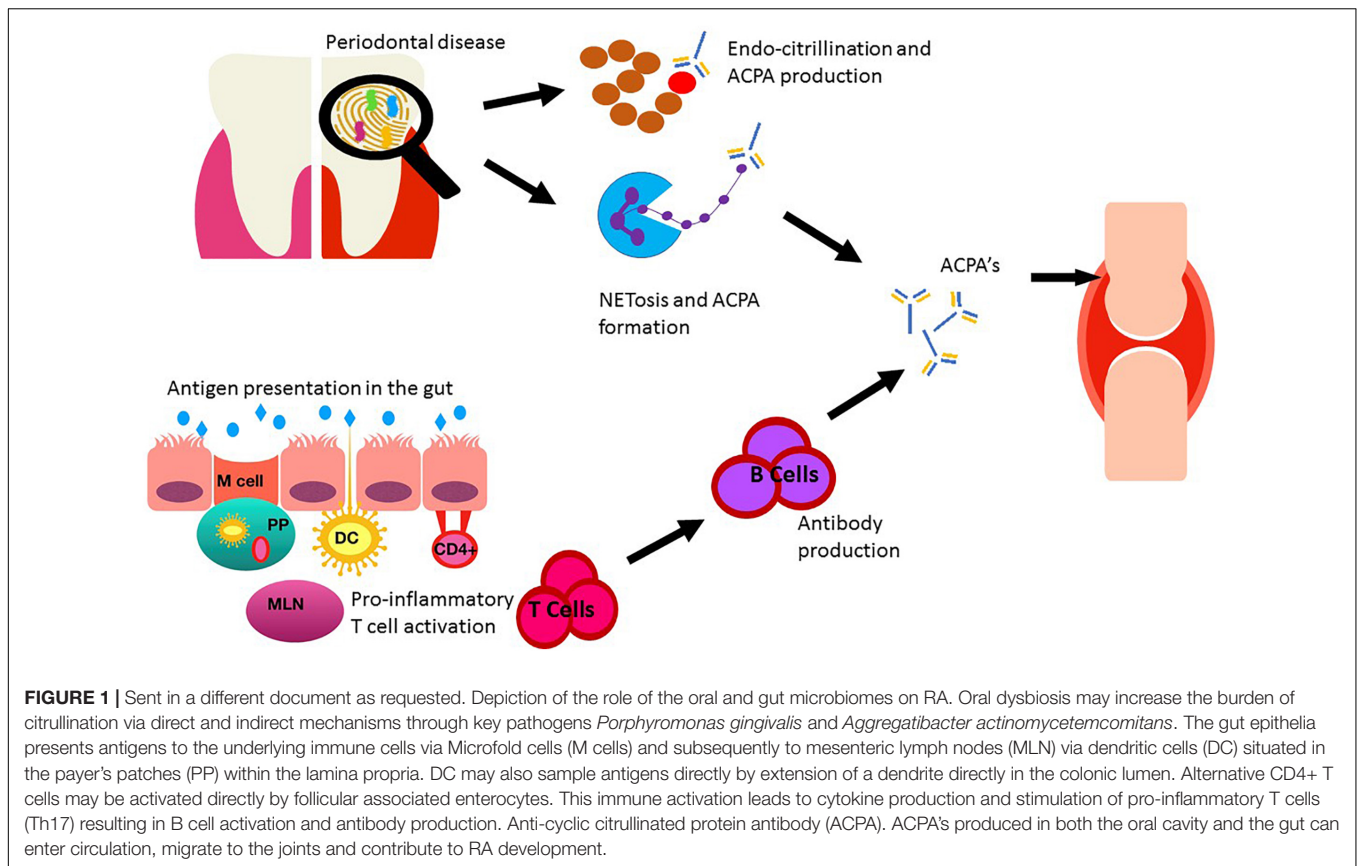
MURINE MODELS OF RA

Although the focus of this review is on human studies, it would be remiss not to cover the three main rodent models [collagen induced arthritis (CIA), K/B×N, and SKG] of RA and microbiome research as these studies offer the unique ability for microbial manipulation, and therefore an attractive avenue for mechanistic insights. Within each mucosal section we have included additional important animal studies. Rogier et al. (2017) used a CIA mouse model to investigate the gut microbiome in the pre-RA state. Briefly the CIA murine model is created via immunization of genetically susceptible (DBA/1) mice with type II collagen resulting in a polyarthritis which is both clinically and histologically similar to RA (Brand et al., 2004). Within the preclinical phases of RA a relative decrease in *Bacteroidetes* and *Bacteroidaceae* was identified, while *Firmicutes* and *Proteobacteria* (*Ruminococcaceae*, *Lachnospiraceae*, and *Desulfovibrionaceae*) were increased during the immune-priming phase of arthritis (Rogier et al., 2017). Following elimination of microbial populations (antibiotics) the abundance of intestinal Th17 cells decreased with subsequent attenuation of arthritis. Dynamic temporal microbial changes in this pre-RA phase have also been demonstrated using CIA mouse models (Jubair et al., 2018), with an initial decrease in *Bacteroidetes* and an increase in *Lactobacillaceae*; however, by day 35 of the model (early induction of arthritis at day 14) *Lactobacillaceae* had returned to day 0–7 levels, while *Lachnospiraceae* significantly increased in abundance. The authors found mucosal IL-17A and IL-22 increased on day 14, corresponding to the decreases in *Bacteroidetes* and increases in *Lactobacillaceae* and subsequently

normalized on day 35, as bacterial abundances of *Bacteroidetes* and *Lactobacillaceae* returned to day 0 levels (Jubair et al., 2018).

Some *Lactobacillaceae* are known to have a regulatory effect on the immune system, for example *Lactobacillus salivarius* and *Lactobacillus plantarum* transferred to mice prior to the induction of CIA reduced Th17 cells and increased Treg cells resulting in reduced arthritis severity (Liu et al., 2016). As discussed later, *L. salivarius* has been associated with new onset RA in humans. Depletion of microbial load using broad spectrum antibiotics resulted in decreased disease duration and decreased antibody production (Jubair et al., 2018) which was true for both early and late antibiotic administration. Of note, later administration of antibiotics, following the second CIA inoculation, had a greater reduction in disease severity. The anti-inflammatory effect of the reduced microbial load has been attributed to decreased glycosylation of the FC portion of mucosal autoantibodies with subsequent decreased complement activation leading to decreased inflammation (Jubair et al., 2018). Pfeifle et al. (2017) has shown antibody glycosylation to be an important factor in the transition between asymptomatic autoimmunity and symptomatic disease in RA patients and in CIA and K/B×N models. Tong et al. (2020) demonstrated the microbiome of pre-RA individuals (ACPA positive) was capable of inducing gut mucosal changes in a CIA mouse model. There was significant decreases in Zo-1 gene expression combined with mucosal damage and increases in mucosal Th17 cells, mice inoculated with the pre-RA microbiome displayed earlier and more severe joint disease in comparison to those inoculated with the microbiome from healthy controls (Tong et al., 2020).

The K/B×N mouse model possess a transgenic T-cell receptor and the MHC class II molecule Ag7 resulting in spontaneous arthritis due to the production of autoantibodies against the ubiquitous protein glucose-6-phosphate isomerase (Ditzel, 2004). Under germ free conditions, autoimmune arthritis in the K/B×N mice was significantly attenuated, with absence of Th17 cells within the gut mucosa. Inoculation with segmented filamentous bacteria (SFB) reinstated the Th17 cell population and the arthritis phenotype (Wu et al., 2010). In keeping with previous experiments demonstrating colonization with SFB and their ability to induce a proinflammatory state (Ivanov et al., 2009). Thompson et al. (2012) has investigated the taxonomic relationships of SFB and demonstrated those observed in vertebrates to be a distinct lineage within the family *clostridiaceae*, suggesting the term *Candidatus Savagella* to be used in future to denote SFB in vertebrates. It is interesting to note that within Thompson et al. (2012) study, SFB observed in arthropods were shown to be a distinct lineage within the family *lachnospiraceae*, which has been implicated in the above CIA models. The presence of SFB has been confirmed in the human gut and shown to be associated with increased IgA levels (Chen et al., 2018). Flak et al. (2019) used K/B×N to gain mechanistic insights into the loss of gut homeostasis and showed that arthritic mice had increased gut permeability due to decreased presence of tight junctions and goblet cells when compared to naive mice. They noted downregulation of the gut-protective mediator D5n-3 DPA (RvD5n-3 DPA) and IL-10 expression corresponding with the above physiological changes



in the gut mucosal. Following inoculation with *P. gingivalis* further decreases of both RvD5n-3 DPA and IL-10 levels were identified with further disruption of the gut permeability, these changes were reversed upon supplementation with RvD5n-3 DPA restoring gut barrier function, suggesting an additional mechanistic role for *P. gingivalis* in RA development.

A third mouse model; the SKG model [a missense mutation in Zap70 resulting in spontaneous arthritis (Sakaguchi et al., 2003)] has demonstrated induction of arthritis following inoculation of SKG mice with the gut microbiome of early RA patients (Maeda et al., 2016). Germ free SKG mice were either inoculated with pooled feces from healthy controls or early RA patients. A predominance of *Prevotella copri* (discussed later in this review) was identified within the early RA patients, which was corroborated within the mice receiving the RA microbiome following inoculation and associated with increased Th17 cells and arthritis severity (Maeda et al., 2016). As previous stated, mouse models provide a malleable environment in which to ascertain mechanistic insights into the microbiome's ability to induce disease, and remain the gold standard of establishing causality in microbiome research (Round and Palm, 2018). However, some caution should be taken given a substantial number of taxa within the human gut fail to colonize the engrafted animal (Zhang et al., 2017), and those that do colonize may foster community structures distinct from the human donor (Staley et al., 2017). Finally, as exemplified by the multifactorial etiology of RA, the ecological factors (diet,

lifestyle, genotype) driving the dysbiosis in humans are lacking in the murine models making it difficult to replicate human-microbiome disease associations (Arrieta et al., 2016).

PERIODONTAL MICROBIOME AND ACPA

Periodontal disease is characterized by environmental risk factors (smoking), genetic risk factors [shared epitope (Marotte et al., 2006)] and persistent inflammation leading to bony destruction, all characteristics shared with RA. We have already highlighted the epidemiological links demonstrating RA patients to have increased prevalence and severity of PD. The fact that PD exists at the time of diagnosis of new RA (Scher et al., 2012; Mankia et al., 2019) suggests it is less likely a consequence of the RA disease process, but possibly an additional target of the disease or a disease initiator. Scher et al. investigated the oral microbiome in new onset RA (NORA) patients prior to disease treatment, and compared it to chronic RA patients and healthy controls. Interestingly there was no difference in the microbiome diversity of the NORA and the other groups, however two taxa, *Prevotella* spp. and *leptotrichia* spp. were enriched in NORA patients regardless of PD status. Investigating groups at risk of developing RA allows us to examine disease chronology and investigate disease initiation, before clinical arthritis occurs. This is a unique time point which is unattainable in most disease

TABLE 1 | Possible mechanism of microbial influence on RA development.

Study	Link to RA	Methodology	Findings
Maresz et al., 2013; Gully et al., 2014; Sandal et al., 2016; Courbon et al., 2019	PPAD citrullination	Rodent arthritis model	Infection with <i>P. gingivalis</i> aggravated arthritic symptoms
Konig et al., 2016	Citrullination via <i>A. actinomycetemcomitans</i>	Mass spectrometry	Neutrophilic hypercitrullination induced by pore forming toxin LtxA.
Moutsopoulos et al., 2012	Pro-inflammatory cytokine production leading to osteoclastic activation	<i>In-vitro</i> cytokine production	Increased Th17 and IL17 production on exposure to <i>P. gingivalis</i>
Sato et al., 2017; Tsukasaki et al., 2018	Pro-inflammatory cytokine production leading to osteoclastic activation	Rodent model	Increased Th17 and IL17 production on exposure to <i>P. gingivalis</i>
Lundberg et al., 2008	Molecular mimicry	ELISA, mass spectrometry	Cross-reactivity between human α -enolase and <i>P. gingivalis</i> α -enolase
Khandpur et al., 2013	Citrullination via NETosis	Neutrophils isolated via sedimentation and quantification via fluorescence microscopy	Increased NETosis in RA patients. NETosis correlated with ACPA presence.
Totaro et al., 2013	Bacterial translocation	PCR	Presence of <i>P. gingivalis</i> DNA in synovial tissue
Taurog et al., 1994	Toll like receptor activation	Rodent model	Arthritis development was dependant on LTR activation by <i>Lactobacillus bifidus</i>
Chen et al., 2016	Disease prediction model based on random forest plots.	16S rRNA sequencing in humans. Rodent model used to investigate causality	<i>Collinsella</i> , <i>Eggerthella</i> , and <i>Faecalibacterium</i> identified as predictor organisms of RA. <i>Collinsella</i> increase disease severity in rodent models
Kim et al., 2018	Osteoclastic activity inhibited by butyrate	Rodent model	Butyrate inhibited HDAC2 in osteoclast and HDAC8 in T cells. Control of Th17/Treg balance.

processes. Mankia et al. demonstrated increased prevalence of PD in ACPA+ at-risk individuals when compared with early RA patients and healthy matched controls (Mankia et al., 2019).

The strongest evidence linking both PD and RA comes in the form of the enzyme PAD. This enzyme has been identified in the organism *P. gingivalis* part of the “red complex” of dental organisms known to cause PD (Mcgraw et al., 1999). Interestingly the genes encoding PAD enzymes in *P. gingivalis* (PPAD) share no sequence homology to human PAD genes and to date *P. gingivalis* is the only bacteria identified containing such genes (Gabarrini et al., 2015). PPAD possesses the same catalytic activity of the human PAD enzymes resulting in citrullination, however PPAD shows preference to the terminal and free arginine residues. This is an important differentiation from human PAD genes (which endocitrullinate) as one of the proposed mechanisms in which *P. gingivalis* induces arthritis is via the release of the virulence factor arginine-gingipain (RgpB) which cleaves host proteins exposing the terminal arginine residue which is then free to undergo citrullination via PPAD with the creation of neo-epitopes and subsequent ACPA positivity (Wegner et al., 2010). This hypothesis is supported by murine models which demonstrated that mice with laboratory induced arthritis had higher autoantibody production and joint destruction in those infected with wild type PPAD compared to those with mutated deficient PPAD genes (Maresz et al., 2013; Gully et al., 2014; Sandal et al., 2016; Courbon et al., 2019). Sandel et al. demonstrated this pathway was restricted via HLA-DRB1 positive mice suggesting that in addition to the presence of

P. gingivalis and its associated expressed virulence factors, a genetic predisposition was also required. Remaining on the theme of citrullination, another oral pathogen has been recently identified as a possible etiological agent, *Aggregatibacter actinomycetemcomitans* (Konig et al., 2016). This organism is typically associated with aggressive PD or endocardial disease. Leukotoxin A (LtxA) is a primary virulence toxin produced by *A. actinomycetemcomitans* capable of inducing pore formation into the cell membrane of neutrophils, the resultant transient membrane permeability can then induce dysregulation of human PAD enzymes due to a rapid influx of calcium leading to increased endogenous citrullination, however not shown to be increased in ACPA positive population progressing to RA see **Figure 1**.

P. gingivalis has also been linked to increased production of Th17 cells (Moutsopoulos et al., 2012), a subset of CD4+ cells that have gained much attention in the field of autoimmunity since their identification in Harrington et al. (2005). The primary role of Th17 cells is fighting bacterial (mainly *Staphylococcus aureus*) and fungal (mainly *Candida albicans*) infections (Holland et al., 2007; De Beaucoudrey et al., 2008). Th17 cells are capable of producing a repertoire of pro-inflammatory cytokines IL-17A, IL-17F, and IL-22 (Marwaha et al., 2012), which in turn can result in bone destruction via osteoclastic activation (Sato et al., 2006). Increased levels of IL-17 have been found in the synovium of RA patients and correlate with disease severity (Cascao et al., 2010). Furthermore, CIA mouse models have demonstrated increased Th17 production and large quantities of IL-17 in lymph nodes draining the affected

TABLE 2 | Identified microbiome perturbations in RA.

Study	Microbiome	Methodology	Findings
Scher et al., 2012	Oral	V1-V2 16S rRNA sequencing	<i>Prevotella</i> spp. and <i>leptotrichia</i> spp. were enriched in NORA
Mankia et al., 2019	Oral	Shotgun metagenomic sequencing	Increased prevalence of periodontitis and <i>P. gingivalis</i> in ACPA+ at-risk individuals.
Scher et al., 2013	Gut	V1-V2 16S rRNA sequencing, Shotgun metagenomic sequencing in a subset of patients	Higher abundance of <i>Prevotella copri</i> in NORA
Zhang et al., 2015	Oral and Gut	Shotgun metagenomic sequencing	Higher abundance of <i>Lactobacillus salivarius</i> in RA patients. <i>Prevotella copri</i> was a function of disease duration.
Round et al., 2011	Oral	V4 16S rRNA sequencing	Higher abundance of <i>Prevotella</i> spp. in at risk RA population
Rodrigues et al., 2019	Gut	qPCR	Higher abundances of <i>Bacteroides</i> spp. and <i>Prevotella</i> spp.
Jeong et al., 2019	Gut	Genus specific 16S rRNA PCR	Higher abundances of <i>Bacteroidales</i> and <i>Prevotella</i> in early RA
Maeda et al., 2016	Gut	V5-V6 16S rRNA sequencing	Higher abundances of <i>Prevotella copri</i> in a subset of RA patients.
Breban et al., 2017	Gut	V3- V4 16S rRNA sequencing	Lower abundance of <i>Prevotellaceae</i> and <i>Paraprevotellaceae</i> in RA than healthy controls
Vahtovuo et al., 2008	Gut	16S rRNA hybridization	Lower abundance of <i>Bifidobacteria</i> and bacteria of the <i>Bacteroides-Porphyromonas-Prevotella</i> group, <i>Bacteroides fragilis</i> subgroup, and <i>Eubacterium rectale-Clostridium coccoides</i> group compared to fibromyalgia patients
Muñiz Pedrego et al., 2019	Gut	Shotgun metagenomic sequencing	Higher abundances of <i>Clostridiaceae</i> in RA group (arthritis group also contained IBD patients with arthralgia)
Chiang et al., 2019	Gut	V1-V3 16S rRNA sequencing	ACPA-positive patients had higher proportions of <i>Blautia</i> , <i>Akkermansia</i> , and <i>Clostridiales</i> than ACPA-negative patients
Picchianti-Diamanti et al., 2018	Gut	V3-V4 16S rRNA sequencing	Higher abundance of <i>Lactobacillales</i> in RA. ACPA positivity was indirectly correlated with <i>Streptococcaceae</i> , <i>Erysipelotrichaceae</i> , <i>Streptococcus</i> , <i>Bacteroides xylanisolvens</i> , and <i>Lachnospira pectinoschiza</i>
Forbes et al., 2018	Gut	V4 16S rRNA sequencing	Higher abundance of <i>Actinomyces</i> , <i>Eggerthella</i> , <i>Clostridium III</i> , <i>Faecalicoccus</i> , and <i>Streptococcus</i> in all disease cohorts including RA

joints in mice infected with *P. gingivalis* PD (Sato et al., 2017; Tsukasaki et al., 2018).

The oral microbiome itself can produce an array of small molecules, some of which share structural homology to self-antigens which may lead to antibody cross reactivity and aberrant targeting of host proteins (i.e., molecular mimicry). Again *P. gingivalis* has been implicated here as its α -enolase protein shares 82% homology to human α -enolase and have been shown to cross-react (Lundberg et al., 2008). Alpha-enolase is consistently identified as an autoantigen (Kinloch et al., 2005) in RA patients. Interestingly higher levels of antibodies against citrullinated α -enolase (anti-CEP-1) were present in individuals, without RA, suffering from chronic PD compared to non PD individuals (De Pablo et al., 2014).

Neutrophil extracellular traps (NETs) primarily act as a defensive mechanisms against invading microorganisms (Kaplan and Radic, 2012). During the process of NETosis the extracellular membrane breaks down allowing the mixing of cellular contents including chromatin and histones proteins with extracellular fluid, creating a matrix capable of affixing invading organisms (Li et al., 2010; Lood et al., 2016). The process of NETosis has recently gained renewed interest in RA (Khandpur et al., 2013), as citrullination of proteins is a key step in NETosis. This process is catalyzed by PAD4 enzymes (Wang et al., 2009) and interestingly individuals suffering from autoimmune conditions display spontaneous NETosis, resulting in the externalization of a number of intracellular molecules which are

subsequently recognized as autoantigens (Grayson and Kaplan, 2016; Demoruelle et al., 2017).

Although we have initially stated the microbiome enacts its autoimmune effects via the mucosal surface, which is typically distant to the target tissues, recently both the oral and gut microbiome have been implicated in the translocation of bacteria to the joints. Clinical microbiologists now appreciate that a transient bacteraemia can occur following minor breaks in the mucosal barrier, including brushing ones' teeth (Maharaj et al., 2012). The possibility of bacterial translocation is increased in the presence of mucosal inflammation such as PD where organisms associated with PD have been identified in the liver and spleen of affected mice (Tsukasaki et al., 2018). Additionally *P. gingivalis* has been shown to persist intracellularly (Li et al., 2008), which may then act as a vehicle to carry this pathogen to joint sites. This hypothesis is supported by the isolation of *P. gingivalis* DNA from the synovium of RA patients (Totaro et al., 2013) suggesting certain bacteria may have a direct inflammatory effect on the joint. If this effect exists it is independent for ACPA as there was no correlation between joint bacteria and ACPA positivity. A summary of possible mechanisms of microbial influence on RA development is provided in **Table 1**.

THE GUT MICROBIOME AND RA

The advent of DNA analyses has expanded our knowledge on the microbiota present within the gut, allowing for the

identification of communities but also potential functional pathways. For example, the human microbiome project has produced >70 million 16S rRNA gene sequences (HMP consortium) and together with MetaHIT a European project has suggested great medical significance of the gut microbiome and aimed at developing genomic databases for the enumeration of bacteria. A delicate balance has evolved to create a mutually beneficial relationship between man and microbe representing a symbiosis within the gut. However, we now know alterations in our gut microbiome (dysbiosis) have been linked to a variety of diseases including RA. The change from symbiosis to dysbiosis is a critical transition from microbiome stability to an alternative state, representative of disease. Investigations into the role of the gut microbiome in the development of RA have focused on identifying perturbations in the gut microbiome, thereby resulting in a local mucosal immune dysregulation which may lead to local inflammation and subsequently systemic inflammation.

The gut microbiome has evolved its own unique innate immune homeostasis, with distinct phenotypic expression between gut and blood borne macrophages. CD14 expression is lacking on intestinal macrophages, a key molecule required for the recognition of lipopolysaccharide on bacterial surfaces (Smith et al., 1997). There is also a distinct down regulation of cytokine expression from macrophages isolated from the colon (Smith et al., 2001). Germ-free animal studies have demonstrated a reduced ability of neutrophils to phagocytise and subsequently release superoxide anions into the lysosome (Ohkubo et al., 1990). Innate lymphoid cells capable of helper T (Th) cell regulation via cytokine production play a vital role in immune homeostasis. These cells resemble Th17 cells with respect to their cytokine profile, producing pro-inflammatory interleukins (IL)-17 and IL-22. Additionally, the gut microbiome plays a regulatory role for the adaptive immune response. CD4⁺ T cells are divided into four major classes depending on their cytokine profile; Th1, Th2, Th17, and T regulatory Cells (Treg) and a careful balance of pro versus anti-inflammatory cells maintain immune homeostasis. Certain bacteria have been associated with the induction of a T cell response, for example *Bacteroides fragilis* induce the differentiation of Treg cells through polysaccharide A present on the bacterial surface resulting in an anti-inflammatory effect that has been shown to have both local mucosal effect but also modulate systemic anti-inflammatory role (Hooper and Macpherson, 2010; Round et al., 2011). Similarly, *Clostridia* spp. (IV and XIVa) have also shown anti-inflammatory effects via IL-10 producing Treg cells after colonization of germ cell mice (Atarashi et al., 2011). The gut microbiome has also been shown to have a pro-inflammatory effect mediated via CD4⁺ cells differentiation in Th17, this differentiation is induced via the presence of SFB (Ivanov et al., 2009).

Given the interplay described and the multiplicative effect via cytokine activity it is reasonable to assume a pivotal role of the gut microbiome in autoimmune conditions. Germ-free animal studies of HLA B27 positive rats (genetic predisposition) demonstrate that without the input from the gut microbiome peripheral joint disease does not develop (Taurog et al.,

1994). Gnotobiotic studies implicate specific bacteria in RA development, monocolonisation with *Lactobacillus bifidus* results in homeostatic imbalance between Treg and Th17 (Abdollahi-Roodsaz et al., 2008). Ivanov et al. (2009) demonstrated a role for SFB specifically *candidatus* spp. resident in the terminal ileum capable to inducing Th17 cell differentiation and subsequent arthritis development.

Biofilm formation within the gut is now receiving more interest as a mechanism of immune dysregulation, tipping the scales between Th17 and Treg cells. Dalpke et al. (2006) described the activation of TLR-9 via bacterial cell contents including DNA, a major constituent of bacterial biofilms (Schlafer et al., 2017). Interestingly biofilm formation has been implicated in the development of systemic lupus erythematosus (SLE), where a structural protein of the biofilm called a curli (amyloid fibril) was capable of binding to bacterial DNA, creating an immunogenic complex inducing an immune response via DC presentation (Gallo et al., 2015). Curli fibers produced by common enteric organisms can activate the NLRP3 inflammasome, leading to the production of IL-1 β through caspase 1 and TLR signaling thereby driving a pro-inflammatory response (Rapsinski et al., 2015). However, Curli fibers also have demonstrated the ability to increase epithelia tight junctions (Oppong et al., 2015) via TLR-2 activation and so further work must be done to explore the action of biofilm on autoimmunity. Mucosal epithelial barrier integrity has been linked to RA pathogenesis in mouse models by Chen et al. (2016), who demonstrated colonization with *collinsella* spp. increased mucosal barrier permeability and Th17 cells. Elements known to influence the mucosal barrier integrity include bacteria, their by-products and diet (Horta-Baas et al., 2017; Guerreiro et al., 2018). Microbial by-products particularly short chain fatty acids (SCFA), including acetate, propionate, and butyrate have been linked to amelioration of arthritis development in CIA models (Mizuno et al., 2017; Kim et al., 2018). Mizuno et al. (2017) showed that oral administration of SCFA was able to decrease disease severity by decreasing Th1 cells, and increasing Treg cells thereby damping the immune response.

The RA Dysbiosis

Using 16S rRNA gene sequencing the microbiome of new onset RA patients, chronic RA patients who are already receiving treatment, established psoriatic arthritis patients and healthy matched controls were analyzed. An overabundance of *P. copri* with new onset RA was found, a predominance of this group was not seen within the microbiome's of long standing arthritis patients or healthy matched controls (Scher et al., 2013). Functional genomic analysis of the new onset RA patients suggests a decrease in vitamin metabolism (biotin, pyroxidol, and folate) due to a lack of these pathways in *Prevotella* sp. This functional shift may represent a pro-inflammatory environment more resistant to treatment given that folate metabolism is a target for methotrexate, a stable in RA treatment. Interestingly Scher et al. demonstrated an inverse relationship between the abundance of *P. copri* and the presence of HLA-DRB1. The authors' hypothesize a minimum threshold of *P. copri* is needed to induce disease, which may be lower in those with accompanying genetic risk, although this theory has been recently

challenged by Wells et al. (2020), discussed further in the causality section of the review. Using metagenomic shotgun sequencing Zhang et al. demonstrated increased quantities of *Lactobacillus* spp. in RA patients at multiple microbiome sites (gut, oral and saliva) which positively correlated with disease activity. *P. copri* abundance was illustrated, within the first year, to be a function of disease duration. Large clustering was identified including *Gordonibacter pamelaeae*, *Clostridium asparagiforme*, *Eggerthella lenta*, and *Lachnospiraceae* bacterium, and smaller clusters containing *Lactobacillus* spp., *Bifidobacterium dentium* and *Ruminococcus lactaris* as over-abundant in the RA microbiome (Zhang et al., 2015).

Recently Alpizar-Rodriguez et al. (2019b) also identified an over-abundance of *P. copri* in individuals at risk of RA, their population included ACPA positive and/or RF positive patients without arthritis comparing them to first degree seronegative relatives. This study demonstrates a dysbiotic microbiome before the onset of clinical arthritis and suggests the gut microbiome may play an active role in RA development. Of note, this study did include individuals with undifferentiated arthritis (likely to include SpA patients) which represents progression of the disease phenotype beyond the pre-arthritis “at-risk” phase (Alpizar-Rodriguez et al., 2019b). Multiple studies describing various dysbiotic bacterial states associated with RA have been published, some demonstrating increased *Prevotellaceae* (Maeda et al., 2016; Jeong et al., 2019; Lee et al., 2019; Rodrigues et al., 2019), some decreased *prevotellaceae* (Vaahtovuori et al., 2008; Breban et al., 2017) and others attributing the dysbiosis to other organisms, such as *Clostridiaceae* (Muñiz Pedrego et al., 2019) *Blautia*, *Akkermansia*, and *Clostridiales* (Chiang et al., 2019), *Lactobacilli* (Liu et al., 2013; Picchianti-Diamanti et al., 2018), *Actinomyces*, *Eggerthella* (Chen et al., 2016; Forbes et al., 2018). **Table 2** contains a summary of microbial perturbations found in RA.

LUNG MICROBIOME AND RA

Pulmonary disease is a common extra-articular manifestation of RA and may affect multiple respiratory structures including lung parenchyma, pleura, airways and vascular compartments (O’dwyer et al., 2013; Shaw et al., 2015). As previously stated, smoking is a well-established risk factor for RA, and often the presence of respiratory symptoms predates the onset of joint disease. Indeed HRCT has demonstrated underlying lung pathology prior to RA onset (Demoruelle et al., 2012). Furthermore, the presence of autoantibodies in the sputum of seronegative individuals (Willis et al., 2013) suggests the lung may act as a site of autoantibody generation. Scher et al. (2016) demonstrated decreased alpha diversity of the lung microbiome (bronchial alveolar lavage) in individuals with newly diagnosed RA compared to healthy controls. The microbial changes identified by Scher et al. (2016) in this cohort resembled the changes present in the lung microbiome of sarcoidosis patients (granulomatous disease not associated with ACPA positivity); involving decreases in the relative abundance of *Burkholderiaceae*, *Actinomycetaceae*, *Spirochaetaceae* and the genera *Actinomyces*, *Treponema*, and *Porphyromonas* suggesting a commonality within lung dysbiosis driving inflammation. Of

note, there was also a correlation between the presence of the genus *Prevotella* in BAL samples and systemic RF titers and the number of ACPA fine specificities.

While there is a distinct lack of lung microbiome studies in RA or pre-RA, both *Prevotella* and *P. gingivalis* have also been identified within the lung microbiome (Erb-Downward et al., 2011; Goleva et al., 2013) of other inflammatory conditions and therefore it is not impossible to assume they could be present within the RA/Pre-RA population. Both *Streptococcus pneumoniae* and *Streptococcus pyogenes* are capable of causing respiratory infections, similar to *P. gingivalis*, both of these pathogens express α -enolase (Pancholi and Fischetti, 1998; Bergmann et al., 2001) and therefore via molecular mimicry could result in ACPA formation within the lung mucosa. It is interesting to note also the number of respiratory infections has been shown to increase prior to the onset of RA (Arleevskaya et al., 2018) and subside upon RA diagnosis and treatment. Additionally, as smoking induces human PAD genes (PAD2 and PAD4) which increases the overall burden of citrullinated proteins (Kilsgård et al., 2012; Damgaard et al., 2015), it has been demonstrated that citrullinated IL-37 resulted in decreased activity against common respiratory pathogens potentially facilitating bacterial infection within the lungs (Kilsgård et al., 2012). Therefore interplay between lifestyle factors and infections could induce autoimmunity with the lung.

CAUSALITY AND THE MICROBIOME

In building the case for the microbiome as a trigger of RA we have relied on several key experimental approaches, specifically aimed at understanding the molecular mechanisms by which the microbiome could trigger autoimmunity. In summary these findings suggest a number of “commensal” organisms capable of inducing ACPA formation, or microbial perturbation resulting in activation and subsequent compensatory immune cascades which could ultimately lead to RA development. Traditional approaches for the assessment of microbial causal relationships required the fulfillment of Koch postulates (Koch, 2010; Duhe, 2011), however these postulates pose a significant hurdle for microbiome studies. Not least of which, the difficulty to culture much of the human microbiome (Browne et al., 2016), furthermore we now appreciate the human host microbiome interactions can be both beneficial or deleterious depending on the organisms abundance and temporality (Cho and Blaser, 2012) which forfeits the major tenants of Koch’s postulates. An alternative approach to help ascribe causality is the use of epidemiology in complex ecosystems like humans, where the putative casual factor is the environment, or in this case, the microbiome. Consideration of the environment as a potential instigator of disease, which may be communicable is integral to the many sights from the field of epidemiology. For example, John Snow considered the father of epidemiology and his description of contaminated drinking water and cholera, to more complex relations of diet and cardiovascular disease or smoking and lung cancer. Epidemiological studies of this nature are expensive and require multiple statistical methods to control for confounders. Furthermore, these latter examples are unpin-

by genetics, amongst other factors, and from this perspective microbial perturbations as an impetus from RA would be highly contextual. As we have highlighted earlier in this article, cross-sectional observational studies have demonstrated microbial changes in individuals with RA and pre-RA compared to healthy controls, with animal studies supporting a causal role for the microbiome and RA development. Of course, it is essential to determine the microbiome features that are causal for RA onset from those that are a consequence of the disease process or treatment, and from those that show statistical association due to confounding.

Mendelian randomization (MR) is increasingly used to overcome the multiple confounding effects of observational studies and has been used as an alternative method to ascribe causality (Sekula et al., 2016; Davies et al., 2018). MR relies on the presence of naturally occurring genetic variants within our human genome, and assigns these as instrumental variables to investigate the effects of a modifiable risk factor (the microbiome) on a disease outcome (RA). Valid genetic instrumental variables for RA studies must fulfill three assumptions; the selected gene must be associated with the microbiome (relevance assumption), must not be associated with any related confounders (independence assumption), and does not affect RA except through the microbiome (exclusion restriction assumption) (Davies et al., 2018). The nature of genetic inheritance which allows the use of randomization introduced during meiosis and fixed at conception allows genetic variants to act as plausible instrumental variables. Inamo has used MR to investigate for a causal relationship between the gut microbiome and RA (Inamo, 2019). Utilizing two datasets from genome-wide association studies; one for the gut microbiome as the exposure and another for RA as the outcome, 26 single nucleotide polymorphisms (SNP) were identified to be associated with decreased gut microbial diversity. One SNP (rs1230666) was found to be independently associated with RA development and therefore removed, following its removal the remaining 25 SNP's failed to demonstrate the microbiome as a causal factor for RA development (Inamo, 2019), suggesting the observed microbial dysbiosis in RA is a secondary phenomenon. However, Alpizar-Rodriguez et al. (2019a) has highlighted that microbial dysbiosis does not always equate to decreases in microbial taxa, and rather is it a compositional shift of the microbiome that is driving the RA dysbiosis (Kishikawa et al., 2020). Therefore MR analysis based a selection of SNP's that are known to affect the gut microbiome by decreasing the numbers of taxa present within the gut is unlikely to yield a causal effect, given an arbitrary decrease of taxa is in contradiction to the current observational studies.

Using the same datasets as Inamo, Lee again used MR to question the causal effects of the microbiome on RA (Lee, 2020). In this study 32 SNPs were identified as instrumental variables, as opposed to original 26 identified by Inamo, presumably by including SNP's known to alter bacterial taxa in either direction, not limiting to those that decrease bacterial taxa only. Following removal of rs1230666 SNP, known to independently influence RA development, the MR analysis did show significance and supported a causal role for the microbiome in RA development. The use of MR to assign causality to the gut microbiome

obviously relies upon the selected SNPs and the strength of their influence on the microbiome, Rothschild et al. (2018) has demonstrated that genetics have a poor effect on microbiome composition. However, a recent study by Wells et al. (2020) has demonstrated that a polygenic risk score for RA was positively associated with the presence of *Prevotella* spp. within the gut microbiome of non-RA patients, they went on to validate their findings within an independent cohort composed of first degree relatives of RA patients carrying the HLA DRB1 risk allele. An inverse relationship between *P. copri* and HLA DRB1 has previously been reported (Scher et al., 2013), here the authors' suggest the differences identified are likely a result of population characteristics or unmeasured confounding (Wells et al., 2020). They also found an association between individuals with preclinical RA and *P. copri*.

Interestingly, there was no association between the polygenic risk score and overall microbial diversity (Wells et al., 2020), again adding weight to the theory that MR analysis based on decreased taxa is unlikely to be an accurate measure of RA dysbiosis.

FUTURE CONSIDERATIONS

There is much interest in the microbiome community to move past the traditional taxonomic description of the microbiome to understanding its functional capacity, which has mainly relied upon metagenomic sequencing which is expensive [although methods to infer function from 16S rRNA are available (Ortiz-Estrada et al., 2019)]. Recently Hillmann et al. (2018) described shallow shotgun sequencing, allowing better taxonomic resolution and functional analysis for a fraction of the cost of whole metagenome shotgun sequencing, although if wishing to identify the rarer taxa which may delineate a disease phenotype then depending on research budget 16S rRNA may still be the better option. It is worth pointing out that some RA studies have relied upon qPCR to identify microbes of interest, which obviously identifies only the organisms carrying the reciprocal primer target sequence, which might create a skewed view of the microbiome in these individuals; it is possible that in the future qPCR might be the technology that is taken to the clinic if a unique microbiome signature indicative of RA disease was identified, but we are not at that stage yet. It has been over 10 years since the first publication of the human microbiome project (Turnbaugh et al., 2007), which has been consolidated by large phenotyped cross-sectional population studies (Falony et al., 2016; Zhernakova et al., 2016). These studies highlight the importance to account for multiple covariates into microbiome research such as diet, gut transit time, medications and intrinsic factors, to date no such RA study has included these important factors and this is a key point that needs to be addressed moving forward.

As we have highlighted in this review mucosal surfaces including oral, gut and lung microbiomes can play an important role in initiating and perpetuating inflammation. It appears that induction of autoimmunity may not occur at a single

site but in fact these microbiomes may be acting in tandem creating a systemic multiplicative effect. A recent study by Schmidt et al. (2019) demonstrated that extensive transmission of bacterial species exists between the oral and gut mucosal sites, demonstrating >40% of bacterial species were prevalent (>10%) in both gut and salivary samples in a population including RA patients. Taken into account future microbiome studies should investigate a homogenous at-risk population, incorporate known factors effecting the microbiome, examine multiple mucosal sites, and ideally provide a longitudinal prospective as individuals progress toward the disease phenotype.

REFERENCES

- Abdollahi-Roodsaz, S., Joosten, L. A., Koenders, M. I., Devesa, I., Roelofs, M. F., Radstake, T. R., et al. (2008). Stimulation of TLR2 and TLR4 differentially skews the balance of T cells in a mouse model of arthritis. *J. Clin. Invest.* 118, 205–216. doi: 10.1172/jci32639
- Ahluwalia, B., Magnusson, M. K., and Öhman, L. (2017). Mucosal immune system of the gastrointestinal tract: maintaining balance between the good and the bad. *Scand. J. Gastroenterol.* 52, 1185–1193. doi: 10.1080/00365521.2017.1349173
- Aho, K., Koskenvuo, M., Tuominen, J., and Kaprio, J. (1986). Occurrence of rheumatoid arthritis in a nationwide series of twins. *J. Rheumatol.* 13, 899–902.
- Alpizar-Rodriguez, D., Lesker, T. R., Gilbert, B., Strowig, T., and Finckh, A. (2019a). Intestinal dysbiosis in RA development: difficulty of establishing causality. Response to: 'non-causal association of gut microbiome on the risk of rheumatoid arthritis: a Mendelian randomisation study' by Inamo. *Ann. Rheum. Dis.* doi: 10.1136/annrheumdis-2019-216637 [Epub ahead of print].
- Alpizar-Rodriguez, D., Lesker, T. R., Gronow, A., Gilbert, B., Raemy, E., Lamacchia, C., et al. (2019b). *Prevotella copri* in individuals at risk for rheumatoid arthritis. *Ann. Rheum. Dis.* 78, 590–593. doi: 10.1136/annrheumdis-2018-214514
- Arleevskaya, M. I., Albina, S., Larionova, R. V., Gabdoulkhakova, A. G., Lemerle, J., and Renaudineau, Y. (2018). Prevalence and incidence of upper respiratory tract infection events are elevated prior to the development of rheumatoid arthritis in first-degree relatives. *Front. Immunol.* 9:2771. doi: 10.3389/fimmu.2018.02771
- Arrieta, M. C., Walter, J., and Finlay, B. B. (2016). Human microbiota-associated mice: a model with challenges. *Cell Host Microbe* 19, 575–578. doi: 10.1016/j.chom.2016.04.014
- Atarashi, K., Tanoue, T., Shima, T., Imaoka, A., Kuwahara, T., Momose, Y., et al. (2011). Induction of colonic regulatory T cells by indigenous *Clostridium* species. *Science* 331, 337–341. doi: 10.1126/science.1198469
- Äyräväinen, L., Leirisalo-Repo, M., Kuuliala, A., Ahola, K., Koivuniemi, R., Meurman, J. H., et al. (2017). Periodontitis in early and chronic rheumatoid arthritis: a prospective follow-up study in Finnish population. *BMJ Open* 7:e011916. doi: 10.1136/bmjopen-2016-011916
- Berglin, E., Johansson, T., Sundin, U., Jidell, E., Wadell, G., Hallmans, G., et al. (2006). Radiological outcome in rheumatoid arthritis is predicted by presence of antibodies against cyclic citrullinated peptide before and at disease onset, and by IgA-Rf at disease onset. *Ann. Rheum. Dis.* 65, 453–458. doi: 10.1136/ard.2005.041376
- Bergmann, S., Rohde, M., Chhatwal, G. S., and Hammerschmidt, S. (2001). alpha-enolase of *Streptococcus pneumoniae* is a plasmin(ogen)-binding protein displayed on the bacterial cell surface. *Mol. Microbiol.* 40, 1273–1287. doi: 10.1046/j.1365-2958.2001.02448.x
- Brand, D. D., Kang, A. H., and Rosloniec, E. F. (2004). The mouse model of collagen-induced arthritis. *Methods Mol. Med.* 102, 295–312. doi: 10.1385/1-59259-805-6:295
- Brandtzaeg, P. (2013). Secretory immunity with special reference to the oral cavity. *J. Oral Microbiol.* 5:20401. doi: 10.3402/jom.v5i0.20401
- Brandtzaeg, P., Farstad, I. N., Johansen, F. E., Morton, H. C., Norderhaug, I. N., and Yamanaka, T. (1999). The B-cell system of human mucosae and exocrine glands. *Immunol. Rev.* 171, 45–87. doi: 10.1111/j.1600-065x.1999.tb01342.x

AUTHOR CONTRIBUTIONS

CR initially drafted the manuscript. KM and PE critical revising of the manuscript. All authors contributed to the article and approved the submitted version.

FUNDING

CR is receiving funding from Versus Arthritis as a clinical research fellow, grant number 22294.

- Breban, M., Tap, J., Leboime, A., Said-Nahal, R., Langella, P., Chiocchia, G., et al. (2017). Faecal microbiota study reveals specific dysbiosis in spondyloarthritis. *Ann. Rheum. Dis.* 76, 1614–1622. doi: 10.1136/annrheumdis-2016-211064
- Brown, T. M., Clark, H. W., Bailey, J. S., and Gray, C. W. (1971). A mechanistic approach to treatment of rheumatoid type arthritis naturally occurring in a gorilla. *Trans. Am. Clin. Climatol. Assoc.* 82, 227–247.
- Browne, H. P., Forster, S. C., Anonye, B. O., Kumar, N., Neville, B. A., Stares, M. D., et al. (2016). Culturing of 'unculturable' human microbiota reveals novel taxa and extensive sporulation. *Nature* 533, 543–546. doi: 10.1038/nature17645
- Carragher, D. M., Rangel-Moreno, J., and Randall, T. D. (2008). Ectopic lymphoid tissues and local immunity. *Semin. Immunol.* 20, 26–42. doi: 10.1016/j.smim.2007.12.004
- Cascao, R., Moura, R. A., Perpetuo, I., Canha, H., Vieira-Sousa, E., Mourao, A. F., et al. (2010). Identification of a cytokine network sustaining neutrophil and Th17 activation in untreated early rheumatoid arthritis. *Arthritis Res. Ther.* 12:R196.
- Castaner, O., Goday, A., Park, Y.-M., Lee, S.-H., Magkos, F., Shiow, S.-A. T. E., et al. (2018). The gut microbiome profile in obesity: a systematic review. *Int. J. Endocrinol.* 2018:4095789.
- Chavanas, S., Mechin, M. C., Takahara, H., Kawada, A., Nachat, R., Serre, G., et al. (2004). Comparative analysis of the mouse and human peptidylarginine deiminase gene clusters reveals highly conserved non-coding segments and a new human gene, Padi6. *Gene* 330, 19–27. doi: 10.1016/j.gene.2003.12.038
- Chen, B., Chen, H., Shu, X., Yin, Y., Li, J., Qin, J., et al. (2018). Presence of segmented filamentous bacteria in human children and its potential role in the modulation of human gut immunity. *Front. Microbiol.* 9:1403. doi: 10.3389/fmicb.2018.01403
- Chen, J., Wright, K., Davis, J. M., Jeraldo, P., Marietta, E. V., Murray, J., et al. (2016). An expansion of rare lineage intestinal microbes characterizes rheumatoid arthritis. *Genome Med.* 8:43.
- Chervonsky, A. V. (2013). Microbiota and autoimmunity. *Cold Spring Harb. Perspect. Biol.* 5:a007294.
- Chiang, H. I., Li, J. R., Liu, C. C., Liu, P. Y., Chen, H. H., Chen, Y. M., et al. (2019). An association of gut microbiota with different phenotypes in Chinese patients with rheumatoid arthritis. *J. Clin. Med.* 8:1770. doi: 10.3390/jcm8111770
- Cho, I., and Blaser, M. J. (2012). The human microbiome: at the interface of health and disease. *Nat. Rev. Genet.* 13, 260–270. doi: 10.1038/nrg3182
- Costello, E. K., Lauber, C. L., Hamady, M., Fierer, N., Gordon, J. I., and Knight, R. (2009). Bacterial community variation in human body habitats across space and time. *Science* 326, 1694–1697. doi: 10.1126/science.1177486
- Courbon, G., Rinaudo-Gaujous, M., Blasco-Baque, V., Auger, I., Caire, R., Mijola, L., et al. (2019). *Porphyromonas gingivalis* experimentally induces periodontitis and an anti-CCP2-associated arthritis in the rat. *Ann. Rheum. Dis.* 78, 594–599. doi: 10.1136/annrheumdis-2018-213697
- Criswell, L. A., Merlino, L. A., Cerhan, J. R., Mikuls, T. R., Mudano, A. S., Burma, M., et al. (2002). Cigarette smoking and the risk of rheumatoid arthritis among postmenopausal women: results from the Iowa Women's Health Study. *Am. J. Med.* 112, 465–471. doi: 10.1016/s0002-9343(02)01051-3
- Dalpke, A., Frank, J., Peter, M., and Heeg, K. (2006). Activation of toll-like receptor 9 by DNA from different bacterial species. *Infect. Immun.* 74, 940–946. doi: 10.1128/iai.74.2.940-946.2006
- Damgaard, D., Friberg Bruun Nielsen, M., Quisgaard Gaunsbaek, M., Palarasah, Y., Svane-Knudsen, V., and Nielsen, C. H. (2015). Smoking is associated with

- increased levels of extracellular peptidylarginine deiminase 2 (PAD2) in the lungs. *Clin. Exp. Rheumatol.* 33, 405–408.
- Davies, N. M., Holmes, M. V., and Davey Smith, G. (2018). Reading Mendelian randomisation studies: a guide, glossary, and checklist for clinicians. *BMJ* 362:k601. doi: 10.1136/bmj.k601
- De Beaucoudrey, L., Puel, A., Filipe-Santos, O., Cobat, A., Ghandil, P., Chrabieh, M., et al. (2008). Mutations in STAT3 and IL12RB1 impair the development of human IL-17-producing T cells. *J. Exp. Med.* 205, 1543–1550.
- De Pablo, P., Dietrich, T., Chapple, I. L., Milward, M., Chowdhury, M., Charles, P. J., et al. (2014). The autoantibody repertoire in periodontitis: a role in the induction of autoimmunity to citrullinated proteins in rheumatoid arthritis? *Ann. Rheum. Dis.* 73, 580–586. doi: 10.1136/annrheumdis-2012-202701
- Deane, K. D., Demoruelle, M. K., Kelmenson, L. B., Kuhn, K. A., Norris, J. M., and Holers, V. M. (2017). Genetic and environmental risk factors for rheumatoid arthritis. *Best Pract. Res. Clin. Rheumatol.* 31, 3–18.
- Demoruelle, M. K., Harrall, K. K., Ho, L., Purmalek, M. M., Seto, N. L., Rothfuss, H. M., et al. (2017). Anti-citrullinated protein antibodies are associated with neutrophil extracellular traps in the sputum in relatives of rheumatoid arthritis patients. *Arthritis Rheumatol.* 69, 1165–1175. doi: 10.1002/art.40066
- Demoruelle, M. K., Weisman, M. H., Simonian, P. L., Lynch, D. A., Sachs, P. B., Pedraza, I. F., et al. (2012). Brief report: airways abnormalities and rheumatoid arthritis-related autoantibodies in subjects without arthritis: early injury or initiating site of autoimmunity? *Arthritis Rheum.* 64, 1756–1761. doi: 10.1002/art.34344
- Ditzel, H. J. (2004). The K/BxN mouse: a model of human inflammatory arthritis. *Trends Mol. Med.* 10, 40–45. doi: 10.1016/j.molmed.2003.11.004
- Du, R. J. (2011). “Koch’s postulates,” in *Encyclopedia of Cancer*, ed. M. Schwab (Berlin: Springer).
- Erb-Downward, J. R., Thompson, D. L., Han, M. K., Freeman, C. M., McCloskey, L., Schmidt, L. A., et al. (2011). Analysis of the lung microbiome in the “healthy” smoker and in COPD. *PLoS One* 6:e16384. doi: 10.1371/journal.pone.0016384
- Falony, G., Joossens, M., Vieira-Silva, S., Wang, J., Darzi, Y., Faust, K., et al. (2016). Population-level analysis of gut microbiome variation. *Science* 352, 560–564.
- Flak, M. B., Colas, R. A., Muñoz-Atienza, E., Curtis, M. A., Dalli, J., and Pitzalis, C. (2019). Inflammatory arthritis disrupts gut resolution mechanisms, promoting barrier breakdown by *Porphyromonas gingivalis*. *JCI Insight* 4:e125191.
- Forbes, J. D., Chen, C.-Y., Knox, N. C., Marrie, R.-A., El-Gabalawy, H., De Kievit, T., et al. (2018). A comparative study of the gut microbiota in immune-mediated inflammatory diseases—does a common dysbiosis exist? *Microbiome* 6:221.
- Foulquier, C., Sebbag, M., Clavel, C., Chapuy-Regaud, S., Al Badine, R., Mechlin, M. C., et al. (2007). Peptidyl arginine deiminase type 2 (PAD-2) and PAD-4 but not PAD-1, PAD-3, and PAD-6 are expressed in rheumatoid arthritis synovium in close association with tissue inflammation. *Arthritis Rheum.* 56, 3541–3553. doi: 10.1002/art.22983
- Gabarrini, G., De Smit, M., Westra, J., Brouwer, E., Vissink, A., Zhou, K., et al. (2015). The peptidylarginine deiminase gene is a conserved feature of *Porphyromonas gingivalis*. *Sci. Rep.* 5:13936.
- Gallo, P. M., Rapsinski, G. J., Wilson, R. P., Oppong, G. O., Sriram, U., Goulian, M., et al. (2015). Amyloid-DNA composites of bacterial biofilms stimulate autoimmunity. *Immunity* 42, 1171–1184. doi: 10.1016/j.immuni.2015.06.002
- Goleva, E., Jackson, L. P., Harris, J. K., Robertson, C. E., Sutherland, E. R., Hall, C. F., et al. (2013). The effects of airway microbiome on corticosteroid responsiveness in asthma. *Am. J. Respir. Crit. Care Med.* 188, 1193–1201. doi: 10.1164/rccm.201304-0775oc
- Grayson, P. C., and Kaplan, M. J. (2016). At the Bench: neutrophil extracellular traps (NETs) highlight novel aspects of innate immune system involvement in autoimmune diseases. *J. Leukoc. Biol.* 99, 253–264. doi: 10.1189/jlb.5bt0615-247r
- Gregersen, P. K., Silver, J., and Winchester, R. J. (1987). The shared epitope hypothesis. An approach to understanding the molecular genetics of susceptibility to rheumatoid arthritis. *Arthritis Rheum.* 30, 1205–1213. doi: 10.1002/art.1780301102
- Guerreiro, C. S., Calado, A., Sousa, J., and Fonseca, J. E. (2018). Diet, microbiota, and gut permeability—the unknown triad in rheumatoid arthritis. *Front. Med.* 5:349. doi: 10.3389/fmed.2018.00349
- Gully, N., Bright, R., Marino, V., Marchant, C., Cantley, M., Haynes, D., et al. (2014). *Porphyromonas gingivalis* peptidylarginine deiminase, a key contributor in the pathogenesis of experimental periodontal disease and experimental arthritis. *PLoS One* 9:e100838. doi: 10.1371/journal.pone.0100838
- Harrington, L. E., Hatton, R. D., Mangan, P. R., Turner, H., Murphy, T. L., Murphy, K. M., et al. (2005). Interleukin 17-producing CD4⁺ effector T cells develop via a lineage distinct from the T helper type 1 and 2 lineages. *Nat. Immunol.* 6, 1123–1132. doi: 10.1038/ni1254
- Hasan, N., and Yang, H. (2019). Factors affecting the composition of the gut microbiota, and its modulation. *PeerJ* 7:e7502. doi: 10.7717/peerj.7502
- Hillmann, B., Al-Ghalith, G. A., Shields-Cutler, R. R., Zhu, Q., Gohl, D. M., Beckman, K. B., et al. (2018). Evaluating the information content of shallow shotgun metagenomics. *mSystems* 3:e00069-18.
- Holland, S. M., Deleo, F. R., Elloumi, H. Z., Hsu, A. P., Uzel, G., Brodsky, N., et al. (2007). STAT3 mutations in the hyper-IgE syndrome. *N. Engl. J. Med.* 357, 1608–1619.
- Horta-Baas, G., Romero-Figueroa, M. D. S., Montiel-Jarquín, A. J., Pizano-Zárate, M. L., García-Mena, J., and Ramírez-Durán, N. (2017). Intestinal dysbiosis and rheumatoid arthritis: a link between gut microbiota and the pathogenesis of rheumatoid arthritis. *J. Immunol. Res.* 2017:4835189.
- Hooper, L. V., and Macpherson, A. J. (2010). Immune adaptations that maintain homeostasis with the intestinal microbiota. *Nat. Rev. Immunol.* 10, 159–169. doi: 10.1038/nri2710
- Huizinga, T. W., Amos, C. I., Van Der Helm-Van Mil, A. H., Chen, W., Van Gaalen, F. A., Jawaheer, D., et al. (2005). Refining the complex rheumatoid arthritis phenotype based on specificity of the HLA-DRB1 shared epitope for antibodies to citrullinated proteins. *Arthritis Rheum.* 52, 3433–3438. doi: 10.1002/art.21385
- Idris, A., Hasnain, S. Z., Huat, L. Z., and Koh, D. (2017). Human diseases, immunity and the oral microbiota—Insights gained from metagenomic studies. *Oral Sci. Int.* 14, 27–32. doi: 10.1016/s1348-8643(16)30024-6
- Inamo, J. (2019). Non-causal association of gut microbiome on the risk of rheumatoid arthritis: a Mendelian randomisation study. *Ann. Rheum. Dis.* doi: 10.1136/annrheumdis-2019-216565 [Epub ahead of print].
- Ivanov, I. T., Atarashi, K., Manel, N., Brodie, E. L., Shima, T., Karaoz, U., et al. (2009). Induction of intestinal Th17 cells by segmented filamentous bacteria. *Cell* 139, 485–498.
- Jeong, Y., Kim, J.-W., You, H. J., Park, S.-J., Lee, J., Ju, J. H., et al. (2019). Gut microbial composition and function are altered in patients with early rheumatoid arthritis. *J. Clin. Med.* 8:693. doi: 10.3390/jcm8050693
- Joshua, V., Chatzidionisyou, K., and Catrina, A. I. (2017). Role of the lung in individuals at risk of rheumatoid arthritis. *Best Pract. Res. Clin. Rheumatol.* 31, 31–41. doi: 10.1016/j.berh.2017.08.002
- Jubair, W. K., Hendrickson, J. D., Severs, E. L., Schulz, H. M., Adhikari, S., Ir, D., et al. (2018). Modulation of inflammatory arthritis in mice by gut microbiota through mucosal inflammation and autoantibody generation. *Arthritis Rheumatol.* 70, 1220–1233. doi: 10.1002/art.40490
- Kamada, N., Seo, S. U., Chen, G. Y., and Nunez, G. (2013). Role of the gut microbiota in immunity and inflammatory disease. *Nat. Rev. Immunol.* 13, 321–335. doi: 10.1038/nri3430
- Kaplan, M. J., and Radic, M. (2012). Neutrophil extracellular traps: double-edged swords of innate immunity. *J. Immunol.* 189, 2689–2695. doi: 10.4049/jimmunol.1201719
- Karlson, E. W., Lee, I. M., Cook, N. R., Manson, J. E., Buring, J. E., and Hennekens, C. H. (1999). A retrospective cohort study of cigarette smoking and risk of rheumatoid arthritis in female health professionals. *Arthritis Rheum.* 42, 910–917. doi: 10.1002/1529-0131(199905)42:5<910::aid-anr9>3.0.co;2-d
- Kasser, U. R., Gleissner, C., Dehne, F., Michel, A., Willershausen-Zonnchen, B., and Bolten, W. W. (1997). Risk for periodontal disease in patients with longstanding rheumatoid arthritis. *Arthritis Rheum.* 40, 2248–2251. doi: 10.1002/art.1780401221
- Kelly, B. J., Imai, I., Bittinger, K., Laughlin, A., Fuchs, B. D., Bushman, F. D., et al. (2016). Composition and dynamics of the respiratory tract microbiome in intubated patients. *Microbiome* 4:7.
- Khandpur, R., Carmona-Rivera, C., Vivekanandan-Giri, A., Gizinski, A., Yalavarthi, S., Knight, J. S., et al. (2013). NETs are a source of citrullinated autoantigens and stimulate inflammatory responses in rheumatoid arthritis. *Sci. Transl. Med.* 5:178ra40. doi: 10.1126/scitranslmed.3005580
- Kilgärd, O., Andersson, P., Malmsten, M., Nordin, S. L., Linde, H. M., Eliasson, M., et al. (2012). Peptidylarginine deiminases present in the airways during

- tobacco smoking and inflammation can citrullinate the host defense peptide LI-37, resulting in altered activities. *Am. J. Respir. Cell Mol. Biol.* 46, 240–248. doi: 10.1165/rcmb.2010-0500oc
- Kim, D. S., Kwon, J.-E., Lee, S. H., Kim, E. K., Ryu, J.-G., Jung, K.-A., et al. (2018). Attenuation of rheumatoid inflammation by sodium butyrate through reciprocal targeting of HDAC2 in osteoclasts and HDAC8 in T cells. *Front. Immunol.* 9:1525. doi: 10.3389/fimmu.2018.01525
- Kinloch, A., Tatzert, V., Wait, R., Peston, D., Lundberg, K., Donatien, P., et al. (2005). Identification of citrullinated alpha-enolase as a candidate autoantigen in rheumatoid arthritis. *Arthritis Res. Ther.* 7, R1421–R1429.
- Kishikawa, T., Maeda, Y., Nii, T., Motooka, D., Matsumoto, Y., Matsushita, M., et al. (2020). Metagenome-wide association study of gut microbiome revealed novel aetiology of rheumatoid arthritis in the Japanese population. *Ann. Rheum. Dis.* 79, 103–111. doi: 10.1136/annrheumdis-2019-215743
- Koch, R. (ed.). (2010). “Die ätiologie der milzbrand-krankheit, begründet auf die entwicklungsgeschichte des bacillus anthracis,” in *Klassische Texte der Wissenschaft*, (Berlin: Springer Spektrum).
- Kong, H. H., Oh, J., Deming, C., Conlan, S., Grice, E. A., Beatson, M. A., et al. (2012). Temporal shifts in the skin microbiome associated with disease flares and treatment in children with atopic dermatitis. *Genome Res.* 22, 850–859. doi: 10.1101/gr.131029.111
- König, M. F. (2020). The microbiome in autoimmune rheumatic disease. *Best Pract. Res. Clin. Rheumatol.* 34:101473. doi: 10.1016/j.berh.2019.101473
- König, M. F., Abusleme, L., Reinholdt, J., Palmer, R. J., Teles, R. P., Sampson, K., et al. (2016). Aggregatibacter actinomycetemcomitans-induced hypercitrullination links periodontal infection to autoimmunity in rheumatoid arthritis. *Sci. Transl. Med.* 8:369ra176. doi: 10.1126/scitranslmed.aaj1921
- Kumar, H., Kawai, T., and Akira, S. (2011). Pathogen recognition by the innate immune system. *Int. Rev. Immunol.* 30, 16–34. doi: 10.3109/08830185.2010.529976
- Kurowska, W., Kuca-Warnawin, E. H., Radzikowska, A., and Maslinski, W. (2017). The role of anti-citrullinated protein antibodies (Acpa) in the pathogenesis of rheumatoid arthritis. *Cent. Eur. J. Immunol.* 42, 390–398. doi: 10.5114/ceji.2017.72807
- Lederberg, J., and McCray, A. T. (2001). ‘Ome sweet ‘Omics—A genealogical treasury of words. *Scientist* 15:8. doi: 10.1089/clinomi.03.09.05
- Lee, J. Y., Mannaa, M., Kim, Y., Kim, J., Kim, G. T., and Seo, Y. S. (2019). Comparative analysis of fecal microbiota composition between rheumatoid arthritis and osteoarthritis patients. *Genes* 10:748. doi: 10.3390/genes10100748
- Lee, Y. H. (2020). Causal association of gut microbiome on the risk of rheumatoid arthritis: a Mendelian randomisation study. *Ann. Rheum. Dis.* doi: 10.1136/annrheumdis-2019-216747 [Epub ahead of print].
- Li, L., Michel, R., Cohen, J., Decarlo, A., and Kozarov, E. (2008). Intracellular survival and vascular cell-to-cell transmission of *Porphyromonas gingivalis*. *BMC Microbiol.* 8:26. doi: 10.1186/1471-2180-8-26
- Li, P., Li, M., Lindberg, M. R., Kennett, M. J., Xiong, N., and Wang, Y. (2010). PAD4 is essential for antibacterial innate immunity mediated by neutrophil extracellular traps. *J. Exp. Med.* 207, 1853–1862. doi: 10.1084/jem.20100239
- Li, S., Yu, Y., Yue, Y., Zhang, Z., and Su, K. (2013). Microbial infection and rheumatoid arthritis. *J. Clin. Cell. Immunol.* 4:174.
- Liu, X., Zhang, J., Zou, Q., Zhong, B., Wang, H., Mou, F., et al. (2016). *Lactobacillus salivarius* isolated from patients with rheumatoid arthritis suppresses collagen-induced arthritis and increases treg frequency in mice. *J. Interferon Cytokine Res.* 36, 706–712. doi: 10.1089/jir.2016.0057
- Liu, X., Zou, Q., Zeng, B., Fang, Y., and Wei, H. (2013). Analysis of fecal *Lactobacillus* community structure in patients with early rheumatoid arthritis. *Curr. Microbiol.* 67, 170–176. doi: 10.1007/s00284-013-0338-1
- Lood, C., Blanco, L. P., Purmalek, M. M., Carmona-Rivera, C., De Ravin, S. S., Smith, C. K., et al. (2016). Neutrophil extracellular traps enriched in oxidized mitochondrial DNA are interferogenic and contribute to lupus-like disease. *Nat. Med.* 22, 146–153. doi: 10.1038/nm.4027
- Luckey, T. D. (1972). Introduction to intestinal microecology. *Am. J. Clin. Nutr.* 25, 1292–1294. doi: 10.1093/ajcn/25.12.1292
- Lundberg, K., Kinloch, A., Fisher, B. A., Wegner, N., Wait, R., Charles, P., et al. (2008). Antibodies to citrullinated alpha-enolase peptide 1 are specific for rheumatoid arthritis and cross-react with bacterial enolase. *Arthritis Rheum.* 58, 3009–3019. doi: 10.1002/art.23936
- Maeda, Y., Kurakawa, T., Umamoto, E., Motooka, D., Ito, Y., Gotoh, K., et al. (2016). Dysbiosis contributes to arthritis development via activation of autoreactive T cells in the intestine. *Arthritis Rheumatol.* 68, 2646–2661. doi: 10.1002/art.39783
- Maharaj, B., Coovadia, Y., and Vayej, A. C. (2012). An investigation of the frequency of bacteraemia following dental extraction, tooth brushing and chewing. *Cardiovasc. J. Afr.* 23, 340–344. doi: 10.5830/cvja-2012-016
- Mankia, K., Cheng, Z., Do, T., Hunt, L., Meade, J., Kang, J., et al. (2019). Prevalence of periodontal disease and periodontopathic bacteria in anti-cyclic citrullinated protein antibody-positive at-risk adults without arthritis. *JAMA Netw. Open* 2:e195394. doi: 10.1001/jamanetworkopen.2019.5394
- Maresz, K. J., Hellvard, A., Sroka, A., Adamowicz, K., Bielecka, E., Koziel, J., et al. (2013). *Porphyromonas gingivalis* facilitates the development and progression of destructive arthritis through its unique bacterial peptidylarginine deiminase (PAD). *PLoS Pathog.* 9:e1003627. doi: 10.1371/journal.ppat.1003627
- Marotte, H., Farge, P., Gaudin, P., Alexandre, C., Mougin, B., and Miossec, P. (2006). The association between periodontal disease and joint destruction in rheumatoid arthritis extends the link between the HLA-DR shared epitope and severity of bone destruction. *Ann. Rheum. Dis.* 65, 905–909. doi: 10.1136/ard.2005.036913
- Marwaha, A. K., Leung, N. J., McMurchy, A. N., and Levings, M. K. (2012). TH17 cells in autoimmunity and immunodeficiency: protective or pathogenic? *Front. Immunol.* 3:129. doi: 10.3389/fimmu.2012.00129
- Mcgraw, W. T., Potempa, J., Farley, D., and Travis, J. (1999). Purification, characterization, and sequence analysis of a potential virulence factor from *Porphyromonas gingivalis*, peptidylarginine deiminase. *Infect. Immun.* 67, 3248–3256. doi: 10.1128/iai.67.7.3248-3256.1999
- Mercado, F. B., Marshall, R. I., Klestov, A. C., and Bartold, P. M. (2001). Relationship between rheumatoid arthritis and periodontitis. *J. Periodontol.* 72, 779–787.
- Mezouar, S., Chantran, Y., Michel, J., Fabre, A., Dubus, J.-C., Leone, M., et al. (2018). Microbiome and the immune system: from a healthy steady-state to allergy associated disruption. *Hum. Microb. J.* 10, 11–20. doi: 10.1016/j.humic.2018.10.001
- Mizuno, M., Noto, D., Kaga, N., Chiba, A., and Miyake, S. (2017). The dual role of short fatty acid chains in the pathogenesis of autoimmune disease models. *PLoS One* 12:e0173032. doi: 10.1371/journal.pone.0173032
- Moutsopoulos, N. M., Kling, H. M., Angelov, N., Jin, W., Palmer, R. J., Nares, S., et al. (2012). *Porphyromonas gingivalis* promotes Th17 inducing pathways in chronic periodontitis. *J. Autoimmun.* 39, 294–303. doi: 10.1016/j.jaut.2012.03.003
- Mowat, A. M. (2003). Anatomical basis of tolerance and immunity to intestinal antigens. *Nat. Rev. Immunol.* 3, 331–341. doi: 10.1038/nri1057
- Muñiz Pedrego, D. A., Chen, J., Hillmann, B., Jeraldo, P., Al-Ghalith, G., Taneja, V., et al. (2019). An increased abundance of clostridiaceae characterizes arthritis in inflammatory bowel disease and rheumatoid arthritis: a cross-sectional study. *Inflamm. Bowel Dis.* 25, 902–913. doi: 10.1093/ibd/izy318
- Nagra, N. S., Robinson, D. E., Douglas, I., Delmestri, A., Dakin, S. G., Snelling, S. J. B., et al. (2019). Antibiotic treatment and flares of rheumatoid arthritis: a self-controlled case series study analysis using CPRD GOLD. *Sci. Rep.* 9:8941.
- Nielen, M. M., Van Schaardenburg, D., Reesink, H. W., Van De Stadt, R. J., Van Der Horst-Bruinsma, I. E., De Koning, M. H., et al. (2004). Specific autoantibodies precede the symptoms of rheumatoid arthritis: a study of serial measurements in blood donors. *Arthritis Rheum.* 50, 380–386. doi: 10.1002/art.20018
- O’dwyer, D. N., Armstrong, M. E., Cooke, G., Dodd, J. D., Veale, D. J., and Donnelly, S. C. (2013). Rheumatoid arthritis (RA) associated interstitial lung disease (ILD). *Eur. J. Intern. Med.* 24, 597–603.
- Ogrendik, M. (2013). Antibiotics for the treatment of rheumatoid arthritis. *Int. J. Gen. Med.* 7, 43–47. doi: 10.2147/ijgm.s56957
- Ohkubo, T., Tsuda, M., Tamura, M., and Yamamura, M. (1990). Impaired superoxide production in peripheral blood neutrophils of germ-free rats. *Scand. J. Immunol.* 32, 727–729. doi: 10.1111/j.1365-3083.1990.tb03216.x
- Oppong, G. O., Rapsinski, G. J., Tursi, S. A., Biesecker, S. G., Klein-Szanto, A. J., Goulian, M., et al. (2015). Biofilm-associated bacterial amyloids dampen inflammation in the gut: oral treatment with curli fibres reduces the severity of hapten-induced colitis in mice. *NPJ Biofilms Microbiomes* 1:15019.
- Ortiz-Estrada, Á. M., Gollas-Galván, T., Martínez-Córdova, L. R., and Martínez-Porchas, M. (2019). Predictive functional profiles using metagenomic 16S rRNA

- data: a novel approach to understanding the microbial ecology of aquaculture systems. *Rev. Aquacult.* 11, 234–245. doi: 10.1111/raq.12237
- Padyukov, L., Silva, C., Stolt, P., Alfredsson, L., and Klareskog, L. (2004). A gene-environment interaction between smoking and shared epitope genes in HLA-DR provides a high risk of seropositive rheumatoid arthritis. *Arthritis Rheum.* 50, 3085–3092. doi: 10.1002/art.20553
- Pancholi, V., and Fischetti, V. A. (1998). alpha-enolase, a novel strong plasmin(ogen) binding protein on the surface of pathogenic streptococci. *J. Biol. Chem.* 273, 14503–14515. doi: 10.1074/jbc.273.23.14503
- Pfeifle, R., Rothe, T., Ipseiz, N., Scherer, H. U., Culemann, S., Harre, U., et al. (2017). Regulation of autoantibody activity by the IL-23-T(H)17 axis determines the onset of autoimmune disease. *Nat. Immunol.* 18, 104–113. doi: 10.1038/ni.3579
- Picchianti-Diamanti, A., Panebianco, C., Salemi, S., Sorgi, M. L., Di Rosa, R., Tropea, A., et al. (2018). Analysis of gut microbiota in rheumatoid arthritis patients: disease-related dysbiosis and modifications induced by etanercept. *Int. J. Mol. Sci.* 19:2938. doi: 10.3390/ijms19102938
- Pischon, N., Pischon, T., Kroger, J., Gulmez, E., Kleber, B. M., Bernimoulin, J. P., et al. (2008). Association among rheumatoid arthritis, oral hygiene, and periodontitis. *J. Periodontol.* 79, 979–986. doi: 10.1902/jop.2008.070501
- Rakieh, C., Nam, J. L., Hunt, L., Hensor, E. M., Das, S., Bissell, L. A., et al. (2015). Predicting the development of clinical arthritis in anti-CCP positive individuals with non-specific musculoskeletal symptoms: a prospective observational cohort study. *Ann. Rheum. Dis.* 74, 1659–1666. doi: 10.1136/annrheumdis-2014-205227
- Rapsinski, G. J., Wynosky-Dolfi, M. A., Oppong, G. O., Tursi, S. A., Wilson, R. P., Brodsky, I. E., et al. (2015). Toll-like receptor 2 and NLRP3 cooperate to recognize a functional bacterial amyloid, curli. *Infect. Immun.* 83, 693–701. doi: 10.1128/iai.02370-14
- Raychaudhuri, S., Sandor, C., Stahl, E. A., Freudenberg, J., Lee, H. S., Jia, X., et al. (2012). Five amino acids in three HLA proteins explain most of the association between MHC and seropositive rheumatoid arthritis. *Nat. Genet.* 44, 291–296. doi: 10.1038/ng.1076
- Rodrigues, G. S. P., Cayres, L. C. F., Gonçalves, F. P., Takaoka, N. N. C., Lengert, A. H., Tansini, A., et al. (2019). Detection of increased relative expression units of *Bacteroides* and *Prevotella*, and decreased *Clostridium leptum* in stool samples from Brazilian rheumatoid arthritis patients: a pilot study. *Microorganisms* 7:413. doi: 10.3390/microorganisms7100413
- Rogier, R., Evans-Marin, H., Manasson, J., Van Der Kraan, P. M., Walgreen, B., Helsen, M. M., et al. (2017). Alteration of the intestinal microbiome characterizes preclinical inflammatory arthritis in mice and its modulation attenuates established arthritis. *Sci. Rep.* 7:15613.
- Rosenbaum, J. T., and Asquith, M. J. (2016). The microbiome: a revolution in treatment for rheumatic diseases? *Curr. Rheumatol. Rep.* 18:62.
- Rothschild, D., Weissbrod, O., Barkan, E., Kurilshikov, A., Korem, T., Zeevi, D., et al. (2018). Environment dominates over host genetics in shaping human gut microbiota. *Nature* 555, 210–215.
- Round, J. L., Lee, S. M., Li, J., Tran, G., Jabri, B., Chatila, T. A., et al. (2011). The Toll-like receptor 2 pathway establishes colonization by a commensal of the human microbiota. *Science* 332, 974–977. doi: 10.1126/science.1206095
- Round, J. L., and Palm, N. W. (2018). Causal effects of the microbiota on immune-mediated diseases. *Sci. Immunol.* 3:eaa01603. doi: 10.1126/sciimmunol.aa01603
- Sakaguchi, N., Takahashi, T., Hata, H., Nomura, T., Tagami, T., Yamazaki, S., et al. (2003). Altered thymic T-cell selection due to a mutation of the Zap-70 gene causes autoimmune arthritis in mice. *Nature* 426, 454–460. doi: 10.1038/nature02119
- Sandal, I., Karydis, A., Luo, J., Prislowsky, A., Whittington, K. B., Rosloniec, E. F., et al. (2016). Bone loss and aggravated autoimmune arthritis in Hla-Drβ1-bearing humanized mice following oral challenge with *Porphyromonas gingivalis*. *Arthritis Res. Ther.* 18:249.
- Sandberg, M. E. C., Bengtsson, C., Klareskog, L., Alfredsson, L., and Saevarsdottir, S. (2015). Recent infections are associated with decreased risk of rheumatoid arthritis: a population-based case-control study. *Ann. Rheum. Dis.* 74, 904–907. doi: 10.1136/annrheumdis-2014-206493
- Sato, K., Suematsu, A., Okamoto, K., Yamaguchi, A., Morishita, Y., Kadono, Y., et al. (2006). Th17 functions as an osteoclastogenic helper T cell subset that links T cell activation and bone destruction. *J. Exp. Med.* 203, 2673–2682. doi: 10.1084/jem.20061775
- Sato, K., Takahashi, N., Kato, T., Matsuda, Y., Yokoji, M., Yamada, M., et al. (2017). Aggravation of collagen-induced arthritis by orally administered *Porphyromonas gingivalis* through modulation of the gut microbiota and gut immune system. *Sci. Rep.* 7:6955.
- Scher, J. U., Joshua, V., Artacho, A., Abdollahi-Roodsaz, S., Öckinger, J., Kullberg, S., et al. (2016). The lung microbiota in early rheumatoid arthritis and autoimmunity. *Microbiome* 4:60.
- Scher, J. U., Sczesnak, A., Longman, R. S., Segata, N., Ubeda, C., Bielski, C., et al. (2013). Expansion of intestinal *Prevotella copri* correlates with enhanced susceptibility to arthritis. *eLife* 2:e01202.
- Scher, J. U., Ubeda, C., Equinda, M., Khanin, R., Buischi, Y., Viale, A., et al. (2012). Periodontal disease and the oral microbiota in new-onset rheumatoid arthritis. *Arthritis Rheum.* 64, 3083–3094. doi: 10.1002/art.34539
- Schlafer, S., Meyer, R. L., Dige, I., and Regina, V. R. (2017). Extracellular DNA contributes to dental biofilm stability. *Caries Res.* 51, 436–442. doi: 10.1159/000477447
- Schmidt, T. S., Hayward, M. R., Coelho, L. P., Li, S. S., Costea, P. I., Voigt, A. Y., et al. (2019). Extensive transmission of microbes along the gastrointestinal tract. *eLife* 8:e42693.
- Sekula, P., Del Greco, M. F., Pattaro, C., and Köttgen, A. (2016). Mendelian randomization as an approach to assess causality using observational data. *J. Am. Soc. Nephrol.* 27, 3253–3265. doi: 10.1681/asn.2016010098
- Sender, R., Fuchs, S., and Milo, R. (2016). Are we really vastly outnumbered? Revisiting the ratio of bacterial to host cells in humans. *Cell* 164, 337–340. doi: 10.1016/j.cell.2016.01.013
- Sharma, S., and Tripathi, P. (2019). Gut microbiome and type 2 diabetes: where we are and where to go? *J. Nutr. Biochem.* 63, 101–108. doi: 10.1016/j.jnutbio.2018.10.003
- Shaw, M., Collins, B. F., Ho, L. A., and Raghu, G. (2015). Rheumatoid arthritis-associated lung disease. *Eur. Respir. Rev.* 24, 1–16.
- Smith, P. D., Janoff, E. N., Mosteller-Barnum, M., Merger, M., Orenstein, J. M., Kearney, J. F., et al. (1997). Isolation and purification of CD14-negative mucosal macrophages from normal human small intestine. *J. Immunol. Methods* 202, 1–11. doi: 10.1016/s0022-1759(96)00204-9
- Smith, P. D., Smythies, L. E., Mosteller-Barnum, M., Sibley, D. A., Russell, M. W., Merger, M., et al. (2001). Intestinal macrophages lack CD14 and CD89 and consequently are down-regulated for LPS- and IgA-mediated activities. *J. Immunol.* 167, 2651–2656. doi: 10.4049/jimmunol.167.5.2651
- Stahl, E. A., Raychaudhuri, S., Remmers, E. F., Xie, G., Eyre, S., Thomson, B. P., et al. (2010). Genome-wide association study meta-analysis identifies seven new rheumatoid arthritis risk loci. *Nat. Genet.* 42, 508–514.
- Staley, C., Kaiser, T., Beura, L. K., Hamilton, M. J., Weingarden, A. R., Bobr, A., et al. (2017). Stable engraftment of human microbiota into mice with a single oral gavage following antibiotic conditioning. *Microbiome* 5:87.
- Sugiyama, D., Nishimura, K., Tamaki, K., Tsuji, G., Nakazawa, T., Morinobu, A., et al. (2010). Impact of smoking as a risk factor for developing rheumatoid arthritis: a meta-analysis of observational studies. *Ann. Rheum. Dis.* 69, 70–81. doi: 10.1136/ard.2008.096487
- Taurog, J. D., Richardson, J. A., Croft, J. T., Simmons, W. A., Zhou, M., Fernandez-Sueiro, J. L., et al. (1994). The germfree state prevents development of gut and joint inflammatory disease in HLA-B27 transgenic rats. *J. Exp. Med.* 180, 2359–2364. doi: 10.1084/jem.180.6.2359
- Thompson, C. L., Vier, R., Mikaelyan, A., Wienemann, T., and Brune, A. (2012). 'Candidatus Arthromitus' revised: segmented filamentous bacteria in arthropod guts are members of Lachnospiraceae. *Environ. Microbiol.* 14, 1454–1465. doi: 10.1111/j.1462-2920.2012.02731.x
- Tilg, H., and Moschen, A. R. (2014). Microbiota and diabetes: an evolving relationship. *Gut* 63, 1513–1521. doi: 10.1136/gutjnl-2014-306928
- Tomasello, G., Zeenny, M. N., Giammanco, M., Di Majo, D., and Traina, G. (2015). Intestinal microbiota mutualism and gastrointestinal diseases. *Euromediterranean Biomed. J.* 10:10.
- Tong, Y., Zhao, Y., Lui, Y., and Luo, Y. (2020). *OP0016 Gut Microbiota Dysbiosis in the High-Risk Individual for RA Triggers the Mucosal Immunity Perturbation and Promotes Rheumatoid Arthritis Development*. Basel: European League Against Rheumatism.

- Totaro, M. C., Cattani, P., Ria, F., Tolusso, B., Gremese, E., Fedele, A. L., et al. (2013). *Porphyromonas gingivalis* and the pathogenesis of rheumatoid arthritis: analysis of various compartments including the synovial tissue. *Arthritis Res. Ther.* 15:R66.
- Tralongo, P., Tomasello, G., Sinagra, E., Damiani, P., Leone, A., Palumbo, V. D., et al. (2014). The role of butyric acid as a protective agent against inflammatory bowel diseases. *Euromediterranean Biomed. J.* 9:11.
- Tsukasaki, M., Komatsu, N., Nagashima, K., Nitta, T., Pluemsakunthai, W., Shukunami, C., et al. (2018). Host defense against oral microbiota by bone-damaging T cells. *Nat. Commun.* 9:701.
- Turnbaugh, P. J., Ley, R. E., Hamady, M., Fraser-Liggett, C. M., Knight, R., and Gordon, J. I. (2007). The human microbiome project. *Nature* 449, 804–810.
- Vahtovuo, J., Munukka, E., Korkeamäki, M., Luukkainen, R., and Toivanen, P. (2008). Fecal microbiota in early rheumatoid arthritis. *J. Rheumatol.* 35, 1500–1505.
- Van De Sande, M. G., De Hair, M. J., Van Der Leij, C., Klarenbeek, P. L., Bos, W. H., Smith, M. D., et al. (2011). Different stages of rheumatoid arthritis: features of the synovium in the preclinical phase. *Ann. Rheum. Dis.* 70, 772–777. doi: 10.1136/ard.2010.139527
- Van De Stadt, L. A., Witte, B. I., Bos, W. H., and Van Schaardenburg, D. (2013). A prediction rule for the development of arthritis in seropositive arthralgia patients. *Ann. Rheum. Dis.* 72, 1920–1926. doi: 10.1136/annrheumdis-2012-202127
- Wang, Y., Li, M., Stadler, S., Correll, S., Li, P., Wang, D., et al. (2009). Histone hypercitrullination mediates chromatin decondensation and neutrophil extracellular trap formation. *J. Cell Biol.* 184, 205–213. doi: 10.1083/jcb.200806072
- Wegner, N., Lundberg, K., Kinloch, A., Fisher, B., Malmstrom, V., Feldmann, M., et al. (2010). Autoimmunity to specific citrullinated proteins gives the first clues to the etiology of rheumatoid arthritis. *Immunol. Rev.* 233, 34–54. doi: 10.1111/j.0105-2896.2009.00850.x
- Wells, P. M., Adebayo, A. S., Bowyer, R. C. E., Freidin, M. B., Finckh, A., Strowig, T., et al. (2020). Associations between gut microbiota and genetic risk for rheumatoid arthritis in the absence of disease: a cross-sectional study. *Lancet Rheumatol.* 2, e418–e427.
- Wells, P. M., Williams, F. M. K., Matey-Hernandez, M. L., Menni, C., and Steves, C. J. (2019). 'ra and the microbiome: do host genetic factors provide the link? *J. Autoimmun.* 99, 104–115. doi: 10.1016/j.jaut.2019.02.004
- Willis, V. C., Demoruelle, M. K., Derber, L. A., Chartier-Logan, C. J., Parish, M. C., Pedraza, I. F., et al. (2013). Sputum autoantibodies in patients with established rheumatoid arthritis and subjects at risk of future clinically apparent disease. *Arthritis Rheum.* 65, 2545–2554.
- Wu, H. J., Ivanov, I. I., Darce, J., Hattori, K., Shima, T., Umesaki, Y., et al. (2010). Gut-residing segmented filamentous bacteria drive autoimmune arthritis via T helper 17 cells. *Immunity* 32, 815–827. doi: 10.1016/j.immuni.2010.06.001
- Wu, R.-Q., Zhang, D.-F., Tu, E., Chen, Q.-M., and Chen, W. (2014). The mucosal immune system in the oral cavity—an orchestra of T cell diversity. *Int. J. Oral Sci.* 6, 125–132. doi: 10.1038/ijos.2014.48
- Zhang, L., Bahl, M. I., Roager, H. M., Fonvig, C. E., Hellgren, L. I., Frandsen, H. L., et al. (2017). Environmental spread of microbes impacts the development of metabolic phenotypes in mice transplanted with microbial communities from humans. *ISME J.* 11, 676–690. doi: 10.1038/ismej.2016.151
- Zhang, X., Zhang, D., Jia, H., Feng, Q., Wang, D., Liang, D., et al. (2015). The oral and gut microbiomes are perturbed in rheumatoid arthritis and partly normalized after treatment. *Nat. Med.* 21, 895–905. doi: 10.1038/nm.3914
- Zhernakova, A., Kurilshikov, A., Bonder, M. J., Tigchelaar, E. F., Schirmer, M., Vatanen, T., et al. (2016). Population-based metagenomics analysis reveals markers for gut microbiome composition and diversity. *Science* 352, 565–569. doi: 10.1126/science.aad3369

Conflict of Interest: PE has provided expert advice for Abbvie, Pfizer, Amgen, Schering-Plough, Roche, BMS, Novartis, Lilly, Gilead, and Genentech.

The remaining authors declare that the research was conducted in the absence of any commercial or financial relationships that could be construed as a potential conflict of interest.

Copyright © 2020 Rooney, Mankia and Emery. This is an open-access article distributed under the terms of the Creative Commons Attribution License (CC BY). The use, distribution or reproduction in other forums is permitted, provided the original author(s) and the copyright owner(s) are credited and that the original publication in this journal is cited, in accordance with accepted academic practice. No use, distribution or reproduction is permitted which does not comply with these terms.



Recent Advances in Pathophysiology, Drug Development and Future Perspectives of SARS-CoV-2

Desh Deepak Singh¹, Ihn Han², Eun-Ha Choi^{2*} and Dharmendra K. Yadav^{3*}

¹ Amity Institute of Biotechnology, Amity University Rajasthan, Jaipur, India, ² Plasma Bioscience Research Center, Applied Plasma Medicine Center, Department of Electrical and Biological Physics, Kwangwoon University, Seoul, South Korea,

³ College of Pharmacy, Gachon University of Medicine and Science, Incheon, South Korea

OPEN ACCESS

Edited by:

Claudia Fiorillo,
University of Florence, Italy

Reviewed by:

Raman Chandrasekar,
Kansas State University, United States

Sunil Kumar,
Sungkyunkwan University,
South Korea

Ravi Mani Tripathi,
Amity University, India

*Correspondence:

Dharmendra K. Yadav
dharmendra30oct@gmail.com

Eun-Ha Choi
choipdp@gmail.com

Specialty section:

This article was submitted to
Molecular Medicine,
a section of the journal
Frontiers in Cell and Developmental
Biology

Received: 05 July 2020

Accepted: 22 September 2020

Published: 06 November 2020

Citation:

Singh DD, Han I, Choi E-H and
Yadav DK (2020) Recent Advances
in Pathophysiology, Drug
Development and Future Perspectives
of SARS-CoV-2.
Front. Cell Dev. Biol. 8:580202.
doi: 10.3389/fcell.2020.580202

The coronavirus (SARS-CoV-2) pandemic is a rapidly transmitting and highly pathogenic disease. The spike protein of SARS-CoV-2 binds to the surface of angiotensin-converting enzyme-2 (ACE2) receptors along the upper respiratory tract and intestinal epithelial cells. SARS-CoV-2 patients develop acute respiratory distress, lymphocytic myocarditis, disseminated intravascular coagulation, lymphocytic infiltration, and other serious complications. A SARS-CoV-2 diagnosis is conducted using quantitative reverse-transcription PCR and computed tomography (CT) imaging. In addition, IgM or IgG antibodies are used to identify acute and convalescent illness. Recent clinical data have been generated by health workers and researchers and have shown that there is an urgent requirement in the effective clinical and treatment of patients, as well as other developments for dealing with SARS-CoV-2 infection. A broad spectrum of clinical trials of different vaccines and drug treatment has been evaluated for use against SARS-CoV-2. This review includes the emergence of SARS-CoV-2 pneumonia as a way to recognize and eliminate any barriers that affect rapid patient care and public health management against the SARS-CoV-2 epidemic based on the natural history of the disease, its transmission, pathogenesis, immune response, epidemiology, diagnosis, clinical presentation, possible treatment, drug and vaccine development, prevention, and future perspective.

Keywords: SARS-CoV-2, pneumonia, pathophysiology, immune response, epidemiology, drug discovery

INTRODUCTION

Coronaviruses are a group of large viruses with positive SS RNA, 160 nm in size, and belonging to the Nidovirales family (Schoeman and Fielding, 2019). The genome size of the SARS-CoV-2 virus is approximately 30 KB. The virion of SARS-CoV-2 is made up of genomic RNA with a structural protein, i.e., nucleocapsid (N) phosphoprotein, which encloses the nucleic acid, a glycoprotein membrane (M) embedded in the lipid bilayer, a spike glycoprotein (S) with petal-shaped peplomers and a small enveloped (E) protein and a polyadenylated tail, followed by 3' ends (McBride et al., 2014; Schoeman and Fielding, 2019). Two-thirds of the SARS-CoV-2 genome made up of a polyprotein (pp1a and pp1b), which is produced after the cleavage of the cysteine protease (PLpro)

and 3C-like serine protease (3CLpro), the resultant non-structured protein, and RNA-dependent RNA polymerase and helicase are synthesized (Narayanan et al., 2015). Six genera of Coronavirus have been discovered, namely, alpha corona, beta, gamma, delta, bafinivirus, and torovirus. Human coronavirus (HCoV) belongs to the alpha and beta coronaviruses, genera 229 E and NL63 belong to the alpha coronavirus, and OC43 and HKU1 belong to the beta coronavirus (**Figures 1, 2**; Owusu et al., 2014). The main hosts and reservoir of these viruses are infected birds and mammals. Being hosts to the largest number of viral genotypes, bats have also become host to large numbers of coronaviruses, and their immune systems can suppress such viruses (Khan, 2013). However, they can transmit these viruses to birds and other mammals. Epidemics of coronaviruses generally occur when the virus transmits from one species to another, as shown in **Figures 1, 2**, which takes place when the viruses acquire mutations in proteins that allow them to bind to the cells of other animals and more easily infect the other cells in the new host. Human coronaviruses are causes of respiratory and gastrointestinal tract infections (Lau et al., 2010). Such viruses have been estimated to account for 5–10% of all adult upper respiratory tract infections such as the common cold, pneumonia, and acute respiratory distress syndrome (ARDS), and causing gastrointestinal infection (Ge et al., 2013; Khan, 2013). There are a wide variety of symptoms of coronavirus infection. Usually, mutations occur when a virus transfers from one species to another, and entirely new coronaviruses can develop through such mutations. Several outbreaks of new coronaviruses (Smith, 2006), the first being severing acute respiratory syndrome (SARS), occurred in 2002 to 2003, which was reported to have been a beta coronavirus from Guangdong province in China (Chan et al., 2003). There are different lineages of beta coronaviruses within SARS lineage B, and this particular virus has previously been transmitted from bats to civets to humans in an outbreak recorded from February to July 2003. In this outbreak, there were more than 8000 total recorded cases and 774 deaths with a fatality rate of 9.6% (Chan-Yeung and Xu, 2003). Another coronavirus outbreak of Middle East Respiratory Syndrome (MERS) occurred in 2012, as shown in **Figures 1, 2** (Zaki et al., 2012), which reportedly began in Saudi Arabia and spread to several other countries. This was also a beta coronavirus and was transmitted from camels to humans (Lau et al., 2013) either by eating camels or drinking camel milk. More than 2400 cases and 858 deaths were recorded with a fatality rate of approximately 34.4%. The new coronavirus, 2019-nCoV (SARS-CoV-2) discovered in Wuhan, Hubei province of China in December 2019, the seventh coronavirus found to cause illness in humans. It is also a novel beta coronavirus and has many similarities with SARS (Chen N. et al., 2020; Huang C. et al., 2020). SARS-CoV-2 was first identified through a cluster of pneumonia cases in Wuhan, China On December 31, 2019, an infectious disease with a cluster of cases of pneumonia occurred in Wuhan, China, which was later identified as novel SARS-CoV-2 (Bernard Stoecklin et al., 2020). By January 31, 2020, 7818 cases had been confirmed in 19 countries, and on May 18, 2020, the WHO declared a coronavirus outbreak as a public health emergency, with 10500,639 cases, 510,736 deaths, and 5,727,094

recovered cases recorded in more than 200 countries. The virus is officially named SARS-CoV-2 because it is genetically extremely like SARS coronavirus, which was responsible for the outbreak in 2002 (Chen and Yu, 2020). It is believed that SARS-CoV-2 was transmitted from a bat to a Pangolin and finally to a human (**Figure 2**). A coronavirus found in a Pangolin showed a 96% genetic match with SARS-CoV-2. The spike protein of the coronavirus allows it to attach to the lining of the respiratory tract and damage the ciliated epithelial cells of the nasopharynx leading to viremia (Xu H. et al., 2020). Severe lung damage can cause ARDS and aseptic shock, which are the main causes of death for people infected and are more likely to occur in those over the age of 60, in smokers, and in people with previous medical conditions such as diabetes, Chronic Obstructive Pulmonary Disease (COPD), Cardiovascular Diseases (CVDs), hepatitis, hypertension, or pregnancy (**Figure 3**; Matthay et al., 2019). During this pandemic, one of the main concerns is the treatment options available. At present, we do not have any drugs approved for SARS-CoV-2 by the FDA, although there are certain drugs used by clinicians for patients with SARS-CoV-2 infection (Adnan, 2020), including redeliver, chloroquine, hydroxychloroquine, lopinavir, ritonavir, and tocilizumab (Abd El-Aziz and Stockand, 2020). None of these drugs are currently used as a prophylactic against SARS-CoV-2 but are administered after infection. It has been observed that chloroquine and hydroxychloroquine, which are antimalarial drugs, are more effective against SARS-CoV-2 (Kruse, 2020). Tocilizumab is most widely used by clinicians, and its IL-6 inhibitors lead to a reduction in cytokines and an acute phase retract. This drug is still under clinical trial for SARS-CoV-2 pneumonia. Lopinavir and ritonavir are two other drugs that have been used despite their limitations. Initially, they were used for HIV infection, and have shown to be active against SARS-CoV-2 in animal studies (Zhao, 2020). All these drugs are used by clinicians based on their severity, clinical complications, and special consent or ethical approval of the competent authority. Previous reviews on COVID-19 have been based on information regarding a specific problem. Limited reviews are available regarding the recent developments of SARS-CoV-2 pneumonia for recognizing and eliminating any barriers that affect the rapid patent care and public health management against the SARS-CoV-2 epidemic. This review aims to discuss recent advances in SARS-CoV-2 in terms of pathophysiology, epidemiology, clinical management, drug discovery, vaccine development, and prospects. This review includes the emergence of SARS-CoV-2, the natural history of the disease, and its transmission, pathogenesis, epidemiology, diagnosis, clinical presentation, possible treatment, drug and vaccine development, and prospects.

PATHOPHYSIOLOGY

SARS-CoV-2 is inhaled through respiratory droplets ($>5 \mu\text{m}$) in the air at up to $<1 \text{ m}$ (less than 3.3 feet) and within close contact (6 feet, or 1.8 m) (Cui et al., 2020). The virus is also inhaled by touching an object or surface with a virus present from an infected person, and then touching the mouth, nose,

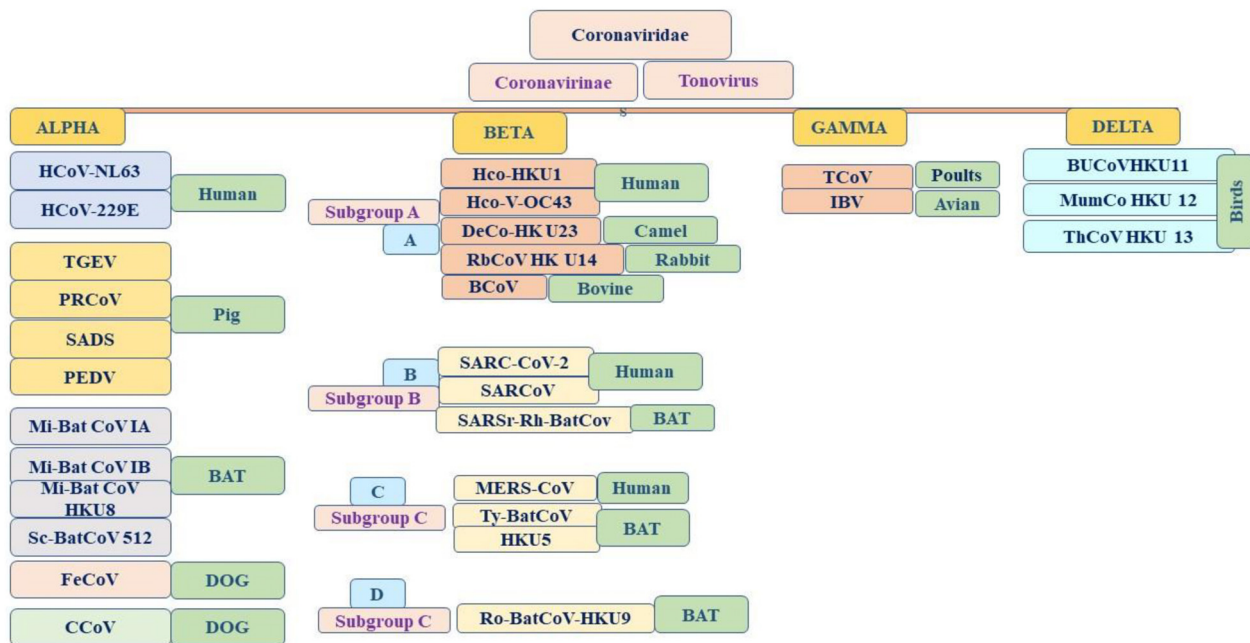


FIGURE 1 | Emergence and taxonomy of coronavirus.

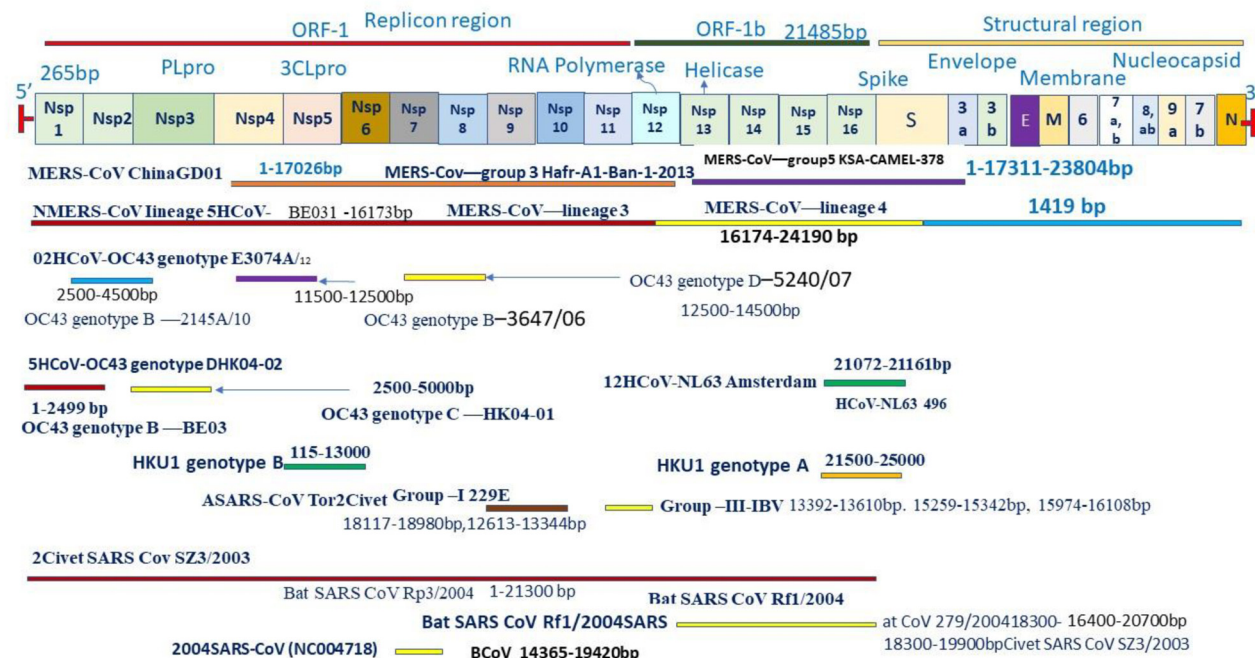


FIGURE 2 | Genome and genetic shift at genomic site coronavirus with zoonotic origin.

or eyes (Figure 4). SARS-CoV-2 causes ARDS and invades two types of cells in the lungs, namely, mucus-producing (Goblet) cells and ciliated cells, allowing it to reproduce (Singhal, 2020). Mucus keeps the lungs from drying out and protects them from pathogens. Cilia pushes the mucus toward the exterior of the

body, clearing debris from the lungs including viruses. Killer cells are the preferred host cells for SARS-CoV and are likely the preferred host cells for SARS-CoV-2 (Figure 3; Chen W. H. et al., 2020; Wang F. et al., 2020). Once a structural protein enters a cell, the genetic, viral material is copied. The invading

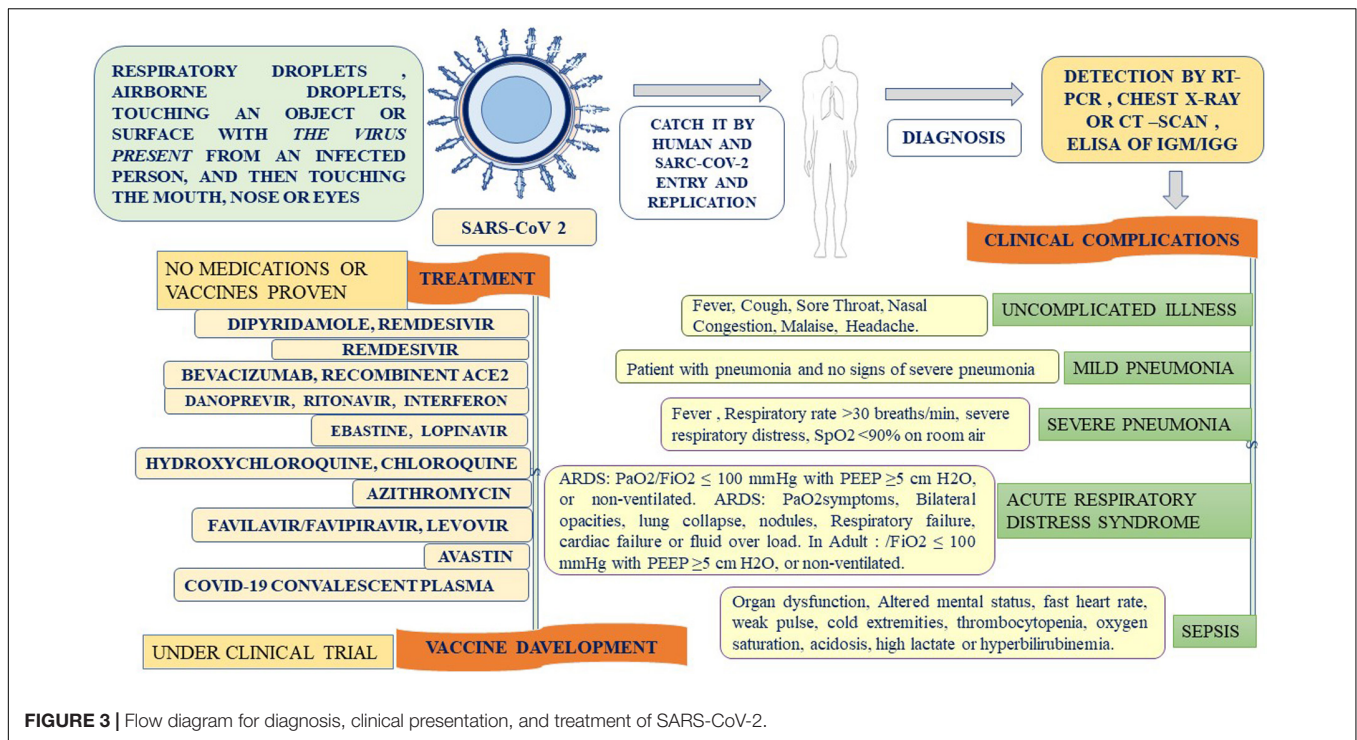


FIGURE 3 | Flow diagram for diagnosis, clinical presentation, and treatment of SARS-CoV-2.

virus blocks the synthesis of this viral genetic material. The invading virus blocks the synthesis of this viral genetic material (Tian et al., 2020). The virus enters the cell through fusion and endocytosis. The virus is partially decomposed and becomes insensitive to the neutralizing antibodies of the host (Belouzard et al., 2012). The host cell receptors, consider the virus to be a normal legend, leading to a receptor aggregation of the virus and the entry of the virus through the endocytosis process (Baig et al., 2020). Virus uncoating occurs inside the cytoplasm along with the release RNA inside the host cells, forming a polyprotein complex (Tian et al., 2020). These polyproteins are cleaved under the action of the protease into the RNA polymerase (Letko et al., 2020). Antigenomic RNA is transcribed from genomic RNA. The hallmark of coronavirus transcription is the production of multiple sub-genomic mRNAs, and during the replication process, two intermediates are formed: First, an intermediate genome forms an antigen and creates a new genome complex (Baig et al., 2020). RNA polymerase acts as an anti-genomic RNA to generate a positive genome strand and the m-RNA. Next, m-RNA acts on the rough endoplasmic reticulum of the host cells to produce a new viral genome (Baig et al., 2020; Letko et al., 2020). Common symptoms of SARS-CoV-2 include fever (>37.3°C), which may not be present in some cases, shortness of breath, coughing, sore throat, insomnia and/or ageusia, muscles ache, nausea/or vomiting, abdominal pain, headache, runny nose, and fatigue (Figure 3; Huang C. et al., 2020). Frequent symptoms at illness onset include fever (83–98%), dry cough (76–82%), and myalgia or fatigue (11–44%), and the incubation period varies from 5 to 14 days. Besides, 14% of patients were observed as having severe symptoms, and 5% were found to be critically ill (Zhou et al., 2020). According to the WHO,

SARS-CoV-2 cases are steadily increasing throughout the world. Early reports suggested that illness severity is associated with age (>60 years old) and comorbidity (Liu B. et al., 2020). Clinical investigations of patients with SARS-CoV-2 have been based on early detection, identification, isolation, and employment of immediate prevention and control with supportive care of the patient through the management of ARDS and hypoxemic conditions with septic shock (Jiang et al., 2020). Special and urgent care is required for pregnant women. Patients are categorized into those with an uncomplicated illness, mild pneumonia, severe pneumonia, ARDS, sepsis, and septic shock (Du et al., 2020). When mucus-producing (goblet) cells and ciliated cells die owing to a collection of new SARS-CoV-2 material, they slough off into the airways, filling them with debris and fluid. Many of those infected experience pneumonia in both lungs (Li et al., 2020). The virus enters the immune system, and the immune cells recognize the virus flooding into the lungs (Jiang et al., 2020). The lung tissues then become inflamed during the normal immune response. The inflammatory process is highly regulated and is confined to the infected area (Liu H. et al., 2020). However, occasionally the immune system overreacts, resulting in damage to the healthy tissues. More cells then die and slough off, further clogging the lungs and worsening pneumonia (Feng Y. et al., 2020). As damage to the lungs increases, stage three begins, potentially resulting in respiratory failure, permanent lung damage, or death. Here, we can see the same lessons with SARS-CoV-2 as with SARS (Cowling and Leung, 2020). SARS create holes in the lungs, which have a honeycomb appearance. This is probably due to an over-reactive immune response, which affects healthy and infected tissue and generates scars that stiffen the lungs (Tan K.S. et al., 2020). Some

patients with this condition may require ventilators to aid in breathing (Chen W. H. et al., 2020). The inflammation also results in alveoli that are more permeable. Alveoli are interfaces of gas exchange, where the lung replaces CO₂ in the blood with fresh oxygen. The increased permeability causes fluid to leak into the lungs (Raoult et al., 2020; Zhou et al., 2020). This decreases the ability of the lungs to oxygenate the blood and in severe cases floods the lungs with fluid, preventing the patient from breathing properly and sometimes resulting in death (Zhang H.-T. et al., 2020). Venous thromboembolism is reduced using mechanical or pharmacological prophylaxis, and catheter-related bloodstream infections are removed by maintaining sterile and aseptic conditions, as well as the removal of the catheters daily (Goossens, 2015). Aseptic shock is the main cause of death for people with this infection and is more likely to occur in those over the age of 60, smokers, and people with previous medical conditions. Individuals with diabetes, cardiovascular disease, heart disease, hypertension, respiratory disease, pregnancy, or an immunocompromised state are high risk for clinical complications and mortality (Figure 3; Liu K. et al., 2020). An overreaction of the immune system causes another type of damage, namely, cytokines recruiting immune cells at the site of infection. Overproduction of cytokines can result in a cytokine storm and cause large-scale inflammation in the whole body of the patient (Puja et al., 2020). Therefore, blood vessels become more permeable and fluid seeps out. This situation makes it difficult for blood and oxygen to reach the patient's body. As a result, multi-organ failure occurs in more severe cases of SARS-CoV-2.

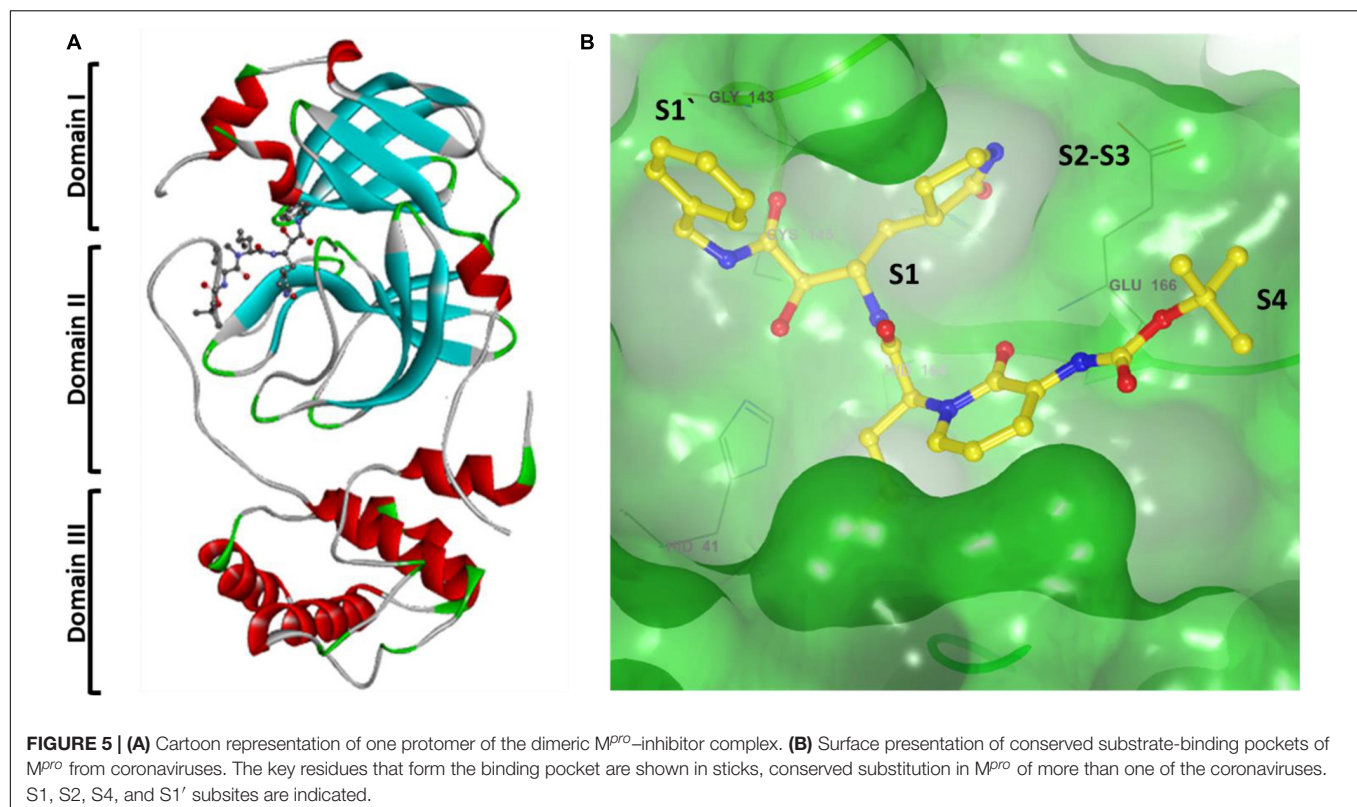
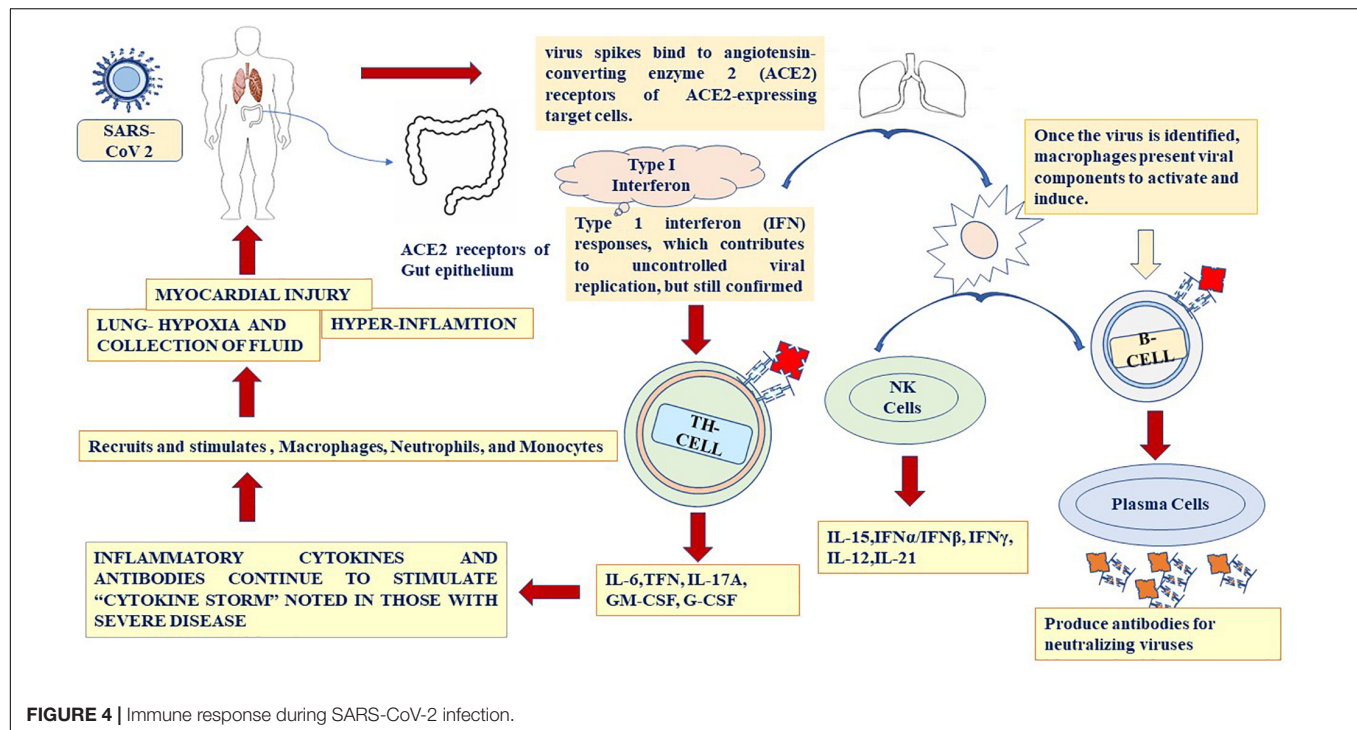
IMMUNE RESPONSE

The site of the initial infection of SARS-CoV-2 is unknown, but the most common effect is damage to the respiratory system owing to the predominance of the angiotensin-converting enzyme 2 (ACE2) receptors in the epithelial lining (Elena et al., 2020). The gastrointestinal tract also has a significantly higher concentration of ACE2, but GI symptoms were seen more in SARS infections and have been quite rare in SARS-CoV-2 infections. The immune response in SARS-CoV-2 patients occurs in two phases: Initially, when the disease is moderate, the immune cells eliminate the virus by producing primary cytokines, which may be beneficial for eliminating the virus but results in inflammation. During the second phase of more severe cases, SARS-CoV-2 patients exhibit significantly high cytokine levels or hyper-inflammation, and in some cases, the lungs become damaged (Figure 4; Azin et al., 2020; Shih-Hwa et al., 2020). Patients in this stage develop ARDS, and worsening damage to the lungs is a major challenge. Some patients with severe respiratory symptoms experience a high viral load in the lungs, and further studies are required to understand the dynamics between viral load dynamics and effective immune response (Zhuobing et al., 2020). Extreme inflammation results in the release of large cytokines in the circulation, which start affecting the secondary organs, and the viral load begins to decrease. In addition to the lungs, the heart rate may also be affected

by systemic inflammation during SARS-CoV-2 infection (Tian et al., 2020). Severe SARS-CoV-2 infections are associated with lymphocytopenia, which is a severe loss of lymphocytes in the bloodstream. Many cytokines are released in SARS-CoV-2 patients and cause a cytokine storm such as IL-6, IL-1, IL-2, IL-10, TNF- α , and IFN- γ . Increased level of IL-6 in the serum leads ARDS and adverse clinical outcome, such as respiratory failure (Tan K.S. et al., 2020; Tan L. et al., 2020). A high level of IL-6 can suppress normal cell activation (Azin et al., 2020). Thus, a cytokine storm may help with the suppression of T-cells in SARS-CoV-2 patients (Puja et al., 2020). Researchers have also suggested that a massive release of cytokines involves a rapid viral replication, leading to apoptosis. This increases the macrophages in the lungs, which in turn amplifies the inflammatory response (Figure 4). Specific cytokines are involved in the SARS-CoV-2 immune response. In severe cases of SARS-CoV-2 infection, increased levels of IL-6, IL-10, TNF- α , and the soluble IL-2 receptor have been found. In another study, elevated levels of IL-7, G-CSF, IP-10, MCP-1, and MIP-1 α were found in patients with a severe SARS-CoV-2 infection (Liu H. et al., 2020). Patients experiencing a cytokine storm may have lung damage and multi-organ failure, with death occurring in some cases. Understanding the mechanism of the immune response by which the cytokine storm can be reduced is critical for the design of future therapies. Targeted immune cell-based therapies may prove beneficial because they focus on a specific cytokine, such as IL-6, IL-10, and TNF- α , without causing a widespread effect on the immune system (Figure 4; Ye et al., 2020). To fully understand the occurrence of a cytokine storm in SARS-CoV-2 patients, inflammation, acute phase, essential immune response, proinflammatory chemokines, immune cell-specific (including B cells, CD8, and natural killer cells), macrophage and microglia, and T-helper-cell cytokine panels need to be conducted on the serum or bronchoalveolar lavage fluid of COVID-19 patients (Zhang H.-T. et al., 2020).

DIAGNOSIS

Lab diagnosis of SARS-CoV-2 is shown in Table 1, where the chest X-ray shows patchy infiltrates, which may be peripheral or concentrated in the lower lung fields, or maybe interstitial infiltrates, an easily progressive problem involving diffusion and infiltration (Hong et al., 2020). To confirm the diagnosis, and (Real-Time Polymerase Chain Reaction) RT-PCR is conducted on a small amount of viral RNA specimen in the respiratory tract (sputum, swab, aspirate, or lavage), or plasma during the early disease stage (Corman et al., 2020). An RT-PCR is also conducted on the urine and stool at a later stage (Xu X. et al., 2020; Zhang J. J. et al., 2020). The cultivation of a coronavirus is extremely difficult; in fact, such viruses grow only in a human tracheal ring organ culture, except for SARS and MERS, which can easily grow on Vero cell lines (Coleman and Frieman, 2015). Antibodies appear after 1 month from infection, and ELISA and immunofluorescence antibody tests (IFATs) are used as a sociological investigation in the spread of the disease into the population. ELISA and immunofluorescence antibody test (IFAT) is used to detect for sociological investigation, which



appears, after 1 month (Addie, 2020). Confirmed cases of SARS-CoV-2 have tested positive regardless of clinical symptoms. Probable cases are considered for those with inconclusive results or when testing cannot be performed under any circumstances

(Jian-Min et al., 2020). Suspected cases are referred to as those patients with clinical symptoms, a history of travel to or residing in an infected area, or have had contact with someone with a confirmed or probable case during 14 days or more up to

28 days before the onset of symptoms or with someone with full clinical signs (Giuseppe and Rossella, 2020). Negative cases are considered individuals who have tested negative at least twice within at least a 48-h time interval with a confirmed or probable test result (Jian-Min et al., 2020). CRISPR (Clusters of Regularly Interspaced Short Palindromic Repeats) is a genome-editing tool. It helps in DNA sequences and functions of the gene (Singh et al., 2019; Verma et al., 2019). CRISPR has potential application in the prevention and diagnosis of disease. CRISPR-Cas 9 and its variants-based diagnostic under process. The expert from the United States published CRISPR based diagnosis method for SARS-CoV-2 in nature Biotechnology (Broughton et al., 2020).

TREATMENT

The repurposing of drugs is an effective outcome-based treatment that also allows significantly enhancing the drug development process (Senanayake, 2020). Most treatment for SARS-CoV-2 has been based on supportive care such as the use of remdesivir, lopinavir/ritonavir, hydroxychloroquine, convalescent plasma, synthetic antibodies, interferons, low dose steroids, azithromycin, IL-6, IL-1 inhibitors, anti-TNF, and various other support treatments according to the clinical complications of the patients (Tables 2, 3; Wu D. et al., 2020). Ritonavir is an anti-HIV drug, and redeliver is an anti-viral drug previously used against the EBOLA virus. Remdesivir was given to the first United States patient with SARS-CoV-2, who began to improve the very next day (Eastman et al., 2020). Remdesivir is an intravenous drug, which has a broad antiviral activity, inhibiting viral replication through a pre-mature termination of the RNA transcription. This drug has shown an *in vitro* activity against SARS-CoV-2 and *in vitro* and *in vivo* activities against related beta coronaviruses, and the drug blocks RNA dependent polymerases (Cao Y.C. et al., 2020). There are various randomized trials underway to evaluate the efficacy of remdesivir for SARS-CoV-2 infection from moderate to severe cases (Beigel et al., 2020). A large-scale clinical trial is ongoing, and some of the results are shown in Tables 2, 3. Chloroquine and hydroxychloroquine are oral prescription drugs used for the treatment of malaria and various inflammatory clinical complications (Ferner and Aronson, 2020). Chloroquine has been used for malaria treatment and chemoprophylaxis, and hydroxychloroquine has been used for rheumatoid arthritis, systemic lupus erythematosus, and porphyria cutanea treatments (Alia and Grant-Kels, 2020). Both are drugs having *in vitro* activity against SARS-CoV-2 and other coronaviruses. Hydroxychloroquine has a higher potency against SARS-CoV-2 infection. Chloroquine has been reported to inhibit the *in vitro* activity of SARS-CoV-2 (Alia and Grant-Kels, 2020). Although published clinical data are limited, hydroxychloroquine in combination with azithromycin is more effective; however, validation is required and clinical trials are ongoing (Yazdany and Kim, 2020). The possibilities of drug toxicity and other clinical side effects should be considered before use. In May of 2020, the WHO stopped the clinical trial of hydroxychloroquine owing to various side effects. Italy, France, Belgium, and other countries also

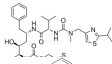
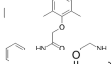
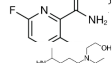
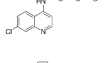
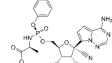
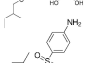
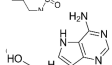
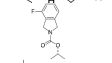
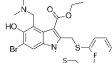
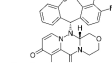
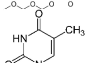
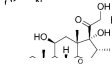
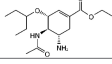
stopped using hydroxychloroquine (Meyerowitz et al., 2020). A study published in the New England Journal of Medicine reported that hydroxychloroquine is of no benefit in SARS-CoV-2 patients (Geleris et al., 2020). In April, the Food Drug Administration (FDA) issued an order to stop using hydroxychloroquine and chloroquine owing to potential cardiac problems (Boulware et al., 2020). Ibuprofen is anti-inflammatory and helps with breathing difficulty in patients. The clinical trial of Ibuprofen started on hospitalized patients with SARS-CoV-2 infections (Sodhi and Etminan, 2020). Monoclonal antibodies were isolated from surviving patients of SARS-CoV-2 and used for testing. During the first week of June in 2020, blood plasma was transferred in approximately 25 patients with SARS-CoV-2 infection at Methodist Hospital in Texas, United States (Salazar et al., 2020). Stem cell-based treatments are also under phase-II and -III clinical trials for use in SARS-CoV-2 infection (Raza and Khan, 2020). Immunosuppressant drugs are also under clinical trials, including baricitinib and an IL-6 inhibitor. In SARS-CoV-2 patients, the immune system becomes overactive and releases a cytokine storm. The FDA has therefore allowed the use of a device that filters cytokines from the blood of patients and improves the immune response. Even in various re-purposed and possibly novel therapies for SARS-CoV-2, developments in the clinical management of the patient is critical. In addition, there are still no future timelines for specific treatment options for SARS-CoV-2 (Zhao, 2020).

Clinicians and researchers are also looking for other options to target the replication or clinical manifestations of SARS-CoV-2. There is an urgent need to develop a sensitive and specific medicine for the various genotypes and stereotypes of SARS-CoV-2, such as cove 229E (HCoV-229E), OC43 (HCoV-OC43), NL63 (HCoV-NL63), and HKU1 (HCoV-HKU1), as shown in Figures 1, 2 (Bleibtreu et al., 2018). Preliminary investigations suggest that RNA a polymerase-based drug may inhibit the multiplication of HCoV infections (Adnan, 2020). There are various possible target RNA-dependent polymerase and helices for application as antiviral developers (Russell et al., 2020), which are produced by a replicase polyprotein and encoded by the ORF at the 5' end and cleaved by 3-C like proteases. The cleavage process occurring during membrane fusion leads to a syncytium formation. The binding of the amino-terminal receptor to the host cell surface leads to conformational changes in the carboxy-terminal, enabling fusion (Li et al., 2020). The structural spike glycoprotein of SARS-CoV-2 can also be targeted. Monoclonal antibodies have been developed using an angiotensin-converting enzyme 2 and are sensitive against SARS-CoV-2 at the site of the amino terminal-receptor binding domain and cause fusion with the host cells (Russell et al., 2020). After completion of SARS-CoV-2 multiplication cycles in the host, a version is released into the extracellular compartment through exocytosis, and viral multiplication cycles are repeated. The structural protein of SARS-CoV-2 may be targeted by small interfering RNA. Existing or earlier used drugs for HCoV-229E, HCoV-OC43, SARS-CoV, and the emerging MERS-curve can be further tested for cytopathies by applying a standard assay (Shen et al., 2019). A known pharmacokinetic and

TABLE 1 | Types of diagnostic approaches in SARS-CoV-2.

Types of diagnostic tests	Mechanism of detection	Source of samples	Result Interpretation	References
Nucleic acid amplification	Real Time PCR and NGS sequencing by using gene specific primer such as N,S,E and RdRP genes two independent sequences need to be detected	Nasal Swab, throat Swab, Bronchoalveolar lavage, blood faces and endotracheal aspirate	SARS-CoV2 Infection	Corman et al., 2020
Antibody based immunoassay	SARS-CoV2 IgM and IgG antibodies detection by ELISA	Serum	Immunity/Overall infection	Addie et al., 2020
Antigen based immunoassay	SARS-CoV2 detection protein	Nasal Swab, throat Swab, Bronchoalveolar lavage, blood faces and endotracheal aspirate	Confirm current SARS-CoV2	Udugama et al., 2020
CT- Imaging	Clinical symptoms (Fever/Cough, epidemiological history imaging CT)	Radiological features	Trade to identify for further target	Zhuobing et al., 2020

TABLE 2 | SARS-CoV-2 candidate drug treatments in Phase III-IV trials.

Drug candidate	Structure of compound	Description	Existing disease approval	Trial sponsor(s)	Expected results	References
Ritonavir		Anti-HIV Drug	Investigational combination	Oxford University WHO, CEPI	Under Clinical trial	Cao B. et al., 2020
Lopinavir		Anti-viral	Investigational combination	Oxford University WHO, CEPI	Under Clinical trial	Cao B. et al., 2020
Favipiravir		Antiviral agent against influenza	Influenza	Fujifilm	Under Clinical trial	Pawelec and Weng, 2020
Hydroxychloroquine or chloroquine		Anti-malarial anti rheumatic	Malaria, rheumatoid arthritis	Coalition for epidemic preparedness innovations CEPI)	Discontinued by WHO Under Clinical trial	Meyerowitz et al., 2020
Remdesivir		Viral RNA-dependent RNA polymerase	Broad spectrum anti-viral drug	NIAID, WHO, Gilead	Under clinical trial	Gordon et al., 2020
Prezcobix		HIV-1 protease inhibitor	HIV infection	Chinese hospital testing (Janssen)	Under clinical trial	Zhang Q. et al., 2020
Galidesivir		Viral replication inhibitor	Antiviral against RNA viruses	BioCryst Pharmaceuticals	Under clinical trial	Jeong et al., 2020
Danoprevir		Inhibitors of NS3/4A	HCV Protease inhibitor	Chinese research sponsors	Under clinical trial	Zhang L. et al., 2020
Umifenovir		Replication inhibitors	Anti-viral used for Influenza	Various trials with Chinese research	Under clinical trial	Huang D. et al., 2020
Baloxavir marboxil (BXM)		Polymerase acidic endonuclease inhibitor	Anti-viral used for Influenza	Various trials with Chinese research		Abed et al., 2020
Levovir		polymerase inhibitor	Anti-viral used for hepatitis B Virus	Bukwang Pharm, South Korea	Under clinical trial	Sae-im, 2020
Dexamethasone		Anti-inflammatory	Rheumatoid arthritis	University of Oxford	Phase-III	Horby, 2020
Oseltamivir		Neuraminidase inhibitor	Prevent Influenza A and B	Roche; REMAP-CAP global trial	Phase-III	Coenen et al., 2020

pharmacodynamic immunoglobulin approach may be employed by exploring the efficacy against SARS-CoV-2 (Shen et al., 2019; Li et al., 2020). In addition, a high throughput analysis of existing compounds can be conducted by using a database and expected antiviral activity along with their immunological and physiological efficacy. Genomic and biophysical based drugs can be developed including viral enzyme-based inhibitors. Moreover, all these drug options can be used with patients of SARS-CoV-2.

INHIBITOR OF SARS-CoV-2 M^{pro}

Recently SARS-CoV-2 M^{pro} X-ray crystal structure elucidated, which showed with an α -ketoamide as a potent inhibitor in the enzyme's active site, and screened for several FDA approved antiviral drugs and thereby blocking the active pocket (Kumar et al., 2020; Zhang N. et al., 2020). The structure of SARS-CoV-2 M^{pro} in the apo form and α -ketoamide bound form shows that the protein makes a crystallographic dimer

TABLE 3 | Development of SARS-CoV-2 Immunoglobulin based treatments option.

Leading candidate	Description	Trial sponsor(s)	Development of stage
Convalescent plasma	Passively transfer antibodies (Immunoglobulin)	USA FDA -Sponsored Expanded access program coordinated by Mayo Clinic	Phase-III
STI-5656 (Abivertinib)	Tyrosine kinase inhibitor	Sorrento Therapeutics	Phase-III
PRO 140 (Leronlimab)	Monoclonal antibody targeted against CCR5 receptor	CytoDyn Inc., United States	Phase-III
PTC299	Dihydroorotate dehydrogenase inhibitors	PTC therapeutics, Inc., South Plainfield, NJ, United States	Phase-III
CD24Fc	Immunomodulator (New drug)	Oncolmmune, Inc., United States	Phase-III
Lenzilumab	Chronic Myelomonocytic leukemia	Targets Colony Stimulating factors (CSF-2); Multiple countries	Phase-III
Tocilizumab	Immunosuppression	Roche holding AG, Basel, Switzerland	Phase-III
Sarilumab	Rheumatoid arthritis	Regeneron-Sanofi, United States	Phase-III
Ravulizumab	Compliment inhibitors	Alexion pharmaceuticals Inc	Phase-III
Losmapimod	MAPK as potent suppressors of DUX4 expression	Fulcrum Therapeutics, United States	Phase-III
Pepcid	H2 blocker	Yamanouchi Pharmaceutical Co., Merck, Japan	Phase-III
Mitigare (Colcrys)	Anti-inflammatory agent	Bill & Melinda Gates Foundation, United States	Phase-III

composed of two monomers of identical conformations. Each protomer is furthermore made up of three domains. The interface of domain I and domain II form the active site of the protein, which is composed of a Cys145-His41 dyad where α -ketoamide derivative bound (**Figures 5A,B**). Domain I (residues 8–101) and domain II (residues 102–184) have an antiparallel β -barrel structure. Domain III (residues 201–303) contains five α -helices arranged into a largely antiparallel globular cluster, and it is connected to domain II by a long loop region (residues 185–200). SARS-CoV-2 M^{pro} has a Cys-His catalytic dyad, and the substrate-binding site is located in a cleft between domain I and domain II. These features are similar to previously reported M^{pro} from other coronaviruses (Anand, 2002; Yang et al., 2003; Xue et al., 2008; Wang et al., 2016; Ren et al., 2020). It is stabilized by several interactions with the active site residues His41 and Cys145 and adjacent residues in substrate binding cleft such as Gly143 and Ser144. Coronaviruses use a chymotrypsin-like a protease (3CLpro) and a papain-like protease (PLpro) to process and cleaves its long polyprotein precursor into individually functional non-structural proteins. The active site residues are thoroughly conserved and make a catalytic Cys145-His41 dyad. The specific subsite residues located in the enzyme active site are named as S1', S1, S2, S3, and S4 depending on their relative position to the cleavage site and subsites P1', P1, P2, P3, and P4 in the polyprotein. Subsite P1 corresponds to the amino acid just before the cleavage site, and position P1 corresponds to the residue immediately after the cleavage site (Anand, 2003; Kiemer et al., 2004). In the M^{pro} of SARS-CoV-2 active site region, the S1' residues are contributed by Cys145, Gly143, and Ser144 which also serve as the oxyanion hole. The S1 residue is His163, while Glu166 and Gln189 located at the S2 position. Bulky Gln189 and Pro168 make the S4 site (**Figure 5A**). The main protease recognizes and binds specific residues at each subsite of the peptide substrate to determine the initiation of proteolysis and the production of non-structural proteins for the formation of the replication-transcription complex.

A previous study proposed that M^{pro} has a substrate-recognition pocket that is highly conserved among all coronaviruses and that this pocket could serve as a drug target for the design of broad-spectrum inhibitors. The recent discovery of new coronaviruses, and the accumulation of structural data for M^{pro} from coronaviruses of various species, provided the opportunity to further examine this hypothesis. Crystal structures of M^{pro} revealed that (Xue et al., 2008; Wang et al., 2016; Ren et al., 2020) most variable regions are the helical domain III and surface loops, and that the substrate-binding pocket (located in a cleft between domain I and domain II) is highly conserved among M^{pro} in all coronaviruses; this suggests that antiviral inhibitors targeting this pocket should have wide-spectrum activity against coronaviruses as shown in **Figure 5B**.

DEVELOPMENT OF MERS-CoV VACCINES

SARS-CoV-2 has caused a global public health crisis, and a vaccine urgently needs to be developed. An effective vaccine will also help control the pandemic situation of the emerging SARS virus and act as an effective treatment against its genotypes and stereotypes (**Figure 2**; Pawelec and Weng, 2020). Researchers have also been investigating live-attenuated vaccines against SARS in animal models, which may be helpful for SARS-CoV-2 (Aurélien et al., 2020). There are three possible targets for the development of a SARS-CoV-2 vaccine. Everyone has different types of immunity level I, particularly during old age and in children or those suffering a non-communicable disease, and it is therefore highly difficult to optimize a single vaccine for all age groups. RNA-based SARS-CoV-2 vaccines are also in development (**Table 4**). Adjuvants may help enhance the immune response when such vaccines are administered to older populations and may reduce the amount of RNA needed in each vaccine (Hotez et al., 2020). After the Wuhan outbreak, Chinese

scientists published the genome sequence of SARS-CoV-2 and started designing a vaccine. Traditional methods required an actual sample of the virus. When an inactivated virus is injected into the body, the immune system is recognized as an antigen. Vaccines can be used as antigens in the body to protect against SARS-CoV-2 (Ojha et al., 2020). For vaccine development, a rapid response after direct injection of antigen into the body is required. These types of vaccines typically send instructions into the cell of the body. Because the cells produce an antigen protein specific to the virus a suitable design is needed. These instructions are in the form of RNA or DNA (Zhang N. et al., 2020). The molecules contain the code for different proteins. This process requires a shorter development time because we do not need to grow the entire virus. Scientists have tried to replicate a SARS-CoV-2-like sequence designed like a cassette tray and slot for use in new virus antigens. Scientists have tried to like COVID-19 that sequence designed like cassette tray and slot in new virus antigens. To deal with SARS-CoV-2, CEPI is funding several teams globally, each independently working from a plate form model. As a nucleic acid-based candidate, NIH (United States) is developing a vaccine on an mRNA platform. They applied a conventional approach using the body's cells rather than a lab test producing antigenic proteins, that's been once made by like SARS-CoV-2. The host immune system then stimulates and develops antibodies to SARS-CoV-2. It can immediately recognize SARS-CoV-2 later and prevent the person from becoming sick. Scientists are also currently working on preventing sickness from SARS-CoV-2 (Wang F. et al., 2020). As the race for a novel and viable vaccine continues for all age groups, we do not know how bad the situation will become. Hopefully, a vaccine will soon be ready for distribution. Normally, a vaccine takes years to reach the clinical stage. However, researchers are working hard using high throughput analyses to identify the SARS-CoV-2 sequence. A small genetic sequence of the virus, received globally, is applied, and a computer algorithm scans the sequence to find tiny motifs in the DNA. A strong immune response is needed to fight against SARS-CoV-2. The moment the genetic code for the 2019 novel coronavirus was released by the Chinese government, the team at INOVIO Pharmaceuticals in California, United States began developing a new DNA medicine to kill it (Arnold, 2020). They identified, such motifs, inserted another piece of plasmid, and amplified it using bacteria to create new DNA. They then purified the DNA and injected it into completely healthy cells of a human body. This DNA acts as a map or picture of the human body. It finds the SARS-CoV-2 and attacks and kills it. There is nothing on the market yet for DNA medicines. This will be ready for human clinical trials by the end of June 2020. Since 2016, Migal Galilee Research Institute, an Israeli company, has been working on a poultry coronavirus. According to an expert in this field, poultry coronaviruses are similar to human coronaviruses, and they are more likely to produce a SARS-CoV-2 vaccine in a short period (Hodgson, 2020). Researchers are optimistic about overcoming the major challenges and safety issues. Recent developments in vaccines against SARS-CoV-2 are shown in **Table 4**.

EPIDEMIOLOGY

Most of the Wuhan cases had links with the wet seafood market. The etiology was studied in a patient who was admitted to a health center and similar types of clinical signs and symptoms were found (Gangqiang et al., 2020). Approximately 40 days later, it was determined that the virus belongs to group 2 coronaviruses of bats and was 70% like the genome of SARS-CoV (Chen W. H. et al., 2020). SARS-CoV-2 is closely related to bat coronaviruses, pangolin coronaviruses, and SARS-CoV. The genome and genetic shift of such coronaviruses are shown in **Figure 2**. A similar type of outbreak occurred during the middle of January of 2003 until the last week of February of the same year, during the Spring Festival, or Lunar New Year, in China (Ali et al., 2020). This newest outbreak also peaked between the first and third weeks of January 2020 (Wu P. et al., 2020). The number of travelers increased by approximately 1.7-fold during the holiday. This is also one of the reasons for the spread of SARS-CoV-2 and difficulty in identifying the disease (Jiang et al., 2020). The first person with SARS-CoV-2 symptoms was observed earlier on December 1, 2019, but was not associated with the seafood market in Wuhan. In the early stage of the cluster, two-thirds of the cases were associated with the wet market (Chan et al., 2020). On March 13, 2020, a non-authenticated report from South China Morning Post stated that a 55-year-old from Hubei was the first observed case on November 17, 2019 (Chan et al., 2020). The fatality was recorded at a rate of 2.3%. The maximum number of cases was observed on February 12, 2020; owing to modifications in the diagnosis, the classification of 13,332 (rather than laboratory) confirmed cases were all recorded as new cases on February 12, 2020, despite being diagnosed during the preceding days and weeks as per the WHO on March 11, 2020. SARS-CoV-2 is affecting more than 185 countries throughout the world. New cases in new countries are still occurring. For the distribution of cases worldwide, 80,849 (51.36%) cases were observed in mainland China, and 76,562 (48.64%) cases were recorded in the rest of the world. On March 11, 2020, the WHO declared a pandemic and the total number of cases increased globally. Positive cases are considered in individuals who have been tested positive for SARS-CoV-2 as per the standard guidelines of the WHO and CDC (Operations Dashboard for ArcGIS, 18 April 2020). During the early stage up to January 23, 2020, approximately 86% of SARS-CoV-2 infected individuals had not been detected, and these infected people were the source for approximately 79% of the later confirmed cases. The numbers of infected people are higher in many countries than the number of reported cases (Li et al., 2020). According to reports published by various countries, testing data showed that an average of 1.4% of their total populations had been infected (Li et al., 2020). Based on preliminary results, 15% tested positive for antibodies in Gageite, North Rhine-Westphalia, Germany. Mothers and pregnant women in New York City also tested positive against SARS-CoV-2, which also suggests that the number of cases presented globally was higher than previously confirmed (Streck, 2020). A low number of cases were observed in China for those below 20 years of age, however

TABLE 4 | Tabular representation of ongoing clinical studies of vaccines for SARS-CoV-2.

Vaccine candidate	Details	Status	Organizations	References
Bacillus Calmette-Guerin (BCG) live-attenuated vaccine for SARS-CoV-2	BCG vaccine may be effective in preventing acute respiratory tract infections in elderly patients, other respiratory infection and sepsis. in the fight against SARS-CoV-2	Phase 3 BRACE trial in Australia, Netherlands	University of Melbourne and Murdoch Children's Research Institute (Australia); Radboud University Medical Center (Netherlands); Faustman Lab at Massachusetts General Hospital (MGH) (United States)	Kamat and Kumari, 2020
mRNA-1273	mRNA-1273, a vaccine candidate based on previous study of SARS and MERS	Phase 2 clinical trial	Kaiser Permanente Washington Health Research Institute	Jackson et al., 2020
Ad5-nCoV	Recombinant novel corona virus vaccine with adenovirus type 5 vector (Ad5)	Phase 2 trial	Tongji Hospital, Wuhan, China	Feng L. et al., 2020
ChAdOx1	SARS-CoV-2, adenovirus vaccine vector MERS vaccine.	Phase 1/2 clinical trial	The University of Oxford	van Doremalen et al., 2020
INO-4800	DNA vaccine for SARS-CoV-2	Phase 1 trial	Inovio Pharmaceuticals	Smith et al., 2020
BNT162	Modified mRNA-based, SARS-CoV-2 vaccine	Phase 1/2 trial	Pfizer and BioNTech	Keech et al., 2020
NVX-CoV2373	Recombinant nanoparticle vaccine candidates for SARS-CoV-2	Phase 1 trial	Novavax, United States	Thanh et al., 2020
CureVac	mRNA-based SARS-CoV-2 vaccine	Under progress	CureVac AG, a clinical stage biopharmaceutical	Wu R. et al., 2020
Vaxart	Oral recombinant SARS-CoV-2 vaccine; gene-based vaccine	Phase 1 clinical	Emergent Biosolutions	Maurya et al., 2020
DNA vaccine candidates	DNA-based vaccine for SARS-CoV-2	Preclinical	Takis Biotech, Italy	Frederiksen et al., 2020
mRNA vaccine	Repurposed SARS vaccine and mRNA vaccine candidate	Lab testing	Sanofi, Paris, France	Ng et al., 2020
DNA plasmid vaccine candidate	Modified vaccinia ankara virus like particles (MVA-VLP) vaccine candidate for SARS-CoV-2	Pre-clinical testing	GeoVax and BravoVax, China	Chen W. H. et al., 2020
Adenovirus-based vector vaccine for SARS-CoV-2	Adenovirus-based vector vaccine for SARS-CoV-2	Animal testing	Greffex Inc., Aurora, CO, United States	Funk et al., 2020
Modified avian coronavirus vaccine	Genetically similar avian coronavirus Infectious Bronchitis Virus	Ready for human trials	MIGAL – Galilee Research Institute, Israel	Zhu et al., 2020
Gene-encoded antibody vaccine candidate	Next-generation, gene-encoded antibody vaccine for SARS-CoV-2	Phase I	Sorrento Therapeutics, Inc., and SmartPharm Therapeutics Inc., United States	Folegatti et al., 2020
DPX- SARS-CoV-2	T-cell activating immunotherapy antigen vaccine	Phase 1 clinical	IMV, Canada	Rabaan et al., 2020
Intranasal DNA-based vaccine candidate	Stimulating an immune response in the nasal cavity	Phase 1 clinical	University of Waterloo Waterloo, ON, Canada	Folegatti et al., 2020
Single-dose patch delivery vaccine	Vaccine candidate for SARS-CoV-2 delivered through a single-dose patch	Testing in Animal	California-based Biotech company Verndari, United States	Sharpe et al., 2020

(Sutton et al., 2020). It is not clear whether this is due to less developed symptoms or a smaller number of infections (China: Age distribution of novel coronavirus patients, 2020). In a China-based study, children were infected by adults, which needs to be validated (Bi et al., 2020). In the current stage, the basic reproduction number (R_0) of SARS-CoV-2 is 5.7, although in January 2020 it was approximately 2.5 (Ward, 2020). This may vary by population and country (Sanche et al., 2020). It is expected that by the third week of May 2020, the value will be 1.0 in many countries. Most infected individuals have recovered and the onset of symptoms and death is 6 to 14 days (Worldwide Sars-Cov-2 Statistics, 2020). Death due to SARS-CoV-2 is considered as a patient who has died after testing positive, according to the WHO and CDC guidelines (New York Times, January 23, 2020).

On January 9, 2020, the first confirmed death from SARS-CoV-2 was reported in China, and the first death outside China was reported on February 1, 2020, in the Philippines (Rothan and Byrareddy, 2020). On February 14, 2020, the first death outside Asia was reported in France. On February 5, 2020, approximately 80% of deaths in China were recorded in those above 60 years in age, with cardiovascular disease, diabetes, or in immunocompromised individuals (Johns Hopkins University SARS-CoV-2 Dataset, April 25, 2020). In some countries, the death rate is higher than normal, such as in the United States (New York City), France (Paris), and Italy. The high mortality rate may be due to strained medical facilities (Coronavirus: Is SARS-CoV-2 cause of all the fatalities in Italy, April 16, 2020). According to data available on the Johns Hopkins University website, the global death rate is 6.8%, which may vary by country. The global case fatality rate is 0.82% and the infection fatality rate is 0.1%, which may vary by country according to the University of Oxford's Centre for Evidence-Based Medicine (Oke and Heneghan, 2020).

PREVENTION

Suspected individuals should be monitored, and their health status, such as fever and difficulty in breathing, should be recorded. In case of any relevant symptoms, the individual should be isolated immediately, and nucleic acid detection for SARS-CoV-2 should be performed using an appropriate sample. Healthy individuals are advised to avoid traveling to disease outbreak areas. In general, people should stay away from crowded places and maintain more than 6 feet or 2 m from anyone with symptoms (Gangqiang et al., 2020). Wearing a surgical mask is recommended owing to the general risk of obtaining SARS-CoV-2, and hand washing is a key and should be done using soap or an alcohol-based hand sanitizer. Besides, people should avoid touching their eyes, nose, or mouth, which are known as the T-Zone and are common entry points for the viruses in the body. For healthcare workers around patients with SARS-CoV-2 (WHO, 2020; Worldwide Sars-Cov-2 Statistics, 2020), the recommendations are to avoid

respiratory droplets and take precautions, which include wearing personal protective gear such as a clean and dry surgical mask and gloves, long sleeve gowns, and eye protection including goggles or a face shield (Eurosurveillance editorial team, 2020). When conducting procedures that result in aerosol-like tracheal intubation, cardiopulmonary resuscitation, or non-invasive ventilation, it is important to wear an N-95 respirator, which prevents 95% of small particles such as respiratory droplets from passing through (Güner et al., 2020).

Prospects

Like any other disease model, the forecast of SARS-CoV-2 aims to determine when the outbreak will stop and how many people suffer or die. We need to employ novel efforts rather than generating premature investigations. Researchers have been working tirelessly since the first phase of the epidemic. At the same time, it is also necessary to develop advanced models to handle the presently available data. Scott Layne, an epidemiologist at the University of California, Los Angeles has proposed a new data bank. In addition, bioinformatician investigators are working to compile a dataset and build an algorithm. Scientists from the University of Montreal have also published chest X-ray and CT scan data for use by other researchers. Johns Hopkins University has developed a server that is regularly updated for further research on the vaccine and drug development. Researchers from Shanghai have developed a server for checking CT scan images to reduce the diagnosis (Zhang Z. et al., 2020). Researchers from the United States have claimed to have identified the effects of SARS-CoV-2 in the lungs during active infection. Wang Y. et al. (2020) has developed an auditory system-based SARS-CoV-2 detection, which is based on the breathing rate. Although this investigation has not yet been validated, the idea is sound. In addition, investigators in Wuhan, China have developed a health calculator using nearly 3,000 electronic health records from patients, achieving more than 90% accuracy (Butt et al., 2020). Some clinicians have used anti-HIV medicine to cure SARS-CoV-2 patients, although other scientists have suggested that nanoparticle-based medicine would be more effective to fight against SARS-CoV-2 (Yan et al., 2020). Many scientists are also working on therapeutic-based approaches. To avoid research gaps in SARS-CoV-2, clinical, and public health strategies need to be implemented using more advanced tools and approaches with international cooperation. Some key points should be monitored for strategic prevention, such as a strategy for identifying contact with infected individuals, the range of virus mutation at the global level, the identification of super spreaders, the association of disease progression level of viral contagion after recovery of positive patients, immunity level between severe and non-severe cases, the immunopathological mechanism of mucous hypersecretion with a cytokine storm, effective clinical biomarkers, effective implication of artificial intelligence, identification of the optimal incubation period, and the development of cost-effective diagnosis treatment and vaccines. There is an urgent requirement to recognize and eliminate any barriers that would affect rapid patient care and public health management against the SARS-CoV-2 pandemic.

Furthermore, improved effectiveness in care is urgently needed and a new approach to international coordination is required.

AUTHOR CONTRIBUTIONS

DDS and DKY conceived and designed the project. IH, E-HC, and DKY collected the data from the literature. DDS, IH, E-HC, and DKY analyzed the data and wrote the manuscript. All authors contributed to the interpretation and discussion of the results, and read and approved the final version of the manuscript.

FUNDING

DKY was thankful to the Basic Science Research Program of the National Research Foundation of Korea (NRF), funded by the Ministry of Education, Science, and Technology, who supported

this study (No. 2017R1C1B2003380). This research was also partially supported by the Leading Foreign Research Institute Recruitment Program through the National Research Foundation of Korea (NRF) funded by the Korea government (MSIP) (NRF-2016K1A4A3914113).

ACKNOWLEDGMENTS

DDS is thankful to Amity Institute of Biotechnology and Amity Institute of Microbial Technology, Amity University Jaipur, Rajasthan, India. DKY is thankful to Gachon Institute of Pharmaceutical Science and the Department of Pharmacy, College of Pharmacy, Gachon University of Medicine and Science, Incheon, South Korea for providing the computational modeling facility. We are also thankful to Chandni Gupta for arranging the references.

REFERENCES

- Abd El-Aziz, T. M., and Stockand, J. D. (2020). Recent progress and challenges in drug development against SARS-CoV-2 coronavirus (SARS-CoV-2) - an update on the status. *Infect. Genet. Evol.* 83:104327. doi: 10.1016/j.meegid.2020.104327
- Abed, Y., Fage, C., Checkmahomed, L., Venable, M.-C., and Boivin, G. (2020). Characterization of contemporary influenza B recombinant viruses harboring mutations of reduced susceptibility to baloxavir marboxil, in vitro and in mice. *Antiviral Res.* 179:104807. doi: 10.1016/j.antiviral.2020.104807
- Addie, D. D. (2020). *Feline Coronavirus and Feline Infectious Peritonitis Diagnosis and Prevention*. Available online at: catvirus.com
- Addie, D. D., le Pote, R. S., Burr, P., Decaro, N., Graham, E., and Hofmann-Lehmann, R. (2020). Utility of feline coronavirus antibody tests. *J. Feline Med. Surg.* 17, 152–162. doi: 10.1177/1098612X14538873
- Adnan, S. (2020). Novel coronavirus-induced NLRP3 inflammasome activation: a potential drug target in the treatment of SARS-CoV-2. *Front. Immunol.* 11:1021. doi: 10.3389/fimmu.2020.01021
- Ali, A., Areeba, A., and Sana, H. (2020). Comparison of epidemiological variations in SARS-CoV-2 Patients inside and outside of china—a meta-analysis. *Front. Public Health* 8:193. doi: 10.3389/fpubh.2020.00193
- Alia, E., and Grant-Kels, J. M. (2020). Does hydroxychloroquine combat SARS-CoV-2? A timeline of evidence. *J. Am. Acad. Dermatol.* 83, e33–e34. doi: 10.1016/j.jaad.2020.04.031
- Anand, K. (2002). Structure of coronavirus main proteinase reveals combination of a chymotrypsin fold with an extra alpha-helical domain. *EMBO J.* 21, 3213–3224. doi: 10.1093/emboj/cdf327
- Anand, K. (2003). Coronavirus main proteinase (3CLpro) structure: basis for design of Anti-SARS Drugs. *Science* 300, 1763–1767. doi: 10.1126/science.1085658
- Arnold, C. (2020). Race for a vaccine. *New Sci.* 245, 44–47. doi: 10.1016/s0262-4079(20)30600-x
- Aurélien, M., Lucie, H., Jean-Luc, S., Jean-Philippe, L., and Michel, B. (2020). Therapeutic options for SARS-CoV-2 -modulation of type I interferon response as a promising strategy? *Cureus* 12:e10480. doi: 10.3389/fpubh.2020.00185
- Azin, T., Mahta, A., Yeganeh, F., Parnian, J., Saba, H., Tess, M. C., et al. (2020). Clinical features, diagnosis, and treatment of SARS-CoV-2 in hospitalized patients: a systematic review of case reports and case series. *Front. Med.* 7:231. doi: 10.3389/fmed.2020.00231
- Baig, A. M., Khaleeq, A., Ali, U., and Syeda, H. (2020). Evidence of the SARS-CoV-2 virus targeting the CNS: tissue distribution, host-virus interaction, and proposed neurotropic mechanisms. *ACS Chem. Neurosci.* 11, 995–998. doi: 10.1021/acscchemneuro.0c00122
- Beigel, J. H., Tomashek, K. M., Dodd, L. E., Mehta, A. K., Zingman, B. S., Kalil, A. C., et al. (2020). Remdesivir for the treatment of SARS-CoV-2 - preliminary report. *New Engl. J. Med.* 2020:NEJMoa2007764. doi: 10.1056/NEJMoa2007764
- Belouzard, S., Millet, J. K., Licitra, B. N., and Whittaker, G. R. (2012). Mechanisms of coronavirus cell entry mediated by the viral spike protein. *Viruses* 4, 1011–1033. doi: 10.3390/v4061011
- Bernard Stoecklin, S., Rolland, P., Silue, Y., Mailles, A., Campese, C., Simondon, A., et al. (2020). First cases of coronavirus disease 2019 (SARS-CoV-2) in France: surveillance, investigations and control measures, January 2020. *Eur. Commun. Dis. Bull.* 25:2000094. doi: 10.2807/1560-7917.ES.2020.25.6.2000094
- Bi, Q., Wu, Y., Mei, S., Ye, C., Zou, X., Zhang, Z., et al. (2020). Epidemiology and transmission of SARS-CoV-2 in 391 cases and 1286 of their close contacts in Shenzhen, China: a retrospective cohort study. *Lancet* 202:287. doi: 10.1016/S1473-3099(20)30287-5
- Bleibtreu, A., Jaureguierry, S., Houhou, N., Boutolleau, D., Guillot, H., Vallois, D., et al. (2018). Clinical management of respiratory syndrome in patients hospitalized for suspected Middle East respiratory syndrome coronavirus infection in the Paris area from 2013 to 2016. *BMC Infect. Dis.* 18:331. doi: 10.1186/s12879-018-3223-5
- Boulware, D. R., Pullen, M. F., Bangdiwala, A. S., Pastick, K. A., Lofgren, S. M., Okafor, E. C., et al. (2020). A randomized trial of hydroxychloroquine as postexposure prophylaxis for Covid-19. *New Engl. J. Med.* 383, 517–525. doi: 10.1056/NEJMoa2016638
- Broughton, J. P., Deng, X., Yu, G., Clare, L. F., Venice, S., Jasmeet, S., et al. (2020). CRISPR-Cas12-based detection of SARS-CoV-2. *Nat. Biotechnol.* 38, 870–874. doi: 10.1038/s41587-020-0513-4
- Butt, C., Gill, J., Chun, D., and Babu, B. A. (2020). Deep learning system to screen coronavirus disease 2019 pneumonia. *Appl. Intell.* 22, 1–7. doi: 10.1007/s10489-020-01714-3
- Cao, B., Wang, Y., Wen, D., Liu, W., Wang, J., Fan, G., et al. (2020). A trial of lopinavir-ritonavir in adults hospitalized with severe SARS-CoV-2. *N. Engl. J. Med.* 382, 1787–1799. doi: 10.1056/NEJMoa2001282
- Cao, Y. C., Deng, Q. X., and Dai, S. X. (2020). Remdesivir for severe acute respiratory syndrome coronavirus 2 causing SARS-CoV-2: an evaluation of the evidence. *Travel Med. Infect. Dis.* 35:101647. doi: 10.1016/j.tmaid.2020.101647
- Chan, J. F.-W., Yuan, S., Kok, K.-H., To, K. K.-W., Chu, H., Yang, J., et al. (2020). A familial cluster of pneumonia associated with the 2019 novel coronavirus indicating person-to-person transmission: a study of a family cluster. *Lancet* 395, 514–523.
- Chan, J. W. M., Ng, C. K., Chan, Y. H., Lee, S., Chu, S., Law, W., et al. (2003). Short term outcome and risk factors for adverse clinical outcomes in adults with severe acute respiratory syndrome (SARS). *Thorax* 58, 686–689.
- Chan-Yeung, M., and Xu, R. H. (2003). SARS: epidemiology. *Respirology* 8(Suppl.), S9–S14. doi: 10.1046/j.1440-1843.2003.00518

- Chen, N., Zhou, M., Dong, X., Qu, J., Gong, F., Yang, H., et al. (2020). Epidemiological and clinical characteristics of 99 cases of 2019 novel coronavirus pneumonia in Wuhan, China: a descriptive study. *Lancet* 395, 507–513.
- Chen, W. H., Strych, U., Hotez, P. J., and Bottazzi, M. E. (2020). The SARS-CoV-2 vaccine pipeline: an overview. *Curr. Trop. Med. Rep.* 2020, 1–4. doi: 10.1007/s40475-020-00201-6
- Chen, X., and Yu, B. (2020). First two months of the 2019 Coronavirus disease (SARS-CoV-2) epidemic in China: real-time surveillance and evaluation with a second derivative model. *Glob. Health Res. Policy* 5:7. doi: 10.1186/s41256-020-00137-4
- Coenen, S., van der Velden, A. W., Cianci, D., Goossens, H., Bongard, E., Saville, B. R., et al. (2020). Oseltamivir for coronavirus illness: post-hoc exploratory analysis of an open-label, pragmatic, randomised controlled trial in European primary care from 2016 to 2018. *Br. J. Gen. Pract.* 70, e444–e449. doi: 10.3399/bjgp20X711941
- Coleman, C. M., and Frieman, M. B. (2015). Growth and quantification of MERS-CoV infection. *Curr. Protoc. Microbiol.* 37, 11–15. doi: 10.1002/9780471729259.mc15e02s37
- Corman, V. M., Landt, O., Kaiser, M., Molenkamp, R., Meijer, A., Chu, D., et al. (2020). Detection of 2019 novel coronavirus (2019-nCoV) by real-time RT-PCR. *Eur. Commun. Dis. Bull.* 25:2000045. doi: 10.2807/1560-7917.ES.2020.25.3.2000045
- Cowling, B. J., and Leung, G. M. (2020). Epidemiological research priorities for public health control of the ongoing global novel coronavirus (2019-nCoV) outbreak. *Eur. Commun. Dis. Bull.* 25:2000110. doi: 10.2807/1560-7917.ES.2020.25.6.2000110
- Cui, P., Chen, Z., Wang, T., Dai, J., Zhang, J., Ding, T., et al. (2020). Severe acute respiratory syndrome coronavirus 2 detection in the female lower genital tract. *Am. J. Obstet. Gynecol.* 223, 131–134. doi: 10.1016/j.ajog.2020.04.038
- Du, Y., Tu, L., Zhu, P., Mu, M., Wang, R., Yang, P., et al. (2020). Clinical features of 85 Fatal cases of SARS-CoV-2 from Wuhan. A retrospective observational study. *Am. J. Respir. Crit. Care Med.* 201, 1372–1379. doi: 10.1164/rccm.202003-0543OC
- Eastman, R. T., Roth, J. S., Brimacombe, K. R., Simeonov, A., Shen, M., Patnaik, S., et al. (2020). Remdesivir: a review of its discovery and development leading to emergency use authorization for treatment of SARS-CoV-2. *ACS Cent. Sci.* 6, 672–683. doi: 10.1021/acscentsci.0c00489
- Elena, C., Carmine, V., and Annibale, A. P. (2020). SARS-CoV-2 infection and circulating ACE2 levels: protective role in women and children. *Front. Pediatr.* 8:206. doi: 10.3389/fped.2020.00206
- Eurosurveillance editorial team (2020). Note from the editors: novel coronavirus (2019-nCoV). *Eurosurveillance* 25:2001231. doi: 10.2807/1560-7917.ES.2020.25.3.2001231
- Feng, L., Wang, Q., Shan, C., Yang, C., Feng, Y., Wu, J., et al. (2020). An adenovirus-vectored COVID-19 vaccine confers protection from SARS-CoV-2 challenge in rhesus macaques. *Nat. Commun.* 11:4207. doi: 10.1038/s41467-020-18077-5
- Feng, Y., Ling, Y., Bai, T., Xie, Y., Huang, J., Li, J., et al. (2020). SARS-CoV-2 with different severities: a multicenter study of clinical features. *Am. J. Respir. Crit. Care Med.* 201, 1380–1388. doi: 10.1164/rccm.202002-0445OC
- Ferner, R. E., and Aronson, J. K. (2020). Chloroquine and hydroxychloroquine in SARS-CoV-2. *BMJ* 369:m1432. doi: 10.1136/bmj.m1432
- Folegatti, P. M., Ewer, K. J., Aley, P. K., Angus, B., Becker, S., Belij-Rammerstorfer, S., et al. (2020). Safety and immunogenicity of the ChAdOx1 nCoV-19 vaccine against SARS-CoV-2: a preliminary report of a phase 1/2, single-blind, randomised controlled trial. *Lancet* 396, 467–478. doi: 10.1016/s0140-6736(20)31604-4
- Frederiksen, L. S. F., Zhang, Y., Foged, C., and Thakur, A. (2020). The long road toward COVID-19 herd immunity: vaccine platform technologies and mass immunization strategies. *Front. Immunol.* 11:1817. doi: 10.3389/fimmu.2020.01817
- Funk, C. D., Laferrière, C., and Ardakani, A. (2020). A snapshot of the global race for vaccines targeting SARS-CoV-2 and the COVID-19 pandemic. *Front. Pharmacol.* 11:937. doi: 10.3389/fphar.2020.00937
- Gangqiang, G., Lele, Y., Kan, P., Yu, C., Dong, X., and Kejing, Y. (2020). New insights of emerging SARS-CoV-2: epidemiology, etiology, clinical features, clinical treatment and prevention. *Front. Cell Dev. Biol.* 8:410. doi: 10.3389/fcell.2020.00410
- Ge, X. Y., Li, J. L., Yang, X. L., Chmura, A. A., Zhu, G., Epstein, J. H., et al. (2013). Isolation and characterization of a bat SARS-like coronavirus that uses the ACE2 receptor. *Nature* 503, 535–538. doi: 10.1038/nature12711
- Geleris, J., Sun, Y., Platt, J., Zucker, J., Baldwin, M., Hripcsak, G., et al. (2020). Observational study of hydroxychloroquine in hospitalized patients with Covid-19. *New Engl. J. Med.* 382, 2411–2418. doi: 10.1056/NEJMoa2012410
- Giuseppe, D. L., and Rossella, D. T. (2020). Coronavirus disease (SARS-CoV-2) in Italy: analysis of risk factors and proposed remedial measures. *Front. Med.* 7:140. doi: 10.3389/fmed.2020.00140
- Goossens, G. A. (2015). Flushing and locking of venous catheters: available evidence and evidence deficit. *Nurs. Res. Pract.* 2015:985686. doi: 10.1155/2015/985686
- Gordon, C. J., Tchesnokov, E. P., Feng, J. Y., Porter, D. P., and Götte, M. (2020). The antiviral compound remdesivir potently inhibits RNA-dependent RNA polymerase from Middle East respiratory syndrome coronavirus. *J. Biol. Chem.* 295, 4773–4779. doi: 10.1074/jbc.AC120.013056
- Güner, R., Hasanoglu, I., and Aktas, F. (2020). SARS-CoV-2: prevention and control measures in community. *Turk. J. Med. Sci.* 50, 571–577. doi: 10.3906/sag-2004-146
- Hodgson, J. (2020). The pandemic pipeline. *Nat. Biotechnol.* 38, 523–532. doi: 10.1038/d41587-020-00005-z
- Hong, K. H., Lee, S. W., Kim, T. S., Hee, J., Lee, J., Kim, S. Y., et al. (2020). Guidelines for laboratory diagnosis of coronavirus disease 2019 (SARS-CoV-2) in Korea. *Ann. Lab. Med.* 40, 351–360. doi: 10.3343/alm.2020.40.5.351
- Horby, P. (2020). Dexamethasone in hospitalized patients with Covid-19: preliminary report. *New Engl. J. Med.* doi: 10.1056/NEJMoa2021436
- Hotez, P. J., Corry, D. B., and Bottazzi, M. E. (2020). SARS-CoV-2 vaccine design: the Janus face of immune enhancement. *Nat. Rev. Immunol.* 20:347.
- Huang, C., Wang, Y., Li, X., Ren, L., Zhao, J., Hu, Y., et al. (2020). Clinical features of patients infected with 2019 novel coronavirus in Wuhan, China. *Lancet* 395, 497–506.
- Huang, D., Yu, H., Wang, T., Yang, H., Yao, R., and Liang, Z. (2020). Efficacy and safety of umifenovir for coronavirus disease 2019 (COVID-19): a systematic review and meta-analysis. *J. Med. Virol.* 2020:jmv.26256. doi: 10.1002/jmv.26256
- Jackson, L. A., Anderson, E. J., Roupheal, N. G., Roberts, P. C., Makhene, M., Coler, R. N., et al. (2020). An mRNA vaccine against SARS-CoV-2: preliminary report. *New Engl. J. Med.* doi: 10.1056/NEJMoa2022483
- Jeong, G. U., Song, H., Yoon, G. Y., Kim, D., and Kwon, Y.-C. (2020). Therapeutic strategies against COVID-19 and structural characterization of SARS-CoV-2: a review. *Front. Microbiol.* 11:1723. doi: 10.3389/fmicb.2020.01723
- Jiang, F., Deng, L., Zhang, L., Cai, Y., Cheung, C. W., and Xia, Z. (2020). Review of the clinical characteristics of Coronavirus disease 2019 (SARS-CoV-2). *J. Gen. Intern. Med.* 35, 1545–1549. doi: 10.1007/s11606-020-05762-w
- Jian-Min, J., Peng, B., Wei, H., Fei, W., Li, X. F., Shi, L., et al. (2020). Gender differences in patients with SARS-CoV-2: focus on severity and mortality. *Front. Public Health* 8:152. doi: 10.3389/fpubh.2020.00152
- Kamat, S., and Kumari, M. (2020). BCG against SARS-CoV-2: second youth of an old age vaccine? *Front. Pharmacol.* 11:1050. doi: 10.3389/fphar.2020.01050
- Keech, C., Albert, G., Cho, I., Robertson, A., Reed, P., Neal, S., et al. (2020). Phase 1-2 trial of a SARS-CoV-2 recombinant spike protein nanoparticle vaccine. *New Engl. J. Med.* 21:44. doi: 10.1056/NEJMoa2026920
- Khan, G. (2013). A novel coronavirus capable of lethal human infections: an emerging picture. *Virol. J.* 10:66. doi: 10.1186/1743-422X-10-66
- Kiemer, L., Lund, O., Brunak, S., and Blom, N. (2004). Blom Coronavirus 3CLproproteinase cleavage sites: possible relevance to SARS virus pathology. *BMC Bioinform.* 5:72. doi: 10.1186/1471-2105-5-72
- Kruse, R. L. (2020). Therapeutic strategies in an outbreak scenario to treat the novel coronavirus originating in Wuhan, China. *F1000Research* 9:72. doi: 10.12688/f1000research.22211.2
- Kumar, Y., Singh, H., and Patel, C. N. (2020). In silico prediction of potential inhibitors for the main protease of SARS-CoV-2 using molecular docking and dynamics simulation based drug-repurposing. *J. Infect. Public Health* 13, 1210–1223. doi: 10.1016/j.jiph.2020.06.016
- Lau, S. K., Li, K. S., Huang, Y., Shek, C. T., Tse, H., Wang, M., et al. (2010). Ecoepidemiology and complete genome comparison of different strains of severe acute respiratory syndrome-related Rhinolophus bat coronavirus in

- China reveal bats as a reservoir for acute, self-limiting infection that allows recombination events. *J. Virol.* 84, 2808–2819. doi: 10.1128/JVI.02219-09
- Lau, S. K., Li, K. S., Tsang, A. K., Lam, C. S., Ahmed, S., Chen, H., et al. (2013). Genetic characterization of Betacoronavirus lineage C viruses in bats reveals marked sequence divergence in the spike protein of pipistrellus bat Coronavirus HKU5 in Japanese pipistrelle: implications for the origin of the novel Middle East respiratory syndrome Coronavirus. *J. Virol.* 87, 8638–8650. doi: 10.1128/JVI.01055-13
- Letko, M., Marzi, A., and Munster, V. (2020). Functional assessment of cell entry and receptor usage for SARS-CoV-2 and another lineage B Betacoronaviruses. *Nat. Microbiol.* 5, 562–569. doi: 10.1038/s41564-020-0688-y
- Li, K., Wu, J., Wu, F., Guo, D., Chen, L., Fang, Z., et al. (2020). The clinical and chest CT features associated with severe and critical SARS-COV-2 pneumonia. *Invest. Radiol.* 55, 327–331. doi: 10.1097/RLL.0000000000000672
- Liu, B., Li, M., Zhou, Z., Guan, X., and Xiang, Y. (2020). Can we use interleukin-6 (IL-6) blockade for coronavirus disease 2019 (SARS-COV-2)-induced cytokine release syndrome (CRS)? *J. Autoimmun.* 111:102452. doi: 10.1016/j.jaut.2020.102452
- Liu, K., Chen, Y., Lin, R., and Han, K. (2020). Clinical features of SARS-COV-2 in elderly patients: a comparison with young and middle-aged patients. *J. Infect.* 80, e14–e18. doi: 10.1016/j.jinf.2020.03.005
- Liu, H., Liu, F., Li, J., Zhang, T., Wang, D., and Lan, W. (2020). Clinical and CT imaging features of the SARS-COV-2 pneumonia: Focus on pregnant women and children. *J. Infect.* 80, e7–e13. doi: 10.1016/j.jinf.2020.03.007
- Matthay, M. A., Zemans, R. L., Zimmerman, G. A., Arabi, Y. M., Beitler, J. R., Mercat, A., et al. (2019). Acute respiratory distress syndrome. *Nat. Rev. Dis. Prim.* 5:572. doi: 10.1038/s41572-019-0069-0
- Maurya, C. K., Misra, R., Sharma, P., Singh, N., Awasthi, H., Agrawal, R., et al. (2020). Novel stem cells and nucleic acid-based vaccine trials against viral outbreak: a systematic evaluation during COVID-2019 pandemic. *Indian J. Clin. Biochem.* 35, 397–409. doi: 10.1007/s12291-020-00907-4
- McBride, R., van Zyl, M., and Fielding, B. C. (2014). The coronavirus nucleocapsid is a multifunctional protein. *Viruses* 6, 2991–3018. doi: 10.3390/v6082991
- Meyerowitz, E. A., Vannier, A., Friesen, M., Schoenfeld, S., Gelfand, J. A., Callahan, M. V., et al. (2020). Rethinking the role of hydroxychloroquine in the treatment of SARS-COV-2. *FASEB J.* 34, 6027–6037. doi: 10.1096/fj.202000919
- Narayanan, K., Ramirez, S. I., Lokugamage, K. G., and Makino, S. (2015). Coronavirus nonstructural protein 1: common and distinct functions in the regulation of host and viral gene expression. *Virus Res.* 202, 89–100. doi: 10.1016/j.virusres.2014.11.019
- Ng, W. H., Liu, X., and Mahalingam, S. (2020). Development of vaccines for SARS-CoV-2. *F1000Research* 9:25998. doi: 10.12688/f1000research.25998
- Ojha, R., Gupta, N., Naik, B., Singh, S., Verma, V. K., Prusty, D., et al. (2020). High throughput and comprehensive approach to develop multi-epitope vaccine against minacious SARS-COV-2. *Eur. J. Pharmaceut. Sci.* 151:105375. doi: 10.1016/j.ejps.2020.105375
- Oke, J., and Heneghan, C. (2020). *Global Covid-19 Case Fatality Rates; Centre for Evidence-Based Medicine*. Oxford: Oxford University.
- Owusu, M., Annan, A., Corman, V. M., Larbi, R., Anti, P., Drexler, J. F., et al. (2014). Human coronaviruses associated with upper respiratory tract infections in three rural areas of Ghana. *PLoS One* 9:e99782. doi: 10.1371/journal.pone.0099782
- Pawelec, G., and Weng, N. P. (2020). Can an effective SARS-CoV-2 vaccine be developed for the older population? *Immun. Age* 17:8. doi: 10.1186/s12979-020-00180-2
- Puja, M., McAuley, D. F., Brown, M., Sanchez, E., Tattersall, R. S., and Manson, J. J. (2020). COVID-19: consider cytokine storm syndromes and immunosuppression. *Cell Stress* 395, 1033–1034. doi: 10.1016/S0140-6736(20)30628-0
- Rabaan, A. A., Al-Ahmed, S. H., Sah, R., Tiwari, R., Yatoo, M. I., Patel, S. K., et al. (2020). SARS-CoV-2/COVID-19 and advances in developing potential therapeutics and vaccines to counter this emerging pandemic. *Ann. Clin. Microbiol. Antimicrob.* 19:38. doi: 10.1186/s12941-020-0038
- Raoult, D., Zumla, A., Locatelli, F., Ippolito, G., and Kroemer, G. (2020). Coronavirus infections: epidemiological, clinical and immunological features and hypotheses. *Cell Stress* 4, 66–75. doi: 10.15696/cst2020.04.216
- Raza, S. S., and Khan, M. A. (2020). Mesenchymal stem cells: a new front emerge in COVID19 treatment. *Cytotherapy* doi: 10.1016/j.jcyt.2020.07.002 [Epub ahead of print].
- Ren, Z., Yan, L., Zhang, N., Guo, Y., Yang, C., Lou, Z., et al. (2020). The newly emerged SARS-Like coronavirus HCoV-EMC also has an “Achilles’ heel”: current effective inhibitor targeting a 3C-like protease. *Protein Cell* 4, 248–250. doi: 10.1007/s13238-013-2841-3
- Rothan, H. A., and Byrareddy, S. N. (2020). The epidemiology and pathogenesis of coronavirus disease (SARS-COV-2) outbreak. *J. Autoimmun.* 109:102433. doi: 10.1016/j.jaut.2020.102433
- Russell, C. D., Millar, J. E., and Baillie, J. K. (2020). Clinical evidence does not support corticosteroid treatment for 2019-nCoV lung injury. *Lancet* 395, 473–475.
- Sae-im, J. (2020). Bukwang to test its antiviral drug against Covid-19. *Korea Biomedical Rev.* Available online at: <http://www.koreabiomed.com/news/articleView.html?idxno=8010>
- Salazar, E., Perez, K. K., Ashraf, M., Chen, J., Castillo, B., Christensen, P. A., et al. (2020). Treatment of SARS-COV-2 patients with convalescent plasma. *Am. J. Pathol.* 323, 1582–1589. doi: 10.1016/j.ajpath.2020.05.014
- Sanche, S., Lin, Y. T., Xu, C., Romero-Severson, E., Hengartner, N., and Ke, R. (2020). High contagiousness and rapid spread of severe acute respiratory syndrome Coronavirus 2. *Emerg. Infect. Dis.* 26:282. doi: 10.3201/eid2607.200282
- Schoeman, D., and Fielding, B. C. (2019). Coronavirus envelope protein: current knowledge. *Virol. J.* 16:69. doi: 10.1186/s12985-019-1182-0
- Senanayake, S. L. (2020). Drug repurposing strategies for COVID-19. *Future Drug Discov.* 2:fdd-2020-0010. doi: 10.4155/fdd-2020-0010
- Sharpe, H. R., Gilbride, C., Allen, E., Belij-Rammerstorfer, S., Bissett, C., Ewer, K., et al. (2020). The early landscape of coronavirus disease 2019 vaccine development in the UK and rest of the world. *Immunology* 160, 223–232. doi: 10.1111/imm.13222
- Shen, L., Niu, J., Wang, C., Huang, B., Wang, W., Zhu, N., et al. (2019). High-throughput screening and identification of potent broad-spectrum inhibitors of Coronaviruses. *J. Virol.* 93:e0023-19. doi: 10.1128/JVI.00023-19
- Shih-Hwa, C., Pei Ching, C., Yanwen, L., Mong-Lien, W., Chian-Hsu, C., Yi-Ping, Y., et al. (2020). Highlight of immune pathogenic response and hematopathologic effect in SARS-CoV, MERS-CoV and SARS-Cov-2 infection. *Front. Immunol.* 11:1022. doi: 10.3389/fimmu.2020.01022
- Singh, D. D., Hawkins, R. D., Lahesmaa, R., and Tripathi, S. K. (2019). CRISPR/Cas9 guided genome and epigenome engineering and its therapeutic applications in immune mediated diseases. *Semin. Cell Dev. Biol.* 96, 32–43.
- Singhal, T. (2020). A review of Coronavirus Disease-2019 (SARS-COV-2). *Indian J. Pediatr.* 87, 281–286. doi: 10.1007/s12098-020-03263-6
- Smith, R. D. (2006). Responding to global infectious disease outbreaks: lessons from SARS on the role of risk perception, communication and management. *Soc. Sci. Med.* 63, 3113–3123. doi: 10.1016/j.socscimed.2006.08.004
- Smith, T. R. F., Patel, A., Ramos, S., Elwood, D., Zhu, X., Yan, J., et al. (2020). Immunogenicity of a DNA vaccine candidate for COVID-19. *Nat. Commun.* 11:2601. doi: 10.1038/s41467-020-16505-0
- Sodhi, M., and Etminan, M. (2020). Safety of ibuprofen in patients with SARS-COV-2: causal or confounded? *Chest* 158, 55–56. doi: 10.1016/j.chest.2020.03.040
- Streck, H. (2020). *Vorläufiges Ergebnis und Schlussfolgerungen der SARS-COV-2 Case-Cluster-Study (Gemeinde Gangelt)*. Available online at: https://www.land.nrw/sites/default/files/asset/document/zwischenenergebnis_covid19_case_study_gangelt_0.pdf?fbclid=IwAR2U147uWQOgf5SK6n1Cewm4UKRSN7dAIYhBX9irdAB6Zzy8klHYKdv80 (accessed April 13, 2020).
- Sutton, D., Fuchs, K., D’Alton, M., and Goffman, D. (2020). Universal screening for SARS-CoV-2 in Women admitted for delivery. *New Engl. J. Med.* 382, 2163–2164. doi: 10.1056/NEJMc2009316
- Tan, K. S., Lim, R. L., Liu, J., Ong, H. H., Tan, V. J., Lim, H. F., et al. (2020). Respiratory viral infections in exacerbation of chronic airway inflammatory diseases: novel mechanisms and insights from the upper airway epithelium. *Front. Cell Dev. Biol.* 8:99. doi: 10.3389/fcell.2020.00099
- Tan, L., Wang, Q., Zhang, D., Ding, J., Huang, Q., Tang, Y. Q., et al. (2020). Lymphopenia predicts disease severity of SARS-COV-2: a descriptive and predictive study. *Signal Transd. Target. Ther.* 5:33. doi: 10.1038/s41392-020-0148-4

- Thanh, L. T., Andreadakis, Z., Kumar, A., Gómez Román, R., Tollefsen, S., Saville, M., et al. (2020). The COVID-19 vaccine development landscape. *Nat. Rev. Drug Discov.* 19, 305–306. doi: 10.1038/d41573-020-00073-5
- Tian, S., Hu, W., Niu, L., Liu, H., Xu, H., and Xiao, S. Y. (2020). Pulmonary pathology of early-phase 2019 novel Coronavirus (SARS-CoV-2) pneumonia in two patients with lung cancer. *J. Thorac. Oncol.* 15, 700–704. doi: 10.1016/j.jtho.2020.02.010
- Udugama, B., Kadhiresan, P., Kozlowski, H. N., Malekjahani, A., Osborne, M., Li, V., et al. (2020). Diagnosing SARS-CoV-2: the disease and tools for detection. *ACS Nano* 14, 3822–3835. doi: 10.1021/acsnano.0c02624
- van Doremalen, N., Lambe, T., Spencer, A., Belij-Rammerstorfer, S., Purushotham, J. N., Port, J. R., et al. (2020). ChAdOx1 nCoV-19 vaccine prevents SARS-CoV-2 pneumonia in rhesus macaques. *bioRxiv* [Preprint]. doi: 10.1038/s41586-020-2608-y
- Verma, R., Sahu, R., Singh, D. D., and Egbo, T. E. (2019). A CRISPR/Cas9 based polymeric nanoparticles to treat/inhibit microbial infections. *Semin. Cell Dev. Biol.* 96, 44–52.
- Wang, F., Chen, C., Tan, W., Yang, K., and Yang, H. N. (2016). Structure of main protease from human Coronavirus NL63: insights for wide spectrum anti-Coronavirus drug design. *Sci. Rep.* 6:677. doi: 10.1038/srep22677
- Wang, F., Kream, R. M., and Stefano, G. B. (2020). An evidence based perspective on mRNA-SARS-CoV-2 vaccine development. *Med. Sci. Monit.* 26:e924700. doi: 10.12659/MSM.924700
- Wang, Y., Wang, Y., Chen, Y., and Qin, Q. (2020). Unique epidemiological and clinical features of the emerging 2019 novel coronavirus pneumonia (SARS-CoV-2) implicate special control measures. *J. Med. Virol.* 92, 568–576. doi: 10.1002/jmv.25748
- Ward, D. (2020). *Sampling Bias: Explaining Variations in Age Distributions of SARS-CoV-2 Cases*. Bern: WardEnvironment.
- WHO (2020). *Ward Environment WHO Director-General's Opening Remarks at the Media Briefing on SARS-CoV-2 - 11 March 2020*. Technical Report.
- Worldwide Sars-Cov-2 Statistics (2020). Available online at: <https://www.who.int/emergencies/diseases/novel-coronavirus-2019/situation-reports> (accessed July 4, 2020).
- Wu, D., Koganti, R., Lambe, U. P., Yadavalli, T., Nandi, S. S., and Shukla, D. (2020). Vaccines and therapies in development for SARS-CoV-2 infections. *J. Clin. Med.* 9:1885. doi: 10.3390/jcm9061885
- Wu, P., Hao, X., Lau, E., Wong, J. Y., Leung, K., Wu, J. T., et al. (2020). Real-time tentative assessment of the epidemiological characteristics of novel coronavirus infections in Wuhan, China, as at 22 January 2020. *Eur. Commun. Dis. Bull.* 25:2000044. doi: 10.2807/1560-7917.ES.2020.25.3.2000044
- Wu, R., Wang, L., Kuo, H. D., Shannar, A., Peter, R., Chou, P. J., et al. (2020). An update on current therapeutic drugs treating SARS-CoV-2. *Curr. Pharmacol. Rep.* 11, 1–15. doi: 10.1007/s40495-020-00216-7
- Xu, H., Zhong, L., Deng, J., Peng, J., Dan, H., Zeng, X., et al. (2020). High expression of ACE2 receptor of 2019-nCoV on the epithelial cells of oral mucosa. *Intern. J. Oral Sci.* 12:8. doi: 10.1038/s41368-020-0074-x
- Xu, X., Han, M., Li, T., Sun, W., Wang, D., Fu, B., et al. (2020). Effective treatment of severe SARS-CoV-2 patients with tocilizumab. *Proc. Natl. Acad. Sci. U.S.A.* 2020:202005615. doi: 10.1073/pnas.2005615117
- Xue, X., Yu, H., Yang, H., Xue, F., Wu, Z., Shen, W., et al. (2008). Structures of two Coronavirus main proteases: implications for substrate binding and antiviral drug design. *J. Virol.* 82, 2515–2527. doi: 10.1128/jvi.02114-07
- Yan, L., Zhang, H.-T., Gonçalves, J., Xiao, Y., Wang, M., Guo, Y., et al. (2020). Prediction of criticality in patients with severe Covid-19 infection using three clinical features: a machine learning-based prognostic model with clinical data in Wuhan. *medRxiv* [Preprint]. doi: 10.1101/2020.02.27.20028027
- Yang, H., Yang, M., Ding, Y., Liu, Y., Lou, Z., Zhou, Z., et al. (2003). The crystal structures of severe acute respiratory syndrome virus main protease and its complex with an inhibitor. *Proc. Natl. Acad. Sci. U.S.A.* 100, 13190–13195. doi: 10.1073/pnas.1835675100
- Yazdany, J., and Kim, A. (2020). Use of Hydroxychloroquine and Chloroquine during the SARS-CoV-2 pandemic: what every clinician should know. *Ann. Intern. Med.* 172, 754–755. doi: 10.7326/M20-1334
- Ye, Q., Wang, B., and Mao, J. (2020). The pathogenesis and treatment of the 'Cytokine Storm' in SARS-CoV-2. *J. Infect.* 80, 607–613. doi: 10.1016/j.jinf.2020.03.037
- Zaki, A. M., Sander, V. B., Theo, M. B., Albert, D. M. E. O., and Ron, A. M. F. (2012). Isolation of a novel coronavirus from a man with pneumonia in Saudi Arabia. *N. Engl. J. Med.* 367, 1814–1820. doi: 10.1056/NEJMoa1211721
- Zhang, H.-T., Zhang, J.-S., Zhang, H.-H., Nan, Y.-D., Zhao, Y., Fu, E.-Q., et al. (2020). Automated detection and quantification of COVID-19 pneumonia: CT imaging analysis by a deep learning-based software. *Eur. J. Nuclear Med. Mol. Imag.* 47:9531. doi: 10.1007/s00259-020-04953-1
- Zhang, J. J., Dong, X., Cao, Y. Y., Ya-Dong, Y., Yi-Bin, Y., You-Qin, Y., et al. (2020). Clinical characteristics of 140 patients infected by SARS-CoV-2 in Wuhan, China. *Allergy* 75, 1730–1741.
- Zhang, N., Li, C., Hu, Y., Li, K., Liang, J., Wang, L., et al. (2020). Current development of SARS-CoV-2 diagnostics, vaccines and therapeutics. *Microb. Infect.* 22, 231–235. doi: 10.1016/j.micinf.2020.05.001
- Zhang, Q., Wang, Y., Qi, C., Shen, L., and Li, J. (2020). Clinical trial analysis of 2019-nCoV therapy registered in China. *J. Med. Virol.* 92, 540–545. doi: 10.1002/jmv.25733
- Zhang, L., Lin, D., Sun, X., Curth, U., Drosten, C., Sauerhering, L., et al. (2020). Crystal structure of SARS-CoV-2 main protease provides a basis for design of improved α -ketoamide inhibitors. *Science* 368, 409–412. doi: 10.1126/science.abb3405
- Zhang, Z., Wang, S., Tu, X., Peng, X., Huang, Y., Wang, L., et al. (2020). A comparative study on the time to achieve negative nucleic acid testing and hospital stays between danoprevir and lopinavir/ritonavir in the treatment of patients with COVID-19. *J. Med. Virol.* 92, 2631–2636. doi: 10.1002/jmv.26141
- Zhao, M. (2020). Cytokine storm and immunomodulatory therapy in SARS-CoV-2: Role of chloroquine and anti-IL-6 monoclonal antibodies. *Intern. J. Antimicrob. Agents* 55:105982. doi: 10.1016/j.ijantimicag.2020.105982
- Zhou, M., Zhang, X., and Qu, J. (2020). Coronavirus disease 2019 (SARS-CoV-2): a clinical update. *Front. Med.* 14, 126–135. doi: 10.1007/s11684-020-0767-8
- Zhu, F.-C., Guan, X.-H., Li, Y.-H., Huang, J.-Y., Jiang, T., Hou, L.-H., et al. (2020). Immunogenicity and safety of a recombinant adenovirus type-5-vectored COVID-19 vaccine in healthy adults aged 18 years or older: a randomised, double-blind, placebo-controlled, phase 2 trial. *Lancet* 396, 479–488. doi: 10.1016/s0140-6736(20)31605-6
- Zhuobing, L., Li, D., Gongqi, C., Chaohui, Z., Li, X., Luo, W., et al. (2020). Clinical time features and chest imaging of 85 patients with SARS-CoV-2 in Zhuhai, China. *Front. Med.* 7:209. doi: 10.3389/fmed.2020.00209

Conflict of Interest: The authors declare that the research was conducted in the absence of any commercial or financial relationships that could be construed as a potential conflict of interest.

Copyright © 2020 Singh, Han, Choi and Yadav. This is an open-access article distributed under the terms of the Creative Commons Attribution License (CC BY). The use, distribution or reproduction in other forums is permitted, provided the original author(s) and the copyright owner(s) are credited and that the original publication in this journal is cited, in accordance with accepted academic practice. No use, distribution or reproduction is permitted which does not comply with these terms.



Exploring Additional Valuable Information From Single-Cell RNA-Seq Data

Yunjin Li¹, Qiyue Xu¹, Duoqiao Wu² and Geng Chen^{1*}

¹ Center for Bioinformatics and Computational Biology, Shanghai Key Laboratory of Regulatory Biology, Institute of Biomedical Sciences, School of Life Sciences, East China Normal University, Shanghai, China, ² Institute of Clinical Science, Zhongshan Hospital, Fudan University, Shanghai, China

OPEN ACCESS

Edited by:

Cornelia Braicu,
Iuliu Hațieganu University of Medicine
and Pharmacy, Romania

Reviewed by:

Guibo Li,
Beijing Genomics Institute (BGI),
China

Vincent Gardeux,
École Polytechnique Fédérale
de Lausanne, Switzerland
Huanming Yang,
Beijing Genomics Institute (BGI),
China

*Correspondence:

Geng Chen
gchen@bio.ecnu.edu.cn;
chengeng6666@gmail.com

Specialty section:

This article was submitted to
Molecular Medicine,
a section of the journal
Frontiers in Cell and Developmental
Biology

Received: 04 September 2020

Accepted: 26 October 2020

Published: 01 December 2020

Citation:

Li Y, Xu Q, Wu D and Chen G
(2020) Exploring Additional Valuable
Information From Single-Cell
RNA-Seq Data.
Front. Cell Dev. Biol. 8:593007.
doi: 10.3389/fcell.2020.593007

Single-cell RNA-seq (scRNA-seq) technologies are broadly applied to dissect the cellular heterogeneity and expression dynamics, providing unprecedented insights into single-cell biology. Most of the scRNA-seq studies mainly focused on the dissection of cell types/states, developmental trajectory, gene regulatory network, and alternative splicing. However, besides these routine analyses, many other valuable scRNA-seq investigations can be conducted. Here, we first review cell-to-cell communication exploration, RNA velocity inference, identification of large-scale copy number variations and single nucleotide changes, and chromatin accessibility prediction based on single-cell transcriptomics data. Next, we discuss the identification of novel genes/transcripts through transcriptome reconstruction approaches, as well as the profiling of long non-coding RNAs and circular RNAs. Additionally, we survey the integration of single-cell and bulk RNA-seq datasets for deconvoluting the cell composition of large-scale bulk samples and linking single-cell signatures to patient outcomes. These additional analyses could largely facilitate corresponding basic science and clinical applications.

Keywords: single-cell RNA-seq, cell-to-cell communication, RNA velocity, copy number variations, non-coding RNAs, cell-type deconvolution

INTRODUCTION

In recent years, single-cell RNA-seq (scRNA-seq) technologies and related bioinformatics methods have been developing and innovating rapidly, which significantly revolutionized our understanding of the expression heterogeneity and transcriptome dynamics of individual cells for diverse species including human (Quadrato et al., 2017), mouse (Brown et al., 2016), zebrafish (Wagner et al., 2018), and *Drosophila* (Karaiskos et al., 2017). The data generated by scRNA-seq can be generally grouped into read-based and unique molecular identifier (UMI)-based, depending on the full-length transcript sequencing [e.g., Smart-seq2 (Picelli et al., 2014)] or 3'/5'-end capturing [such as 10× Chromium (Zheng et al., 2017), and Drop-seq (Macosko et al., 2015)] protocols used (Chen et al., 2019). A series of preprocessing steps are required for overcoming the high noise of raw scRNA-seq data to obtain robust results from downstream analysis. Quality control (QC) of scRNA-seq data is important to remove the low-quality cells resulting from RNA degradation, break of the cell membrane, or multicells to avoid misinterpretation of downstream results, which have been reviewed recently (Luecken and Theis, 2019). Then normalization is needed to eliminate the influence of technical effects on molecular counts (e.g., sequencing depth) to make gene

expression comparable between cells. For the two main types of data generated from the full-length transcript and 3'/5'-end enrichment scRNA-seq protocols, distinct normalization methods are needed. It is recommended to take gene length into account for full-length transcript scRNA-seq data (such as the common approach of TPM normalization), while disparate methods like *scrna* (Lun et al., 2016) are required for normalizing 3'/5'-tag scRNA-seq data (Luecken and Theis, 2019). However, normalization cannot directly address the biases of technical noises (e.g., batch effect and dropout) and biological covariates (such as cell cycle); further data processing like batch effect correction and imputation may be needed to mitigate such effects according to the data properties and research goals.

After data preprocessing, a range of common analyses can be conducted, like cell type/state identification and annotation, trajectory inference, alternative splicing detection, gene regulatory network (GRN) reconstruction, which has been reviewed by us and other colleagues (Chen et al., 2019; Luecken and Theis, 2019). Because scRNA-seq data usually involve many cells and thousands of genes, feature selection and dimensionality reduction methods are needed to reduce the dimensionality of high-dimensional datasets to lighten the computational burden of downstream analysis (Andrews and Hemberg, 2018). Generally, 500–5,000 highly variable genes are often used depending on the data complexity in feature selection approaches (Yip et al., 2019). Linear [e.g., principal component analysis (PCA)] or non-linear [such as t-distributed stochastic neighbor embedding [t-SNE (van der Maaten and Hinton, 2008)]] and uniform approximation and projection (UMAP) (Diaz-Papkovich et al., 2019) dimensionality reduction methods can be used to further reduce the data dimension and visualize the data in two or three dimensions (Moon et al., 2018).

Based on the data with reduced dimensions, the cell clusters are typically identified in single-cell analysis. Methods for clustering (such as *k*-means) or community detection (e.g., *K*-nearest neighbor graph) are often applied to determine the clusters according to the expression similarity of genes (Duò et al., 2018; Kiselev et al., 2019). Once the clusters of single cells are determined, marker genes can be identified through differential expression (DE) analysis to annotate the clusters with meaningful biological insight. Moreover, for the scRNA-seq data generated from full-length transcript sequencing protocols, the alternative splicing changes between distinct cell clusters can be further investigated as we summarized previously (Chen et al., 2019). On the other hand, for the single-cell datasets involving developmental or differentiation process, trajectory inference methods can be utilized to infer the order of cells along developmental trajectories. Saelens et al. (2019) benchmarked dozens of trajectory inference tools and revealed that these methods are complementary with variable performances depending on the dataset dimensions and trajectory topology. Additionally, cellular differentiation and cell state transition processes are controlled by the underlying GRNs. An increasing number of approaches have been developed to infer the GRNs from scRNA-seq data generally based on the assumption that the genes with similar expression profiles could be regulated by a common transcription factor [such as SCENIC

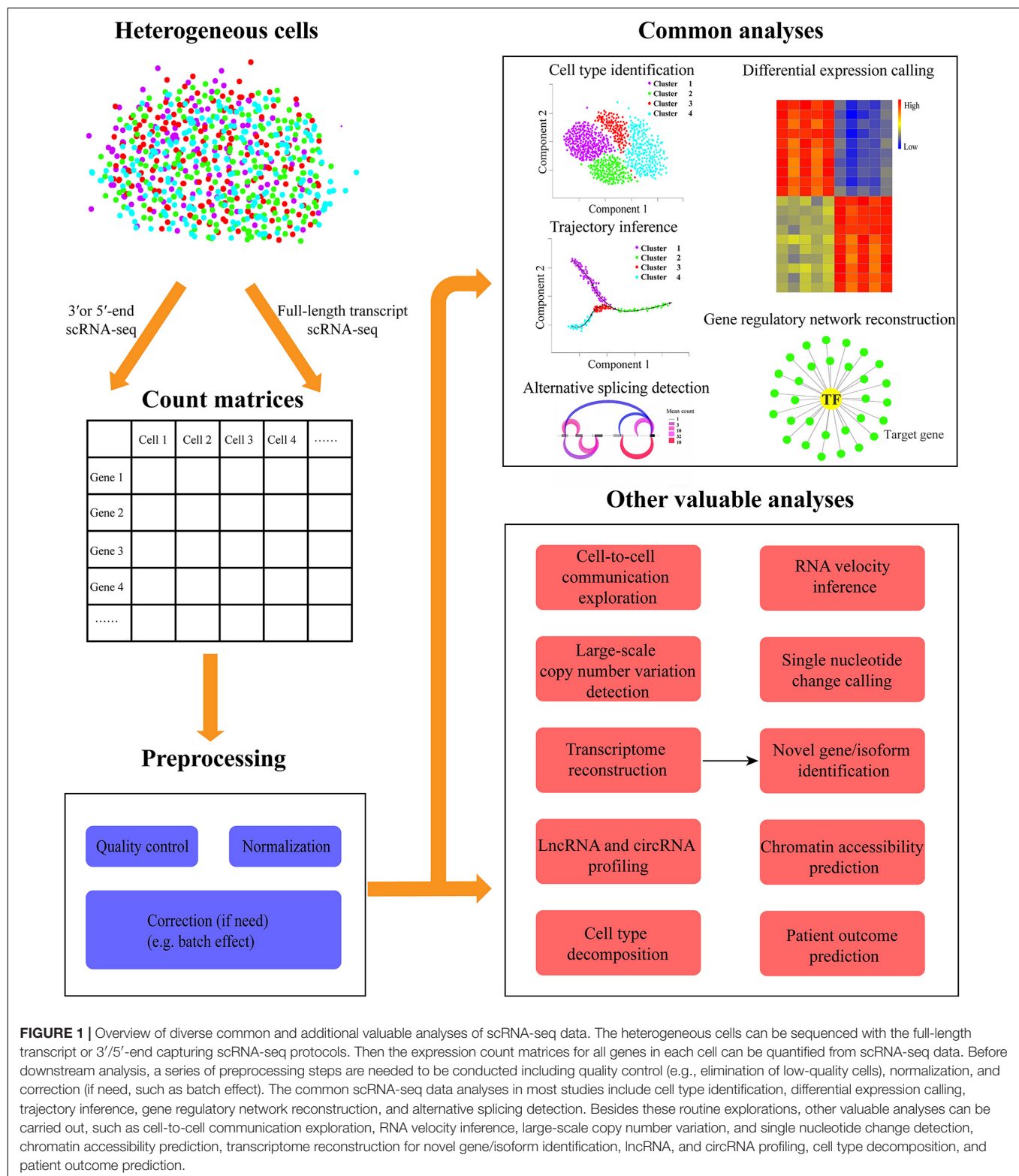
(Aibar et al., 2017)], but more efforts are needed to improve the accuracy of these analytical approaches (Chen and Mar, 2018; Fiers et al., 2018; Pratapa et al., 2020).

However, besides those common analyses, many other valuable explorations can be conducted to gain additional insights into scRNA-seq data (Figure 1). In this review, we first describe the progress and related methods for cell-cell communication network inference, RNA velocity analysis, interrogation of chromosomal-scale copy number variations (CNVs) and single nucleotide variations, as well as novel gene/isoform identification. Then we summarize the integration of single-cell and bulk RNA-seq data to cost-effectively analyze a large sample size. In particular, we discuss their implications and potential challenges as well as future directions.

CELL-TO-CELL COMMUNICATION NETWORK INFERENCE

Cells often do not function independently but can communicate with each other and change their behaviors by transmitting and receiving signals within their environment. In multicellular organisms, cell signaling is critical for joining different cell types together to form tissues (e.g., brain, lung, muscle, and liver). Specifically, autocrine (interact with the same or similar cells) and paracrine (communicate with nearby cells) signaling networks within and across cell types play fundamental roles for cells working together to coordinate diverse organismal processes. Moreover, an abundance of cell fate decisions are made to react to extracellular signals from the interactions between secreted ligands and cell-surface receptors in the local environment (Watabe and Miyazono, 2009). Especially for cancers, the tumor microenvironment is typically composed of various cell types (including malignant, immune, and stromal cells). Understanding the cell-to-cell communication/interaction network among distinct cell populations can facilitate the elucidation of underlying mechanisms for tumorigenesis, tumor progression, metastasis, therapy resistance, and immune infiltration (Hanahan and Weinberg, 2011). Defects in cell-to-cell interaction have been demonstrated to be associated with different cancers (Haass et al., 2004), autoimmune (Gorelik and Flavell, 2000), and metabolic diseases (Hotamisligil, 2006).

ScRNA-seq enables expression quantification of transcripts encoding ligands and their cognate receptors in each cell, which provides unprecedented opportunities for decoding the diversity, complexity, and dynamics of intercellular communication networks (Figure 2). An increasing number of studies investigated the cell-to-cell communications between distinct cell populations and uncovered meaningful biological insights. For example, interlineage communications mediated by ligand-receptor complexes among single cells can regulate liver bud development (Camp et al., 2017), and functionally important ligand-receptor interactions associated with cancer metastasis were recently identified in head and neck squamous cell carcinoma (Puram et al., 2017). We also detected a set of intercellular communications between macrophages and cancer stem-like cells (CSCs) in glioma that the expression levels



of involved ligands and receptors are significantly correlated with the survival of patients (Yuan et al., 2019). Moreover, lung basophils were found to widely communicate with both immune and non-immune compartments (Cohen et al., 2018),

and cell-cell interactions were useful in identifying the cell types of human placenta (Pavlicev et al., 2017). Interaction network analysis between distinct cell types within the melanoma microenvironment highlighted that tumor cell composition is

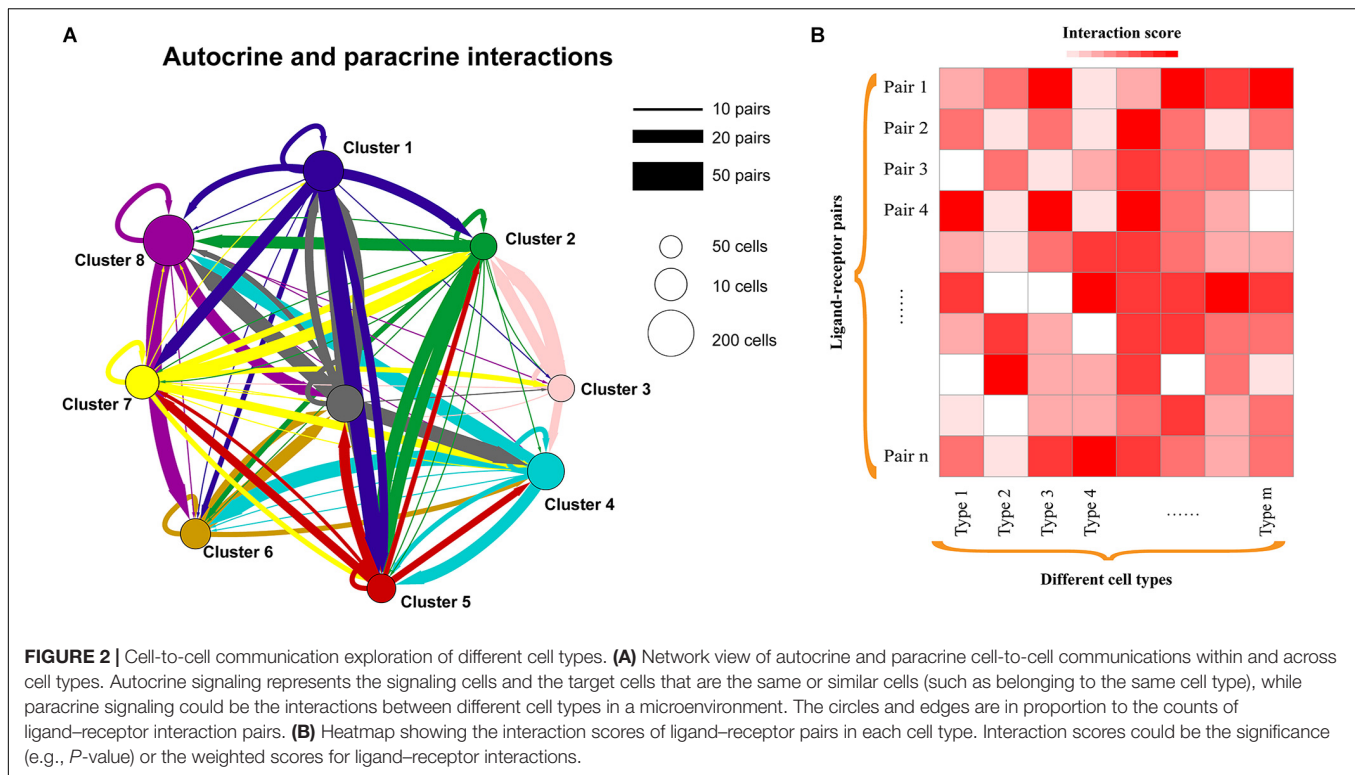


FIGURE 2 | Cell-to-cell communication exploration of different cell types. **(A)** Network view of autocrine and paracrine cell-to-cell communications within and across cell types. Autocrine signaling represents the signaling cells and the target cells that are the same or similar cells (such as belonging to the same cell type), while paracrine signaling could be the interactions between different cell types in a microenvironment. The circles and edges are in proportion to the counts of ligand-receptor interaction pairs. **(B)** Heatmap showing the interaction scores of ligand-receptor pairs in each cell type. Interaction scores could be the significance (e.g., *P*-value) or the weighted scores for ligand-receptor interactions.

critical for diagnostic and therapeutic strategies (Tirosh et al., 2016a). Additionally, extensive intercellular communication networks were observed between diverse mouse heart cell types, which contributed to the transcriptional program of sexual dimorphism (Skelly et al., 2018).

To identify the potential interactions within or between cell subpopulations from scRNA-seq data, an increasing number of computational methods have been developed based on the expression abundance of ligand and receptor pairs (Table 1). For instance, Kumar et al. (2018) proposed a computational approach to characterize cell-cell communications across the cell types in a microenvironment (such as tumor ecosystem) by scoring the ligand-receptor interactions between two cell types as the product of average expression of ligands and receptors in corresponding cell types. PyMINer integrates ligand and receptor information, protein-protein interactions as well as pathway analyses to build the autocrine-paracrine signaling networks (Tyler et al., 2019). scTensor defines the cell-cell interactions as directed hypergraphs (nodes are cell types, and edges represent ligand-receptor pairs) and can infer many-to-many interactions with tensor decomposition (Tsuyuzaki et al., 2019). iTALK identifies the intercellular crosstalk signals based on curated ligand-receptor pairs and can visualize the results in different plot formats like Circos, network, and errorbar (Wang Y. et al., 2019). Moreover, CellPhoneDB provides a repository of curated receptors, ligands, and their interactions, and can allow users to search particular ligand/receptor or predict enriched cellular interactions with inquired scRNA-seq data efficiently (Efremova et al., 2020). CellChat quantitatively infers intercellular communication networks using mass action models,

which also enables the visualization of cellular interactions (Jin et al., 2020a). Additionally, SingleCellSignalR allows the assessment of the confidence of predicted ligand-receptor (Cabello-Aguilar et al., 2020), while NicheNet can enable a functional understanding of cell-cell communications by providing the information on how ligand-receptor interactions influence the target gene expression (Browaeys et al., 2020). However, the study for systematic performance evaluation of these methods is currently lacking. Moreover, the available approaches for inferring cell-cell interactions are generally based on the known and/or curated ligand-receptor pairs; the interactions mediated by unknown ligand-receptor pairs will be missed. When interpreting the resulting cell-cell communications between cell types, especially the number of interactions, it would be better to consider the missing interactions. Therefore, dissecting the cellular communications in health and disease states will largely benefit the elucidation of the underlying molecular mechanisms.

RECONSTRUCTION OF SPATIAL CELLULAR COMMUNICATIONS AND GENE EXPRESSION

Additionally, the spatial organization of cells is closely associated with diverse cell functions and behaviors including cell-cell interactions, but such information is usually missing from scRNA-seq data as the cells are needed to be dissociated before sequencing. Interestingly, novoSpaRc was recently developed to enable *de novo* spatial reconstruction of gene expression using

TABLE 1 | Computational approaches for additional analyses of scRNA-seq data.

Categories	Suitable scRNA-seq protocols	Tools	URL	References
Cell to cell communication	Full-length transcript or 3'/5'-tag sequencing	PyMINER	https://bitbucket.org/scotttyler892/pyminer_release	Tyler et al., 2019
		scTensor	https://rdrr.io/bioc/scTensor/	Tsuyuzaki et al., 2019
		iTALK	https://github.com/Coolgenome/iTALK	Wang Y. et al., 2019
RNA velocity	Full-length transcript or 3'/5'-tag sequencing	CellPhoneDB	https://github.com/Teichlab/cellphonedb	Efremova et al., 2020
		velocity	https://github.com/velocyto-team/velocyto.R	La Manno et al., 2018
		scVelo	https://github.com/theislab/scvelo	Bergen et al., 2019
Copy number variation	Full-length transcript or 3'/5'-tag sequencing	inferCNV	https://github.com/broadinstitute/inferCNV	Patel et al., 2014
		HoneyBADGER	https://github.com/JEFworks/HoneyBADGER	Fan et al., 2018
Chromatin accessibility	Full-length transcript sequencing or 3'/5'-tag sequencing	BIRD	https://github.com/WeiqiangZhou/BIRD	Zhou et al., 2017
Single nucleotide variants	Full-length transcript sequencing	SAMtools	http://samtools.sourceforge.net/	Li, 2011
		Strelka2	https://github.com/Illumina/strelka	Kim et al., 2018
		FreeBayes	https://github.com/ekg/freebayes	Garrison and Marth, 2012
RNA editing	Full-length transcript sequencing	GIREFI	https://github.com/zhqjingit/giremi	Zhang and Xiao, 2015
		REDIttools	https://github.com/BioinfoUNIBA/REDIttools	Picardi and Pesole, 2013
Transcriptome reconstruction	Full-length transcript sequencing	TransComb (genome-guided)	https://zenodo.org/record/61994#.XiEfaOgzaUk	Liu J. T. et al., 2016
		StringTie (genome-guided and <i>de novo</i>)	https://ccb.jhu.edu/software/stringtie/	Pertea et al., 2015
		Cufflinks (genome-guided)	http://cole-trapnell-lab.github.io/cufflinks/	Trapnell et al., 2010
		Trinity (<i>de novo</i>)	https://github.com/trinityrnaseq/trinityrnaseq/wiki	Grabherr et al., 2011
		Trans-ABYSS (<i>de novo</i>)	https://github.com/bcgsc/transabyss	Robertson et al., 2010
		rnaSPAdes (<i>de novo</i>)	http://cab.spbu.ru/software/rnaspades/	Bushmanova et al., 2019
Coding potential assessment	Full-length transcript sequencing	CPAT	http://rna-cpat.sourceforge.net/	Wang et al., 2013
		LncRNA-ID	https://github.com/zhangy72/LncRNA-ID	Achawanantakun et al., 2015
Circular RNA identification	Total RNA (poly (A+) and poly (A-) RNAs) sequencing	LGC	http://bigd.big.ac.cn/biocode/tools/BT000004	Wang G. Y. et al., 2019
		find_circ2	https://github.com/rajewsky-lab/find_circ2	Memczak et al., 2013
Cell composition deconvolution	Full-length transcript or 3'/5'-tag sequencing	CircExplorer2	https://circexplorer2.readthedocs.io/en/latest/	Zhang et al., 2016
		CIRI2	https://sourceforge.net/projects/ciri/	Gao et al., 2018
		CMP	https://cran.r-project.org/web/packages/scBio/index.html	Frishberg et al., 2019
Survival analysis	Full-length transcript or 3'/5'-tag sequencing	MuSiC	https://github.com/xuranw/MuSiC	Wang X. R. et al., 2019
		DWLS	https://bitbucket.org/yuanlab/dwls	Tsoucas et al., 2019
		CIBERSORTx	https://cibersortx.stanford.edu/	Newman et al., 2019
		Cox regression	https://github.com/therneau/survival	Li, 2003

scRNA-seq data alone (Nitzan et al., 2019). Specifically, CSOmap cannot only predict the cellular interactions but also can infer the cell spatial organizations *de novo* from single-cell transcriptomic data (Ren et al., 2020). Furthermore, the sequencing-based or image-based spatial technologies that can preserve the spatial coordinates of cells have achieved great progress (Mayr et al.,

2019). Integrative analysis of the spatial and scRNA-seq data may enable us to gain novel insights into cell–cell communications by constructing the spatial expression patterns of signaling ligands and receptors using transfer learning or deep learning approaches (Efremova and Teichmann, 2020). For instance, SpaOTsc can allow the inference of spatial gene expression patterns and spatial

cell–cell communications by incorporating scRNA-seq and spatial data (Cang and Nie, 2020). With the innovation of scRNA-seq and spatial transcriptomics as well as the computational algorithms, the accuracy of intercellular communication network inference will be improved as well. Specifically, such analysis may shed light on the signaling mechanisms of cellular behaviors and responses under various conditions like tumor progression, development, or differentiation.

IDENTIFICATION OF LARGE-SCALE COPY NUMBER VARIATIONS

Besides cellular communication detection, scRNA-seq data can be used to identify different types of genomic variations. Intratumoral heterogeneity is a ubiquitous feature for various cancer types, which contributes to tumor progression and therapy failure (Kreso and Dick, 2014). One of the well-studied sources of intratumoral heterogeneity is genetic variation, such as single nucleotide variations and CNVs that are the gains or losses of genomic sequences larger than one kilobase in size (Vogelstein et al., 2013). CNVs play an essential role in generating both physiological and pathological phenotypes through altering corresponding gene transcription or disrupting neighboring or distant non-coding regulatory regions; some of them could have pathogenic roles in common and rare cancers (Shlien and Malkin, 2009).

As large-scale CNVs may cause the gain or loss of many genes, they can result in the upregulation or downregulation of the genes in the affected regions. It has been shown that scRNA-seq data can provide informative large-scale CNV evidence for corresponding cells (**Figure 3A**). For instance, Patel et al. (2014) revealed coherent chromosomal-scale CNV pattern in glioblastoma by averaging relative expression levels of genes over large chromosomal regions and comparing with a set of reference normal cells using their method of inferCNV. With a similar approach, somatic large-scale CNVs were examined in metastatic melanoma (Tirosh et al., 2016a), oligodendroglioma (Tirosh et al., 2016b), as well as head and neck cancer (Puram et al., 2017) at single-cell resolution, which allowed researchers to effectively distinguish malignant cells from non-malignant ones. Recently, another computational method that integrated the hidden Markov model with a Bayesian approach, called HoneyBADGER, has also been developed for identifying the CNVs and loss of heterozygosity in single cells based on the allele and expression information inferred from scRNA-seq data (Fan et al., 2018) (**Table 1**). Since genomic instability is a hallmark of diverse cancers (Negrini et al., 2010; Ferguson et al., 2015), detecting the somatic large-scale CNVs in single cells could discriminate tumor cells from normal ones and gain insights into their roles in tumorigenesis. However, attention should be paid to the sparsity and noise of scRNA-seq data because currently available scRNA-seq approaches are generally with high-dropout property, which may result in false positives and influence the CNV detection. Collectively, scRNA-seq provides an alternative and cost-effective way for exploring large-scale CNVs in individual cells. It is valuable for unraveling the

evolutionary complexity of tumors and understanding cancer development and progression.

ANALYSIS OF SINGLE NUCLEOTIDE VARIANTS AND RNA EDITING

In addition to CNV detection, single nucleotide variants (SNVs) and RNA editing events could also be inferred from single-cell transcriptomic data. SNVs are the most prevalent type of genetic variation and are closely associated with diverse normal and disease phenotypes. The influences of SNVs could manifest on gene expression by *cis* and/or *trans* effects (Bryois et al., 2014), and a multitude of SNVs have been linked to tumor evolution (Navin et al., 2011). Importantly, SNVs in progenitors could be inherited by all the daughter cells during DNA replication, thus systematic SNV calling in single cells is one promising strategy for delineating cellular heterogeneity and phylogenetic relationships, especially for cancer evolution (Navin et al., 2010; Abbosh et al., 2017; Ju et al., 2017; Martincorena et al., 2017). Although single-cell exome sequencing or whole-genome sequencing technologies can be used to interrogate SNVs, such approaches could introduce substantial error rates due to inherent technical limitations (Xu et al., 2012; Zafar et al., 2016), and they are highly expensive for sequencing a large number of cells. By contrast, scRNA-seq is more affordable, and the SNVs detected from single-cell transcriptomic data could be interesting since they are expressed, and their functions are easier to elucidate. A range of studies have revealed intriguing findings by exploring SNVs from scRNA-seq data using the tools originally developed for bulk sequencing data (Tirosh et al., 2016b; Enge et al., 2017; Fan et al., 2018; Poirion et al., 2018; Ding et al., 2019). For example, Enge et al. (2017) gained insights into aging-related genetic and transcriptional processes of the human pancreas by analyzing the somatic mutation patterns with single-cell transcriptomic data. A linear modeling framework, SSRGE, was recently proposed to detect the effective and expressed SNVs that are associated with gene expression from scRNA-seq data, which could facilitate the subpopulation identification and genotype–phenotype relationship determination (Poirion et al., 2018). Moreover, Ding et al. (2019) developed a method for trajectory inference based on the SNPs inferred from scRNA-seq data.

Currently, few tools were specially designed for SNV calling based on single-cell transcriptomic data. However, Liu et al. (2019) systematically evaluated the performance of traditional variant callers on scRNA-seq datasets and recommended SAMtools (Li, 2011), Strelka2 (Kim et al., 2018), and FreeBayes (Garrison and Marth, 2012) to call SNVs for the data with low supporting reads, with sufficient read depths, and with high variant allele frequencies, respectively (**Table 1**). SAMtools calls the SNVs directly based on the sequencing data with a statistic model, while Strelka2 employs a mixture model to alleviate the effects of context-specific variation, and FreeBayes uses a Bayesian statistical framework to model multiallelic loci. With these tools, the SNVs in each cell can be predicted by treating each cell as a sample like bulk data. Notably, low read depths that

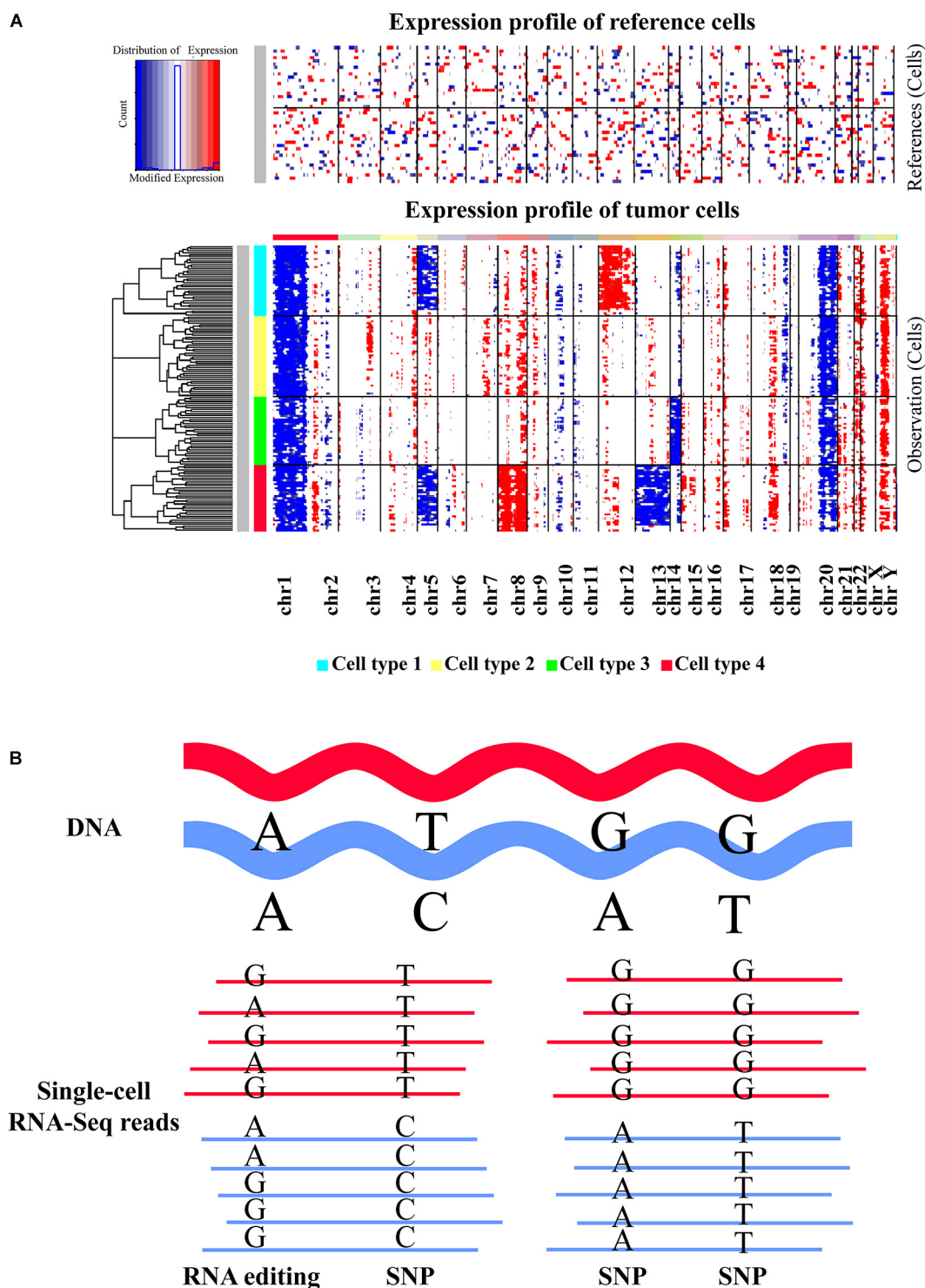


FIGURE 3 | Inference of large-scale copy number alterations and single nucleotide changes based on scRNA-seq data. **(A)** Representative heatmap displaying the large-scale copy number variations (CNVs) identified in different cell types with scRNA-seq data. Top panel shows that no significant large-scale CNVs were identified in reference normal cells, whereas chromosomal-scale deletions (blue) and gains (red) were observed for several chromosomes in different cell subtypes of tumor cells (second panel). The heatmap was created by inferCNV. **(B)** Graphic view of single nucleotide variations and RNA editing events. The reads of scRNA-seq data generated from full-length transcript sequencing protocols are mapped to the reference genome first. Then specific SNV calling tools or RNA-editing detection approaches can be applied to determine the SNVs or RNA-editing events based on the alignment result. Both SNV and RNA editing identifications are mainly suitable for the scRNA-seq methods that can generate full-length transcripts. Moreover, sequencing depth could be an important factor influencing the detection accuracy.

resulted from the biologically low expressions and/or technical bias (e.g., dropout events) could reduce the sensitivity of SNV detection. Therefore, the innovation of scRNA-seq strategies to minimize the dropout events will greatly improve the accuracy of SNV inference (Liu et al., 2019). Moreover, novel SNV calling methods that are specifically designed for scRNA-seq are also crucial for correcting the technical bias and increase the sensitivity and specificity of variant calling. Overall, detecting SNVs from single-cell transcriptomic data could provide another layer of cellular heterogeneity among single cells besides gene expression (**Figure 3B**), which could be useful for lineage tracing and subpopulation identification as well as genotype–phenotype linkage inference (Poirion et al., 2018; Tang, 2020).

Unlike genomic SNVs, RNA editing is a posttranscriptional process that made nucleotide changes on RNA sequences, and adenosine-to-inosine (A-to-I) editing is the most common type in general (Nishikura, 2010) (**Figure 3B**). RNA editing has been considered as a crucial mechanism for increasing the molecular diversity and regulating the function of proteins (Maas et al., 2006; Park et al., 2012). The known functional impacts of RNA editing mainly include amino acid sequence changes, alternative splicing alteration, RNA stability influence, and alternations on miRNA sequence or miRNA targeting sequence (Nishikura, 2016). Furthermore, aberrant RNA editing events could be correlated with the etiology or progression of various diseases, such as amyotrophic lateral sclerosis, astrocytoma, hepatocellular carcinoma, and metastatic melanoma (Slotkin and Nishikura, 2013; Kung et al., 2018; Kanata et al., 2019). Although sequencing the genome and transcriptome from the same sample/cell can theoretically enable more accurate RNA editing detection, such data are relatively uncommon and costly. Several computational tools are available for robustly identifying RNA editing sites using bulk RNA-Seq data alone, such as GIREMI (Zhang and Xiao, 2015), the pipeline proposed by Ramaswami et al. (2013), and REDIttools (Picardi and Pesole, 2013) (**Table 1**). However, the approaches specifically developed for scRNA-seq data are currently lacking, and a few studies investigated the RNA editome in individual cells. Recently, Ding et al. (2019) suggested that an abundance of SNVs identified from scRNA-seq data by their method are likely to be RNA-editing events. Since aberrant RNA editing events could be correlated with the etiology or progression of many diseases including cancers (Slotkin and Nishikura, 2013; Kung et al., 2018; Kanata et al., 2019), exploring the RNA editome in single cells can facilitate a better understanding of their functional implications to cellular heterogeneity and clinical utility in diseases. Considering that RNA editing detection depends closely on the sequencing depth, applying the tools originally designed for bulk data to single-cell data should be careful due to the inherent technical noise and low sequencing depth of current scRNA-seq protocols. There is an urgent need to develop robust methods for identifying RNA editing events with single-cell data. Consequently, exploring the RNA editome in single cells will be more feasible with the improvement of single-cell sequencing and specialized algorithms, which will benefit the elucidation of the functional implications of RNA editing to cellular variations and disease development.

EXPLORING RNA VELOCITY

scRNA-seq data have also been used to predict the future transcriptional state of single cells (termed RNA velocity) by deducing their directed dynamic transcriptome changes (**Figure 4A**). RNA regulation involves multiple stages including transcription, RNA maturation, and RNA degradation; thus, the abundance of RNAs is a strong indicator of cell state. Previous bulk RNA-seq study has shown that gene splicing and degradation can be effectively estimated based on the relative abundance of unspliced and spliced RNAs (Zeisel et al., 2011; Gaidatzis et al., 2015). Thus, similar signals could be also decoded from individual cells with single-cell transcriptomic data (Svensson and Pachter, 2018). La Manno et al. (2018) proposed a model named *velocyto* (**Table 1**) to estimate the rate of change in mRNA abundance (RNA velocity) to predict the future transcriptional state of individual cells by distinguishing between spliced and unspliced mRNAs with scRNA-seq data. This RNA velocity inference method has been applied to an increasing number of researches. For instance, RNA velocity analysis revealed dynamic transcriptional changes of immune cells in hepatocellular carcinoma (Zhang et al., 2019) and could also allow effective identification of the major directions of cell progression for murine neural crest cells (Soldatov et al., 2019). Moreover, Kanton et al. (2019) successfully uncovered the differentiation of neural progenitor cells in human development with RNA velocity exploration, but *velocyto* could not efficiently process large datasets and even may run out of memory (e.g., cell number > 40,000). More recently, Bergen et al. developed a likelihood-based dynamical model, *scVelo* (can handle > 300,000 cells), to infer the RNA velocity of cells by solving the full transcriptional dynamics (Bergen et al., 2019), which is 10 times faster and less memory consuming than that of *velocyto* (La Manno et al., 2018).

RNA velocity inference could predict the direction of cell transition within and between cell clusters/states. By contrast, pseudotime/trajectory analysis aims to identify the paths between cell clusters/subtypes, which does not automatically infer a direction like RNA velocity prediction. However, RNA velocity analysis can benefit trajectory inference or pseudotemporal ordering that aims to deduce the order of cells along developmental paths by overlaying the directionality of velocity to trajectories to better predict cell fate decisions (La Manno et al., 2018). Therefore, integrative analysis of single-cell RNA velocity and trajectory/pseudotime could provide deeper insights into various dynamic cellular processes in development and evolution, such as lineage decisions and gene regulation.

INFERRING CHROMATIN ACCESSIBILITY

Besides transcriptome profiling, scRNA-seq could also provide the potential for decoding the chromatin accessibility of transcribed regions in single cells (**Figure 4B**). Chromatin accessibility is essential for establishing and maintaining cellular identity by governing cell- or context-specific gene expression

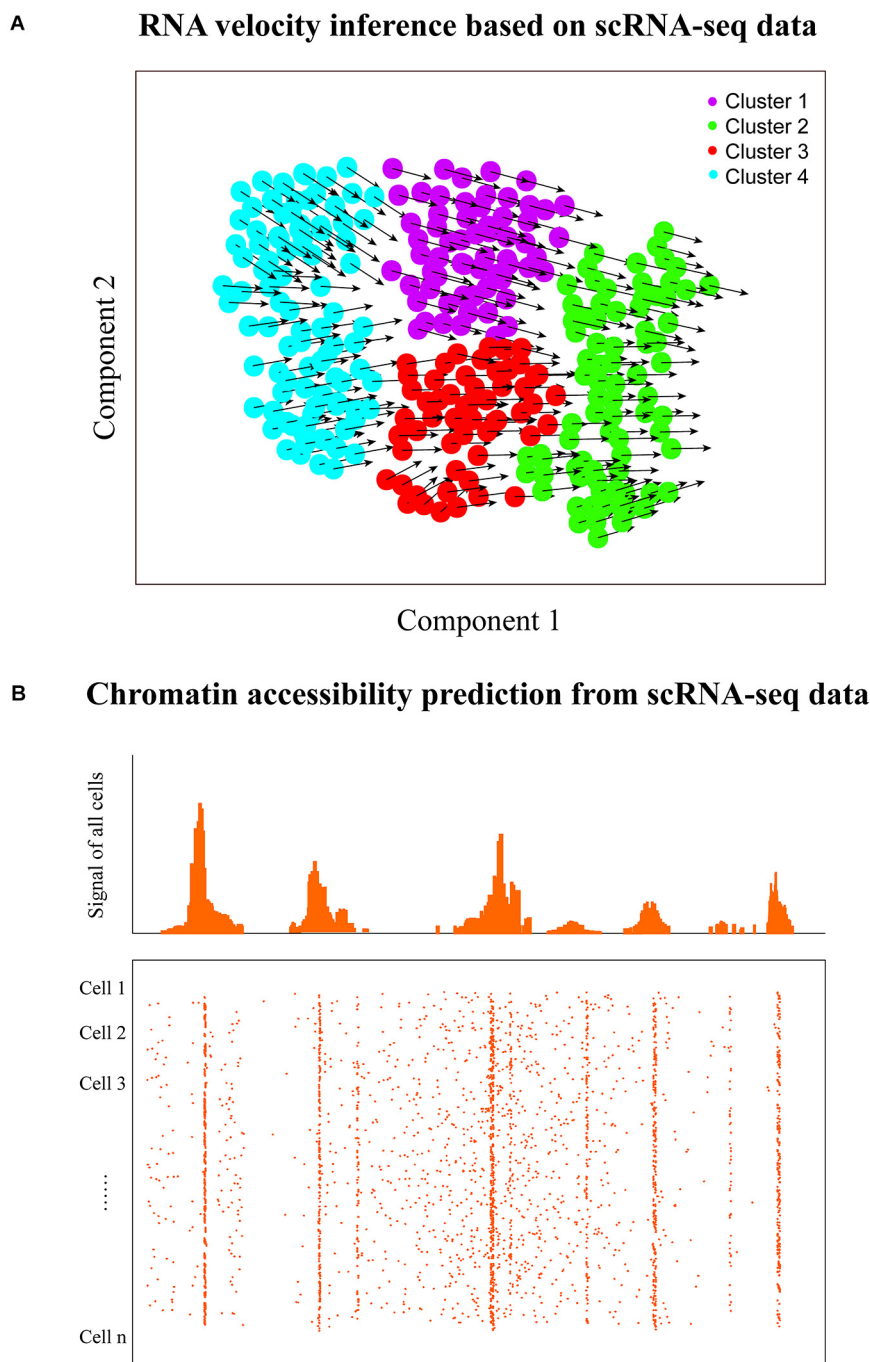


FIGURE 4 | RNA velocity and chromatin accessibility analyses. **(A)** RNA velocity inference of single cells to predict their future transcriptional states. The velocity of gene expression could be represented as the mRNA abundance over time, which enables the prediction of future transcriptional state of cells (the arrows denote the directionality). **(B)** Graphic view of chromatin accessibility prediction with scRNA-seq data. Transcriptome and regulome could have bidirectional interplay because of the feedback, thus scRNA-seq has the potential to predict the chromatin accessibility of transcribed regions using the corresponding computational approach. However, it is worth noting that the chromatin accessibility of non-transcribed regions cannot be predicted with scRNA-seq.

(Pennacchio et al., 2013; Klemm et al., 2019). The landscape of chromatin accessibility broadly reflects the regulatory capacity and is dynamically changing in response to developmental cues and environmental stimulation (Klemm et al., 2019).

Some single-cell technologies are emerging to measure the chromatin accessibility of individual cells including single-cell ATAC-seq (Cusanovich et al., 2015), single-cell DNase-seq (Jin et al., 2015), and single-cell THSseq (Lake et al., 2018).

Moreover, Yu et al. (2020) recently proposed a software, scATAC-pro, for quality estimation and visualization of single-cell chromatin accessibility sequencing data generated by different experimental protocols.

Determining the accessible genome is crucial for understanding the regulatory program of gene expression control. Many studies have demonstrated that the transcriptional activities of genes can be predicted based on the activities of associated regulatory elements (Natarajan et al., 2012; Kumar et al., 2013), but few researches investigated to what extent activities of regulatory elements can be inferred from the RNA-seq data. Gene transcription needs the chromatin to be open and accessible; thus, bidirectional interplay exists between transcriptome and regulome due to the feedback (Neph et al., 2012; Voss and Hager, 2014). Previously, Zhou et al. (2017) demonstrated that their method of BIRD (**Table 1**) can effectively predict the activities of genome-wide regulatory elements measured by DNase I hypersensitivity based on bulk gene expression profiles. Since scRNA-seq technologies enable capturing the gene transcriptional signals in each cell, it may be also possible to predict the regulome of cells based on single-cell transcriptomic data. Recently, Zhou et al. (2019) further suggested that the chromatin accessibility of the genome could be inferred from the scRNA-seq data of a small number of cells. But currently available methods for inferring chromatin accessibility from single-cell transcriptomic data are very few. Both experimental chromatin accessibility profiling technologies and computational methods that predict chromatin accessibility from scRNA-seq data will continue to improve. It remains an open question as to which method will be more accurate. To answer that question, a systematic and independent benchmark study in the future will be required.

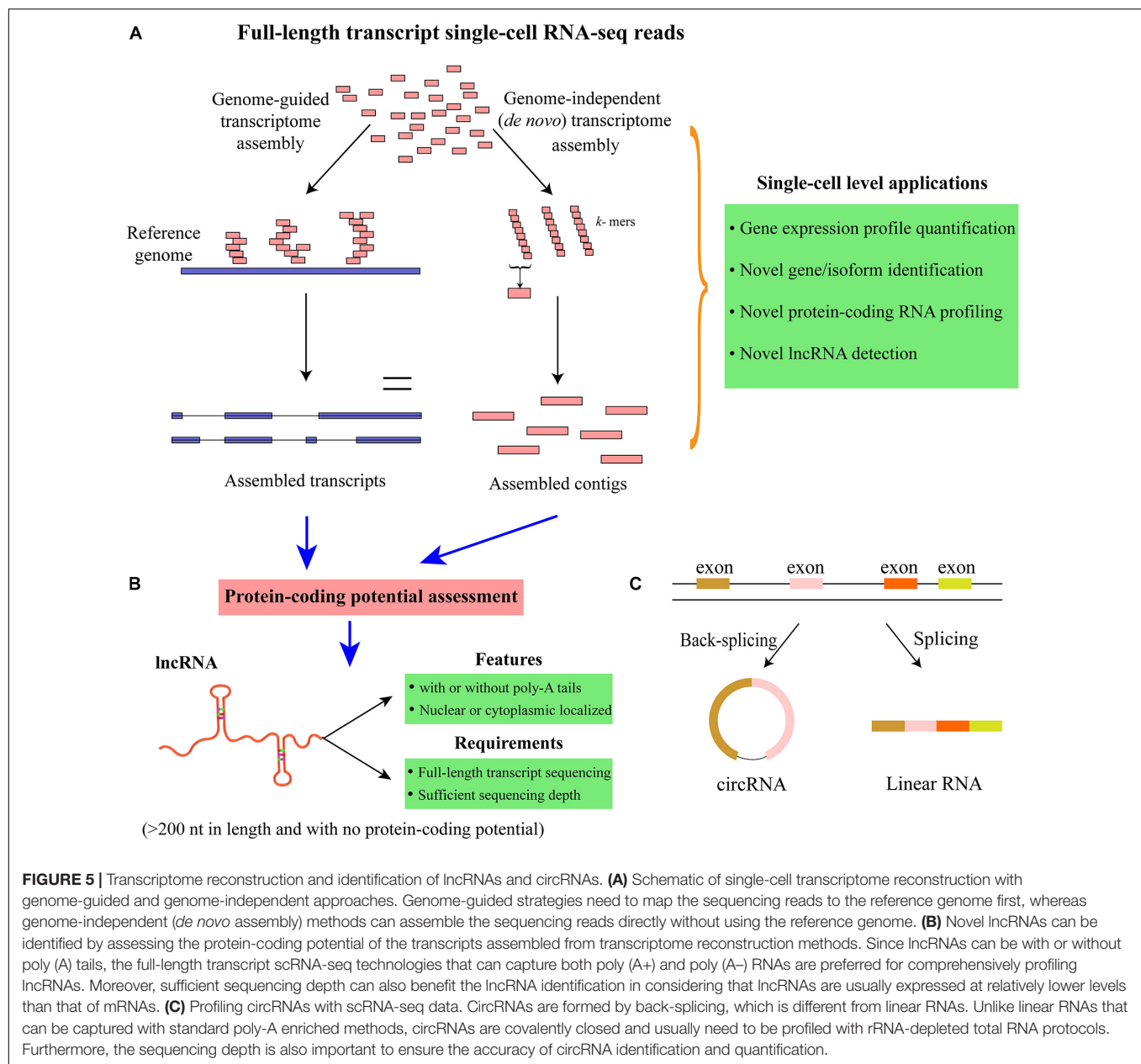
Specifically, the data from single-cell RNA-seq and chromatin profiling technologies can be combined to delineate cellular heterogeneity and elucidate transcriptional regulatory mechanisms. For instance, the computational tool of SOMatic enables the integrative analysis of scATAC-seq and scRNA-seq data for gene regulatory network reconstruction (Jansen et al., 2019). ScAI can deconvolute the cellular heterogeneity based on single-cell transcriptomic and epigenomic profiles (Jin et al., 2020b). Additionally, MAESTRO supports cell clustering and automatic cell-type annotation as well as transcriptional regulator inference for both scRNA-seq and scATAC-seq datasets (Wang et al., 2020). These analyses will help us better elucidate the underlying mechanisms of gene regulation and cellular gene expression heterogeneity.

TRANSCRIPTOME RECONSTRUCTION FOR NOVEL GENE/ISOFORM IDENTIFICATION

For full-length transcript scRNA-seq data, transcriptome reconstruction at the single-cell level is promising to identify cell-type-specific genes/isoforms. Currently, the annotated genes and isoforms for many species including humans are still far

from complete, and a multitude of novel protein-coding and non-coding genes/isoforms remain to be uncovered (Chen et al., 2013). One major reason accounting for this is that gene expression is often spatial and temporal specific; thus, those unannotated genes/isoforms could be only expressed in specific conditions and/or cell types/states. Since gene expression is usually heterogeneous at the single-cell level, different cell subpopulations may express unique and unannotated genes and/or isoforms that could not be identified with bulk RNA-seq data. Thus, scRNA-seq provides great potential for identifying and annotating the novel genes and isoforms.

Transcriptome reconstruction is the most popular strategy for detecting all the expressed genes and isoforms in a particular sample (Garber et al., 2011; Chen et al., 2017). The approaches for transcriptome reconstruction can be mainly grouped into the following two categories: genome-guided and *de novo* (genome independent) transcriptome assembly (Garber et al., 2011) (**Figure 5A** and **Table 1**). Generally, genome-guided strategies [such as TransComb (Liu J. T. et al., 2016), StringTie (Pertea et al., 2015), and Cufflinks (Trapnell et al., 2010)] assemble the overlapping reads aligned to the reference genome into transcripts, which is suitable for the organisms with the available qualified reference genome. By contrast, *de novo* transcriptome assembly methods [e.g., Trinity (Grabherr et al., 2011), Trans-ABYSS (Robertson et al., 2010), and rnaSPAdes (Bushmanova et al., 2019)] often utilize de Bruijn graph to directly assemble the reads into transcripts without the need of reference genome. When a qualified reference genome is available, genome-guided approaches are the choice due to their higher sensitivity than *de novo* assembly methods. However, for cancer cells, large-scale rearrangement events may exist in the genome and/or transcriptome; a combination use of these two different strategies may generate a more comprehensive set of transcripts (Garber et al., 2011). After transcriptome reconstruction, the coding potential of those assembled transcripts can be assessed to group them into protein-coding or non-coding RNAs. Although the available transcriptome reconstruction approaches are mainly designed for bulk RNA-seq data, some studies have applied them to scRNA-seq data and successfully identified many novel genes/transcripts (Yan et al., 2013; Fan et al., 2015; Liu S. J. et al., 2016; Wu et al., 2019). For example, Yan et al. (2013) integrated genome-independent and genome-guided assembly methods to predict the new transcripts and detected a set of novel long non-coding RNAs (lncRNAs) that are functionally important in human embryos. Notably, transcriptome assembly is mainly applicable to the scRNA-seq approaches that can sequence the full-length of transcripts [e.g., Smart-Seq2 (Picelli et al., 2014), SUPeR-seq (Fan et al., 2015), and RamDA-seq (Hayashi et al., 2018)] rather than the protocols that only capture the 3'/5'-end of transcripts. Moreover, novel algorithms for reconstructing single-cell transcriptome may be essential to overcome the noise and low coverage of scRNA-seq data. Overall, conducting single-cell transcriptome reconstruction is promising for identifying the novel genes and isoforms (including both protein-coding and non-coding RNAs) expressed in specific cell



types/states, which may transform our understanding of the complexity of single-cell transcriptome.

PROFILING LONG NON-CODING RNAs AND CIRCULAR RNAs

After transcriptome reconstruction, novel lncRNAs could be identified from single cells. lncRNAs are the transcripts with >200 nucleotides in length and have no protein-coding potential. It has been shown that lncRNAs are fundamental regulators and involved in a wide range of biological processes and pathways related to transcriptional and posttranscriptional regulation as well as chromatin remodeling (Mercer et al., 2009;

Slack and Chinnaiyan, 2019). Moreover, lncRNAs can play critical roles in a variety of human diseases, and some of them could be important biomarkers for many cancers (Ransohoff et al., 2018). Additionally, the expression of lncRNAs is more tissue- and cell-type specific than that of mRNAs (Ransohoff et al., 2018); thus, scRNA-seq provides unprecedented opportunities for profiling and annotating the cell-type-specific lncRNAs. To identify lncRNAs with RNA-seq data, the aforementioned transcriptome reconstruction is usually conducted to define the map of all expressed transcription units first (Figure 5B). Then a variety of methods can be applied to discriminate lncRNAs from protein-coding RNAs, such as CPAT (Wang et al., 2013), lncRNA-ID (Achawanantakun et al., 2015), and LGC (Wang G. Y. et al., 2019) (Table 1). CPAT employs a

logistic regression model to discriminate between non-coding and protein-coding transcripts, while lncRNA-ID utilizes the machine learning model of random forest, and LGC is based on the feature relationship between the length of open reading frame (ORF) and GC content. The protein-coding potential assessment tools have been widely used in numerous studies to predict the protein-coding potential of transcripts, which have been reviewed previously (Han et al., 2016; Lorenzi et al., 2019).

An increasing number of studies have explored the lncRNA expression profiles and functions at the single-cell level. For example, Fan et al. (2015) developed SUPeR-seq to sequence both poly (A+) and ploy (A-) RNAs and identified hundreds of novel lncRNAs that showed developmental stage-specific expression in mouse. The random (AnchorX-T₁₅N₆) primers were used in SUPeR-seq to enable the simultaneous capture of both polyadenylated and non-polyadenylated RNAs from individual cells. Moreover, novel lncRNAs associated with human early embryonic development were identified (Yan et al., 2013), and cell-type-specific lncRNAs were observed to be abundantly expressed in human neocortex (Liu S. J. et al., 2016). Besides, Wu et al. (2019) detected over 3,000 lncRNAs using the scRNA-seq data of human bone marrow and revealed that a fraction of them could play crucial roles in dysplastic hematopoiesis. It is worth noting that lncRNAs can localize in the nucleus and cytoplasm, and are usually less abundant than mRNAs, and can be expressed simultaneously with relevant protein-coding genes. If cells can be directly lysed without RNA extraction and sequenced with substantial depth, it may allow more comprehensive lncRNA identification. Furthermore, lncRNAs can be with or without poly (A) tails; thus, the full-length transcript scRNA-seq technologies that enable total RNA [including poly (A+) and ploy (A-) RNAs] capturing [e.g., SUPeR-seq (Fan et al., 2015), MATQ-seq (Sheng et al., 2017), and RamDA-seq (Hayashi et al., 2018)] are more suitable for comprehensive lncRNA profiling, whereas those single-cell protocols that only sequence poly (A+) RNAs will miss the lncRNAs without poly-A tails. However, currently available scRNA-seq strategies that can provide whole gene body coverage are still suffering certain bias at the 3'/5'-end of transcripts; further improvement of these technologies will greatly benefit single-cell lncRNA profiling.

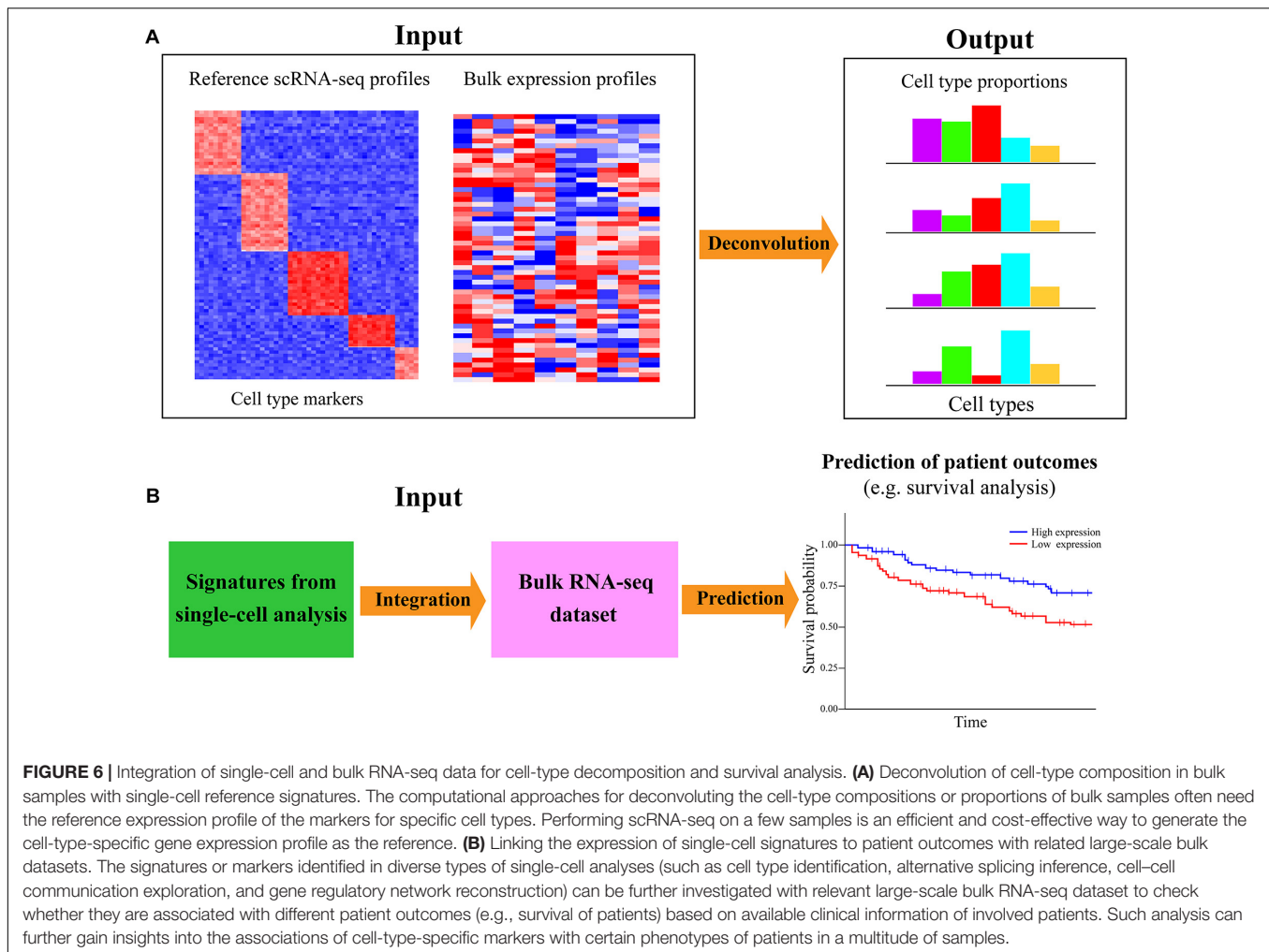
Additionally, circular RNAs (circRNAs) are an essential class of circularized non-coding RNAs, which are formed by back-splicing of linear pre-mRNAs (Figure 5C). CircRNAs can act as sponges for miRNAs or proteins, interfere with pre-mRNA processing, and even produce polypeptides (Lasda and Parker, 2014; Li et al., 2018). Moreover, a multitude of circRNAs have been associated with a variety of human cancers, and some of them could be important biomarkers for cancer diagnosis or prognosis (Greene et al., 2017). However, the specific functions for the great majority of circRNAs in biological systems are still unknown. Multitudinous studies have identified and annotated circRNAs with different bioinformatic pipelines based on bulk RNA-seq data (Memczak et al., 2013; Jakobi and Dieterich, 2019). However, circRNA exploration at the single-cell level is just emerging. Since circRNAs are covalently closed continuous loop and do not have poly (A) tail, they cannot be profiled with standard poly (A) enrichment protocols. Recently, an abundance

of circRNAs involved in the early embryonic development of mice was identified using SUPeR-seq protocol to sequence total RNAs from individual cells (Fan et al., 2015). Furthermore, Verboom et al. (2019) proposed SMARTer technology for conducting single-cell strand-specific total RNA sequencing and detected over 500 circRNAs in neuroblastoma cell lines. A range of computational methods are available for identifying circRNAs with RNA-seq data [such as find_circ2 (Memczak et al., 2013), CircExplorer2 (Zhang et al., 2016), and CIRI2 (Gao et al., 2018)], which have been reviewed recently (Jakobi and Dieterich, 2019) (Table 1). These tools could be applicable to explore the circRNAs in single cells. The commonly used bulk sequencing strategies for circRNA detection are ribosomal RNA (rRNA)-depleted total RNA and poly (A)-depletion methods, but none of them can guarantee that the enriched RNAs are exclusively circular as some other types of ncRNAs would be also captured (Kristensen et al., 2019). By contrast, the scRNA-seq protocols for profiling circRNAs are still in the early phases of development, and the bioinformatic methods specially designed for single-cell circRNA exploration are still lacking. Furthermore, the reliable identification and quantification of circRNAs generally need a substantial sequencing depth to obtain sufficient supporting reads spanning the back-splice junction region of circRNAs.

Currently, available scRNA-seq protocols are still with high technical noise, and the sequencing depth for each cell is relatively low in consideration of the cost, which hinders the identification of lncRNA and circRNA. Additionally, the computational methods specially developed to process single-cell transcriptomic data by taking the data sparsity and noise into account for lncRNA and circRNA investigation are currently lacking. With the development of both single-cell total RNA sequencing methods and related computational approaches, exploring the lncRNAs and circRNAs in individual cells, will be more feasible. These advancements will largely promote the profiling and functional characterization of lncRNAs and circRNAs in different cell types/states under various conditions.

CELL COMPOSITION DECONVOLUTION OF BULK SAMPLES USING SINGLE-CELL DATA

The aforementioned analyses are mainly based on scRNA-seq data alone; single-cell transcriptomic data can also be analyzed with the bulk RNA-seq dataset to infer the cell-type proportions/compositions for a large number of bulk samples (Figure 6A). ScRNA-seq has great advantages in dissecting the heterogeneity of cellular compositions within a given sample; however, such researches were mainly focused on a limited number of samples/individuals in consideration of cost effectiveness and scalability. Bulk RNA-seq is still the primary workhorse for dissecting gene expression for a host of samples in biomedical research due to the low cost and technical simplicity. For investigating the cell-subset specific information in a plethora of samples, an attractive approach is to directly decode the cell-type composition of large-scale heterogeneous bulk samples



via deconvolution algorithms (Shen-Orr and Gaujoux, 2013). Such a strategy is not only cost effective but could also preserve both whole-system level perspective and cell-based view of cell heterogeneity. For example, Li T. et al. (2017) have explored the composition of different tumor-infiltrating immune subsets in 32 cancer types of The Cancer Genome Atlas (TCGA). Moreover, Donovan et al. (2020) deconvoluted the cellular composition of 28 distinct human tissues from Genotype-Tissue Expression (GTEx) project (Aguet et al., 2017), which allowed cell-type-specific functional investigation for the impacts of genetic variation on gene expression.

Currently, a dozen of deconvolution approaches are available for inferring the composition of cell types from bulk RNA-seq data (Cobos et al., 2018), such as CMP (Frishberg et al., 2019), MuSiC (Wang X. R. et al., 2019), DWLS (Tsoucas et al., 2019), and CIBERSORTx (Newman et al., 2019) (Table 1). CMP uses linear regression to estimate the expression abundance of reference cells in the given bulk samples, while MuSiC weights the genes exhibiting cross-subject and cross-cell consistency to transfer cell-type-specific gene expression profile across different datasets. DWLS employs a weighted least squares method to estimate cell-type proportions, and CIBERSORTx is based on the machine

learning method to determine cell type abundance and cell-type-specific gene expression. A systematic comparison of the performance for recently developed deconvolution approaches is very valuable, but such a study is currently lacking. Existing deconvolution tools generally rely on the prior knowledge of reference expression profiles of known cell-type signatures, which can be obtained from the scRNA-seq data of one or a few samples (Figure 6A). At present, it is still highly expensive and time consuming to sequence a multitude of samples using scRNA-seq. Therefore, deconvoluting cell-type compositions from large-scale bulk RNA-seq dataset with a small sample size of single-cell transcriptomic data as the reference is an economically practical and time-saving way. Such analysis is valuable for identifying the cell types vulnerable to disease and detect the cellular targets of disease/cancer.

LINKING SINGLE-CELL SIGNATURE TO PATIENT OUTCOMES WITH BULK DATA

Another important joint analysis of scRNA-seq and bulk RNA-seq data is to associate the signatures identified in single-cell

transcriptomic data exploration to predict patient outcomes. Intratumoral heterogeneity is a pivotal determinant of tumor biology, survival, and treatment response of patients. A major goal of cancer profiling studies is to identify the genetic biomarkers that are predictive for the survival status of cancer patients. The advance in scRNA-seq largely facilitates the biomarker/signature detection at a higher resolution beyond traditional bulk data. Such single-cell signatures can be screened out from different types of single-cell analyses, such as cell clustering, differential expression calling, alternative splicing exploration, and gene regulatory network inference. Specifically, important signatures could be identified from the scRNA-seq data of the tumor ecosystem to potentially predict cancer stage, therapy response, disease-free interval, metastatic probability, or overall patient survival. Although it may not be practical to perform scRNA-seq on an abundance of patients for prognosis prediction, those publicly accessible bulk datasets with available clinical information are valuable resources for such analysis. It is an alternative way to assess whether the single-cell signatures could be useful biomarkers for predicting patient outcomes (**Figure 6B**).

A host of studies have used the bulk datasets from public databases like TCGA (Weinstein et al., 2013) and Gene Expression Omnibus (GEO) to determine the association between the expression level of single-cell signatures and the patient survival of corresponding cancers. For example, signatures from scRNA-seq analysis were successfully applied to predict the overall survival of patients for TCGA melanoma (Nirschl et al., 2017) and hepatocellular carcinoma (Zheng et al., 2018). Furthermore, Li H. P. et al. (2017) identified single-cell biomarkers that can stratify the colorectal tumors from TCGA and GEO databases into subgroups with divergent survival. For survival analysis, Raman et al. (2019) revealed that highly variable results are usually obtained from different methods, and Cox regression (Li, 2003) is superior to other compared approaches based on tests of reliability, accuracy, and robustness. Cox regression is a flexible method that can improve the accuracy of estimation between gene expression level and patient survival by enabling the inclusion of multiple covariates to accommodate explanatory variables. It is worth noting that the single-cell signatures are used to build a model, while the actual data using the model is the bulk RNA-seq data. The continuous decreasing cost and time for scRNA-seq will make single-cell transcriptomic profiling on a large sample size become more affordable and practicable, which will greatly benefit the association analysis between single-cell signatures and patient outcomes. Consequently, the signatures/biomarkers screened out from diverse kinds of single-cell analyses could be further linked to the patient outcomes with related bulk datasets and clinical information to assess their associations and clinical value.

CONCLUSION AND OUTLOOK

ScRNA-seq is widely applied to diverse organisms to dissect a range of biological questions related to developmental biology,

oncology, immunology, neurology, and microbiology at the single-cell resolution. Besides those routine analyses conducted in most studies (e.g., cell type identification, alternative splicing detection, trajectory, and GRN inference), much more other valuable information can be mined from scRNA-seq data. As we summarized in this review, cell-to-cell communications, RNA velocity, and large-scale CNVs and chromatin accessibility could be effectively extracted from single-cell transcriptomic data. Nucleotide sequence changes of SNVs and RNA editing events also could be derived from scRNA-seq experiments to enable multiple modalities. Moreover, transcriptome reconstruction with full-length transcript scRNA-seq data is promising for identifying and annotating the novel genes and isoforms mainly expressed in certain cell types/states. The innovation and optimization of scRNA-seq protocols that can effectively capture both poly (A+) and poly (A-) RNAs with increased throughput will improve the feasibility of profiling and characterizing of lncRNAs and circRNAs at single-cell resolution. Additionally, the results of scRNA-seq analysis can be further explored with traditional bulk RNA-seq data to deconvolute the cell compositions in a multitude of bulk samples or assess the association between single-cell signatures and patient outcomes in a cost-effective way.

Notably, the accuracy of any kind of single-cell analysis largely depends on the quality of single-cell sequencing data (e.g., cell quality, sequencing quality, coverage, and depth) as well as the performance of corresponding bioinformatics algorithms. Special attention needs to be paid to the noise and sparsity of scRNA-seq data, and stringent criteria may be needed to minimize the false positives. Besides, since there is a general lack of studies for benchmarking the computational approaches of the single-cell analyses we summarized in this review, it would be useful to conduct such researches in the future. In consideration of the absence of a gold-standard method, running more than one bioinformatic tools could be an effective way to reduce the number of false positives. Additionally, performance comparison for several commonly used scRNA-seq technologies revealed that if the research goal aims to pursue the highest sensitivity, the low-throughput methods that can produce full-length transcripts (e.g., Smart-seq2) are significantly better than the high-throughput approaches that mainly capture the 3'/5'-end of transcripts (like 10x Chromium) (Ziegenhain et al., 2017; Ding et al., 2020). Future comparative analysis for the newly developed single-cell transcriptome profiling protocols will be very helpful to provide better guidance in experimental designs. The fast evolution of both scRNA-seq approaches and bioinformatics methods will make the single-cell analyses we discussed become more feasible. We anticipate that these useful analyses will add much more value to scRNA-seq data and largely facilitate biomedical and clinical researches.

On the other hand, the states of single cells are determined by the intricate interplay of various molecules from multi-omic levels, such as genomics, transcriptomics, proteomics, and epigenomics. Integrative analysis of multi-omic data will enable a much more comprehensive and systematic view of each cell, which will greatly benefit the study of a variety

of normal development and disease processes. An increasing number of single-cell protocols have been developed to measure different modalities including genome (Vitak et al., 2017), epigenome (Mulqueen et al., 2018), proteome (Darmanis et al., 2016), and chromatin accessibility (Cusanovich et al., 2015), as well as profile spatial (Wang et al., 2018) or lineage (Raj et al., 2018) information. Furthermore, some assays can even simultaneously capture multimodal data from the same cell (Stuart and Satija, 2019). Additionally, the third-generation sequencing technologies like nanopore can sequence RNA and DNA with super long reads (Rand et al., 2017; Garalde et al., 2018); such technological advances and improvements will effectively accelerate the refinement of single-cell multi-omic approaches. As single-cell technology matures (including sensitivity, coverage, and throughput) and the continuous decrease in cost, multi-omic studies will be more feasible and affordable. Collectively, we envision that the advances of multi-omic assays coupled with novel computational approaches will enable a more comprehensive understanding and elucidation of

diverse cellular processes and significantly transform the single-cell biology.

AUTHOR CONTRIBUTIONS

GC conceived the manuscript. GC, YL, QX, and DW wrote the review. YL plotted all the figures. GC provided guidance on the writing and direction of the review. GC and YL revised and finalized the manuscript. All authors contributed to the article and approved the submitted version.

FUNDING

This work was supported by the National Natural Science Foundation of China (31771460, 32070680, and 91629103) and the National Key Research and Development Program of China (2016YFC0902100).

REFERENCES

- Abbosh, C., Birkbak, N. J., Wilson, G. A., Jamal-Hanjani, M., Constantin, T., Salari, R., et al. (2017). Phylogenetic ctDNA analysis depicts early-stage lung cancer evolution. *Nature* 545, 446–451. doi: 10.1038/nature22364
- Achawanantakun, R., Chen, J., Sun, Y. N., and Zhang, Y. (2015). LncRNA-ID: long non-coding RNA Identification using balanced random forests. *Bioinformatics* 31, 3897–3905. doi: 10.1093/bioinformatics/btv480
- Aguet, F., Brown, A. A., Castel, S. E., Davis, J. R., He, Y., Jo, B., et al. (2017). Genetic effects on gene expression across human tissues. *Nature* 550, 204–213. doi: 10.1038/nature24277
- Aibar, S., González-Blas, C. B., Moerman, T., Huynh-Thu, V. A., Imrichova, H., Hulselmans, G., et al. (2017). SCENIC: single-cell regulatory network inference and clustering. *Nat. Methods* 14, 1083–1086. doi: 10.1038/nmeth.4463
- Andrews, T. S., and Hemberg, M. (2018). Identifying cell populations with scRNASeq. *Mol. Aspects Med.* 59, 114–122. doi: 10.1016/j.mam.2017.07.002
- Bergen, V., Lange, M., Peidli, S., Wolf, F. A., and Theis, F. J. (2019). Generalizing RNA velocity to transient cell states through dynamical modeling. *bioRxiv [Preprint]* doi: 10.1101/820936
- Browaeys, R., Saelens, W., and Saeys, Y. (2020). NicheNet: modeling intercellular communication by linking ligands to target genes. *Nat. Methods* 17, 159–162. doi: 10.1038/s41592-019-0667-5
- Brown, T. I., Carr, V. A., LaRocque, K. F., Favila, S. E., Gordon, A. M., Bowles, B., et al. (2016). Oligodendrocyte heterogeneity in the mouse juvenile and adult central nervous system. *Science* 352, 1323–1326.
- Bryois, J., Buil, A., Evans, D. M., Kemp, J. P., Montgomery, S. B., Conrad, D. F., et al. (2014). Cis and trans effects of human genomic variants on gene expression. *PLoS Genet.* 10:e1004461. doi: 10.1371/journal.pgen.1004461
- Bushmanova, E., Antipov, D., Lapidus, A., and Prjibelski, A. D. (2019). rnaSPAdes: a de novo transcriptome assembler and its application to RNA-Seq data. *Gigascience* 8:giz100.
- Cabello-Aguilar, S., Alame, M., Kon-Sun-Tack, F., Fau, C., Lacroix, M., and Colinge, J. (2020). SingleCellSignalR: inference of intercellular networks from single-cell transcriptomics. *Nucleic Acids Res.* 48:e55. doi: 10.1093/nar/gkaa183
- Camp, J. G., Sekine, K., Gerber, T., Loeffler-Wirth, H., Binder, H., Gac, M., et al. (2017). Multilineage communication regulates human liver bud development from pluripotency. *Nature* 546, 533–538. doi: 10.1038/nature22796
- Cang, Z., and Nie, Q. (2020). Inferring spatial and signaling relationships between cells from single cell transcriptomic data. *Nat. Commun.* 11:2084.
- Chen, G., Ning, B. T., and Shi, T. L. (2019). Single-cell RNA-seq technologies and related computational data analysis. *Front. Genet.* 10:317. doi: 10.3389/fgene.2019.00317
- Chen, G., Shi, T. L., and Shi, L. M. (2017). Characterizing and annotating the genome using RNA-seq data. *Sci. China Life Sci.* 60, 116–125. doi: 10.1007/s11427-015-0349-4
- Chen, G., Wang, C., Shi, L. M., Qu, X. F., Chen, J. W., Yang, J. M., et al. (2013). Incorporating the human gene annotations in different databases significantly improved transcriptomic and genetic analyses. *RNA* 19, 479–489. doi: 10.1261/rna.037473.112
- Chen, S. N., and Mar, J. C. (2018). Evaluating methods of inferring gene regulatory networks highlights their lack of performance for single cell gene expression data. *BMC Bioinformatics* 19:232. doi: 10.1186/s12859-018-2217-z
- Cobos, F. A., Vandesompele, J., Mestdag, P., and De Preter, K. (2018). Computational deconvolution of transcriptomics data from mixed cell populations. *Bioinformatics* 34, 1969–1979. doi: 10.1093/bioinformatics/bty019
- Cohen, M., Giladi, A., Gorki, A. D., Solodkin, D. G., Zada, M., Hladik, A., et al. (2018). Lung single-cell signaling interaction map reveals basophil role in macrophage imprinting. *Cell* 175, 1031.e18–1044.e18.
- Cusanovich, D. A., Daza, R., Adey, A., Pliner, H. A., Christiansen, L., Gunderson, K. L., et al. (2015). Multiplex single-cell profiling of chromatin accessibility by combinatorial cellular indexing. *Science* 348, 910–914. doi: 10.1126/science.aab1601
- Darmanis, S., Gallant, C. J., Marinescu, V. D., Niklasson, M., Segerman, A., Flamourakis, G., et al. (2016). Simultaneous multiplexed measurement of RNA and proteins in single cells. *Cell Rep.* 14, 380–389. doi: 10.1016/j.celrep.2015.12.021
- Diaz-Papkovich, A., Anderson-Trocmé, L., Ben-Eghan, C., and Gravel, S. (2019). UMAP reveals cryptic population structure and phenotype heterogeneity in large genomic cohorts. *PLoS Genet.* 15:e1008432. doi: 10.1371/journal.pgen.1008432
- Ding, J., Adiconis, X., Simmons, S. K., Kowalczyk, M. S., Hession, C. C., Marjanovic, N. D., et al. (2020). Systematic comparison of single-cell and single-nucleus RNA-sequencing methods. *Nat. Biotechnol.* 38, 737–746.
- Ding, J., Lin, C., and Bar-Joseph, Z. (2019). Cell lineage inference from SNP and scRNA-Seq data. *Nucleic Acids Res.* 47:e56. doi: 10.1093/nar/gkz146
- Donovan, M., D'Antonio-Chronowska, A., D'Antonio, M., and Frazer, K. (2020). Cellular deconvolution of GTEx tissues powers discovery of disease and cell-type associated regulatory variants. *Nat. Commun.* 11:955.
- Duò, A., Robinson, M. D., and Soneson, C. (2018). A systematic performance evaluation of clustering methods for single-cell RNA-seq data. *F1000Res* 7:1141. doi: 10.12688/f1000research.15666.1
- Efremova, M., and Teichmann, S. A. (2020). Computational methods for single-cell omics across modalities. *Nat. Methods* 17, 14–17. doi: 10.1038/s41592-019-0692-4

- Efremova, M., Vento-Tormo, M., Teichmann, S. A., and Vento-Tormo, R. (2020). CellPhoneDB: inferring cell-cell communication from combined expression of multi-subunit ligand-receptor complexes. *Nat. Protoc.* 15, 1484–1506. doi: 10.1038/s41596-020-0292-x
- Enge, M., Arda, H. E., Mignardi, M., Beausang, J., Bottino, R., Kim, S. K., et al. (2017). Single-cell analysis of human pancreas reveals transcriptional signatures of aging and somatic mutation patterns. *Cell* 171, 321.e14–330.e14.
- Fan, J., Lee, H. O., Lee, S., Ryu, D. E., Lee, S., Xue, C., et al. (2018). Linking transcriptional and genetic tumor heterogeneity through allele analysis of single-cell RNA-seq data. *Genome Res.* 28, 1217–1227. doi: 10.1101/gr.228080.117
- Fan, X. Y., Zhang, X. N., Wu, X. L., Guo, H. S., Hu, Y. Q., Tang, F. C., et al. (2015). Single-cell RNA-seq transcriptome analysis of linear and circular RNAs in mouse preimplantation embryos. *Genome Biol.* 16:148.
- Ferguson, L. R., Chen, H., Collins, A. R., Connell, M., Damia, G., Dasgupta, S., et al. (2015). Genomic instability in human cancer: molecular insights and opportunities for therapeutic attack and prevention through diet and nutrition. *Semin. Cancer Biol.* 35, S5–S24.
- Fiers, M. W. E. J., Minnoye, L., Aibar, S., Gonzalez-Blas, C. B., Atak, Z. K., and Aerts, S. (2018). Mapping gene regulatory networks from single-cell omics data. *Brief. Funct. Genomics* 17, 246–254. doi: 10.1093/bfpg/ebx046
- Frishberg, A., Peshes-Yaloz, N., Cohn, O., Rosentul, D., Steuerman, Y., Valadarsky, L., et al. (2019). Cell composition analysis of bulk genomics using single-cell data. *Nat. Methods* 16, 327–332. doi: 10.1038/s41592-019-0355-5
- Gaidatzis, D., Burger, L., Florescu, M., and Stadler, M. B. (2015). Analysis of intronic and exonic reads in RNA-seq data characterizes transcriptional and post-transcriptional regulation. *Nat. Biotechnol.* 33, 722–729. doi: 10.1038/nbt.3269
- Gao, Y., Zhang, J. Y., and Zhao, F. Q. (2018). Circular RNA identification based on multiple seed matching. *Brief. Bioinform.* 19, 803–810. doi: 10.1093/bib/bbx014
- Garalde, D. R., Snell, E. A., Jachimowicz, D., Sipos, B., Lloyd, J. H., Bruce, M., et al. (2018). Highly parallel direct RNA sequencing on an array of nanopores. *Nat. Methods* 15, 201–206. doi: 10.1038/nmeth.4577
- Garber, M., Grabherr, M. G., Guttman, M., and Trapnell, C. (2011). Computational methods for transcriptome annotation and quantification using RNA-seq. *Nat. Methods* 8, 469–477. doi: 10.1038/nmeth.1613
- Garrison, E., and Marth, G. (2012). Haplotype-based variant detection from short-read sequencing. *Quant. Biol.*
- Gorelik, L., and Flavell, R. A. (2000). Abrogation of TGFβ signaling in T cells leads to spontaneous T cell differentiation and autoimmune disease. *Immunity* 12, 171–181. doi: 10.1016/s1074-7613(00)80170-3
- Grabherr, M. G., Haas, B. J., Yassour, M., Levin, J. Z., Thompson, D. A., Amit, I., et al. (2011). Full-length transcriptome assembly from RNA-Seq data without a reference genome. *Nat. Biotechnol.* 29, 644–652. doi: 10.1038/nbt.1883
- Greene, J., Baird, A. M., Brady, L., Lim, M., Gray, S. G., McDermott, R., et al. (2017). Circular RNAs: biogenesis, function and role in human diseases. *Front. Mol. Biosci.* 4:38. doi: 10.3389/fmolb.2017.00038
- Haass, N. K., Smalley, K. S. M., and Herlyn, M. (2004). The role of altered cell-cell communication in melanoma progression. *J. Mol. Histol.* 35, 309–318. doi: 10.1023/b:hijo.0000032362.35354.bb
- Han, S. Y., Liang, Y. C., Li, Y., and Du, W. (2016). Long noncoding RNA identification: comparing machine learning based tools for long noncoding transcripts discrimination. *Biomed. Res. Int.* 2016:8496165.
- Hanahan, D., and Weinberg, R. A. (2011). Hallmarks of cancer: the next generation. *Cell* 144, 646–674. doi: 10.1016/j.cell.2011.02.013
- Hayashi, T., Ozaki, H., Sasagawa, Y., Umeda, M., Danno, H., and Nikaido, I. (2018). Single-cell full-length total RNA sequencing uncovers dynamics of recursive splicing and enhancer RNAs. *Nat. Commun.* 9:619.
- Hotamisligil, G. S. (2006). Inflammation and metabolic disorders. *Nature* 444, 860–867. doi: 10.1038/nature05485
- Jakobi, T., and Dieterich, C. (2019). Computational approaches for circular RNA analysis. *Wiley Interdiscip. Rev. RNA* 10:e1528. doi: 10.1002/wrna.1528
- Jansen, C., Ramirez, R. N., El-Ali, N. C., Gomez-Cabrero, D., Tegner, J., Merckenschlager, M., et al. (2019). Building gene regulatory networks from scATAC-seq and scRNA-seq using linked self organizing maps. *PLoS Comput. Biol.* 15:e1006555. doi: 10.1371/journal.pcbi.1006555
- Jin, S., Guerrero-Juarez, C. F., Zhang, L., Chang, I., Myung, P., Plikus, M. V., et al. (2020a). Inference and analysis of cell-cell communication using CellChat. *bioRxiv [Preprint]* doi: 10.1101/2020.07.21.214387
- Jin, S., Zhang, L., and Nie, Q. (2020b). scAI: an unsupervised approach for the integrative analysis of parallel single-cell transcriptomic and epigenomic profiles. *Genome Biol.* 21:25.
- Jin, W. F., Tang, Q. S., Wan, M. M., Cui, K. R., Zhang, Y., Ren, G., et al. (2015). Genome-wide detection of DNase I hypersensitive sites in single cells and FFPE tissue samples. *Nature* 528, 142–146. doi: 10.1038/nature15740
- Ju, Y. S., Martincorena, I., Gerstung, M., Petljak, M., Alexandrov, L. B., Rahbari, R., et al. (2017). Somatic mutations reveal asymmetric cellular dynamics in the early human embryo. *Nature* 543, 714–718.
- Kanata, E., Llorens, F., Dafou, D., Dimitriadis, A., Thune, K., Xanthopoulos, K., et al. (2019). RNA editing alterations define manifestation of prion diseases. *Proc. Natl. Acad. Sci. U.S.A.* 116, 19727–19735. doi: 10.1073/pnas.1803521116
- Kanton, S., Boyle, M. J., He, Z. S., Santel, M., Weigert, A., Sanchis-Calleja, F., et al. (2019). Organoid single-cell genomic atlas uncovers human-specific features of brain development. *Nature* 574, 418–422. doi: 10.1038/s41586-019-1654-9
- Karaïskos, N., Wahle, P., Alles, J., Boltengagen, A., Ayoub, S., Kipar, C., et al. (2017). The drosophila embryo at single-cell transcriptome resolution. *Science* 358, 194–199.
- Kim, S., Scheffler, K., Halpern, A. L., Bekritsky, M. A., Noh, E., Kallberg, M., et al. (2018). Strelka2: fast and accurate calling of germline and somatic variants. *Nat. Methods* 15, 591–594. doi: 10.1038/s41592-018-0051-x
- Kiselev, V. Y., Andrews, T. S., and Hemberg, M. (2019). Challenges in unsupervised clustering of single-cell RNA-seq data. *Nat. Rev. Genet.* 20, 310–310. doi: 10.1038/s41576-019-0095-5
- Klemm, S. L., Shipony, Z., and Greenleaf, W. J. (2019). Chromatin accessibility and the regulatory epigenome. *Nat. Rev. Genet.* 20, 207–220. doi: 10.1038/s41576-018-0089-8
- Kreso, A., and Dick, J. E. (2014). Evolution of the cancer stem cell model. *Cell Stem Cell* 14, 275–291. doi: 10.1016/j.stem.2014.02.006
- Kristensen, L. S., Andersen, M. S., Stagsted, L. V. W., Ebbesen, K. K., Hansen, T. B., and Kjems, J. (2019). The biogenesis, biology and characterization of circular RNAs. *Nat. Rev. Genet.* 20, 675–691.
- Kumar, M. P., Du, J. Y., Lagoudas, G., Jiao, Y., Sawyer, A., Drummond, D. C., et al. (2018). Analysis of single-cell RNA-seq identifies cell-cell communication associated with tumor characteristics. *Cell Rep.* 25, 1458.e4–1468.e4.
- Kumar, V., Muratani, M., Rayan, N. A., Kraus, P., Lufkin, T., Ng, H. H., et al. (2013). Uniform, optimal signal processing of mapped deep-sequencing data. *Nat. Biotechnol.* 31, 615–622. doi: 10.1038/nbt.2596
- Kung, C. P., Maggi, L. B., and Weber, J. D. (2018). The role of RNA editing in cancer development and metabolic disorders. *Front. Endocrinol.* 9:762. doi: 10.3389/fendo.2018.00762
- La Manno, G., Soldatov, R., Zeisel, A., Braun, E., Hochgerner, H., Petukhov, V., et al. (2018). RNA velocity of single cells. *Nature* 560, 494–498.
- Lake, B. B., Chen, S., Sos, B. C., Fan, J., Kaeser, G. E., Yung, Y. C., et al. (2018). Integrative single-cell analysis of transcriptional and epigenetic states in the human adult brain. *Nat. Biotechnol.* 36, 70–80. doi: 10.1038/nbt.4038
- Lasda, E., and Parker, R. (2014). Circular RNAs: diversity of form and function. *RNA* 20, 1829–1842. doi: 10.1261/rna.047126.114
- Li, H. (2011). A statistical framework for SNP calling, mutation discovery, association mapping and population genetical parameter estimation from sequencing data. *Bioinformatics* 27, 2987–2993. doi: 10.1093/bioinformatics/btr509
- Li, H. P., Courtois, E. T., Sengupta, D., Tan, Y. L., Chen, K. H., Goh, J. J. L., et al. (2017). Reference component analysis of single-cell transcriptomes elucidates cellular heterogeneity in human colorectal tumors. *Nat. Genet.* 49, 708–718. doi: 10.1038/ng.3818
- Li, T., Fan, J., Wang, B., Traugh, N., Chen, Q., Liu, J. S., et al. (2017). TIMER: a web server for comprehensive analysis of tumor-infiltrating immune cells. *Cancer Res.* 77, e108–e110.
- Li, J. C. A. (2003). Modeling survival data: extending the cox model. *Sociol. Method Res.* 32, 117–120.
- Li, X., Yang, L., and Chen, L. L. (2018). The biogenesis, functions, and challenges of circular RNAs. *Mol. Cell* 71, 428–442. doi: 10.1016/j.molcel.2018.06.034

- Liu, F. L., Zhang, Y. Y., Zhang, L., Li, Z. Y., Fang, Q., Gao, R. R., et al. (2019). Systematic comparative analysis of single-nucleotide variant detection methods from single-cell RNA sequencing data. *Genome Biol.* 20:242.
- Liu, J. T., Yu, T., Jiang, T., and Li, G. J. (2016). TransComb: genome-guided transcriptome assembly via combing junctions in splicing graphs. *Genome Biol.* 17:213.
- Liu, S. J., Nowakowski, T. J., Pollen, A. A., Lui, J. H., Horlbeck, M. A., Attenello, F. J., et al. (2016). Single-cell analysis of long non-coding RNAs in the developing human neocortex. *Genome Biol.* 17:67.
- Lorenzi, L., Cobos, F. A., Decock, A., Everaert, C., Helmsmoortel, H., Lefever, S., et al. (2019). Long noncoding RNA expression profiling in cancer: challenges and opportunities. *Gene Chromosome Canc.* 58, 191–199. doi: 10.1002/gcc.22709
- Lueken, M. D., and Theis, F. J. (2019). Current best practices in single-cell RNA-seq analysis: a tutorial. *Mol. Syst. Biol.* 15:e8746.
- Lun, A. T. L., Bach, K., and Marioni, J. C. (2016). Pooling across cells to normalize single-cell RNA sequencing data with many zero counts. *Genome Biol.* 17:75.
- Maas, S., Kawahara, Y., Tamburro, K. M., and Nishikura, K. (2006). A-to-I RNA editing and human disease. *RNA Biol.* 3, 1–9. doi: 10.4161/rna.3.1.2495
- Macosko, E. Z., Basu, A., Satija, R., Nemesh, J., Shekhar, K., Goldman, M., et al. (2015). Highly parallel genome-wide expression profiling of individual cells using nanoliter droplets. *Cell* 161, 1202–1214. doi: 10.1016/j.cell.2015.05.002
- Martincoren, I., Raine, K. M., Gerstung, M., Dawson, K. J., Haase, K., Van Loo, P., et al. (2017). Universal patterns of selection in cancer and somatic tissues. *Cell* 171, 1029.e21–1041.e21.
- Mayr, U., Serra, D., and Liberali, P. (2019). Exploring single cells in space and time during tissue development, homeostasis and regeneration. *Development* 146:dev176727. doi: 10.1242/dev.176727
- Memczak, S., Jens, M., Elefsinioti, A., Torti, F., Krueger, J., Rybak, A., et al. (2013). Circular RNAs are a large class of animal RNAs with regulatory potency. *Nature* 495, 333–338. doi: 10.1038/nature11928
- Mercer, T. R., Dinger, M. E., and Mattick, J. S. (2009). Long non-coding RNAs: insights into functions. *Nat. Rev. Genet.* 10, 155–159.
- Moon, K. R., Stanley, J. S., Burkhardt, D., van Dijk, D., Wolf, G., and Krishnaswamy, S. (2018). Manifold learning-based methods for analyzing single-cell RNA-sequencing data. *Curr. Opin. Syst. Biol.* 7, 36–46. doi: 10.1016/j.coisb.2017.12.008
- Mulqueen, R. M., Pokholok, D., Norberg, S. J., Torkenczy, K. A., Fields, A. J., Sun, D. C., et al. (2018). Highly scalable generation of DNA methylation profiles in single cells. *Nat. Biotechnol.* 36, 428–431. doi: 10.1038/nbt.4112
- Natarajan, A., Yardimci, G. G., Sheffield, N. C., Crawford, G. E., and Ohler, U. (2012). Predicting cell-type-specific gene expression from regions of open chromatin. *Genome Res.* 22, 1711–1722. doi: 10.1101/gr.135129.111
- Navin, N., Kendall, J., Troge, J., Andrews, P., Rodgers, L., McIndoo, J., et al. (2011). Tumour evolution inferred by single-cell sequencing. *Nature* 472, 90–94. doi: 10.1038/nature09807
- Navin, N., Krasnitz, A., Rodgers, L., Cook, K., Meth, J., Kendall, J., et al. (2010). Inferring tumor progression from genomic heterogeneity. *Genome Res.* 20, 68–80. doi: 10.1101/gr.099622.109
- Negrini, S., Gorgoulis, V. G., and Halazonetis, T. D. (2010). Genomic instability - an evolving hallmark of cancer. *Nat. Rev. Mol. Cell Bio.* 11, 220–228. doi: 10.1038/nrm2858
- Neph, S., Stergachis, A. B., Reynolds, A., Sandstrom, R., Borenstein, E., and Stamatoiyannopoulos, J. A. (2012). Circuitry and dynamics of human transcription factor regulatory networks. *Cell* 150, 1274–1286. doi: 10.1016/j.cell.2012.04.040
- Newman, A. M., Steen, C. B., Liu, C. L., Gentles, A. J., Chaudhuri, A. A., Scherer, F., et al. (2019). Determining cell type abundance and expression from bulk tissues with digital cytometry. *Nat. Biotechnol.* 37, 773–782. doi: 10.1038/s41587-019-0114-2
- Nirschl, C. J., Suárez-Fariñas, M., Izar, B., Prakadan, S., Dannenfeller, R., Tirosh, I., et al. (2017). IFN γ -dependent tissue-immune homeostasis is co-opted in the tumor microenvironment. *Cell* 170, 127.e15–141.e15.
- Nishikura, K. (2010). Functions and regulation of RNA editing by ADAR deaminases. *Annu. Rev. Biochem.* 79, 321–349. doi: 10.1146/annurev-biochem-060208-105251
- Nishikura, K. (2016). A-to-I editing of coding and non-coding RNAs by ADARs. *Nat. Rev. Mol. Cell Bio.* 17, 83–96. doi: 10.1038/nrm.2015.4
- Nitzan, M., Karaikos, N., Friedman, N., and Rajewsky, N. (2019). Gene expression cartography. *Nature* 576, 132–137. doi: 10.1038/s41586-019-1773-3
- Park, E., Williams, B., Wold, B. J., and Mortazavi, A. (2012). RNA editing in the human ENCODE RNA-seq data. *Genome Res.* 22, 1626–1633. doi: 10.1101/gr.134957.111
- Patel, A. P., Tirosh, I., Trombetta, J. J., Shalek, A. K., Gillespie, S. M., Wakimoto, H., et al. (2014). Single-cell RNA-seq highlights intratumoral heterogeneity in primary glioblastoma. *Science* 344, 1396–1401. doi: 10.1126/science.1254257
- Pavlicev, M., Wagner, G. P., Chavan, A. R., Owens, K., Maziarz, J., Dunn-Fletcher, C., et al. (2017). Single-cell transcriptomics of the human placenta: inferring the cell communication network of the maternal-fetal interface. *Genome Res.* 27, 349–361. doi: 10.1101/gr.207597.116
- Pennacchio, L. A., Bickmore, W., Dean, A., Nobrega, M. A., and Bejerano, G. (2013). Enhancers: five essential questions. *Nat. Rev. Genet.* 14, 288–295. doi: 10.1038/nrg3458
- Perte, M., Perte, G. M., Antonescu, C. M., Chang, T. C., Mendell, J. T., and Salzberg, S. L. (2015). StringTie enables improved reconstruction of a transcriptome from RNA-seq reads. *Nat. Biotechnol.* 33, 290–295. doi: 10.1038/nbt.3122
- Picardi, E., and Pesole, G. (2013). REDIttools: high-throughput RNA editing detection made easy. *Bioinformatics* 29, 1813–1814. doi: 10.1093/bioinformatics/btt287
- Picelli, S., Faridani, O. R., Bjorklund, A. K., Winberg, G., Sagasser, S., and Sandberg, R. (2014). Full-length RNA-seq from single cells using Smart-seq2. *Nat. Protoc.* 9, 171–181. doi: 10.1038/nprot.2014.006
- Poirion, O., Zhu, X., Ching, T., and Garmire, L. X. (2018). Using single nucleotide variations in single-cell RNA-seq to identify subpopulations and genotype-phenotype linkage. *Nat. Commun.* 9:4892.
- Pratap, A., Jaliha, A. P., Law, J. N., Bharadwaj, A., and Murali, T. M. (2020). Benchmarking algorithms for gene regulatory network inference from single-cell transcriptomic data. *Nat. Methods* 17, 147–154. doi: 10.1038/s41592-019-0690-6
- Puram, S. V., Tirosh, I., Parikh, A. S., Patel, A. P., Yizhak, K., Gillespie, S., et al. (2017). Single-cell transcriptomic analysis of primary and metastatic tumor ecosystems in head and neck cancer. *Cell* 171, 1611.e24–1624.e24.
- Quadrato, G., Nguyen, T., Macosko, E. Z., Sherwood, J. L., Yang, S. M., Berger, D. R., et al. (2017). Cell diversity and network dynamics in photosensitive human brain organoids. *Nature* 545, 48–53. doi: 10.1038/nature22047
- Raj, B., Wagner, D. E., McKenna, A., Pandey, S., Klein, A. M., Shendure, J., et al. (2018). Simultaneous single-cell profiling of lineages and cell types in the vertebrate brain. *Nat. Biotechnol.* 36, 442–450. doi: 10.1038/nbt.4103
- Raman, P., Zimmerman, S., Rathi, K. S., de Torrenté, L., Sarmady, M., Wu, C., et al. (2019). A comparison of survival analysis methods for cancer gene expression RNA-Sequencing data. *Cancer Genet.* 235–236, 1–12. doi: 10.1016/j.cancergen.2019.04.004
- Ramaswami, G., Zhang, R., Piskol, R., Keegan, L. P., Deng, P., O'Connell, M. A., et al. (2013). Identifying RNA editing sites using RNA sequencing data alone. *Nat. Methods* 10, 128–132. doi: 10.1038/nmeth.2330
- Rand, A. C., Jain, M., Eizenga, J. M., Musselman-Brown, A., Olsen, H. E., Akeson, M., et al. (2017). Mapping DNA methylation with high-throughput nanopore sequencing. *Nat. Methods* 14, 411–413. doi: 10.1038/nmeth.4189
- Ransohoff, J. D., Wei, Y. N., and Khavari, P. A. (2018). The functions and unique features of long intergenic non-coding RNA. *Nat. Rev. Mol. Cell Bio.* 19, 143–157. doi: 10.1038/nrm.2017.104
- Ren, X., Zhong, G., Zhang, Q., Zhang, L., Sun, Y., and Zhang, Z. (2020). Reconstruction of cell spatial organization from single-cell RNA sequencing data based on ligand-receptor mediated self-assembly. *Cell Res.* 30, 763–778. doi: 10.1038/s41422-020-0353-2
- Robertson, G., Schein, J., Chiu, R., Corbett, R., Field, M., Jackman, S. D., et al. (2010). De novo assembly and analysis of RNA-seq data. *Nat. Methods* 7, 909–912.
- Saelens, W., Cannoodt, R., Todorov, H., and Saeys, Y. (2019). A comparison of single-cell trajectory inference methods. *Nat. Biotechnol.* 37, 547–554. doi: 10.1038/s41587-019-0071-9
- Sheng, K., Cao, W., Niu, Y., Deng, Q., and Zong, C. (2017). Effective detection of variation in single-cell transcriptomes using MATQ-seq. *Nat. Methods* 14, 267–270. doi: 10.1038/nmeth.4145
- Shen-Orr, S. S., and Gaujoux, R. (2013). Computational deconvolution: extracting cell type-specific information from heterogeneous samples. *Curr. Opin. Immunol.* 25, 571–578. doi: 10.1016/j.coi.2013.09.015
- Shlien, A., and Malkin, D. (2009). Copy number variations and cancer. *Genome Med.* 1:62.

- Skelly, D. A., Squiers, G. T., McLellan, M. A., Bolisetty, M. T., Robson, P., Rosenthal, N. A., et al. (2018). Single-cell transcriptional profiling reveals cellular diversity and intercommunication in the mouse heart. *Cell Rep.* 22, 600–610. doi: 10.1016/j.celrep.2017.12.072
- Slack, F. J., and Chinnaiyan, A. M. (2019). The role of non-coding RNAs in oncology. *Cell* 179, 1033–1055. doi: 10.1016/j.cell.2019.10.017
- Slotkin, W., and Nishikura, K. (2013). Adenosine-to-inosine RNA editing and human disease. *Genome Med.* 5:105. doi: 10.1186/gm508
- Soldatov, R., Kaucak, M., Kastriti, M. E., Petersen, J., Chontorotzea, T., Englmaier, L., et al. (2019). Spatiotemporal structure of cell fate decisions in murine neural crest. *Science* 364:eaas9536.
- Stuart, T., and Satija, R. (2019). Integrative single-cell analysis. *Nat. Rev. Genet.* 20, 257–272. doi: 10.1038/s41576-019-0093-7
- Svensson, V., and Pachter, L. (2018). RNA velocity: molecular kinetics from single-cell RNA-seq. *Mol. Cell* 72, 7–9. doi: 10.1016/j.molcel.2018.09.026
- Tang, L. (2020). Integrating lineage tracing and single-cell analysis. *Nat. Methods* 17:359. doi: 10.1038/s41592-020-0802-3
- Tirosch, I., Izar, B., Prakadan, S. M., Wadsworth, M. H., Treacy, D., Trombetta, J. J., et al. (2016a). Dissecting the multicellular ecosystem of metastatic melanoma by single-cell RNA-seq. *Science* 352, 189–196.
- Tirosch, I., Venteicher, A. S., Hebert, C., Escalante, L. E., Patel, A. P., Yizhak, K., et al. (2016b). Single-cell RNA-seq supports a developmental hierarchy in human oligodendrogloma. *Nature* 539, 309–313.
- Trapnell, C., Williams, B. A., Pertea, G., Mortazavi, A., Kwan, G., van Baren, M. J., et al. (2010). Transcript assembly and quantification by RNA-Seq reveals unannotated transcripts and isoform switching during cell differentiation. *Nat. Biotechnol.* 28, 511–515. doi: 10.1038/nbt.1621
- Tsoucas, D., Dong, R., Chen, H. D., Zhu, Q., Guo, G. J., and Yuan, G. C. (2019). Accurate estimation of cell-type composition from gene expression data. *Nat. Commun.* 10:2975.
- Tsuyuzaki, K., Ishii, M., and Nikaido, I. (2019). Uncovering hypergraphs of cell-cell interaction from single cell RNA-sequencing data. *bioRxiv [Preprint]* doi: 10.1101/566182
- Tyler, S. R., Rott, P. G., Sun, X. S., Yi, Y. L., Xie, W. L., Winter, M. C., et al. (2019). PyMINER Finds Gene and Autocrine-Paracrine Networks from Human Islet scRNA-Seq. *Cell Rep.* 26, 1951.e8–1964.e8.
- van der Maaten, L., and Hinton, G. (2008). Visualizing data using t-SNE. *J. Mach. Learn. Res.* 9, 2579–2605.
- Verboom, K., Everaert, C., Bolduc, N., Livak, K. J., Yigit, N., Rombaut, D., et al. (2019). SMARTer single cell total RNA sequencing. *Nucleic Acids Res.* 47:e93.
- Vitak, S. A., Torkenczy, K. A., Rosenkrantz, J. L., Fields, A. J., Christiansen, L., Wong, M. H., et al. (2017). Sequencing thousands of single-cell genomes with combinatorial indexing. *Nat. Methods* 14, 302–308. doi: 10.1038/nmeth.4154
- Vogelstein, B., Papadopoulos, N., Velculescu, V. E., Zhou, S., Diaz, L. A., and Kinzler, K. W. (2013). Cancer genome landscapes. *Science* 339, 1546–1558. doi: 10.1126/science.1235122
- Voss, T. C., and Hager, G. L. (2014). Dynamic regulation of transcriptional states by chromatin and transcription factors. *Nat. Rev. Genet.* 15, 69–81. doi: 10.1038/nrg3623
- Wagner, D. E., Weinreb, C., Collins, Z. M., Briggs, J. A., Megason, S. G., and Klein, A. M. (2018). Single-cell mapping of gene expression landscapes and lineage in the zebrafish embryo. *Science* 360, 981–987. doi: 10.1126/science.aar4362
- Wang, C., Sun, D., Huang, X., Wan, C., Li, Z., Han, Y., et al. (2020). Integrative analyses of single-cell transcriptome and regulome using MAESTRO. *Genome Biol.* 21:198.
- Wang, G. Y., Yin, H. Y., Li, B. Y., Yu, C. L., Wang, F., Xu, X. J., et al. (2019). Characterization and identification of long non-coding RNAs based on feature relationship. *Bioinformatics* 35, 2949–2956. doi: 10.1093/bioinformatics/bt z008
- Wang, X. R., Park, J., Susztak, K., Zhang, N. R., and Li, M. Y. (2019). Bulk tissue cell type deconvolution with multi-subject single-cell expression reference. *Nat. Commun.* 10:380.
- Wang, Y., Wang, R., Zhang, S., Song, S., Jiang, C., Han, G., et al. (2019). iTALK: an R package to characterize and illustrate intercellular communication. *bioRxiv [Preprint]* doi: 10.1101/507871
- Wang, L., Park, H. J., Dasari, S., Wang, S. Q., Kocher, J. P., and Li, W. (2013). CPAT: coding-potential assessment tool using an alignment-free logistic regression model. *Nucleic Acids Res.* 41:e74. doi: 10.1093/nar/gk t006
- Wang, X., Allen, W. E., Wright, M. A., Sylvestrak, E. L., Samusik, N., Vesuna, S., et al. (2018). Three-dimensional intact-tissue sequencing of single-cell transcriptional states. *Science* 361:eaat5691. doi: 10.1126/science.aat5691
- Watabe, T., and Miyazono, K. (2009). Roles of TGF-beta family signaling in stem cell renewal and differentiation. *Cell Res.* 19, 103–115. doi: 10.1038/cr.2008.323
- Weinstein, J. N., Collisson, E. A., Mills, G. B., Shaw, K. R. M., Ozenberger, B. A., Ellrott, K., et al. (2013). The cancer genome atlas pan-cancer analysis project. *Nat. Genet.* 45, 1113–1120. doi: 10.1038/ng.2764
- Wu, Z. J., Gao, S. G., Zhao, X., Chen, J. G., Keyvanfar, K., Feng, X. M., et al. (2019). Long noncoding RNAs of single hematopoietic stem and progenitor cells in healthy and dysplastic human bone marrow. *Haematologica* 104, 894–906. doi: 10.3324/haematol.2018.208926
- Xu, X., Hou, Y., Yin, X. Y., Bao, L., Tang, A. F., Song, L. T., et al. (2012). Single-cell exome sequencing reveals single-nucleotide mutation characteristics of a kidney tumor. *Cell* 148, 886–895. doi: 10.1016/j.cell.2012.02.025
- Yan, L. Y., Yang, M. Y., Guo, H. S., Yang, L., Wu, J., Li, R., et al. (2013). Single-cell RNA-Seq profiling of human preimplantation embryos and embryonic stem cells. *Nat. Struct. Mol. Biol.* 20, 1131–1139. doi: 10.1038/nsmb.2660
- Yip, S. H., Sham, P. C., and Wang, J. W. (2019). Evaluation of tools for highly variable gene discovery from single-cell RNA-seq data. *Brief. Bioinform.* 20, 1583–1589. doi: 10.1093/bib/bby011
- Yu, W., Uzun, Y., Zhu, Q., Chen, C., and Tan, K. (2020). scATAC-pro: a comprehensive workflow for single-cell chromatin accessibility sequencing data. *Genome Biol.* 21:94. doi: 10.1186/s13059-020-02008-0
- Yuan, D. S., Tao, Y. R., Chen, G., and Shi, T. L. (2019). Systematic expression analysis of ligand-receptor pairs reveals important cell-to-cell interactions inside glioma. *Cell Commun. Signal* 17:48.
- Zafar, H., Wang, Y., Nakhleh, L., Navin, N., and Chen, K. (2016). Monovar: single-nucleotide variant detection in single cells. *Nat. Methods* 13, 505–507. doi: 10.1038/nmeth.3835
- Zeisel, A., Kostler, W. J., Molotski, N., Tsai, J. M., Krauthgamer, R., Jacob-Hirsch, J., et al. (2011). Coupled pre-mRNA and mRNA dynamics unveil operational strategies underlying transcriptional responses to stimuli. *Mol. Syst. Biol.* 7:529. doi: 10.1038/msb.2011.62
- Zhang, Q., and Xiao, X. (2015). Genome sequence-independent identification of RNA editing sites. *Nat. Methods* 12, 347–350. doi: 10.1038/nmeth.3314
- Zhang, Q. M., He, Y., Luo, N., Patel, S. J., Han, Y. J., Gao, R. R., et al. (2019). Landscape and dynamics of single immune cells in hepatocellular carcinoma. *Cell* 179, 829.e20–845.e20.
- Zhang, X. O., Dong, R., Zhang, Y., Zhang, J. L., Luo, Z., Zhang, J., et al. (2016). Diverse alternative back-splicing and alternative splicing landscape of circular RNAs. *Genome Res.* 26, 1277–1287. doi: 10.1101/gr.202895.115
- Zheng, G. X. Y., Terry, J. M., Belgrader, P., Ryvkin, P., Bent, Z. W., Wilson, R., et al. (2017). Massively parallel digital transcriptional profiling of single cells. *Nat. Commun.* 8:14049.
- Zheng, H. P., Pomyen, Y., Hernandez, M. O., Li, C. Y., Livak, F., Tang, W., et al. (2018). Single-cell analysis reveals cancer stem cell heterogeneity in hepatocellular carcinoma. *Hepatology* 68, 127–140. doi: 10.1002/hep.29778
- Zhou, W. Q., Ji, Z. C., Fang, W. X., and Ji, H. K. (2019). Global prediction of chromatin accessibility using small-cell-number and single-cell RNA-seq. *Nucleic Acids Res.* 47:e121. doi: 10.1093/nar/gkz716
- Zhou, W. Q., Sherwood, B., Ji, Z. C., Xue, Y. C., Du, F., Bai, J. W., et al. (2017). Genome-wide prediction of DNase I hypersensitivity using gene expression. *Nat. Commun.* 8:1038.
- Ziegenhain, C., Vieth, B., Parekh, S., Reinus, B., Guillaumet-Adkins, A., Smets, M., et al. (2017). Comparative analysis of single-cell RNA sequencing methods. *Mol. Cell* 65, 631.e4–643.e4. doi: 10.1016/j.molcel.2017.01.023

Conflict of Interest: The authors declare that the research was conducted in the absence of any commercial or financial relationships that could be construed as a potential conflict of interest.

Copyright © 2020 Li, Xu, Wu and Chen. This is an open-access article distributed under the terms of the Creative Commons Attribution License (CC BY). The use, distribution or reproduction in other forums is permitted, provided the original author(s) and the copyright owner(s) are credited and that the original publication in this journal is cited, in accordance with accepted academic practice. No use, distribution or reproduction is permitted which does not comply with these terms.



***b3galt6* Knock-Out Zebrafish Recapitulate β 3GalT6-Deficiency Disorders in Human and Reveal a Trisaccharide Proteoglycan Linkage Region**

Sarah Delbaere¹, Adelbert De Clercq¹, Shuji Mizumoto², Fredrik Noborn^{3,4}, Jan Willem Bek¹, Lien Alluyn¹, Charlotte Gistelincx⁵, Delfien Syx¹, Phil L. Salmon⁶, Paul J. Coucke¹, Göran Larson^{3,4}, Shuhei Yamada², Andy Willaert^{1†} and Fransiska Malfait^{1*†}

OPEN ACCESS

Edited by:

Mario Antonio Bianchet,
Johns Hopkins University,
United States

Reviewed by:

Ross F. Coltery,
Medical College of Wisconsin,
United States
Joseph M. Chambers,
Manchester University, United States

***Correspondence:**

Fransiska Malfait
Fransiska.Malfait@UGent.be

[†]These authors have contributed
equally to this work

Specialty section:

This article was submitted to
Molecular Medicine,
a section of the journal
Frontiers in Cell and Developmental
Biology

Received: 22 August 2020

Accepted: 17 November 2020

Published: 10 December 2020

Citation:

Delbaere S, De Clercq A,
Mizumoto S, Noborn F, Bek JW,
Alluyn L, Gistelincx C, Syx D,
Salmon PL, Coucke PJ, Larson G,
Yamada S, Willaert A and Malfait F
(2020) *b3galt6* Knock-Out Zebrafish
Recapitulate β 3GalT6-Deficiency
Disorders in Human and Reveal
a Trisaccharide Proteoglycan Linkage
Region.
Front. Cell Dev. Biol. 8:597857.
doi: 10.3389/fcell.2020.597857

¹ Department of Biomolecular Medicine, Center for Medical Genetics Ghent, Ghent University Hospital, Ghent University, Ghent, Belgium, ² Department of Pathobiochemistry, Faculty of Pharmacy, Meijo University, Nagoya, Japan, ³ Department of Laboratory Medicine, Sahlgrenska Academy at the University of Gothenburg, Gothenburg, Sweden, ⁴ Laboratory of Clinical Chemistry, Sahlgrenska University Hospital, Gothenburg, Sweden, ⁵ Department of Orthopaedics and Sports Medicine, University of Washington, Seattle, WA, United States, ⁶ Bruker MicroCT, Kontich, Belgium

Proteoglycans are structurally and functionally diverse biomacromolecules found abundantly on cell membranes and in the extracellular matrix. They consist of a core protein linked to glycosaminoglycan chains via a tetrasaccharide linkage region. Here, we show that CRISPR/Cas9-mediated *b3galt6* knock-out zebrafish, lacking galactosyltransferase II, which adds the third sugar in the linkage region, largely recapitulate the phenotypic abnormalities seen in human β 3GalT6-deficiency disorders. These comprise craniofacial dysmorphism, generalized skeletal dysplasia, skin involvement and indications for muscle hypotonia. In-depth TEM analysis revealed disturbed collagen fibril organization as the most consistent ultrastructural characteristic throughout different affected tissues. Strikingly, despite a strong reduction in glycosaminoglycan content, as demonstrated by anion-exchange HPLC, subsequent LC-MS/MS analysis revealed a small amount of proteoglycans containing a unique linkage region consisting of only three sugars. This implies that formation of glycosaminoglycans with an immature linkage region is possible in a pathogenic context. Our study, therefore unveils a novel rescue mechanism for proteoglycan production in the absence of galactosyltransferase II, hereby opening new avenues for therapeutic intervention.

Keywords: *b3galt6*, zebrafish, trisaccharide linkage region, proteoglycans, linkeropathies

INTRODUCTION

Proteoglycans (PGs) comprise a group of complex biomacromolecules, consisting of a core protein and one or multiple glycosaminoglycan (GAG) side chains, that are ubiquitously expressed in the extracellular matrix (ECM) and on cell surfaces and basement membranes in vertebrate and invertebrate species (Prydz and Dalen, 2000; Selleck, 2000; Couchman and Pataki, 2012;

Lindahl et al., 2015). Besides their structural role, PGs act as mediators between the ECM and intracellular signaling pathways and contribute to development and tissue homeostasis, influencing a variety of cellular processes including cell fate determination, cell proliferation, migration, adhesion, differentiation, and survival (Malfait et al., 2013).

The PG superfamily is, depending on the composition of the GAG chains, subdivided into heparan sulfate (HS) and chondroitin/dermatan sulfate (CS/DS) PGs. These GAG chains are linear polysaccharides, composed of a repeated disaccharide unit consisting of an uronic acid and amino sugar. HSPGs, such as perlecan, syndecan and glypican, consist of repeating glucuronic acid (GlcA)-*N*-acetyl-glucosamine (GlcNAc) disaccharides. CSPGs consist of repeating GlcA-*N*-acetyl-galactosamine (GalNAc) disaccharides. DS is a stereoisomer of CS, in which GlcA is epimerized to iduronic acid (IdoA). In mammalian tissues, CS and DS chains are often present as hybrid CS-DS chains on PGs (e.g. decorin, biglycan) (Sugahara et al., 2003). Tightly controlled modifications, such as epimerization and sulfation reactions, further increase the structural and functional diversity of the HS and CS/DS PGs (Kusche-Gullberg and Kjellen, 2003; Bui et al., 2010). GAG biosynthesis of both HSPGs and CS/DS PGs is initiated in the endoplasmic reticulum and Golgi apparatus by the formation of a common tetrasaccharide linkage region (glucuronic acid-galactose-galactose-xylose-*O*-) (GlcA-Gal-Gal-Xyl-*O*-) via *O*-glycosylation of a serine residue of the core protein (**Figure 1A**; Prydz and Dalen, 2000; Couchman and Pataki, 2012; Lindahl et al., 2015). The first step in the biosynthesis of this tetrasaccharide linkage region is catalyzed by xylosyltransferases (XylTs) encoded by the paralogs *XYLT1* [MIM 608124] and *XYLT2* [MIM 608125] (Gotting et al., 2000). Two Gal residues are subsequently added by, respectively, galactosyltransferase I (GalT-I or β 4GalT7 encoded by *B4GALT7* [MIM 604327]) and galactosyltransferase II (GalT-II or β 3GalT6 encoded by *B3GALT6* [MIM 615291]) (Almeida et al., 1999; Bai et al., 2001). Further addition of a GlcA by glucuronosyltransferase I (GlcAT-I encoded by *B3GAT3*) [MIM 606374] completes the formation of the linkage region (Kitagawa et al., 1998).

The cellular machinery required for GAG biosynthesis and modification is conserved over a broad range of eukaryotic organisms (Wen et al., 2014). The particular importance of a correct initiation of GAG synthesis is underscored by the identification of a series of severe, overlapping and multisystemic genetic human disorders that result from deficient activity of any of these “linkage-enzymes,” collectively coined as “linkeropathies” (Guo et al., 2013; Nakajima et al., 2013; Jones et al., 2015). The most frequently reported linkeropathy results from galactosyltransferase II deficiency, caused by biallelic pathogenic variants in *B3GALT6*. This leads to two clinically overlapping conditions, spondylodysplastic Ehlers-Danlos syndrome (EDS) (spEDS-*B3GALT6*) and spondyloepimetaphyseal dysplasia with joint laxity type I (SEMD-JL1) (Malfait et al., 2013; Nakajima et al., 2013), both of which are characterized by variable degrees of spondyloepimetaphyseal bone dysplasia (with postnatal growth restriction, bowing of long bones, hypo- or dysplasia of iliac and long bones, and vertebral body changes),

kyphoscoliosis, bone fragility with spontaneous fractures, joint hypermobility in conjunction with joint contractures, hypotonia with delayed motor development, skin fragility, and craniofacial dysmorphisms, including midfacial hypoplasia and dysplastic teeth (Malfait et al., 2013, 2017; Nakajima et al., 2013). The severe and pleiotropic phenotype suggests a critical role for *B3GALT6* in the development and homeostasis of various connective tissues. Pathogenic variants in *B3GALT6* either result in mislocalization and/or reduced amounts of active galactosyltransferase II (Ritelli et al., 2015). Previous studies on several biallelic *B3GALT6* variants showed that they resulted in a barely detectable *in vitro* galactosyltransferase II enzymatic activity, but intriguingly HS and CS/DS GAG synthesis was partially preserved *in cellulo* (Van Damme et al., 2018). While some variants may have a greater deleterious effect on the *in vitro* than on the *in cellulo* enzymatic activity, it is currently unknown whether there are rescue mechanisms at play to partially compensate for the galactosyltransferase II activity.

In recent years, zebrafish have emerged as an excellent tool to model disease and to increase our understanding of developmental processes and disease mechanisms. Zebrafish share 70% of their genes with humans (Santoriello and Zon, 2012) and the advantages of their use are reflected by their large breed size, short lifecycle and low husbandry costs (Dooley and Zon, 2000). Zebrafish has proven to be a relevant genetic model for the study of PG biosynthesis since many enzymes involved in this process are strongly conserved between human and zebrafish (Eames et al., 2010), and a number of zebrafish models for defective PG synthesis (including *fam20b*^{b1125}, *xylt1*^{b1189}, or *b3gat3*^{hi307}), provided novel knowledge on PG function in bone and cartilage formation (Amsterdam et al., 2004; Nissen et al., 2006; Eames et al., 2010, 2011).

In this study, we generated *b3galt6* knock-out (KO) zebrafish as a model for spEDS-*B3GALT6* and SEMD-JL1. These models were used to investigate the structure and amount of different GAG disaccharides and the PG linkage region composition in these disorders. Furthermore, in-depth phenotypic characterization of *b3galt6*^{-/-} zebrafish was done to reveal to which extent key features of the human disorders are recapitulated and to further elucidate the function of galactosyltransferase II in vertebrate musculoskeletal development.

RESULTS

CRISPR/Cas9-Mediated *b3galt6* Knock-Out in Zebrafish Leads to Reduced HS and CS/DS Glycosaminoglycan Concentrations in Bone, Muscle, and Skin

Similar to its human ortholog, zebrafish *b3galt6* (NM_001045225.1) is a single-exon gene (**Figure 1B**). Human and zebrafish galactosyltransferase II (β 3GalT6/*B3galt6*) protein sequence display 82.5% amino acid (AA) similarity, with the highest AA conservation in the luminal domain (**Figure 1C**).

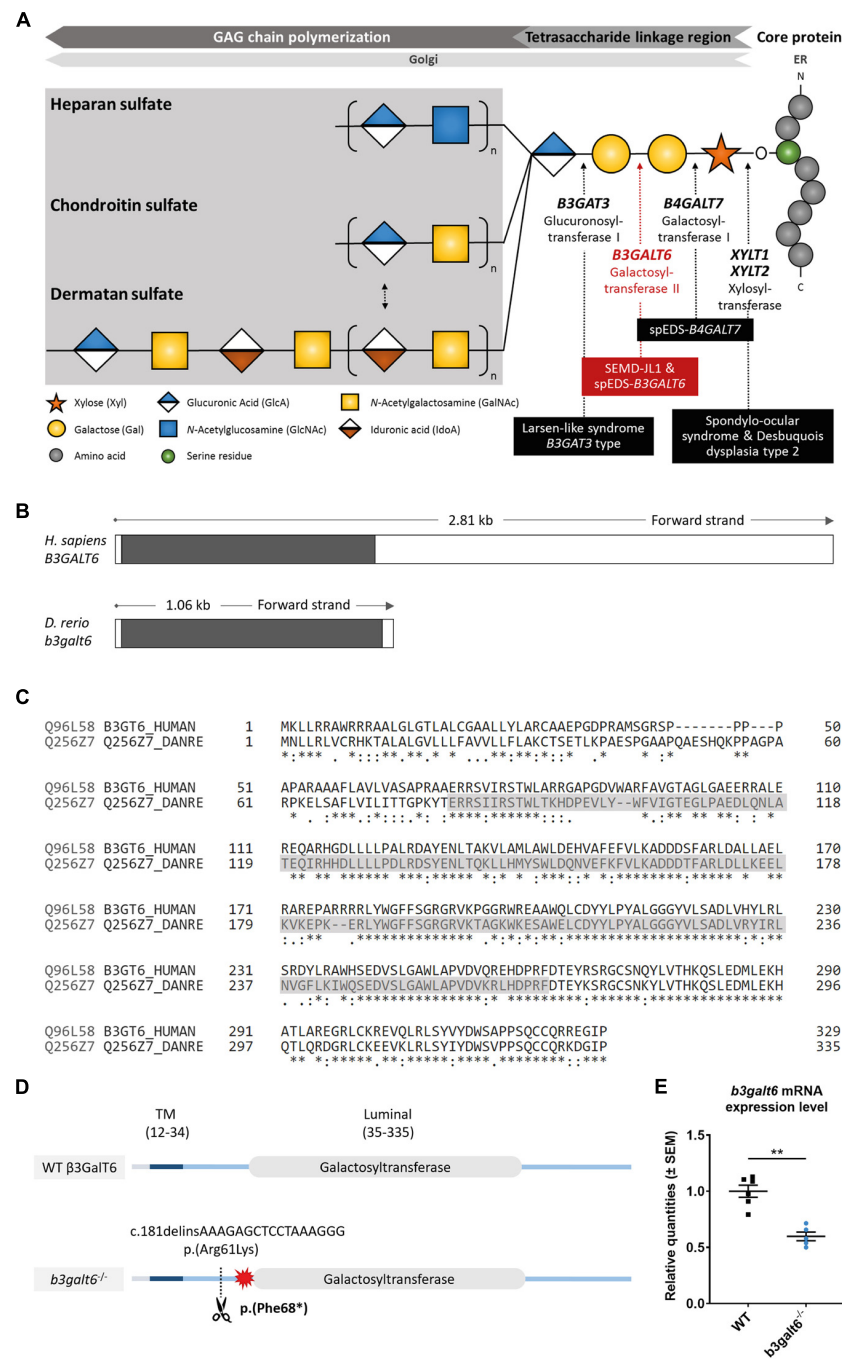


FIGURE 1 | Schematic representation of the GAG biosynthesis and the evolutionary conservation of the zebrafish and human *b3gal6/B3GALT6* gene and *B3gal6/β3GalT6* protein. **(A)** Simplified schematic representation of the PG linkage and GAGs biosynthesis. PG core proteins are synthesized in the endoplasmic reticulum and undergo further modification in the Golgi apparatus. First, a tetrasaccharide linkage region is synthesized that originates from the addition of a Xyl onto a serine residue of the core protein. Subsequent addition of two Gals and one GlcA residues completes this process. Depending on the addition of GlcNAc or GalNAc to the terminal GlcA residue of the linkage region, HS or CS/DS PGs will be formed, respectively. The elongation of the GAG chain continues by repeated addition of uronic acid and amino sugar residues. The GAG chain is then further modified by epimerization and sulfation (not shown). The main genes encoding for the enzymes involved in the linkage region biosynthesis are indicated in bold and biallelic mutations in these genes result in different linkopathies. Disorders resulting from deficiency of the enzymes in the linkage region biosynthesis are indicated in black boxes. The deficient enzyme ($\beta 3\text{GalT6}$) and the related disorder studied here are depicted in red (e.g., spEDS-B3GALT6 and SEMD-JL1). **(B)** Schematic representation of the genomic structure of the *H. sapiens B3GALT6* (NM_080605.4) and *D. rerio b3gal6* (NM_001045225.1) genes. The white and black boxes represent the untranslated regions and the single *B3GALT6/b3gal6* exon, respectively. The zebrafish *b3gal6* (Continued)

FIGURE 1 | Continued

gene resides on chromosome 11, spans a region of 1.06 kb and has not been duplicated during teleost evolution. **(C)** Amino acid (AA) sequence alignment (Clustal Omega) between *H. sapiens* β 3GalT6 (Uniprot: Q96L58) and *D. rerio* B3galt6 (Uniprot: Q256Z7). The luminal galactosyltransferase domain is highlighted in gray. Conservation of AA sequences is shown below the alignment: "*" residues identical in all sequences in the alignment; "." conserved substitutions; " " semi-conserved substitutions; "space" no conservation. **(D)** Schematic representation of the cmg20 allele in *b3galt6* mutants. *b3galt6* consists of three parts, a cytosolic domain (AA 1-11), a transmembrane domain (TM, AA 12-34) and a luminal domain (AA 35-335). The location of the CRISPR/Cas9-generated indel variant is indicated by a scissor symbol and the resulting premature termination codon (PTC) is depicted by a red star. **(E)** RT-qPCR analysis of relative *b3galt6* mRNA expression levels in *b3galt6*^{-/-} adult zebrafish (0.597 ± 0.03919) ($n = 5$) compared to WT siblings (1 ± 0.05395) ($n = 6$). Data are expressed as mean \pm SEM. A Mann-Whitney U test was used to determine significance, ** $P < 0.01$.

In order to investigate the consequences of zebrafish B3galt6-deficiency on GAG biosynthesis, we generated two *b3galt6* KO zebrafish models using CRISPR/Cas9 gene editing. The first KO model carries the c.181delinsAAAGAGCTCCTAAAGGG indel mutation (cmg20 allele), leading to a premature termination codon (PTC) [p.(Phe68*)], located upstream to the catalytic domain (**Figure 1D**). RT-qPCR showed a 40.3% reduction of *b3galt6* mRNA expression in homozygous adult *b3galt6* KO zebrafish compared to wild-type (WT) siblings (**Figure 1E**). For the remainder of this manuscript, this model will be referred to as *b3galt6*^{-/-}. The second KO model carries a four base pair deletion (c.398_401del) (cmg22 allele), predicted to generate a PTC [p.(Asn139*)] in the catalytic domain (NM_001045225.1). This mutant was solely used for validation purposes (**Supplementary Figure S1**). Both *b3galt6* KO zebrafish were produced at an expected Mendelian ratio and survived into adulthood. Unfortunately, commercial antibodies, which were only available against human β 3GalT6, did not work in our hands and precluded the investigation of zebrafish B3galt6 protein levels and localization.

To examine the activity of B3galt6 in different *b3galt6*^{-/-} tissues, concentrations of CS, DS, and HS disaccharides extracted from bone, muscle and skin from WT and *b3galt6*^{-/-} zebrafish were quantified using a combination of enzymatic digestion and anion-exchange HPLC (**Supplementary Figures S2–S5** and **Supplementary Tables S1–S4**). Overall, a generalized decrease in HS, CS and DS concentration was detected in all examined tissues of *b3galt6*^{-/-} zebrafish. In the GAG fractions prepared from bone, the disaccharide concentration of the CS/DS and CS moieties was significantly decreased by, respectively, 55 and 64%, compared to WT zebrafish (**Table 1** and **Supplementary Tables S1, S2**). DS moieties were undetectable in bone of *b3galt6*^{-/-} zebrafish, whereas their concentration was 50.5 pmol/mg protein in bone of WT zebrafish (**Table 1** and **Supplementary Table S3**). A non-significant decrease in the disaccharide concentration of the HS moiety was observed in *b3galt6*^{-/-} mutant bone (**Table 1** and **Supplementary Table S4**), compared to WT. In GAG fractions prepared from *b3galt6*^{-/-} muscle, CS/DS, CS, and DS disaccharide moieties were generally lower than in WT muscle (**Table 1** and **Supplementary Tables S1–S3**). Due to the low concentrations close to the detection limit, a significant reduction could only be detected for the DS moiety (72% reduction) (**Table 1** and **Supplementary Table S3**). In addition, a significant decrease in HS disaccharide moieties by 56% was noted in *b3galt6*^{-/-} muscle compared to WT muscle (**Table 1** and **Supplementary Table S4**). In the GAG fractions prepared from *b3galt6*^{-/-} skin, the concentration of all

TABLE 1 | Concentrations of GAG disaccharides in wild-type and *b3galt6*^{-/-} zebrafish tissues.

	pmol/mg protein (Average \pm SE)			
	CS/DS	CS	DS	HS
Bone				
Wild-type	774.2 \pm 19.9	728.4 \pm 148.1	50.5 \pm 8.1	178.6 \pm 19.8
<i>b3galt6</i> ^{-/-}	346.1 \pm 20.0*	279.9 \pm 4.8**	N.D.	137.1 \pm 39.7 ^{ns}
Muscle				
Wild-type	9.3 \pm 0.4	2.1 \pm 0.4	14.5 \pm 1.1	30.8 \pm 1.2
<i>b3galt6</i> ^{-/-}	5.7 \pm 3.1 ^{ns}	N.D.	4.1 \pm 1.0*	13.5 \pm 4.0**
Skin				
Wild-type	236.2 \pm 26.5	175.1 \pm 25.3	75.9 \pm 7.9	55.1 \pm 4.5
<i>b3galt6</i> ^{-/-}	55.4 \pm 15.2*	47.9 \pm 13.5**	33.8 \pm 6.3**	21.0 \pm 2.8**

Student's *t*-test (vs. wild-type) ($n = 3$), N.D., not detected (< 1 pmol/mg protein), * $P < 0.01$, ** $P < 0.05$, ns: not significant, SE: standard error.

disaccharide moieties was significantly reduced compared to WT (**Table 1** and **Supplementary Tables S1–S4**). The disaccharide concentration of the CS/DS, CS, DS and HS moieties were decreased by, respectively, 77, 73, 55, and 62% compared to WT (**Table 1** and **Supplementary Tables S1–S4**). No altered sulfation patterns were observed in disaccharide moieties when comparing unique GAG chains between WT and *b3galt6*^{-/-} zebrafish samples (**Supplementary Tables S1–S4**).

Despite the strong reduction in disaccharide concentrations observed in *b3galt6*^{-/-} zebrafish, low amounts of GAGs were still produced in the mutants. Similar results were obtained for the second *b3galt6* KO zebrafish (cmg22 allele) (**Supplementary Table S5**). RT-qPCR revealed no significant upregulation of other galactosyltransferase(s) member(s) from the *b3galt* family (*b3galt1a*, *b3galt2*, *b3galt4*, *b3galt5*) or of other linkage-enzymes (*xylt1*, *xylt2*, *b4galt7* and *b3gat3*) (**Supplementary Figure S6**), suggesting that altered expression of these genes did not compensate for the reduced *b3galt6* mRNA levels.

B3galt6-Deficiency Leads to the Biosynthesis of a Non-canonical (GlcA-Gal-Xyl-O-) Trisaccharide Linkage Region in Zebrafish

In order to explain why *b3galt6*^{-/-} zebrafish can still produce GAG chains on PG core proteins, we investigated the composition of the linkage region. To this purpose, whole zebrafish extracts were enriched for all PGs, their GAG chains depolymerized with bacterial lyases, the core proteins digested

with trypsin and the remaining glycopeptides subjected to nano-scale liquid chromatography-tandem mass spectrometry (nLC-MS/MS) using a recently developed glycoproteomic approach (Noborn et al., 2015; Persson et al., 2019). Potential structural differences in PG linkage regions in WT versus $b3galt6^{-/-}$ zebrafish are thus elucidated through the combined identities of peptide backbones and GAG linkage region structures. The glycoproteomic analysis identified two CS-glycopeptides derived from biglycan (UniProt: A8BBH0) in both the WT and $b3galt6^{-/-}$ zebrafish. These CS-glycopeptides displayed different linkage region structures in WT compared with $b3galt6^{-/-}$ zebrafish (Figure 2). While the peptide in the WT zebrafish was modified with a hexasaccharide structure (Figure 2A), the peptide in the $b3galt6^{-/-}$ zebrafish was modified with a pentasaccharide structure (Figure 2B), supporting the hypothesis that $b3galt6^{-/-}$ zebrafish produces a non-canonical trisaccharide linkage region. The precursor ion (m/z 1281.7922; 3+) in the WT zebrafish equated to a mass of a peptide (DQEEGSAVEPYKPEHPTCPFGCR) modified with a hexasaccharide structure, with the peptide containing two carbamidomethyl (CAM) modifications. Furthermore, the hexasaccharide structure was modified with one sulfate group (SO_3^-) on the subterminal GalNAc residue [$GlcAGalNAc-H_2O + SO_3 + H$] $^+$, and one phosphate group (HPO_3^-) on the Xyl residue (Supplementary Figure S7). In contrast, the precursor ion (m/z 1227.7765; 3+) in the $b3galt6^{-/-}$ zebrafish equated to a mass of the same peptide but modified with a pentasaccharide structure, with two phosphate/sulfate groups, with the peptide containing two CAM modifications. The difference in mass between the WT and $b3galt6^{-/-}$ precursor ions corresponds to 162.08 Da, equating to the mass of a hexose (galactose) residue (162 Da). Additional HS- and CS-glycopeptides with the expected tetrasaccharide linkage region were found in the WT. In the $b3galt6^{-/-}$, no HS-modified structures were identified but additional CS-glycopeptides with the non-canonical trisaccharide linkage region were found. Supplementary Table S6 shows a complete list of all glycopeptides identified in both WT and $b3galt6^{-/-}$ zebrafish. PGs harboring a tetrasaccharide linkage region were never detected in the $b3galt6^{-/-}$ adult zebrafish samples and no trisaccharide linkage region was detected in WT zebrafish samples.

These observations suggest that B3GAT3/GlcAT-I can transfer a GlcA residue not only to Gal-Gal-Xyl, but also to a Gal-Xyl substrate. This was confirmed by an *in vitro* GlcAT-I assay, which showed that GlcAT-I is indeed capable of adding a GlcA to a Gal-Xyl-*p*-nitrophenyl, which was chemically synthesized, thus to a substrate ending with a single galactose (Supplementary Figure S8).

$b3galt6^{-/-}$ Zebrafish Show Early Onset, Progressive Morphological Abnormalities and Delay of Cartilage and Bone Formation, Reminiscent of Human spEDS-B3GALT6

One of the clinical hallmarks of human spEDS-B3GALT6 is the pronounced skeletal involvement with the presence

of spondyloepimetaphyseal dysplasia with postnatal growth restriction, bowing of long bones, hypoplasia of iliac bones, femoral head dysplasia, vertebral body changes, kyphoscoliosis and bone fragility with spontaneous fractures (Table 2). To evaluate the development of cartilage and bone associated with B3galt6-deficiency in zebrafish, phenotypic characterization of $b3galt6^{-/-}$ zebrafish was performed in juvenile (20 dpf, days post fertilization) and adult stages (4 months).

At 20 dpf, the average weight (W), standard length (SL) and Fulton's condition factor (K), which is used as a measure for the relative proportion of SL to W (Nash et al., 2006), were not significantly different between $b3galt6^{-/-}$ and WT siblings (Figure 3A), although for SL there was a trend toward smaller mutants ($P = 0.0640$). Several externally visible morphological anomalies could be observed in 20 dpf $b3galt6^{-/-}$ zebrafish as compared to their WT siblings, including a shorter, more compact head, a shorter and rounder frontal region, a shorter parietal/occipital region and a malformed posterior edge of the opercular apparatus (Figure 3B). Alcian blue (AB) cartilage staining showed no morphological abnormalities, but developmental delay of the head and pectoral and caudal fin endoskeleton was noted (Figure 3B and Supplementary Table S7), with cartilage elements being absent or in early development in $b3galt6$ KO, while these structures were already fully developed in WT sibling zebrafish. Alizarin red (AR) mineral staining showed delayed mineralization in all regions of the head, the pectoral fin girdle and the caudal fin (Figure 3B and Supplementary Table S8), further confirming developmental retardation. In addition, malformations of different mineralized bones, such as the parasphenoid, branchiostegal rays, supracleithrum, and the subopercle bone could be detected in the head of $b3galt6^{-/-}$ zebrafish larvae (Supplementary Figure S9). The vertebral column, i.e., the vertebral centra and their associated elements (neural and haemal arches), did not show delayed mineralization in $b3galt6^{-/-}$ zebrafish larvae, but malformation of the associated elements and fusions of preural vertebrae were observed at a much higher frequency in the $b3galt6^{-/-}$ mutants. Kyphosis, scoliosis and lordosis were also more frequently observed and pronounced in $b3galt6^{-/-}$ larvae compared to WT siblings (Supplementary Figure S10 and Supplementary Table S8). A similar phenotype was observed in the second $b3galt6$ KO model (cmg22 allele), confirming the specificity of the displayed phenotype (Supplementary Figure S11).

At the adult stage (4 months), $b3galt6^{-/-}$ zebrafish had a significantly reduced average SL (1.834 ± 0.077 cm), and W (0.1196 ± 0.014 g), when compared to their WT siblings (2.371 ± 0.049 cm, and 0.2497 ± 0.016 g, respectively), while the Fulton's condition factor (K) indicated that SL and W were normally proportioned to each other (Figure 4A). A similar phenotype was observed in the second $b3galt6$ KO model (cmg22 allele), confirming the specificity of the displayed phenotype (Supplementary Figure S1).

The head malformations, which were already observed in 20 dpf $b3galt6^{-/-}$ zebrafish, showed further progression, with a more pronounced smaller, rounded head and an abnormal

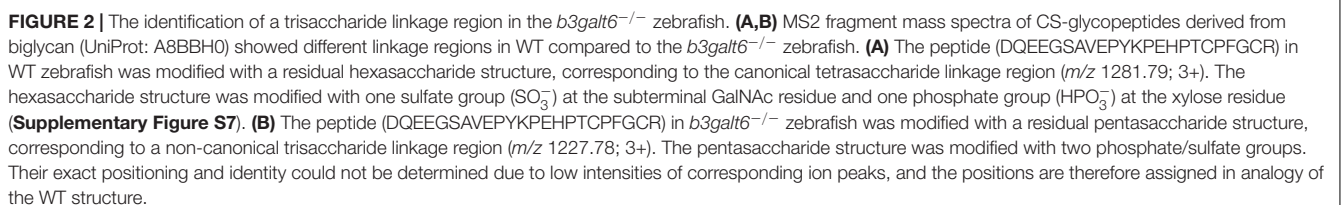


TABLE 2 | Clinical features and ultrastructural and biochemical abnormalities observed in spEDS-*B3GALT6* and SEMD-JL1 individuals compared to the *b3galt6*^{-/-} zebrafish model.

	Human		Zebrafish
	spEDS- <i>B3GALT6</i>	SEMD-JL1	<i>b3galt6</i> ^{-/-} mutant
General morphology			
Short stature	22/30	11/14	Reduced body length
Craniofacial dysmorphisms (e.g., midfacial hypoplasia, micrognathia)	25/30	12/14	Deformed, small and round head with shorter parietal/occipital region and underdeveloped olfactory region
Dental abnormalities	14/30	n.a.	Smaller teeth
Musculoskeletal involvement			
Bowing of limbs, metaphyseal widening or vertebral body changes	20/30	14/14	Deformities of the fin skeleton
Bone fragility with spontaneous fractures	19/30	0/3	Extra intramembranous bone, lower degree of collagen type I fibril organization and higher TMD after correction for smaller size
Joint contractures (especially hands)	23/30	5/14	Pectoral fins point upwards
Joint hypermobility	26/30	6/14	n.a.
Kyphoscoliosis	23/30	13/14	Kyphosis and scoliosis
Muscle hypotonia	18/30	1/14	Reduced critical swimming speed and endurance
Skin features			
Skin hyperextensibility	19/30	2/14	n.a.
Biochemical findings			
Reduced GAG synthesis	9/9	4/4 (3/4; <HS but >CS/DS)	Reduced GAG production
Ultrastructural findings			
Loosely packed collagen fibrils	1/1	n.a.	Disturbed collagen fibril organization in bone and loosely packed collagen fibrils in the dermis

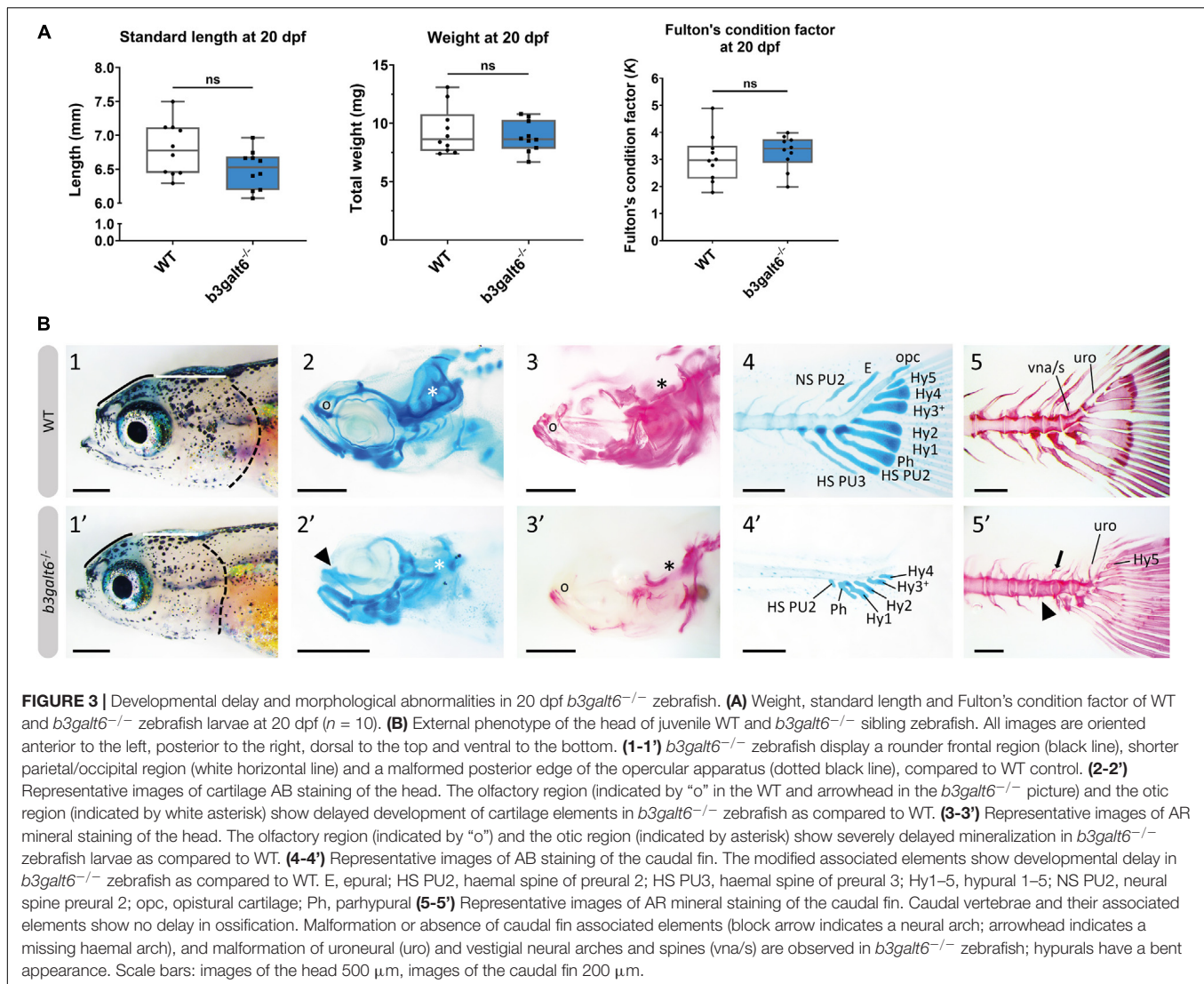
n.a., not available; GAG, glycosaminoglycan. The columns "spEDS-*B3GALT6*" and "SEMD-JL1" summarize the most important clinical features of all hitherto reported patients for whom this data was available (Van Damme et al., 2018; Caraffi et al., 2019).

compaction of the opercular apparatus (**Figure 4B**). In addition, a reduced surface area of the fins, with a crenelated postero-distal fin edge was observed in the mutant animals. The pectoral fins were pointing in an abnormal upwards angle (**Figure 4B**). In addition, an altered pigmentation pattern was observed, mainly on the ventral part of the body where the dark stripes showed interruptions (**Figure 4B**).

Further progression of the larval phenotype was also confirmed by AR staining of the mineralized skeleton in adult (4 months) *b3galt6*^{-/-} zebrafish. The olfactory region was underdeveloped (**Figure 5A**), the cranial roof bones and sutures were deformed (**Supplementary Figure S12**) and the opercular apparatus was smaller and compacted in KO zebrafish (**Figure 5A** and **Supplementary Figure S12**). The fifth ceratobranchial arch and its attached teeth were smaller in *b3galt6*^{-/-} zebrafish (**Figure 5B**). In the pectoral fins of *b3galt6*^{-/-} zebrafish the radials were smaller, had an irregular shape, and were often fused (**Figure 5B**). The autocentra, i.e., the inner layer of the vertebral centra in the vertebral column and caudal fin (Arratia and Schultze, 1992) of KO zebrafish had a normal hourglass shape, but the associated elements often showed presence of extra intramembranous bone (**Figure 5** and **Supplementary Figure S12**) and extra bony elements (**Figure 5A**). Fusions were observed in preural vertebrae (**Figure 5A** and **Supplementary Figures S12B,C**).

Lordosis and scoliosis was variably observed in the caudal region of the vertebral column of *b3galt6*^{-/-} mutant zebrafish (**Supplementary Figures S12B,C**). Extra mineralization was observed at the edge (growth zone) of *b3galt6*^{-/-} scales (**Figure 5B**). Notably, variation in the severity of the skeletal malformations in *b3galt6*^{-/-} zebrafish was observed.

Subsequent quantitative μ CT analysis of 4 months old zebrafish revealed multifaceted effects of *B3galt6*-deficiency on vertebral morphology and mineralization. Most notably, the volume of vertebral centrum, haemal and neural associated elements was significantly reduced throughout the entire vertebral column in *b3galt6*^{-/-} zebrafish ($P < 0.01$), with more pronounced differences in the abdominal region (**Figure 6**). Tissue mineral density (TMD) was not significantly different in the *b3galt6*^{-/-} vertebral bodies compared to WT siblings. However, TMD in zebrafish is proportionally related to standard length (Parichy et al., 2009; McMenamin et al., 2016), and *b3galt6*^{-/-} zebrafish exhibited a significantly reduced body size compared to the WT siblings. We therefore normalized the μ CT data to standard length using the normalization procedure outlined by Hur et al. (2017). In this procedure, phenotypic data in WT sibling controls was scaled using the mean standard length of *b3galt6*^{-/-} zebrafish as the reference length. Remarkably, after normalization, a significant increase in TMD of centrum, haemal and neural associated elements was noted in *b3galt6*^{-/-} zebrafish



compared to WT controls ($P < 0.001$, $P < 0.01$, and $P < 0.01$, respectively) (Supplementary Figure S13).

***b3galt6* Knock-Out Zebrafish Display a Disturbed Organization of Type I Collagen Fibrils in Skin, Bone, and Intervertebral Space**

Transmission electron microscopy (TEM) studies on the dermis of spEDS- $B3\text{GALT6}$ patients revealed an abnormal collagen fibril architecture with loosely packed collagen fibrils of variable size and shape (Malfait et al., 2013). We therefore studied the effect of loss of galactosyltransferase II activity on collagen fibril architecture. TEM sections of skin biopsies of $b3galt6^{-/-}$ zebrafish showed an abnormal dermal collagen fibril architecture characterized by loosely packed collagen fibrils and larger and more interfibrillar spaces compared to WT siblings (Figure 7A). In addition, at the level of the scales a thicker epidermal layer was observed and electron dense structures were present in the interfibrillar spaces (Figure 7A). Next, we examined

the intervertebral region and adjacent vertebral centra in the vertebral column of 5 months old zebrafish by means of TEM. In general, the type I collagen fibers in $b3galt6^{-/-}$ zebrafish displayed a lower degree of organization (Figure 7B). This was observed in immature collagen layers, deposited by osteoblasts in the outer edges of the intervertebral space, but also in the mature type I collagen layers of the intervertebral ligament and in the autocentrum, the inner layer of the vertebral bone, where a lack of the typical plywood-like organization was seen. Detailed investigation of TEM sections of the vertebral bone revealed presence of several electron dense spots of unknown origin in knock-outs. These "dark spots" may reflect extrafibrillar hydroxyapatite crystals (Figure 7B).

Mass spectrometry analysis of type I collagen modification in bone derived from the vertebral column showed no significant difference in hydroxylation status of the $\alpha 1(\text{I})$ K87 and C-telopeptide lysine residues (Supplementary Table S9). These lysine residues are conserved in zebrafish and human type I collagen and are crucial for intermolecular crosslinking of collagen fibrils in bone matrix (Gistelink et al., 2017).

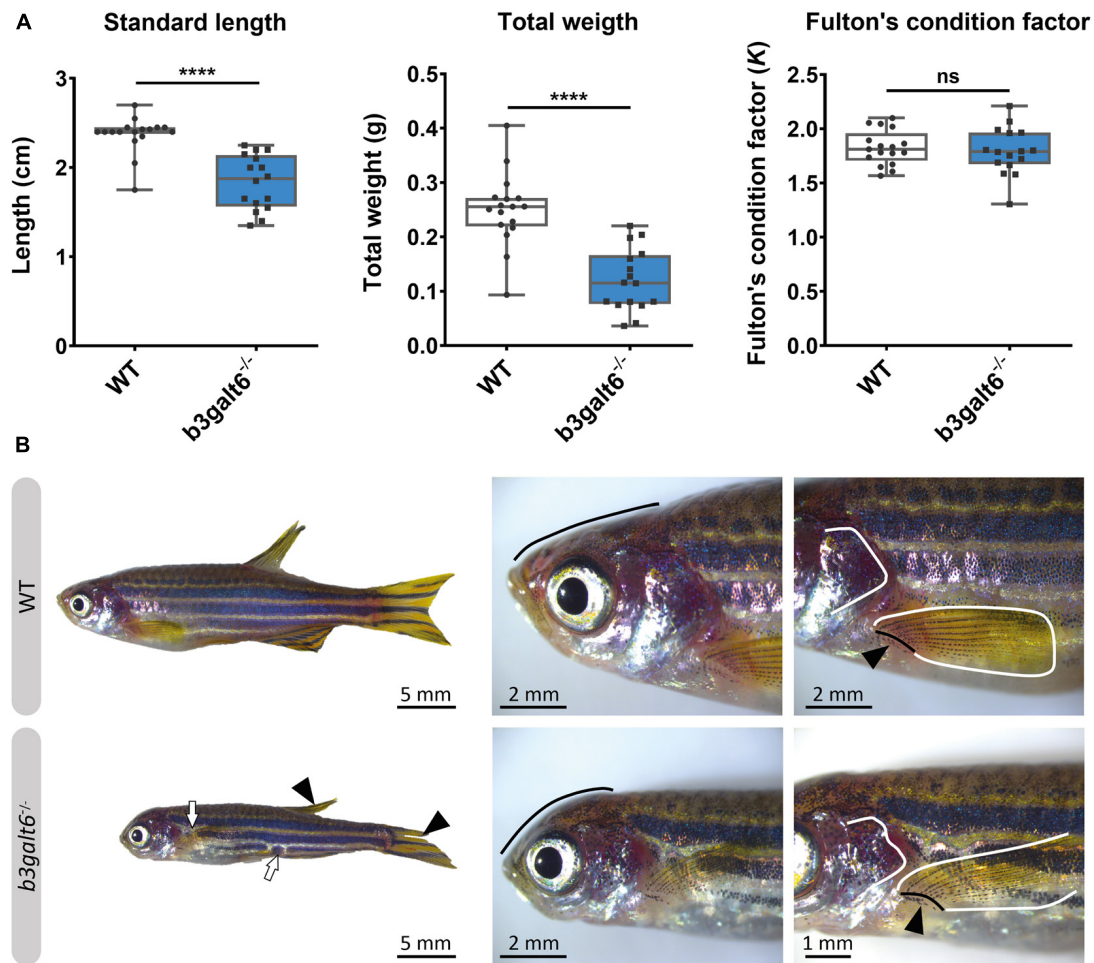


FIGURE 4 | Characterization of the external phenotype of adult $b3galt6^{-/-}$ zebrafish. **(A)** $b3galt6^{-/-}$ zebrafish ($n = 16$) had a significantly shorter standard length (SL) compared to their WT siblings ($n = 17$). The weight (W) was significantly lower in the mutant zebrafish. The Fulton's condition factor [$K = 100 \cdot (W/SL^3)$] was not significantly different between $b3galt6^{-/-}$ zebrafish and WT siblings. Data are expressed as box plots with min-to-max whiskers on which each individual data point is plotted. An unpaired t -test with Welch's correction was used to determine significance. **** $P < 0.0001$, ns: not significant. **(B)** Adult $b3galt6^{-/-}$ zebrafish exhibit morphological abnormalities compared to their WT siblings; $b3galt6^{-/-}$ zebrafish display interruptions of the blue horizontal stripes (white arrows), smaller fins (arrowhead), aberrations of the head shape (black line), of the shape of the opercular apparatus (white line indicates the posterior edge) and of the pectoral fin (black line and arrow indicate the fin rays at the base of the fin, white line shows the outline of the fin).

***b3galt6* Knock-Out Zebrafish Display Ultrastructural Muscle Abnormalities and Lower Endurance**

Human spEDS-*B3GALT6* patients often suffer from muscle hypotonia with a delay in motor development. In view of the observed reduction in the concentration of the different GAG moieties in muscle of $b3galt6^{-/-}$ zebrafish, we investigated the function and the ultrastructural appearance of muscle.

First, the critical swimming speed (U_{crit}) and endurance of the zebrafish were assessed by means of a custom-made swim tunnel. The U_{crit} , defined as the maximum velocity that the tested zebrafish could sustain for at least 5 min (Plaut, 2000), was significantly lower in $b3galt6^{-/-}$ zebrafish (30.1 ± 2.39 cm/s) compared to length-matched WT (41.61 ± 1.942 cm/s) ($P < 0.01$) (Figure 8A). The stamina of each zebrafish was determined by

an effort test where it was tested how long zebrafish could swim at high speed (37 cm/s) after a 3 min warm-up. This effort test showed that the $b3galt6^{-/-}$ zebrafish performed less well compared to length-matched WT zebrafish, indicating a lower endurance (Figure 8B).

The muscle tissue in the zebrafish trunk was further investigated at the ultrastructural level. Toluidine blue-stained semi-thin cross sections revealed that the endomysium, a layer of connective tissue ensheating the muscle fibers, was enlarged along the horizontal myoseptum of $b3galt6^{-/-}$ zebrafish, although no clear differences in muscle fiber diameter were noted (Figure 8C). Ultra-thin parasagittal sections, investigated by TEM, showed that the length of the sarcomeres, the smallest basic units of striated muscle, as well as the length of the A and I band were significantly increased in the $b3galt6^{-/-}$ zebrafish (Figure 8D).

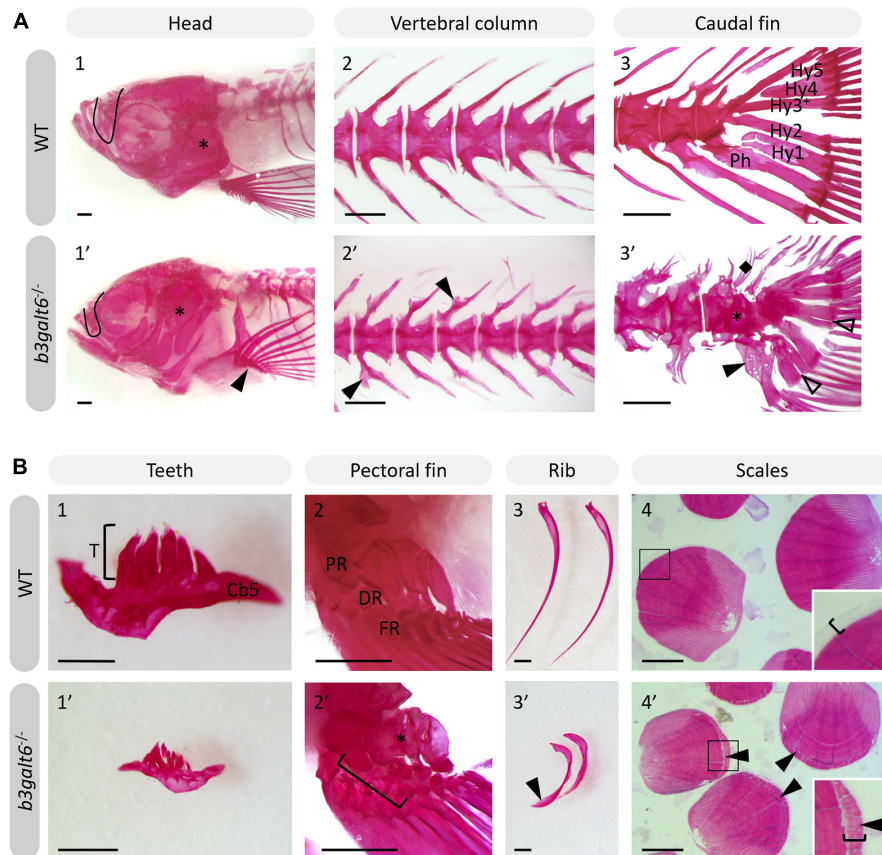
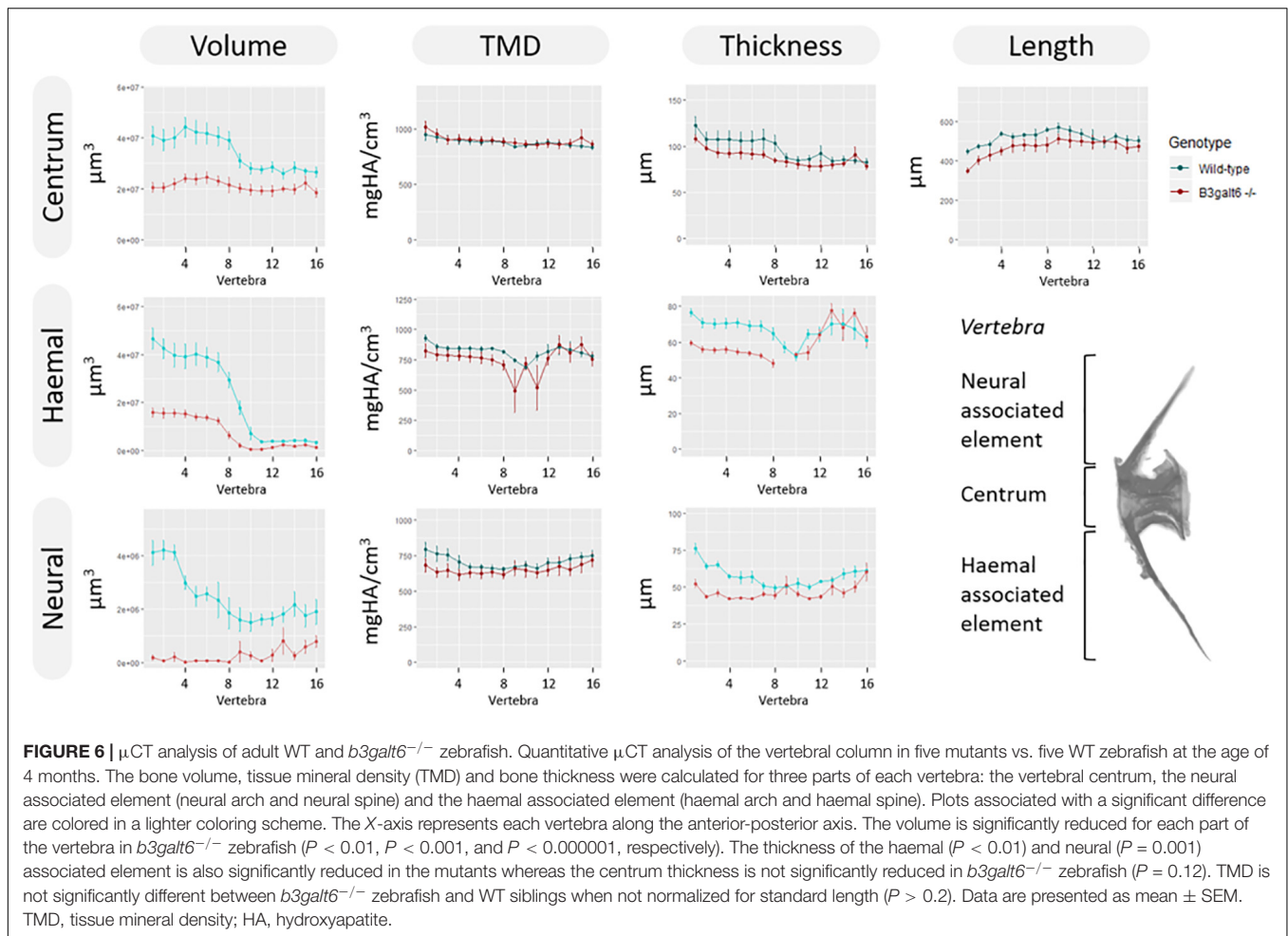


FIGURE 5 | Alizarin red stained mineralized bone in WT and $b3galt6^{-/-}$ adult zebrafish. The mineralized bones in the skeleton were studied in 4 months old WT and mutant zebrafish after AR mineral staining. **(A)** $b3galt6^{-/-}$ zebrafish display malformation of the cranium, vertebral column and caudal fin. **(A1-1')** The cranium shows an underdeveloped olfactory region (black line) and a smaller compacted opercular bone (asterisk). **(A2-2')** The vertebral column shows extra intramembranous outgrowths located where the distal tip of the neural and haemal arches fuse to a neural and haemal spine, respectively (arrowheads). **(A3-3')** In the caudal fin fusion of preural vertebrae is observed (asterisk). Associated elements show intramembranous outgrowths (arrowhead) and the presence of extra bony elements (diamond). The distal tip of the hypurals is sometimes split (transparent arrowhead). Structures indicated in the WT caudal fin: Hy1-5, hypural 1-5, Ph, parhypural. **(B)** Details of mineralized structures in $b3galt6^{-/-}$ zebrafish. **(B1-1')** The fifth ceratobranchial arch and its teeth are smaller in KO zebrafish. **(B2-2')** The proximal (PR) and distal radials (DR) have irregular shapes in mutant zebrafish. Proximal (asterisk) and distal radials are sometimes fused. The bracket indicates a fusion between a proximal and distal radial, and the first fin ray (FR). **(B3-3')** Ribs also show extra intramembranous bone (black arrowhead). **(B4-4')** More mineralization was observed at the growth zone (bracket) of the scales in mutant zebrafish (arrowhead). Scale bars = 500 μ m.

DISCUSSION

In this study we developed two viable $b3galt6$ KO zebrafish models using CRISPR/Cas9 mutagenesis, and performed an in-depth characterization of the biochemical, ultrastructural and phenotypical consequences of β 3GalT6-deficiency on different tissues, including skin, cartilage, mineralized bone and muscle. These models currently represent the only vertebrate models available for the study of the pathogenetic consequences of β 3GalT6-deficiency on tissue development and homeostasis. In both models we detected a significant reduction, yet not a complete absence in $b3galt6$ mRNA expression (**Figure 1E**). One possible explanation is the absence of canonical nonsense-mediated decay (NMD) in the single-exon $b3galt6$ gene, due to a lack of exon junction complexes (EJCs) (Wittkopp et al., 2009). We were unable to examine the effect of the mutations on β 3GalT6 protein levels and localization due to the unavailability

of a suitable antibody. Nevertheless, since the *cmg20* and *cmg22* alleles are predicted to introduce a PTC, respectively, upstream and in the catalytic domain, residual translation of some mRNA into a truncated protein is not expected to lead to the production of an active enzyme. β 3GalT6 is a key enzyme in the biosynthesis of the common linkage region of PGs, and reduced levels of active enzyme are thus expected to equally affect the biosynthesis of HS and CS/DS GAG chains. We therefore quantified the disaccharide concentrations in bone, muscle and skin of adult $b3galt6^{-/-}$ zebrafish by means of a combination of enzymatic digestion and anion-exchange HPLC. This revealed a distinct, and relatively proportional decrease in the concentration of CS, DS, hybrid CS/DS and HS moieties in all examined tissues, compared to age-matched WT zebrafish (**Table 1**). Nonetheless, low amounts of GAGs were still produced in the KO zebrafish in absence of upregulation of other galactosyltransferase member(s) from the *b3galt* family or



by other linkage-enzymes (**Supplementary Figure S6**). Together with the previous demonstration that the other five $\beta 3\text{GalT}$ human enzymes (e.g., $\beta 3\text{GalT1}$, $\beta 3\text{GalT2}$, $\beta 3\text{GalT3}/\beta 3\text{GalNacT1}$, $\beta 3\text{GalT4}$, and $\beta 3\text{GalT5}$) are involved in the biosynthesis of glycoproteins and glycolipids (Bai et al., 2001), compensation for galactosyltransferase II deficiency in zebrafish by other $\beta 3\text{galT}$ family members is unlikely. Chinese hamster ovary $B3\text{galT6}$ KO cells were also shown to be capable of producing GAGs, in contrast to $Xylt2$, $B4\text{galT7}$ or $B3\text{galT3}$ KO cells (Chen et al., 2018). The recent identification of the presence of a non-canonical trisaccharide linkage region, lacking one Gal residue (GlcA-Gal-Xyl-O-), as a minor constituent in the PG bikunin in the urine of healthy human individuals (Persson et al., 2019), prompted us to examine the composition of the GAG linkage region in our $\beta 3\text{galT6}$ KO zebrafish models, by analyzing protein extracts from adult $\beta 3\text{galT6}^{-/-}$ and WT zebrafish via LC-MS/MS. This led to the striking finding that the few detected PGs in the $\beta 3\text{galT6}^{-/-}$ zebrafish all presented with a trisaccharide PG linkage region, consisting of only one Gal (**Figure 2B** and **Supplementary Table S6**). Further *in vitro* analysis indicated that GlcAT-I/ $\beta 3\text{GAT3}$ is capable of adding a GlcA to Gal-Xyl-O- (**Supplementary Figure S8**). This observation might explain the phenotypic differences observed between GalT-II/ $\beta 3\text{GALT6}$

deficiency and deficiencies of the other linkage region enzymes, for which such a rescue mechanism might be absent. This hypothesis is supported by the lack of GAGs in the Chinese hamster ovary $Xylt2$, $B4\text{galT7}$ or $B3\text{galT3}$ KO cells and by the lethal phenotype observed in the $B4\text{galT7}$ KO zebrafish model (Delbaere et al., 2020b). At present, we have no information on the length of the GAG chains attached to the trisaccharide linkage region or the composition and the possible modifications of these HS and CS/DS chains. As such, the GAG structure, length and modifications in the $\beta 3\text{galT6}^{-/-}$ zebrafish might be different from the ones in WT zebrafish.

HSPGs and CS/DSPGs are essential macromolecules for the development, signaling and homeostasis of many tissues. It therefore comes as no surprise that defects in linkage region biosynthesis can affect many organs. Endochondral ossification of cartilage (forming chondral bones) for example is a multi-staged process that must be coordinated in space and time. CS/DSPGs and HSPGs, which have key roles in modulating signaling events during vertebrate skeletal development, are expressed in a spatially and temporally highly controlled manner (Eames et al., 2011), thus regulating the timing of endochondral ossification. Genetic defects disrupting PG synthesis or structure have been shown to disrupt the timing of skeletal development.

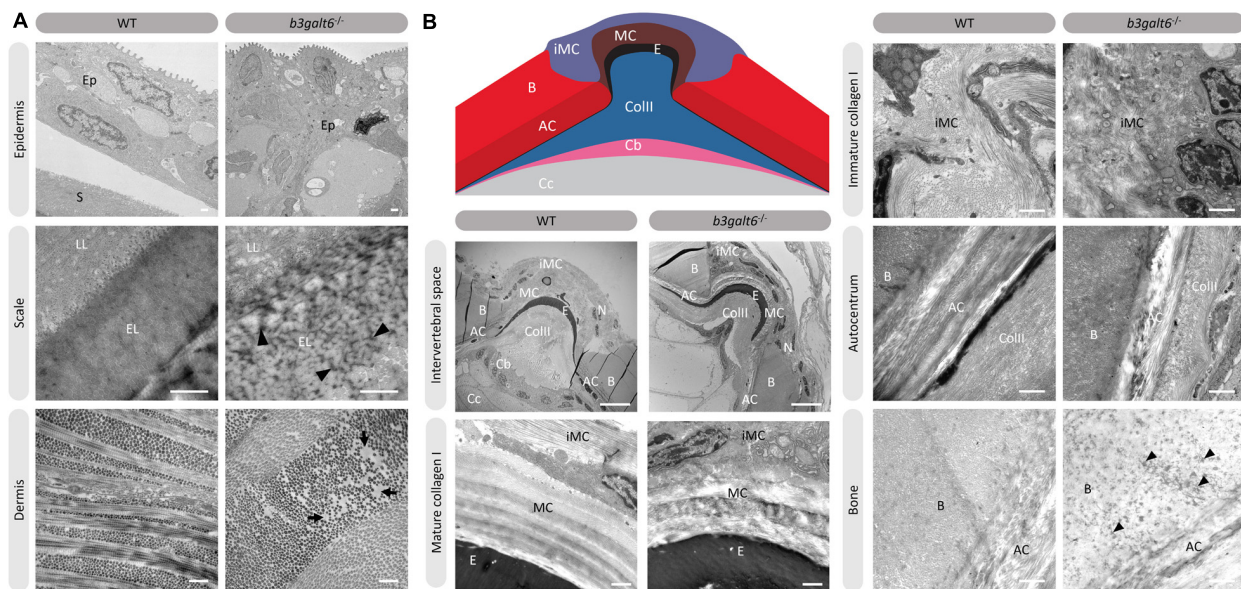
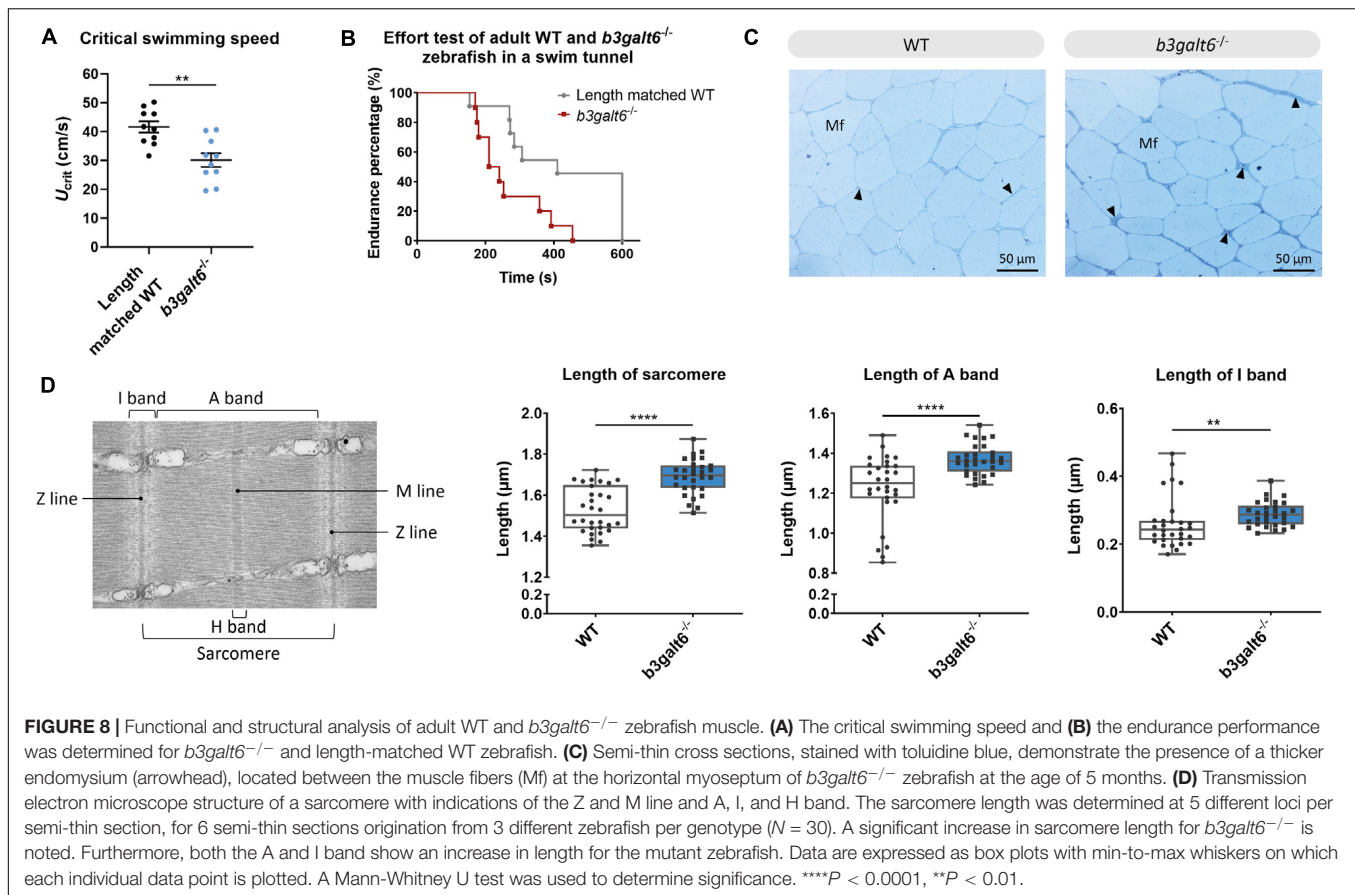


FIGURE 7 | Collagen fibrillar architecture in 5 months old adult zebrafish. **(A)** Skin from 5 months old WT and $b3galt6^{-/-}$ adult zebrafish. The epidermis (Ep), the outer layer of the skin covering the scales (S) of zebrafish, appears thicker in $b3galt6^{-/-}$ zebrafish compared to the epidermis of WT zebrafish. A mature zebrafish scale consists of several layers. The limiting layer of the scale (LL) is rich in fine granules that in some areas are linearly arranged, forming dense layers. This matrix contrasts with that of the external layer(s) (EL) below. Structures resembling extrafibrillar crystals (arrowhead) are noted in the external layer of the mutant scale, which are rare in WT zebrafish sections. Upon investigation of the dermis of $b3galt6^{-/-}$ mutants, increased interfibrillar spaces are noted (arrows), which are absent in the dermis of WT adults. Scale bars = 500 nm. **(B)** Schematic representation and TEM images of the zebrafish intervertebral space. Schematic representation of the zebrafish intervertebral space. AC, aut centrum; B, bone; Cb, chordoblasts; Cc, chordocytes; CollII, type II collagen; E, elastin; IMC, immature collagen type I layer; MC, mature collagen type I layer. Starting from the central body axis, several recognizable structures are present in the intervertebral space along a proximo-distal axis: (i) notochord tissue consisting of chordocytes and chordoblasts, (ii) the notochord sheath consisting of a type II collagen layer and an external elastic membrane, (iii) and a connective tissue ligament consistent of a mature and an immature type I collagen layer. The mature type I collagen layer is organized in a typical plywood-like pattern and is continuous with the inner layer of the vertebral bone, i.e., the aut centrum, which also shows a plywood-like organization. The immature type I collagen layers consist of loose collagen fibers connecting the outer layer of vertebral bones. Notice the higher number of nuclei (N) in the $b3galt6^{-/-}$ zebrafish at the intervertebral space. Mature collagen (MC) displays a typical plywood-like organization, in WT zebrafish but not in comparable regions for $b3galt6^{-/-}$ mutant zebrafish. Cross section and longitudinal type I collagen regions are less clearly demarcated and smaller in immature collagen (IMC) from $b3galt6^{-/-}$ zebrafish compared to WT siblings. It is more difficult to pinpoint the different layers of the aut centrum (AC) in the KO compared to WT zebrafish. Bone (B) from the $b3galt6^{-/-}$ zebrafish shows electron dense structures (arrowhead). Scale bars = 10 μm for the intervertebral space and 1 μm for the other images.

Two zebrafish models with abnormal PG linkage region biosynthesis, i.e., the *fam20b* and *xylt1*-deficient models, revealed partial decrease in CSPGs, which are predominantly present in cartilage, and accelerated endochondral ossification, showing that CSPGs can negatively regulate skeletogenic timing (Eames et al., 2011). On the other hand, a strong reduction in CSPGs and partial decrease in HSPGs was noted in *b3gat3* mutant zebrafish, but this led to a delay in endochondral ossification and short and disorganized cartilaginous structures (Holmborn et al., 2012). Our $B3galt6$ -deficient zebrafish models also show a delay in skeletal development at juvenile stages. At 20 dpf, a delay was noticed in the development of cartilage and mineralized bony elements of the craniofacial structures, the pectoral and caudal fin endoskeleton (Figure 3B and Supplementary Tables S7, S8), and these abnormalities had progressed in adult zebrafish. The reduced body length, misshapen cranial bones and smaller teeth observed in the head skeleton, and general skeletal dysplasia with kyphosis and scoliosis seen in the vertebral column of $b3galt6^{-/-}$ adult zebrafish is reminiscent of the skeletal phenotype observed in human $\beta 3\text{GalT6}$ -deficient individuals (Table 2).

In addition to skeletal dysplasia, we also observed abnormalities in bone mineralization. Adult mutant zebrafish stained with AR showed the presence of extra intramembranous bone and extra bony elements on the associated elements of the vertebral centra. On the other hand, quantitative μCT analysis of the vertebral column and associated elements revealed a generalized reduction in bone volume and thickness, and a relative increase in TMD after correction for reduced body length of the mutant zebrafish (Figure 6 and Supplementary Figure S13). Although it is not clear so far if the increased fracture risk in *spEDS-B3GALT6* patients can be attributed to a lower bone volume combined with a higher TMD, such hypothesis has been put forward for the brittle bone disorder Osteogenesis Imperfecta (OI) based on observations in both patients and animal models (Gistelincq et al., 2016; Fiedler et al., 2018). In the Chihuahua (*coll1a1^{chi/+}*) OI zebrafish model the intrafibrillar mineral platelets were shown to be smaller and more densely packed, leading to an increased mineral to matrix ratio, and consequently a reduced elastic modulus-to-hardness ratio, a measure for fracture toughness (Viguet-Carrin et al., 2006;



Bishop, 2016; Fiedler et al., 2018). In addition, in both OI patients and the mouse model *oim*, reduced collagen matrix organization was shown to lead to the formation of extrafibrillar crystals, which are larger compared to intrafibrillar crystals (Viguet-Carrin et al., 2006). Eventually, additional minerals stabilize the tissue, but they do so at the cost of increased brittleness of the bone (Grabner et al., 2001). In accordance, in $b3galT6^{-/-}$ zebrafish we observed an irregular collagen organization interspersed with large interfibrillar spaces and electron dense spots on ultra-thin sections of skin and bone via TEM. The “dark spots” observed in the vertebral bone could be remnants of extrafibrillar mineral aggregates, contributing to increased mineralization but also increased brittleness of the skeleton.

Abnormalities in collagen fibril organization were observed in many mutant zebrafish tissues. Besides vertebral bone, irregular collagen organization was also observed in the intervertebral space, intervertebral ligament, and the dermis (Figure 7). This strongly resembles the previously reported abnormal dermal collagen fibril architecture in the skin from a $\beta 3\text{GalT6}$ -deficient individual (Malfait et al., 2013). This could be attributed to abnormalities in GAG chains of small leucine-rich PGs (SLRPs), such as the DSPGs decorin and biglycan, which are known to be of particular importance for regulating collagen fibril organization in connective tissues through their core protein and GAG chains (Kalamajski and Oldberg, 2010). SLRPs are also thought to influence collagen cross-linking patterns, but

the mechanism by which they do so remain largely unknown (Kalamajski and Oldberg, 2010). Although similar hydroxylation levels were observed at K87 and the C-telopeptide of the type I collagen $\alpha 1$ chain in $b3galT6^{-/-}$ and WT adult zebrafish (Supplementary Table S9), we cannot rule out that type I collagen cross-linking might still be affected.

In view of the observation that human $\beta 3\text{GalT6}$ -deficient individuals often present quite severe muscle hypotonia with delayed gross motor development and reduced endurance, we also studied the effect of $\beta 3\text{GalT6}$ -deficiency on GAG synthesis in muscle, and on muscle function and ultrastructure (Figure 8). Similar to the other examined tissues, HS and CS/DS GAG concentrations were severely reduced in muscle tissue. It is known that the ECM in skeletal muscle plays an important role in muscle fiber force transmission, maintenance and repair. Numerous PGs, including the HSPGs syndecans 1–4, glypican-1, perlecan and agrin, and CS/DSPGs, such as decorin and biglycan, are present in muscle ECM. Besides their structural role, many of them are known to bind growth factors (e.g., TGF β). Those growth factors can be stored and released by the negatively charged GAGs. Certain enzymes in the ECM can cleave GAG chains, thereby releasing associated growth factors, allowing their interaction in cell signaling and mechanotransduction (Gillies and Lieber, 2011). The significant decrease in critical swimming speed (U_{crit}) and endurance observed in the $b3galT6^{-/-}$ zebrafish suggest decreased muscle function (Figures 8A,B). Further

evidence for an intrinsic muscle dysfunction in the $b3\text{galt6}^{-/-}$ model comes from semi-thin muscle sections, showing an enlargement of the connective tissue sheet surrounding the muscle fibers (Figure 8C). Nevertheless, we cannot exclude that the observed skeletal malformations and/or other abnormalities, such as respiratory or neuronal dysfunction, could also influence the outcome of these tests.

Taken together, we generated and characterized the first $b3\text{galt6}$ KO zebrafish models and show that their phenotype largely mimics that of human $\beta 3\text{GALT6}$ -deficiency. A strong reduction in HS, CS and DS GAG concentration was observed in $b3\text{galt6}^{-/-}$ zebrafish. Yet, we did observe a small amount of GAGs being produced with a unique trisaccharide PG linkage region. Furthermore, we showed that a lack of $\beta 3\text{galt6}$ causes disturbances in collagen fibril organization in skin, ligament and bone, with the latter also showing abnormalities in mineralization, and leads to structural and functional abnormalities of the muscle. These KO zebrafish can serve as useful models to further unravel the underlying pathogenic mechanisms of this complex multisystemic disorder and serve as a tool for the development and evaluation of possible therapeutic interventions, such as the stimulation of intrinsic compensational mechanisms for the production of PGs.

Future studies will focus on verifying the presence of a trisaccharide linkage region in samples (e.g., urine) from human spEDS- $\beta 3\text{GALT6}$ patients. In addition, the hypothesis that $\beta 3\text{gat3}$ is responsible for the remaining GAG synthesis in our $b3\text{galt6}^{-/-}$ model should be further explored by inactivating $\beta 3\text{gat3}$ in our $b3\text{galt6}^{-/-}$ model via knock-down or knock-out approaches, followed by GAG analysis. Potential therapeutic avenues to explore include stimulation of $\beta 3\text{gat3}$ expression, or enzyme replacement therapy (ERT). For patients with an inborn error of metabolism, such as Gaucher disease and mucopolysaccharidosis, ERT is a well-known therapeutic approach and has already been proven successful (Ferreira and Gahl, 2017). Other (but less straightforward) therapeutic avenues in human are stimulation of residual enzyme via co-enzyme treatment or enzyme enhancement therapy, bone-marrow transplantation or correcting the product deficiency by providing alternate substrate. Nevertheless, we should first investigate the human situation before starting to explore these avenues.

MATERIALS AND METHODS

Zebrafish Maintenance

Wild-type (AB strain) and $b3\text{galt6}$ knock-out zebrafish lines were reared and maintained by standard protocols (Gistelink et al., 2018). All animal studies were performed in agreement with EU Directive 2010/63/EU for animals, permit number: ECD 16/18. All zebrafish used in a single experiment were bred at the same density. All efforts were made to minimize pain, distress and discomfort.

Alcian Blue and Alizarin Red Staining

Twenty-day-old larvae ($n = 10$) and 5 months old WT and $b3\text{galt6}^{-/-}$ ($n = 5$) adult zebrafish were stained as

previously described (Delbaere et al., 2020b). See **Supplementary Information** for details.

μ CT Scanning Analysis

Whole-body μ CT scans of 4 months old WT ($n = 5$) and $b3\text{galt6}^{-/-}$ ($n = 5$) siblings were acquired on a SkyScan 1275 (Bruker, Kontich, Belgium) using the following scan parameters: 0.25 mm aluminum filter, 50 kV, 160 μ A, 65 ms integration time, 0.5° rotation step, 721 projections/360°, 5 m 57 s scan duration and 21 μ m voxel size. DICOM files of individual zebrafish were segmented in MATLAB using custom FishCuT software and data were analyzed and corrected for standard length in the R statistical environment, as previously described (Hur et al., 2017).

Histology and Transmission Electron Microscopy

Zebrafish bone, consisting of the last transitional vertebra and two consecutive caudal vertebrae (Morin-Kensicki et al., 2002; Bird and Mabey, 2003), skin, at the lateral line below the dorsal fin, and muscle samples, located dorsolateral underneath the dorsal fin, dissected from 5 months old WT ($n = 5$) and $b3\text{galt6}^{-/-}$ ($n = 5$) zebrafish, were fixed and embedded in epon following the procedures outlined by Huyssseune and Sire (1992).

Swim Tunnel Experiments

Ten WT (5 months) and ten $b3\text{galt6}^{-/-}$ zebrafish (8 months), were selected based on their similar (not significantly different) length and weight. The critical swimming speed (U_{crit}) was measured in a swim tunnel for both WT and $b3\text{galt6}^{-/-}$ zebrafish as previously described (Brett, 1964). Furthermore, the endurance of each zebrafish was tested by means of an effort test in the swim tunnel. Each zebrafish had a 3 min warm-up and after the third minute, the speed increased until 37 cm/s for maximum 7 min. When the zebrafish was not able to swim anymore, the test was stopped.

Collagen Crosslinking Analysis

The collagen crosslinking was analyzed in the dissected vertebral column (excluding Weberian apparatus and urostyle) from 5 months old wild-type ($n = 5$) and $b3\text{galt6}^{-/-}$ ($n = 5$) siblings as described before in Gistelink et al. (2016).

Disaccharide Composition Analysis of CS, DS, and HS Chains

The level of total disaccharides from CS, DS, and HS in bone, muscle and skin tissues from 9 months old zebrafish ($n = 5$) were determined as described previously (Mizumoto et al., 2009; Mizumoto and Sugahara, 2012).

Glycopeptide Preparation and Analysis LC-MS/MS Sample Preparation

CS- and HS-glycopeptides were purified from 6 months old WT ($n = 3$) and $b3\text{galt6}^{-/-}$ ($n = 3$) zebrafish using a combination of extraction, trypsin digestion and anion exchange chromatography, slightly modified (see

Supplementary Information) from previously described protocols (Noborn et al., 2015, 2016).

LC-MS/MS Analysis

The samples were analyzed on an Orbitrap Fusion mass spectrometer coupled to an Easy-nLC 1200 liquid chromatography system (Thermo Fisher Scientific, Waltham, MA) (see **Supplementary Information**). Nanospray Flex ion source was operated in positive ionization mode and three separate higher-energy collision-induced dissociation (HCD) MS/MS spectra were recorded for each precursor ion (Noborn et al., 2015, 2016).

LC-MS/MS Data Analysis

The glycopeptide files were analyzed using both manual interpretation and automated Mascot searches for GAG-glycopeptides. The files were manually interpreted using the Xcalibur software (Thermo Fisher Scientific). Database searches were performed against *Danio rerio* in the UniProtKB/Swiss-Prot database and NCBI using Mascot Distiller (version 2.6.1.0, Matrix Science, London, United Kingdom) and an in-house Mascot server (version 2.5.1). Glycan structures with very small mass differences were manually evaluated at the MS2-level.

GlcAT-I Assay

GlcA-transferase assay was carried out by the methodology as previously described (Kitagawa et al., 1998; Baasanjav et al., 2011; Job et al., 2016), with slight modifications.

Detailed information regarding the procedures used is provided in **Supplementary Material** and Methods.

DATA AVAILABILITY STATEMENT

The original contributions presented in the study are included in the article/**Supplementary Material**, further inquiries can be directed to the corresponding author.

ETHICS STATEMENT

The animal study was reviewed and approved by the Ethische Commissie Dierproeven Faculteit Geneeskunde en Gezondheidswetenschappen Universiteit Gent. All animal studies were performed in agreement with EU Directive 2010/63/EU for animals, permit number: ECD 16/18.

REFERENCES

Almeida, R., Levery, S. B., Mandel, U., Kresse, H., Schwientek, T., Bennett, E. P., et al. (1999). Cloning and expression of a proteoglycan UDP-galactose:beta-xylotriose 4-epimerase. A seventh member of the human beta-4-galactosyltransferase gene family. *J. Biol. Chem.* 274, 26165–26171. doi: 10.1074/jbc.274.37.26165

AUTHOR CONTRIBUTIONS

SD, AW, and FM designed the study and wrote the manuscript. SD, AD, SM, FN, JB, LA, and CG performed the research. SM, PS, GL, and SY contributed new reagents and analytic tools. SD, AD, SM, FN, JB, LA, CG, DS, PS, PC, GL, SY, AW, and FM analyzed the data. All authors reviewed the manuscript.

FUNDING

DS and FM were a postdoctoral fellow and a senior clinical investigator, respectively, of the Research Foundation Flanders (FWO), Belgium. This work was supported by a Methusalem Grant (BOFMET2015000401) from the Ghent University to Prof. Anne De Paepe, by grants from the FWO to DS (12Q5917N) and to FM (1842318N) and by grant (2017-00955) from the Swedish Research Council to FN and GL. CG was supported at the UW by a post-doctoral fellowship of the Belgian American Educational Fund (BAEF). This work was further supported by a Grant-in-Aid for Scientific Research (C) 19K07054 (to SM) from the Japan Society for the Promotion of Science, Japan; by the Takeda Science Foundation (to SM); Grant-in Aid for Research Center for Pathogenesis of Intractable Diseases from the Research Institute of Meijo University (SM and SY).

ACKNOWLEDGMENTS

We would like to thank the TEM facility of the Nematology Research Unit, member of the UGent TEM-Expertise Center (life sciences). We are grateful to Hanna De Saffel and Petra Vermassen for their technical assistance on processing the TEM samples. The LC-MS/MS analyses were performed at the BioMS node at the Proteomics Core Facility, Sahlgrenska Academy, University of Gothenburg with support from the Swedish National Infrastructure for Biological Mass Spectrometry (BioMS), funded by the Swedish Research Council. This manuscript has been released as a pre-print at bioRxiv (Delbaere et al., 2020a).

SUPPLEMENTARY MATERIAL

The Supplementary Material for this article can be found online at: <https://www.frontiersin.org/articles/10.3389/fcell.2020.597857/full#supplementary-material>

Amsterdam, A., Nissen, R. M., Sun, Z., Swindell, E. C., Farrington, S., and Hopkins, N. (2004). Identification of 315 genes essential for early zebrafish development. *Proc. Natl. Acad. Sci. U.S.A.* 101, 12792–12797. doi: 10.1073/pnas.0403929101

Arratia, G., and Schultze, H. P. (1992). Reevaluation of the caudal skeleton of certain actinopterygian fishes: III. Salmonidae. Homologization of caudal skeletal structures. *J. Morphol.* 214, 187–249. doi: 10.1002/jmor.1052140209

- Baasanjav, S., Al-Gazali, L., Hashiguchi, T., Mizumoto, S., Fischer, B., Horn, D., et al. (2011). Faulty initiation of proteoglycan synthesis causes cardiac and joint defects. *Am. J. Hum. Genet.* 89, 15–27. doi: 10.1016/j.ajhg.2011.05.021
- Bai, X., Zhou, D., Brown, J. R., Crawford, B. E., Hennet, T., and Esko, J. D. (2001). Biosynthesis of the linkage region of glycosaminoglycans: cloning and activity of galactosyltransferase II, the sixth member of the beta 1,3-galactosyltransferase family (beta 3GalT6). *J. Biol. Chem.* 276, 48189–48195. doi: 10.1074/jbc.m107339200
- Bird, N. C., and Mabee, P. M. (2003). Developmental morphology of the axial skeleton of the zebrafish, *Danio rerio* (Ostariophysi: Cyprinidae). *Dev. Dyn.* 228, 337–357. doi: 10.1002/dvdy.10387
- Bishop, N. (2016). Bone material properties in Osteogenesis imperfecta. *J. Bone Miner. Res.* 31, 699–708. doi: 10.1002/jbmr.2835
- Brett, J. R. (1964). The respiratory metabolism and swimming performance of young sockeye salmon. *J. Fish. Res. Board Can.* 21, 1183–1226. doi: 10.1139/f64-103
- Bui, C., Ouzzine, M., Talhaoui, I., Sharp, S., Prydz, K., Coughtrie, M. W., et al. (2010). Epigenetics: methylation-associated repression of heparan sulfate 3-O-sulfotransferase gene expression contributes to the invasive phenotype of H-EMC-SS chondrosarcoma cells. *FASEB J.* 24, 436–450. doi: 10.1096/fj.09-136291
- Caraffi, S. G., Maini, I., Ivanovski, I., Pollazzon, M., Giangioffe, S., Valli, M., et al. (2019). severe peripheral joint laxity is a distinctive clinical feature of Spondylodysplastic-Ehlers-danlos syndrome (EDS)-B4GALT7 and spondylodysplastic-EDS-B3GALT6. *Genes* 10:799. doi: 10.3390/genes10100799
- Chen, Y. H., Narimatsu, Y., Clausen, T. M., Gomes, C., Karlsson, R., Steentoft, C., et al. (2018). The GAGome: a cell-based library of displayed glycosaminoglycans. *Nat. Methods* 15, 881–888. doi: 10.1038/s41592-018-0086-z
- Couchman, J. R., and Pataki, C. A. (2012). An introduction to proteoglycans and their localization. *J. Histochem. Cytochem.* 60, 885–897. doi: 10.1369/0022155412464638
- Delbaere, S., De Clercq, A., Mizumoto, S., Noborn, F., Bek, J. W., Alluyn, L., et al. (2020a). b3gal6 knock-out zebrafish recapitulate β 3GalT6-deficiency disorders in human and reveal a trisaccharide proteoglycan linkage region. *bioRxiv* [Preprint]. doi: 10.1101/2020.06.22.165316
- Delbaere, S., Van Damme, T., Syx, D., Symoens, S., Coucke, P., Willaert, A., et al. (2020b). Hypomorphic zebrafish models mimic the musculoskeletal phenotype of beta4GalT7-deficient Ehlers-Danlos syndrome. *Matrix Biol.* 89, 59–75. doi: 10.1016/j.matbio.2019.12.002
- Dooley, K., and Zon, L. I. (2000). Zebrafish: a model system for the study of human disease. *Curr. Opin. Genet. Dev.* 10, 252–256. doi: 10.1016/s0959-437x(00)00074-5
- Eames, B. F., Singer, A., Smith, G. A., Wood, Z. A., Yan, Y. L., He, X., et al. (2010). UDP xylose synthase 1 is required for morphogenesis and histogenesis of the craniofacial skeleton. *Dev. Biol.* 341, 400–415. doi: 10.1016/j.ydbio.2010.02.035
- Eames, B. F., Yan, Y. L., Swartz, M. E., Levic, D. S., Knapik, E. W., Postlethwait, J. H., et al. (2011). Mutations in fam20b and xylt1 reveal that cartilage matrix controls timing of endochondral ossification by inhibiting chondrocyte maturation. *PLoS Genet.* 7:e1002246. doi: 10.1371/journal.pgen.1002246
- Ferreira, C. R., and Gahl, W. A. (2017). Lysosomal storage diseases. *Transl. Sci. Rare Dis.* 2, 1–71.
- Fiedler, I. A. K., Schmidt, F. N., Wolfel, E. M., Plumeyer, C., and Milovanovic, P. (2018). Severely impaired bone material quality in chihuahua zebrafish resembles classical dominant human Osteogenesis imperfecta. *J. Bone Miner. Res.* 33, 1489–1499. doi: 10.1002/jbmr.3445
- Gillies, A. R., and Lieber, R. L. (2011). Structure and function of the skeletal muscle extracellular matrix. *Muscle Nerve* 44, 318–331. doi: 10.1002/mus.22094
- Gistelink, C., Gioia, R., Gagliardi, A., Tonelli, F., Marchese, L., Bianchi, L., et al. (2017). Zebrafish collagen type I: molecular and biochemical characterization of the major structural protein in bone and skin. *Sci. Rep.* 6:21540.
- Gistelink, C., Kwon, R. Y., Malfait, F., Symoens, S., Harris, M. P., Henke, K., et al. (2018). Zebrafish type I collagen mutants faithfully recapitulate human type I collagenopathies. *Proc. Natl. Acad. Sci. U.S.A.* 115, E8037–E8046.
- Gistelink, C., Witten, P. E., Huysseune, A., Symoens, S., Malfait, F., Larionova, D., et al. (2016). Loss of Type I collagen telopeptide Lysyl hydroxylation causes musculoskeletal abnormalities in a zebrafish model of bruck syndrome. *J. Bone Miner. Res.* 31, 1930–1942. doi: 10.1002/jbmr.2977
- Gotting, C., Kuhn, J., Zahn, R., Brinkmann, T., and Kleesiek, K. (2000). Molecular cloning and expression of human UDP-d-Xylose:proteoglycan core protein beta-d-xylosyltransferase and its first isoform XT-II. *J. Mol. Biol.* 304, 517–528. doi: 10.1006/jmbi.2000.4261
- Grabner, B., Landis, W. J., Roschger, P., Rinnerthaler, S., Peterlik, H., Klaushofer, K., et al. (2001). Age- and genotype-dependence of bone material properties in the osteogenesis imperfecta murine model (oim). *Bone* 29, 453–457. doi: 10.1016/s8756-3282(01)00594-4
- Guo, M. H., Stoler, J., Lui, J., Nilsson, O., Bianchi, D. W., Hirschhorn, J. N., et al. (2013). Redefining the progeroid form of Ehlers-Danlos syndrome: report of the fourth patient with B4GALT7 deficiency and review of the literature. *Am. J. Med. Genet. A* 161A, 2519–2527.
- Holmborn, K., Habicher, J., Kasza, Z., Eriksson, A. S., Filipek-Gorniok, B., Gopal, S., et al. (2012). On the roles and regulation of chondroitin sulfate and heparan sulfate in zebrafish pharyngeal cartilage morphogenesis. *J. Biol. Chem.* 287, 33905–33916. doi: 10.1074/jbc.m112.401646
- Hur, M., Gistelink, C. A., Huber, P., Lee, J., Thompson, M. H., Monstad-Rios, A. T., et al. (2017). MicroCT-based phenomics in the zebrafish skeleton reveals virtues of deep phenotyping in a distributed organ system. *eLife* 6:e26014.
- Huysseune, A., and Sire, J. Y. (1992). Bone and cartilage resorption in relation to tooth development in the anterior part of the mandible in cichlid fish: a light and TEM study. *Anat. Rec.* 234, 1–14. doi: 10.1002/ar.1092340102
- Job, F., Mizumoto, S., Smith, L., Couser, N., Brazil, A., Saal, H., et al. (2016). Functional validation of novel compound heterozygous variants in B3GAT3 resulting in severe osteopenia and fractures: expanding the disease phenotype. *BMC Med. Genet.* 17:86. doi: 10.1186/s12881-016-0344-9
- Jones, K. L., Schwarze, U., Adam, M. P., Byers, P. H., and Mefford, H. C. (2015). A homozygous B3GAT3 mutation causes a severe syndrome with multiple fractures, expanding the phenotype of linkeropathy syndromes. *Am. J. Med. Genet. A* 167A, 2691–2696. doi: 10.1002/ajmg.a.37209
- Kalamajski, S., and Oldberg, A. (2010). The role of small leucine-rich proteoglycans in collagen fibrillogenesis. *Matrix Biol.* 29, 248–253. doi: 10.1016/j.matbio.2010.01.001
- Kitagawa, H., Tone, Y., Tamura, J., Neumann, K. W., Ogawa, T., Oka, S., et al. (1998). Molecular cloning and expression of glucuronyltransferase I involved in the biosynthesis of the glycosaminoglycan-protein linkage region of proteoglycans. *J. Biol. Chem.* 273, 6615–6618. doi: 10.1074/jbc.273.12.6615
- Kusche-Gullberg, M., and Kjellen, L. (2003). Sulfotransferases in glycosaminoglycan biosynthesis. *Curr. Opin. Struct. Biol.* 13, 605–611. doi: 10.1016/j.sbi.2003.08.002
- Lindahl, U., Couchman, J., Kimata, K., and Esko, J. D. (2015). “Proteoglycans and sulfated glycosaminoglycans,” in *Essentials of Glycobiology*, 3rd Edn, eds A. Varki, R. D. Cummings, J. D. Esko, P. Stanley, G. W. Hart, M. Aebi, et al. (Cold Spring Harbor, NY: Cold Spring Harbor Laboratory Press), 207–221.
- Malfait, F., Francomano, C., Byers, P., Belmont, J., Berglund, B., Black, J., et al. (2017). The 2017 international classification of the Ehlers-Danlos syndromes. *Am. J. Med. Genet. C Semin. Med. Genet.* 175, 8–26.
- Malfait, F., Kariminejad, A., Van Damme, T., Gauche, C., Syx, D., Merhi-Soussi, F., et al. (2013). Defective initiation of glycosaminoglycan synthesis due to B3GALT6 mutations causes a pleiotropic Ehlers-Danlos-Syndrome-like connective tissue disorder. *Am. J. Hum. Genet.* 92, 935–945. doi: 10.1016/j.ajhg.2013.04.016
- McMenamin, S. K., Chandless, M. N., and Parichy, D. M. (2016). Working with zebrafish at postembryonic stages. *Methods Cell Biol.* 134, 587–607. doi: 10.1016/bs.mcb.2015.12.001
- Mizumoto, S., Mikami, T., Yasunaga, D., Kobayashi, N., Yamauchi, H., Miyake, A., et al. (2009). Chondroitin 4-O-sulfotransferase-1 is required for somitic muscle development and motor axon guidance in zebrafish. *Biochem. J.* 419, 387–399. doi: 10.1042/bj20081639
- Mizumoto, S., and Sugahara, K. (2012). Glycosaminoglycan chain analysis and characterization (glycosylation/epimerization). *Methods Mol. Biol.* 836, 99–115. doi: 10.1007/978-1-61779-498-8_7
- Morin-Kensicki, E. M., Melancon, E., and Eisen, J. S. (2002). Segmental relationship between somites and vertebral column in zebrafish. *Development* 129, 3851–3860.
- Nakajima, M., Mizumoto, S., Miyake, N., Kogawa, R., Iida, A., Ito, H., et al. (2013). Mutations in B3GALT6, which encodes a glycosaminoglycan linker region

- enzyme, cause a spectrum of skeletal and connective tissue disorders. *Am. J. Hum. Genet.* 92, 927–934. doi: 10.1016/j.ajhg.2013.04.003
- Nash, R., Valencia, A. H., and Geffen, A. J. (2006). The origin of Fulton's condition factor - Setting the record straight. *Fisheries* 31, 236–238.
- Nissen, R. M., Amsterdam, A., and Hopkins, N. (2006). A zebrafish screen for craniofacial mutants identifies *wdr68* as a highly conserved gene required for endothelin-1 expression. *BMC Dev. Biol.* 6:28. doi: 10.1186/1471-213X-6-28
- Noborn, F., Gomez Toledo, A., Green, A., Nasir, W., Sihlbom, C., Nilsson, J., et al. (2016). Site-specific identification of heparan and chondroitin sulfate glycosaminoglycans in hybrid proteoglycans. *Sci. Rep.* 6:34537. doi: 10.1038/srep34537
- Noborn, F., Gomez Toledo, A., Sihlbom, C., Lengqvist, J., Fries, E., Kjellen, L., et al. (2015). Identification of chondroitin sulfate linkage region glycopeptides reveals prohormones as a novel class of proteoglycans. *Mol. Cell Proteom.* 14, 41–49. doi: 10.1074/mcp.m114.043703
- Parichy, D. M., Elizondo, M. R., Mills, M. G., Gordon, T. N., and Engeszer, R. E. (2009). Normal table of postembryonic zebrafish development: staging by externally visible anatomy of the living fish. *Dev. Dyn.* 238, 2975–3015. doi: 10.1002/dvdy.22113
- Persson, A., Nilsson, J., Vorontsov, E., Noborn, F., and Larson, G. (2019). Identification of a non-canonical chondroitin sulfate linkage region trisaccharide. *Glycobiology* 29, 366–371. doi: 10.1093/glycob/cwz014
- Plaut, I. (2000). Effects of fin size on swimming performance, swimming behaviour and routine activity of zebrafish *Danio rerio*. *J. Exp. Biol.* 203(Pt 4), 813–820.
- Prydz, K., and Dalen, K. T. (2000). Synthesis and sorting of proteoglycans - commentary. *J. Cell Sci.* 113, 193–205.
- Ritelli, M., Chiarelli, N., Zoppi, N., Dordoni, C., Quinzani, S., Traversa, M., et al. (2015). Insights in the etiopathology of galactosyltransferase II (GalT-II) deficiency from transcriptome-wide expression profiling of skin fibroblasts of two sisters with compound heterozygosity for two novel B3GALT6 mutations. *Mol. Genet. Metab. Rep.* 2, 1–15. doi: 10.1016/j.ymgmr.2014.11.005
- Santoriello, C., and Zon, L. I. (2012). Hooked! modeling human disease in zebrafish. *J. Clin. Invest.* 122, 2337–2343. doi: 10.1172/jci60434
- Selleck, S. B. (2000). Proteoglycans and pattern formation: sugar biochemistry meets developmental genetics. *Trends Genet.* 16, 206–212. doi: 10.1016/s0168-9525(00)01997-1
- Sugahara, K., Mikami, T., Uyama, T., Mizuguchi, S., Nomura, K., and Kitagawa, H. (2003). Recent advances in the structural biology of chondroitin sulfate and dermatan sulfate. *Curr. Opin. Struct. Biol.* 13, 612–620. doi: 10.1016/j.sbi.2003.09.011
- Van Damme, T., Pang, X., Guillemin, B., Gulberti, S., Syx, D., De Rycke, R., et al. (2018). Biallelic B3GALT6 mutations cause spondylodysplastic Ehlers-Danlos syndrome. *Hum. Mol. Genet.* 27, 3475–3487. doi: 10.1093/hmg/ddy234
- Viguet-Carrin, S., Garnero, P., and Delmas, P. D. (2006). The role of collagen in bone strength. *Osteoporos. Int.* 17, 319–336. doi: 10.1007/s00198-005-2035-9
- Wen, J., Xiao, J., Rahdar, M., Choudhury, B. P., Cui, J., Taylor, G. S., et al. (2014). Xylose phosphorylation functions as a molecular switch to regulate proteoglycan biosynthesis. *Proc. Natl. Acad. Sci. U.S.A.* 111, 15723–15728. doi: 10.1073/pnas.1417993111
- Wittkopp, N., Huntzinger, E., Weiler, C., Sauliere, J., Schmidt, S., Sonawane, M., et al. (2009). Nonsense-mediated mRNA decay effectors are essential for zebrafish embryonic development and survival. *Mol. Cell Biol.* 29, 3517–3528. doi: 10.1128/mcb.00177-09

Conflict of Interest: PS was employed by the company Bruker MicroCT.

The remaining authors declare that the research was conducted in the absence of any commercial or financial relationships that could be construed as a potential conflict of interest.

Copyright © 2020 Delbaere, De Clercq, Mizumoto, Noborn, Bek, Alluyn, Gistelinc, Syx, Salmon, Coucke, Larson, Yamada, Willaert and Malfait. This is an open-access article distributed under the terms of the Creative Commons Attribution License (CC BY). The use, distribution or reproduction in other forums is permitted, provided the original author(s) and the copyright owner(s) are credited and that the original publication in this journal is cited, in accordance with accepted academic practice. No use, distribution or reproduction is permitted which does not comply with these terms.



N6-Methyladenosine Induced miR-34a-5p Promotes TNF- α -Induced Nucleus Pulposus Cell Senescence by Targeting SIRT1

Hao Zhu^{1,2†}, Bao Sun^{1†}, Liang Zhu¹, Guoyou Zou² and Qiang Shen^{1*}

¹ Department of Orthopaedics, The Affiliated Shanghai General Hospital of Nanjing Medical University, Shanghai, China,

² Department of Orthopaedics, Yancheng First Hospital, Affiliated Hospital of Nanjing University Medical School, Yancheng, China

OPEN ACCESS

Edited by:

Roland Wohlgemuth,
Lodz University of Technology, Poland

Reviewed by:

Daniela Carlisi,
University of Palermo, Italy
Wenbin Hua,
Huazhong University of Science
and Technology, China
William K. K. Wu,
Chinese University of Hong Kong,
China

*Correspondence:

Qiang Shen
shenshsy@163.com

[†] These authors have contributed
equally to this work

Specialty section:

This article was submitted to
Molecular Medicine,
a section of the journal
Frontiers in Cell and Developmental
Biology

Received: 16 December 2020

Accepted: 15 February 2021

Published: 05 March 2021

Citation:

Zhu H, Sun B, Zhu L, Zou G and
Shen Q (2021) N6-Methyladenosine
Induced miR-34a-5p Promotes
TNF- α -Induced Nucleus Pulposus
Cell Senescence by Targeting SIRT1.
Front. Cell Dev. Biol. 9:642437.
doi: 10.3389/fcell.2021.642437

Low back pain is tightly associated with intervertebral disc degeneration (IVDD) and aberrant nucleus pulposus (NP) is a critical cause. miRNAs N6-methyladenosine (m6A) modification accounts for the TNF- α -induced senescence of NP cells. The aim of this study was to investigate whether m6A modification regulates TNF- α -mediated cell viability, cell cycle arrest, and cell senescence and how it works. The results showed that METTL14 expression positively correlated with m6A and TNF- α expression in HNPCs. The knockdown of METTL14 led to the inhibition of the TNF- α -induced cell senescence. METTL14 overexpression promoted cell senescence. METTL14 regulated the m6A modification of miR-34a-5p and interacted with DGCR8 to process miR-34a-5p. The miR-34a-5p inhibitor inhibited the cell cycle senescence of HNPCs. miR-34a-5p was predicted to interact with the SIRT1 mRNA. SIRT1 overexpression counteracted the miR-34a-5p-promoted cell senescence. METTL14 participates in the TNF- α -induced m6A modification of miR-34a-5p to promote cell senescence in HNPCs and NP cells of IVDD patients. Downregulation of either METTL14 expression or miR-34a-5p leads to the inhibition of cell cycle arrest and senescence. SIRT1 mRNA is an effective binding target of miR-34a-5p, and SIRT1 overexpression mitigates the cell cycle arrest and senescence caused by miR-34a-5p.

Keywords: N6-methyladenosine, IVDD, miR-34a-5p, cell senescence, SIRT1

INTRODUCTION

Lower back pain (LBP) is the most common chronic pain that affects at least 80% of Americans in their lifetime (Freburger et al., 2009). In general, LBP can be caused by a muscle sprain or strain injury as well as certain diseases, including spinal cord cancer, ruptured or herniated disc sciatica arthritis, kidney infections, and spine infections. It has been revealed that LBP is strongly associated with intervertebral disc degeneration (IVDD) and degenerative disc disease is identified to be the main cause of LBP (Luoma et al., 2000; Morgan et al., 2014). However, despite some reports of treatment to mitigate the pain and symptoms, no effective therapeutic regimen toward IVDD has been established considering that LBP is multifactorial (Froud et al., 2014).

Intervertebral disc mainly comprises of inner nucleus pulposus (NP) and surrounded annulus fibrosus, in which NP is the inner core of the vertebral disc (Pattappa et al., 2012). Comprised of a jelly-like material mainly formed by water and a loose collagen fiber network, NP is essential to maintain intervertebral disc height and mechanical properties (Frost et al., 2019). NP is also characterized to be responsible for controlling the synthesis and decomposition of the NP extracellular matrix (ECM) (Hwang et al., 2014). Moreover, abnormal apoptosis of NP cells (NPCs) is correlated with the pathology of IVDD. The degeneration was mainly manifested by the apoptosis of NP cells, in which the levels of cleaved caspase-3 and Bax were upregulated while the expression of Bcl-2 was downregulated (Kepler et al., 2013; Jiao et al., 2018; Li Z. et al., 2019). Aberrant apoptosis and senescence of NP cells play significant roles in the process of IVDD (Zhao et al., 2006; Jiang et al., 2013; Chen et al., 2018). During the apoptosis of NPCs, tumor necrosis factor (TNF)- α represents a key pro-inflammatory cytokine to promote the induction of apoptosis (Xie et al., 2019). Thus, TNF- α has been commonly recognized as a contributor to IVDD (Wang et al., 2017). Additionally, researchers have unveiled the role of TNF- α in the premature senescence of rat NP cells (Li P. et al., 2017). Through the PI3K/Akt signaling, TNF- α promoted senescence of NP cells.

Non-coding RNAs (ncRNAs), including microRNAs (miRNAs), long non-coding RNAs (lncRNAs), and circular RNAs, have critical contributions to IVDD (Li et al., 2018; Zhu et al., 2019; Xiang et al., 2020). They participate in the regulation of the proliferation of human NP cells (HNPCs) and the synthesis of ECM as well as the degradation-regeneration balance of the ECM in IVDD. Recently, a comprehensive analysis of altered methylation level of miRNA and lncRNAs in IVDD patients was conducted, which verified that N6-methyladenosine (m6A) methylation was one of the most abundant internal RNA modifications in IVDD (Wang X. et al., 2020). A growing number of studies have characterized the critical role of mRNA m6A modification in human diseases (Weng et al., 2018; Han et al., 2019; Han et al., 2020). However, the role of this modification in the pathogenesis of IVDD is fully mysterious. Additionally, the silent mating type information regulator 2 homolog-1 (SIRT1) played a protective role in IVDD and preserves the normal NP cell phenotype (Zhang et al., 2011; Feng et al., 2016; Wang Y. et al., 2020). The mechanism behind has not been explicated yet. In this study, we report the Methyltransferase like (METTL)14-dependent m6A methylation of miR-34a-5p in IVDD patients. Through regulating the processing of miR-34a-5p that targeted SIRT1, METTL14-dependent m6A methylation promoted the TNF- α -induced cell senescence of human NP cells (HNPCs). Our research provided novel insights into the mechanism of IVDD development.

MATERIALS AND METHODS

Clinical Sample Collection

The study was approved by the medical ethics committee of The Affiliated Shanghai General Hospital of Nanjing Medical

University and was conducted in accordance with the Declaration of Helsinki. Written informed consents were obtained from all participants. From March 2015 to April 2018, degenerative nucleus pulposus (NP) samples were collected from 30 patients with intervertebral disc degeneration (IVDD) of low (0–3), moderate (4–6), and high (8–10) degenerative grades ($n = 10$ per group) using the Rutgers score (Nakazawa et al., 2018), who underwent operations at The Affiliated Shanghai General Hospital of Nanjing Medical University. Normal NP samples were collected as controls from ten volunteers. The NP tissues were prepared using the culture medium followed by washing with phosphate-buffered saline under sterile conditions. The prepared samples were then used for the qRT-PCR assay.

Cell Culture and Treatment

HNPCs were isolated and cultured as per the previous report (Dudek et al., 2017). Annulus fibrosus was first washed with sterile phosphate-buffered saline (PBS) 3 times and then meticulously eliminated from the human intervertebral disc tissues. The medium was changed every 3 days. Cultured cells were passaged when reaching a confluence of 80–90%. Cells of the second or third generation were used for further assays. Cells were treated with different doses of TNF- α (SRP2102; Sigma-Aldrich, St Louis, MO, United States) for 24 h at 37°C and 95% humidity in an atmosphere of 5% CO₂. Cells without treatment were used as control.

Cell Transfection

pLKO.1 lentiviral vectors containing shRNA targeting human METTL14 were synthesized by Sangon Biotech (Shanghai, China). Human METTL14 or SIRT1 ectopic expression vector was constructed using the pLVX-Puro or pcDNA3.1(+) vector, respectively. HEK293T cells were cultured in 6-well plates and those were transfected with pLKO.1-METTL14-shRNA (shRNA), pLVX-Puro-METTL14 (METTL14), or pcDNA3.1(+)-SIRT1 (SIRT1) using the Lipofectamine reagent as per the manufacturer's protocol. Post-transfection shRNA and METTL14 vectors were collected and were used for transduction. Cells without transduction or transfection were used as control. Cells transduced with pLKO.1-scramble shRNA (shNC), blank pLVX-Puro, or transfected with blank pcDNA3.1(+) vector were used as the negative control.

miR-34a-5p mimic (5'-UGGCAGUGUCUUAGCUGGUUGU-3'), miR-34a-5p inhibitor (5'-ACAACCAGCUAAGACA CUGCCA-3'), and miR-34a-5p negative control (NC, 5'-CAGUACUUUUGUGUAGUACAA-3') were synthesized by Genepharma Technologies (Shanghai, China). Transfection was performed using Lipofectamine 2,000 (Invitrogen) as per the manufacturer's instructions. Cells without transfection were used as control.

Cell Cycle Assay

After treatment, HNPCs were spun down at $1,000 \times g$ for 5 min and fixed with 700 μ L of pre-cooled absolute ethanol. RNase A (1 mg/mL, 100 μ L) was added to the fixed cells for 30-min incubation in darkness. The resulting cells were further stained with 50 μ g/mL of propidium iodide (PI, 400 μ L) for

10 min. FACSscan flow cytometry (Becton Dickinson, Franklin Lakes, NJ) was then performed using the Cell Quest software (Becton Dickinson).

SA β -Galactosidase Staining

After treatment, HNPCs were washed with PBS 3 times and stained with freshly prepared SA- β -Gal staining solution following the manufacturer's protocol (Beyotime Biotechnology Ltd., Shanghai, China). The stained cells were then observed under a microscope.

Co-immunoprecipitation

Cell lysates were prepared with the Radioimmunoprecipitation assay (RIPA) lysis buffer. Antibodies, including anti-METTL14 (ab252562; Abcam, Cambridge, MA, United States), anti-DGCR8 (ab90579; Abcam) or normal IgG antibody (sc-2027; Santa Cruz Biotechnology, Inc.), were incubated with the cell lysates followed by incubation with Protein A/G PLUS-Agarose beads (sc-2003; Santa Cruz Biotechnology, Inc.) for 2 h at 4°C. After washing with the lysis buffer 3 times, the samples were subjected to Western blot analysis using anti-METTL14 (ab223090; Abcam) and anti-DGCR8 (ab191875; Abcam) antibodies.

m6A Content Analysis

m⁶A in total RNA was analyzed with the m6A RNA Methylation Assay Kit as per the manufacturer's protocol (Abcam, ab185912).

RNA Immunoprecipitation Assays

Using the Magna RIP RNA-Binding Protein Immunoprecipitation kit (Millipore), RNA immunoprecipitation (RIP) assays were carried out following the manufacturer's protocol. Total RNA (input control) and isotype control (IgG) were detected simultaneously. RNAs were extracted for reverse transcription and qRT-PCR.

Luciferase Reporter Assay

SIRT1 3'-UTR region containing a putative miR-34a-5p binding site was cloned into the pGL3 vector. For SIRT1 luciferase reporter assay, the HNPCs were transfected with miR-34a-5p mimic, miR-34a-5p inhibitor, and pGL3-SIRT1-WT or pGL3-SIRT1-MUT plasmid and pRL-TK vector (Promega) expressing the renilla luciferase with Lipofectamine 2,000. The relative luciferase activity was determined and normalized to the Renilla luciferase activity 48 h after transfection according to the standard protocol.

RNA Isolation and Quantitative RT-PCR

Total RNA of HNPCs was extracted using TRIzol reagent (Invitrogen) and the RNeasy Mini Kit (Qiagen, Hilden, Germany). Reverse transcription was conducted using PrimeScriptTMRT reagent Kit with gDNA Eraser (Takara, Beijing, China). The resulting products were used for qRT-PCR amplification with SYBR Premix Ex TaqTM GC (Takara). GAPDH or U6 was used as the normalization control. The primers for qRT-PCR are listed in **Table 1**. The fold changes of mRNA or miRNA were determined by the $2^{-\Delta\Delta CT}$ method.

TABLE 1 | Primes sequences used in this study.

Gene	Sequences (5'-3')
TNF- α -forward	GGTATGAGCCCATCTATCTG
TNF- α -reverse	AGGGCAATGATCCCAAAG
METTL3-forward	CCTTTGCCAGTTCGTTAGTC
METTL3-reverse	TCCTCCTTGGTTCCATAGTC
METTL14-forward	CTGGGAATGAAGTCAGGATAG
METTL14-reverse	CCAGGGTATGGAACGTAATAG
WTAP-forward	AAAGCAGTGAGTGGGAAAG
WTAP-reverse	AGCGGCAGAAGTATTGAAG
SIRT1-forward	ACCTCCTCATTGTTATTGG
SIRT1-reverse	TTACAGGGTTACAGCAAAG
pri-miR-34a-forward	AGTTGCTGAAGGTGGTGGTC
pri-miR-34a-reverse	ACATGCGTGCCTGTAGTCC
GAPDH-forward	AATCCCATCACCATTCTTC
GAPDH-reverse	AGGCTGTTGTCACTACTTC
miR-200c-3p-forward	CGCGTAATACTGCCGGGTAAT
miR-200c-3p-reverse	AGTGCAGGGTCCGAGGTATT
miR-27a-3p-forward	GCGCGTTACAGTGGCTAAG
miR-27a-3p-reverse	AGTGCAGGGTCCGAGGTATT
miR-34a-5p-forward	GCGGTGGCAGTGTCTTAGCT
miR-34a-5p-reverse	AGTGCAGGGTCCGAGGTATT
miR-15b-5p-forward	GCGGTAGCAGCACATCATGG
miR-15b-5p-reverse	AGTGCAGGGTCCGAGGTATT
pre-miR-34a-forward	CCTAGAAGTGCTGCACGTTGTG
pre-miR-34a-reverse	AGTGCAGGGTCCGAGGTATT
U6-forward	CTCGCTTCGGCAGCACCA
U6-reverse	AACGCTTCACGAATTTGCGT

Western Blot

The cell lysates were prepared using the radioimmunoprecipitation assay lysis buffer (Beyotime, Shanghai, China). The quantitation of protein in the samples was performed using the bicinchoninic acid (BCA) Protein Assay Kit (Beyotime). For SDS-PAGE, 20 μ g of protein sample was loaded to each well followed by the transmembrane onto polyvinylidene fluoride membranes (Millipore, Billerica, MA, United States). The blocking of the membrane was conducted by incubating with 5% fat-free milk and then primary antibodies against METTL3 (ab195352; Abcam), METTL14 (ab223090; Abcam), WTAP (ab195380; Abcam), SIRT1 (ab110304; Abcam), and GAPDH (#5174, Cell Signaling Technology) overnight at 4°C. The blots were then washed in Tris-buffered Saline Tween-20 (TBST) three times and then incubated with secondary antibodies (A0208, A0216; Beyotime, Shanghai, China). The blots were examined by chemiluminescence using the Enhanced Chemiluminescence Detection kit (Pierce Biotechnology, Rockford, IL, United States). After exposure, the intensity of bands was analyzed by Image-Pro Plus 6.0 software.

Statistical Analysis

All statistical analyses were performed using GraphPad Prism 8.0.2 (GraphPad Software, San Diego, CA, United States). Data were shown as mean \pm standard deviation (SD) from the triplicates of independent experiments. The difference between

different groups was analyzed using a two-sided Student's *t*-test and ANOVA. *P*-values < 0.05 were considered significant.

RESULTS

The Level of m6A Modification Is Positively Correlated With TNF- α in IVDD Patients

TNF- α is the main pro-inflammatory cytokines principally associated with the progression of IVDD (Purmessur et al., 2013). To verify the relationship between TNF- α and the m6A methylation in IVDD patients, we first examined the level of m6A methylation in the NP tissues from the patients and discovered an increase in the level of m6A modification (Figure 1A). Therefore, we further implemented screening of the expression of genes related to m6A methylation, including *METTL3*, *METTL14*, and *Wilms tumor 1-associated protein* (Figures 1B–D). With the increase of the IVDD grades, all the genes exhibited higher expression than the normal group. Meanwhile, TNF- α expression increased along with the IVDD grades (Figure 1E). To better determine the correlation between the expression of TNF- α and m6A modification-related genes, we calculated Pearson correlation coefficients for each gene by plotting the TNF- α mRNA level against the m6A level or the mRNA level of the genes (Figures 1F–I). Among the three genes, TNF- α and *METTL14* ($r = 0.7299$, $P < 0.001$) were more correlated than the other two, which is similar to the correlation between TNF- α expression and the m6A methylation level. Similar phenomena were also observed in HNPCs. With the increase in the stimulation concentrations of TNF- α , the level of m6A methylation was significantly elevated (Figure 1J). Accordingly, compared with the untreated HNPCs, the *METTL14* mRNA level and the protein level in the treatment groups had also experienced significant increases (Figures 1K,L). As a result, it is indicated that the *METTL14*-mediated m6A modification is positively correlated with TNF- α in IVDD models.

METTL14 Knockdown Inhibits TNF- α -Induced Cell Cycle Arrest and Senescence

The discovery of the positive correlation between the expression of *METTL14* and TNF- α in IVDD models motivated us to further explore the impact of *METTL14* on TNF- α -induced NP cellular processes. We developed three shRNAs (shRNA 1–3) to silence *METTL14* in HNPCs, which significantly reduced the expression of the mRNA and protein compared with the controls (Figures 2A,B). Especially, shRNA 1 and 2 showed better inhibitory potency according to the Western blot result (Figure 2B). In the cell viability assay, TNF- α treatment reduced the cell viability while the use of the two shRNAs to TNF- α -treated HNPCs significantly restored the cell viability (Figure 2C). A further investigation indicated that the suppression of the *METTL14* expression affected the TNF- α -induced cell cycle arrest (Figures 2D,E). TNF- α caused the

cell cycle arrest of HNPCs at the G0–G1 stage. In comparison, shRNA1 and 2 significantly drove the cells to enter the S and G2–M phases. Additionally, the knockdown of *METTL14* enabled the inhibition of TNF- α -induced cell senescence (Figure 2F). Using a senescence-associated (SA) β -galactose assay, we observed that the blue-dyed precipitates had been considerably diminished in the shRNA-treatment groups. From the results above, it is suggested that *METTL14* knockdown significantly inhibits TNF- α -induced cell viability inhibition, cell cycle arrest, and cell senescence.

METTL14 Overexpression Promotes Cell Cycle Arrest and Senescence

To further evaluate the influence of *METTL14* on cell cycle arrest and senescence, we overexpressed *METTL14* in HNPCs without the TNF- α treatment (Figures 3A,B). Interestingly, despite the absence of TNF- α , the overexpression of *METTL14* led to reduced cell viability (Figure 3C). Likewise, *METTL14* overexpression remarkably influenced the cell cycle (Figures 3D,E). *METTL14* overexpression enhanced the cell cycle arrest, which brought up the percentage of the cells of the G0–G1 phase by 20% (50% for Vector vs. 70% for *METTL14*). Accordingly, the cell percentage of S and G2–M phases declined. With regard to the efficiency, the overexpression of *METTL14* was even comparable to the TNF- α treatment (Figures 3D,E). When using the SA β -galactose assay to identify the cell senescence of *METTL14*-overexpressing HNPCs, we observed promoted cell senescence (Figure 3F), which was similar to the TNF- α treatment. Therefore, the *METTL14* overexpression assays substantiated that *METTL14* inhibited cell viability and promote cell cycle arrest and senescence.

METTL14-Dependent m6A Methylation Regulates the Processing of miR-34a by DGCR8

METTL14 can interact with DGCR8 to positively regulate the primary miRNA process in an m6A-dependent manner (Ma et al., 2017). In our case, we intended to pursue the downstream target of the *METTL14*-DGCR8 axis. To this end, we first established the interaction between DGCR8 and *METTL14* in HNPCs by co-immunoprecipitation (Figure 4A). Moreover, in *METTL14*-overexpressing HNPCs we also saw a significant increase in the binding between *METTL14* and DGCR8 (Figure 4B). The findings above solidified that *METTL14* mediated pri-miRNA processing by regulating the recognition and binding of DGCR8 to pri-miRNAs.

Furthermore, we detected the association between the four miRNAs, which were upregulated in TNF- α -treated HNPCs and in NP tissues from IVDD patients (Cao and Chen, 2017; Kang et al., 2017; Cheng et al., 2018; Xiang et al., 2020), and *METTL14* (Figure 4C). Compared with the other three miRNAs, the miR-34a-5p level skyrocketed (>3.5-fold) accompanying the overexpression of *METTL14* (Figure 4D). Accordingly, the suppression of *METTL14*

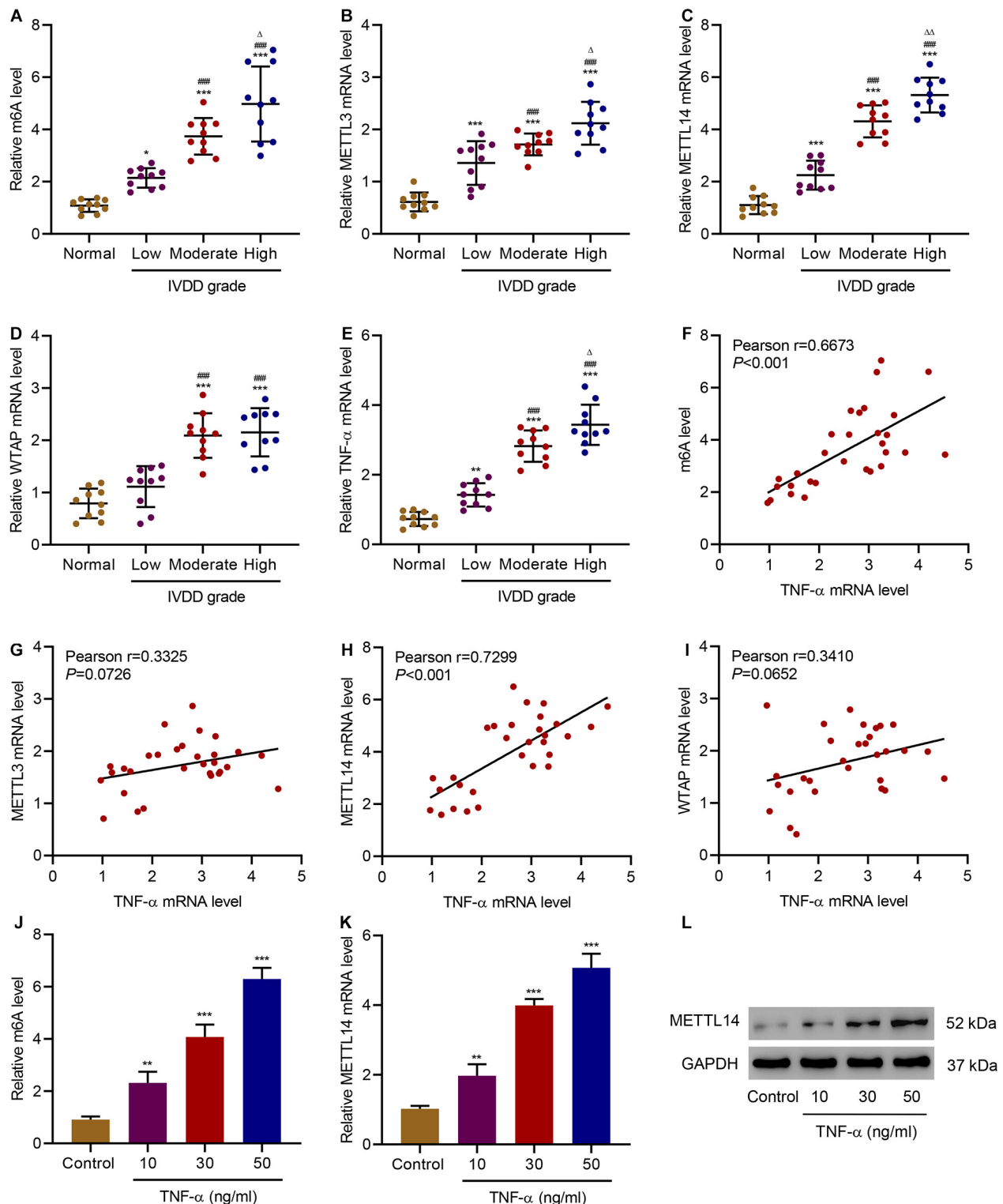


FIGURE 1 | Correlation between TNF- α and m6A modification in IVDD patients. **(A)** The m6A level and expression of **(B)** METTL3, **(C)** METTL14, **(D)** WTAP, and **(E)** TNF- α in normal controls and IVDD patients. **(F–I)** Pearson correlation scatter plots in IVDD patients ($n = 30$). **(J)** The m6A level and **(K,L)** expression of METTL14 in HNPCs treated with different doses of TNF- α . * $P < 0.05$, ** $P < 0.01$, *** $P < 0.001$ compared with normal control; ### $P < 0.001$ compared with low grade; $\Delta P < 0.05$, $\Delta\Delta P < 0.01$ compared with moderate grade.

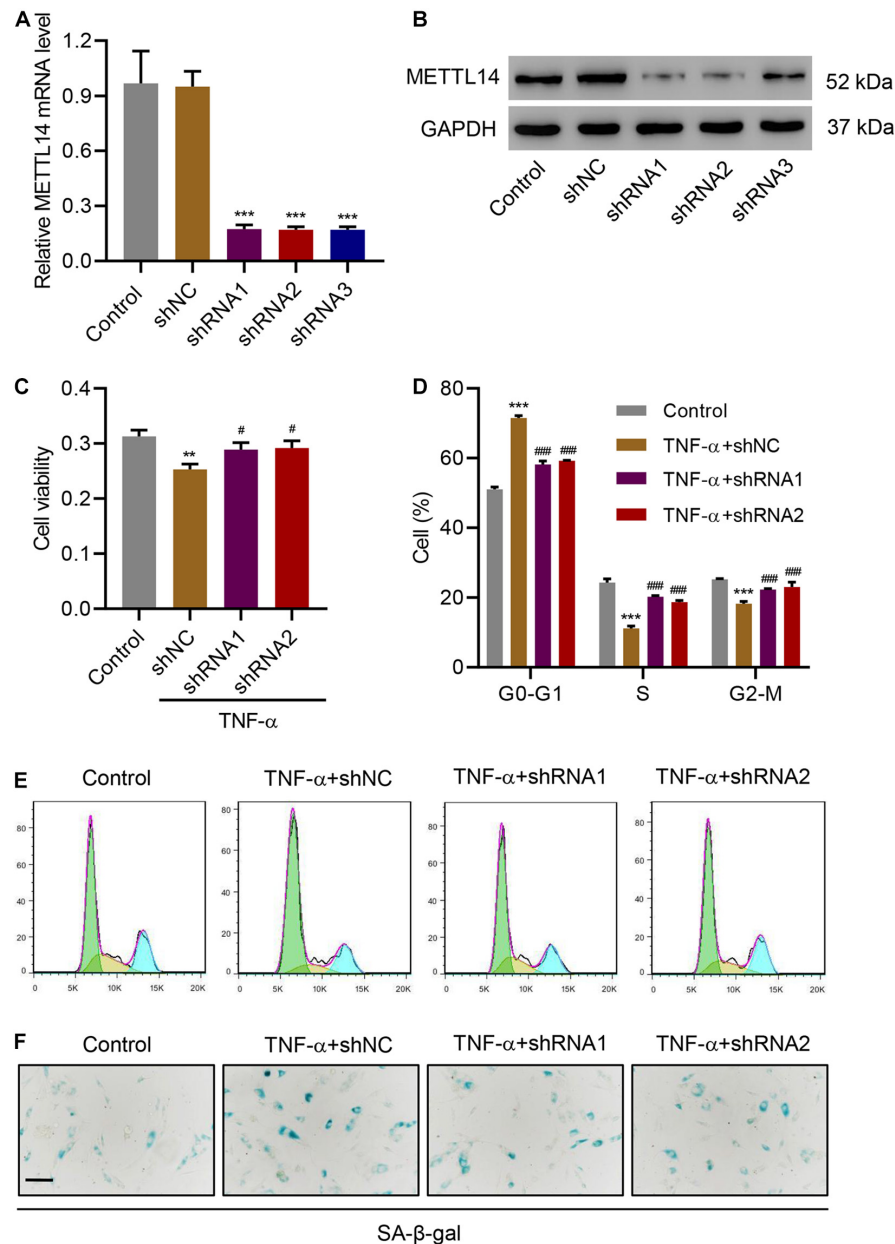


FIGURE 2 | METTL14 silencing inhibits TNF- α -induced cell cycle arrest and senescence. **(A,B)** Expression of METTL14 in HNPCs transduced with METTL14 shRNA vectors. **(C)** Cell viability, **(D,E)** cell cycle, and **(F)** SA- β -gal staining of HNPCs transduced with METTL14 shRNA vectors and treated with 30 ng/mL TNF- α for 24 h. Scale bar: 50 μ m. $**P < 0.01$, $***P < 0.001$ compared with control; $###P < 0.001$ compared with TNF- α + shNC.

by the specific shRNAs significantly reduced the miR-34a-5p relative level. When subjected to the TNF- α treatment, HNPCs exhibited remarkably high expression of miR-34a-5p and pre-miR-34 but low level of pri-miR-34, indicating that miR-34 was processed (Figure 4E). The addition of METTL14 shRNAs tremendously mitigated the TNF- α -induced increase in mRNA levels of miR-34a-5p and pre-miR-34. Furthermore, the relative pri-miR-34a m6A level was also enhanced by TNF- α , which was abolished by METTL14 knockdown (Figure 4F). Conversely, the overexpression

of METTL14 promoted the formation of miR-34a-5p and pre-miR-34 (Figure 4G). The relative level of pri-miR-34a m6A showed a fourfold increase when METTL14 was overexpressed (Figure 4H).

As a result, the level of METTL14 exhibited a positive correlation with that of miR-34a-5p in NP tissues of IVDD patients (Figure 4I). The regulation of the pri-miR-34a level was tightly associated with the interaction between METTL14 and DGCR8 (Figures 4J,K). The DGCR binding level as well as the m6A modification level was significantly promoted by METTL14,

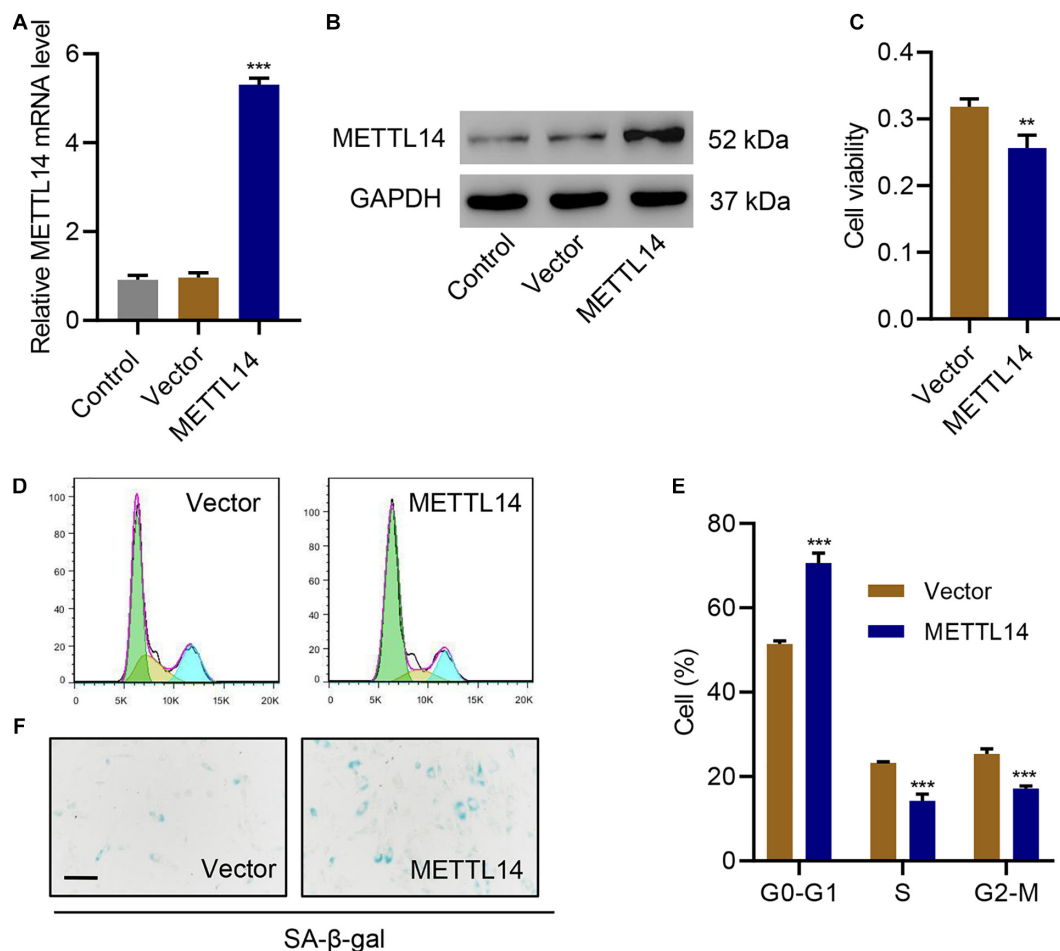


FIGURE 3 | METTL14 overexpression promotes cell cycle arrest and senescence. **(A,B)** Expression of METTL14 in HNPCs transduced with the METTL14 expression vector. **(C)** Cell viability, **(D,E)** cell cycle, and **(F)** SA-β-gal staining of HNPCs transduced with a METTL14 expression vector for 24 h. Scale bar: 50 μm. ** $P < 0.01$, *** $P < 0.001$ compared with vector.

indicating that METTL14 played a vital role in the maturation of pri-miR-34a. Taken together, these results indicate that the METTL14 promoted the processing of pri-miR-34a by DGCR8 in an m6A manner.

miR-34a-5p Inhibitor Rescues the Cell Cycle Arrest and Senescence Induced by METTL14 Overexpression

To verify the potential function of miR-34a-5p in IVDD, we introduced the corresponding miRNA inhibitor in the METTL14-overexpressing HNPCs. The miR-34a-5p inhibitor considerably counteracted the effects of METTL14 overexpression on cell senescence of HNPCs (**Figure 5**). The cell viability (**Figure 5A**), cell cycle arrest (**Figures 5B,C**), and cell senescence (**Figure 5D**) were largely rescued by the inhibitor. As a result, evidenced by the data, the METTL14-induced cell cycle arrest and senescence can be recovered by the miR-34a-5p inhibitor, thus manifesting the indispensable role of miR-34a-5p in regulating METTL14-dependent cell senescence.

miR-34a-5p Promotes Cell Cycle Arrest and Senescence by Targeting SIRT1

Using the mRNA interaction prediction server¹, we predicted the potential interaction between the miR-34a-5p and the 3'-UTR of SIRT1 mRNA (**Figure 6A**). To better analyze the interaction, we devised a dual-luciferase assay using the SIRT1 wildtype mRNA (SIRT1-WT) and the SIRT1 3'-UTR mutant mRNA (SIRT1-MUT) in HNPCs that were treated with the miR-34a-5p inhibitor or the miR-34a-5p mRNA mimic (**Figure 6B**). In the SIRT1-WT group, the inhibitor approximately generated a 9-fold drastic increase in luciferase activity. By contrast, the mimic led to lower luciferase activity. Instead of inducing changes in luciferase activities, in the SIRT1-MUT group, no matter whether the inhibitor or the mimic failed to generate any signal, indicating that the mutation of 3'-UTR jeopardized the interaction between miR34a-5p and SIRT1 mRNA. Furthermore, SIRT1 mRNA expression can be influenced by miR-34a-5p

¹<http://www.microrna.org/>

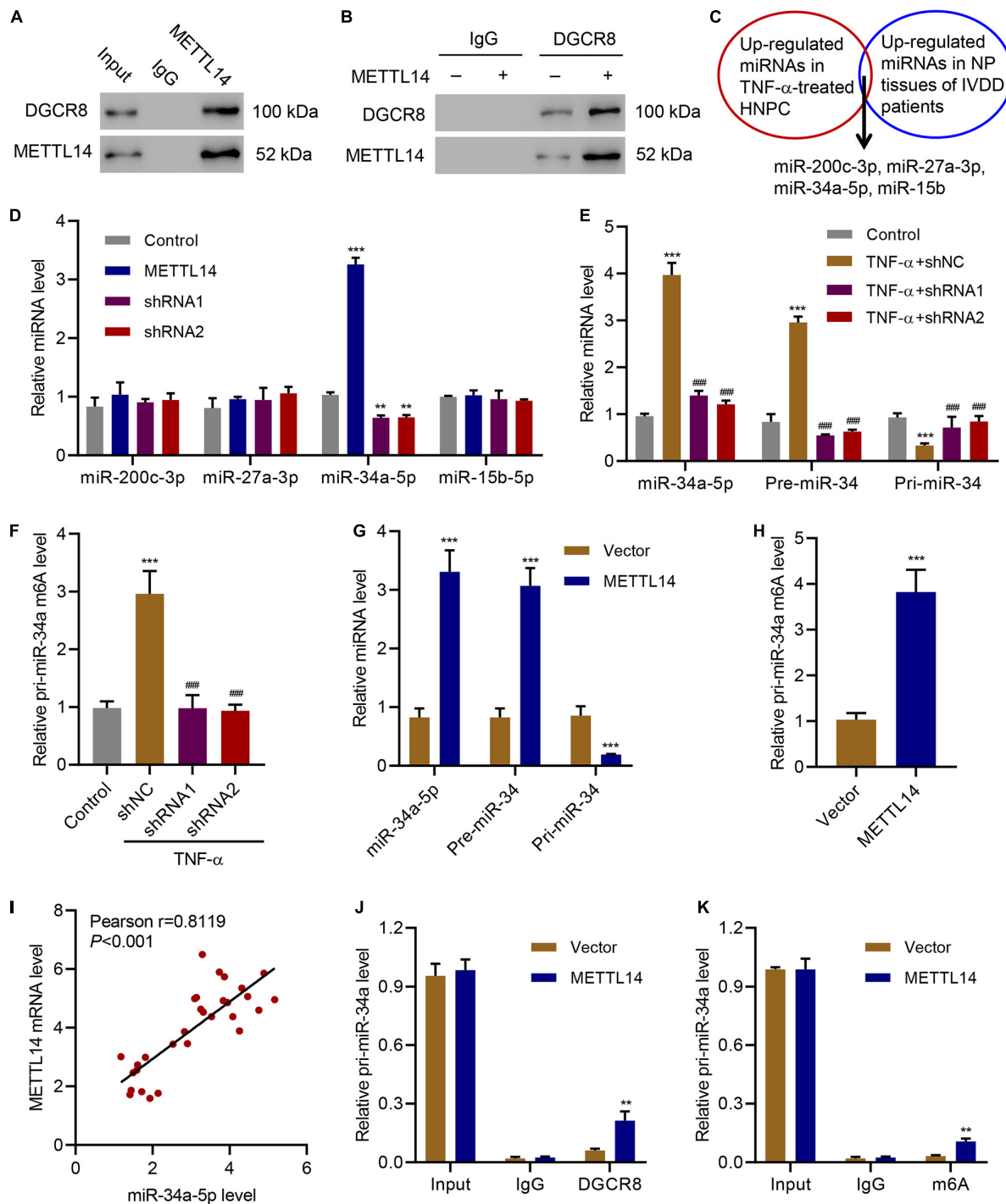


FIGURE 4 | METTL14-dependent m6A methylation regulates the processing of miR-34a by DGCR8. **(A)** Co-immunoprecipitation of the METTL14-interacting protein DGCR8. IgG antibody was used as the control for the immunoprecipitation. **(B)** Immunoprecipitation of DGCR8 in cells overexpressing METTL14 or not. Western blot was conducted using the antibodies depicted. **(C)** Four up-regulated miRNAs were searched out according to their expression levels in TNF- α -treated HNPC cells and in NP tissues of IVDD patients. **(D)** Expression of miR-200c-3p, miR-27a-3p, miR-34a-5p and miR-15b-5p in HNPC cells transduced with METTL14 shRNA vectors or overexpression vector. **(E)** Expression of pri-miR-34a, pre-miR-34a, and miR-34a-5p and **(F)** the levels of pri-miR-34a m6A in HNPC cells transduced with METTL14 shRNA vectors and treated with 30 ng/mL TNF- α for 24 h. **(G)** Expression of pri-miR-34a, pre-miR-34a, and miR-34a-5p and **(H)** the levels of pri-miR-34a m6A in HNPC cells transduced with a METTL14 expression vector for 24 h. **(I)** Pearson correlation scatter plots in IVDD patients ($n = 30$). Immunoprecipitation of **(J)** DGCR8-associated and **(K)** m6A modified RNA from HNPC cells transduced with METTL14 expression vector followed by qRT-PCR to detect pri-miR-34 binding to DGCR8 and to assess the pri-miR-34a m6A modification level, respectively. ** $P < 0.01$, *** $P < 0.001$ compared with control or vector. ### $P < 0.001$ compared with TNF- α + shNC.

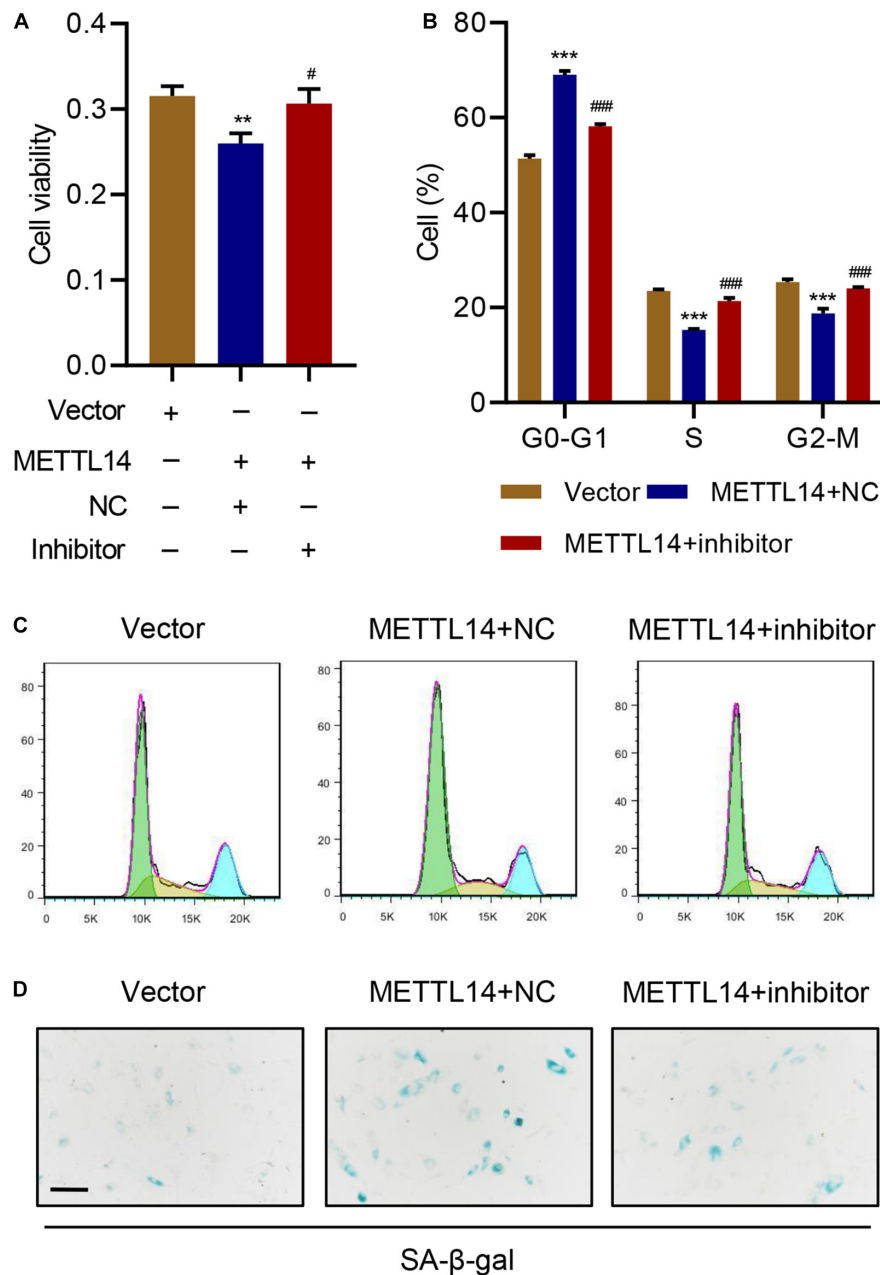


FIGURE 5 | miR-34a-5p inhibitor rescues the cell cycle arrest and senescence induced by METTL14 overexpression. **(A)** Cell viability, **(B,C)** cell cycle, and **(D)** SA-β-gal staining of HNPC cells transduced with the METTL14 expression vector and transfected with miR-34a-5p inhibitor for 24 h. Scale bar: 50 μm. ** $P < 0.01$, *** $P < 0.001$ compared with vector.### $P < 0.001$ compared with METTL14 + NC.

(Figure 6C). The miR-34a-5p inhibitor significantly promoted SIRT1 expression in HNPCs while the mimic considerably suppressed the expression. We next overexpressed SIRT1 in HNPCs to determine the effects of SIRT1 on cell senescence of HNPCs in the presence of the inhibitor or the mimic of miR-34a-5p (Figures 6D,E). The miR-34a-5p mimic lowered the cell viability of HNPCs. However, SIRT1 overexpression in HNPCs largely restored the cell viability despite the presence of the miR-34a-5p mimic (Figure 6F). SIRT1 overexpression

was also active in attenuating the miR-34a-5p-induced cell cycle arrest, in which more HNPCs entered S and G2-M phases (Figure 6G,H). Cell senescence of HNPCs caused by miR-34a-5p was reversed by SIRT1 overexpression as well (Figure 6I). Based on these findings, we established the relationship between the level of SIRT1 mRNA and the levels of miR-34a-5p and METTL14 mRNA in NP tissues of IVDD patients (Figures 6J,K). SIRT1 expression was negatively correlated with either the miR-34a-5p level or the METTL14 mRNA level.

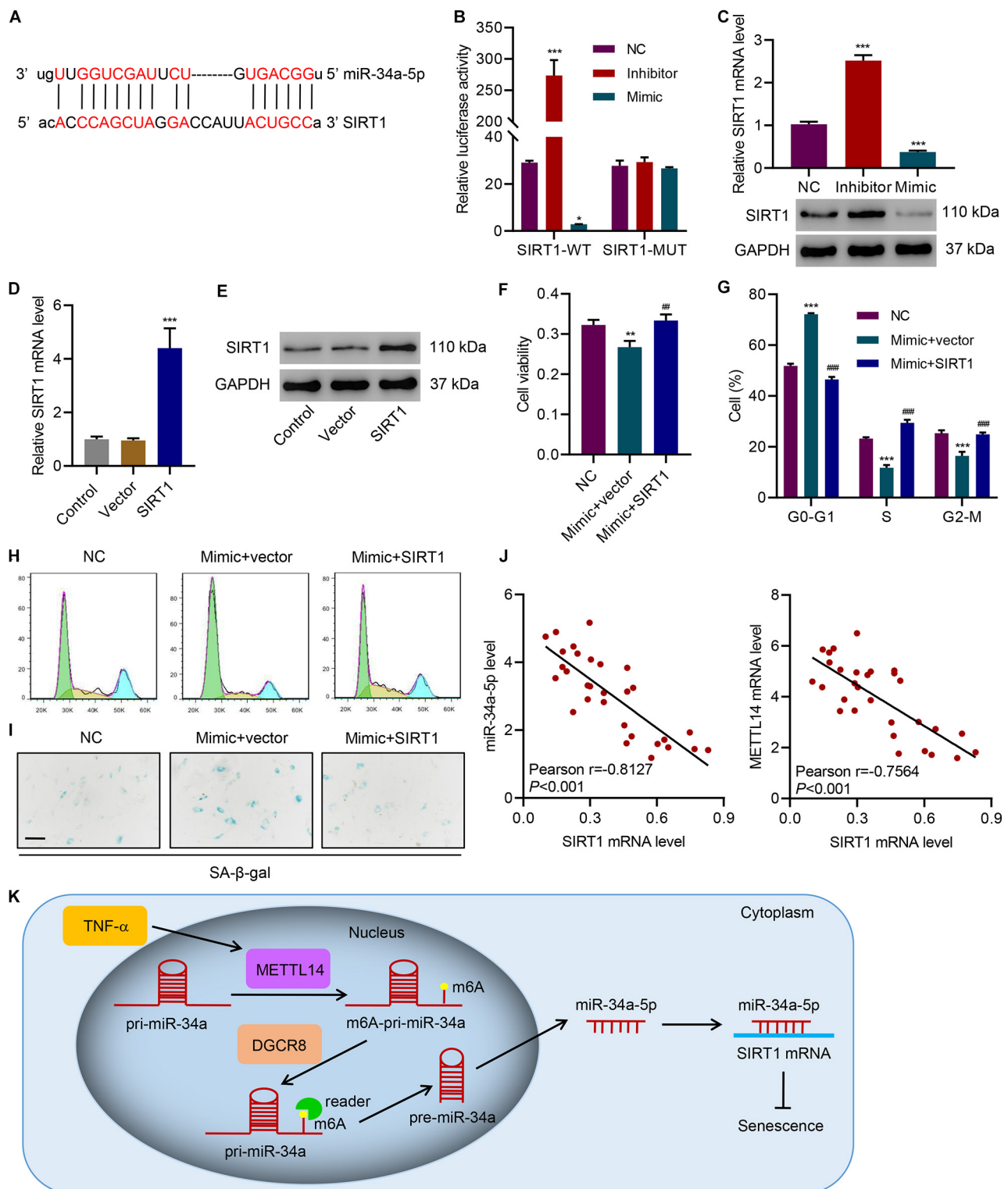


FIGURE 6 | miR-34a-5p promotes cell cycle arrest and senescence by targeting SIRT1. **(A)** Predictive miR-34a-5p binding sites in the 3'-UTR of SIRT1 mRNA. **(B)** Dual-luciferase reporter assays demonstrated that SIRT1 was the direct target of miR-34a-5p. **(C–E)** Expression of SIRT1 in HNPC cells transfected with miR-34a-5p inhibitor, miR-34a-5p mimic, or SIRT1 expression vector. **(F)** Cell viability, **(G,H)** cell cycle, and **(I)** SA-β-gal staining of HNPC cells transfected with miR-34a-5p mimic and a SIRT1 expression vector for 24 h. **(J)** Pearson correlation scatter plots in IVDD patients (n = 30). Scale bar: 50 μm. **(K)** Diagram of the mechanism. *P < 0.05, **P < 0.01, ***P < 0.001 compared with NC or vector. ##P < 0.01, ###P < 0.001 compared with mimic + vector.

Therefore, our results demonstrate that SIRT1 served as a critical target in process of the miR-34a-5p-promoted cell cycle arrest and senescence.

DISCUSSION

miRNA has been found closely associated with cellular process regulation, cell function, and diseases (Bhaskaran and Mohan, 2014). The modification of miRNAs, especially methylation, can largely affect the functions of mRNA, which further regulates cellular processes and biological activities (Bianchi et al., 2017). Recent reports link IVDD with miRNAs, suggesting that miRNAs can act as potential therapeutic targets (Li et al., 2015; Zhou et al., 2017). Herein, we have devised various assays to clarify the mechanism of m6A methylation promoted cell senescence in IVDD.

The level of m6A modification significantly increased in the HNPCs, which was correlated with the level of TNF- α in IVDD patients. m6A modification has been characterized as the most prevalent internal mRNA modification in mammalian cells, which accounts for regulating various important biological processes (Zhang et al., 2019). Rising evidence is confirming the role of m6A in cell development and cancers (Fazi and Fatica, 2019; Chen and Wong, 2020). Li et al. have characterized the function of m6A methylation in controlling the proliferation of human glioma cells by influencing apoptosis (Li F. et al., 2019). Yang et al. have reported the m6A-modulated proliferation and apoptosis of lens epithelial cells (Yang et al., 2020). However, there is no previous report on the relation between m6A methylation and IVDD. Our discovery of a high level of m6A modification in NP tissues of IVDD patients expands the scope of related research. More importantly, we have identified that METTL14, one of the “writer” protein, was more tightly associated with m6A modification, the expression of which was positively correlated with the level of m6A methylation as well as the TNF- α . Jian et al. (2020) have reported the mechanism of METTL14-promoted endothelial inflammation and atherosclerosis through driving FOXO1 m6A modifications. They proved the major role of METTL14 in TNF- α -induced endothelial cell inflammation. As a process tightly associated with inflammation, cell senescence includes irreversible cell cycle arrest (Stojanovic et al., 2020). In our study, we have clearly illustrated the role of METTL14 in cell senescence, which solidifies the function of METTL14 in TNF- α -induced inflammation. With the increased expression of this writer protein, cell viability decreased while cell cycle arrest and senescence were significantly promoted.

The identification of METTL14 as the main regulator of m6A modification in IVDD models allowed us to further explore the mechanism behind it. Studies have shown that METTL14 actively participates in the processing of miRNAs by interacting with DGCR8 (Feng et al., 2010; Ma et al., 2017). Accordingly, our co-immunoprecipitation assay also confirmed the interaction between METTL14 and DGCR8 in HNPCs, which proves that METTL14 played a role in regulating miRNA maturation in IVDD models. Interestingly, through an in-depth

screening of miRNA change in either HNPCs or NP tissues of IVDD patients, we identified several upregulated miRNAs, in which miR-34a-5p showed a positive correlation with the m6A modification level. When varying the METTL14 level in HNPCs, we were able to capture the regulation of the miR-34a-5p processing. Similar to the processing of miR-126 (Feng et al., 2010) and miR-19a (Zhang et al., 2020), METTL14 positively modulated the maturation of miR-34. Thus, the RNA levels of pre-miR-34 and miR-34a-5p were significantly elevated in contrast to the mitigated pri-miR-34 level. The m6A methylation of pri-miR-34 was found active under the circumstance of METTL14 overexpression.

Previous studies have discussed the mechanism of m6A-promoted cell senescence (Li Q. et al., 2017; Wu et al., 2020). The METTL3/METTL14-mediated m6A methylation can enhance p21 expression which is further promoted. oxidative stress-induced cellular senescence (Li Q. et al., 2017). Through interacting with Lamin A, METTL3/14 can be properly localized in the nuclear speckles to achieve the regulatory function (Wu et al., 2020). Our study has deepened the current understanding of m6A modification in cell senescence. Mainly regulated by METTL14, m6A-involved cell senescence was originated from the methylation of miR-34a-5p followed by the interaction with the 3'-UTR of the SIRT mRNA. During the process, the maturation of the mRNA was largely promoted, reflected by the escalated levels of miR-34a-5p and pre-miR-34 and reduced level of pri-miR-34. The role of METTL3 in the regulation of senescence.

It is noted that miRNAs can play vital roles in cell senescence (Li et al., 2009; Faraonio et al., 2012; Baker et al., 2019). miR-34a-5p has been identified as a possible cause of cell senescence in HNPCs in our study. Xia et al. have characterized the mechanism of miR-34a-5p-induced cardiac senescence-related injury. It is shown that miR-34a-5p serves as an exosomal transfer RNA and the inhibition of miR-34a-5p mitigated the pro-senescent effect in cardiomyocytes and subsequently alleviated the irreversible cell cycle arrest (Xia et al., 2020). miR-34a-5p is also found involved in regulating the switch between senescence and apoptosis in non-small cell lung cancer (Gupta et al., 2020). Herein, we have presented that the inhibition of miR-34a-5p significantly decreases the senescence of HNPCs. As a result, miR-34a-5p demonstrates prevalent senescent effects in varieties of tissues and organs, which can be a major biological function of this miRNA.

Additionally, Maes et al. (2009) used a miRNA microarray assay to reveal the upregulation of miR-34 in senescent cells. We advanced the results and proved that this miRNA was further processed through the METTL14-DGCR8 axis. Our data have demonstrated that miR-34a-5p induced cell senescence by targeting the downstream factor SIRT1. SIRT1 localizes in both the nucleus and cytoplasm to function in many crucial biological activities, including lifespan extension, ADP-ribosyl-transferase, DNA repair, cell cycle arrest, and cellular senescence (Lee et al., 2019). The sequence of miR-34a-5p was predicted to pair with that of the 3'-UTR of SIRT1. The use of the miR-34a-5p mimic resulted in typical senescence that was largely inhibited by overexpressing SIRT1. In IVDD patients, SIRT1 expression

was negatively correlated with the levels of the METTL14 mRNA and miR-34a-5p. Therefore, our findings reinforce the idea that SIRT1 prevents cell senescence.

Our data were mainly obtained from the *in vitro* model of HNPCs, which can be further explored in *in vivo* IVDD models. Due to limited studies in the related field, the concrete mechanism of METTL14-mediated m6A modification and maturation of miR-34a has not been fully elucidated. Efficient disruption of the interaction between miR-34a-5p and SIRT1 in both *in vitro* and *in vivo* levels to alleviate IVDD still requires more sophisticated and intensive investigations. Additionally, the interaction between METTL14 and DGRC8 is also worth dedicated studies to uncover the entire axis.

Our current study reveals that m6A-modified miR-34a-5p promotes induced NPC senescence by targeting SIRT1, which represents the first attempt to discover the association between miRNA modification and cell senescence in IVDD models (Figure 6K). By characterizing the role of the miR-34a-5p-SIRT1 axis in cell senescence, we have proposed a potential direction for developing an IVDD therapy by disrupting the interaction between miR-34a-5p and SIRT1 or inhibiting METTL14.

REFERENCES

- Baker, J. R., Vuppusetty, C., Colley, T., Hassibi, S., Fenwick, P. S., Donnelly, L. E., et al. (2019). MicroRNA-570 is a novel regulator of cellular senescence and inflammaging. *FASEB J.* 33, 1605–1616. doi: 10.1096/fj.201800965R
- Bhaskaran, M., and Mohan, M. (2014). MicroRNAs: history, biogenesis, and their evolving role in animal development and disease. *Vet. Pathol.* 51, 759–774. doi: 10.1177/0300985813502820
- Bianchi, M., Renzini, A., Adamo, S., and Moresi, V. (2017). Coordinated actions of microRNAs with other epigenetic factors regulate skeletal muscle development and adaptation. *Int. J. Mol. Sci.* 18:840. doi: 10.3390/ijms18040840
- Cao, Z., and Chen, L. (2017). Inhibition of miR-27a suppresses the inflammatory response via the p38/MAPK pathway in intervertebral disc cells. *Exp. Ther. Med.* 14, 4572–4578. doi: 10.3892/etm.2017.5053
- Chen, M., and Wong, C. M. (2020). The emerging roles of N6-methyladenosine (m6A) deregulation in liver carcinogenesis. *Mol. Cancer* 19:44. doi: 10.1186/s12943-020-01172-y
- Chen, Y., Zheng, Z., Wang, J., Tang, C., Khor, S., Chen, J., et al. (2018). Berberine suppresses apoptosis and extracellular matrix (ECM) degradation in nucleus pulposus cells and ameliorates disc degeneration in a rodent model. *Int. J. Biol. Sci.* 14, 682–692. doi: 10.7150/ijbs.24081
- Cheng, X., Zhang, G., Zhang, L., Hu, Y., Zhang, K., Sun, X., et al. (2018). Mesenchymal stem cells deliver exogenous miR-21 via exosomes to inhibit nucleus pulposus cell apoptosis and reduce intervertebral disc degeneration. *J. Cell Mol. Med.* 22, 261–276. doi: 10.1111/jcmm.13316
- Dudek, M., Yang, N., Ruckshanthi, J. P., Williams, J., Borysiewicz, E., Wang, P., et al. (2017). The intervertebral disc contains intrinsic circadian clocks that are regulated by age and cytokines and linked to degeneration. *Ann. Rheum. Dis.* 76, 576–584. doi: 10.1136/annrheumdis-2016-209428
- Faraonio, R., Salerno, P., Passaro, F., Sedia, C., Iaccio, A., Bellelli, R., et al. (2012). A set of miRNAs participates in the cellular senescence program in human diploid fibroblasts. *Cell Death Differ.* 19, 713–721. doi: 10.1038/cdd.2011.143
- Fazi, F., and Fatica, A. (2019). Interplay between N (6)-methyladenosine (m6A) and non-coding RNAs in cell development and cancer. *Front. Cell Dev. Biol.* 7:116. doi: 10.3389/fcell.2019.00116
- Feng, C., Liu, H., Yang, M., Zhang, Y., Huang, B., and Zhou, Y. (2016). Disc cell senescence in intervertebral disc degeneration: causes and molecular pathways. *Cell Cycle* 15, 1674–1684. doi: 10.1080/15384101.2016.1152433

DATA AVAILABILITY STATEMENT

The original contributions presented in the study are included in the article/supplementary material, further inquiries can be directed to the corresponding author/s.

ETHICS STATEMENT

The studies involving human participants were reviewed and approved by The Affiliated Shanghai General Hospital of Nanjing Medical University. The patients/participants provided their written informed consent to participate in this study.

AUTHOR CONTRIBUTIONS

HZ and BS conceived and designed the work. BS, LZ, and GZ performed the research and collected and analyzed the data. HZ and QS collected human tissue samples and wrote the manuscript. BS, LZ, and QS provided technical assistance. All authors read and approved the final manuscript.

- Feng, R., Chen, X., Yu, Y., Su, L., Yu, B., Li, J., et al. (2010). miR-126 functions as a tumour suppressor in human gastric cancer. *Cancer Lett.* 298, 50–63. doi: 10.1016/j.canlet.2010.06.004
- Freburger, J. K., Holmes, G. M., Agans, R. P., Jackman, A. M., Darter, J. D., Wallace, A. S., et al. (2009). The rising prevalence of chronic low back pain. *Arch. Intern. Med.* 169, 251–258. doi: 10.1001/archinternmed.2008.543
- Frost, B. A., Camarero-Espinosa, S., and Foster, E. J. (2019). Materials for the spine: anatomy, problems, and solutions. *Materials (Basel)* 12:253. doi: 10.3390/ma12020253
- Froud, R., Patterson, S., Eldridge, S., Seale, C., Pincus, T., Rajendran, D., et al. (2014). A systematic review and meta-synthesis of the impact of low back pain on people's lives. *BMC Musculosk. Disord.* 15:50. doi: 10.1186/1471-2474-15-50
- Gupta, S., Silveira, D. A., and Mombach, J. C. M. (2020). ATM/miR-34a-5p axis regulates a p21-dependent senescence-apoptosis switch in non-small cell lung cancer: a Boolean model of G1/S checkpoint regulation. *FEBS Lett.* 594, 227–239. doi: 10.1002/1873-3468.13615
- Han, J., Wang, J. Z., Yang, X., Yu, H., Zhou, R., Lu, H. C., et al. (2019). METTL3 promote tumor proliferation of bladder cancer by accelerating pri-miR221/222 maturation in m6A-dependent manner. *Mol. Cancer* 18:110. doi: 10.1186/s12943-019-1036-9
- Han, M., Liu, Z., Xu, Y., Liu, X., Wang, D., Li, F., et al. (2020). Abnormality of m6A mRNA Methylation Is Involved in Alzheimer's Disease. *Front. Neurosci.* 14:98. doi: 10.3389/fnins.2020.00098
- Hwang, P. Y., Chen, J., Jing, L., Hoffman, B. D., and Setton, L. A. (2014). The role of extracellular matrix elasticity and composition in regulating the nucleus pulposus cell phenotype in the intervertebral disc: a narrative review. *J. Biomech. Eng.* 136:021010. doi: 10.1115/1.4026360
- Jian, D., Wang, Y., Jian, L., Tang, H., Rao, L., Chen, K., et al. (2020). METTL14 aggravates endothelial inflammation and atherosclerosis by increasing FOXO1 N6-methyladenosine modifications. *Theranostics* 10, 8939–8956. doi: 10.7150/thno.45178
- Jiang, L., Zhang, X., Zheng, X., Ru, A., Ni, X., Wu, Y., et al. (2013). Apoptosis, senescence, and autophagy in rat nucleus pulposus cells: implications for diabetic intervertebral disc degeneration. *J. Orthop. Res.* 31, 692–702. doi: 10.1002/jor.22289
- Jiao, S., Li, J., Liu, B., Yang, M., Xiu, J., and Qu, D. (2018). Nucleus pulposus cell apoptosis is attenuated by CDMP-2 through regulating oxidative damage under the hyperosmotic environment. *Biosci. Rep.* 38:BSR20181176. doi: 10.1042/BSR20181176

- Kang, L., Yang, C., Yin, H., Zhao, K., Liu, W., Hua, W., et al. (2017). MicroRNA-15b silencing inhibits IL-1 β -induced extracellular matrix degradation by targeting SMAD3 in human nucleus pulposus cells. *Biotechnol. Lett.* 39, 623–632. doi: 10.1007/s10529-016-2280-3
- Kepler, C. K., Ponnappan, R. K., Tannoury, C. A., Risbud, M. V., and Anderson, D. G. (2013). The molecular basis of intervertebral disc degeneration. *Spine J.* 13, 318–330. doi: 10.1016/j.spinee.2012.12.003
- Lee, S. H., Lee, J. H., Lee, H. Y., and Min, K. J. (2019). Sirtuin signaling in cellular senescence and aging. *BMB Rep.* 52, 24–34. doi: 10.5483/BMBRep.2019.52.1.290
- Li, F., Zhang, C., and Zhang, G. (2019). m6A RNA methylation controls proliferation of human glioma cells by influencing cell apoptosis. *Cytogenet. Genome Res.* 159, 119–125. doi: 10.1159/000499062
- Li, G., Luna, C., Qiu, J., Epstein, D. L., and Gonzalez, P. (2009). Alterations in microRNA expression in stress-induced cellular senescence. *Mech. Ageing Dev.* 130, 731–741. doi: 10.1016/j.mad.2009.09.002
- Li, P., Gan, Y., Xu, Y., Song, L., Wang, L., Ouyang, B., et al. (2017). The inflammatory cytokine TNF- α promotes the premature senescence of rat nucleus pulposus cells via the PI3K/Akt signaling pathway. *Sci. Rep.* 7:42938. doi: 10.1038/srep42938
- Li, Q., Li, X., Tang, H., Jiang, B., Dou, Y., Gorospe, M., et al. (2017). NSUN2-mediated m5C methylation and METTL3/METTL14-mediated m6A methylation cooperatively enhance p21 translation. *J. Cell Biochem.* 118, 2587–2598. doi: 10.1002/jcb.25957
- Li, Z., Chen, X., Xu, D., Li, S., Chan, M. T. V., and Wu, W. K. K. (2019). Circular RNAs in nucleus pulposus cell function and intervertebral disc degeneration. *Cell Prolif.* 52:e12704. doi: 10.1111/cpr.12704
- Li, Z., Li, X., Chen, C., Li, S., Shen, J., Tse, G., et al. (2018). Long non-coding RNAs in nucleus pulposus cell function and intervertebral disc degeneration. *Cell Prolif.* 51:e12483. doi: 10.1111/cpr.12483
- Li, Z., Yu, X., Shen, J., Chan, M. T., and Wu, W. K. (2015). MicroRNA in intervertebral disc degeneration. *Cell Prolif.* 48, 278–283. doi: 10.1111/cpr.12180
- Luoma, K., Riihimäki, H., Luukkonen, R., Raininko, R., Viikari-Juntura, E., and Lamminen, A. (2000). Low back pain in relation to lumbar disc degeneration. *Spine (Phila Pa 1976)* 25, 487–492. doi: 10.1097/00007632-200002150-00016
- Ma, J. Z., Yang, F., Zhou, C. C., Liu, F., Yuan, J. H., Wang, F., et al. (2017). METTL14 suppresses the metastatic potential of hepatocellular carcinoma by modulating N(6)-methyladenosine-dependent primary MicroRNA processing. *Hepatology* 65, 529–543. doi: 10.1002/hep.28885
- Maes, O. C., Sarojini, H., and Wang, E. (2009). Stepwise up-regulation of microRNA expression levels from replicating to reversible and irreversible growth arrest states in WI-38 human fibroblasts. *J. Cell Physiol.* 221, 109–119. doi: 10.1002/jcp.21834
- Morgan, P., Spiridonov, S., Goebel, R., Nissi, M., Frei, R., and Ellermann, J. (2014). MR Imaging with T2*-mapping for improved acetabular cartilage assessment in FAI—a case report with arthroscopic correlation. *Orthop. Traumatol. Surg. Res.* 100, 971–973. doi: 10.1016/j.otsr.2014.09.014
- Nakazawa, K. R., Walter, B. A., Laudier, D. M., Krishnamoorthy, D., Mosley, G. E., Spiller, K. L., et al. (2018). Accumulation and localization of macrophage phenotypes with human intervertebral disc degeneration. *Spine J.* 18, 343–356. doi: 10.1016/j.spinee.2017.09.018
- Pattappa, G., Li, Z., Peroglio, M., Wismer, N., Alini, M., and Grad, S. (2012). Diversity of intervertebral disc cells: phenotype and function. *J. Anat.* 221, 480–496. doi: 10.1111/j.1469-7580.2012.01521.x
- Purmessur, D., Walter, B. A., Roughley, P. J., Laudier, D. M., Hecht, A. C., and Iatridis, J. (2013). A role for TNF α in intervertebral disc degeneration: a non-recoverable catabolic shift. *Biochem. Biophys. Res. Commun.* 433, 151–156. doi: 10.1016/j.bbrc.2013.02.034
- Stojanovic, S. D., Fiedler, J., Bauersachs, J., Thum, T., and Sedding, D. G. (2020). Senescence-induced inflammation: an important player and key therapeutic target in atherosclerosis. *Eur. Heart J.* 41, 2983–2996. doi: 10.1093/eurheartj/ehz919
- Wang, C., Yu, X., Yan, Y., Yang, W., Zhang, S., Xiang, Y., et al. (2017). Tumor necrosis factor- α : a key contributor to intervertebral disc degeneration. *Acta Biochim. Biophys. Sin. (Shanghai)* 49, 1–13. doi: 10.1093/abbs/gmw112
- Wang, X., Chen, N., Du, Z., Ling, Z., Zhang, P., Yang, J., et al. (2020). Bioinformatics analysis integrating metabolomics of m(6)A RNA microarray in intervertebral disc degeneration. *Epigenomics* 12, 1419–1441. doi: 10.2217/epi-2020-0101
- Wang, Y., Wang, H., Zhuo, Y., Hu, Y., Zhang, Z., Ye, J., et al. (2020). SIRT1 alleviates high-magnitude compression-induced senescence in nucleus pulposus cells via PINK1-dependent mitophagy. *Aging (Albany N. Y.)* 12, 16126–16141. doi: 10.18632/aging.103587
- Weng, H., Huang, H., Wu, H., Qin, X., Zhao, B. S., Dong, L., et al. (2018). METTL14 inhibits hematopoietic stem/progenitor differentiation and promotes leukemogenesis via mRNA m(6)A modification. *Cell Stem Cell* 22, 191–205.e199. doi: 10.1016/j.stem.2017.11.016
- Wu, Z., Shi, Y., Lu, M., Song, M., Yu, Z., Wang, J., et al. (2020). METTL3 counteracts premature aging via m6A-dependent stabilization of MIS12 mRNA. *Nucleic Acids Res.* 48, 11083–11096. doi: 10.1093/nar/gkaa816
- Xia, W., Chen, H., Chen, D., Ye, Y., Xie, C., and Hou, M. (2020). PD-1 inhibitor inducing exosomal miR-34a-5p expression mediates the cross talk between cardiomyocyte and macrophage in immune checkpoint inhibitor-related cardiac dysfunction. *J. Immunother. Cancer* 8:e001293. doi: 10.1136/jitc-2020-001293
- Xiang, Q., Kang, L., Wang, J., Liao, Z., Song, Y., Zhao, K., et al. (2020). CircRNA-CIDN mitigated compression loading-induced damage in human nucleus pulposus cells via miR-34a-5p/SIRT1 axis. *EBioMedicine* 53:102679. doi: 10.1016/j.ebiom.2020.102679
- Xie, L., Huang, W., Fang, Z., Ding, F., Zou, F., Ma, X., et al. (2019). CircERCC2 ameliorated intervertebral disc degeneration by regulating mitophagy and apoptosis through miR-182-5p/SIRT1 axis. *Cell Death Dis.* 10:751. doi: 10.1038/s41419-019-1978-2
- Yang, J., Liu, J., Zhao, S., and Tian, F. (2020). N(6)-methyladenosine METTL3 Modulates the proliferation and apoptosis of lens epithelial cells in diabetic cataract. *Mol. Ther. Nucleic Acids* 20, 111–116. doi: 10.1016/j.omtn.2020.02.002
- Zhang, B. Y., Han, L., Tang, Y. F., Zhang, G. X., Fan, X. L., Zhang, J. J., et al. (2020). METTL14 regulates M6A methylation-modified primary miR-19a to promote cardiovascular endothelial cell proliferation and invasion. *Eur. Rev. Med. Pharmacol. Sci.* 24, 7015–7023. doi: <doi>
- Zhang, C., Fu, J., and Zhou, Y. (2019). A review in research progress concerning m6A methylation and immunoregulation. *Front. Immunol.* 10:922. doi: 10.3389/fimmu.2019.00922
- Zhang, Z., Kakutani, K., Maeno, K., Takada, T., Yurube, T., Doita, M., et al. (2011). Expression of silent mating type information regulator 2 homolog 1 and its role in human intervertebral disc cell homeostasis. *Arthritis Res. Ther.* 13:R200. doi: 10.1186/ar3533
- Zhao, C. Q., Jiang, L. S., and Dai, L. Y. (2006). Programmed cell death in intervertebral disc degeneration. *Apoptosis* 11, 2079–2088. doi: 10.1007/s10495-006-0290-7
- Zhou, X., Chen, L., Grad, S., Alini, M., Pan, H., Yang, D., et al. (2017). The roles and perspectives of microRNAs as biomarkers for intervertebral disc degeneration. *J. Tissue Eng. Regen. Med.* 11, 3481–3487. doi: 10.1002/term.2261
- Zhu, J., Zhang, X., Gao, W., Hu, H., Wang, X., and Hao, D. (2019). lncRNA/circRNAmiRNAmRNA ceRNA network in lumbar intervertebral disc degeneration. *Mol. Med. Rep.* 20, 3160–3174. doi: 10.3892/mmr.2019.10569

Conflict of Interest: The authors declare that the research was conducted in the absence of any commercial or financial relationships that could be construed as a potential conflict of interest.

Copyright © 2021 Zhu, Sun, Zhu, Zou and Shen. This is an open-access article distributed under the terms of the Creative Commons Attribution License (CC BY). The use, distribution or reproduction in other forums is permitted, provided the original author(s) and the copyright owner(s) are credited and that the original publication in this journal is cited, in accordance with accepted academic practice. No use, distribution or reproduction is permitted which does not comply with these terms.



Umbilical Cord Blood-Derived Exosomes From Very Preterm Infants With Bronchopulmonary Dysplasia Impaired Endothelial Angiogenesis: Roles of Exosomal MicroRNAs

OPEN ACCESS

Edited by:

Zhiguo Chen,
Capital Medical University, China

Reviewed by:

Hamed Mirzaei,
Kashan University of Medical
Sciences, Iran
Amelia Eva Aranega,
University of Jaén, Spain

*Correspondence:

Xin-qi Zhong
zhongxq2016@gzhmu.edu.cn
Jing Zheng
jzheng@wisc.edu
Qi-liang Cui
cuiql_paper@126.com

† These authors have contributed
equally to this work

Specialty section:

This article was submitted to
Molecular Medicine,
a section of the journal
Frontiers in Cell and Developmental
Biology

Received: 03 December 2020

Accepted: 22 February 2021

Published: 25 March 2021

Citation:

Zhong X-q, Yan Q, Chen Z-g,
Jia C-h, Li X-h, Liang Z-y, Gu J,
Wei H-l, Lian C-y, Zheng J and Cui Q-l
(2021) Umbilical Cord Blood-Derived
Exosomes From Very Preterm Infants
With Bronchopulmonary Dysplasia
Impaired Endothelial Angiogenesis:
Roles of Exosomal MicroRNAs.
Front. Cell Dev. Biol. 9:637248.
doi: 10.3389/fcell.2021.637248

Xin-qi Zhong^{1,2*†}, Qin Yan^{3†}, Zhuang-gui Chen^{4†}, Chun-hong Jia¹, Xiu-hong Li⁵,
Zi-yan Liang¹, Jian Gu¹, Hui-ling Wei¹, Chang-yu Lian¹, Jing Zheng^{6*} and Qi-liang Cui^{1,2*}

¹ Department of Neonatology, Third Affiliated Hospital of Guangzhou Medical University, Guangzhou, China, ² Key Laboratory for Major Obstetric Diseases of Guangdong Province, Guangzhou, China, ³ Department of Gynecology, Shanghai First Maternity and Infant Hospital, Tongji University School of Medicine, Shanghai, China, ⁴ Department of Pediatrics and Department of Allergy, The Third Affiliated Hospital, Sun Yat-sen University, Guangzhou, China, ⁵ Department of Maternal and Child Health, School of Public Health, Sun Yat-sen University, Guangzhou, China, ⁶ Department of Obstetrics and Gynecology, University of Wisconsin-Madison, Madison, WI, United States

Premature infants have a high risk of bronchopulmonary dysplasia (BPD), which is characterized by abnormal development of alveoli and pulmonary vessels. Exosomes and exosomal miRNAs (EXO-miRNAs) from bronchoalveolar lavage fluid are involved in the development of BPD and might serve as predictive biomarkers for BPD. However, the roles of exosomes and EXO-miRNAs from umbilical cord blood of BPD infants in regulating angiogenesis are yet to be elucidated. In this study, we showed that umbilical cord blood-derived exosomes from BPD infants impaired angiogenesis *in vitro*. Next-generation sequencing of EXO-miRNAs from preterm infants without (NBPD group) or with BPD (BPD group) uncovered a total of 418 differentially expressed (DE) EXO-miRNAs. These DE EXO-miRNAs were primarily enriched in cellular function-associated pathways including the PI3K/Akt and angiogenesis-related signaling pathways. Among those EXO-miRNAs which are associated with PI3K/Akt and angiogenesis-related signaling pathways, BPD reduced the expression of hsa-miR-103a-3p and hsa-miR-185-5p exhibiting the most significant reduction (14.3% and 23.1% of NBPD group, respectively); BPD increased hsa-miR-200a-3p expression by 2.64 folds of the NBPD group. Furthermore, overexpression of hsa-miR-103a-3p and hsa-miR-185-5p in normal human umbilical vein endothelial cells (HUVECs) significantly enhanced endothelial cell proliferation, tube formation, and cell migration, whereas overexpressing hsa-miR-200a-3p inhibited these cellular responses. This study demonstrates that exosomes derived from umbilical cord blood of BPD infants impair angiogenesis, possibly via DE EXO-miRNAs, which might contribute to the development of BPD.

Keywords: bronchopulmonary dysplasia, microRNA, angiogenesis, exosome, preterm infants

INTRODUCTION

Very preterm infants (VPI, gestational age <32 weeks) account for 10% of preterm birth infants, and its prevalence keeps increasing in the world (Blencowe et al., 2013). Bronchopulmonary dysplasia (BPD) is one of the most severe respiratory complications in VPI, leading to fetal developmental delay and mortality (Reiterer et al., 2019). Development of BPD is attributed to a wide range of factors including use of ventilator, hyperoxia therapy, and other perinatal risk factors (Jobe and Bancalari, 2001). However, pathogenesis and the underlying mechanisms of BPD remain elusive.

The main pathological features of BPD include developmental retardation of alveoli and microvascular dysfunction (Kalikkot Thekkeveedu et al., 2017). The BPD-impaired pulmonary microvascular endothelium is primarily induced by hyperoxia (Buczynski et al., 2013). The decreased expression of pro-angiogenesis factors, such as vascular endothelial growth factor (VEGF) in BPD patients, is associated with pulmonary vasculature dysfunction (Bhatt et al., 2001; Alvira, 2016). In neonatal rats, BPD also impairs function of lung endothelial progenitor cells which are essential for lung microvascular growth and development (Alphonse et al., 2014). In addition, the number of endothelial progenitor cells decreased in the umbilical cord blood of the preterm infants with subsequent development of BPD (Bertagnolli et al., 2017). It is well-known that suppression of angiogenesis restrains the alveolarization during lung development in rats (Jakkula et al., 2000). On the other hand, improvement of pulmonary angiogenesis is beneficial for the alveolar development, which might prevent the development of BPD in animal models (Stenmark and Balasubramaniam, 2005). Thus, identifying the intrinsic factors which induce angiogenesis impairment will advance our understanding of BPD development and help us develop novel therapies and predictors for BPD.

Exosomes are nanosized extracellular vesicles with sizes ranging from 30 to 120 nm in diameter. Exosomes express a set of markers, such as cluster of differentiation 63 (CD63), Alix/apoptosis-linked gene-2 (ALG-2)-interacting protein X (Alix), and tumor susceptibility gene 101 protein (TSG101) (Willms et al., 2016; Salomon and Rice, 2017). Exosomes contain a number of signaling molecules including microRNAs (miRNAs), proteins, and messenger RNAs, which can be delivered as signaling molecules between cells. The function of exosomes varies in different cell types (Ghaemmghami et al., 2020; Hashemian et al., 2020; Sadri Nahand et al., 2020; Amiri et al., 2021). Specially, exosomes derived from endothelial progenitor cells can promote the angiogenesis of pulmonary microvascular endothelial cells (Zhang et al., 2019). Exosomes derived from mesenchymal stromal cells (MSC) strengthen the tube formation of human umbilical vein endothelial cells (HUVECs) and promote the vascularization and alveolarization in BPD rats (Braun et al., 2018). It has been reported that maternal living environment, hereditary background, and perinatal circumstances can significantly alter the composition of exosomes from umbilical cord blood (Lura et al., 2018). Till now, it remains unclear whether exosomes in umbilical cord

blood affect fetal pulmonary angiogenesis, contributing to the development of BPD.

MicroRNAs (miRNAs) are one of the main components of exosomes which have been implicated in numerous disorders including BPD (Zhang et al., 2015; Lal et al., 2018). Thus, exosome-derived miRNAs are potential candidates as the therapeutic targets and the biomarkers and prognosis markers for BPD (Mianehsaz et al., 2019; Asgarpour et al., 2020; Nahand et al., 2020a,b). Recent evidence has shown that maternal and umbilical exosomes contain an array of miRNAs that critically regulate angiogenesis (Jia et al., 2018). Exosomes isolated from bronchoalveolar lavage fluid of BPD mice can reduce the expression of miR-876-3p, suggesting that exosomal miR-876-3p could serve as a miRNA biomarker of severe BPD and may be used as a target for treating BPD (Lal et al., 2018). However, it remains unknown if exosomal miRNA profiles of umbilical cord blood differ between the BPD-susceptible (BPD group) and BPD-resistant (NBPD group) very preterm infants and if these differences contribute to impaired angiogenesis in BPD. In contrast to the much invasive and harmful approach of obtaining neonatal bronchoalveolar lavage fluid, collection of umbilical cord blood is non-invasive and safer for preterm infants.

In this study, we hypothesized that the differential expression of umbilical cord blood-depleted EXO-miRNAs between the BPD group and NBPD group is a major contributing factor of abnormal angiogenesis in BPD. Angiogenesis is a complex process in which endothelial cell proliferation and migration are essential steps (Folkman and Shing, 1992). Several well-known pro-angiogenic factors, such as basic fibroblast growth factors (bFGF) and vascular endothelial growth factor (VEGF), and platelet-derived endothelial cell growth factor (PF-ECGF), stimulate angiogenesis through promoting endothelial cell proliferation and migration (Klagsbrun and D'Amore, 1991). Endothelial cell proliferation and migration are the most common indicators for *in vitro* angiogenesis (Nowak-Sliwinska et al., 2018). Thus, this study used endothelial cell proliferation and migration assays as well as tube formation *in vitro* to evaluate angiogenesis. We determined the effects of umbilical cord blood-derived exosomes collected from the BPD and NBPD of very preterm infants on angiogenesis. Differentially expressed (DE) EXO-miRNA profiles between these two groups were analyzed. We also determined the effects of the DE EXO-miRNAs on endothelial angiogenesis. We identified a set of DE EXO-miRNAs in umbilical cord blood-derived exosomes from BPD and NBPD infants and provided new insights for the developing diagnosis and therapeutic strategies for BPD.

MATERIALS AND METHODS

Study Subjects and Biospecimen Collection

Patients with very preterm delivery (28–31⁺₆ weeks) were recruited at the Department of Neonatology, the Third Affiliated Hospital of Guangzhou Medical University, China. Patient recruitments and blood sample collection were approved by

the Ethics Review Board of the Third Affiliated Hospital of Guangzhou Medical University. All experiments were performed in accordance with the ethical standards as laid down in the 1964 Helsinki Declaration and its later amendments or comparable ethical standards.

The inclusion criteria of the subjects are as follows: pregnant women without complications such as preeclampsia, gestational diabetes mellitus, premature rupture of membranes, and vaginal bleeding, and without adverse pregnancy history and multiple pregnancy or infectious diseases including vaginitis, gingivitis, respiratory tract infection, and urinary tract infection. Participants and corresponding infants were divided into BPD group or NBPD group depending on whether the infants developed BPD or not.

Umbilical cord vein blood (~20 ml) was collected immediately after parturition and kept at 4°C for 30 min, followed by centrifugation (3000 rpm at 4°C for 15 min) to obtain serum samples. The serum was aliquoted and stored at -80°C until further analysis.

Exosome Isolation

The serum sample (2 ml/infant) was centrifuged at 16,000 g at 4°C for 20 min to remove any remaining cells and cell debris. The supernatant was filtered through a 0.22-μm filter and diluted with 1 ml sterile PBS. Next, polyethylene glycol 6000 (PEG6000, Sigma-Aldrich, United States) was added to the supernatant mixture (1:4). Afterward, the mixture was gently vortexed and kept in 4°C for 60 min, followed by centrifuging at 10,000 g for 20 min. The exosome pellet was resuspended in 200–500 μl sterile PBS (pH = 7.4) and stored it at -80°C.

Exosome Identification

Exosome suspension (5 μl/infant) was diluted into a total volume of 10 μl, fixed with 2% paraformaldehyde (PFA), and stained with 2% uranyl acetate solution for 1 min, followed by air drying. The morphology of exosome was observed by a transmission electron microscope (JEOL-JEM1400, JEOL Ltd., United States) at an acceleration voltage of 80 kV. The size distribution of exosomes was determined by nanoparticle tracking analysis (NTA). The sample (5 μl) was diluted step by step with PBS (5 μl). Then, the NTA measurements were performed using a Particle Metrix ZetaView instrument (Particle Metrix GmbH, Germany) with laser and video camera module (Particle Metrix GmbH, Germany). Flow mode with tracking of the Brownian motion of nanoparticles was used. The expression of exosomal surface marker proteins (TSG101 and Alix) was determined by Western blotting.

Cell Culture and Exosome Treatments

Human umbilical vein endothelial cells were obtained from Cellcook (Guangzhou, China). HUVECs were cultured and passaged in high-glucose Dulbecco's Modified Eagle Medium (DMEM, Thermo Fisher Scientific, United States) supplemented with 10% fetal bovine serum (FBS, Gibco, United States). Endothelial cells were starved for 16 h and then treated with exosomes (50 μg/ml) or an equivalent vehicle for various

times before performing cell proliferation, migration, and tube formation assays.

MiRNA Transfection

MicroRNA transfection was conducted as described (Zhou et al., 2017). Hsa-miR-103a-3p mimic, hsa-miR-185-5p mimic, hsa-miR-200a-3p mimic, and miRNA mimic negative control were purchased from Sangon Biotech (Shanghai, China). The sequences of miRNA mimics are listed in **Table 1**. HUVECs were transfected with miRNA mimics (200 pmol) and equivalent mimic negative controls using Lipofectamine 2000 reagent (Thermo Fisher Scientific, United States) according to the manufacturer's instructions. Overexpression of miRNAs was confirmed by qRT-PCR after 24 h of miRNA mimic transfection. Effects of these miRNA mimics on angiogenesis were assessed after 48 h of miRNA mimic transfection.

Western Blotting

Human umbilical vein endothelial cells were lysed in RIPA buffer (50 mM Tris-base, 150 mM NaCl, 0.1% SDS, 0.5% sodium deoxycholate, 1% Triton X-100, pH 6.7), followed by centrifugation to obtain total protein samples. The protein concentration in the sample was measured using BCA assay kit (Thermo Fisher Scientific, United States). Protein samples were electrophoresed in sodium dodecyl sulfate-polyacrylamide (SDS-PAGE) gel and transferred to polyvinylidene fluoride membranes (PVDF, Millipore, Billerica, United States). Blots were blocked with 5% skim milk in Tris-buffered saline containing 0.1% Tween-20 (TBST) for 1 h at room temperature. Then, the membranes were incubated with primary antibodies (anti-TSG101: ab125011, Abcam, 1:5000; anti-Alix: #2171, CST, 1:1000) at 4°C overnight, followed by incubation with the horseradish peroxidase-conjugated secondary antibodies (horseradish peroxidase-conjugated anti-mouse: ab205719, Abcam, 1:1000; horseradish peroxidase-conjugated anti-rabbit: ab6721, Abcam, 1:1000) at 37°C for 1 h. The blots were developed using Chemiluminescent ECL reagent (Forevergen, China), and their gray values were analyzed using Image J software (NIH, United States).

Cell Proliferation Assay

Cells (1×10^6 cells/ml) were seeded into 96-well plates and subjected to the indicated treatments. When the treatment period was over, CCK-8 (10 μl, Beyotime Company, China) was added into each well and the plate was further incubated for additional 4 h. Afterward, optical density (OD) at 490 nm was read by microplate reader (Shanghai Flash Spectrum Biological Technology Company, China).

TABLE 1 | MiRNA mimic sequences.

miRNA mimics	Sequences
hsa-miR-103a-3p	AGCAGCAUUGUACAGGGCUAUGA
hsa-miR-185-5p	UGGAGAGAAAGGCAGUUCUGA
hsa-miR-200a-3p	UAACACUGUCUGGUAACGAUGU

Tube Formation Assay

Forty-eight-well plates were coated with Matrigel (BD Biosciences, United States) according to the manufacturer's instructions. HUVEC cells (1.6×10^4 per well) were seeded on Matrigel-coated plates and treated with exosomes or equivalent vehicle. For the miRNA overexpression experiments, HUVECs (1.6×10^4 per well) transfected with corresponding miRNA mimic were seeded on Matrigel-coated plates. Cells were then incubated at 37°C with 5% CO_2 . Three fields were captured in microscope (Olympus BX51, Japan) randomly at 6 h after treatments, and the tube formation was analyzed using the Image J software (NIH, United States).

Cell Migration Assay

Cell migration assay was performed using transwell ($8.0 \mu\text{m}$ pore size, Corning, NY, United States) according to the manufacturer's instructions. HUVECs were adjusted to the cell density of 1×10^6 cells/ml. Then, $100 \mu\text{l}$ cell suspension was added to the upper chambers and $600 \mu\text{l}$ complete medium was added to the lower chambers. Cells in the upper chambers were treated with exosomes or equivalent vehicle for 16 h. Cell seeding procedures were the same as above to study the migration of HUVECs transfected with miRNA mimic, but there was no exosome treatment. Migrated cells were fixed with 4% paraformaldehyde and stained with 1% crystal violet. Cell migration images were taken using a Nikon Eclipse Ti microscope (Tokyo, Japan). The number of migrated cells was counted using Image J software (NIH, United States).

Next-Generation Sequencing (NGS) and Bioinformatics Analysis

Total RNAs of exosomes were obtained using MiniBEST Universal RNA Extraction Kit (Takara, Japan). The concentration and quality of total RNA was determined by NanoDrop ND1000 (Thermo Fisher Scientific, United States). Reverse transcription reaction and gene library preparation were performed using NEBNext® Multiplex Small RNA Library (E7300L, NEB, United States) according to the manufacturer's instructions, followed by assessment of the final library product using the Agilent Bioanalyzer 2100 system (Agilent, United States). The library was then sequenced in the Illumina HiSeq 4000 platform using the 150 bp paired-end sequencing strategy. Cluster 3.0 software (United States) was used to generate a heat map of DE miRNA between the two groups ($\text{FDR} \leq 0.001$ and $|\text{Log2Ratio}| \geq 1$). Gene ontology (GO) enrichment was analyzed using Gene Ontology Enrichment Analysis Software Toolkit (GOEAST) with default parameters, including the molecular functions, biological processes, and cellular components. KEGG Orthology Based Annotation System (KOBAS) software was used to analyze the Kyoto Encyclopedia of Genes and Genomes (KEGG) signaling pathways for the differential expressions of miRNAs.

qRT-PCR Analysis

EXO-miRNAs were purified using a SeraMir Exosome RNA Purification Kit (System Biosciences, Mountain View, CA, United States), followed by miRNA cDNA generation using the

TaqMan microRNA assay kit (Applied Biosystems, Foster City, CA, United States) according to the manufacturer's instructions. Total RNAs of cultured cells were extracted using Trizol Reagent (Invitrogen, United States). Revert Aid first-strand cDNA synthesis kit (Fermentas, Life Sciences, Canada) was then used to generate cDNA. qRT-PCR analysis was performed using SYBR Premix Ex Taq™ II in the ABI PRISM® 7900HT System (Takara Biotechnology, Japan). Relative standard curve method ($2^{-\Delta\Delta\text{CT}}$) was used to determine the relative mRNA expression. The miRNA-specific forward primers were synthesized in Sangon Biotech (Shanghai, China) and the universal reverse primer provided by the TaqMan microRNA assay kit. U6 small nuclear RNA was used for normalization. The sequences of miRNA PCR primers were indicated in **Table 2**.

Potential Target Gene Evaluation

The target genes of hsa-miR-185-5p were predicted using mirtargetbase¹. qRT-PCR was used to verify cyclin-dependent kinase 6 (CDK6) and DNA methyltransferase 1 (DNMT1) in HUVECs after 24 h of overexpression of hsa-miR-185-5p. A previous study showed that miR-185-5p suppressed the expression of vascular endothelial growth factor A (VEGFA) in human ovarian microvascular endothelial cells (Matthay and Abman, 2018). Thus, we also tested if VEGFA was the target gene of hsa-miR-185-5p. The primer sequences of these target genes are shown in **Supplementary Table 1**.

Statistical Analysis

Quantitative data were presented as the Mean \pm SD. The unpaired Student's *t*-test was carried out to analyze the differences between two groups. One-way ANOVA followed by Bonferroni's *post hoc* test was used to compare the statistically

¹<http://mirtarbase.cuhk.edu.cn/php/index.php>

TABLE 2 | Primer sequence for miRNA qPCR.

Primers	Sequences
hsa-miR-103a-3p-RT	GTCGTATCCAGTGCAGGGTCCGAGGTATT CGCACTGGATACGACTCATAG
hsa-miR-103a-3p-F	GCGAGCAGCATTGTACAGGG
hsa-miR-17-5p-RT	GTCGTATCCAGTGCAGGGTCCGAGGTATTTCGC ACTGGATACGACCTACCT
hsa-miR-17-5p-F	GCGCAAAGTGCTTACAGTGC
hsa-miR-185-5p-RT	GTCGTATCCAGTGCAGGGTCCGAGGTATTTCGCA CTGGATACGACTCAGGA
hsa-miR-185-5p-F	GCGTGGAGAGAAAGGCAGT
hsa-miR-200a-3p-RT	GTCGTATCCAGTGCAGGGTCCGAGGTATTTCGCA CTGGATACGACACATCG
hsa-miR-200a-3p-F	GCGTAACACTGTCTGGTAA
hsa-miR-20b-5p-RT	GTCGTATCCAGTGCAGGGTCCGAGGTATTTCGCAC TGGATACGACCTACCT
hsa-miR-20b-5p-F	GCGCAAAGTGCTCATAGTGC
hsa-miR-765-RT	GTCGTATCCAGTGCAGGGTCCGAGGTATTTC GCACTGGATACGACCATCAC
hsa-miR-765-F	GCGTGGAGGAGAAGGAAG
Universe-R	GTGCAAGGGTCCGAGGT

significant differences between the means of three or more groups. Qualitative data in basic demographic information were compared using the Chi-square test. All statistical analyses were performed using SPSS 22 software. $P < 0.05$ indicates a statistically significant difference.

RESULTS

Participants' Clinical Characteristics

Demographic characteristics of maternal and preterm infants in BPD and NBPD groups are shown in Table 3. No significant differences were found in maternal age, sex ratio, incident rate of gestational diabetes, and Apgar score between BPD and NBPD infants. The gestational age of the BPD group was significantly smaller ($P < 0.05$) than that of the NBPD group, while the maternal body mass index (BMI) of the BPD group were significantly ($P < 0.05$) higher than that of the NBPD group. The birth weight, birth length, and head circumference of infants in the BPD group significantly ($P < 0.05$) decreased when compared with the NBPD group.

Exosome Characteristics of NBPD and BPD Groups

Exosome-surface markers, Alix and CD63, were confirmed in the vesicles of both groups (Figure 1A). The vesicles had an oval- or round-shaped appearance with a vesicle-like structure, as well as having a deep-stained lipid bilayer membrane in TEM images (Figure 1B). The diameter of the vesicles of both groups ranged from 30 to 150 nm, and the size distributions were comparable in both groups (Figure 1C). The results indicated that the isolated nanoparticles were exosomes, and they were comparable between two groups in term of the morphology, size, and size distribution.

Exosomes of the BPD Group Impaired Endothelial Cell Proliferation, Migration, and Tube Formation

We determined the effects of exosomes from NBPD and BPD groups on endothelial cell proliferation, migration, and tube formation (Figure 2). As shown in Figure 2A, exosomes from the NBPD group significantly ($P < 0.05$) increased cell proliferation when compared with the vehicle control group

using an equivalent volume of PBS, whereas exosomes from the BPD group significantly ($P < 0.05$) inhibited cell proliferation when compared with the NBPD group at 24 h and 48 h. Exosomes from both NBPD and BPD groups inhibited ($P < 0.05$) endothelial migration when compared with vehicle control, and the inhibitory effect was further enhanced in the BPD vs. NBPD groups (Figures 2B,C). We also found that exosomes from the BPD group significantly ($P < 0.05$) reduced tube formation when compared with NBPD group (Figures 2D,E).

Differential Expression of miRNA in Exosomes From NBPD and BPD Groups

We carried out NGS and bioinformatic analysis to determine the differential expression of EXO-miRNAs between NBPD and BPD groups. We obtained 20,912,199 and 20,435,555 clean reads in the NBPD and BPD groups, respectively, indicating that data had a desirable quality (Supplementary Table 2). As shown in Figures 3A,B, the length distribution of EXO-miRNAs in both NBPD and BPD groups dominantly ranged from 19 to 24 nucleotides (nt) with a peak at 22 nt, and it was comparable between two groups. A total of 2588 EXO-miRNAs were identified from both groups (Supplementary Table 3). A total of 418 DE EXO-miRNAs were found (Figure 3C and Supplementary Table 4), among which 328 miRNAs were upregulated while 90 miRNAs were downregulated. GO and KEGG analysis were performed on predicted target genes of DE EXO-miRNAs to exhibit the functional annotation. As shown in Figure 3D, most of the target genes were involved in biological processes, cellular component, and molecular function. Regarding the terms of the biological process, the most dominant categories were cellular process, single-organism process, biological process, and metabolic process. In the terms of cellular component, the major categories included cell, cell part, and organelle. The most enriched categories in the terms of molecular function were binding, catalytic activity, and nucleic acid binding transcription factor activity. The top 20 enriched pathways according to KEGG results are shown in Figure 3E. We found that the most enriched pathways were the cancer-related pathways, PI3K-Akt signaling pathway, pathways related to HTLV-I infection, microRNA in cancer, and proteoglycans in cancer, as well as MAPK signaling pathway.

MiRNA-mRNA Network and Validation of DE miRNAs Which Are Related to the PI3K-Akt Signaling Pathway

Based on the above KEGG results, we selected EXO-miRNAs related to both the PI3K-Akt signaling pathway and inflammation pathway to generate the miRNA-mRNA interaction network. As shown in Figure 4, 13 miRNAs were involved in these pathways and nine of these miRNAs were predicted to have more than three binding sites with their target genes. To validate DE miRNAs in the exosomes, six EXO-miRNAs were chosen, including hsa-miR-103a-3p, hsa-miR-17-5p, hsa-miR-185-5p, hsa-miR-200a-3p, hsa-miR-20b-5p, and hsa-miR-765 for qRT-PCR analysis. As shown in Figures 5A-F, the expression of hsa-miR-765 was decreased

TABLE 3 | The demographic characteristics of patients.

Variables	NBPD	BPD	<i>P</i> value
Study population (N)	14	12	
Maternal age (years)	30.5 ± 3.2	29.6 ± 2.9	0.453
Gestational age (weeks)	31.4 ± 2.3	29.9 ± 1.0	0.032
Maternal BMI	20.5 ± 2.8	23.3 ± 3.9	0.047
Sex ratio (M/F)	10/4	4/8	0.052
Birth weight (kg)	1.7 ± 0.6	1.1 ± 0.3	0.002
Birth length (cm)	41.9 ± 5.7	37.4 ± 2.6	0.021
Head circumference (cm)	29.1 ± 2.5	26.7 ± 1.8	0.011
Apgar score	9.7 ± 0.5	9.3 ± 0.9	0.200

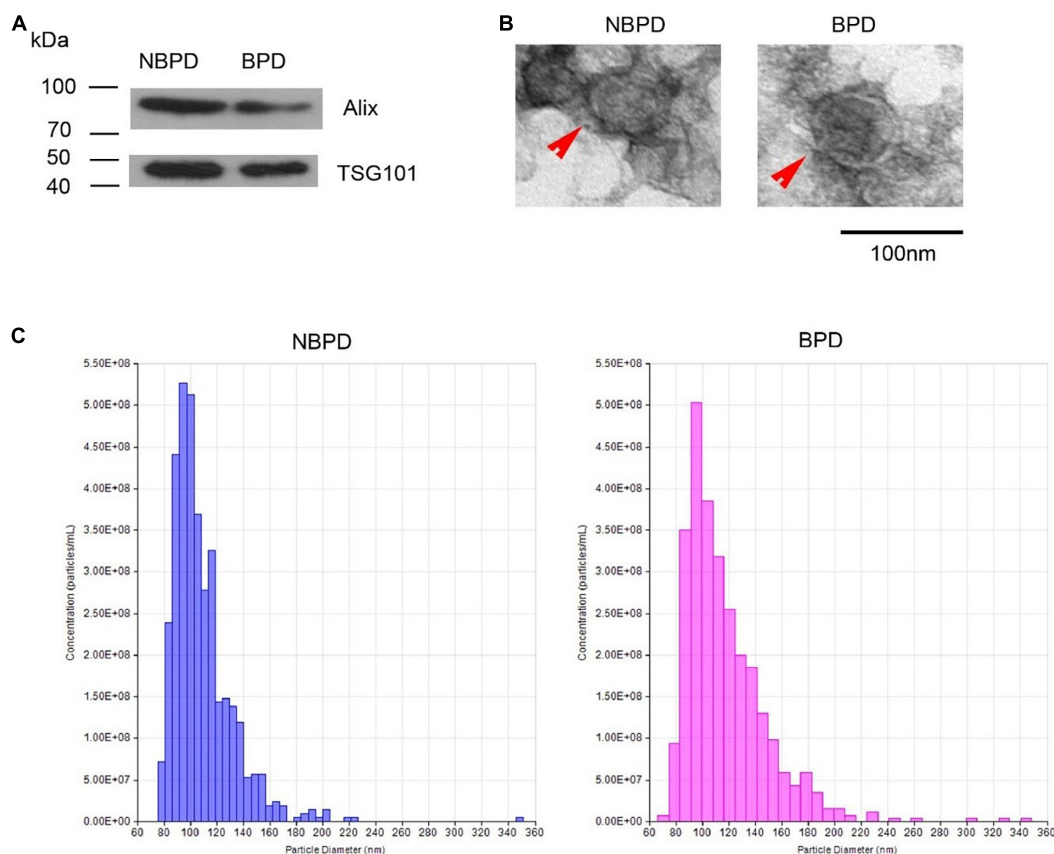


FIGURE 1 | Exosome identification. **(A)** Expression of exosomal markers was determined by Western blotting. **(B)** Representative images showing morphology of exosome (red arrow) under transmission electron microscopy. **(C)** Nanoparticle size distribution measured by NTA. $n = 3$.

in exosomes from the BPD group when compared with the NBPD group, which was opposite to the NGS results. Other five miRNAs (hsa-miR-103a-3p, hsa-miR-17-5p, hsa-miR-185-5p, miR-200a-3p, and hsa-miR-20b-5p) and) showed similar change trends as in NGS analysis. In addition, among the six validated miRNAs, hsa-miR-103a-3p, and hsa-miR-185-5p showed the most significant reduction, while hsa-miR-200a-3p was the only one showing the increase. We further selected these three miRNAs to validate their expression in exosomes isolated from additional samples from the NBPD and BPD groups which were not used for sequencing. We found that expressions of hsa-miR-103a-3p, hsa-miR-185-5p, and hsa-miR-200a-3p were also consistent with the NGS results (Figures 5G–I).

Effects of PI3K-Akt Signaling Pathway-Related DE EXO-miRNAs on *in vitro* Angiogenesis

We further used miRNA mimics to overexpress three EXO-miRNAs (has-sa-miR-103a-3p, hsa-miR-185-5p, and hsa-miR-200a-3p) to study their functions in endothelial cells (Figures 6A–C). We observed that transfection of three EXO-miRNA mimics elevated the levels of corresponding

miRNAs (Figures 6A–C). Overexpression of hsa-miR-103a-3p and hsa-miR-185-5p significantly ($P < 0.05$) enhanced endothelial cell proliferation (Figures 6D,E). In contrast, overexpression of hsa-miR-200a-3p significantly ($P < 0.05$) inhibited endothelial cell proliferation (Figure 6F). Overexpression of hsa-miR-103a-3p and hsa-miR-185-5p dramatically ($P < 0.05$) promoted endothelial cell migration, whereas overexpression of hsa-miR-200a-3p significantly ($P < 0.05$) suppressed cell migration (Figures 6G,H). Similarly, overexpression of hsa-miR-103a-3p and hsa-miR-185-5p significantly ($P < 0.05$) enhanced tube formation, whereas overexpression of hsa-miR-200a-3p suppressed ($P < 0.05$) tube formation (Figure 7). These data uncovered the important function of EXO-miRNAs in regulation of endothelial cell function and angiogenesis.

Hsa-miR-185-5p Negatively Regulated CDK6 mRNA Expression in HUVECs

A total of 39 target genes were predicted for hsa-miR-185-5p in HUVECs (Supplementary Table 5). As shown in Figure 8, hsa-miR-185-5p mimics significantly ($P < 0.05$) reduced CDK6, but not DNMT1 and VEGFA mRNA levels as compared with mimics negative control (mimics NC).

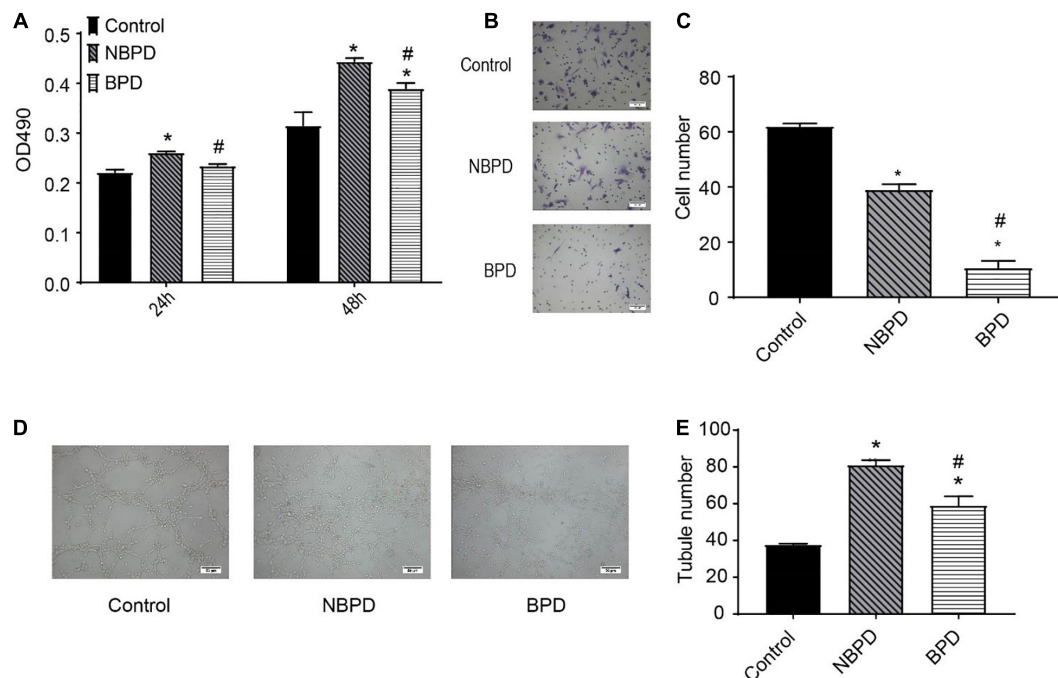


FIGURE 2 | Effects of umbilical cord blood-derived exosomes on endothelial proliferation, migration, and tube formation. **(A)** HUVECs were treated with exosomes (50 μ g/ml) from NBPD and BPD infants or vehicle for 24 h and 48 h, respectively. Cell proliferation was determined using CCK-8. **(B,C)** HUVECs were treated as indicated for 16 h, and number of migrated cells was determined by transwell. $^{*}P < 0.05$ versus control and NBPD group, respectively. $N = 3$. Scale bar = 30 μ m. **(D,E)** HUVECs were treated with exosomes or vehicle as indicated. Tube formation was determined at 6 h after treatments (scale bar = 50 μ m). $^{*}, \# P < 0.05$ versus control and NBPD, respectively. $n = 3$.

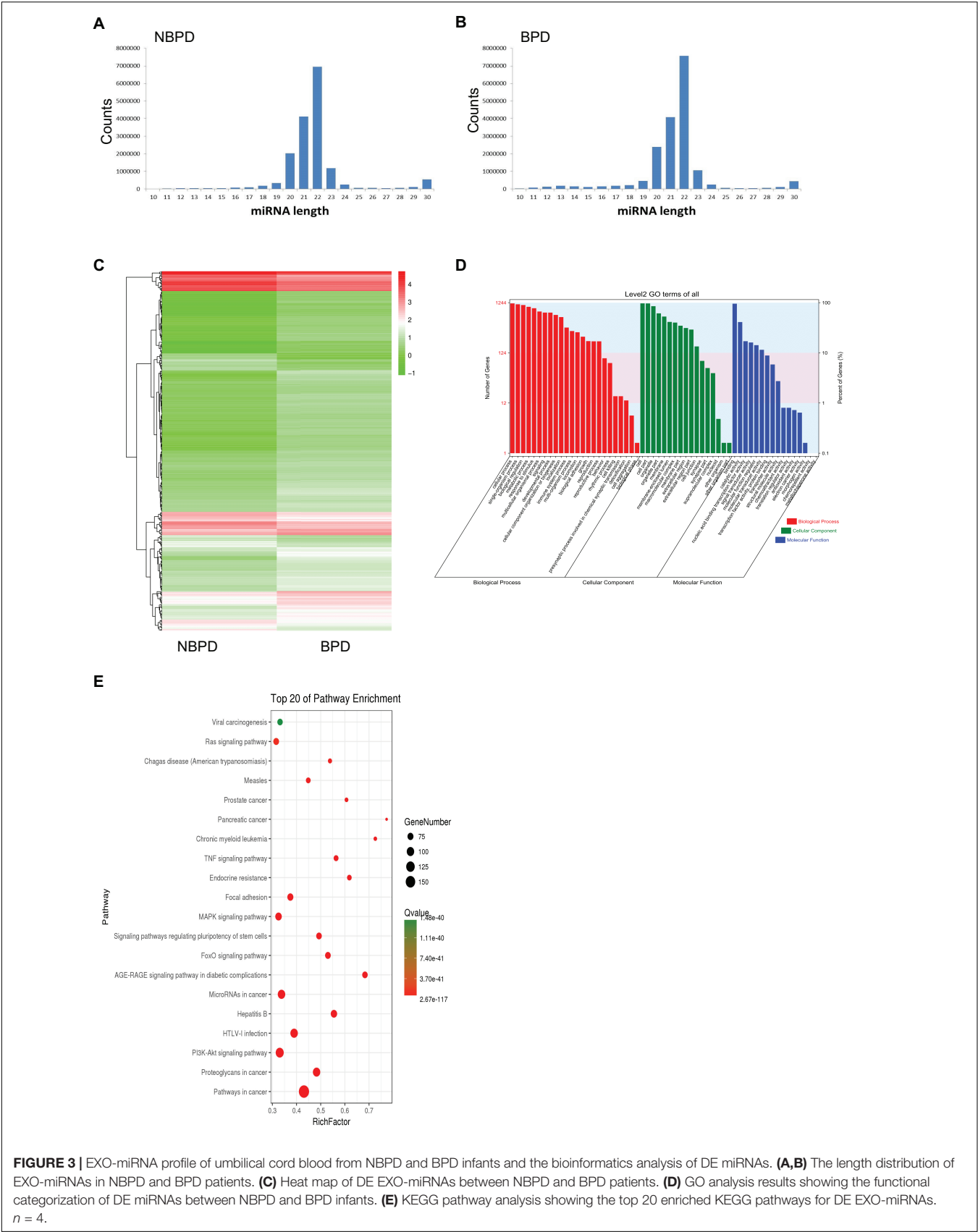
DISCUSSION

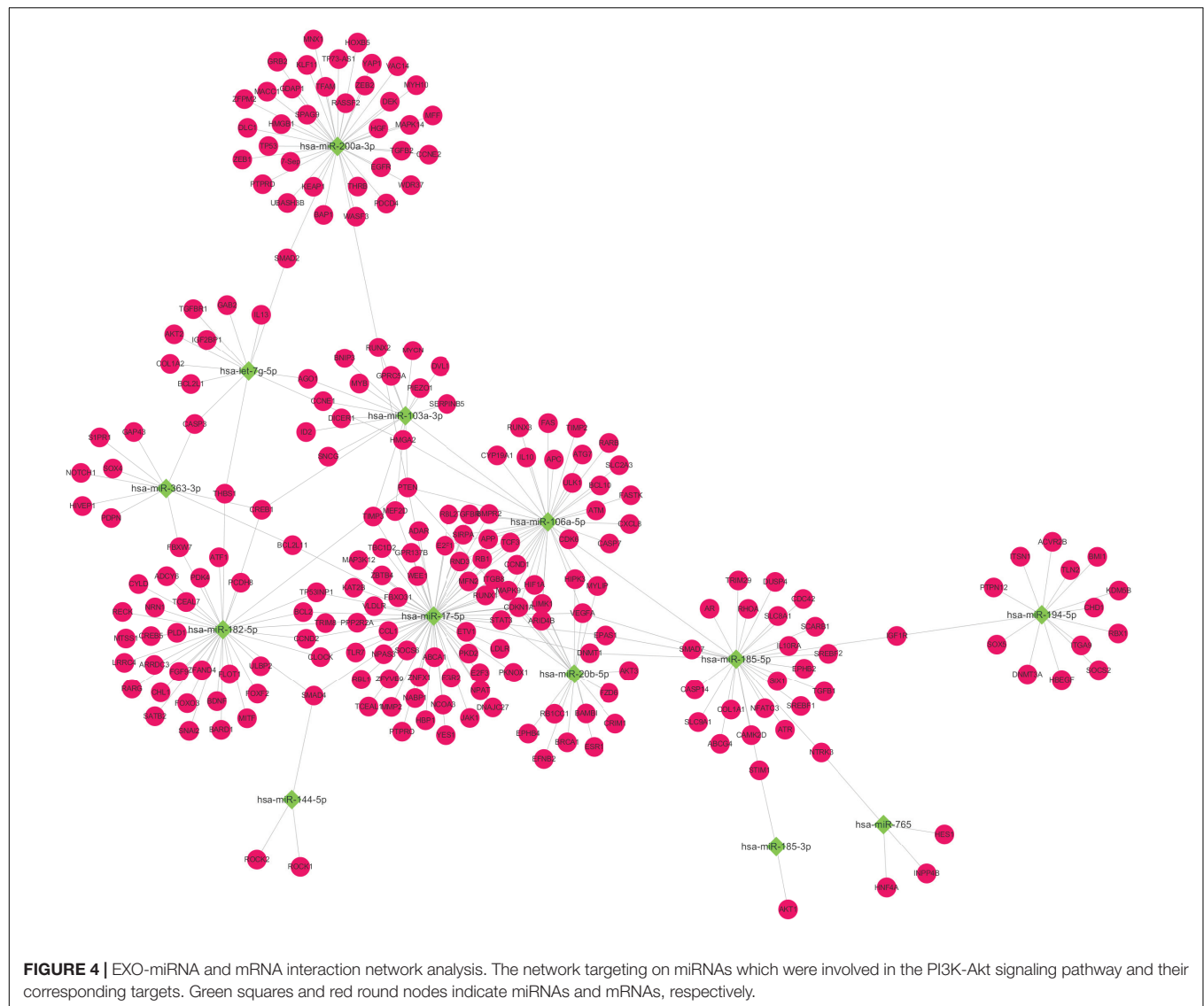
To the best of our knowledge, this is the first report demonstrating the roles of the DE EXO-miRNAs in umbilical cord blood from VPI with BPD. We found that exosomes isolated from umbilical cord blood of the BPD group significantly impaired endothelial angiogenesis when compared with the NBPD group. We also identified a set of DE EXO-miRNA in the BPD group with 90 downregulated (e.g., hsa-miR-103a-3p and hsa-miR-185-5p) and 328 upregulated (e.g., hsa-miR-200a-3p) miRNAs in BPD infants. These DE EXO-miRNAs are highly related to the PI3K-Akt signaling pathway. We further observed that overexpression of hsa-miR-103a-3p and hsa-miR-185-5p enhanced the proliferation, migration, and tube formation of endothelial cells, whereas overexpression of hsa-miR-200a-3p inhibited these angiogenic responses. We also identified CDK6 as a target gene of hsa-miR-185-5p. These data support that exosomes from VPI with BPD impair angiogenesis via EXO-miRNAs, which might lead to adverse outcomes of VPI with BPD. Future investigations are urgent to elucidate the potential of these DE EXO-miRNAs as the predictive biomarkers and therapeutic targets for VPI with BPD.

Therapeutic approaches for respiratory care, such as application of antenatal steroids and surfactant, continuous positive airway pressure therapy, and advanced ventilator device, have greatly improved the survival of preterm infants (Matthay and Abman, 2018). However, the increased survival of preterm

infants potentially increases the incidence of BPD (Stoll et al., 2015). Thus, there is an urgent need to find the biomarkers and effective therapeutic strategies for BPD. Exosome-based therapy has emerged as a potential tool for neonatal lung injury, including BPD (Willis et al., 2018). This is supported by the observation that exosomes derived from mesenchymal stem cells (MSC) protect against experimental BPD in mice (Panfoli et al., 2016), while exosomes derived from endothelial progenitor cells improve angiogenic activity of pulmonary microvascular endothelial cells in the *in vitro* model of BPD induced by hyperoxia (Zhang et al., 2019). Umbilical cord blood is an important source of these stem cells and exosomes. Exosomes isolated from umbilical cord blood can promote angiogenesis and wound healing (Hu et al., 2018), implying that exosomes derived from umbilical cord blood might participate in lung development. However, the exact roles of exosomes derived from preterm infants' umbilical cord blood in the development of BPD remains elusive.

Bronchopulmonary dysplasia changes the contents and size of exosomes in the body fluids of infants as compared with the full-term control (Lal et al., 2018). In contrast, our results showed that the exosomes' size between two groups is comparable. We found that exosomes derived from umbilical cord blood in the NBPD group promoted endothelial angiogenic responses, indicating that umbilical cord blood-derived exosomes from NBPD contains pro-angiogenic factors similar to those in the full-term infants (Hu et al., 2018). Our observation that exosomes





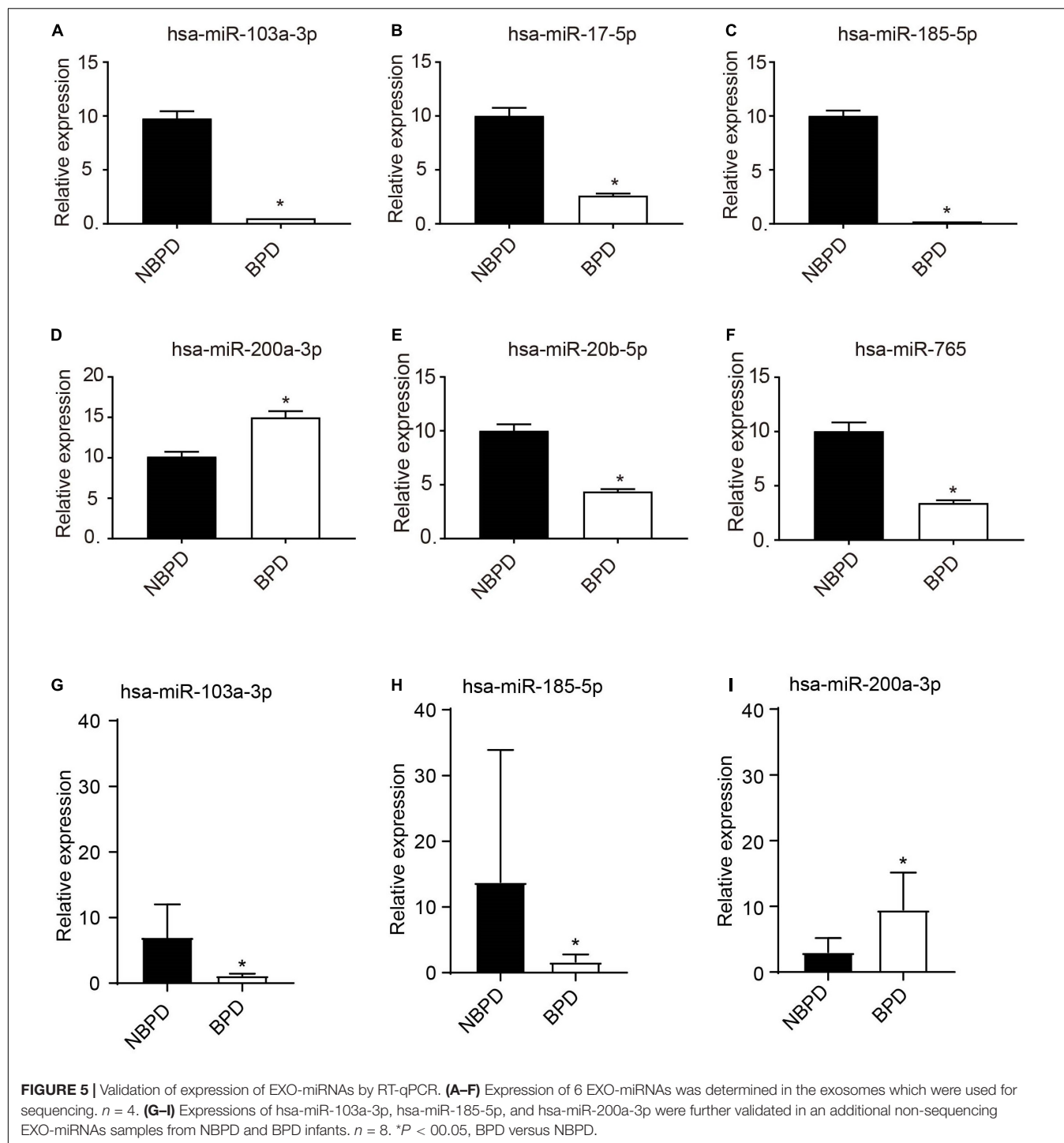
from the BPD group impaired endothelial angiogenic responses suggests that the contents of bioactive molecules in exosomes of BPD are detrimental to the fetal vascular function. This is supported by a recent report by Genschmer et al. (2019) who showed that exosomes from the tracheal aspirate of intubated neonates with severe BPD could transfer mice into the BPD phenotype. Thus, the contents of exosomes could be the potential therapeutic targets and biomarkers of BPD development.

EXO-miRNA expression has been profiled in the body fluids of both human infants and animals with BPD (Bhaskaran et al., 2012; Braun et al., 2018). Developing a non-invasive procedure is ethically critical to obtaining clinical samples to investigate the role of miRNAs in the BPD development. This study demonstrates, for the first time, that collecting EXO-miRNA from umbilical cord blood from the very preterm infants with BPD and without BPD is a non-invasive and safe approach.

We have identified a set of DE EXO-miRNAs. These DE miRNAs identified in our study are distinct from those

previously reported in the bronchoalveolar lavage fluid of infants with and without BPD (Lal et al., 2018). The discrepancy may be due to different cell and tissue origins of miRNAs (Landskroner-Eiger et al., 2013).

The DE EXO-miRNAs identified in the present study were predicted to potentially regulate a variety of signaling pathways, including PI3K-Akt signaling pathway, HTLV-I infection, and MAPK signaling pathway. Among these pathways, PI3K-Akt, inflammatory, and MAPK signaling pathways are closely related to angiogenesis (Sun et al., 2018). Among DE EXO-miRNAs that participated in these angiogenesis-relevant pathways, our data revealed that hsa-miR-103a-3p and hsa-miR-185-5p decreased most significantly and hsa-miR-200a-3p was the only miRNA which showed an increase in expression in the BPD samples. In addition, this study also showed that both hsa-miR-103a-3p and hsa-miR-185-5p overexpression significantly promoted endothelial cell proliferation, migration, and tube formation, but overexpression of hsa-miR-200a-3p



exerted opposite effects on these angiogenesis indexes. Our results indicate that umbilical cord blood-derived exosomes from VPI with BPD impaired angiogenesis, which was potentially through dysregulation of hsa-miR-103a-3p, hsa-miR-185-5p, and hsa-miR-200a-3p.

Overexpression of hsa-miR-103a-3p is associated with the metastasis of breast cancer (Chang et al., 2016) and many other types of cancer (Liang et al., 2015; Fu et al., 2020).

Hsa-miR-103a-3p expression is negatively regulated by inflammation (Cheng and Wang, 2020). As inflammation is a major cause of the pathogenesis of BPD, it is possible that inflammation in BPD decreased EXO-hsa-miR-103a-3p in umbilical cord blood from BPD infants. Given that hsa-miR-103a-3p responded to hypoxia and targeted argonaute 1 (AGO1) to promote angiogenesis (Chen et al., 2013), and EXO-miR-103a increases angiogenesis in gastric cancer

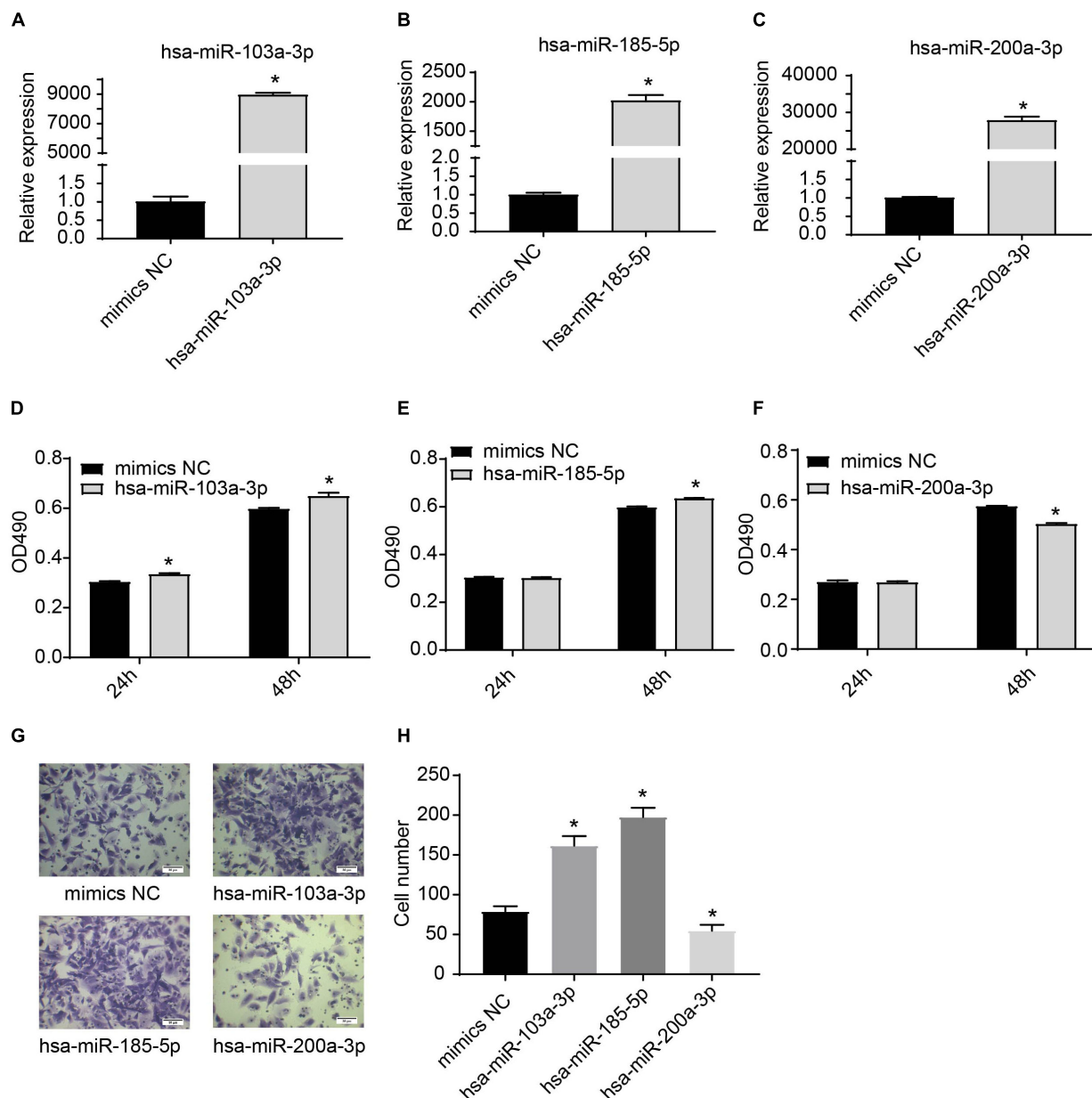


FIGURE 6 | Effects of hsa-miR-103a-3p, hsa-miR-185-5p, and hsa-miR-200a-3p mimics on endothelial cell proliferation and migration. **(A–C)** Overexpression of hsa-miR-103a-3p, hsa-miR-185-5p, and hsa-miR-200a-3p in HUVECs. HUVECs were transfected with miRNA mimics for 24 h, and expression of miRNAs was determined by RT-qPCR. **(D–F)** Cell proliferation was determined at 24 h and 48 h after miRNA mimic transfection. Hsa-miR-103a-3p and hsa-miR-185-5p overexpression promoted endothelial cell proliferation, whereas hsa-miR-200a-3p overexpression suppressed endothelial cell proliferation. **(G,H)** Cell migration was determined at 6 h after miRNA mimic transfection. Hsa-miR-103a-3p and hsa-miR-185-5p overexpression promoted endothelial cell migration. Hsa-miR-200a-3p overexpression inhibited cell migration. * $P < 0.05$, versus mimics NC group. $n = 3$.

targeting c-MYB (Liang et al., 2015), downregulation of exosomal hsa-miR-103a-3p in the BPD group is likely to suppress fetal angiogenesis. Our finding that hsa-miR-185-5p overexpression promotes angiogenesis is inconsistent with the previous report, which demonstrates that miR-185-5p suppresses the expression of vascular endothelial growth factor A (VEGFA), inhibiting angiogenesis in human ovarian microvascular endothelial cells (Wei and Zhao, 2020). In our

study, hsa-miR-185-5p overexpression did not significantly change VEGFA mRNA expression in HUVECs. One explanation for this discrepancy is that the different endothelial cell types (human ovarian microvascular endothelial cells vs. HUVECs) were used. We identified CDK6 mRNA as a target of hsa-miR-185-5p. CDK6 can either promote or inhibit cell proliferation depending on its interaction with CDK4/6 inhibitor p16^{ink4a} (Kollmann et al., 2013). The roles of

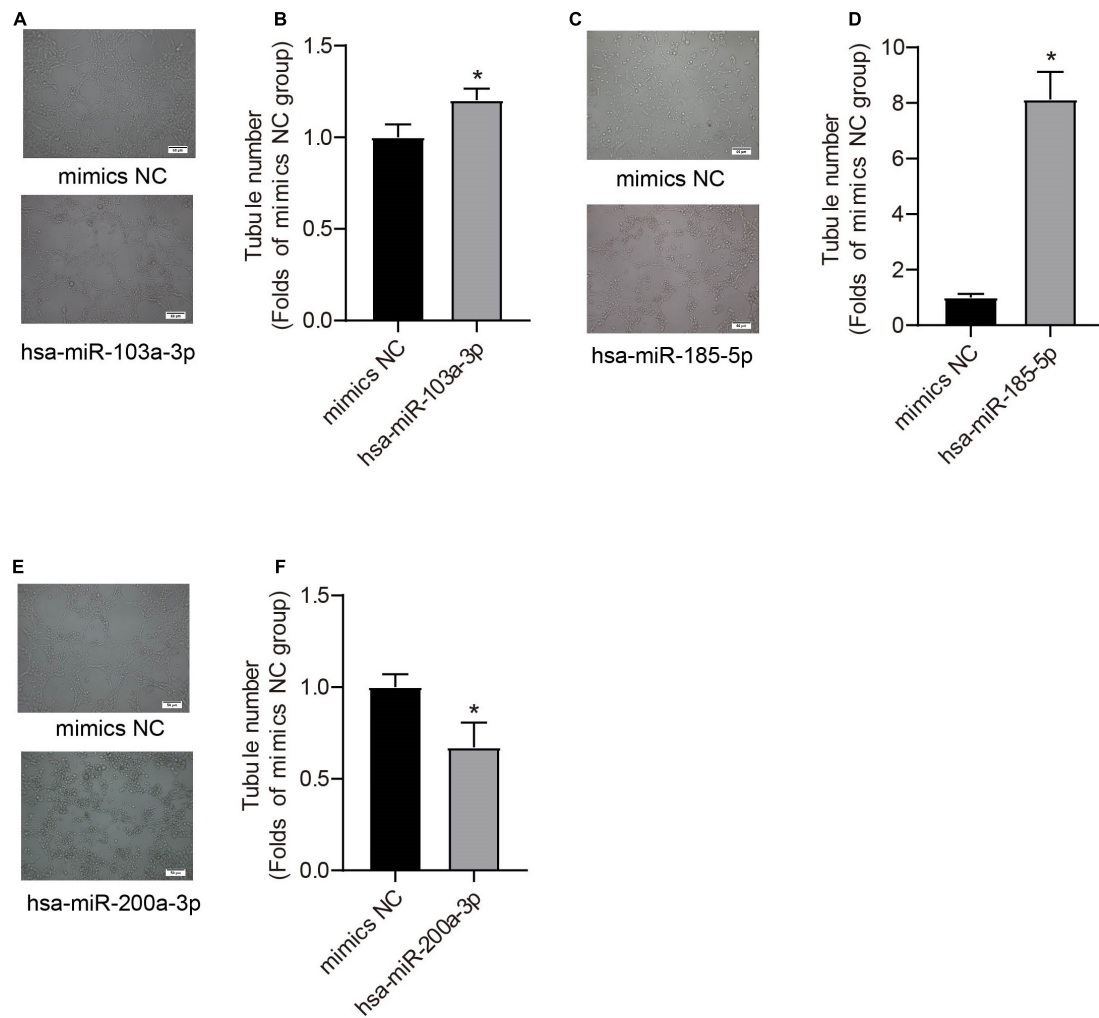


FIGURE 7 | Effects of hsa-miR-103a-3p, hsa-miR-185-5p, and hsa-miR-200a-3p mimics on endothelial tube formation. Tube formation was determined at 48 h after miRNA mimic transfection. Hsa-miR-103a-3p (**A,B**) and hsa-miR-185-5p (**C,D**) overexpression increased endothelial tube formation, whereas hsa-miR-200a-3p overexpression (**E,F**) reduced tubule number. * $P < 0.05$, versus mimics NC group. $n = 3$.

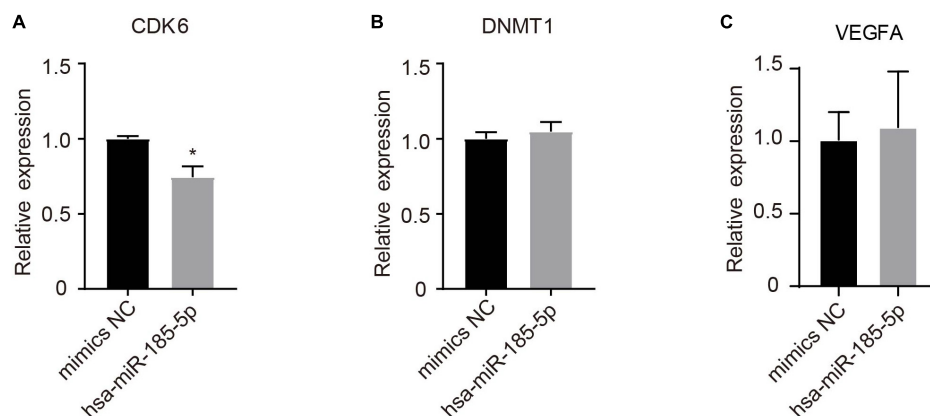


FIGURE 8 | Determination of potential target genes of hsa-185-5p in HUVECs. Cells were transfected with hsa-185-5p mimics or mimics negative control for 24 h. CDK6 (**A**), DNMT1 (**B**), and VEGFA (**C**) mRNA levels were determined using qRT-PCR. $n = 3$, * versus mimics NC, $P < 0.05$.

hsa-miR-185-5p/CDK6 signaling in angiogenesis have yet to be dissected. Consistent with our results, Chang et al. also found that overexpression of miR-200a-3p impaired angiogenesis (Chang et al., 2020). Our results show that overexpression of hsa-miR-103a-3p and hsa-miR-185-5p might rescue PBD-impaired fetal angiogenesis. However, further investigation is needed to reveal the role of their target genes in regulating angiogenesis in PBD.

DATA AVAILABILITY STATEMENT

The datasets presented in this study can be found in online repositories. The names of the repository/repositories and accession number(s) can be found below: NCBI GEO, accession number GSE166762.

ETHICS STATEMENT

The studies involving human participants were reviewed and approved by the Ethics Review Board of the Third Affiliated Hospital of Guangzhou Medical University. Written informed consent to participate in this study was provided by the participants' legal guardian/next of kin.

REFERENCES

- Alphonse, R. S., Vadivel, A., Fung, M., Shelley, W. C., Critser, P. J., Ionescu, L., et al. (2014). Existence, functional impairment, and lung repair potential of endothelial colony-forming cells in oxygen-induced arrested alveolar growth. *Circulation* 129, 2144–2157. doi: 10.1161/CIRCULATIONAHA.114.009124
- Alvira, C. M. (2016). Aberrant pulmonary vascular growth and remodeling in bronchopulmonary Dysplasia. *Front. Med. (Lausanne)* 3:21. doi: 10.3389/fmed.2016.00021
- Amiri, A., Pourhanifeh, M. H., Mirzaei, H. R., Nahand, J. S., Moghooei, M., Sahebnaag, R., et al. (2021). Exosomes and lung cancer: roles in pathophysiology, diagnosis and therapeutic applications. *Curr. Med. Chem.* 28, 308–328. doi: 10.2174/0929867327666200204141952
- Asgarpour, K., Shojaei, Z., Amiri, F., Ai, J., Mahjoubin-Tehran, M., Ghasemi, F., et al. (2020). Exosomal microRNAs derived from mesenchymal stem cells: cell-to-cell messages. *Cell Commun. Signal.* 18:149. doi: 10.1186/s12964-020-00650-6
- Bertagnoli, M., Nuyt, A. M., Thebaud, B., and Luu, T. M. (2017). Endothelial progenitor cells as prognostic markers of preterm birth-associated complications. *Stem Cells Transl. Med.* 6, 7–13. doi: 10.5966/sctm.2016-0085
- Bhaskaran, M., Xi, D., Wang, Y., Huang, C., Narasaraaju, T., Shu, W., et al. (2012). Identification of microRNAs changed in the neonatal lungs in response to hyperoxia exposure. *Physiol. Genomics* 44, 970–980. doi: 10.1152/physiolgenomics.00145.2011
- Bhatt, A. J., Pryhuber, G. S., Huyck, H., Watkins, R. H., Metlay, L. A., and Maniscalco, W. M. (2001). Disrupted pulmonary vasculature and decreased vascular endothelial growth factor, Flt-1, and TIE-2 in human infants dying with bronchopulmonary dysplasia. *Am. J. Respir. Crit. Care Med.* 164(10 Pt 1), 1971–1980. doi: 10.1164/ajrccm.164.10.2101140
- Blencowe, H., Cousens, S., Chou, D., Oestergaard, M., Say, L., Moller, A. B., et al. (2013). Born too soon: the global epidemiology of 15 million preterm births. *Reprod. Health* 10(Suppl. 1):S2.
- Braun, R. K., Chetty, C., Balasubramaniam, V., Centanni, R., Haraldsdottir, K., Hematti, P., et al. (2018). Intraperitoneal injection of MSC-derived exosomes

AUTHOR CONTRIBUTIONS

X-QZ, JZ, and Q-LC conceived this study and designed the experiments. X-QZ wrote the manuscript. JZ, Z-GC, and Q-LC revised the manuscript. X-QZ, Z-GC, and QY performed the experiments. C-HJ, Z-YL, and JG collected the samples and recorded clinical data. X-HL, H-LW, and C-YL analyzed the data and revised the manuscript. All authors contributed to the article and approved the submitted version.

FUNDING

This study was supported by the Natural Science Fund of Guangdong Province (No. 2018A030310188 to X-QZ), the basic and applied research project of Guangzhou Science and Technology Bureau (No. 202002030339 to X-QZ), and the Science and Technology Program of Guangzhou (No. 201704020179 to Z-GC).

SUPPLEMENTARY MATERIAL

The Supplementary Material for this article can be found online at: <https://www.frontiersin.org/articles/10.3389/fcell.2021.637248/full#supplementary-material>

- prevent experimental bronchopulmonary dysplasia. *Biochem. Biophys. Res. Commun.* 503, 2653–2658. doi: 10.1016/j.bbrc.2018.08.019
- Buczynski, B. W., Maduekwe, E. T., and O'Reilly, M. A. (2013). The role of hyperoxia in the pathogenesis of experimental BPD. *Semin. Perinatol.* 37, 69–78. doi: 10.1053/j.semperi.2013.01.002
- Chang, H., Li, Z. B., Wu, J. Y., and Zhang, L. (2020). Circ-100338 induces angiogenesis after myocardial ischemia-reperfusion injury by sponging miR-200a-3p. *Eur. Rev. Med. Pharmacol. Sci.* 24, 6323–6332.
- Chang, J. T., Wang, F., Chapin, W., and Huang, R. S. (2016). Identification of MicroRNAs as breast cancer prognosis markers through the cancer genome atlas. *PLoS One* 11:e0168284. doi: 10.1371/journal.pone.0168284
- Chen, Z., Lai, T. C., Jan, Y. H., Lin, F. M., Wang, W. C., Xiao, H., et al. (2013). Hypoxia-responsive miRNAs target argonaute 1 to promote angiogenesis. *J. Clin. Invest.* 123, 1057–1067. doi: 10.1172/JCI65344
- Cheng, M., and Wang, Y. (2020). Downregulation of HMGB1 by miR-103a-3p promotes cell proliferation, alleviates apoptosis and in inflammation in a cell model of osteoarthritis. *Iran. J. Biotechnol.* 18:e2255. doi: 10.30498/IJB.2020.129470.2255
- Folkman, J., and Shing, Y. (1992). Angiogenesis. *J. Biol. Chem.* 267, 10931–10934.
- Fu, M., Chen, C. W., Yang, L. Q., Yang, W. W., Du, Z. H., Li, Y. R., et al. (2020). MicroRNA103a3p promotes metastasis by targeting TPD52 in salivary adenoid cystic carcinoma. *Int. J. Oncol.* 57, 574–586.
- Genschmer, K. R., Russell, D. W., Lal, C., Szul, T., Bratcher, P. E., Noerager, B. D., et al. (2019). Activated PMN exosomes: pathogenic entities causing matrix destruction and disease in the lung. *Cell* 176, 113–126.e15. doi: 10.1016/j.cell.2018.12.002
- Ghaemmaghami, A. B., Mahjoubin-Tehran, M., Movahedpour, A., Morshedi, K., Sheida, A., Taghavi, S. P., et al. (2020). Role of exosomes in malignant glioma: microRNAs and proteins in pathogenesis and diagnosis. *Cell Commun. Signal.* 18:120. doi: 10.1186/s12964-020-00623-9
- Hashemian, S. M., Pourhanifeh, M. H., Fadaei, S., Velayati, A. A., Mirzaei, H., and Hamblin, M. R. (2020). Non-coding RNAs and exosomes: their role in the pathogenesis of sepsis. *Mol. Ther. Nucleic Acids* 21, 51–74. doi: 10.1016/j.omtn.2020.05.012

- Hu, Y., Rao, S. S., Wang, Z. X., Cao, J., Tan, Y. J., Luo, J., et al. (2018). Exosomes from human umbilical cord blood accelerate cutaneous wound healing through miR-21-3p-mediated promotion of angiogenesis and fibroblast function. *Theranostics* 8, 169–184. doi: 10.7150/thno.21234
- Jakkula, M., Le Cras, T. D., Gebb, S., Hirth, K. P., Tudor, R. M., Voelkel, N. F., et al. (2000). Inhibition of angiogenesis decreases alveolarization in the developing rat lung. *Am. J. Physiol. Lung Cell. Mol. Physiol.* 279, L600–L607. doi: 10.1152/ajplung.2000.279.3.L600
- Jia, L., Zhou, X., Huang, X., Xu, X., Jia, Y., Wu, Y., et al. (2018). Maternal and umbilical cord serum-derived exosomes enhance endothelial cell proliferation and migration. *FASEB J.* 32, 4534–4543. doi: 10.1096/fj.201701337RR
- Jobe, A. H., and Bancalari, E. (2001). Bronchopulmonary dysplasia. *Am. J. Respir. Crit. Care Med.* 163, 1723–1729. doi: 10.1164/ajrccm.163.7.2011060
- Kalikot Thekkevedu, R., Guaman, M. C., and Shivanna, B. (2017). Bronchopulmonary dysplasia: a review of pathogenesis and pathophysiology. *Respir. Med.* 132, 170–177. doi: 10.1016/j.rmed.2017.10.014
- Klagsbrun, M., and D'Amore, P. A. (1991). Regulators of angiogenesis. *Annu. Rev. Physiol.* 53, 217–239. doi: 10.1146/annurev.ph.53.030191.001245
- Kollmann, K., Heller, G., Schneckenleithner, C., Warsch, W., Scheicher, R., Ott, R. G., et al. (2013). A kinase-independent function of CDK6 links the cell cycle to tumor angiogenesis. *Cancer Cell* 24, 167–181. doi: 10.1016/j.ccr.2013.07.012
- Lal, C. V., Olave, N., Travers, C., Rezonzew, G., Dolma, K., Simpson, A., et al. (2018). Exosomal microRNA predicts and protects against severe bronchopulmonary dysplasia in extremely premature infants. *JCI Insight* 3:e93994. doi: 10.1172/jci.insight.93994
- Landskroner-Eiger, S., Moneke, I., and Sessa, W. C. (2013). miRNAs as modulators of angiogenesis. *Cold Spring Harb. Perspect. Med.* 3:a006643. doi: 10.1101/cshperspect.a006643
- Liang, J., Liu, X., Xue, H., Qiu, B., Wei, B., and Sun, K. (2015). MicroRNA-103a inhibits gastric cancer cell proliferation, migration and invasion by targeting c-Myb. *Cell Prolif.* 48, 78–85. doi: 10.1111/cpr.12159
- Lura, M. P., Gorlanova, O., Muller, L., Proietti, E., Vienneau, D., Reppucci, D., et al. (2018). Response of cord blood cells to environmental, hereditary and perinatal factors: a prospective birth cohort study. *PLoS One* 13:e0200236. doi: 10.1371/journal.pone.0200236
- Matthay, M. A., and Abman, S. H. (2018). Exosome-based therapy for bronchopulmonary dysplasia. *Am. J. Respir. Crit. Care Med.* 197, 10–12. doi: 10.1164/rccm.201709-1796ED
- Mianehsaz, E., Mirzaei, H. R., Mahjoubin-Tehran, M., Rezaei, A., Sahebhasagh, R., Pourhanifeh, M. H., et al. (2019). Mesenchymal stem cell-derived exosomes: a new therapeutic approach to osteoarthritis? *Stem Cell Res. Ther.* 10:340. doi: 10.1186/s13287-019-1445-0
- Nahand, J. S., Mahjoubin-Tehran, M., Moghoofei, M., Pourhanifeh, M. H., Mirzaei, H. R., Asemi, Z., et al. (2020a). Exosomal miRNAs: novel players in viral infection. *Epigenomics* 12, 353–370. doi: 10.2217/epi-2019-0192
- Nahand, J. S., Vandchali, N. R., Darabi, H., Doroudian, M., Banafshe, H. R., Moghoofei, M., et al. (2020b). Exosomal microRNAs: novel players in cervical cancer. *Epigenomics* 12, 1651–1660. doi: 10.2217/epi-2020-0026
- Nowak-Sliwinska, P., Alitalo, K., Allen, E., Anisimov, A., Aplin, A. C., Auerbach, R., et al. (2018). Consensus guidelines for the use and interpretation of angiogenesis assays. *Angiogenesis* 21, 425–532. doi: 10.1007/s10456-018-9613-x
- Panfoli, I., Ravera, S., Podesta, M., Cossu, C., Santucci, L., Bartolucci, M., et al. (2016). Exosomes from human mesenchymal stem cells conduct aerobic metabolism in term and preterm newborn infants. *FASEB J.* 30, 1416–1424. doi: 10.1096/fj.15-279679
- Reiterer, F., Scheuchenecker, A., Resch, B., Maurer-Fellbaum, U., Avian, A., and Urlesberger, B. (2019). Bronchopulmonary dysplasia in very preterm infants: outcome up to preschool age, in a single center of Austria. *Pediatr. Int.* 61, 381–387. doi: 10.1111/ped.13815
- Sadri Nahand, J., Bokharai-Salim, F., Karimzadeh, M., Moghoofei, M., Karampoor, S., Mirzaei, H. R., et al. (2020). MicroRNAs and exosomes: key players in HIV pathogenesis. *HIV Med.* 21, 246–278. doi: 10.1111/hiv.12822
- Salomon, C., and Rice, G. E. (2017). Role of exosomes in placental homeostasis and pregnancy disorders. *Prog. Mol. Biol. Transl. Sci.* 145, 163–179. doi: 10.1016/bs.pmbts.2016.12.006
- Stenmark, K. R., and Balasubramaniam, V. (2005). Angiogenic therapy for bronchopulmonary dysplasia: rationale and promise. *Circulation* 112, 2383–2385. doi: 10.1161/CIRCULATIONAHA.105.574061
- Stoll, B. J., Hansen, N. I., Bell, E. F., Walsh, M. C., Carlo, W. A., Shankaran, S., et al. (2015). Trends in care practices, morbidity, and mortality of extremely preterm neonates, 1993–2012. *JAMA* 314, 1039–1051. doi: 10.1001/jama.2015.10244
- Sun, L. L., Li, W. D., Lei, F. R., and Li, X. Q. (2018). The regulatory role of microRNAs in angiogenesis-related diseases. *J. Cell. Mol. Med.* 22, 4568–4587. doi: 10.1111/jcmm.13700
- Wei, J., and Zhao, Y. (2020). MiR-185-5p protects against angiogenesis in polycystic ovary syndrome by targeting VEGFA. *Front. Pharmacol.* 11:1030. doi: 10.3389/fphar.2020.01030
- Willis, G. R., Mitsialis, S. A., and Kourembanas, S. (2018). “Good things come in small packages”: application of exosome-based therapeutics in neonatal lung injury. *Pediatr. Res.* 83, 298–307. doi: 10.1038/pr.2017.256
- Willms, E., Johansson, H. J., Mager, I., Lee, Y., Blomberg, K. E., Sadik, M., et al. (2016). Cells release subpopulations of exosomes with distinct molecular and biological properties. *Sci. Rep.* 6:22519. doi: 10.1038/srep22519
- Zhang, J., Li, S., Li, L., Li, M., Guo, C., Yao, J., et al. (2015). Exosome and exosomal microRNA: trafficking, sorting, and function. *Genom. Proteom. Bioinform.* 13, 17–24. doi: 10.1016/j.gpb.2015.02.001
- Zhang, X., Lu, A., Li, Z., Sun, J., Dai, D., and Qian, L. (2019). Exosomes secreted by endothelial progenitor cells improve the bioactivity of pulmonary microvascular endothelial cells exposed to hyperoxia in vitro. *Ann. Transl. Med.* 7:254. doi: 10.21037/atm.2019.05.10
- Zhou, C., Zou, Q. Y., Li, H., Wang, R. F., Liu, A. X., Magness, R. R., et al. (2017). Preeclampsia downregulates MicroRNAs in fetal endothelial cells: roles of miR-29a/c-3p in endothelial function. *J. Clin. Endocrinol. Metab.* 102, 3470–3479. doi: 10.1210/jc.2017-00849

Conflict of Interest: The authors declare that the research was conducted in the absence of any commercial or financial relationships that could be construed as a potential conflict of interest.

Copyright © 2021 Zhong, Yan, Chen, Jia, Li, Liang, Gu, Wei, Lian, Zheng and Cui. This is an open-access article distributed under the terms of the Creative Commons Attribution License (CC BY). The use, distribution or reproduction in other forums is permitted, provided the original author(s) and the copyright owner(s) are credited and that the original publication in this journal is cited, in accordance with accepted academic practice. No use, distribution or reproduction is permitted which does not comply with these terms.

Advantages of publishing in Frontiers



OPEN ACCESS

Articles are free to read
for greatest visibility
and readership



FAST PUBLICATION

Around 90 days
from submission
to decision



HIGH QUALITY PEER-REVIEW

Rigorous, collaborative,
and constructive
peer-review



TRANSPARENT PEER-REVIEW

Editors and reviewers
acknowledged by name
on published articles

Frontiers

Avenue du Tribunal-Fédéral 34
1005 Lausanne | Switzerland

Visit us: www.frontiersin.org

Contact us: frontiersin.org/about/contact



REPRODUCIBILITY OF RESEARCH

Support open data
and methods to enhance
research reproducibility



DIGITAL PUBLISHING

Articles designed
for optimal readership
across devices



FOLLOW US

@frontiersin



IMPACT METRICS

Advanced article metrics
track visibility across
digital media



EXTENSIVE PROMOTION

Marketing
and promotion
of impactful research



LOOP RESEARCH NETWORK

Our network
increases your
article's readership